

AD706211

NO COPY



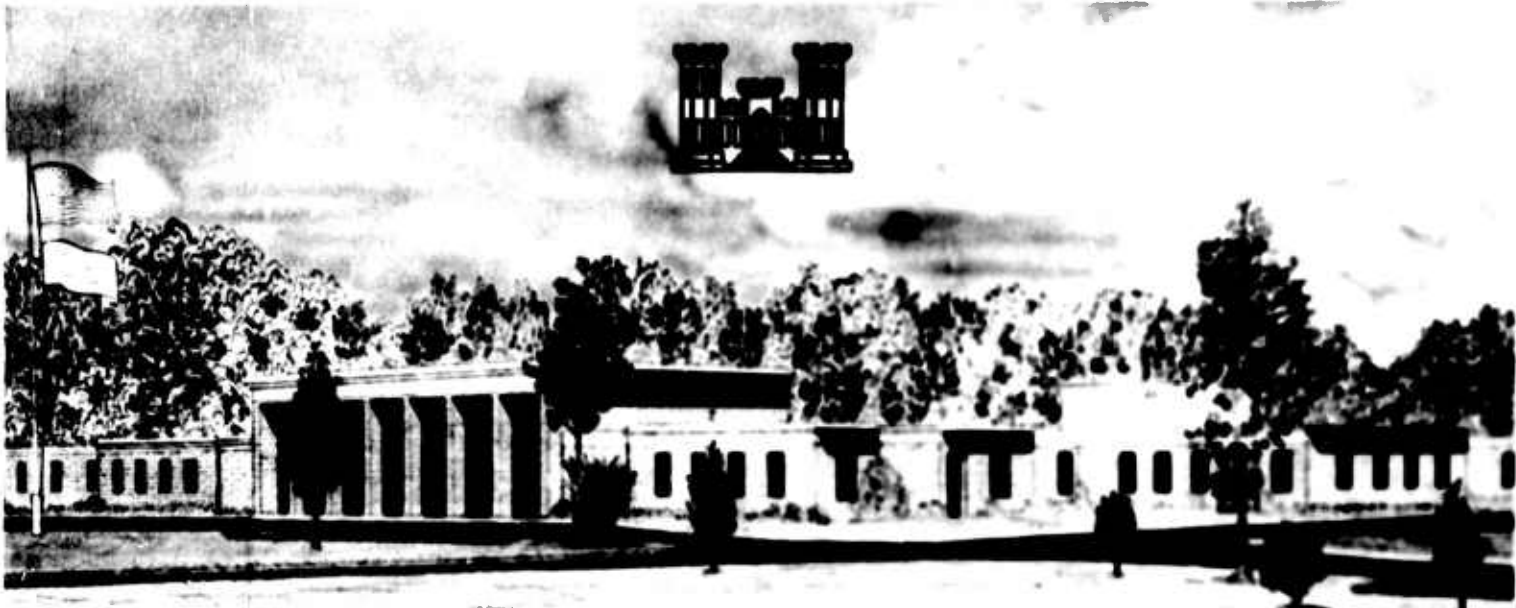
TECHNICAL REPORT N-70-7

AN EXPERIMENTAL INVESTIGATION OF SOIL-STRUCTURE INTERACTION IN A COHESIVE SOIL

Volume II

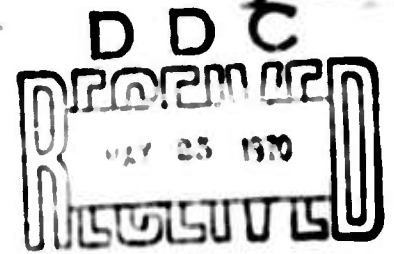
by

G. E. Jester



March 1970

Sponsored by Defense Atomic Support Agency



Conducted by U. S. Army Engineer Waterways Experiment Station, Vicksburg, Mississippi

This document has been approved for public release and sale; its distribution is unlimited

**Destroy this report when it is no longer needed.
Do not return it to the originator.**

**The findings in this report are not to be construed as an official
Department of the Army position unless so designated
by other authorized documents.**



TECHNICAL REPORT N-70-7

**AN EXPERIMENTAL INVESTIGATION OF
SOIL-STRUCTURE INTERACTION IN A
COHESIVE SOIL**

Volume II

by

G. E. Jester



March 1970

Sponsored by **Defense Atomic Support Agency**
NWER Subtask SC210

Conducted by **U. S. Army Engineer Waterways Experiment Station, Vicksburg, Mississippi**

ARMY-MRC VICKSBURG, MISS.

This document has been approved for public release and sale; its distribution is unlimited

CONTENTS

	<u>Page</u>
BIBLIOGRAPHY-----	336
TABLES 1 THROUGH 7-----	350
FIGURES 1 THROUGH 99-----	365
APPENDIX A PROPERTIES OF COMPACTED BUCKSHOT CLAY; WALL FRICTION REDUCTION; SOIL, GAGE, AND TEST DEVICE PLACEMENT-----	460
APPENDIX B DESIGN OF SPRING-RING TEST DEVICE-----	515
APPENDIX C OSCILLOGRAPH RECORDS FROM THE DYNAMIC TESTS-----	528

BIBLIOGRAPHY

- Abbott, P. A. (1966), Nonlinear Static Arching for Vertically Buried Prismatic Structures, AFWL TR 65-160, University of New Mexico for Air Force Weapons Laboratory, Kirtland AFB, New Mexico.
- Adine, A., and Dai, P. (1963), "An Approximate Study of Arching in Soil," Computation of Underground Structural Response, Chapter 5, p. 123-139; DASA 1386, edited by A. Ang and N. M. Newmark for Defense Atomic Support Agency.
- Aggarwal, H. R., Soldate, A. M., and Hook, J. F. (1963), A Theoretical Analysis of Stress Wave Interaction in a Model Soil, final report. AFSWC-TDR-63-43, National Engineering Science Company for Air Force Special Weapons Center, Kirtland AFB, New Mexico.
- Ahlers, E. B. (1961), Experimental Methods of Determining the Behavior of Underground Structures under Dynamic Loads, Armour Research Foundation, Chicago, Illinois.
- Airy, W. (1897), "The Pressure of Grain," Minutes of Proceedings of the Institute of Civil Engineers, Vol. 81, Paper No. 3049.
- Allgood, J. R. (1965), The Behavior of Shallow-Buried Cylinders, Technical Report R344, U. S. Naval Civil Engineering Laboratory, Port Hueneme, California.
- Allgood, J. R., and Seabold, R. H. (1965), Shallow Buried Model Arches Subjected to a Traveling-Wave Load, Technical Report R375, U. S. Naval Civil Engineering Laboratory, Port Hueneme, California.
- American Society of Civil Engineers (1961), Design of Structures to Resist Nuclear Weapons Effects, Manuals of Engineering Practice No. 42, New York, New York.
- Ang, A., and Newmark, N. M. (1963), Computation of Underground Structural Response, DASA 1386, Department of Civil Engineering, University of Illinois, Urbana, Illinois.
- Baker, W. J., and Janza, F. J. (1966), Investigation of Flash X-ray Techniques in Soil Dynamics and Interaction Problems,

AFWL-TR-66-50, U. S. Air Force Weapons Laboratory, Kirtland AFB, New Mexico.

- Baron, M. L., and Parnes, R. (1962), Further Studies on the Diffraction of a Pressure Wave by an Elastically Lined Cylindrical Cavity in an Elastic Medium, SR-72, Paul Weidlinger for the Mitre Corporation.
- Bedesem, W. B. (1964), A Continuum Theory of Soil-Structural Interaction in Granular Media, Ph. D. Thesis, University of Illinois, Urbana, Illinois.
- Bedesem, W. B., Das, Y. C., and Robinson, A. R. (1964), Quasi-Static Theory of Soil-Structure Interaction, AFWL-TDR-64-91, prepared by the University of Illinois for Air Force Weapons Laboratory, Kirtland AFB, New Mexico.
- Berdan, D., and Bernhard, R. K. (1950), "Pilot Studies of Soil Density Measurements by Means of X-Rays," Proceedings of the American Society for Testing and Materials, Vol. 50, pp 1328-1342.
- Bloedow, F. H. (1962), Radiographic Instrumentation Study, final report AFSWC-TDR-62-44, Air Force Special Weapons Center, Kirtland AFB, New Mexico.
- Boynton Associates (1960), Operation Manual for 250 PSI 4-Foot Diameter Dynamic Load Generator, La Canada, California.
- Brecht, W. A., and Wahl, A. M. (1952), The Radially Tapered Disk Spring, Paper APM-52-4, American Society of Mechanical Engineers, New York, New York.
- Caquot, A. I. (1934), Equilibre des Massifs a Frottement Interne, Gauthier-Villars, Paris.
- Caquot, A. I., and Kérisel, J. (1949), Traité De Mécanique Des Sols, Gauthier-Villars, Paris.
- Caquot, A. I. (1957), "Pressure in Elevators," ("La Pression Dans Les Silos,") Proceedings of the Fourth International Conference on Soil Mechanics and Foundation Engineering, Vol. II, pp 191-195 (Translation No. 64-11, U. S. Army Engineer Waterways Experiment Station, by Jan C. Van Tienhoven, December 1964).

- Carlson, R. W. (1936), Development and Analysis of a Device for Measuring Compressive Stress in Concrete, Sc. D. Thesis, Massachusetts Institute of Technology, Cambridge, Massachusetts.
- Carlson, R. W., and Pirtz, D. (1953), "Development of a Device for the Direct Measurement of Compressive Stress," Proceedings, American Concrete Institute, Title No. 49-15, Vol. 49, pp 201-215, Detroit, Michigan.
- Carroll, W. F. (1963), Dynamic Bearing Capacity of Soils, Report 5; Vertical Displacements of Spread Footings on Clay: Static and Impulsive Loadings, Technical Report No. 3-599, U. S. Army Engineer Waterways Experiment Station, Vicksburg, Mississippi.
- Chelapati, C. V. (1964), Arching in Soil Due to the Deflection of a Rigid Horizontal Strip, Technical Note N-591, U. S. Naval Civil Engineering Laboratory, Port Hueneme, California.
- Chiapetta, R. L., and Constantino, C. J. (1967), A Bibliography on the Response of Earth Media and Buried Structures to Ground Shock Loading, IIT Research Institute Project Report M 6177, also published as U. S. Army Engineer Waterways Experiment Station, Vicksburg, Mississippi, Contract Report No. 3-168.
- Christensen, R. W., and Tien Hsing Wu (1964), "Analysis of Clay Deformation as a Rate Process," Journal of the Soil Mechanics and Foundation Division, American Society of Civil Engineers, Proceedings, Vol. 90, SM 6, pp 125-157.
- Costantino, C. J., Robinson, R. R., and Salmon, M. A. (1964), "A Simplified Soil Structure Interaction Model to Investigate the Response of Buried Silos and Cylinders," Proceedings of the Symposium on Soil Structure Interaction, University of Arizona, Tucson, Arizona, pp 303-314.
- Costantino, C. J. (1966), Response of Crushable Foam Encased Buried Cylinders, Ph. D. Thesis, Illinois Institute of Technology, Chicago, Illinois.
- Crandall, S. H., and Dahl, N. C. (1959), An Introduction to the Mechanics of Solids, McGraw-Hill, Inc., New York, New York.
- Davis, H. E., and Woodward, J. R. (1949), "Some Laboratory Studies

of Factors Pertaining to the Bearing Capacity of Soils," Highway Research Board Proceedings, Vol 29, pp 467-476.

- Dorris, A. F. (1965), Response of Horizontally Oriented Buried Cylinders to Static and Dynamic Loading, Technical Report 1-682, Vicksburg, Mississippi, U. S. Army Engineer Waterways Experiment Station.
- Drake, J. L., Considerations for Determining Airblast-Induced Soil Stress, U. S. Army Engineer Waterways Experiment Station, Vicksburg, Mississippi (in preparation).
- Engesser, Fr. (1882), "Ueber den Erddruck Gegen Innere Stützwände (Tunnelwände)," Deutsche Bauzeitung, No. 16, pp 91-93.
- Finn, W. D. (1960), Stresses in Soil Masses Under Various Boundary Conditions, Ph. D. Thesis, University of Washington.
- Gardner, G. C. (1963), "The Best Hopper Profile for Cohesive Material," Chemical Engineering Science, Vol. 18, No. 1, pp 35-39.
- Gravesen, S. (1959), "Elastic Half-Space Covered by a Stiff Plate with a Circular Piston," Bulletin No. 10, Laboratory for Building Research, Technical University of Denmark, Copenhagen.
- Haase, M. C. (1967), X-Radiography of Unopened Soil Cores, Miscellaneous Paper No. 3-918, U. S. Army Engineer Waterways Experiment Station, Vicksburg, Mississippi.
- Hadala, P. F. (1965), Dynamic Bearing Capacity of Soils, Report 4, Investigation of a Dimensionless Load-Displacement Relation for Footings on Clay, Technical Report No. 3-599, U. S. Army Engineer Waterways Experiment Station, Vicksburg, Mississippi.
- Hadala, P. F. (1967a), The Effects of Placement Method on the Response of Soil Stress Gages, Technical Report No. 3-803, U. S. Army Engineer Waterways Experiment Station, Vicksburg, Mississippi.
- Hadala, P. F. (1967b), Sidewall Friction Reduction in Static and Dynamic Small Blast Load Generator Tests, Technical Report, U. S. Army Engineer Waterways Experiment Station, Vicksburg, Mississippi (in preparation).
- Hadala, P. F. (1967c), Spectral Analysis of Fundamental Studies

Tests, Memorandum on DASA's Program, 20 June 1967, U. S. Army Engineer Waterways Experiment Station, Vicksburg, Mississippi (not publicly distributed).

- Havers, J. A. (1963), Structural Materials for Hardened Personnel Shelters, IIT Research Institute for Office of Civil Defense, Department of Defense, Washington, D. C.
- Hendron, A. J. (1963), The Behavior of Sand in One-Dimensional Compression, Ph. D. dissertation, Dept. of Civil Engineering, University of Illinois, Urbana, Illinois.
- Hendron, A. J. (1968), An Experimental Study of Arching In Clay, Technical Report, U. S. Army Engineer Waterways Experiment Station, Vicksburg, Mississippi (in preparation).
- Höeg, Kaare (1966), Pressure Distribution on Underground Structural Cylinders, AFWL TR-65-98, Massachusetts Institute of Technology for Air Force Weapons Laboratory, Kirtland AFB, New Mexico.
- Hughes, G. T., Locker, J. G., and Stewart, W. D. (1965), Bibliography of Soil Dynamics and Soil Structure Interaction During Dynamic or Similar Loadings, DR-170, Department of Civil Engineering, Royal Military College of Canada, Kingston, Ontario.
- Hvorslev, M. J. (1949), Subsurface Exploration and Sampling of Soils for Civil Engineering Purposes, report on research project of ASCE, edited and printed by U. S. Army Engineer Waterways Experiment Station, Vicksburg, Mississippi.
- Hvorslev, M. Juul (1966), Comments on Research Proposal, private communications with author, U. S. Army Engineer Waterways Experiment Station, Vicksburg, Mississippi.
- Ingram, J. K. (1965), "The Development of a Free-Field Soil Stress Gage for Static and Dynamic Measurements," Instruments and Apparatus for Soil and Rock Mechanics, ASTM STP 392, also issued as U. S. Army Engineer Waterways Experiment Station, Vicksburg, Mississippi, Technical Report No. 1-814.
- Ingram, L. F. (1967), Instrumentation for Earth Stresses and Motions Produced by Explosions, Miscellaneous Paper No. 1-885, U. S. Army Engineer Waterways Experiment Station, Vicksburg, Mississippi.

- Jackson, J. G., Jr., and Hadala, P. F. (1964), Dynamic Bearing Capacity of Soils, Report 3; The Application of Similitude to Small-Scale Footing Tests, Technical Report No. 3-599, U. S. Army Engineer Waterways Experiment Station, Vicksburg, Mississippi.
- Jaky, J. (1948), "Pressure in Silos," Second International Conference on Soil Mechanics and Foundation Engineering, Proceedings, Vol. 1, pp 103-107.
- Jamieson, J. A. (1904), "Grain Pressures in Deep Bins," Engineering News, Vol. 51, pp 236-239.
- Janssen, H. A. (1895), "Versuche über Getreidedrucks in Silozellen," Verein Deutscher Ingenieure, Zeitschrift, Vol. 39.
- Jenike, A. W., Elsey, P. J., and Woolley, R. H. (1958), "Flow of Bulk Solids Progress Report," Bulletin No. 96, Utah Engineering Experiment Station, (Revised Reprint July, 1959), Salt Lake City, Utah.
- Jenike, A. W (1964), "Storage and Flow of Solids," Bulletin No. 123, Utah Engineering Experiment Station, University of Utah, Salt Lake City, Utah.
- Johnson, S. J. (1961), An Alternative Method for Determining the Constrained Modulus and the Coefficient of Elastic Vertical Compression, report by Moron, Proctor, Mueser, and Rutledge for Ballistic Systems Division of U. S. A. Force.
- Kallstenius, Torsten (1959), "A Study of the Flow Pattern When Emptying a Vessel," Proceedings No. 47, Royal Swedish Geotechnical Institute, pp 67-70, Appendix, to "Measurements in Grain Silos During Filling and Emptying," by Werner Bergau, Stockholm.
- Kane, H., Davisson, M. T., Oleson, R. E., and Sinnamon, G. K. (1964), A Study of the Behavior of a Clay Under Rapid and Dynamic Loading in the One-Dimensional and Triaxial Tests, final report, RTD TDR 63-3116, University of Illinois for Air Force Weapons Laboratory, Kirtland AFB, New Mexico.
- Kennedy, T. E., Dynamic Response of Buried Concrete Arches, Project 3.2, OPERATION SNOWBALL, Technical Report, U. S. Army Engineer Waterways Experiment Station, Vicksburg, Mississippi (in preparation).

- Kogler, F., and Scheidig, A. (1927), "Druckverteilung im Baugrunde-I. Die Ergebnisse neuerer Versuche," Die Bautechnik, 5. Jahrgang, Heft 29, pp 418-421, Berlin, Germany.
- Kvapil, Rudolf (1965), "Gravity Flow of Granular Materials in Hoppers and Bins," International Journal of Rock Mechanics and Mining Science, Vol. 2, pp 25-41, Pergamon Press.
- Lenczner, D. (1966), "Cohesive Arching of Bulk Materials in Bunkers and Silos," Civil Engineering and Public Works Review, Vol. 61, No. 724, pp 1393, 1395-1396.
- Mason, H. G., Criner, O. H., Waissar, R., and Wallace, N. R. (1963), A Study of the Dynamic Soil-Structure Interaction Characteristics of Real Soil Media, RTD TDR-63-3075, United Research Services for Air Force Weapons Laboratory, Kirtland AFB, New Mexico.
- Mason, H. G. (1965), Effects of Structural Compressibility on Active and Passive Arching in Soil-Structure Interaction, final report, DASA 1718, URS Corporation for Defense Atomic Support Agency, Washington, D. C.
- McNulty, J. W. (1965), An Experimental Study of Arching in Sand, Technical Report No. 1-674, U. S. Army Engineer Waterways Experiment Station, Vicksburg, Mississippi.
- Melin, J. W., and Sutcliffe, S. (1959), Development of Procedures for Rapid Computation of Dynamic Structural Response, SRS 171, Department of Civil Engineering, University of Illinois, Urbana, Illinois.
- Merritt, J. L., and Newmark, N. M. (1964), "Effects on Underground Structures and Equipment," Nuclear Geoplosics, Part V, DASA 1285(V), Stanford Research Institute, Menlo Park, California.
- Monfore, G. E. (1950), "An Analysis of the Stress Distributions in and Near Stress Gages Embedded in Elastic Solids," Structural Research Laboratory Report No. SP 26, U. S. Bureau of Reclamation, Denver, Colorado.
- Mosborg, R. J., and Talda, P. M. (1966), An Experimental Investigation of the Arching Phenomenon Occurring Over a Buried Rectangular Plate, AFWI TR-65-78, prepared by University of

Illinois for Air Force Weapons Laboratory, Kirtland AFB,
New Mexico.

- Mow, C. C. (1964), Dynamic Response of Lined and Unlined Underground Openings, Memorandum RM-3962-PR, The Rand Corporation, Santa Monica, California.
- Newmark, N. M. (1949), Methods of Analysis for Structures Subjected to Dynamic Loading, report to Physical Vulnerability Division, Directorate of Intelligence, U. S. Air Force.
- Newmark, N. M., Briscoe, J. W., and Merritt, J. L. (1960), Analysis and Design of Flexible Underground Structures, Volume I, prepared for U. S. Army Engineer Waterways Experiment Station, Vicksburg, Mississippi.
- Newmark, Hansen and Associates (1961), Protective Construction Review Guide-Hardening, Vol. 1, prepared for the Office of the Assistant Secretary of Defense.
- Newmark, N. M., and Hall, W. J. (1962), Preliminary Design Methods for Underground Protective Structures, AFSWC-TDR-62-6, prepared by University of Illinois for Air Force Special Weapons Center, Kirtland AFB, New Mexico.
- Newmark, N. M., and Haltiwanger, J. D. (1962), Principles and Practices for Design of Hardened Structures, AFSWC-TDR-62-138, prepared by University of Illinois for Air Force Special Weapons Center, Kirtland AFB, New Mexico.
- Newmark, N. M. (1964), "The Basis of Current Criteria for the Design of Underground Protective Construction," Proceedings of the Symposium on Soil-Structure Interaction, University of Arizona, Tucson, Arizona, pp 1-24.
- Neuber, Heinz (1946), Theory of Notch Stresses, Edwards Bros., Ann Arbor, Michigan.
- Peck, R. B., Hanson, W. E., and Thornburn, T. H. (1953), Foundation Engineering, John Wiley & Sons, Inc., New York, New York.
- Peck, R. B. (1960), "Soft Ground Tunneling," From Theory to Practice in Soil Mechanics, selections from the writings of Karl Terzaghi, John Wiley and Sons, Inc., New York, New York.

- Perry, Edward B. (1968), The Effect of Shallow Burial on the Load-Displacement-Time Response of Square Footings in Clay Under Impulsive Loading, M.S. Thesis, Department of Civil Engineering, Mississippi State University, State College, Mississippi.
- Richardson, A. M., Jr. (1965), The Response of Soils to Dynamic Loading, Report 16; Effective Stress Versus Strength, Saturated Fat Clay, Massachusetts Institute of Technology Research Project 63-20, also published as U. S. Army Engineer Waterways Experiment Station, Vicksburg, Mississippi, Contract Report No. 3-26.
- Richardson, A. M., Jr., and Whitman, R. V. (1963), Effect of Strain Rate upon Undrained Shear Resistance of a Saturated Fat Clay, P03-15, Massachusetts Institute of Technology.
- Richart, F. E., Jr. (1959), Arching in Granular Elastic Media, final report on Project 5810, Engineering and Industrial Experiment Station, University of Florida.
- Richmond, O. (1963), "Gravity Hopper Design," Mechanical Engineering, Vol. 85, No. 1, pp 46-49.
- Robinsky, E. I., and Morrison, C. F. (1964), "Sand Displacement and Compaction Around Model Friction Piles," Canadian Geotechnical Journal, Vol. 1, No. 2, pp 81-93.
- Roscoe, K. H., Arthur, J. R. F., and James, R. G. (1963), "The Determination of Strains in Soils by an X-Ray Method," (Part 2), Civil Engineering and Public Works Review, Vol. 58, No. 685, pp 1009-1012.
- Schindler, L. (1967), An Improved Facility for Testing Soils in One-Dimensional Compression, paper submitted to the Symposium on Wave Propagation and Dynamic Properties of Earth Materials, Albuquerque, New Mexico.
- Seazan, Lynn (1966), One-Dimensional Stress Wave Propagation in Soils, DASA Report 1757, prepared by Stanford Research Institute, Menlo Park, California.
- Seely, F. B., and Smith, J. O. (1952), Advanced Mechanics of Materials, 2nd ed., John Wiley & Sons, Inc., New York, New York.
- Selig, E. T. (1960), "An Analytical Method for the Design of

Underground Structures," Shock, Vibration and Associated Environments, Bulletin No. 28, Part III, pp 37-47, Office of the Secretary of Defense, Research and Engineering, Washington, D. C.

- Selig, E. T. (1961a), "A Technique for Observing Structure-Soil Interaction," Materials Research and Standards, Vol. 1, No. 9, pp 717-719.
- Selig, E. T., McKee, K. E., and Vey. Eben (1961b), "Underground Structures Subject to Air Overpressure," Transactions of the American Society of Civil Engineers, Vol. 126, Part I, pp 1627-1649.
- Sirieys, P. M. (1964), "Champs de Contraintes Autour des Tunnels Circulaires en Elastoplasticite," Rock Mechanics and Engineering Geology, Vol. II, No. 1, pp 68-75.
- Spangler, M. G. (1948), "Underground Conduits - An Appraisal of Modern Research," Transactions of the American Society of Civil Engineers, Vol. 113, No. 2337, New York.
- Spangler, M. G. (1956), "Stresses in Pressure Pipelines and Protective Casing Pipes," Journal of the Structural Division, Proceedings of the American Society of Civil Engineers, Vol. 82, No. 1054, Ann Arbor, Michigan.
- Steen, Leo L. (1966a), "Revised Procedure for Lining Small Blast Load Generator Specimens to Reduce Sidewall Friction," Memorandum for Blast Load Generator Soils Laboratory Files, U. S. Army Engineer Waterways Experiment Station, Vicksburg, Mississippi.
- Steen, Leo L. (1966b), "Compaction Methods for Various Degrees of Saturation of Buckshot Clay," Memorandum for Blast Load Generator Soils Laboratory Files, U. S. Army Engineer Waterways Experiment Station, Vicksburg, Mississippi.
- Sylwestrowicz, W. (1953), "Experimental Investigation of the Behavior of Soil Under a Punch or Footing," Journal of the Mechanics and Physics of Solids, Vol. I, pp 258-264.
- Taylor, D. W. (1945), Review of Pressure Distribution Theories, Pressure Cell Investigation and Pressure Distribution Data, Massachusetts Institute of Technology, Cambridge, Massachusetts.

- Teng, Wayne C. (1962), Foundation Design, Prentice-Hall, Inc., Englewood Cliffs, New Jersey.
- Terzaghi, Karl (1919), "Die Erddruckerscheinungen in örtlich beanspruchten Schüttungen und die Entstehung Von 'Tragkörpern'," Osterreichische Wochenschrift für öffentlichen Baudienst, Nos. 17-19, pp 194-199, 206-210, and 218-223.
- Terzaghi, Karl (1936a), "A Fundamental Fallacy in Earth Pressure Computations," Journal of the Boston Society of Civil Engineers, Vol. 23, No. 2, pp 71-88.
- Terzaghi, Karl (1936b), "Arching in Sands," Engineer News-Record, Vol. 116, pp 690-693.
- Terzaghi, Karl (1936c), "Stress Distribution in Dry and in Saturated Sand Above a Yielding Trap-Door," First International Conference on Soil Mechanics and Foundation Engineering, Vol. 1, pp 307-311, Cambridge, Massachusetts.
- Terzaghi, Karl (1943), Theoretical Soil Mechanics, John Wiley & Sons, Inc., New York, New York.
- Terzaghi, Karl, and Peck, R. B. (1948), Soil Mechanics in Engineering Practice, John Wiley & Sons, Inc., New York, New York.
- Terzaghi, Karl, and Richart, F. E., Jr. (1952), "Stresses in Rock About Cavities," Geotechnique, Vol. 3, No. 2, pp 57-90.
- Triandafilidis, G. E., Hampton, D., and Spanovich, N. (1964), Experimental Study of Arching Stresses on Buried Vertical Cylinders, RTD TDR-63-31.06, University of New Mexico for Air Force Weapons Laboratory, Kirtland AFB, New Mexico.
- Tschebotarioff, G. P. (1951), Soil Mechanics, Foundations, and Earth Structures, McGraw-Hill, Inc., New York, New York.
- Tschebotarioff, G. P. (1954), Discussion of Field Study of Sheet-Pile Bulkhead (ASCE Proceedings Separate No. 155) by Duke, C. M., presented at ASCE Meeting, 1950, Los Angeles, ASCE Proceedings Separate No. 379.
- Turnbull, W. J., and Foster, C. R. (1958), "Stabilization of Materials

- by Compaction," Transactions, American Society of Civil Engineers, Vol. 123, pp 1-26.
- U. S. Army Engineer Waterways Experiment Station (1944), Soil Pressure Cell Investigation, interim report, Technical Memorandum No. 210-1, Vicksburg, Mississippi.
- U. S. Army Engineer Waterways Experiment Station (1958), Geological Investigation of the Yazoo Basin, Technical Report No. 3-480, Vicksburg, Mississippi, revised March 1968.
- U. S. Army Engineer Waterways Experiment Station (1963), Status Report for Blast Load Generator Facility, Vicksburg, Mississippi.
- U. S. Corps of Engineers (1965), Laboratory Soils Testing, EM 1110-2-1906.
- Van Horn, D. A., and Tener, R. K. (1963a), A Study of Loads on Underground Structures, Project 434-S, Iowa Engineering Experiment Station, Ames, Iowa.
- Van Horn, D. A. (1963b), A Study of Loads on Underground Structures, Part I, an annotated bibliography, DASA 1406, Iowa Engineering Experiment Station, Iowa State University, Ames, Iowa.
- Van Horn, D. A. (1964), "A Study of Loads on Underground Structures," Proceedings of the Symposium on Soil-Structure Interaction, University of Arizona, Tucson, Arizona, pp 256-282.
- Voellmy, Adolph (1937), Imbedded Pipes, Static Analysis of Buried Conduits with Consideration of the Elasticity (English translation by Professor and Mrs. Edward Allen, 1961-1962, Ames, Iowa).
- Walker, D. M. (1966), "An Approximate Theory for Pressures and Arching in Hoppers," Chemical Engineering Science, Vol. 21, Oxford, England, pp 975-997.
- Watkins, R. K. (1957), Characteristics of the Modulus of Passive Resistance of Soil, Ph. D. Thesis, Iowa State College, Ames, Iowa.
- Watkins, R. K. (1964), "Structural Design Trends in Buried Flexible Conduits," Proceedings of the Symposium on Soil-Structure

- Interaction, University of Arizona, Tucson, Arizona, pp 246-255.
- Watkins, R. K. (1966), Structural Design of Buried Circular Conduits, U. S. Army Engineer Waterways Experiment Station, Vicksburg, Mississippi.
- Whiffin, A. C., and Morris, S. A. H. (1962), "Piezoelectric Gauge for Measuring Dynamic Stresses Under Roads," The Engineer, Vol. 213, No. 5544, pp 741-746.
- Whipple, C. R. (1961), The Dynamic Response of Shallow-Buried Arches Subjected to Blast Loading, Ph. D. Thesis, Department of Civil Engineering, University of Illinois, Urbana, Illinois.
- Whitman, R. V., Roberts, J. E., and Shieh-Wen Mao (1960), The Response of Soils to Dynamic Loadings, Report 4; One-Dimensional Compression and Wave Velocity Tests, prepared by Massachusetts Institute of Technology for U. S. Army Engineer Waterways Experiment Station, Vicksburg, Mississippi, and Defense Atomic Support Agency, Contract Report No. 3-26, DASA 1199.
- Whitman, R. V., Richardson, A. M., Jr., and Nasim, N. M. (1962a), The Response of Soils to Dynamic Loadings, Report 10; Strength of Saturated Fat Clay, Massachusetts Institute of Technology Research Project R62-22, also published as U. S. Army Engineer Waterways Experiment Station, Vicksburg, Mississippi, Contract Report No. 3-26.
- Whitman, R. V., Getzler, Zvi, and Höeg, Kaare (1962b), The Response of Soils to Dynamic Loadings, Report 12; Static Tests Upon Thin Domes Buried in Sand, Massachusetts Institute of Technology Research Project R62-41, also published as U. S. Army Engineer Waterways Experiment Station, Vicksburg, Mississippi, Contract Report No. 3-26.
- Whitman, R. V. (1963), The Response of Soils to Dynamic Loadings, Report 17; Stress-Strain-Time Behavior of Soil in One-Dimensional Compression, Massachusetts Institute of Technology Research Report R63-25, also published as U. S. Army Engineer Waterways Experiment Station, Vicksburg, Mississippi, Contract Report No. 3-26.
- Wiedermann, A. H. (1960), Concepts of Preliminary Design of Structure Projects for Underground Nuclear Detonations, Appendix B; The

Interaction of Buried Structures with Ground Shock, AFSWC-TR-60-3, Armour Research Foundation for Air Force Special Weapons Center, Kirtland AFB, New Mexico.

Wiehle, C. K. (1965), Soil-Structure Interaction Under Dynamic Load, final report, DASA 1711, URS 645-7, URS Corporation, Burlingame, California.

Yoshiharo, T., Robinson, A. R., and Merritt, J. L. (1963), Interaction of Plane Elastic Waves with an Elastic Cylindrical Shell, University of Illinois, Structural Research Series No. 261, for the Office of Naval Research.

Table 1
Summary of Static Tests

Test No.	Pressure		Depth of Cover in. H/E	K _T psi/in.	M _S psi	K _S psi/in.	K _T K _S		Maximum Arching				Avg Soils Data		Remarks			
	P _S	P					Planned	Actual	ΔP psi	$\frac{\Delta P}{q_u}$	$\frac{P_T}{P_S}$	$\frac{\Delta U}{E} \times 1000$	$\frac{D_T}{E} \times 100$	$\frac{d_t}{E} \times 1000$		MC%	$\frac{q_u}{2}$, psi	
1	37.8	38.0	2	1/3	NA	4700	940	NA	NA	-24.5	-1.67	0.35	-73.01	8.64	-78.33	26.0	-14.70	Top of test device lowered
2	37.5	28.3	6	1	NA	1700	340	NA	NA	-37.04	-2.32	0.02	-21.17	2.72	-26.67	24.3	16.97	Top of test device lowered
	37.5	26.5	--	--	NA	2040	404	NA	NA	+8.7	+0.54	1.24	+74.17	7.29	+82.67	--	--	Top of test device raised
	34.8	27.1	--	--	NA	1740	348	NA	NA	-33.5	-2.10	0.04	-78.00	8.80	-81.67	--	--	Lowering top of device 2d time
3	37.5	27.7	18	3	NA	1870	375	NA	NA	-36.5	-2.02	0.03	-11.84	2.13	-16.00	24.7	18.06	Top of test device lowered
	37.5	30.0	--	--	NA	1130	226	NA	NA	+7.8	+0.43	1.21	+15.17	1.47	+25.83	--	--	Raising top of device
	50.0	40.6	18	3	NA	1640	328	NA	NA	-49.3	-2.73	0.01	-26.51	10.24	-24.17	--	--	Top of test device lowered 2d time
4	75.0	67.2	6	1	NA	1700	340	NA	NA	-45.2	-3.32	0.40	-77.17	7.85	-81.83	25.2	13.61	Top of test device lowered
	75.0	66.2	--	--	NA	1650	330	NA	NA	+36.1	+2.65	1.48	+71.67	6.97	+82.67	--	--	Raising top of device
	75.0	67.8	6	1	NA	1690	338	NA	NA	-50.6	-3.72	0.33	-78.83	8.35	-82.17	--	--	Lowering top of device 2d time
5	37.6	--	6	1	NA	UNK	UNK	NA	NA	+38.8	+2.79	2.03	+61.18	6.06	+72.88	25.5	13.89	Top of device raised
	37.5	--	--	--	NA	UNK	UNK	NA	NA	-36.4	-2.62	0.03	-58.51	4.85	-24.63	--	--	Top of device lowered
6	37.5	33.2	6	1	189	1570	314	0.5	0.60	-14.1	-1.04	0.62	-2.17	13.72	-20.67	24.7	13.61	Spring system used, pressure raised
	38.5	36.2	--	--	189	1550	310	0.5	0.61	-15.9	-1.17	0.59	-2.17	15.32	-21.67	--	--	Raised pressure 2d time
	38.0	39.0	--	--	189	1525	305	0.5	0.62	-11.9	-0.87	0.69	-0.67	16.67	-23.00	--	--	Max load after 15.5 hr creep allowed
	38.7	39.0	--	--	189	1565	313	0.5	0.60	-12.1	-0.89	0.69	-1.17	17.19	-23.50	--	--	Max load after 51.8 hr creep allowed
	38.5	39.0	--	--	189	1565	313	0.5	0.60	-11.9	-0.87	0.69	-1.50	17.22	-23.50	--	--	Max load after 62.6 hr creep allowed
7	37.5	46.2	6	1	958	3830	766	3.0	1.25	-5.6	-0.42	0.85	-4.00	14.68	-6.00	25.7	13.47	Spring system used, pressure raised
8	175.0	--	18	3	522	6150	1230	0.7	0.42	-54.0	-4.9	0.74	-27.67	31.26	-41.33	27.3	11.11	Spring system used, first reached max load on top of device
	240.0	--	--	--	532	7950	1590	0.7	0.33	-58.0	-5.2	0.76	-40.17	33.16	-57.50	--	--	Max load on top of device at max P _S
	240.0	--	--	--	532	7450	1490	0.7	0.36	-35.0	3.2	0.85	-45.01	33.94	-60.33	--	--	Max load of top of device after creep allowed

Note: P_S, surface pressure; P, soil pressure at 35-in. level; H/B, ratio of depth of cover to diameter of device (6 in.); K_T, test device stiffness; K_S, soil stiffness; ΔP, differential pressure (P_T - P_S); q_u, unconfined compressive strength of soil; P_T, average force acting on top of test device; ΔU, differential deflection (D_T - D_S); D_T, total deflection of test device (d_b + d_t); d_t, deflection of top with respect to base of test device; WC, water content of soil in percent of dry weight. +(-) pressure on top of device higher (lower) than surface pressure or deflection of top of device is less (more) than the soil in the "free field" at the same level.

Table 2
Summary of Dynamic Tests

Test No.	Peak Pressure, psi P _s	Depth of Cover in. H/E	k _T psi/in.	t msec	ΔP psi	ΔP q _u	Maximum Load on Top of Device				Dimensionless Parameters		d _t × 1000 B	Soil Modulus M _s , psi		Soil Stiffness K _s , psi/in.		K _T K _s		Avg Soil Data	
							F _s *	F _T P/S	AD B × 1000	D _t B × 100	Strain	Velocity		Strain	Velocity	Planned	Actual	K _T K _s	K _T K _s	W _C %	q _u psi
11	37.0	18	3	4.07	13	-9.5	-0.61	-11.67	4.05	-11.33	2700	1390-3040	540	276-608	0.70	0.75	25.0	15.42			
12	70.0	18	3	4.00	12	-11.5	-10.67	3.02	-10.17	2980	2060-4595	596	---	0.70	0.62	26.1	14.58				
13	151.0	18	3	4.25	12.5	-32.0	-19.67	10.52	-10.50	3760	2670-3190	752	532-638	0.70	0.57	26.2	12.78				
14	245.0	18	3	6.13	10	-35.0	-23.2	23.7	-51.50	4650	2980-4250	930	596-850	0.70	0.66	25.5	15.28				
15	39.0	223.0**	2	1/3	7	-59.0	-22.0	13.8	-48.33	5820	---	1164	---	0.70	0.53	25.8	10.83				
16	37.5	32.0	6	1	14	-6.0	-0.53	3.48	-13.83	2500	345-1235	300	69-247	0.70	1.18	25.6	16.25				
17	40.5	44.0	18	3	4.07	-11.5	-8.50	5.27	-11.00	3100	1235-1825	620	247-365	0.70	0.57	24.9	19.72				
18	310.0	270.0	42	7	6.13	-13.0	-11.00	4.20	-12.17	3550	---	710	---	0.70	0.57	25.4	14.85				
19	157.0	140.0	6	1	4.28	-47.0	-30.00	29.83	-56.33	5280	3430-6240	1056	686-1248	0.70	0.58	25.0	17.64				
20	33.0	32.0	6	1	105	-26.5	-17.50	9.97	-55.00	4600	---	920	382	0.70	0.54	25.0	17.64				
21	35.5	34.5	6	1	280	-30.0	-20.00	19.33	-52.67	4000	---	800	---	0.70	0.54	25.0	17.64				
22	38.4	34.0	6	1	575	-22.0	-1.70	0.81	-20.00	4000	---	800	---	0.70	0.54	25.0	17.64				
23	33.3	23.0	6	1	17.5	-23.5	-3.50	3.08	-14.00	1830	935-1430	366	187-286	0.20	0.29	26.6	12.22				
24	31.7	---	6	1	4,246	-26.5	-6.67	4.27	-15.33	1790	---	358	---	0.20	0.29	26.6	12.22				
25	53.5	---	6	1	4,246	-20.0	-10.00	5.43	-10.33	1940	1470-2570	388	294-514	0.50	0.72	25.3	19.44				
26	33.5	---	6	1	317,000	-21.0	(-3.67)	(2.35)	(8.67)	(3320)	---	656	---	0.42	(0.42)	---	---				
27A	31.0	---	6	1	317,000	-22.0	-1.13	0.37	-9.33	3280	---	656	---	0.88	0.88	26.9	16.25				
27B	41.5	---	6	1	317,000	-11.0	-5.67	1.30	-13.00	3280	920-1055	656	184-211	1.00	0.90	25.0	16.67				
27C	64.0	---	6	1	317,000	-14.0	-0.86	2.93	-7.67	3210	---	642	---	0.03	0.03	24.4	17.04				
28	35.8	---	6	1	1,500	-33.3	-2.00	5.70	-23.17	3760	1220-2460	752	244-292	0.60	4.51	24.0	23.68				
						+10.0	+3.33	1.40	-1.22	4700	---	940	---	9.60	4.14	24.0	23.68				
						+25.5	+8.33	3.38	-2.17	5120	2050	1024	410	9.60	4.14	24.0	23.68				
						+7.5	+15.33	2.97	-0.02	4700	600-1385	940	120-277	566.0	337.0	26.0	14.58				
						+11.5	+2.00	1.63	-0.01	4160	---	832	---	566.0	361.0	24.6	17.64				
						+8.0	+2.00	2.83	-0.03	4190	---	838	---	566.0	378.0	23.9	19.03				
						+15.4	+16.7	8.00	-0.04	3440	---	688	---	566.0	461.0	23.9	19.17				
						-5.0	-7.50	2.55	-3.17	2975	1550-2760	595	310-552	3.0	2.52	26.4	14.58				

* P, approximate soil pressure at 35-in. level at time indicated; other symbols are defined in table 1.

** Parameters measured at the time of maximum arching; after peak soil pressure has arrived at 35-in. level but before reflections appear to have had appreciable effects.

† Parameters measured which appear to be of equal value for comparison purposes.

Table 3

Characteristics of Test Device

Test No.	Spring Stiffness				Components of Spring				Total Wt of Top Active Rings lb	Wt of Top +50% of Active Rings lb	Calculated Properties Without Damping				Observed Results of Damping Test in Air				Natural Frequency Hertz
	K lb/in.	k _T psi/in.	K _T X 10 ³	No.	No. Active	Size	No. Spacers	No.			Period T, msec	Damping Mass M, lb in./sec ²	Frequency f, Hertz	Wt in Motion lb	Damping, C lb/in./sec	Critical Damping C _c , lb/in./sec	Period T, msec	Damped Frequency Hertz	
1	NA	--	--	NA	NA	NA	NA	NA	13.36	3.55	--	NA	--	NA	NA	NA	NA		
2	NA	--	--	NA	NA	NA	NA	NA	13.36	3.96	--	NA	--	NA	NA	NA	NA		
3	NA	--	--	NA	NA	NA	NA	NA	13.36	3.96	--	NA	--	NA	NA	NA	NA		
4	NA	--	--	NA	NA	NA	NA	NA	13.36	3.96	--	NA	--	NA	NA	NA	NA		
5	NA	--	--	NA	NA	NA	NA	NA	13.36	3.96	--	NA	--	NA	NA	NA	NA		
6	5,340	190	0.950	20	13	1/8	5	1/4	11.72	3.60	5.51	NA	--	NA	NA	NA	NA		
7	31,750	1,124	5.680	12	5	1/4	4	1/4	9.34	4.51	6.00	NA	--	NA	NA	NA	NA		
8	14,700	522	2.621	20	14	1/8	7	1/4	11.85	3.62	5.71	NA	--	NA	NA	NA	NA		
11	11,500	407	2.035	20	18	1/8	7	1/4	11.88	3.02	5.71	NA	--	NA	NA	NA	NA		
12	11,330	401	2.005	20	18	1/8	7	1/4	11.91	3.02	5.71	NA	--	NA	NA	NA	NA		
13	11,950	425	2.125	20	17	1/8	7	1/4	11.91	3.02	5.56	NA	--	NA	NA	NA	NA		
14	17,300	613	3.065	20	18	1/8	8	1/8	11.73	3.01	5.62	NA	--	NA	NA	NA	NA		
15	11,330	401	2.005	20	18	1/8	7	1/4	12.45	3.51	6.20	NA	--	NA	NA	NA	NA		
16	11,330	401	2.005	20	18	1/8	7	1/4	12.45	3.51	6.20	NA	--	NA	NA	NA	NA		
17	11,500	407	2.035	20	18	1/8	7	1/4	11.88	3.02	5.71	NA	--	NA	NA	NA	NA		
18	17,300	613	3.065	20	18	1/8	8	1/8	11.73	3.01	5.62	NA	--	NA	NA	NA	NA		
19	12,075	428	2.14	20	17	1/8	7	1/4	11.91	3.02	5.56	NA	--	NA	NA	NA	NA		
20	2,960	105	0.525	42	40	1/16	11	1/8	11.57	2.86	5.54	NA	--	NA	NA	NA	NA		
21	7,900	280	1.400	20	13	1/8	6	1/4	11.82	3.61	5.54	NA	--	NA	NA	NA	NA		
22	16,250	575	2.875	12	10	1/4	4	1/4	13.05	3.32	6.30	NA	--	NA	NA	NA	NA		
23	495	17.5	0.0875	42	40	1/16	7	1/8	11.46	2.86	5.49	NA	--	NA	NA	NA	NA		
24	120,000	4,246	22.330	12	8	1/4	7	1/4	13.18	3.93	6.35	NA	--	NA	NA	NA	NA		
25	120,000	4,246	22.330	12	8	1/4	7	1/4	13.18	3.93	6.35	NA	--	NA	NA	NA	NA		
26	8,950,000	317,000	1,585.0						11.30	2.61	5.41	NA	--	NA	NA	NA	NA		
27	8,950,000	317,000	1,585.0						11.30	2.61	5.41	NA	--	NA	NA	NA	NA		
28	42,390	1,500	7,500	12	10	1/4	5	1/4	13.08	3.32	6.32	NA	--	NA	NA	NA	NA		

* Estimated.

Table 4

Summary of Buckshot Clay Properties

Test No.	Unconfined-Compression Test Data										Laboratory Specimens			
	Hvorslev Specimens					Posttest Average					Pretest Average		Posttest Average	
	Above		Over Device		Outside Device		Above 35-in. Level		All Samples		Pretest		Posttest	
	Avg Entire Specimen	35-in. Level	WC %	$q_u/2$ psi	WC %	$q_u/2$ psi	WC %	$q_u/2$ psi	WC %	$q_u/2$ psi	WC %	$q_u/2$ psi	WC %	$q_u/2$ psi
	Dry Density pcf	Saturation %												
1	95.4	92.6	--	15.97	24.3	--	17.22	24.5	--	15.97	25.6	15.28	25.7	--
2	95.0	87.8	--	18.06	24.7	--	18.06	24.7	--	--	--	--	--	--
3	97.2	91.2	--	13.61	25.2	--	13.75	24.9	--	--	--	--	--	--
4	94.9	87.9	--	13.89	25.5	--	13.20	26.1	--	--	--	--	--	--
5	92.5	86.9	--	13.61	24.7	--	13.40	25.3	--	20.83	24.0	19.72	24.8	16.91
6	93.7	87.1	--	13.47	25.7	--	13.89	25.5	--	14.58	25.8	17.78	25.0	--
7	93.9	87.9	--	11.11	27.3	--	11.11	27.0	--	14.17	26.9	13.75	27.0	--
8	92.8	91.0	--	15.42	25.0	--	15.23	24.9	--	19.72	24.9	--	--	--
11	94.0	86.2	--	14.58	26.1	--	14.58	26.0	--	15.56	25.9	15.56	25.9	--
12	94.3	91.4	--	12.78	26.2	--	12.85	26.6	--	15.00	26.2	15.56	26.2	--
13	92.7	87.6	--	15.28	25.5	--	14.44	25.4	--	18.33	25.5	18.40	25.5	--
14	96.0	91.5	--	10.83	25.8	--	10.56	26.4	--	15.28	25.8	13.61	26.3	--
15	92.4	87.7	--	16.25	25.6	--	14.72	25.4	--	20.42	26.0	17.78	26.1	--
16	92.8	86.9	--	19.72	24.9	--	18.33	26.1	--	--	--	--	--	--
17	--	--	--	14.85	25.4	--	14.17	25.4	--	14.17	25.0	18.33	25.3	--
18	94.1	87.1	--	17.64	25.0	--	16.95	25.2	--	20.84	24.0	19.86	24.2	--
19	95.9	91.7	--	12.22	26.6	--	12.50	26.8	--	15.97	26.5	15.83	26.7	--
20	92.6	88.8	--	19.44	25.3	--	19.44	25.3	--	23.34	25.5	22.64	25.5	--
21	94.0	88.1	--	16.25	26.9	--	15.28	27.0	--	19.86	26.8	19.72	26.8	--
22	27.0	87.9	--	16.67	25.0	--	18.20	24.6	--	19.31	24.9	20.14	24.8	--
23	24.7	91.5	--	17.08	24.4	--	16.67	24.6	--	21.67	24.4	21.81	24.3	--
24	24.5	91.0	--	22.34	24.2	--	23.12	24.3	--	21.11	24.4	19.72	24.6	--
25	--	--	--	14.58	26.0	--	15.28	26.2	--	14.72	26.5	16.53	26.5	--
26	26.6	91.8	--	17.64	24.6	--	16.39	24.5	--	19.03	23.9	19.17	23.9	--
27A	24.3	90.9	--	19.03	23.9	--	19.17	23.9	--	17.36	24.2	17.64	24.4	--
27B	--	--	--	14.57	26.4	--	14.57	26.6	--	14.90	26.3	17.35	26.3	--
27C	--	--	--	--	--	--	--	--	--	--	--	--	--	--
28	26.8	88.4	--	--	--	--	--	--	--	--	--	--	--	--
A	23.3	88.4	--	--	--	--	--	--	--	--	--	--	--	--
B	27.2	91.7	--	--	--	--	--	--	--	--	--	--	--	--
C	32.1	85.1	--	--	--	--	--	--	--	--	--	--	--	--
D	25.4	94.6	--	--	--	--	--	--	--	--	--	--	--	--
E	25.6	94.0	--	13.61	25.8	--	15.97	25.2	--	--	--	--	--	--

Note: WC, water content; q_u , unconfined compressive strength.

Table 5 (Concluded)

t hr:min	Pressure psi		Deflections, in.					Force Per Unit Area Acting on Top of Device, psi			Dimensionless Parameters			
	P _S	P _s	D _S	d _b	d _t	D _T	ΔD	P _C	P _T	ΔP	Pressure		Deflection	
											$\frac{\Delta P}{e_u}$	$\frac{P_T}{P_S}$	$\frac{\Delta D}{B} \times 1000$	$\frac{D_T}{B} \times 100$
<u>Test 8 (Continued)</u>														
5:18	175.0		1.709	1.627	0.248	1.875	-0.166	NA	129.0	-54.0	-4.9	0.74	-27.67	31.26
5:41	200.0		1.722	1.635	0.280	1.915	-0.193		146.0	-54.0	-4.9	0.73	-32.17	31.92
5:58	215.0		1.733	1.640	0.303	1.943	-0.210		158.0	-57.0	-5.1	0.73	-35.01	32.39
6:54	216.0		1.737	1.641	0.317	1.958	-0.221		163.0	-53.0	-4.8	0.75	-36.84	32.64
7:18	240.0		1.748	1.644	0.345	1.989	-0.241		182.0	-58.0	-5.2	0.76	-40.17	33.16
22:00	240.0		1.766	1.674	0.362	2.036	-0.270		205.0	-35.0	-3.2	0.85	-45.01	33.94
22:08	235.0		1.764	1.671	0.361	2.032	-0.268		204.0	-31.0	-2.8	0.87	-44.68	33.87
22:23	230.0		1.764	1.671	0.361	2.032	-0.268		204.0	-26.0	-2.3	0.89	-44.68	33.87
22:36	225.0		1.764	1.670	0.360	2.030	-0.266		202.0	-23.0	-2.1	0.90	-44.34	33.84
22:45	220.0		1.767	1.673	0.359	2.032	-0.265		201	-19.0	-1.7	0.91	-44.18	33.87
22:58	215.0		1.767	1.673	0.356	2.029	-0.262		195.0	-20.0	-1.8	0.91	-43.68	33.82
23:13	210.0		1.766	1.672	0.354	2.026	-0.260		191.0	-19.0	-1.7	0.91	-43.34	33.77
23:26	205.0		1.766	1.672	0.352	2.024	-0.258		189.0	-16.0	-1.4	0.92	-43.01	33.74
23:40	200.0		1.764	1.672	0.350	2.022	-0.258		186.0	-14.0	-1.3	0.93	-43.01	33.71
23:58	195.0		1.764	1.671	0.347	2.018	-0.254		183.0	-12.0	-1.1	0.94	-42.34	33.64
24:06	190.0		1.764	1.671	0.344	2.015	-0.251		181.0	-9.0	-0.8	0.95	-41.84	33.59
24:27	165.0		1.765	1.671	0.328	1.999	-0.234		171.0	+6.0	+0.5	1.04	-39.01	33.32
24:39	140.0		1.764	1.672	0.305	1.977	-0.213		159.0	+19.0	+1.7	1.14	-35.51	32.96
24:56	115.0		1.764	1.672	0.274	1.946	-0.182		143.0	+28.0	+2.5	1.24	-30.34	32.44
25:11	90.0		1.767	1.673	0.243	1.916	-0.149		127.0	+37.0	+3.3	1.41	-24.84	31.94
25:28	65.0		1.767	1.674	0.202	1.876	-0.109		105.0	+40.0	+3.6	1.62	-18.17	31.27
25:48	40.0		1.766	1.645	0.145	1.790	-0.024		76.0	+36.0	+3.2	1.90	-4.00	29.84
26:03	15.0		1.752	1.513	0.075	1.568	+0.164		39.0	+24.0	+2.2	2.60	+27.33	26.47
26:34	0		1.034	0.984	0.008	0.992	+0.042		4.0	+4.0	+0.4	--	+7.00	16.54
27:03	0		0.973	0.943	0.005	0.948	+0.025		3.0	+3.0	+0.3	--	+4.17	15.80

Gage not functioning properly

Table 6 (Concluded)

t msec	Pressure psi		Deflections, in.					Force per Unit Area Acting on Top of Device, psi					Dimensionless Parameters							
	P _S	P _T	D _S	d _b	d _t	D _T	ΔD	Damping	Inertia	Spring	P _T	ΔP	Pressure		Deflection					
													$\frac{\Delta P}{q_u}$	$\frac{P_T}{P_S}$	$\frac{\Delta D}{B} \times 1000$	$\frac{D_T}{B} \times 100$				
<u>Test 27C</u>																				
2	46.5		0	0	0.250†	0.25 × 10 ⁻⁴	-0.25 × 10 ⁻⁴						+4.6	8.0	12.60	-34.0	-1.77	0.27	-0.004	0.0004
3	52.5		0.010	0.010	0.600	0.010	-0.6 × 10 ⁻⁴						+9.9	19.0	28.90	-23.5	-1.73	0.55	-0.010	0.1700
4	60.5		0.070	0.050	1.900	0.050	+0.020						+9.6	52.6	62.20	+1.5	+0.08	1.03	+3.300	0.8300
6	64.0		0.240	0.210	2.200	0.210	+0.030						+4.6	67.9	72.50	+8.5	+0.44	1.13	+5.000	3.5000
7	64.0		0.330	0.290	2.300	0.290	+0.040						+3.1	72.3	75.40	+11.5	+0.60	1.18	+6.700	4.8000
8	63.8		0.410	0.350	2.400	0.350	+0.060						+2.1	76.7	78.80	+15.0	+0.78	1.24	+10.000	5.8000
10	63.5		0.580	0.480	2.500	0.480	+0.100						-1.5	80.4	78.90	+15.4	+0.80	1.24	+16.700	8.0000
12	63.0		0.730	0.610	2.600	0.610	+0.120						-4.2	82.6	78.40	+15.4	+0.80	1.24	+20.000	10.2000
14*	63.0		0.860	0.740	2.600	0.740	+0.120						-5.0	84.0	79.00	+16.0	+0.83	1.25	+20.000	12.3000
16*	62.7		0.930	0.820	2.600	0.820	+0.110						-4.6	83.3	78.70	+16.0	+0.83	1.26	+18.300	13.7000
20*	62.0		0.950	0.850	2.400	0.850	+0.100						-2.3	76.0	73.70	+11.5	+0.60	1.19	+16.700	14.2000
100**	44.0		0.910	0.850	1.200	0.850	+0.060						0	54.8	54.80	+11.0	+0.57	1.25	+10.000	14.2000
500	0		0.634	0.586	0	0.586	+0.048						0	0	0	0	0	--	+8.000	9.8000

Test 28

Most of instrumentation lost during test

* Results measurably affected by reflections.
 ** Affected by reflections and/or reduced surface pressure.
 † Multiply value by 10⁻⁴

Table 7

Rate of Pressure Rise and Rise Time at 35-in. Level

Test No.	Fonnet Gages		Channel No.	Soil Near Device		Period of Test Device T, ms	Damped Amplification Factor for $\frac{P_r/F_s}{t_r} \div \times AF$	K_T/K_S^*					
	Rate of Rise South Bonnet psi/ms	Rate of Rise North Bonnet psi/ms		Rate of Rise psi/ms	Rate of Rise Rise Time t_r , ms				Rise Time t_o , ms	t_r/T	t_o/T	t_r	t_o
11	41	--	S11	5.82	6.80	4.75	1.07	0.75	1.06	1.21	0.69	0.60	0.75
12	55	31	S11	11.4	6.08	3.58	0.95	0.56	1.03	1.42	0.81	0.59	0.62
13	94	188	S11	28.6	5.48	2.78	0.80	0.41	1.14†	1.49†	0.67	0.52	0.57
14	224	222	S11	91.5	2.24	0.70	0.38	0.12	1.36	1.45	0.62	0.58	0.66
15	40	41	S11	24.6	1.25	0.75	0.19	0.12	1.71	1.73	0.50	0.49	0.80
16	32	35	S11	8.3	3.05	2.90	0.47	0.45	1.52	1.53	0.47	0.46	0.65
17	40	36	S11	10.0	5.65	3.90	0.89	0.61	1.08	1.36	0.66	0.52	0.57
18	268	343	S11	123.0	3.00	0.75	0.50	0.13	1.30	1.44	0.63	0.57	0.58
19	146	92	S11	58.5	2.50	1.25	0.37	0.18	1.52†	1.61†	0.55	0.52	0.54
20	39	28	S10	10.1	3.25	1.75	0.23	0.12	1.56	1.60	0.18	0.17	0.29
21	54	54	S10	18.6	2.50	1.60	0.30	0.19	1.59†	1.66†	0.28	0.26	0.72
22	51	53	S10	11.9	3.44	1.70	0.54	0.27	1.32	1.47	0.53	0.48	0.88
23	--	25	S11	5.46	3.60	1.80	0.11	0.05	1.63	1.64	0.00	0.00	0.03
24	30	27	S8**	13.8	4.30	4.00	2.62	2.42	1.06	1.08	1.39	1.42	4.51
25	44	41	S5	19.4	2.35	1.65	1.42	1.00	1.14	1.00	1.55	1.36	4.14
26	30	29	S18	10.4	2.90	2.00	12.1	8.34	1.00	1.00	1.24	1.24	337.0
27							No Record						
28	30	51	S10	12.3	3.60	2.00	0.92	0.51	1.04	1.31	0.89	1.13	2.52

Note: t_r = time to maximum pressure (no reflection). t_o = time to first pressure peak (steep part of pressure trace).

* Extrapolated from table 2.

** Close-in gage lost.

† No damping tests--estimated value.

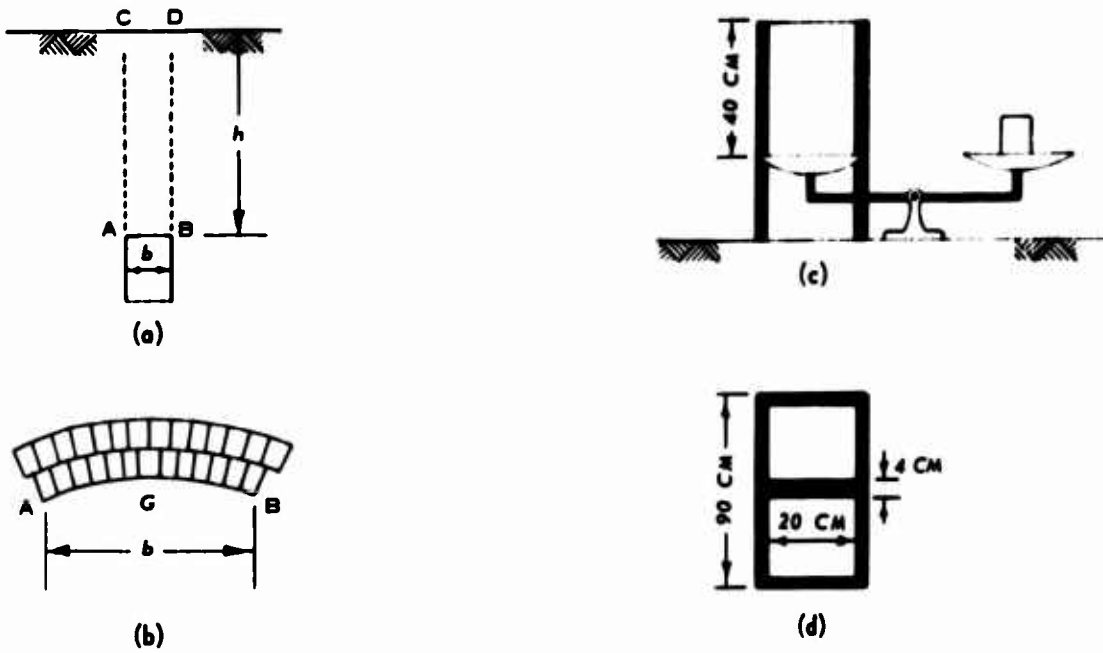
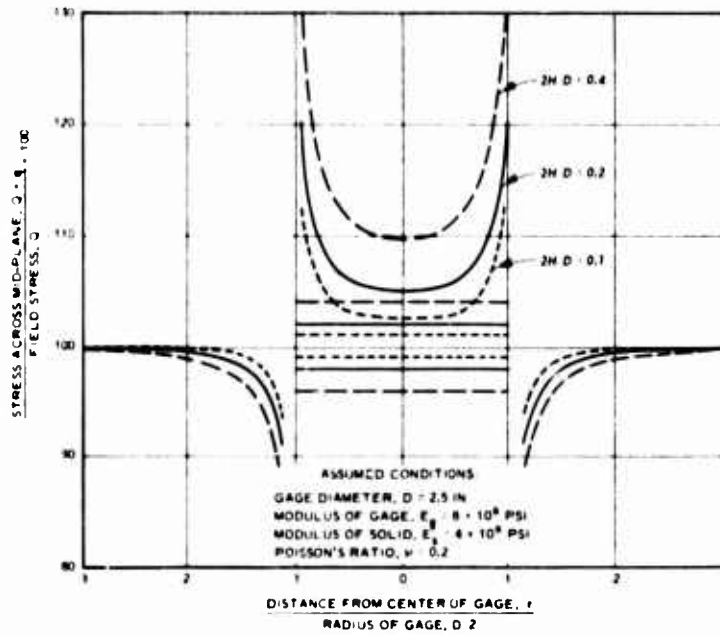


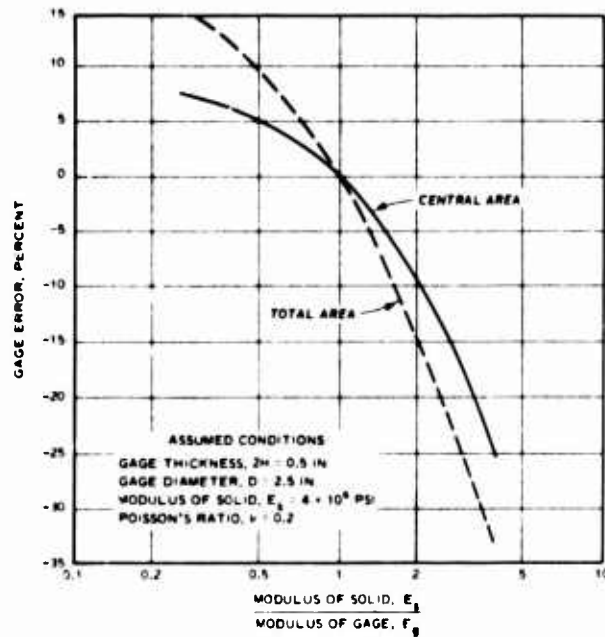
Fig. 1. Analytical and experimental study by Engesser



Fig. 2. Earth pressure phenomena in locally stressed fills by Terzaghi (1919)



a. EFFECTS OF GEOMETRY



b. EFFECTS OF MODULUS

Fig. 3. Monfore's distribution of pressure as determined by elastic analysis

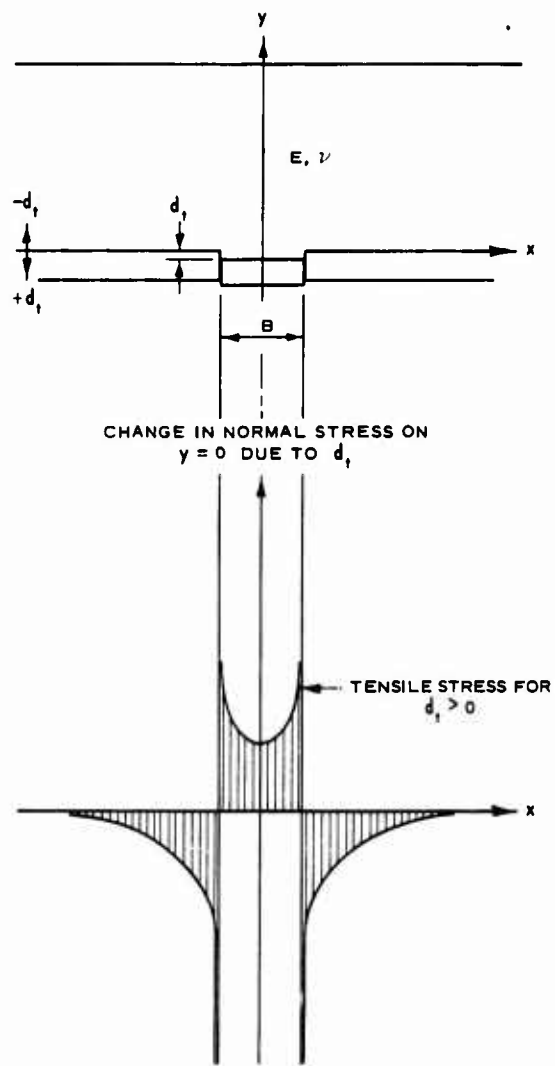
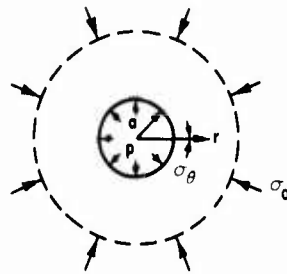
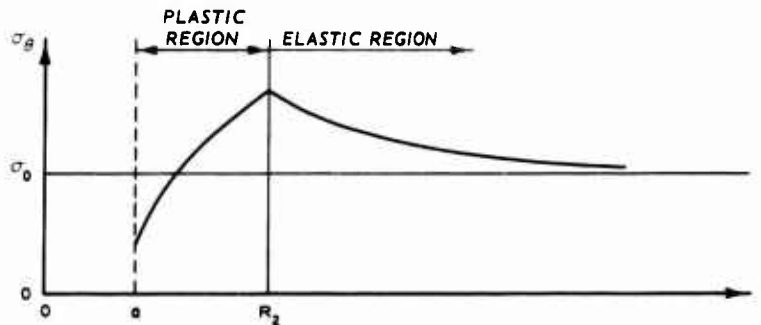


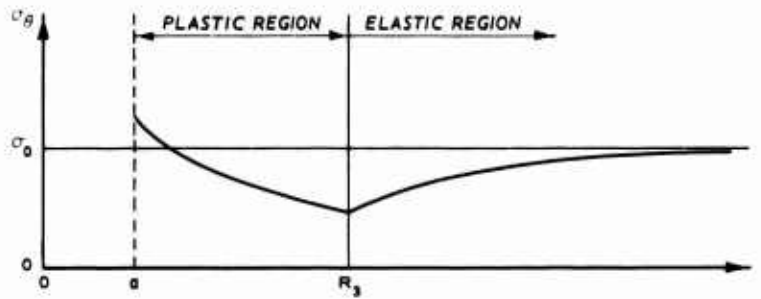
Fig. 4. Distribution of arching stresses from an elastic solution by Finn



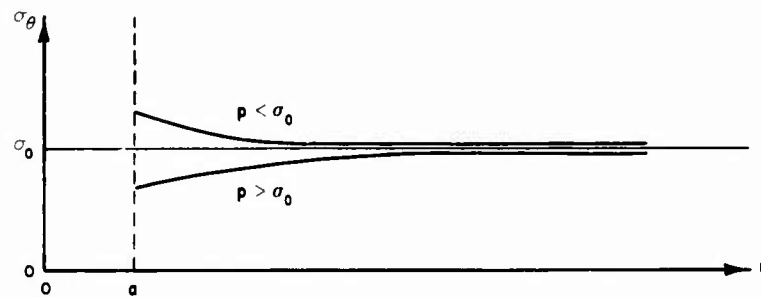
(a) GEOMETRY AND BOUNDARY CONDITIONS



(b) ACTIVE ARCHING - $p \ll \sigma_0$

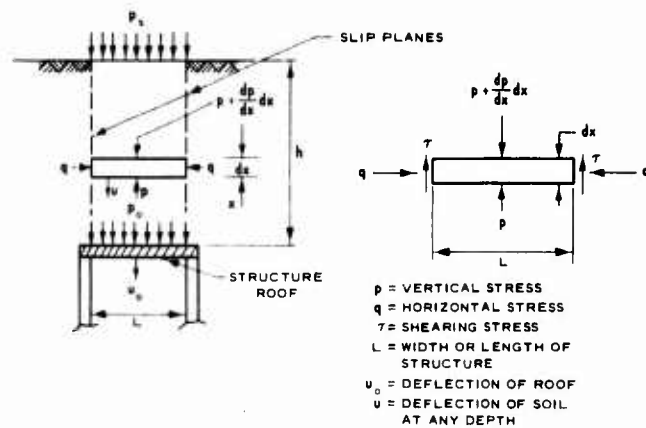


(c) PASSIVE ARCHING - $p \gg \sigma_0$

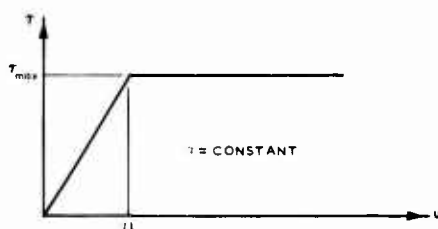


(d) ELASTIC SITUATION - $p \approx \sigma_0$

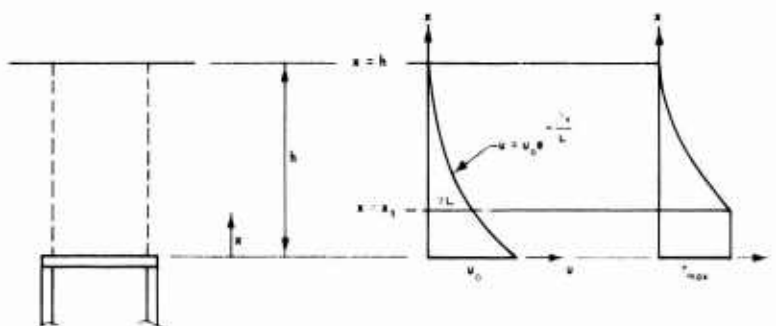
Fig. 5. Circumferential stress distribution from an elastoplastic solution by Sirieys as modified by Hendron (1968)



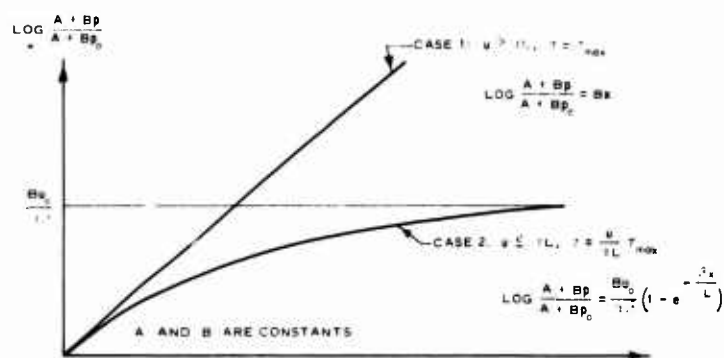
a. ASSUMED FORCE FIELD



b. ASSUMED VARIATION OF SHEARING STRESS VERSUS DISPLACEMENT



c. VARIATION OF DISPLACEMENT AND SHEARING STRESS WITH DEPTH



d. VARIATION OF STRESS WITH DEPTH

Fig. 6. Calculation of arching loads by Newmark and Halmiwanger

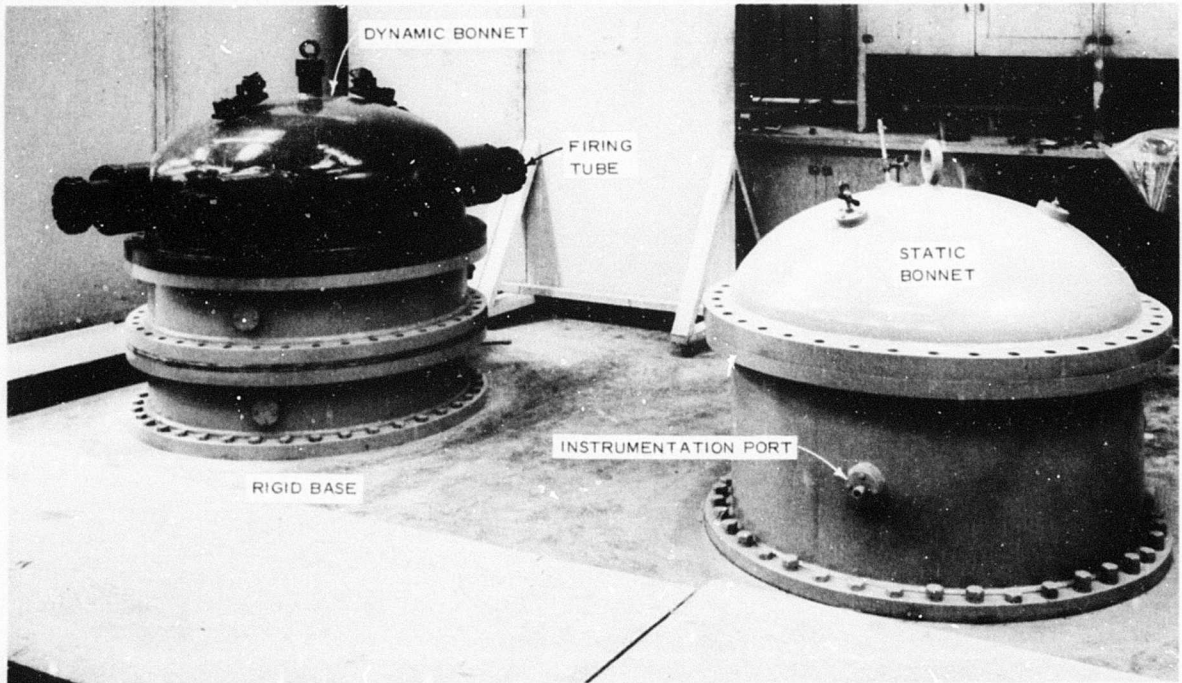
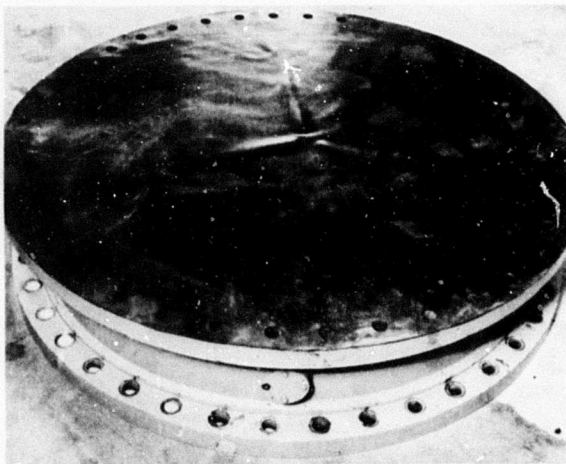
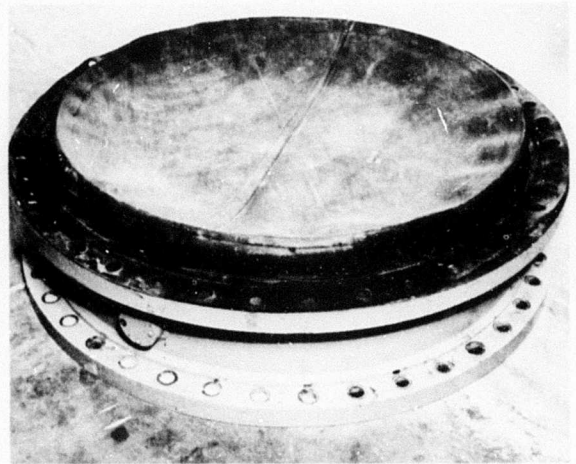


Fig. 7. Small Blast Load Generator facilities (SBLG)



a. Normal diaphragm



b. "Rolled top" diaphragm

Fig. 8. Protective diaphragms

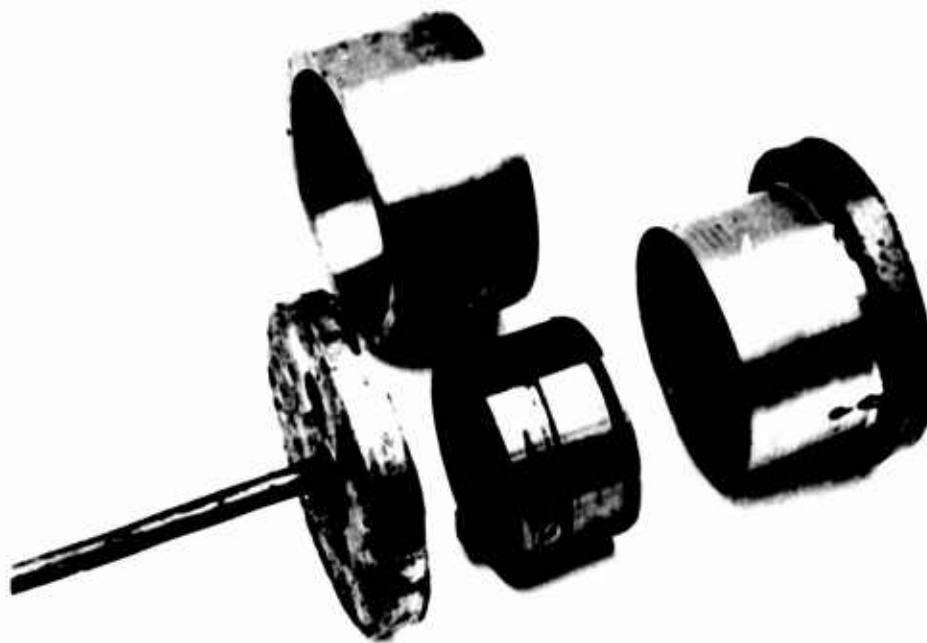
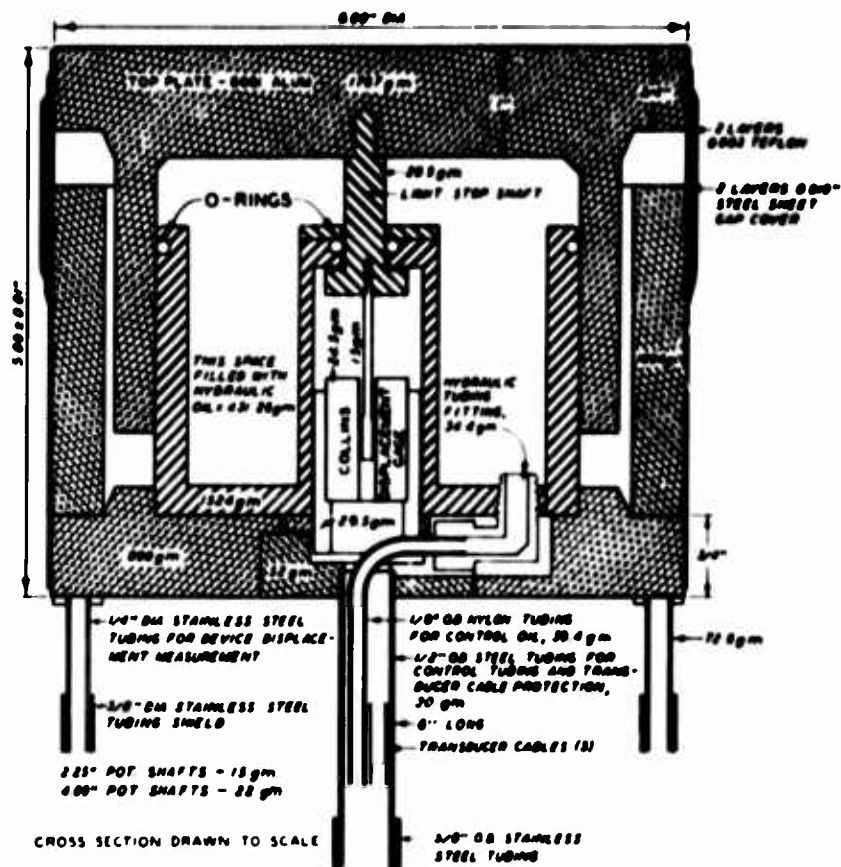


Fig. 9. Hydraulically controlled test device

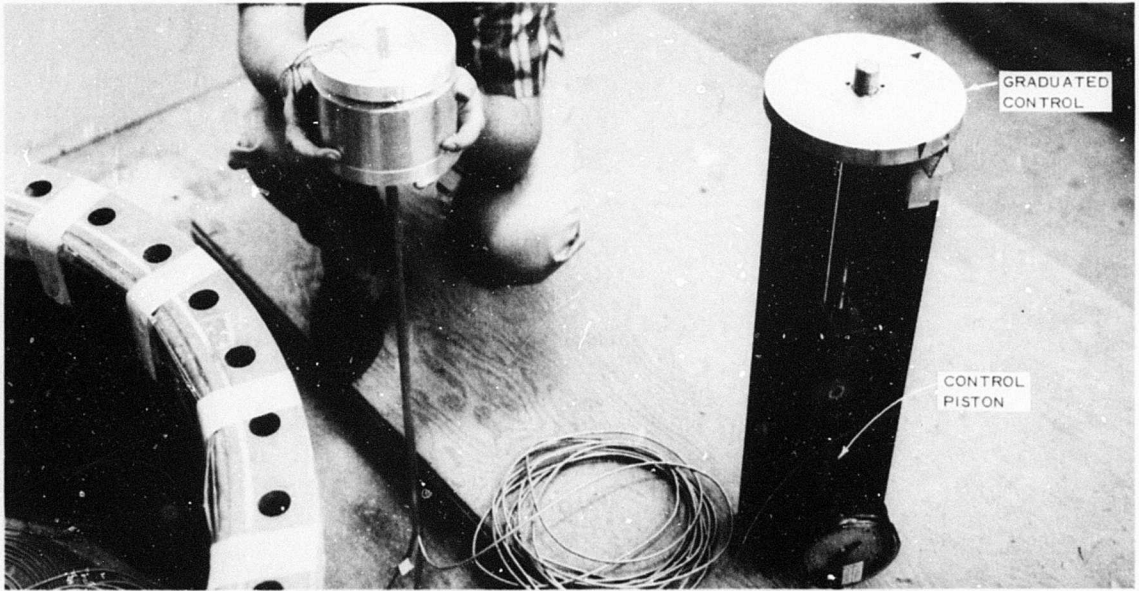


Fig. 10. Hydraulically controlled test device and control piston

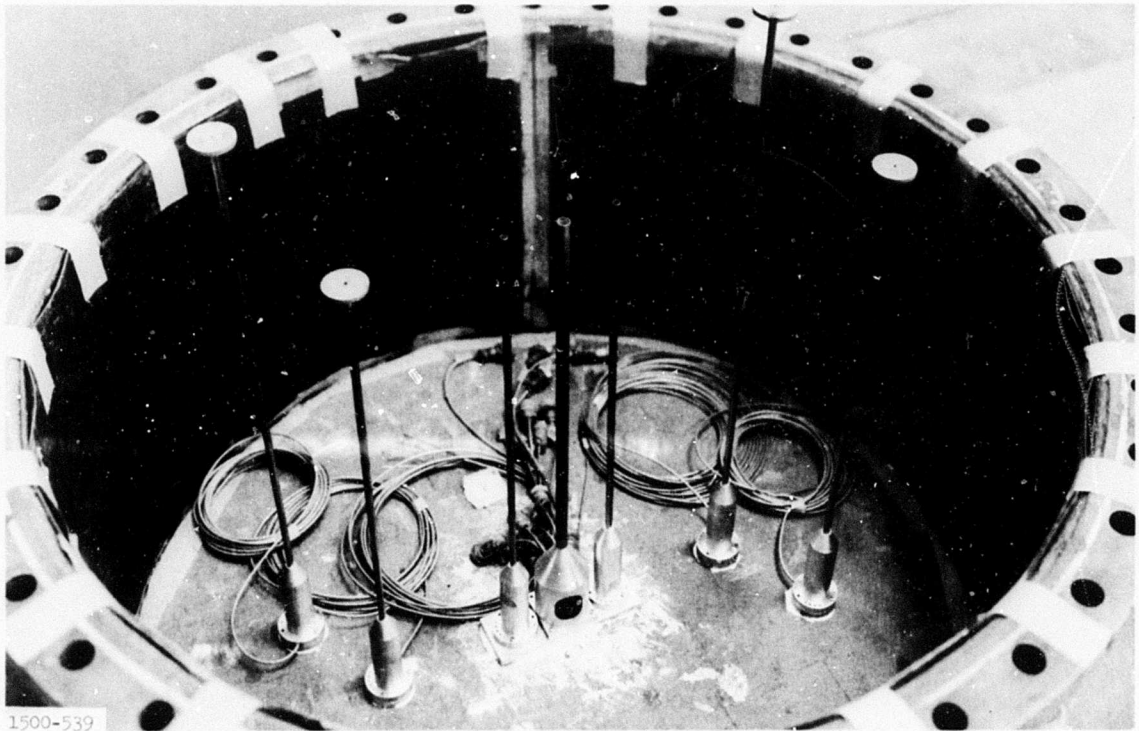


Fig. 11. Base of test chamber with deflection control rods and conduits installed

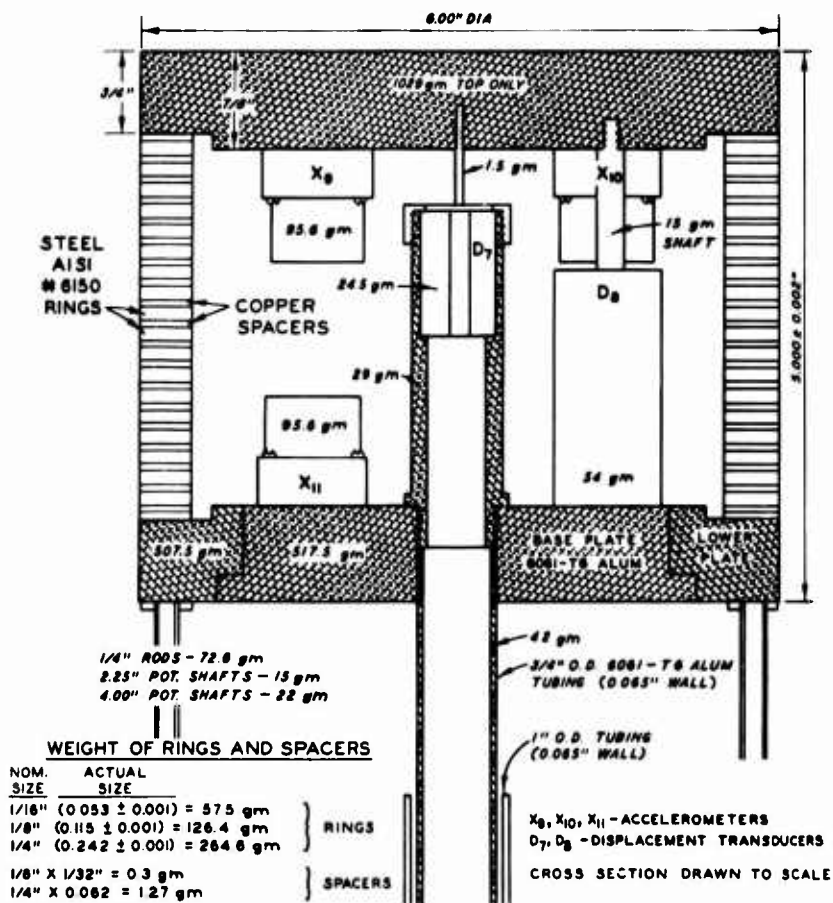
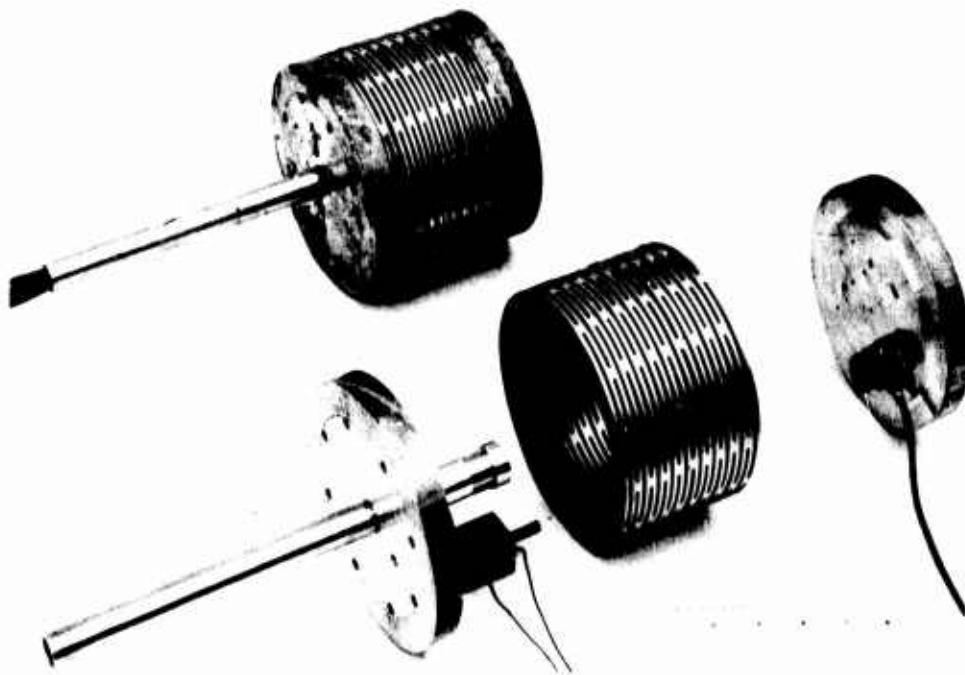


Fig. 12. Spring-ring test device

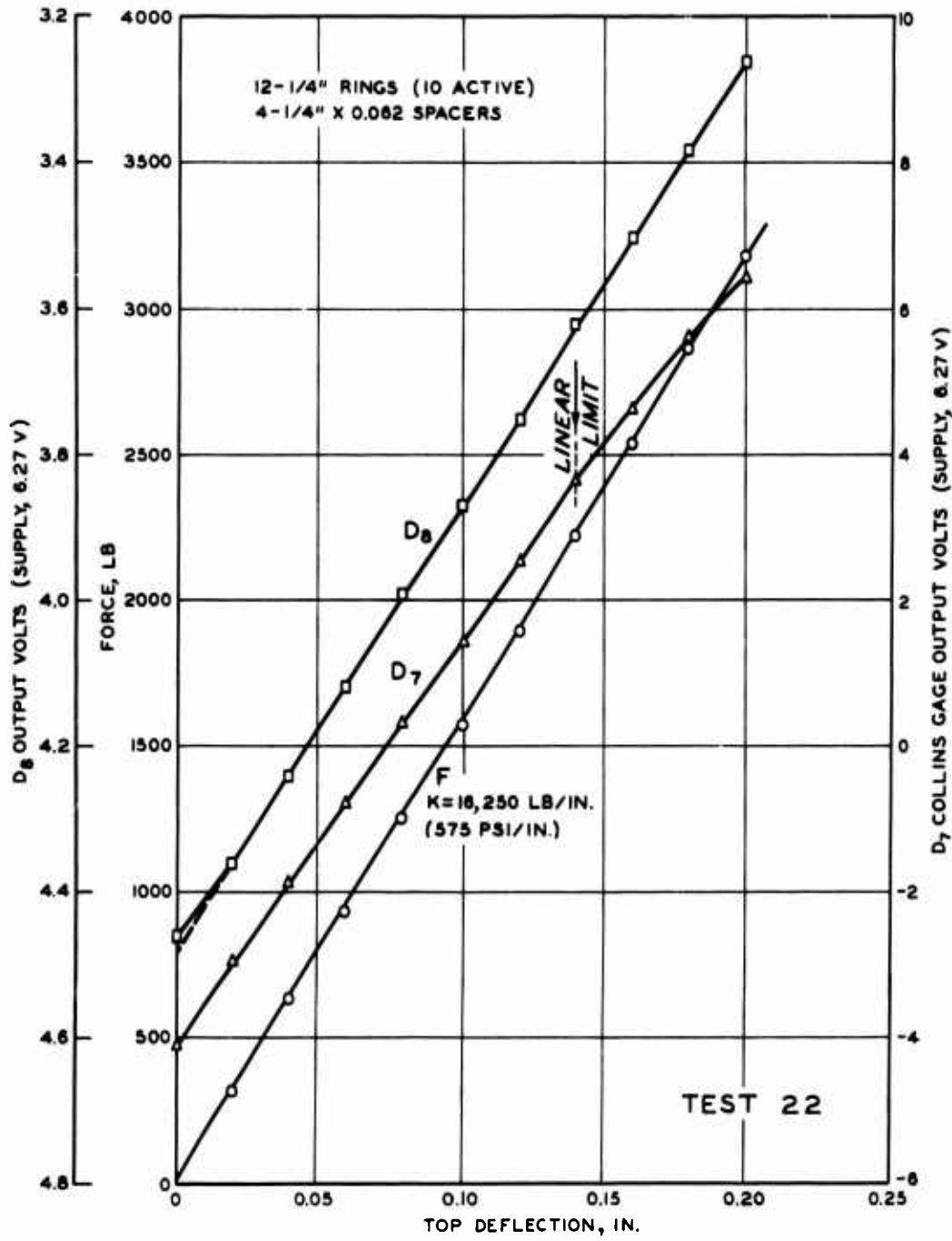


Fig. 13. Typical static calibration curve for spring-ring test device

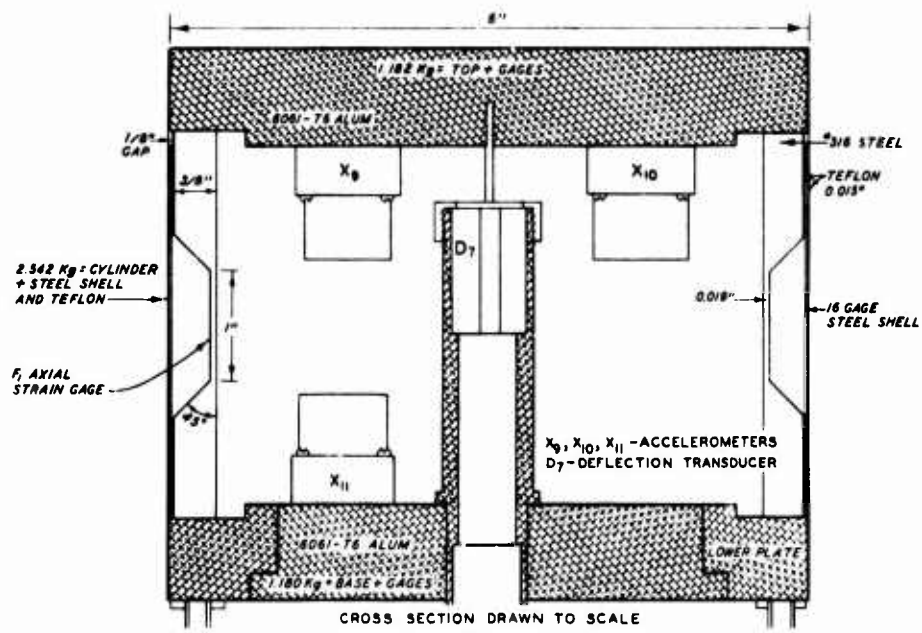
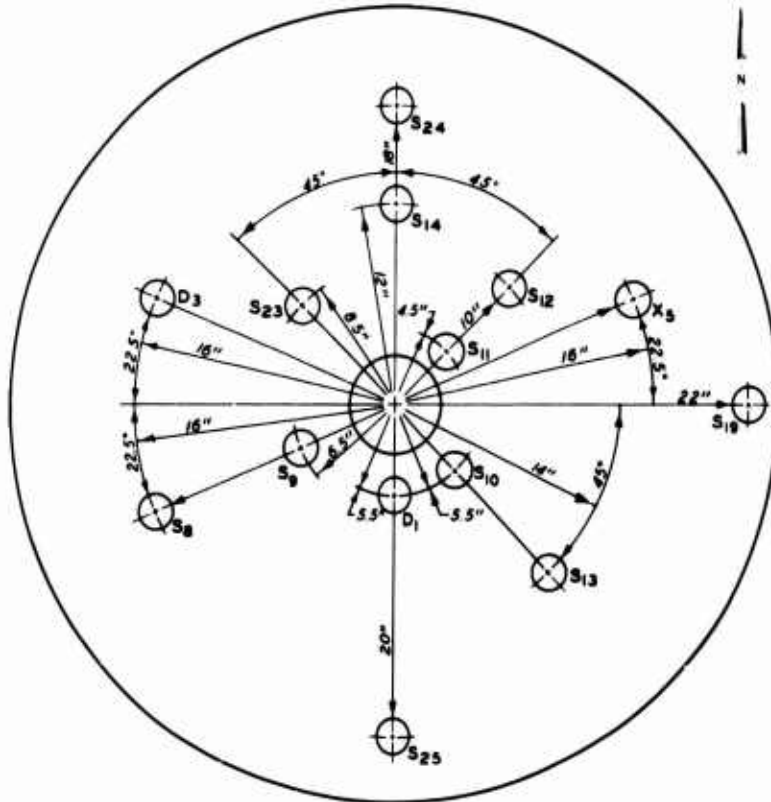
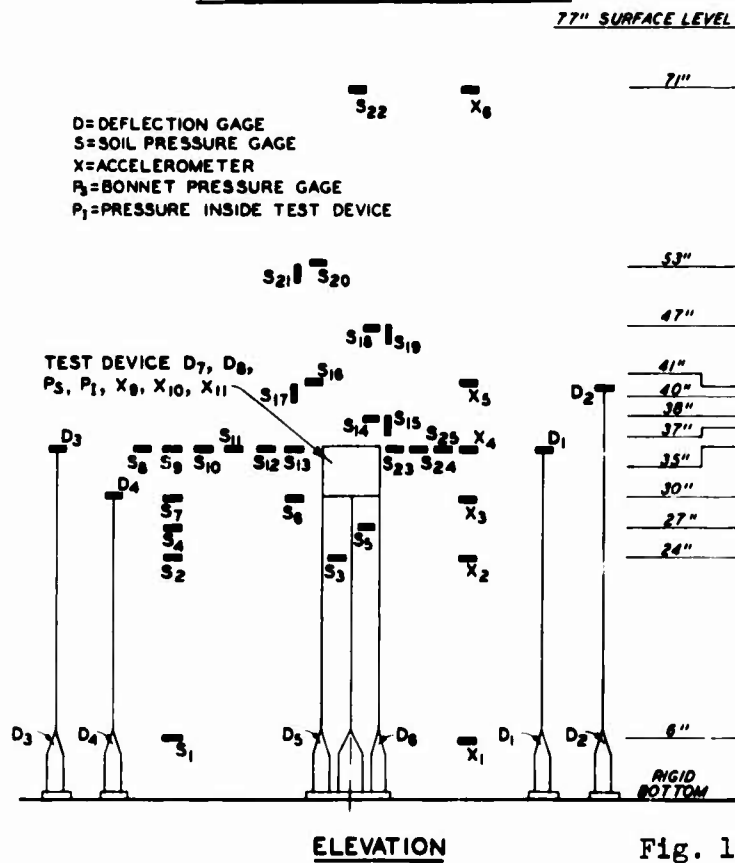


Fig. 14. "Rigid" test device



PLAN VIEW OF 35 -IN. LEVEL



ELEVATION

Fig. 15. Typical gage location diagrams

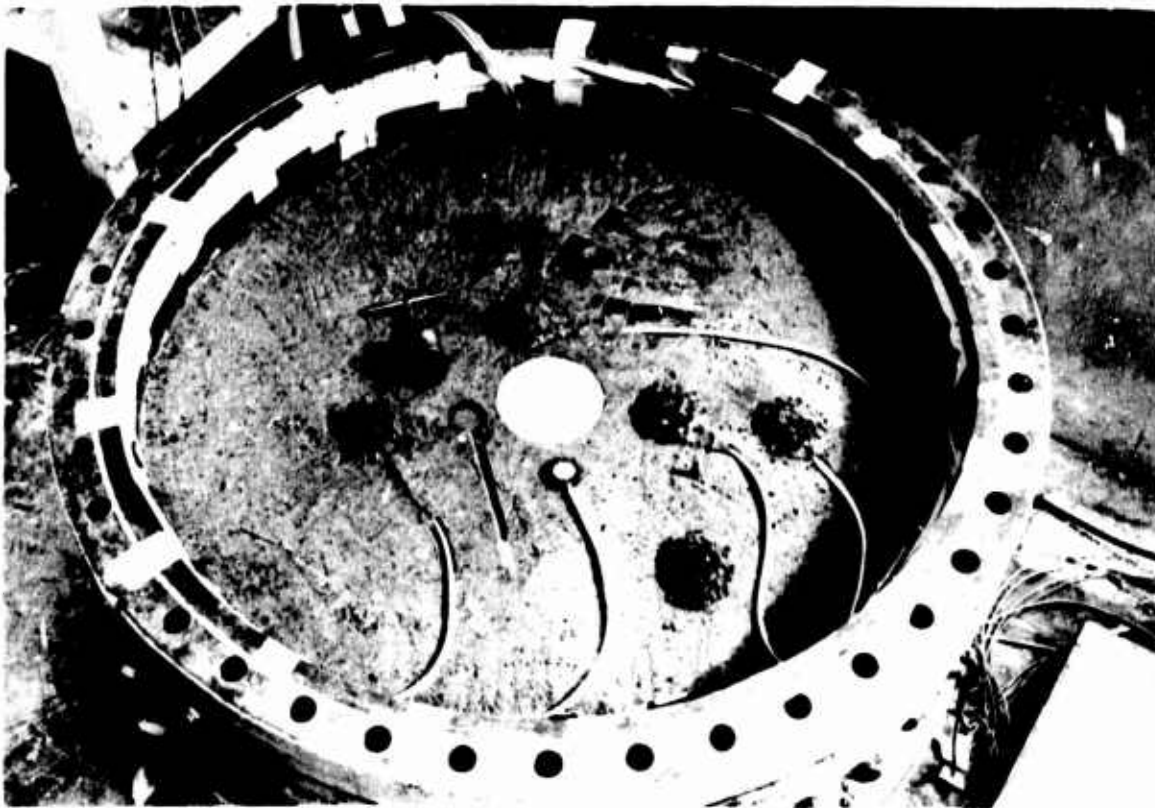


Fig. 16. Soil pressure gage placement at the 35-in. level

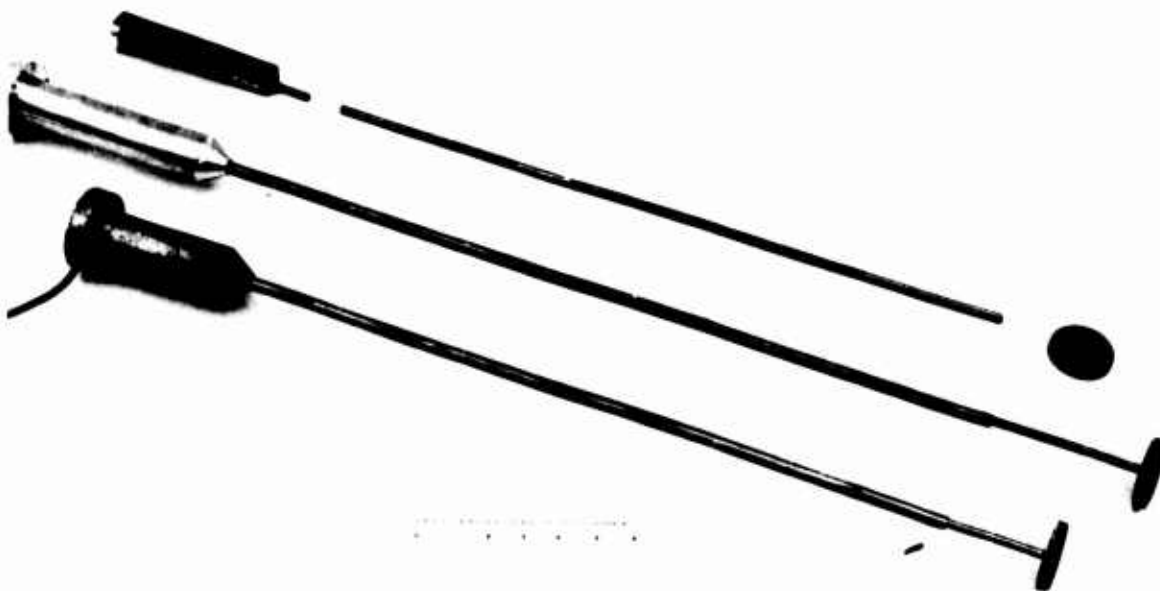


Fig. 17. WES soil deflection measuring device

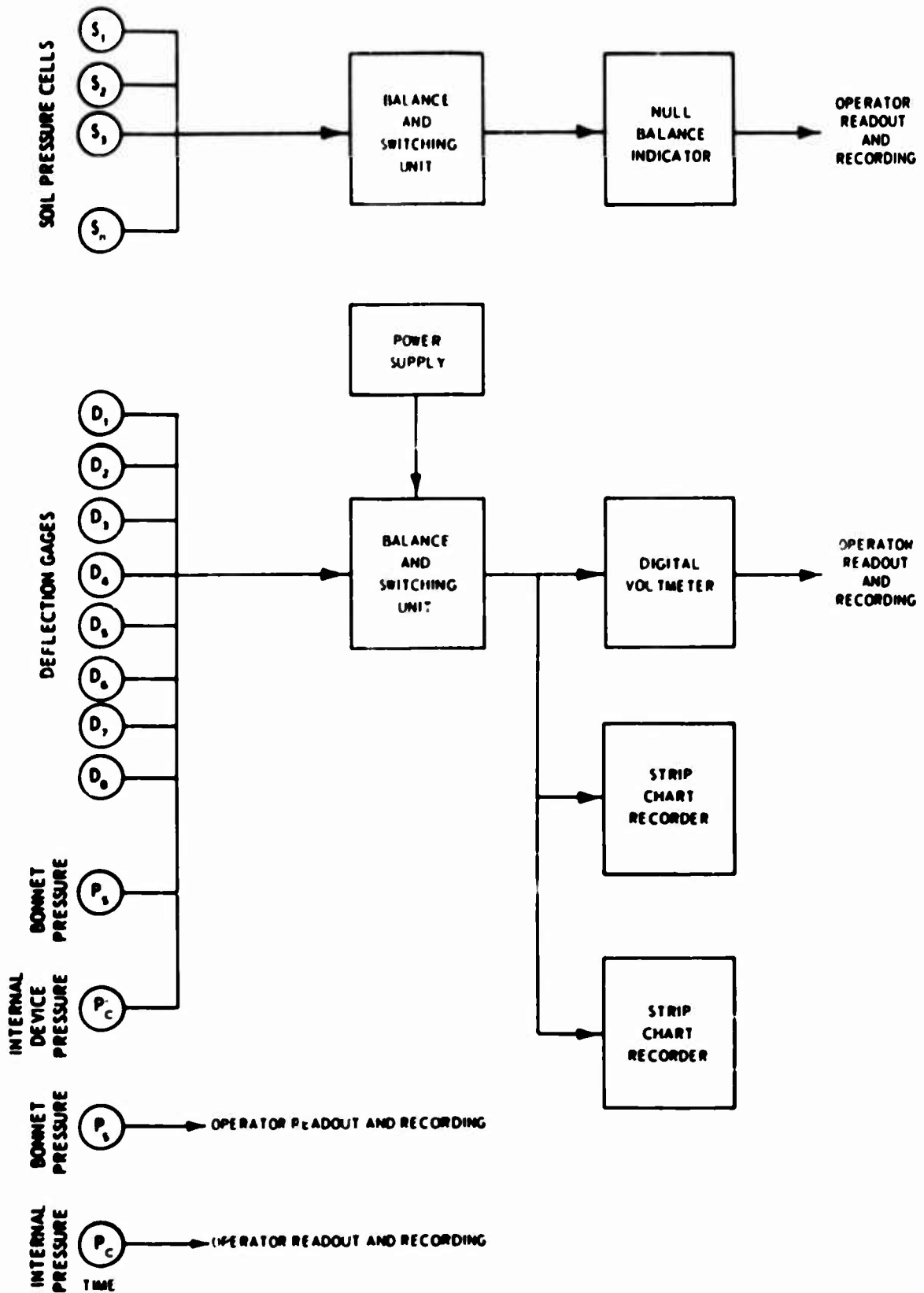


Fig. 18. Block diagram of measurement and control system used for static tests

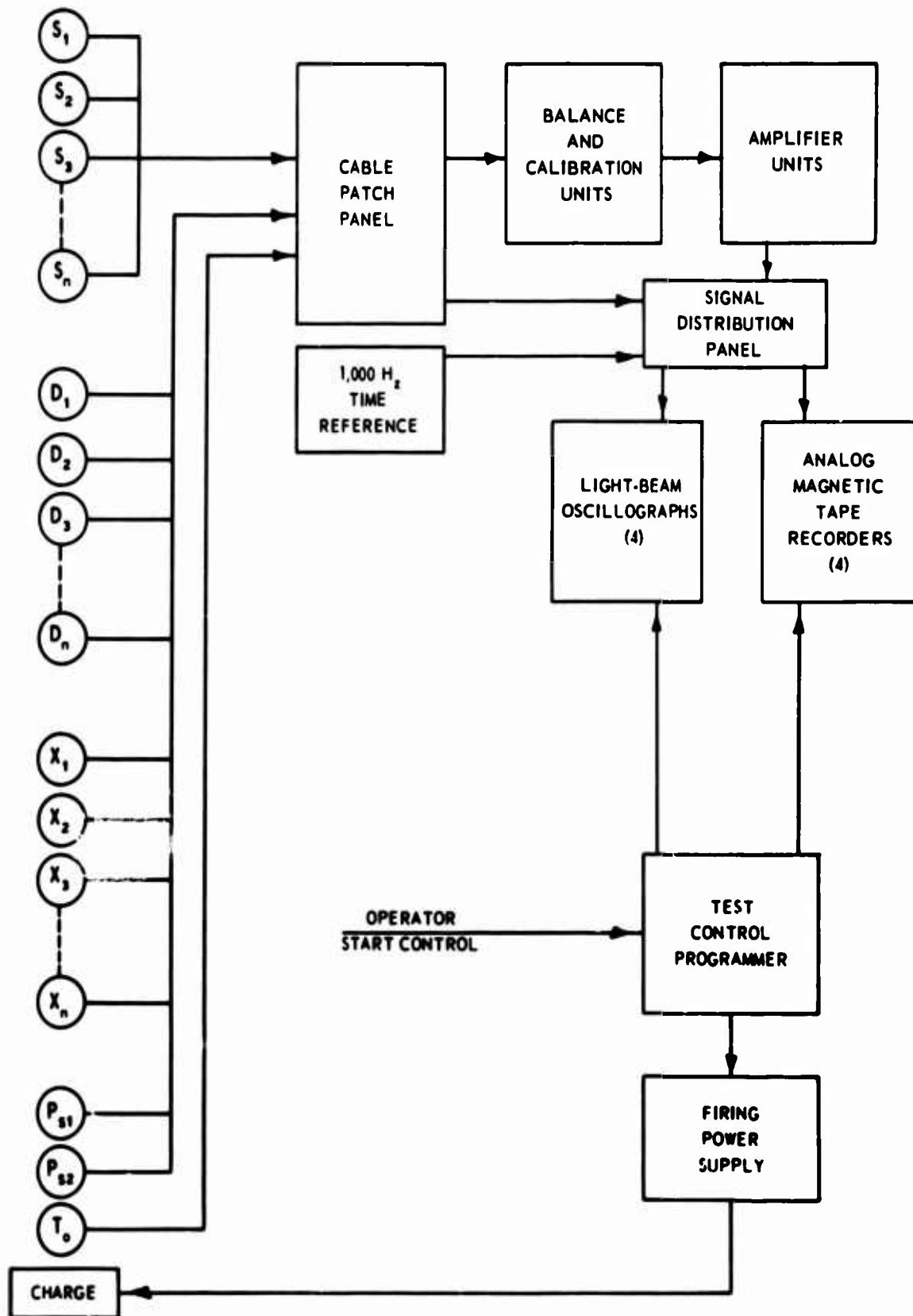


Fig. 19. Block diagram of measurement and control system used for dynamic tests

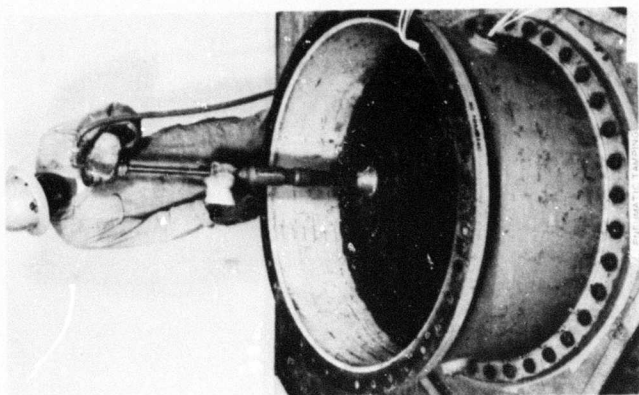
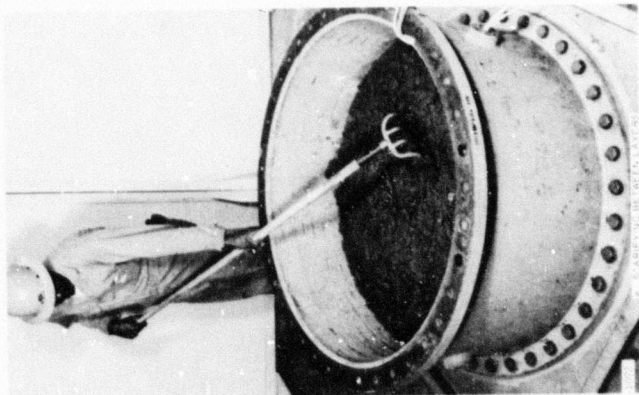
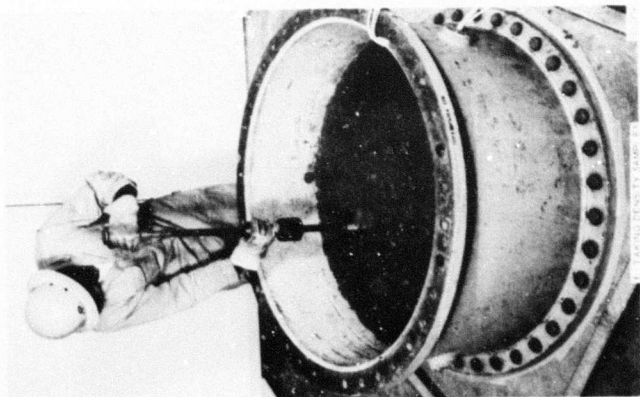
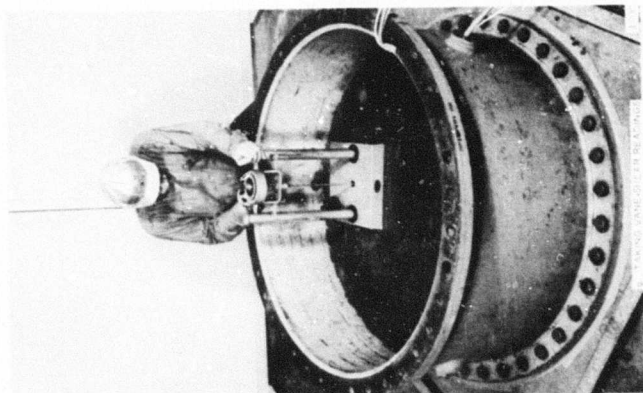
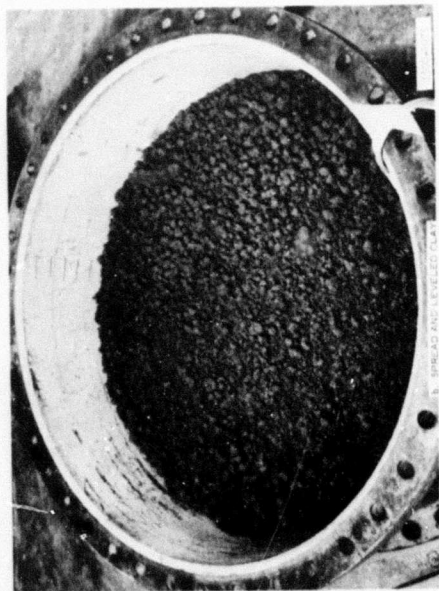
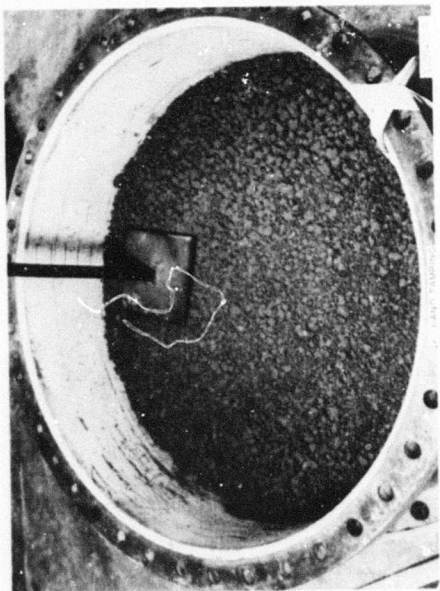


Fig. 20. Placement of buckshot clay in WES Small Blast Load Generator

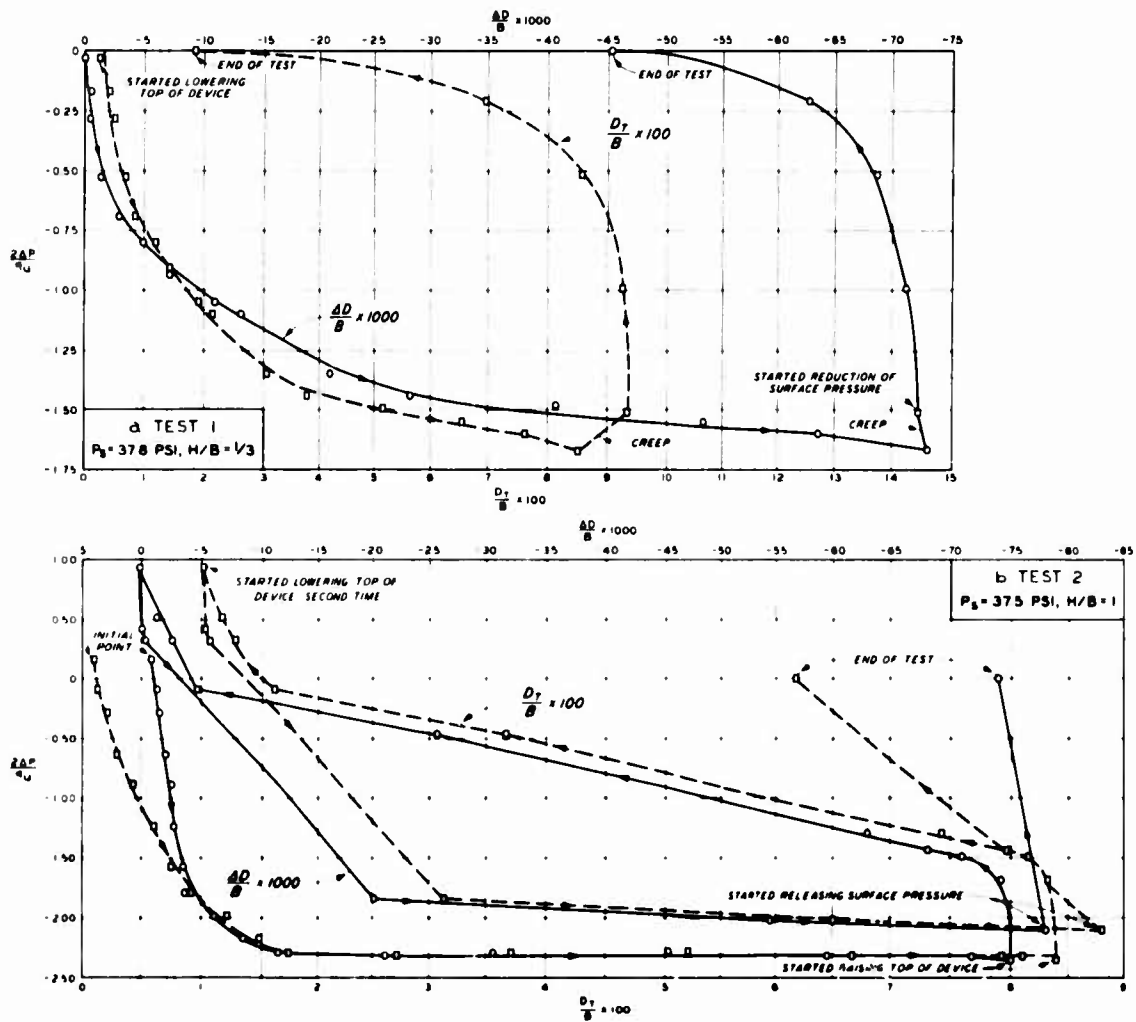


Fig. 21. Dimensionless plot of pressure versus deflection for static Tests 1 and 2

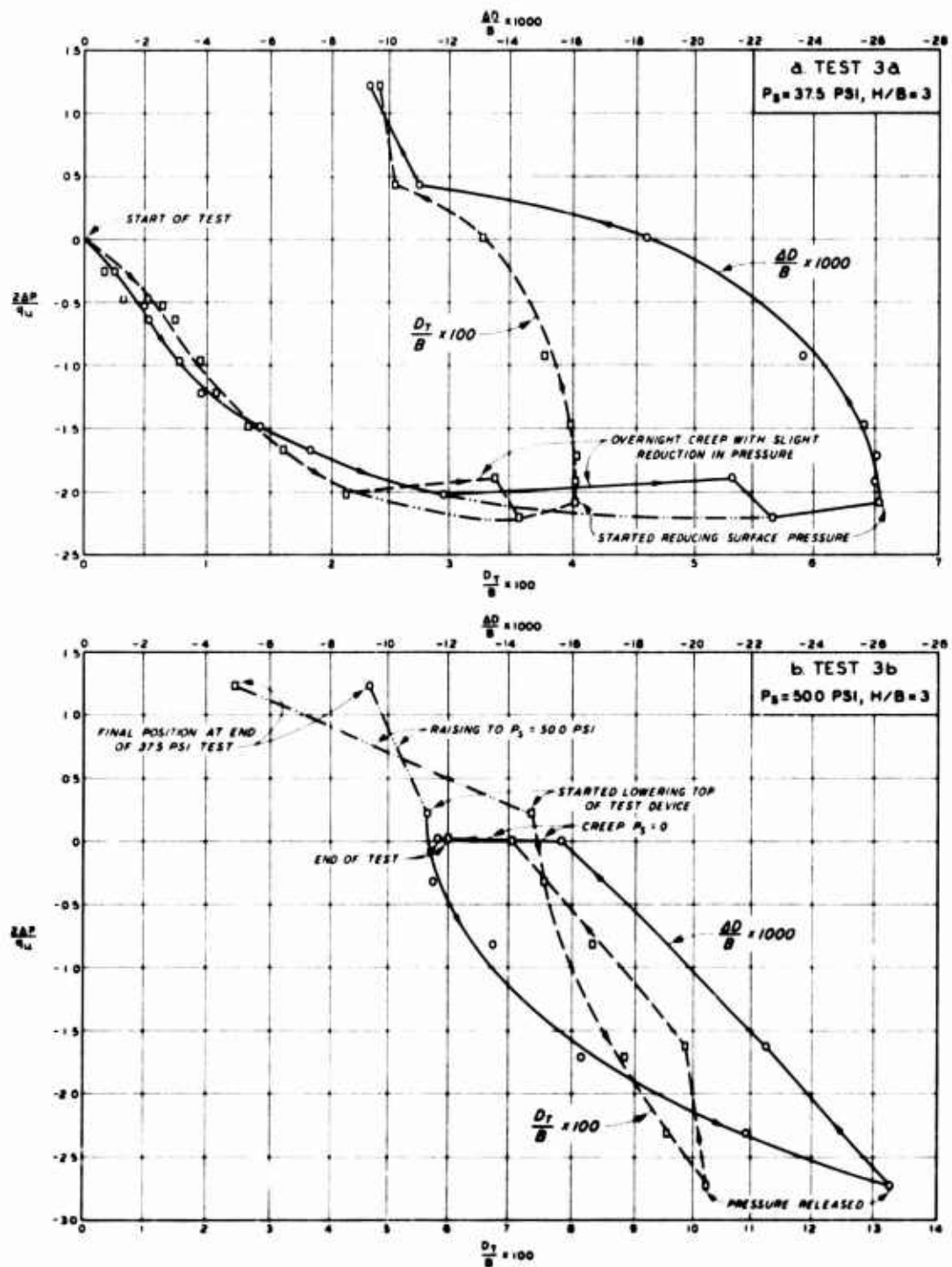


Fig. 22. Dimensionless plot of pressure versus deflection for static Test 3

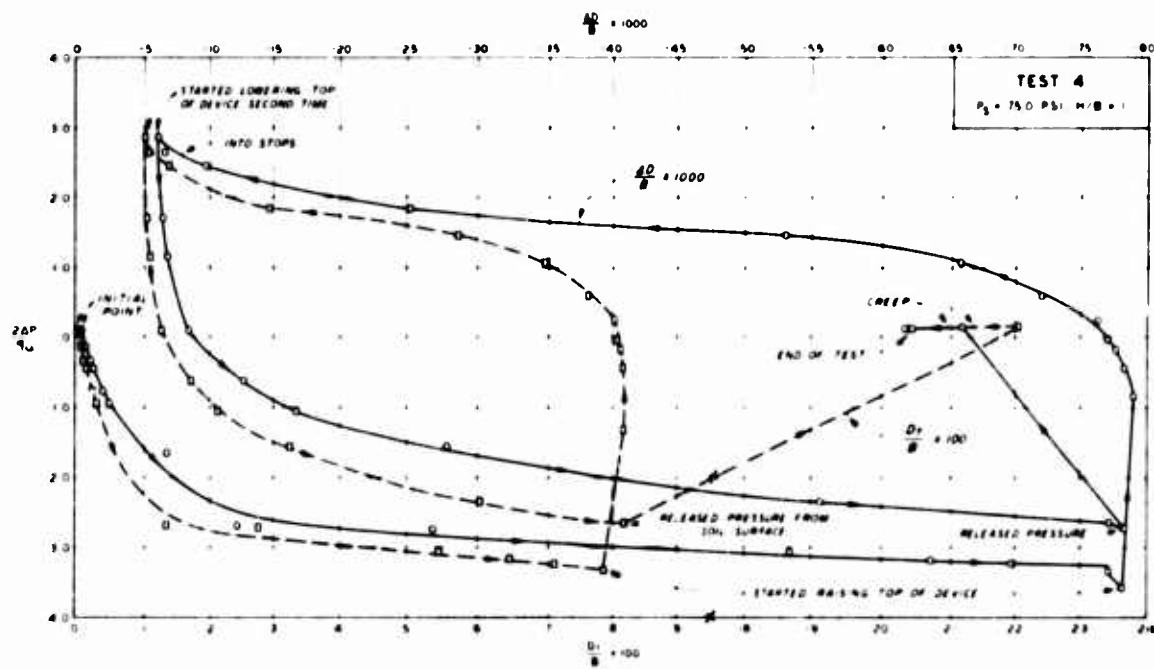


Fig. 23. Dimensionless plot of pressure versus deflection for static Test 4

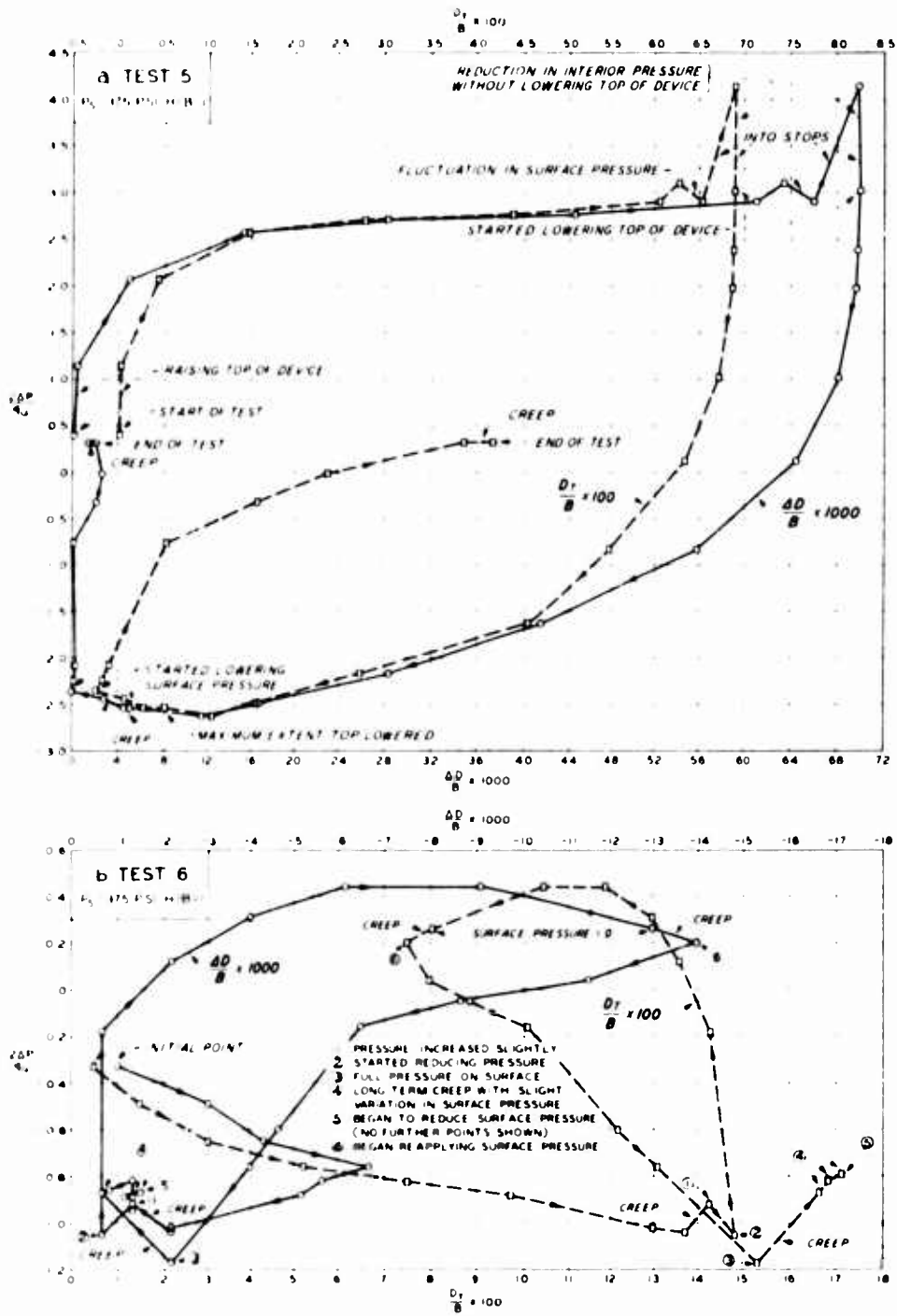


Fig. 24. Dimensionless plot of pressure versus deflection for static Tests 5 and 6

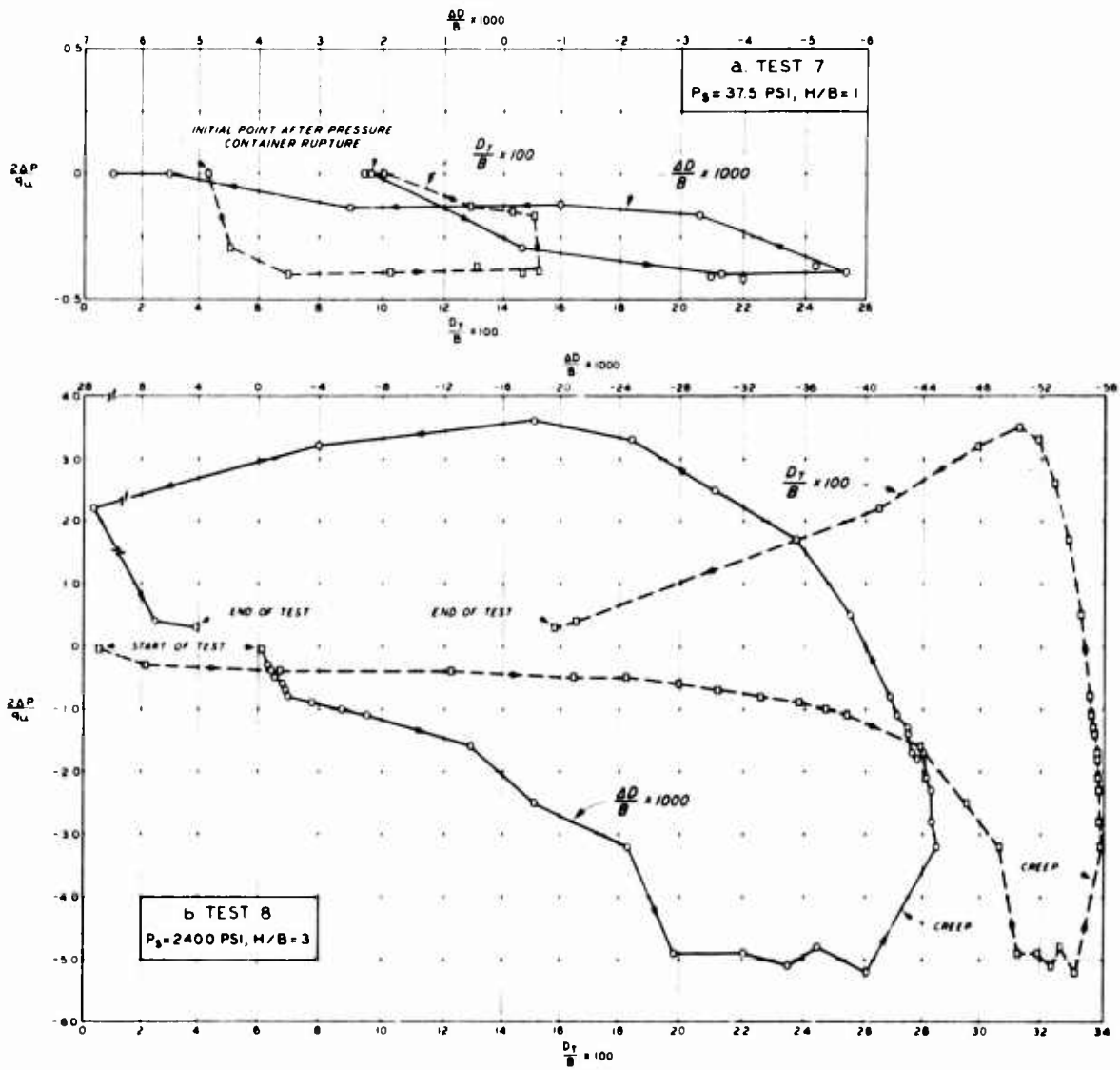


Fig. 25. Dimensionless plot of pressure versus deflection for static Tests 7 and 8

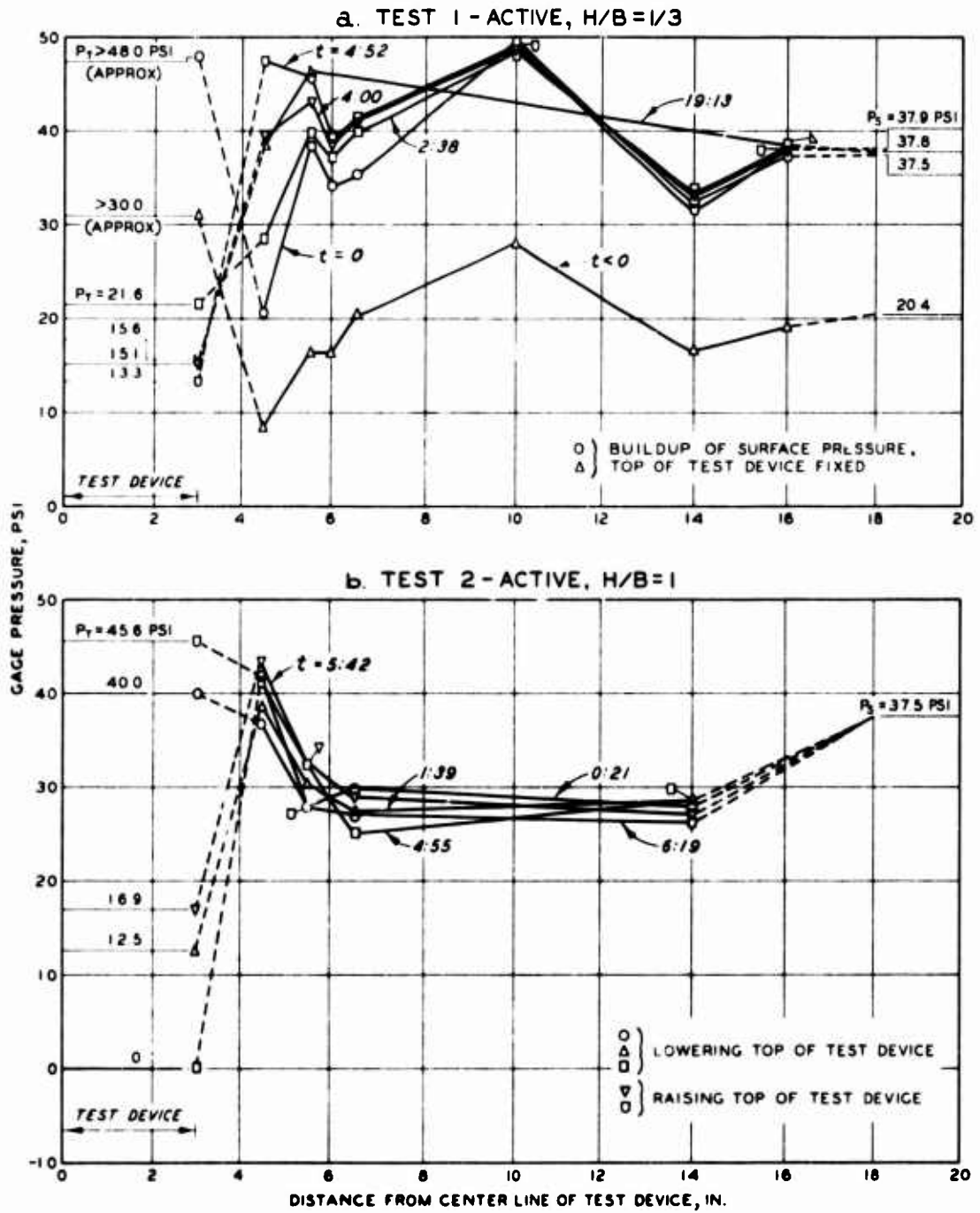


Fig. 26. Change in vertical soil stress at the 35-inch level due to deflection of the top of test device, Tests 1 and 2

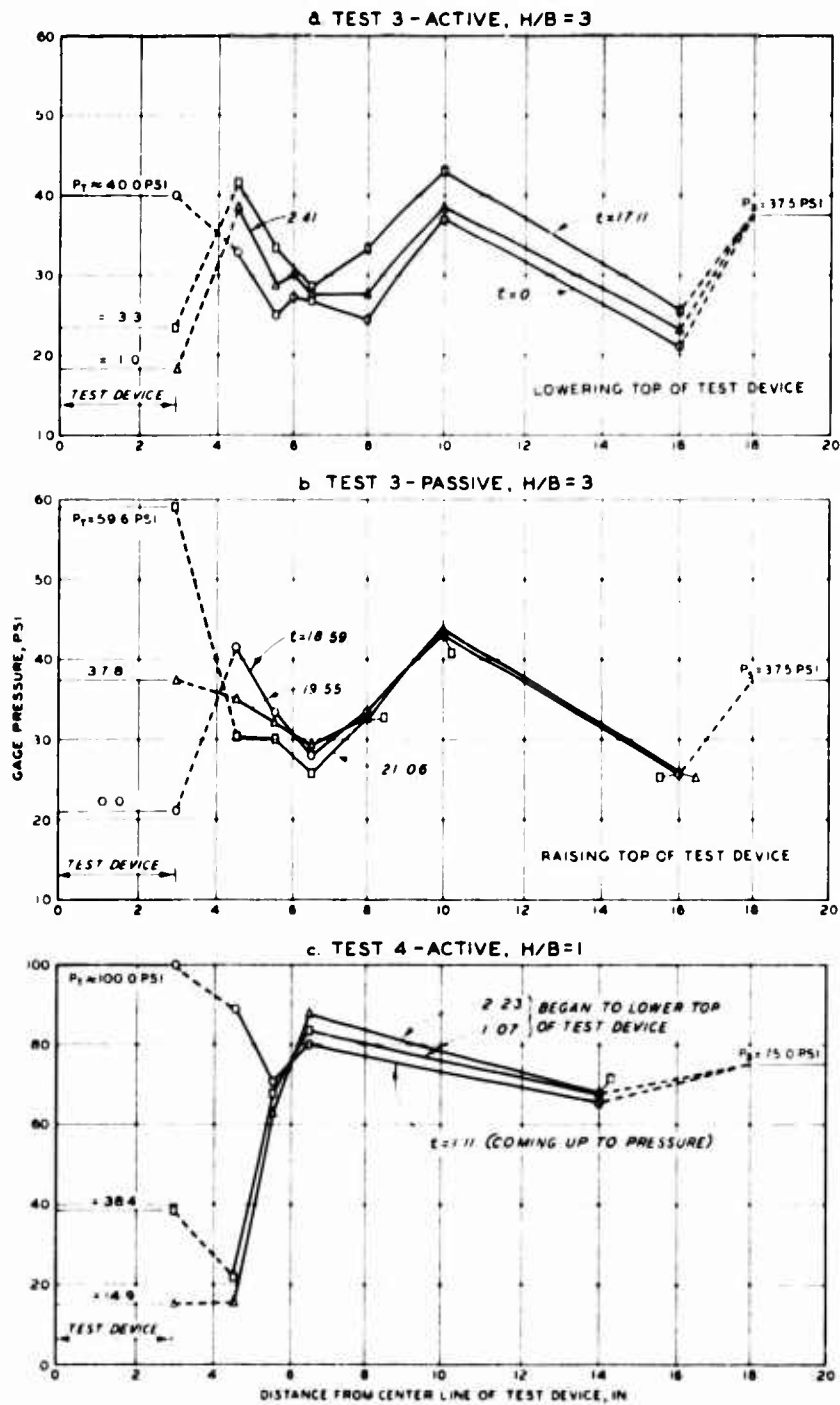


Fig. 27. Change in vertical soil stress at the 35-inch level due to deflection of the top of test device, Tests 3 and 4

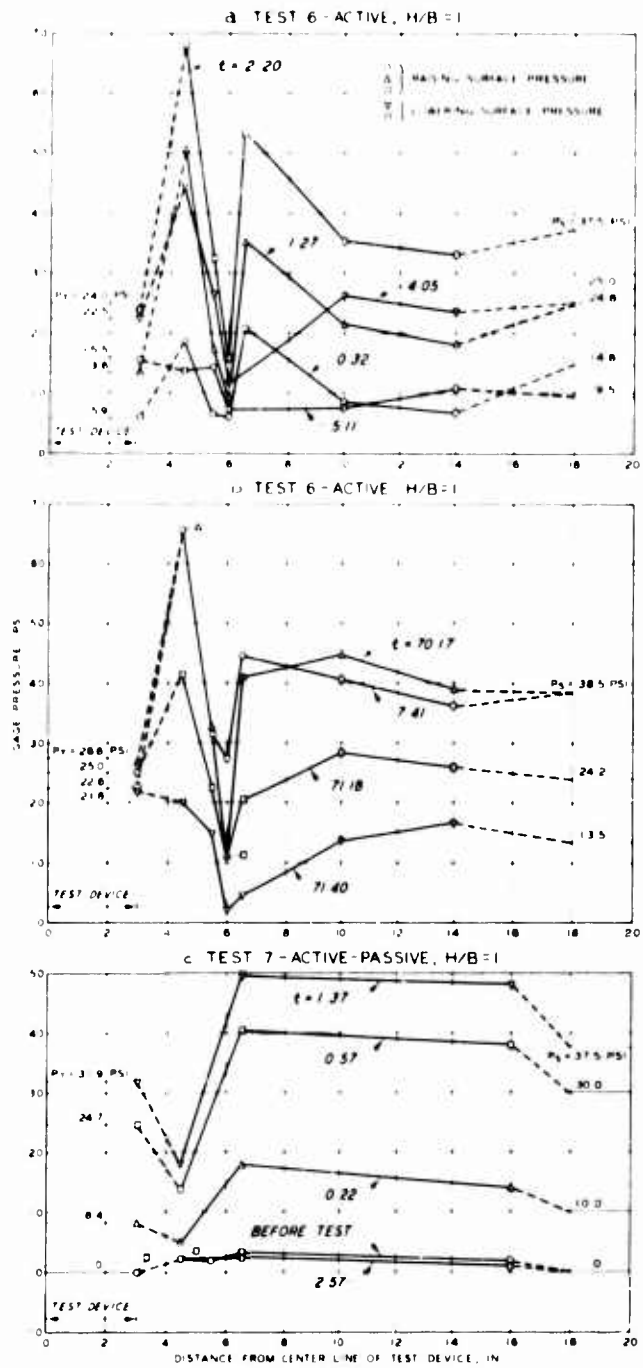


Fig. 28. Change in vertical soil stress at the 35-inch level due to deflection of top of test device, Tests 6 and 7

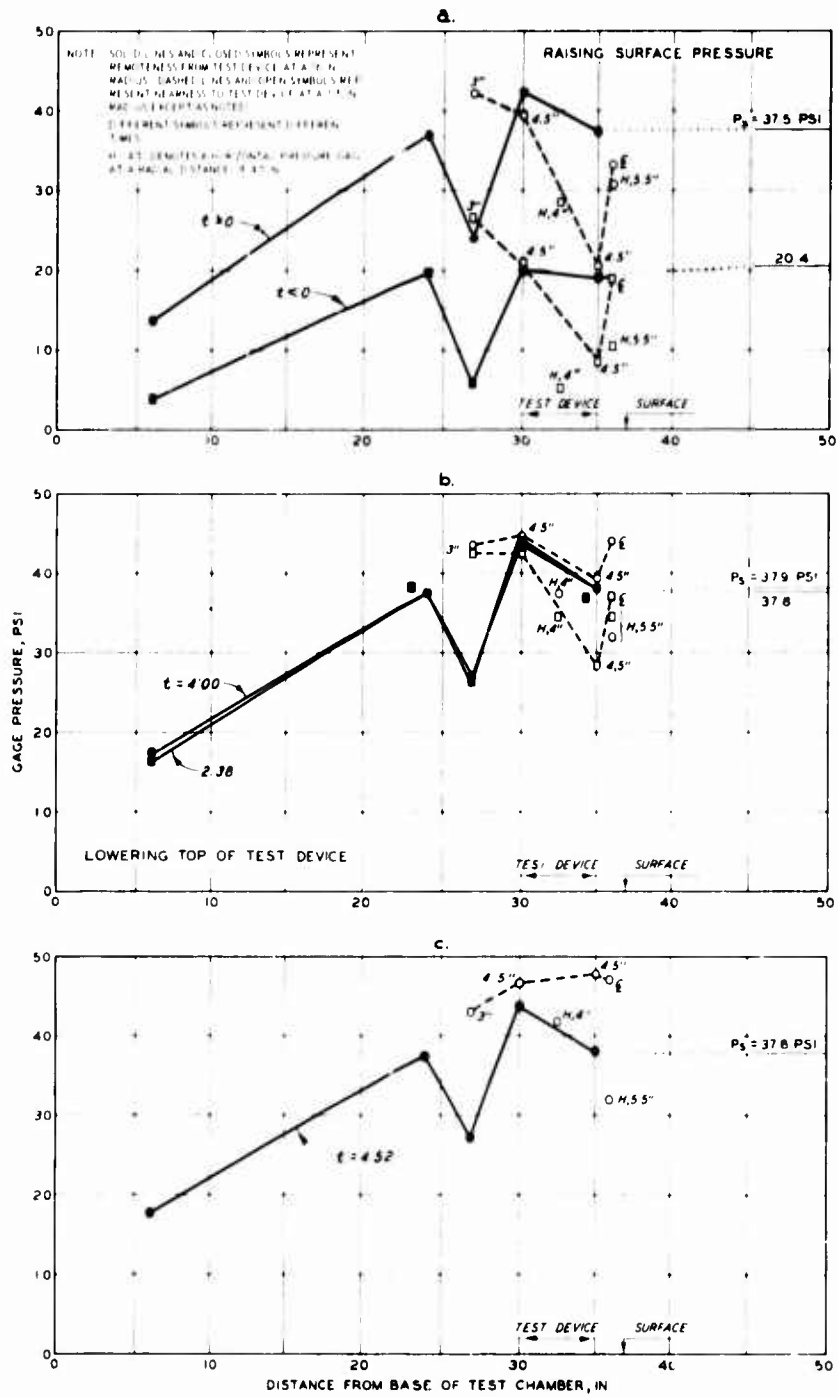


Fig. 29. Change in distribution of vertical soil stress with depth, Test 1; $H/B = 1/3$

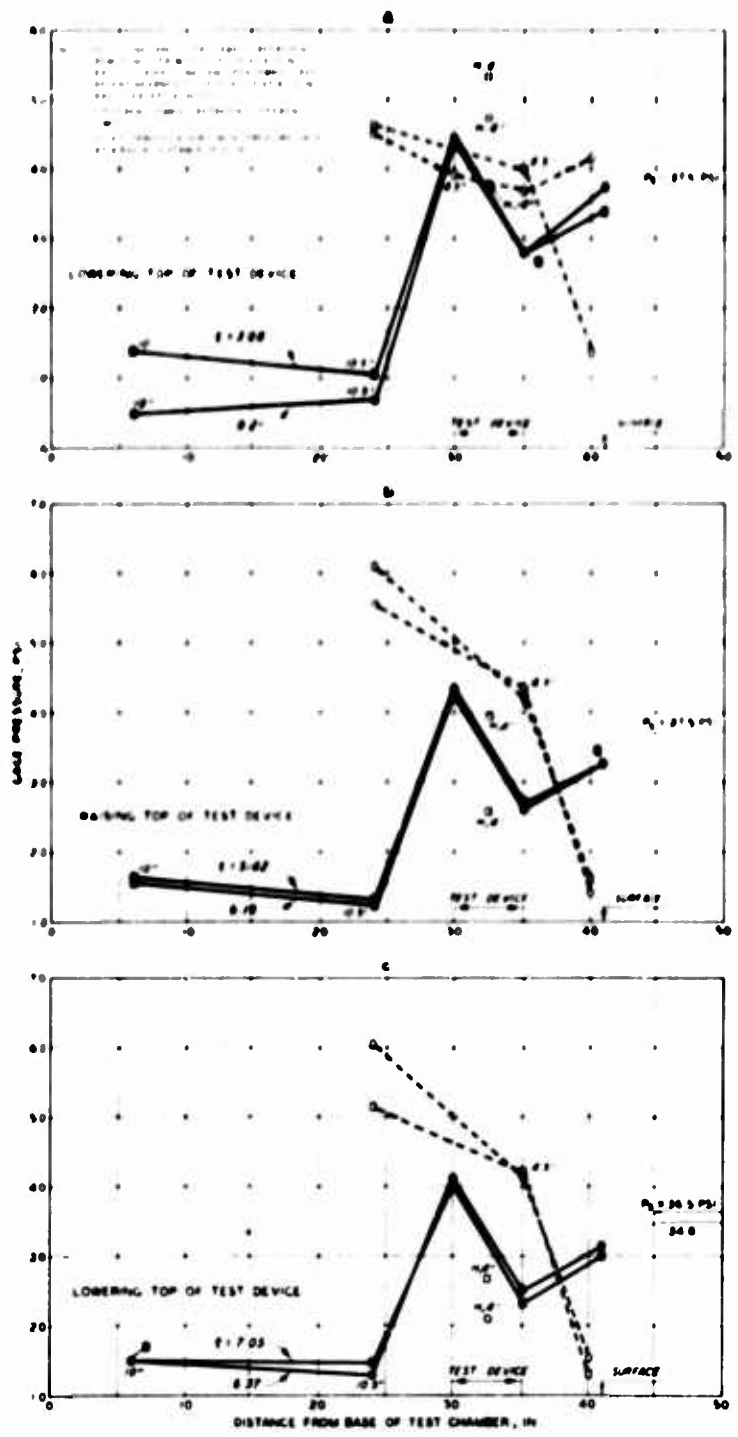


Fig. 30. Change in distribution of vertical soil stress with depth, Test 2; H/B = 1

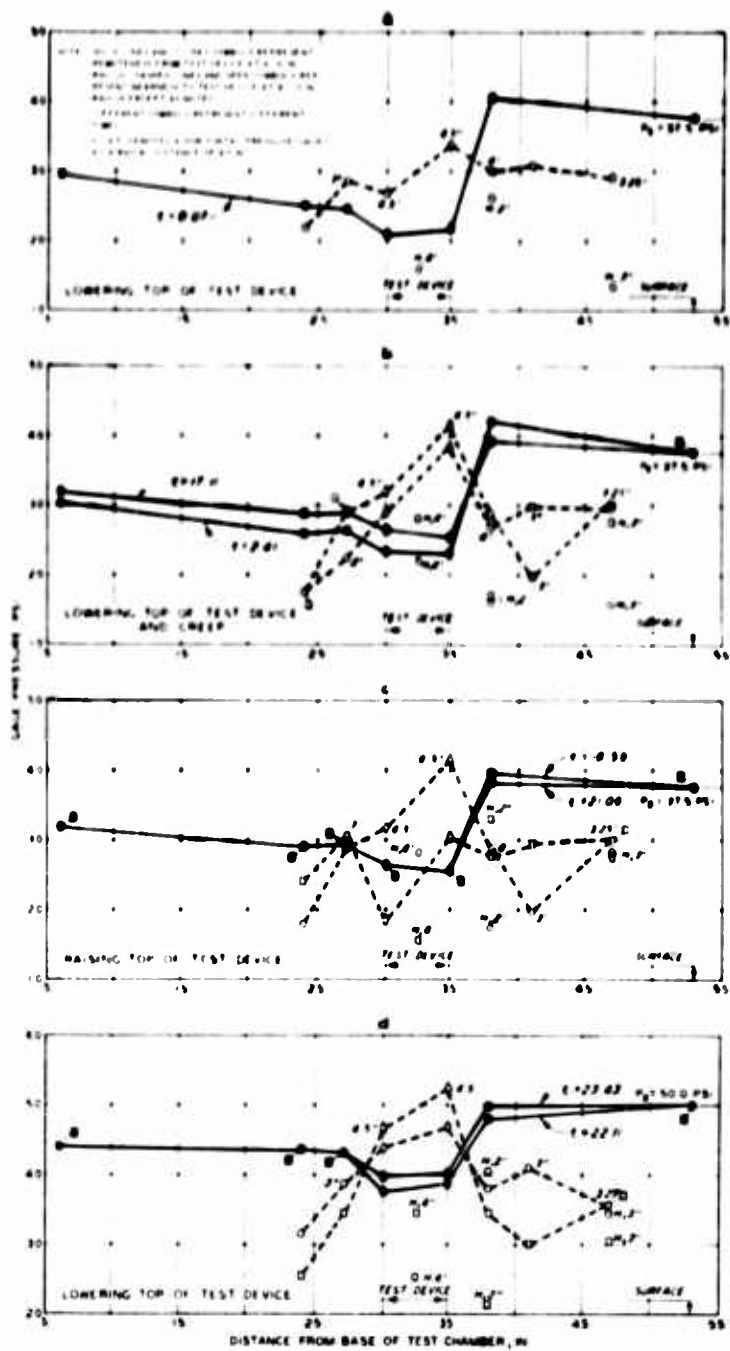
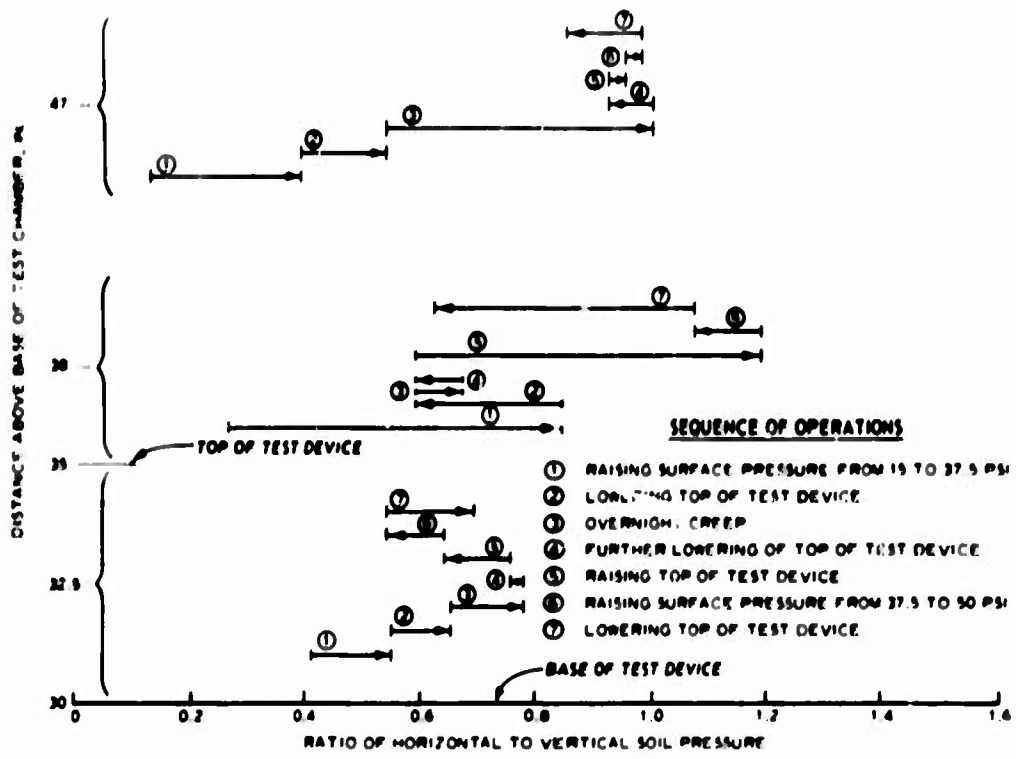
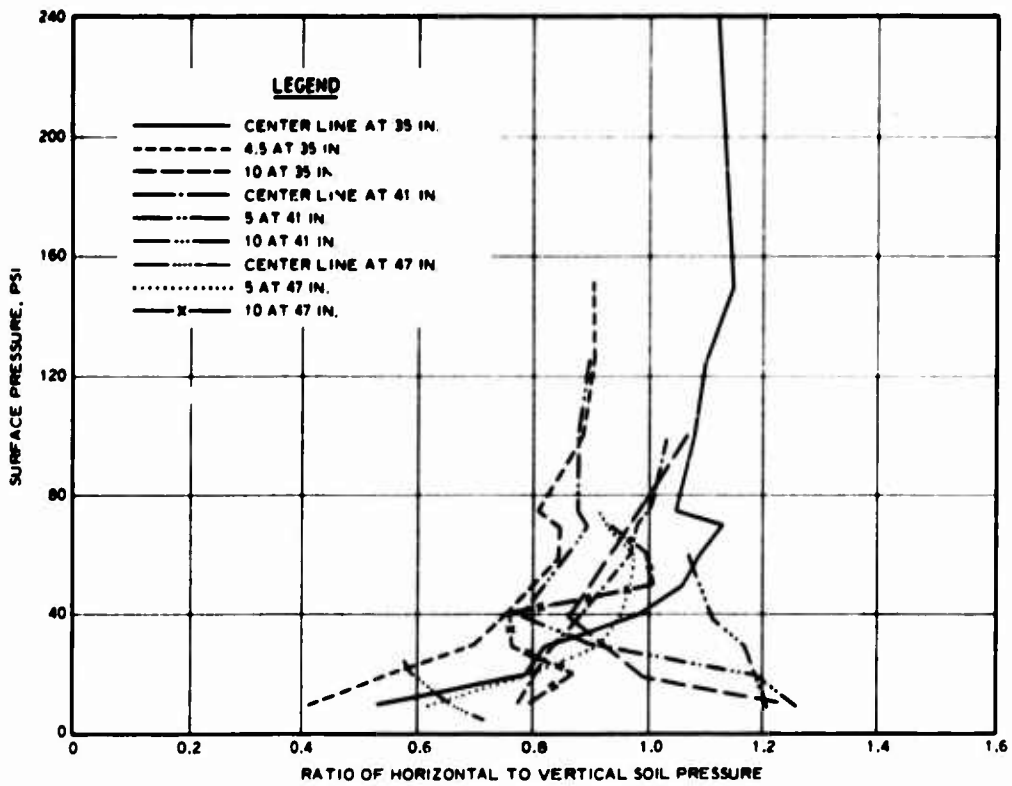


Fig. 31. Change in distribution of vertical soil stress with depth, Test 3; $H/B = 3$

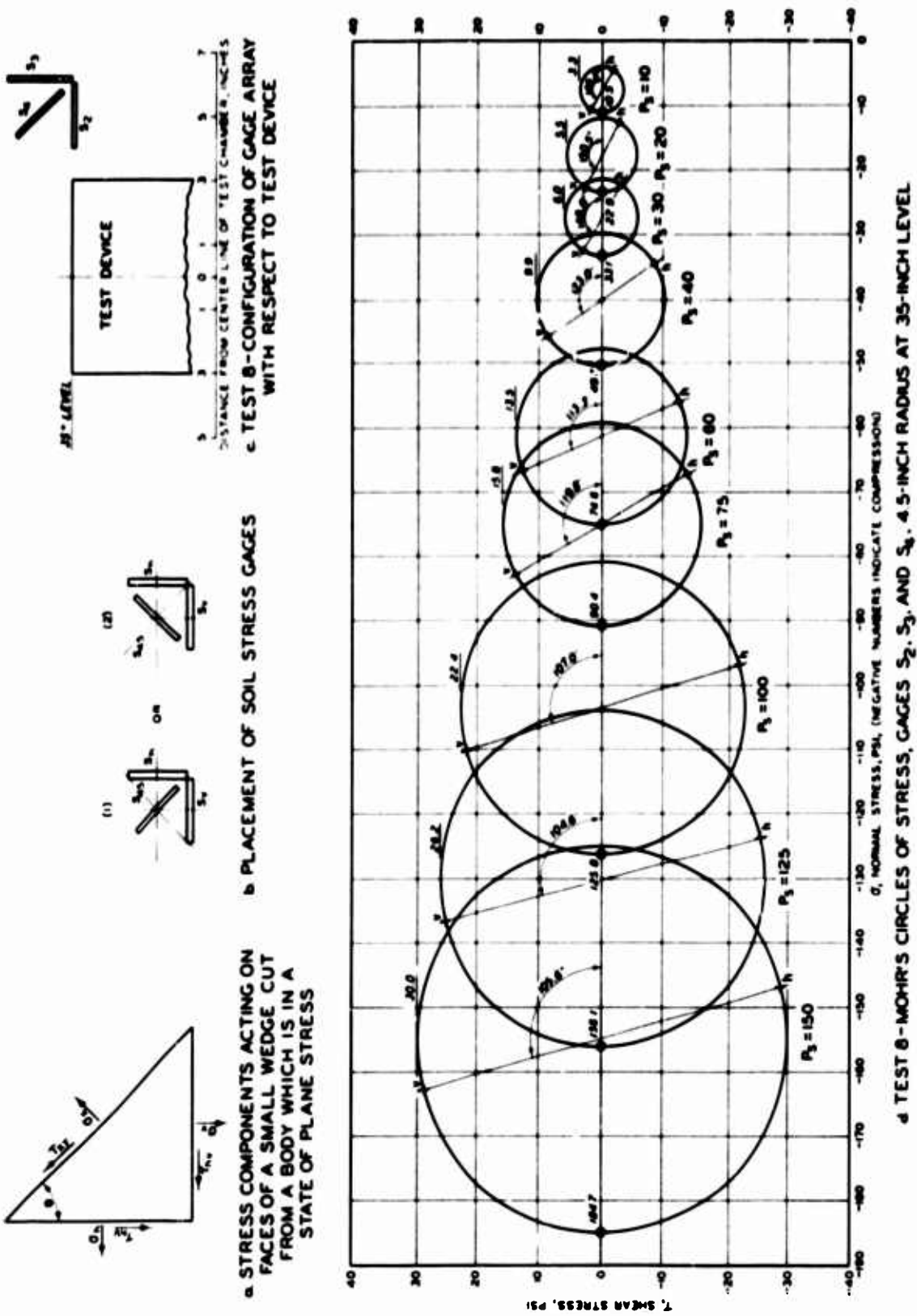


a. TEST 3



b. TEST 3

Fig. 32. Variation of horizontal to vertical soil pressure ratio with structural deflection and surface pressure



a STRESS COMPONENTS ACTING ON FACES OF A SMALL WEDGE CUT FROM A BODY WHICH IS IN A STATE OF PLANE STRESS

b PLACEMENT OF SOIL STRESS GAGES

c TEST B-CONFIGURATION OF GAGE ARRAY WITH RESPECT TO TEST DEVICE

d TEST B-MOHR'S CIRCLES OF STRESS, GAGES S_2 , S_3 , AND S_4 , 4.5-INCH RADIUS AT 35-INCH LEVEL

Fig. 33. Determination of stress components

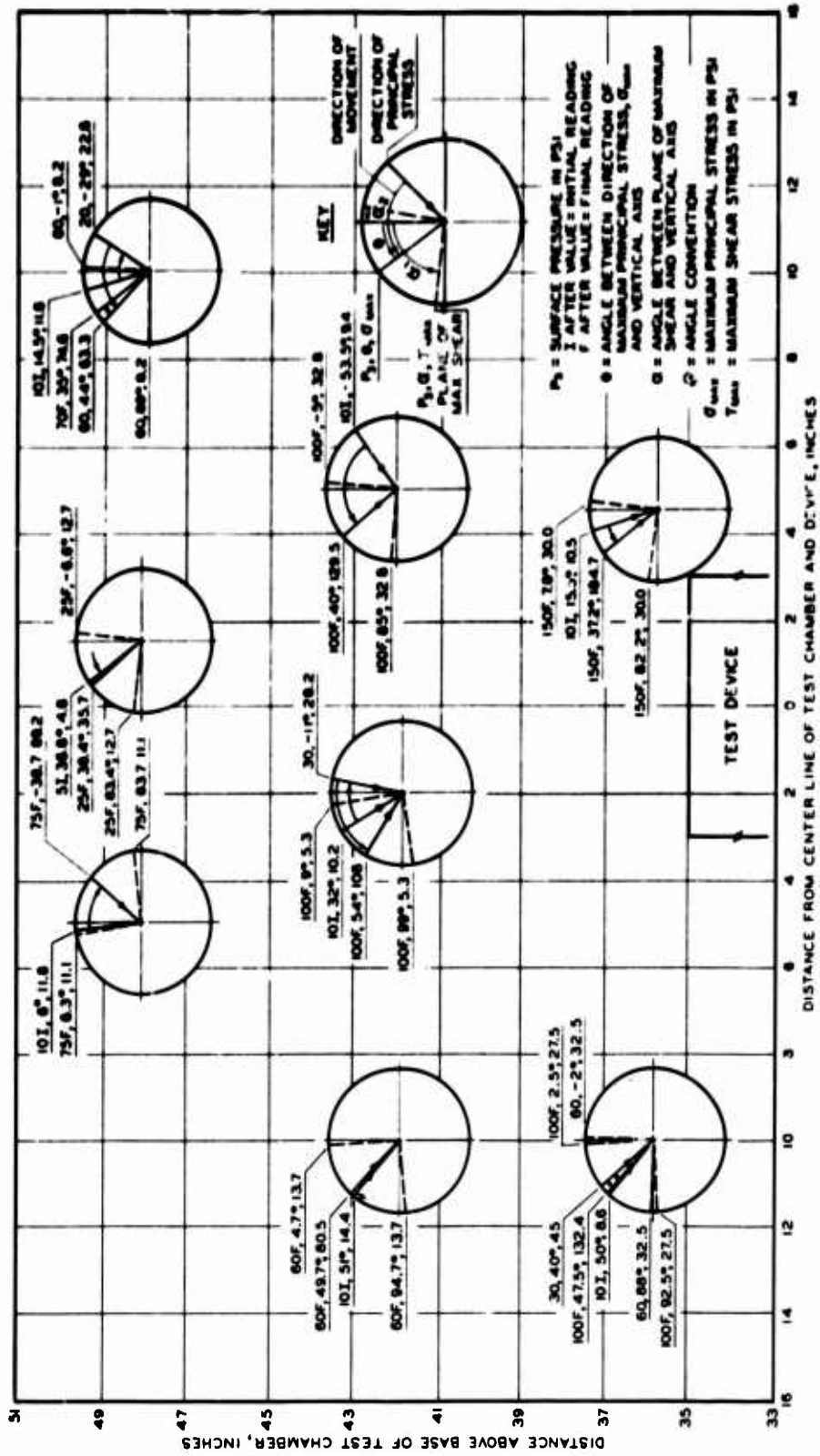


Fig. 34. Directions of principal stresses and location of planes of maximum shear, Test 8



Fig. 35. Soil and structure deflections versus time; Test 1, $H/B = 1/3$, $P_S = 37.5$ psi

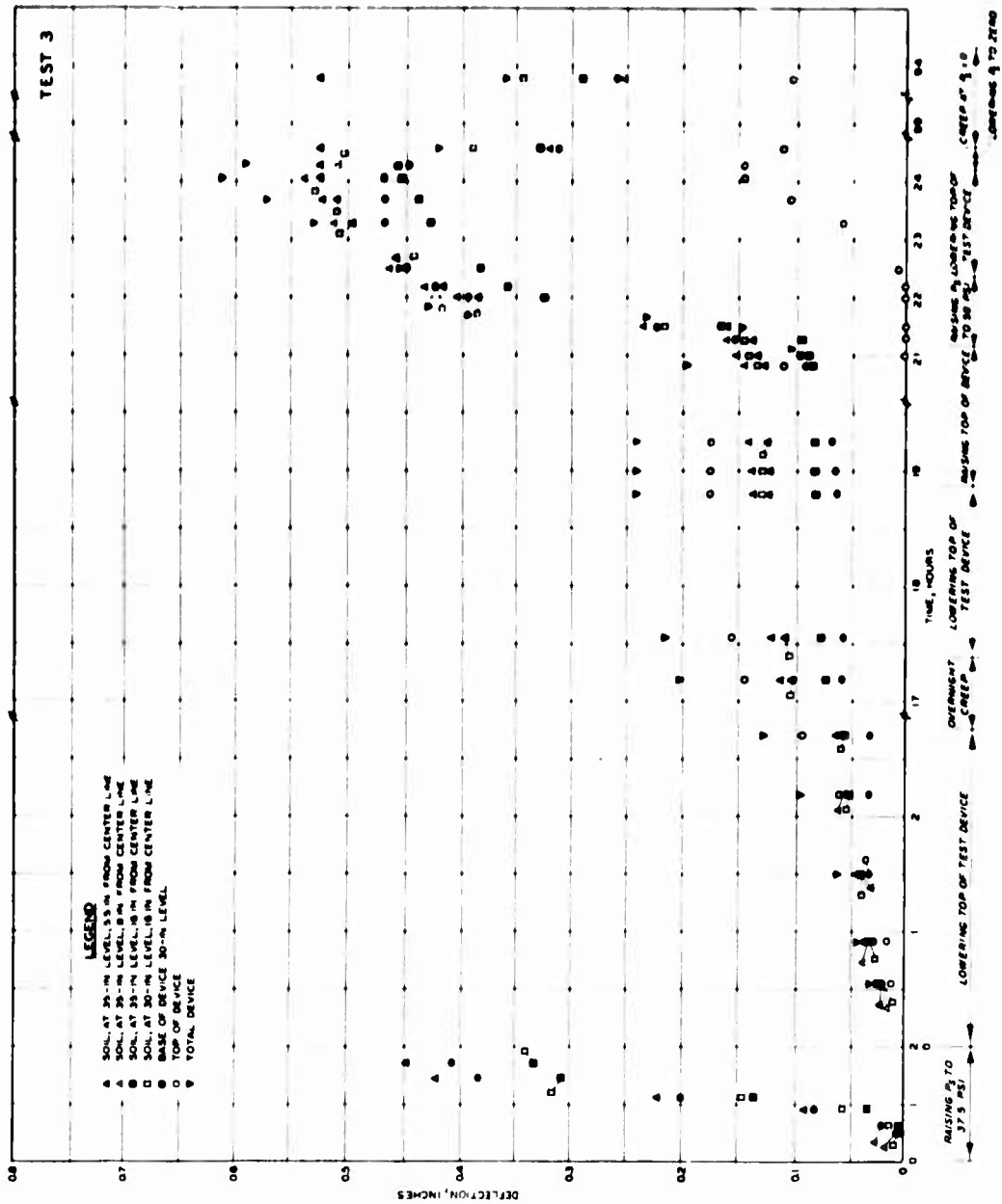


Fig. 36. Soil and structure deflections versus time; Test 3, H/B = 3,
 $P_g = 37.5$ psi

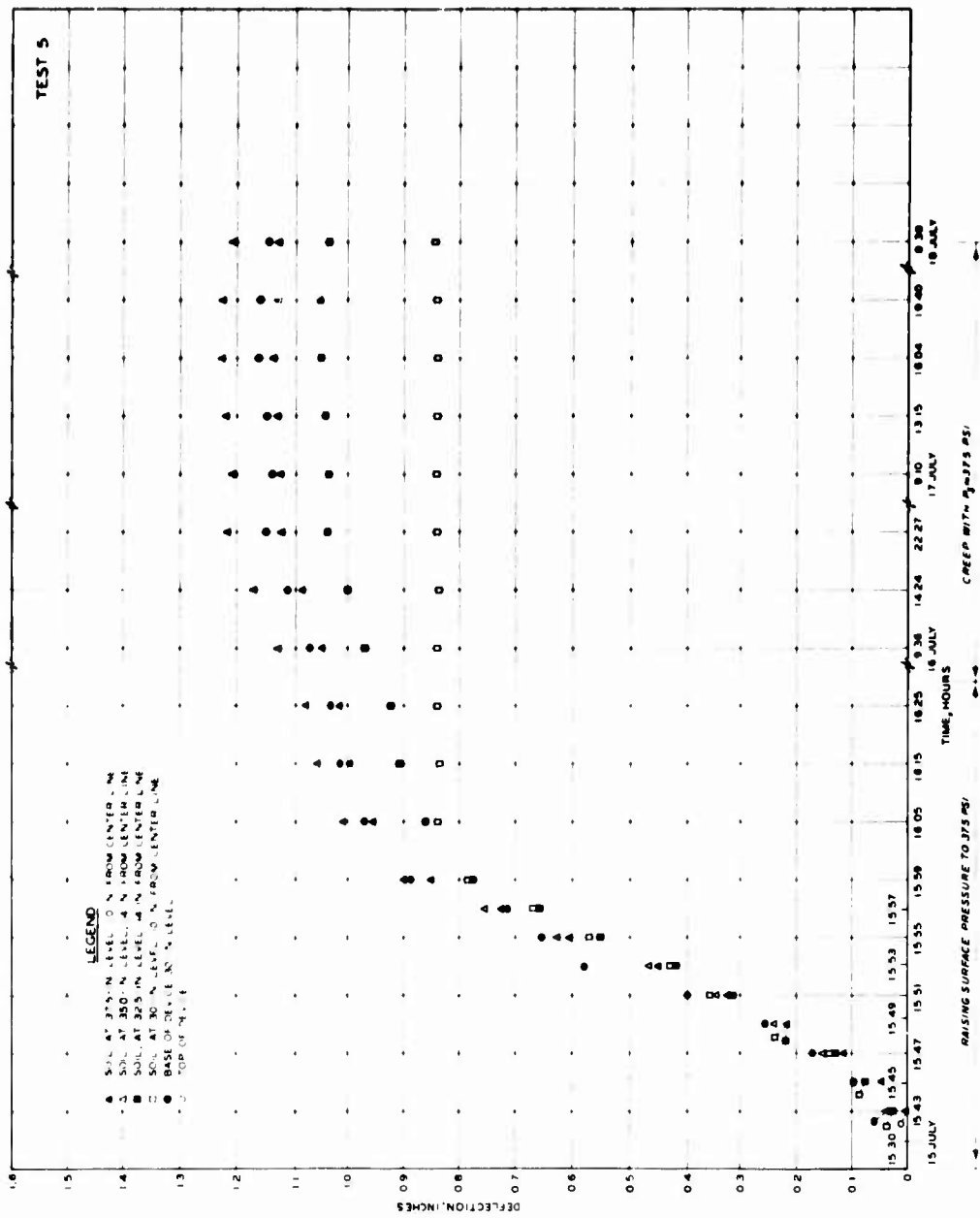


Fig. 37. Soil and structure deflections versus time; Test 5, $H/B = 1$, $P_s = 37.5$ psi

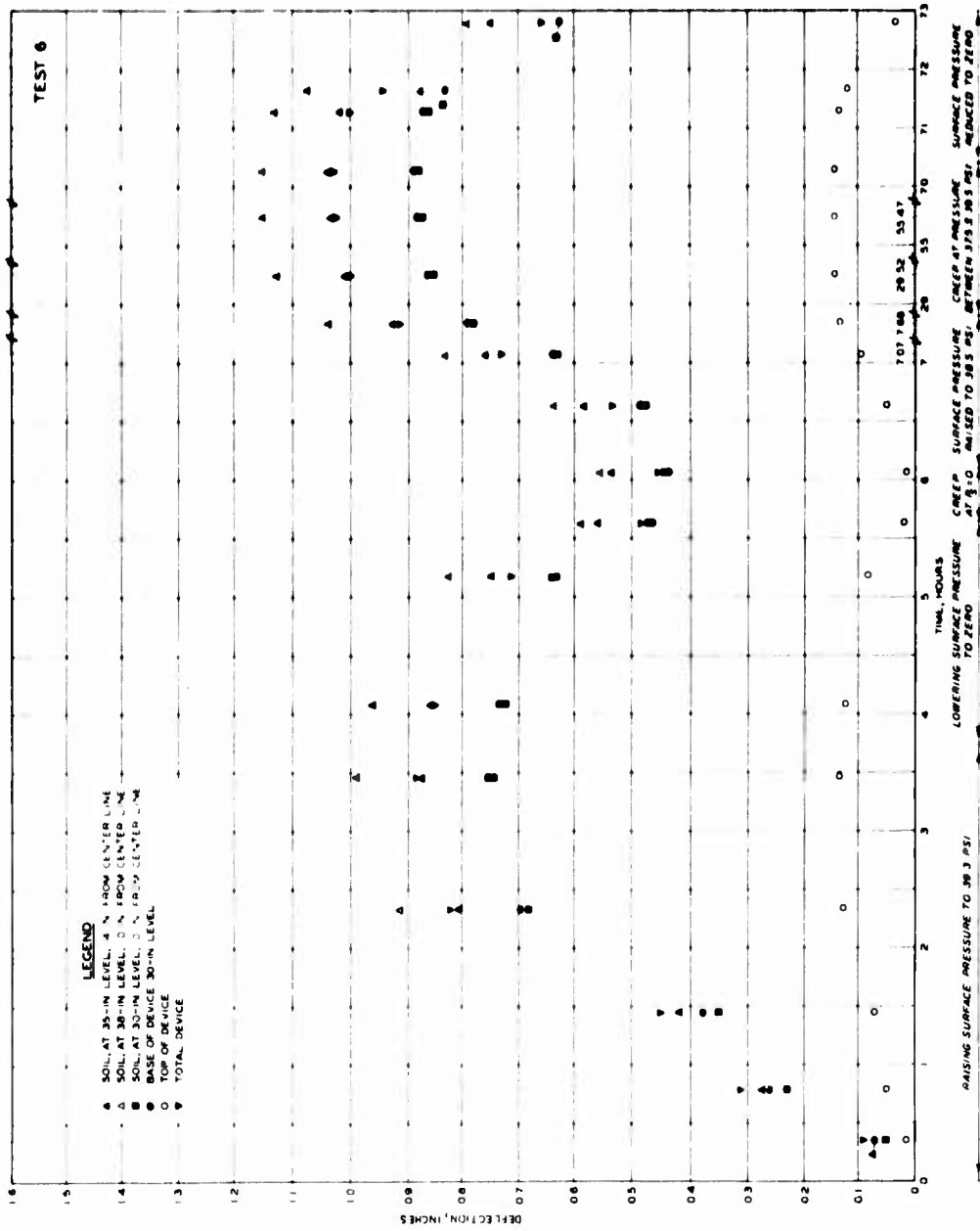


Fig. 38. Soil and structure deflections versus time; Test 6, $H/B = 1$,
 $P_S = 39.3$ psi

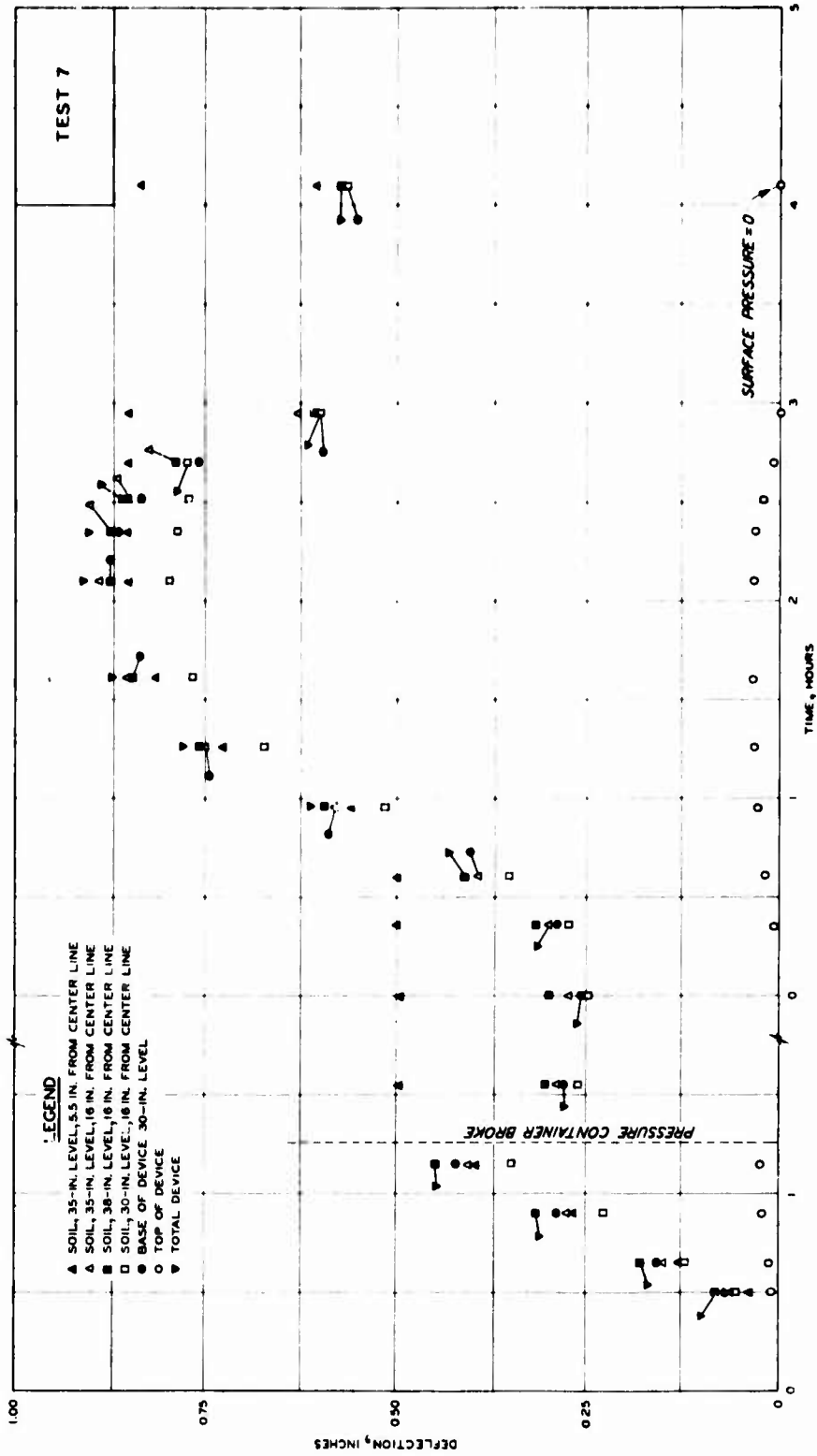


Fig. 39. Soil and structure deflections versus time; Test 7, $H/B = 1$,
 $P_S = 37.5$ psi

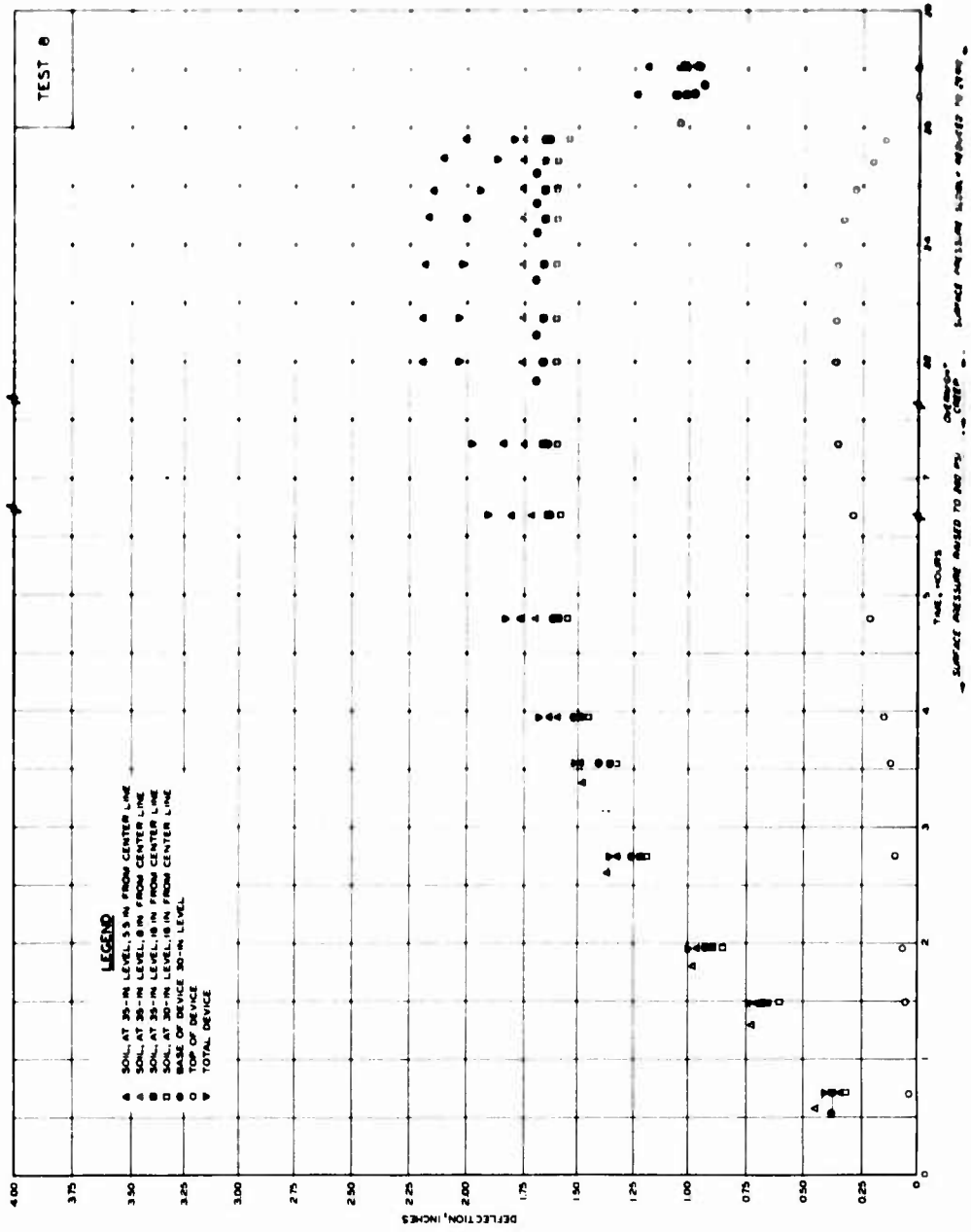
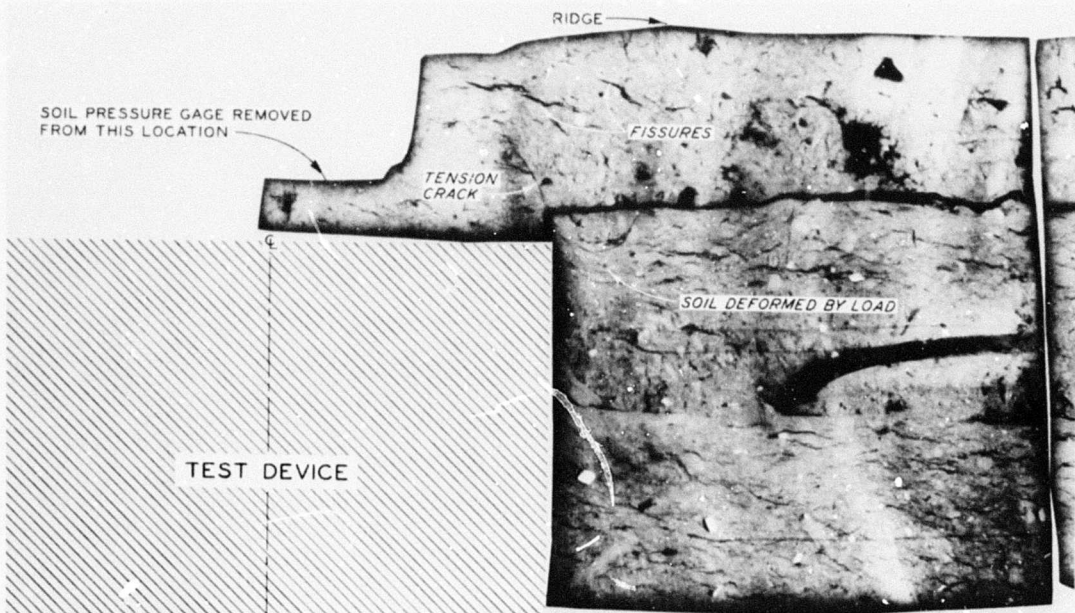


Fig. 40. Soil and structure deflections versus time; Test 8, $H/B = 3$, $P_S = 240$ psi



a. Oblique view of soil surface



b. Cross-section radiograph of depression

Fig. 41. Depression in the soil surface above test device, Test 1; $H/B = 1/3$, $P_S = 37.8$ psi

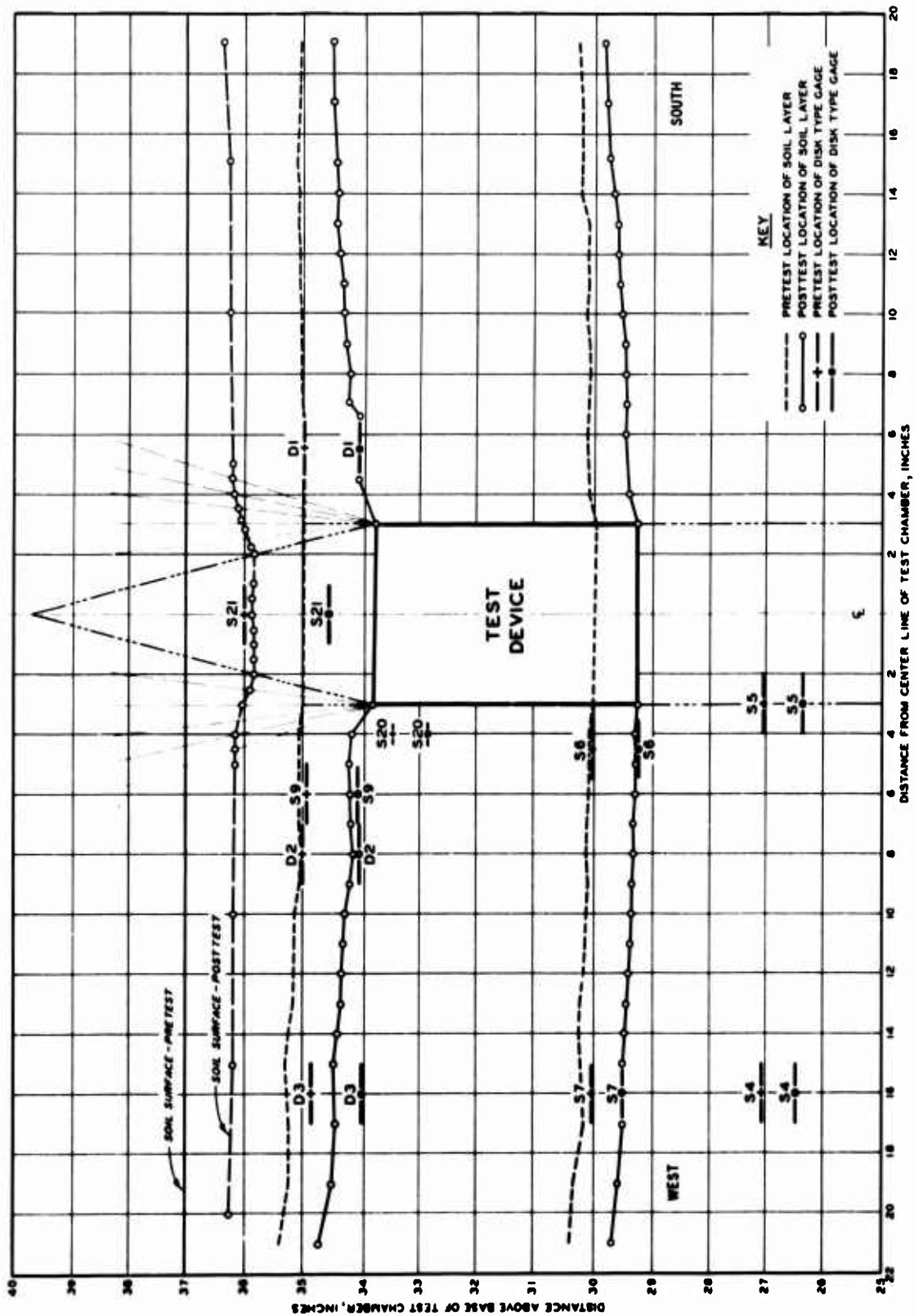
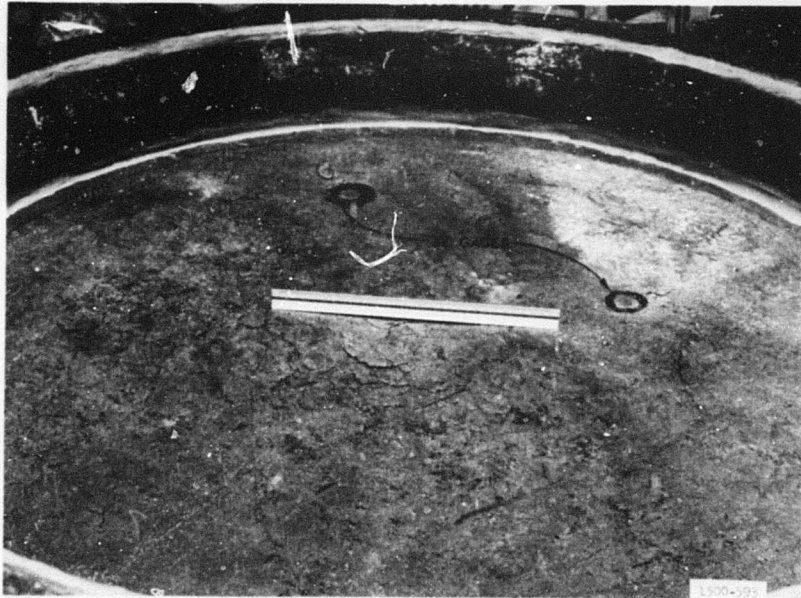
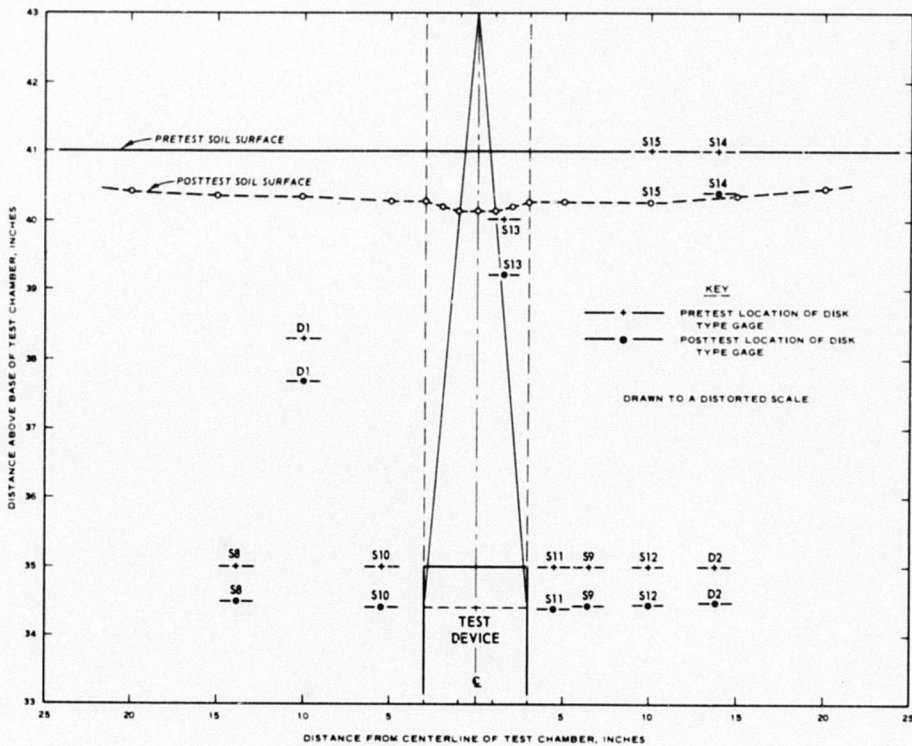


Fig. 42. Cross-section view of soil deformation, Test 1; $H/B = 1/3$, $P_S = 37.8$ psi



a. Oblique view of soil surface



b. Cross-section view of soil deformation

Fig. 43. Depression in soil surface above test device, Test 2;
 $H/B = 1$, $P_S = 37.5$ psi



Fig. 44. Radiograph of soil deformation pattern, Test 3;
 $H/B = 3, P_s = 37.5 \text{ psi}$

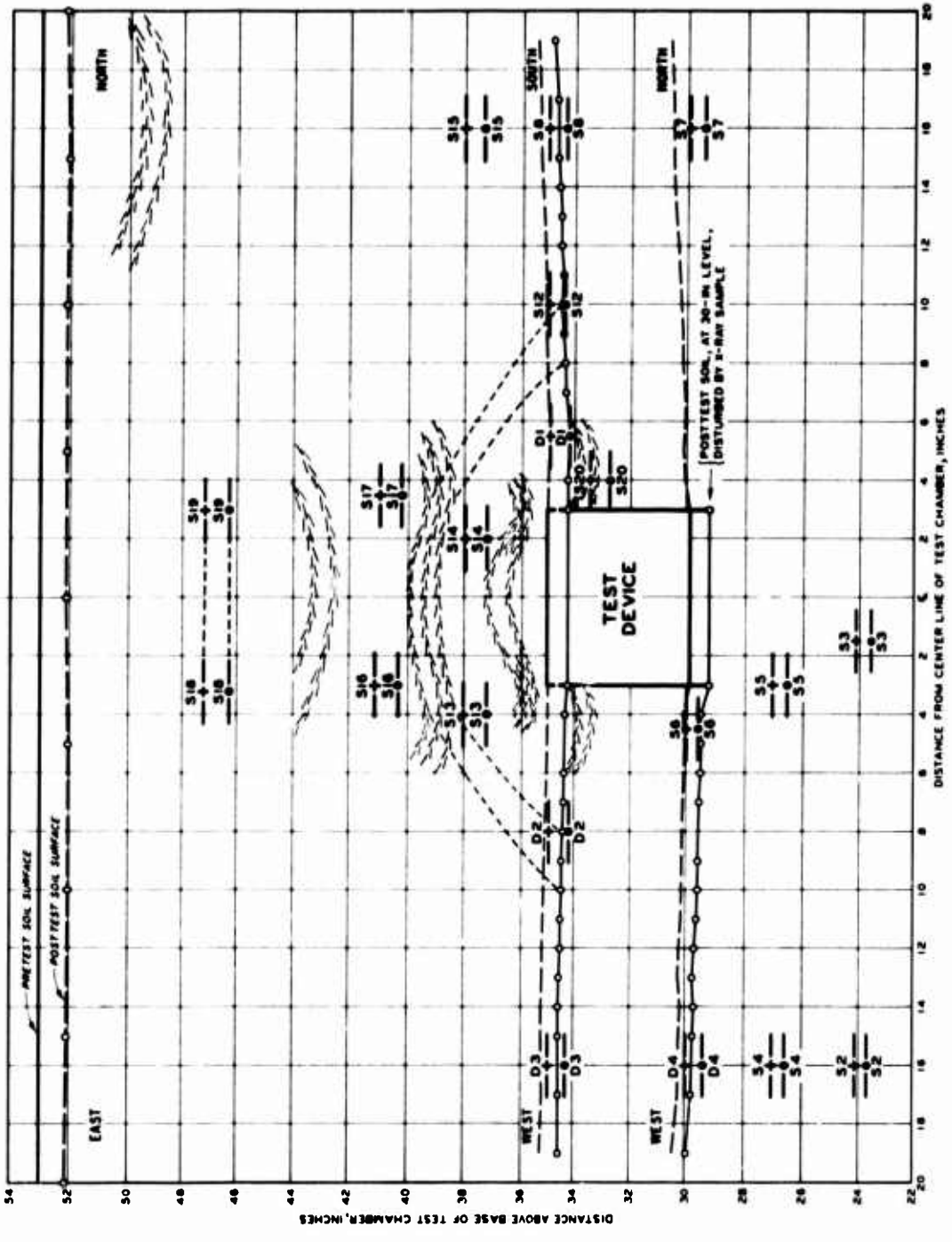
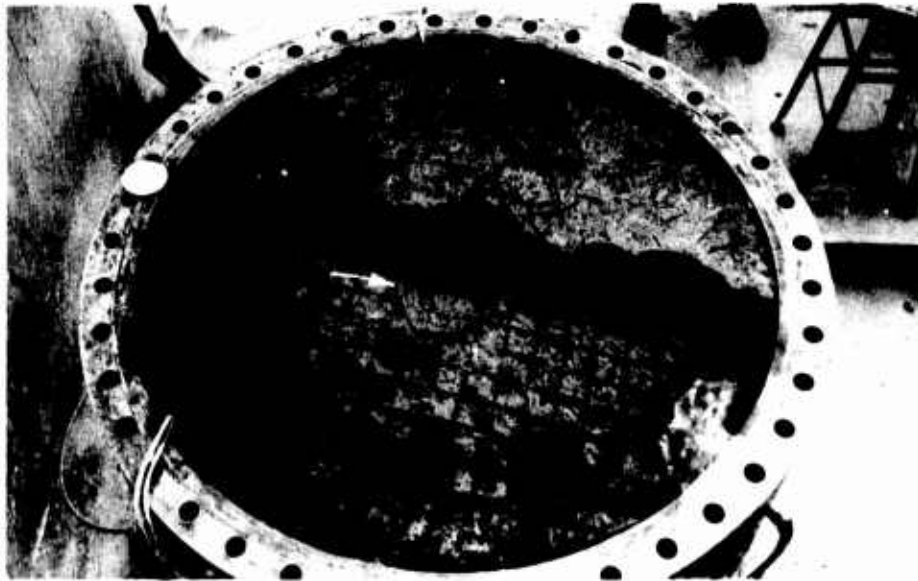
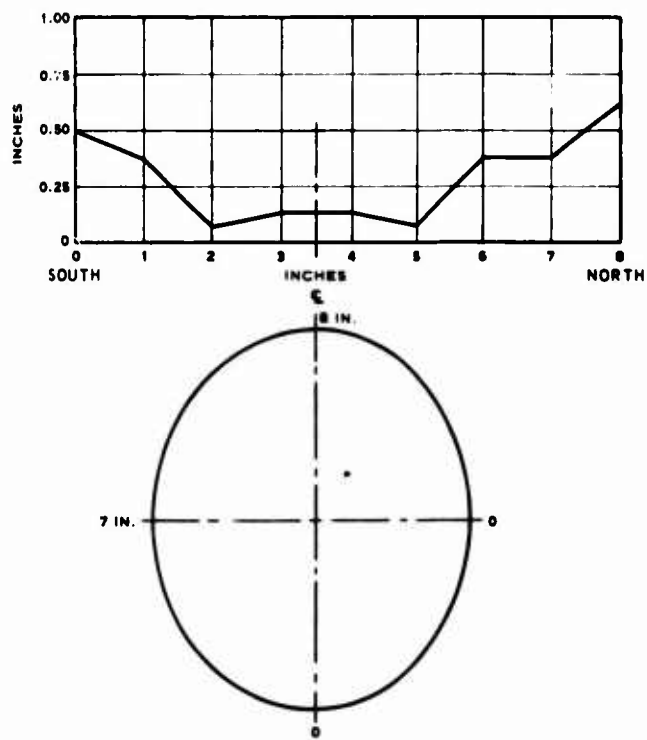


Fig. 45. Sketch of soil deformation patterns found in radiograph and visual inspection, Test 3; $H/B = 3$, $P_g = 37.5$ psi



a. Oblique view of 38-inch soil level

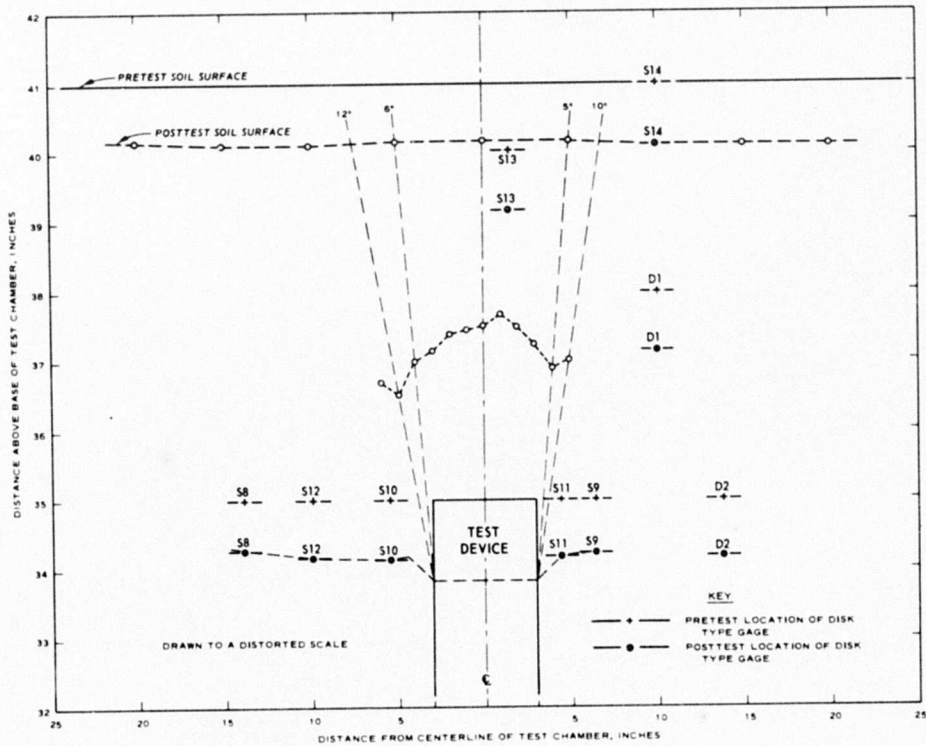


b. Profile of depression at 38-inch level

Fig. 46. Depression above test device, Test 4A;
 $H/B = 1$, $P_S = 75$ psi



a. Oblique view of 38-inch soil level

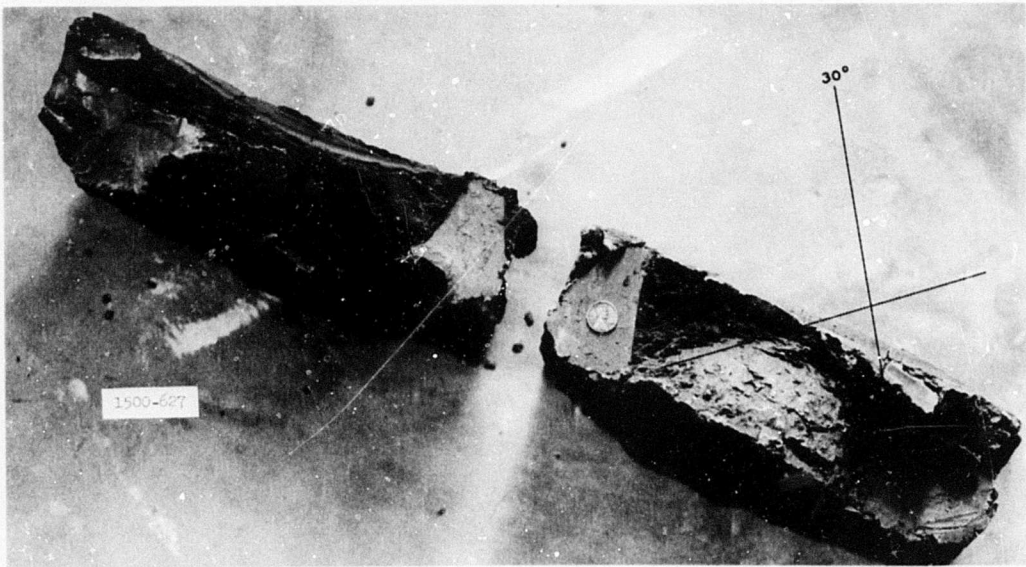


b. Profile of soil deformations

Fig. 47. Hump above test device, Test 4B; $H/B = 1$, $P_S = 75$ psi



a. Oblique view of soil surface



b. Cutaway view of 35- to 38-inch soil level

Fig. 48. Soil deformations, Test 5; $H/B = 1$, $P_S = 37.5$ psi

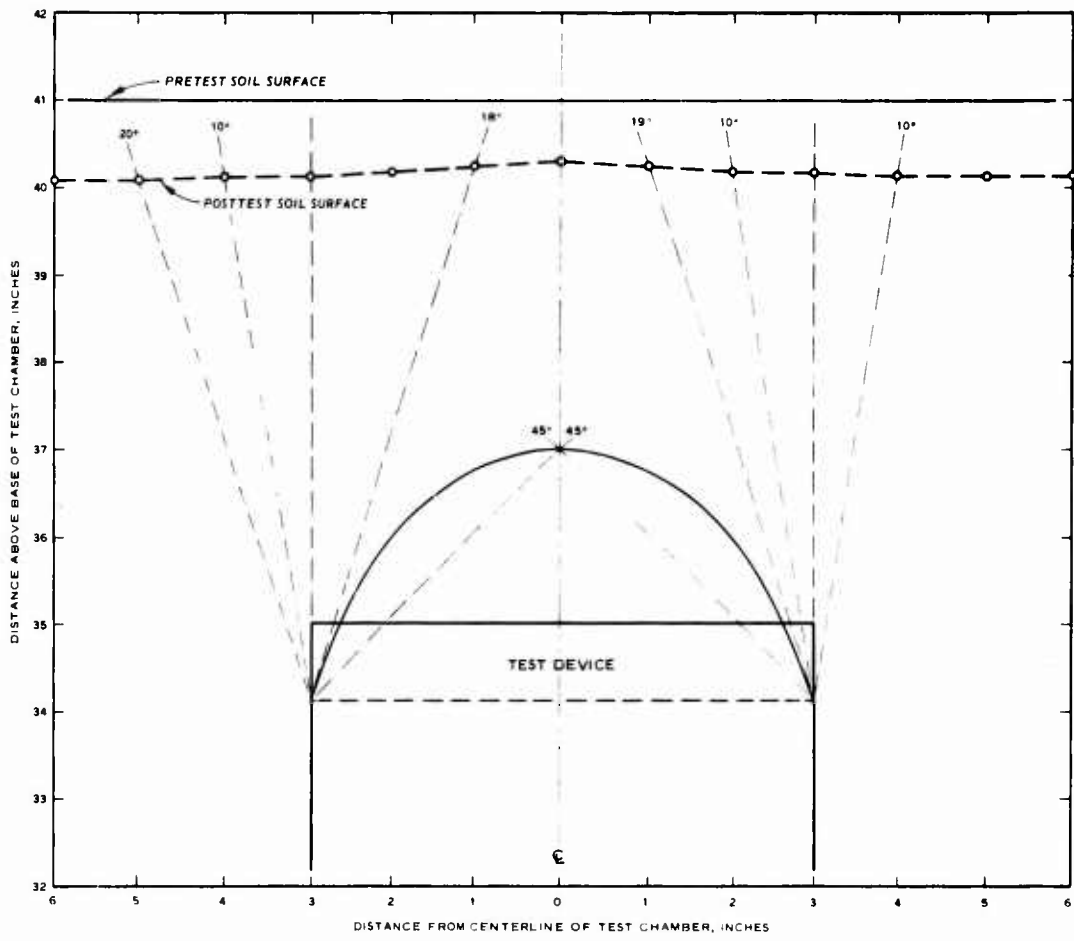
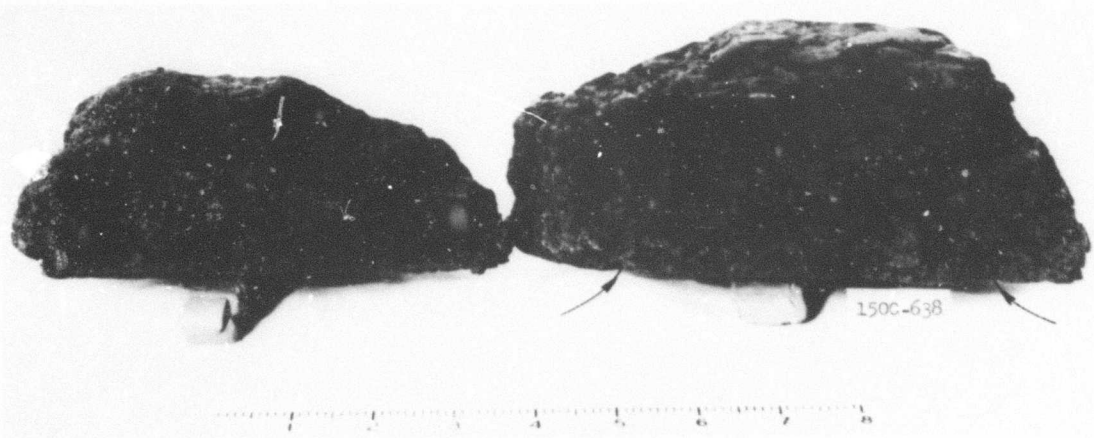
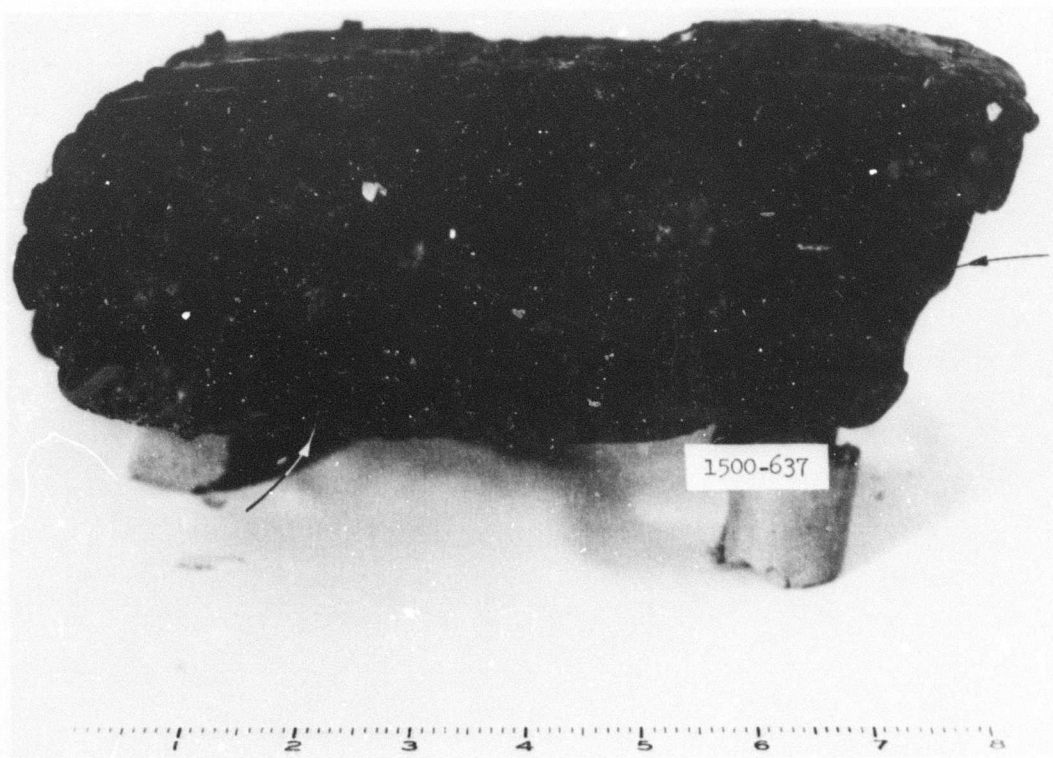


Fig. 49. Profile of soil deformations, Test 5;
 $H/B = 1$, $P_s = 37.5$ psi



a. Soil directly above test device



b. Soil between 6- and 14-inch radii

Fig. 50. Posttest soil samples removed from 35- to 38-inch layer,
Test 6; $H/B = 1$, $P_S = 37.5$ psi

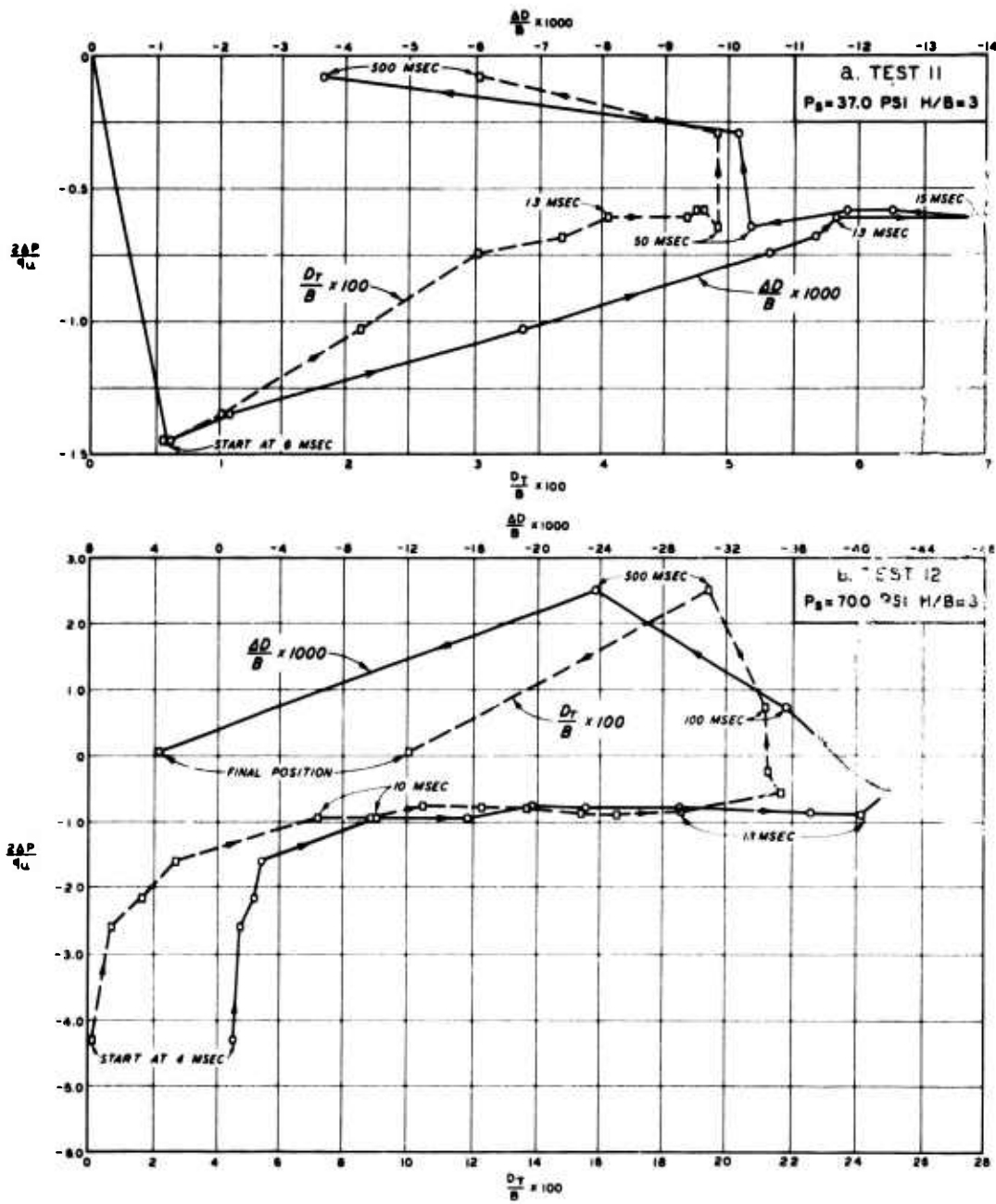


Fig. 51. Dimensionless plot of pressure versus deflection for dynamic Tests 11 and 12

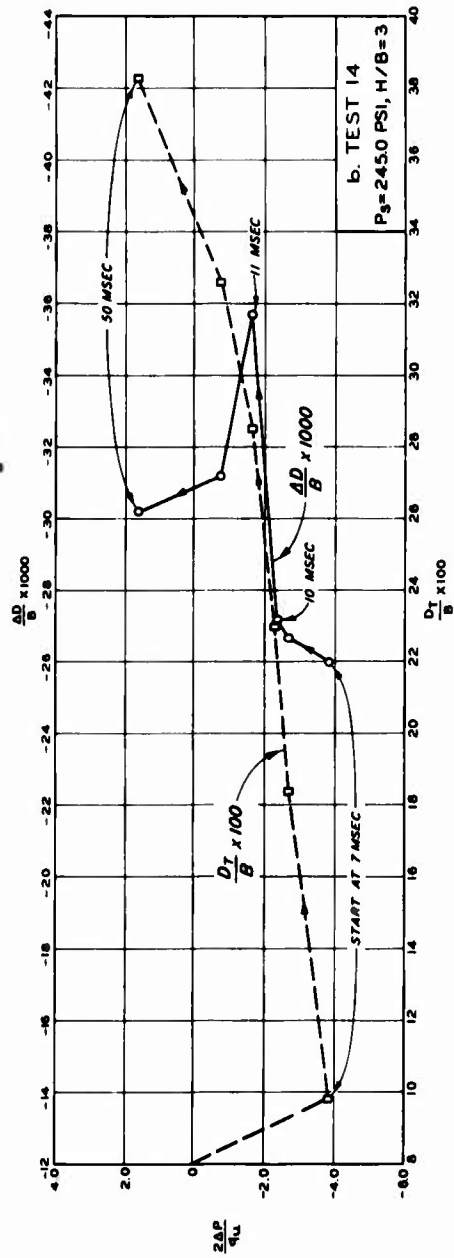
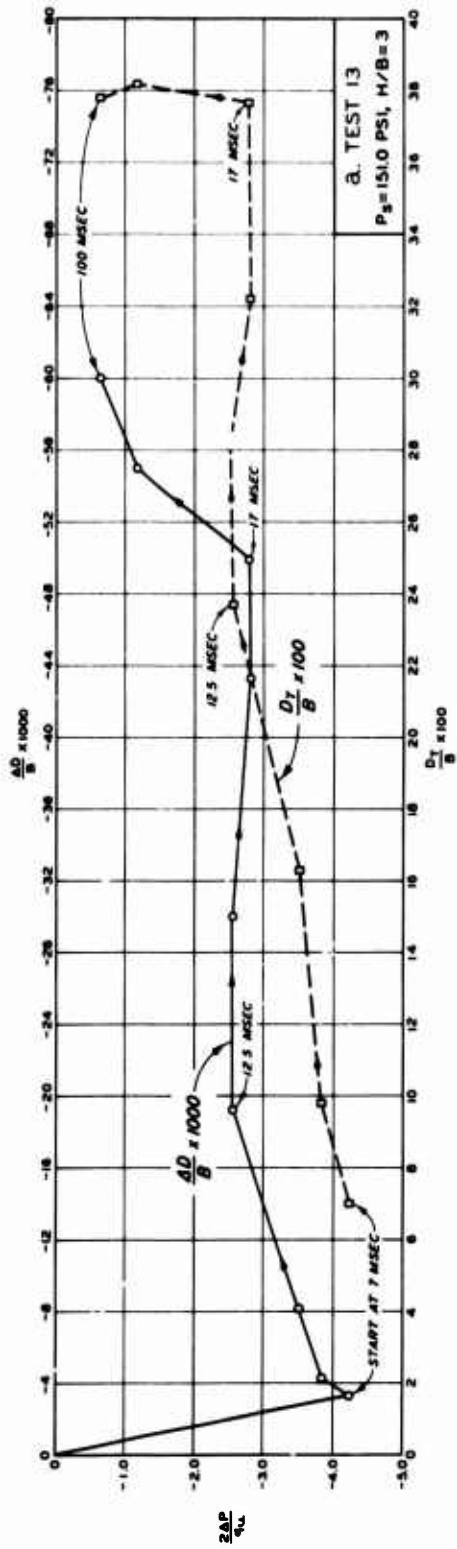


Fig. 52. Dimensionless plot of pressure versus deflection for dynamic Tests 13 and 14

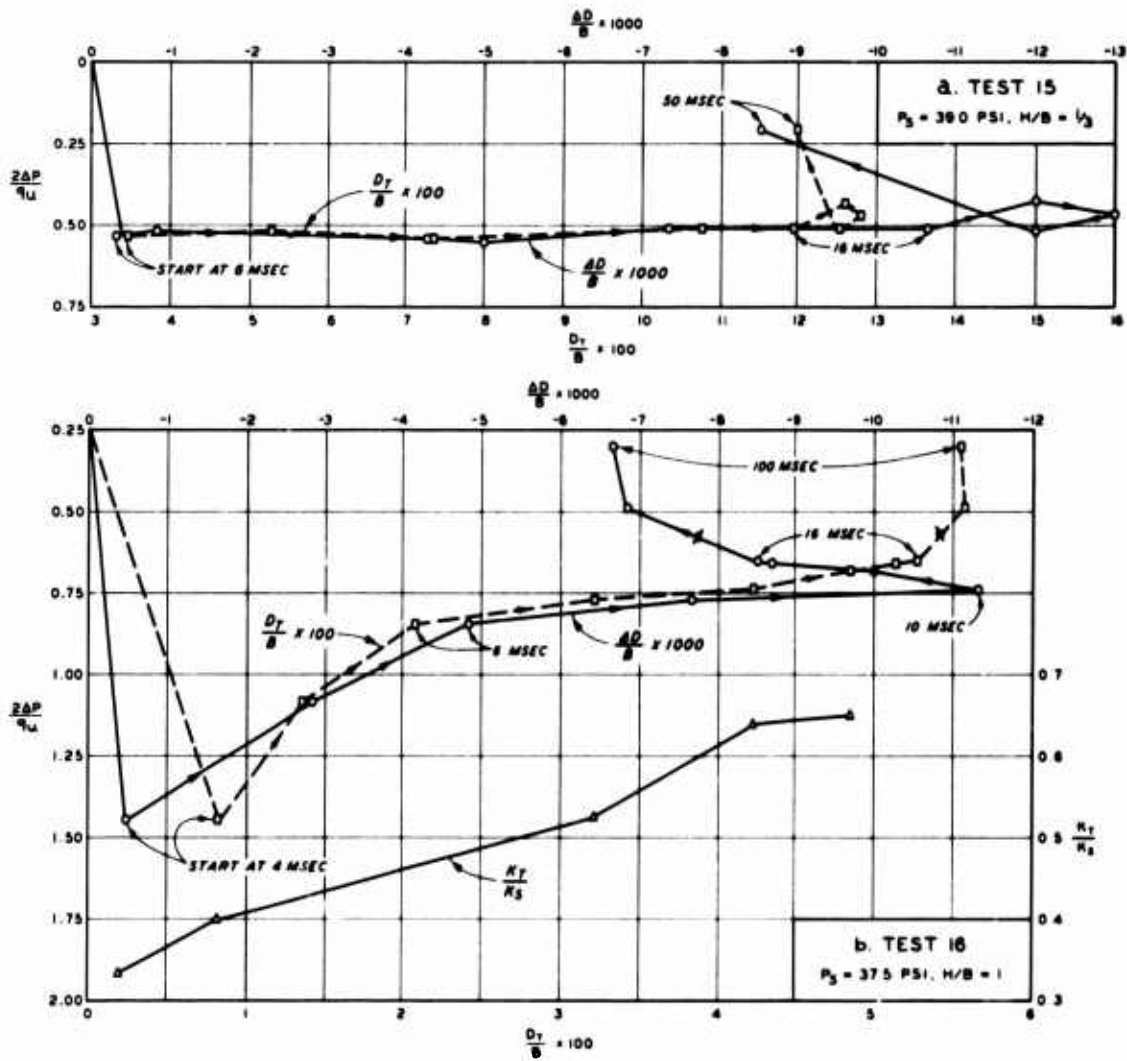


Fig. 53. Dimensionless plot of pressure versus deflection for dynamic Tests 15 and 16

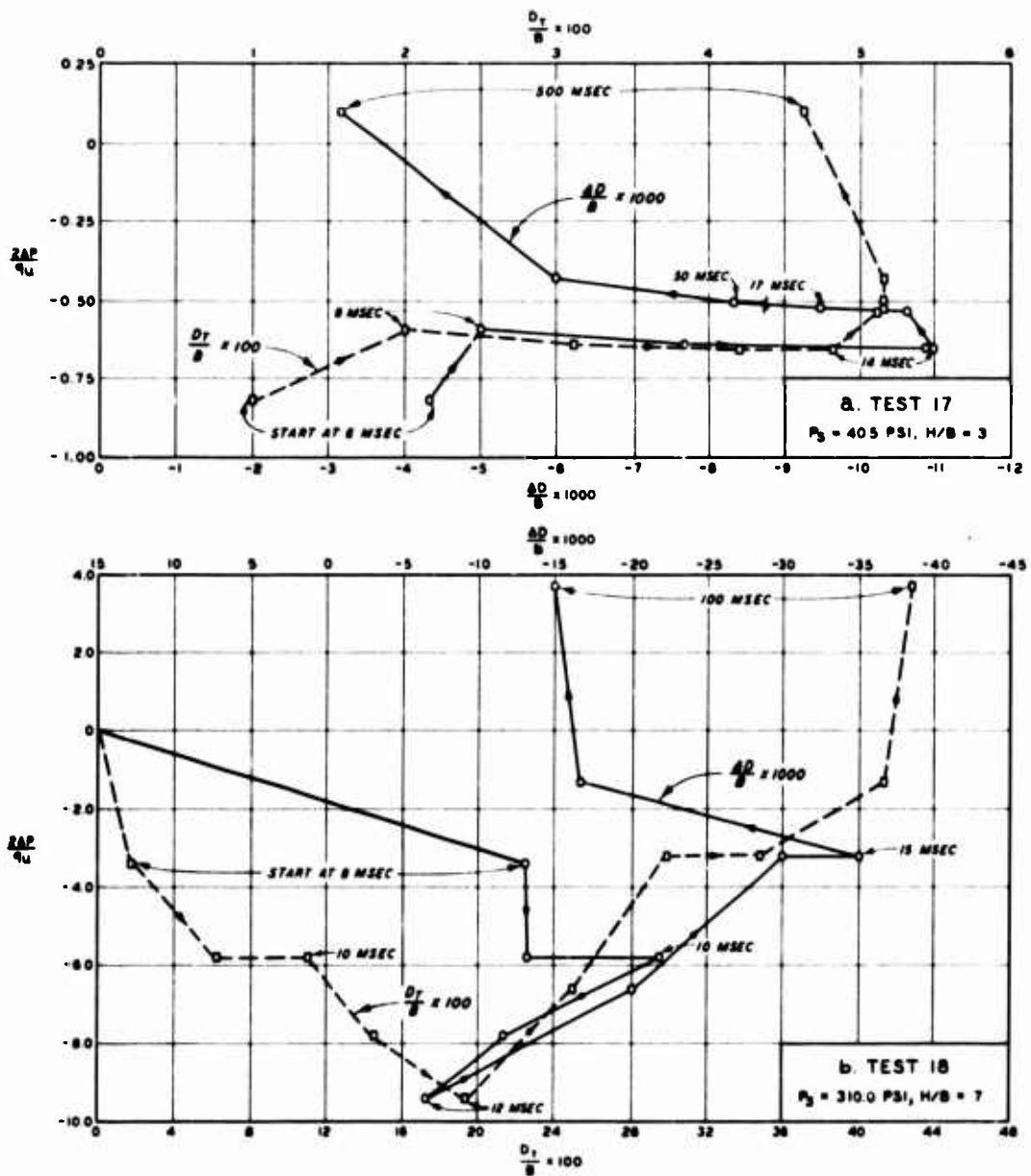


Fig. 54. Dimensionless plot of pressure versus deflection for dynamic Tests 17 and 18

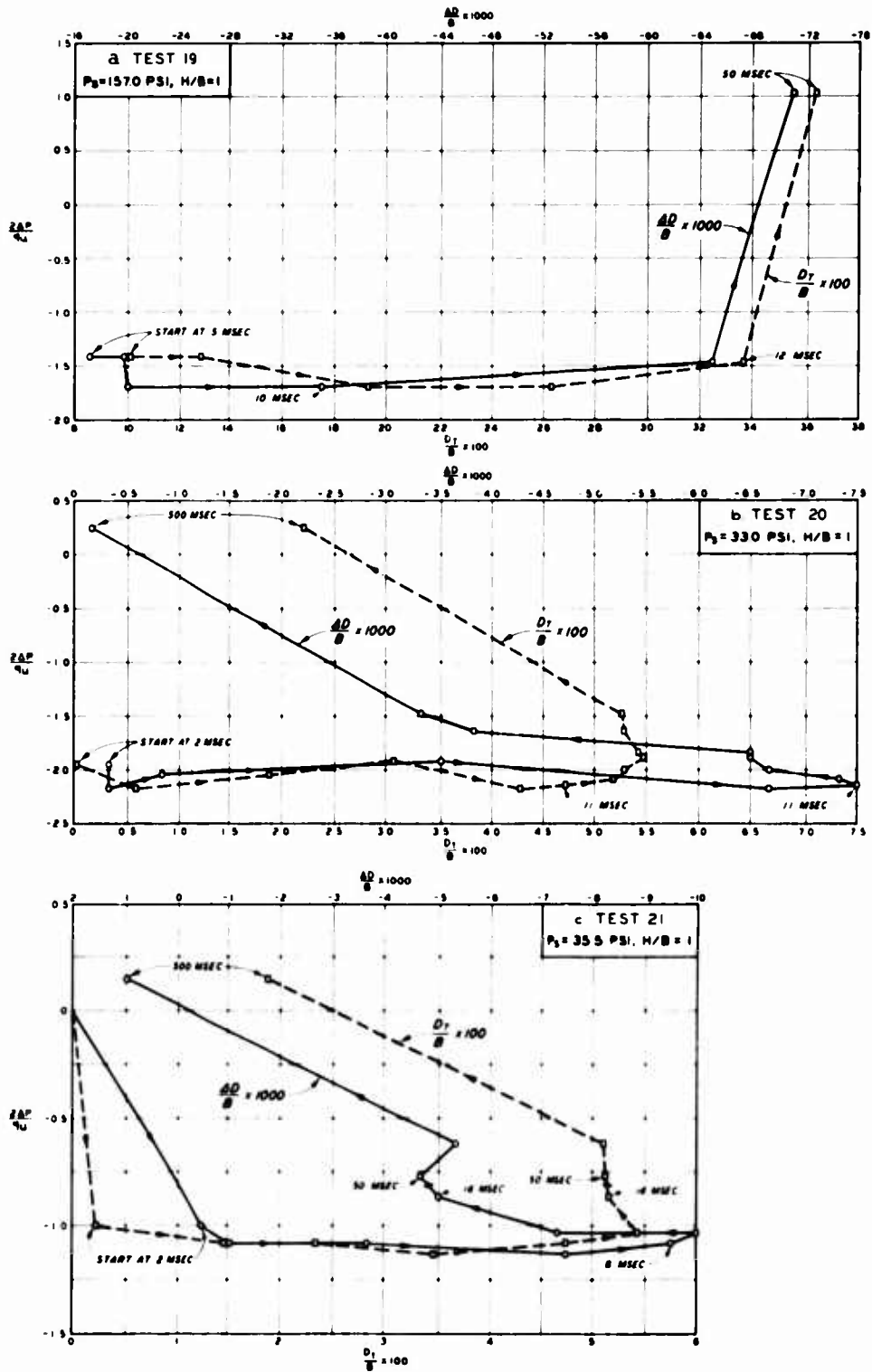


Fig. 55. Dimensionless plot of pressure versus deflection for dynamic Tests 19, 20, and 21

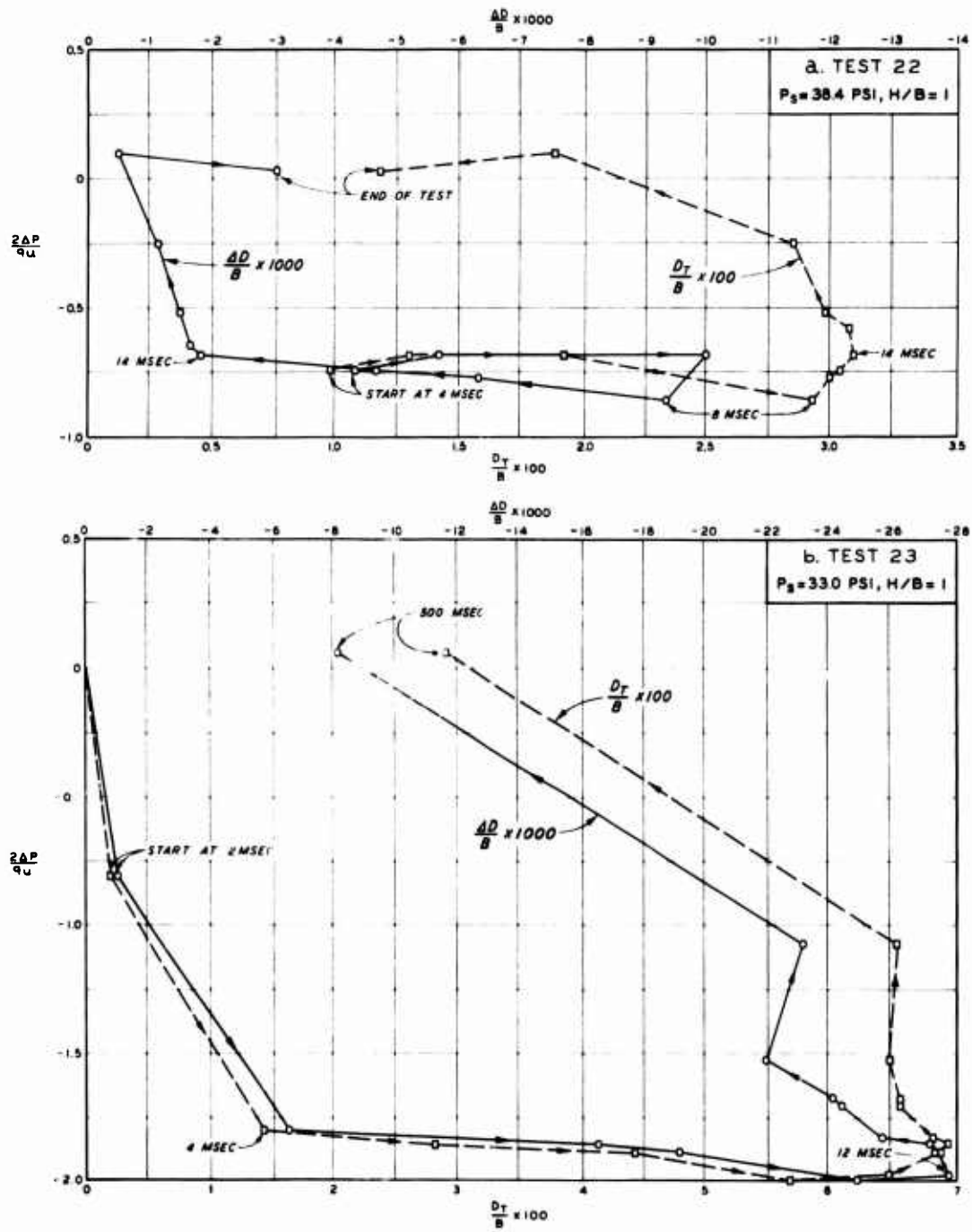


Fig. 56. Dimensionless plot of pressure versus deflection for dynamic Tests 22 and 23

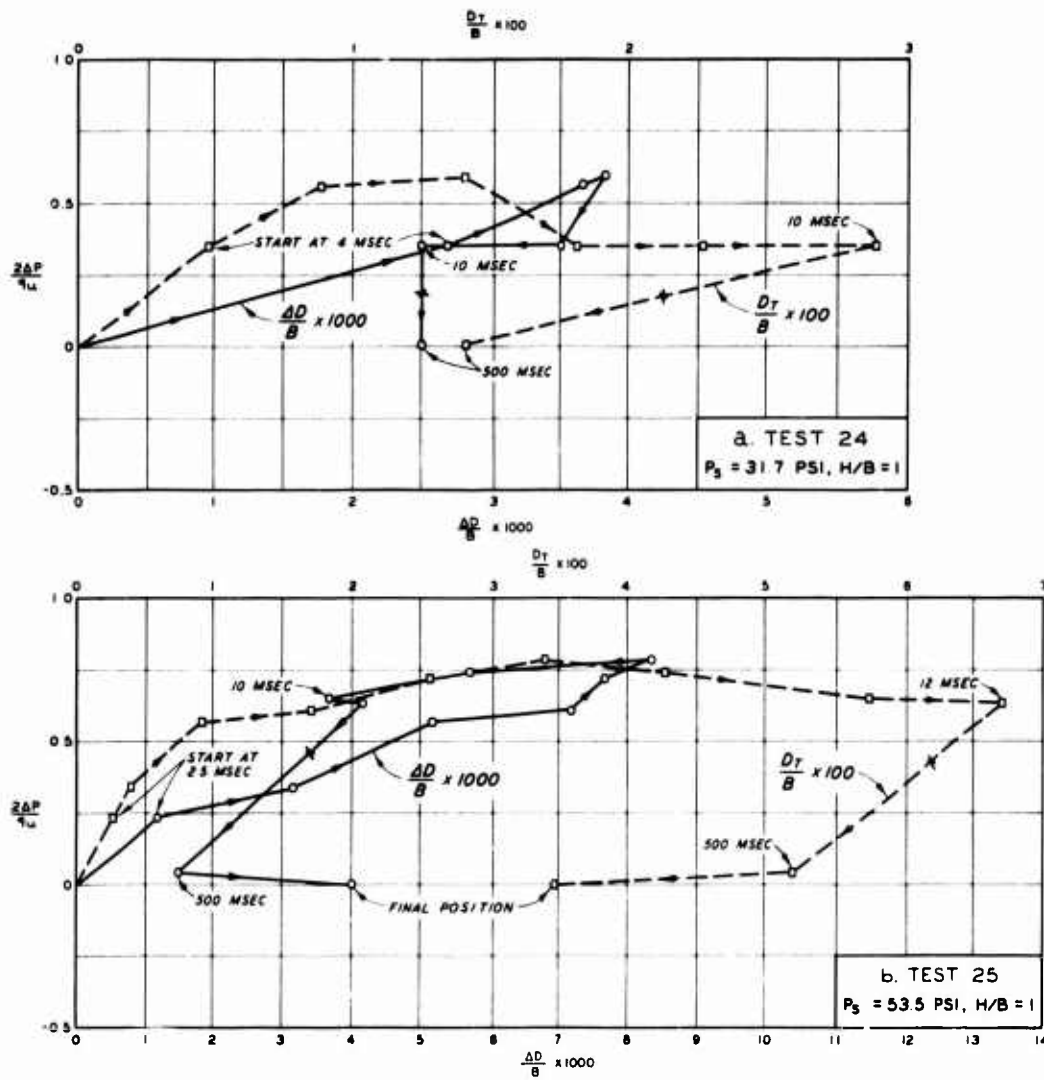


Fig. 57. Dimensionless plot of pressure versus deflection for dynamic Tests 24 and 25

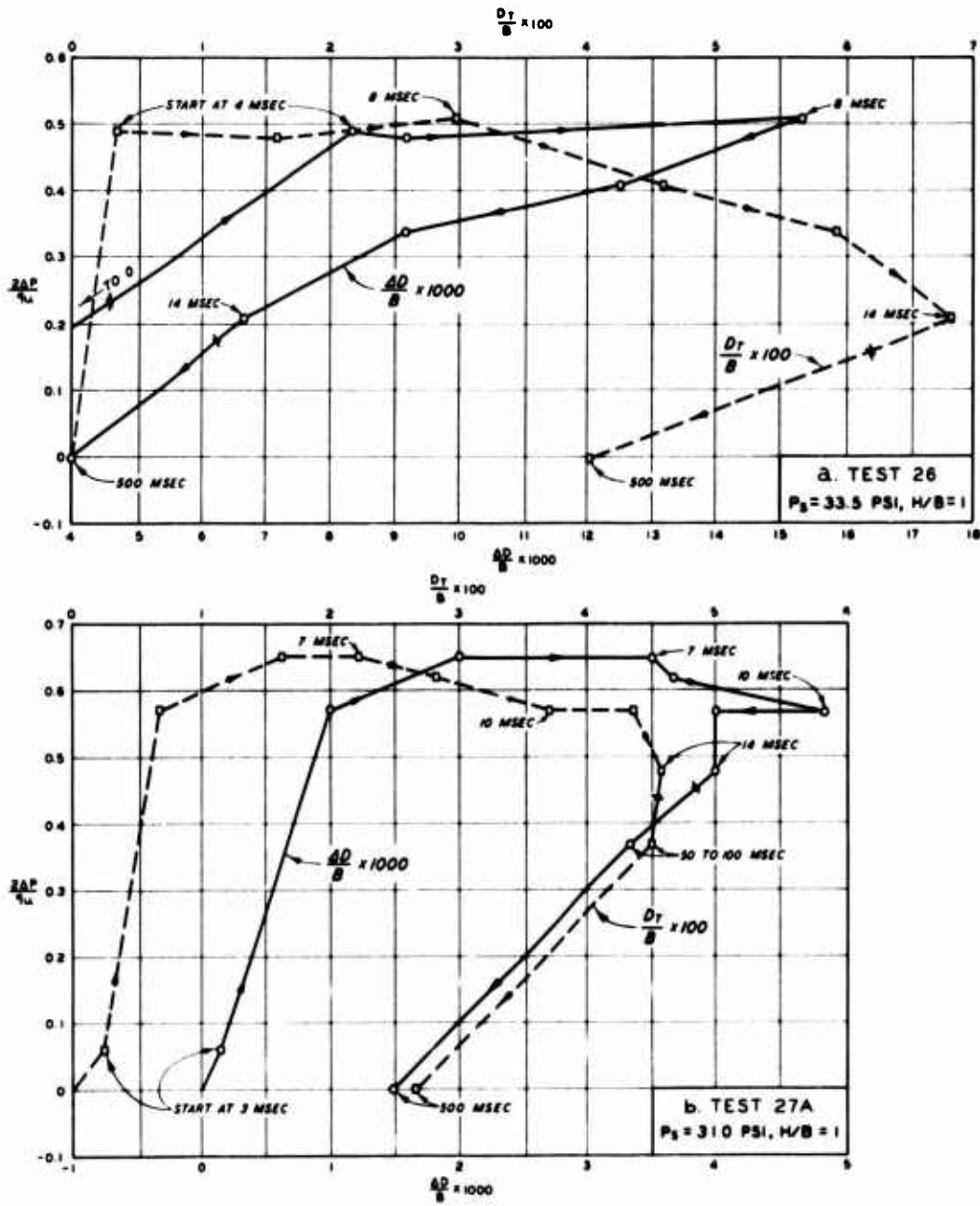


Fig. 58. Dimensionless plot of pressure versus deflection for dynamic Tests 26 and 27A

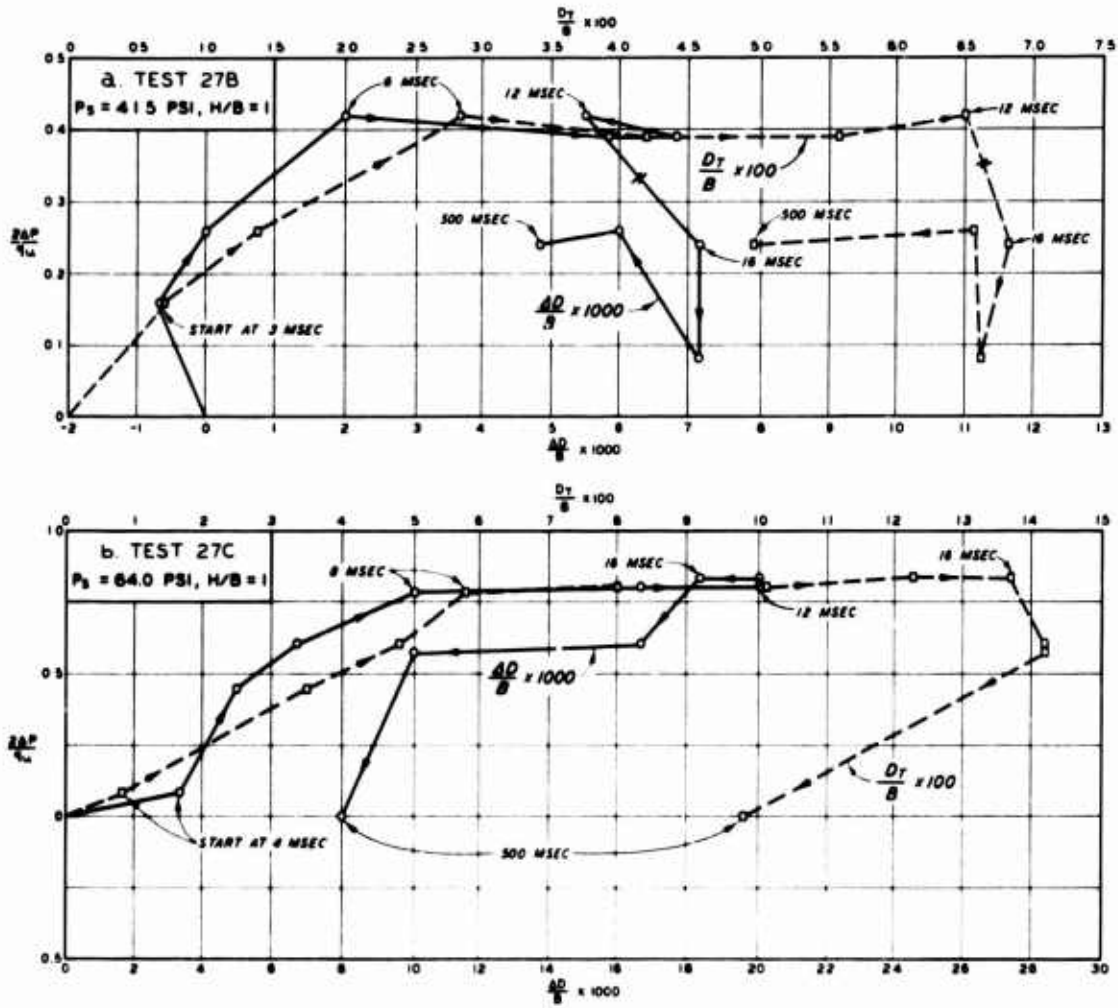


Fig. 59. Dimensionless plot of pressure versus deflection for dynamic Tests 27B and 27C

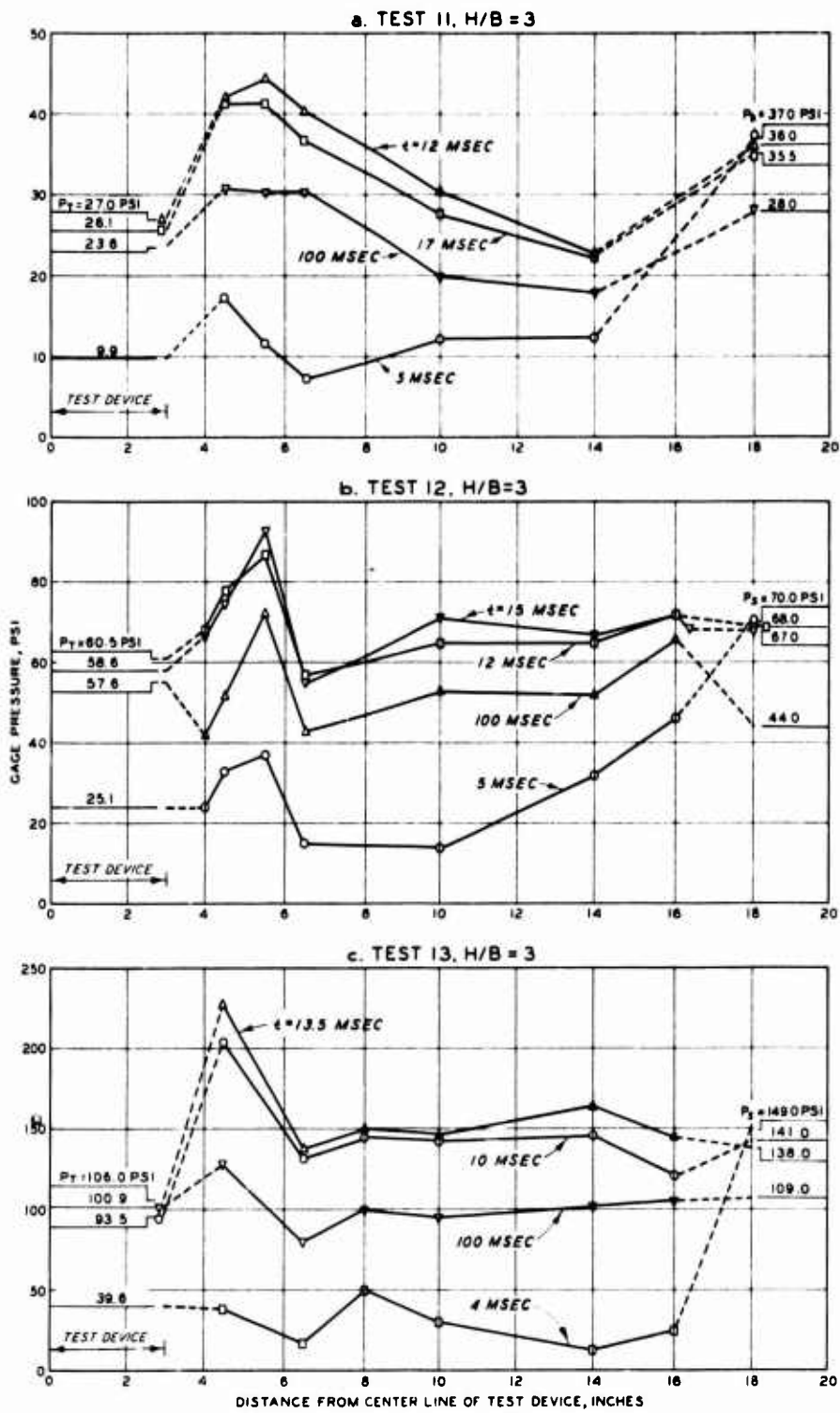


Fig. 60. Variation of vertical soil stress with time at the 35-inch level, Tests 11, 12, and 13

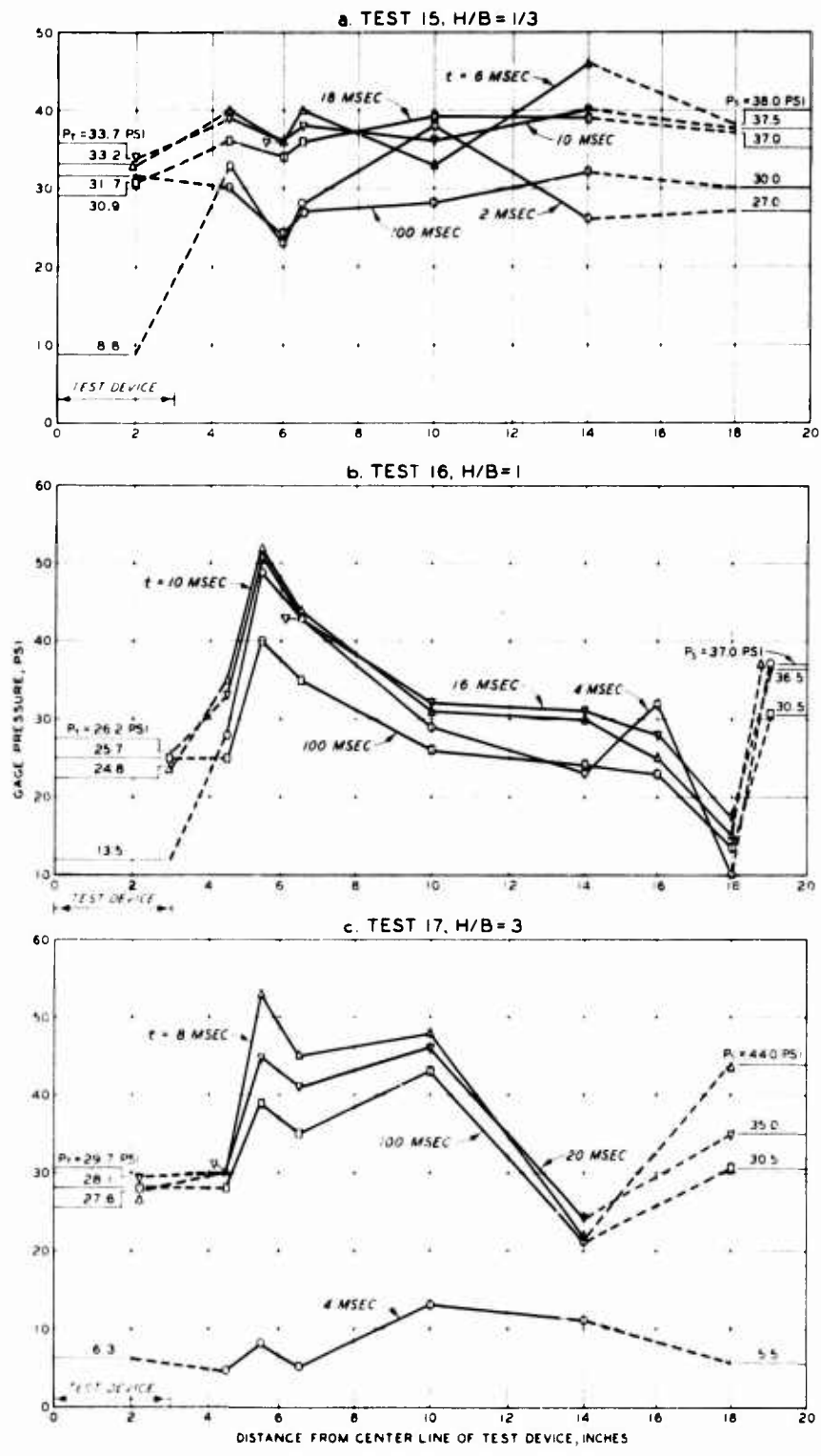


Fig. 61. Variation of vertical soil stress with time at the 35-inch level, Tests 15, 16, and 17

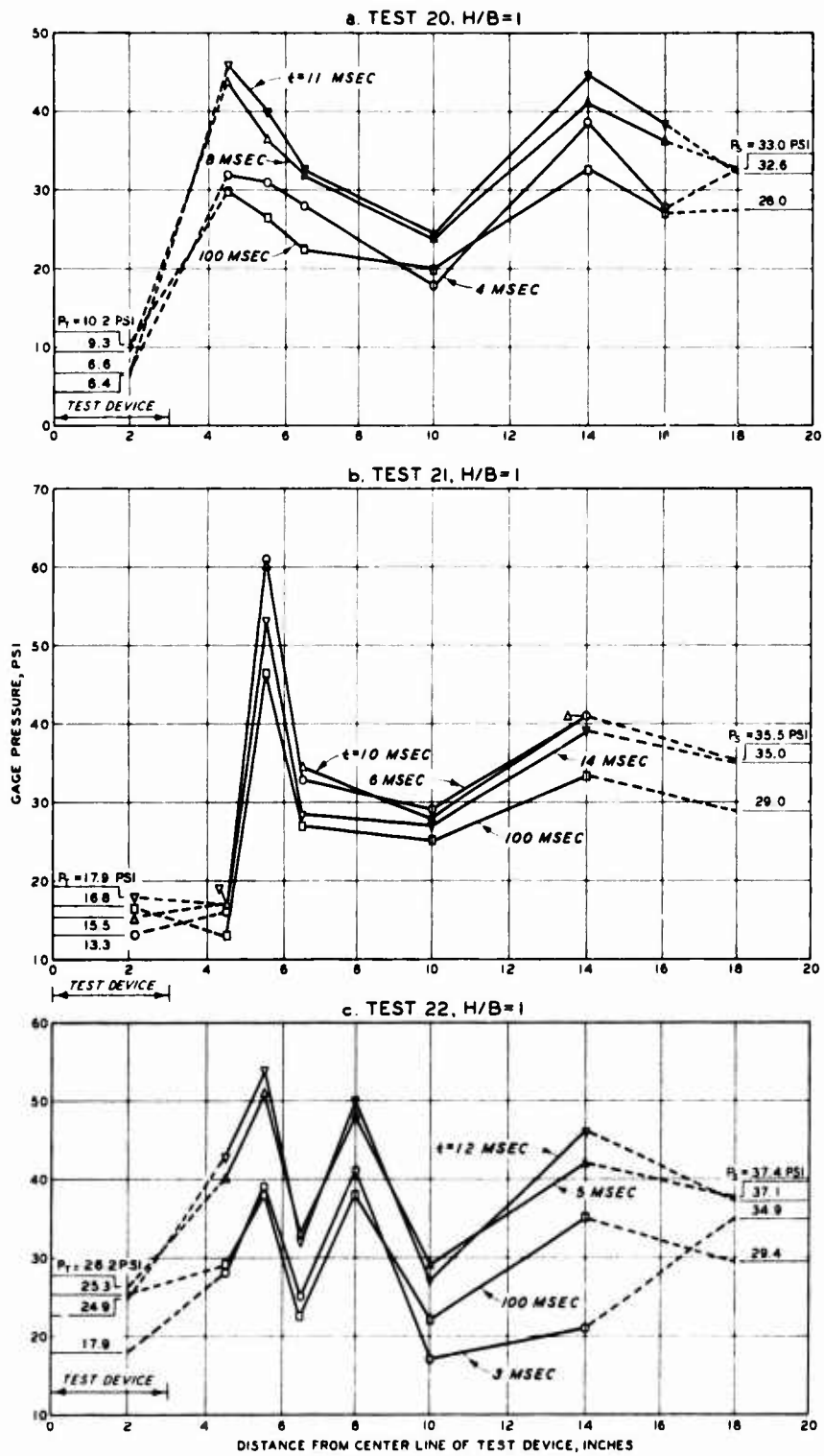


Fig. 62. Variation of vertical soil stress with time at the 35-inch level, Tests 20, 21, and 22

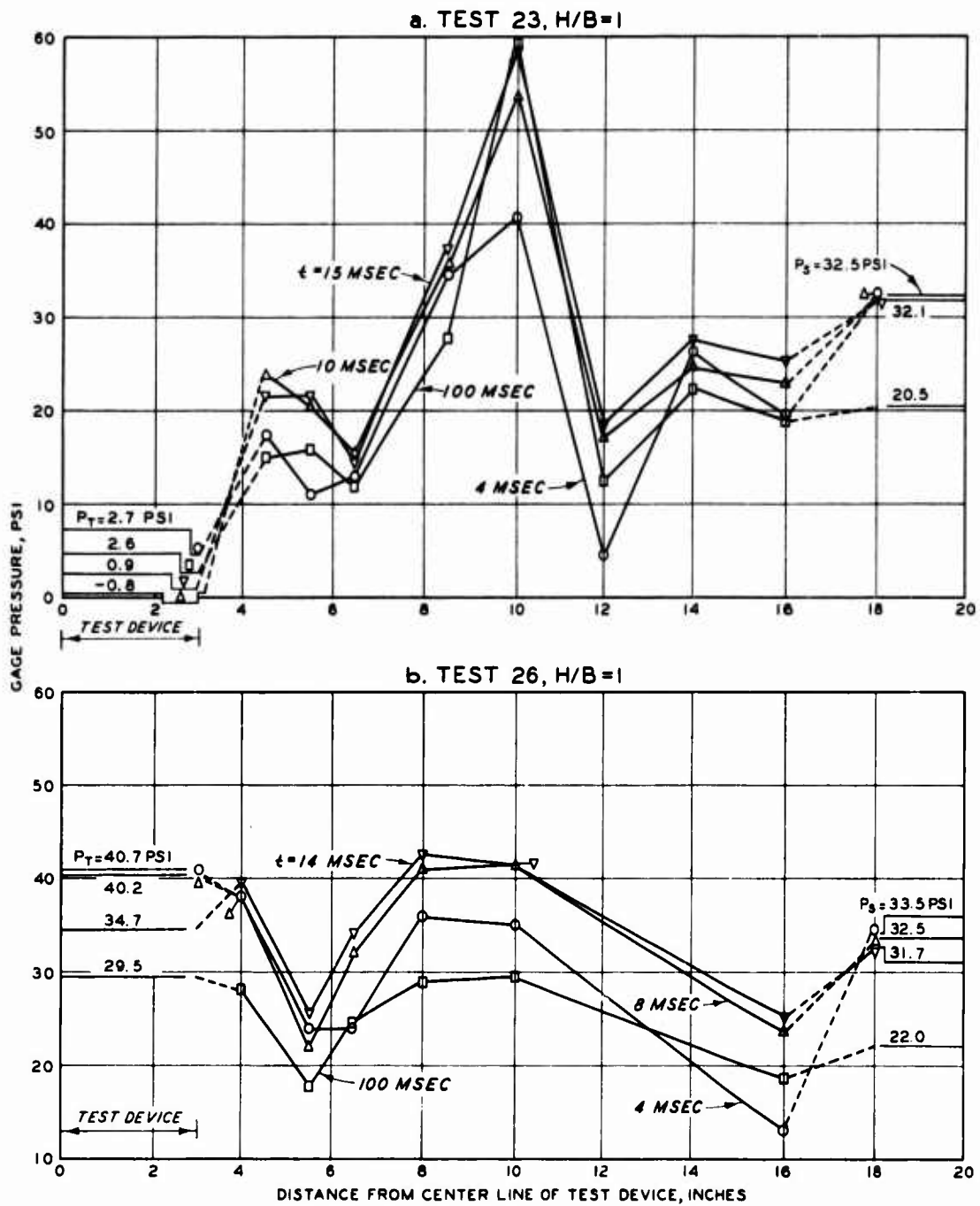


Fig. 63. Variation of vertical soil stress with time at the 35-inch level, Tests 23 and 26

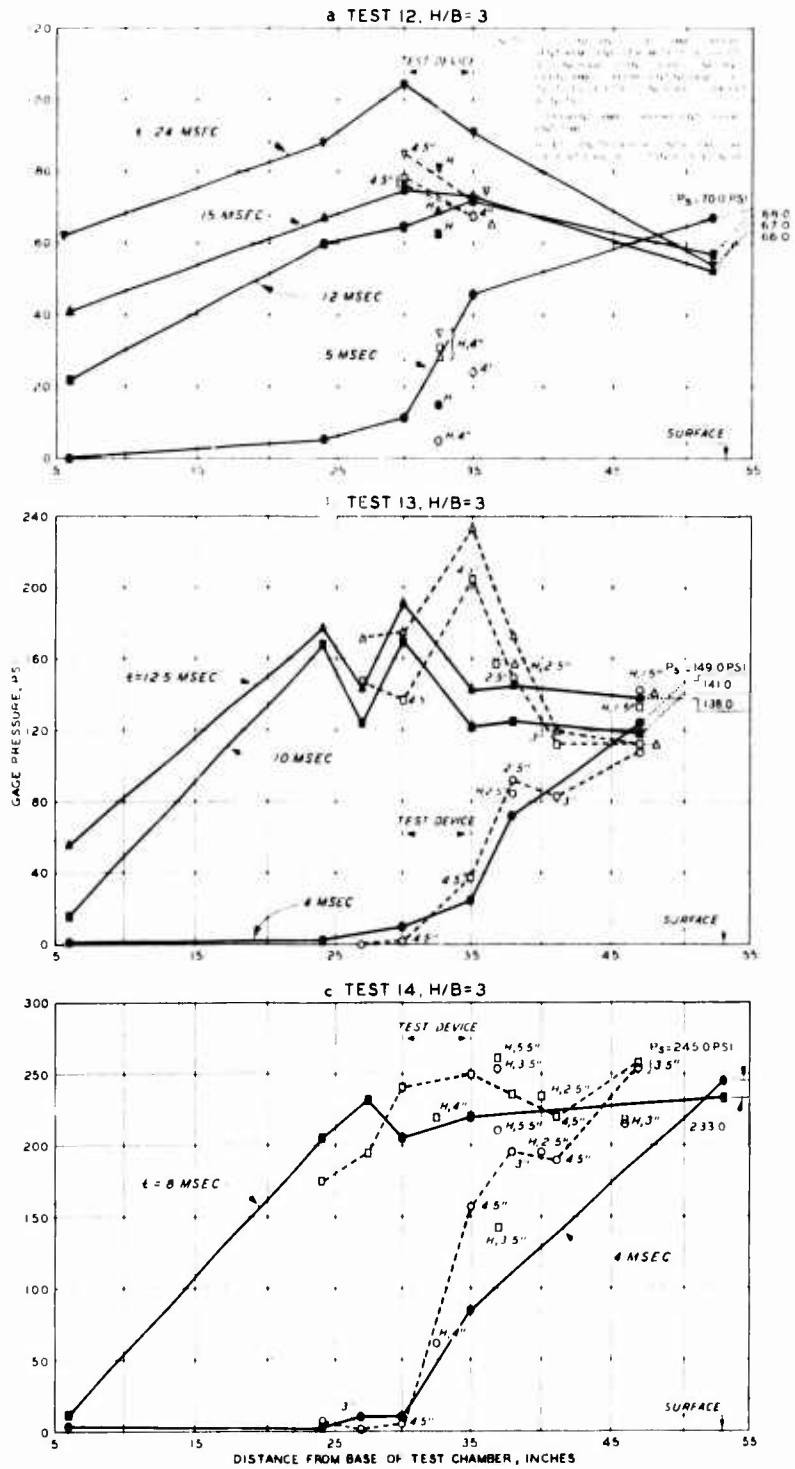


Fig. 64. Variation of soil stress with depth and time, Tests 12, 13, and 14

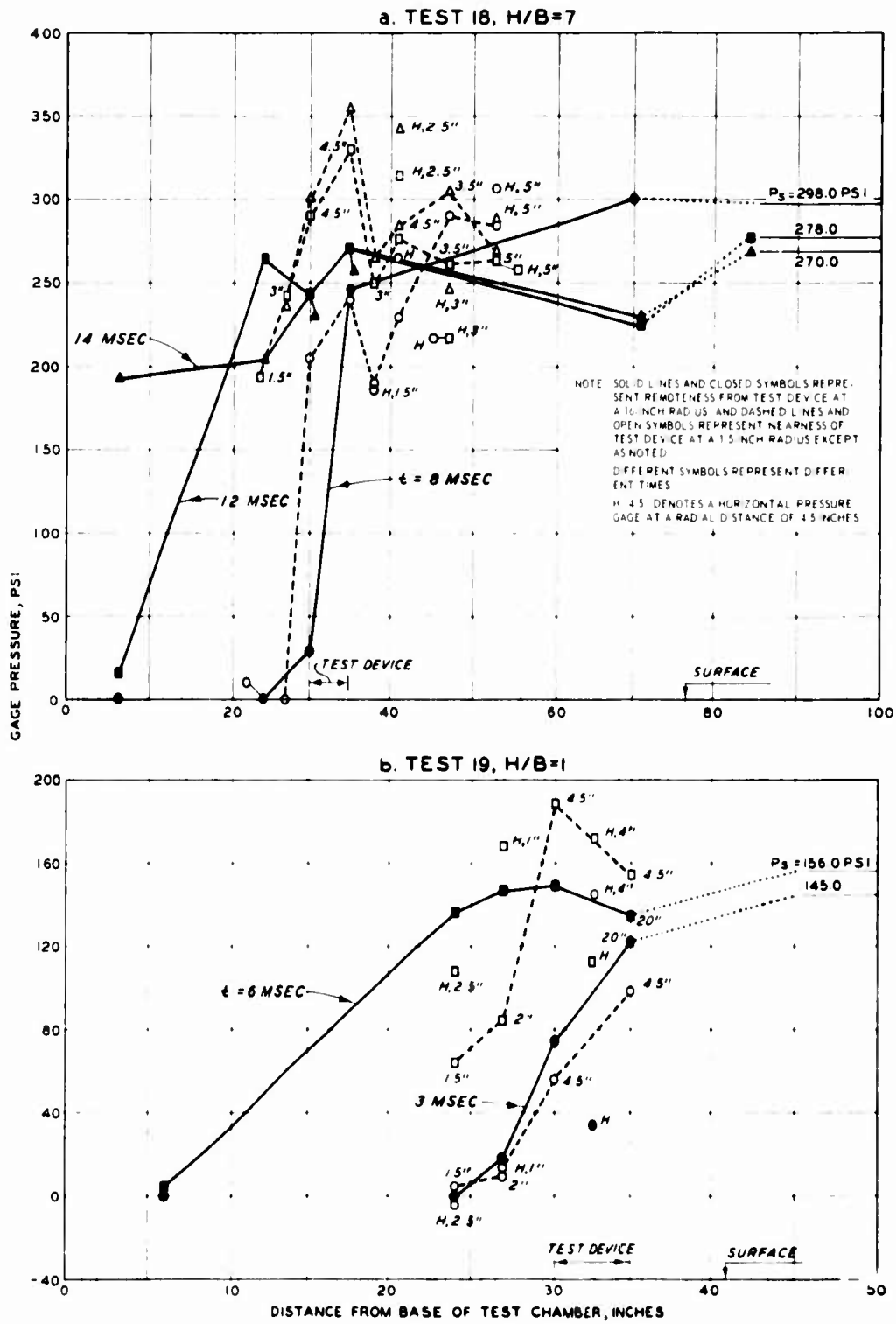


Fig. 65. Variation of soil stress with depth and time, Tests 18 and 19

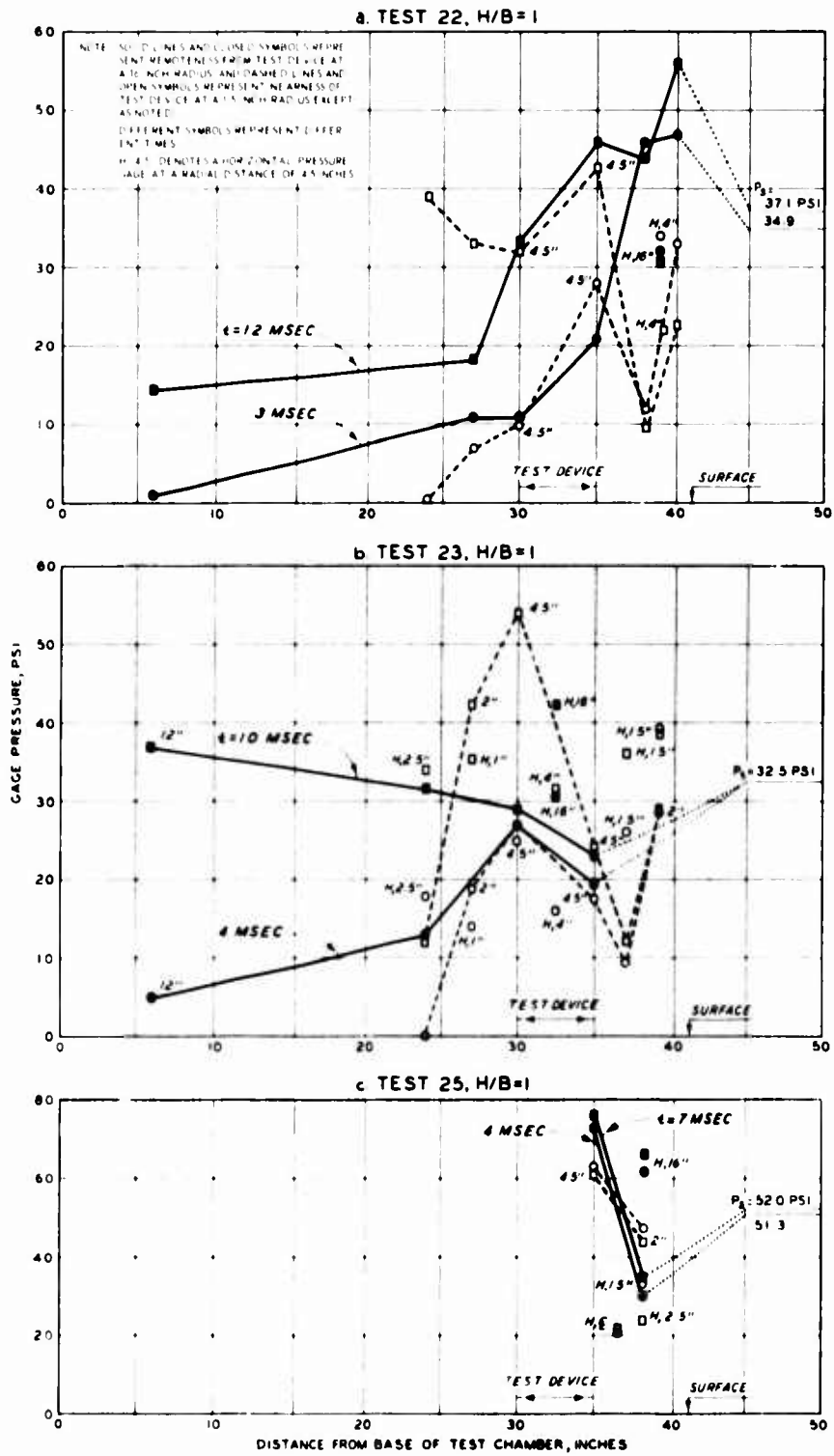


Fig. 66. Variation of soil stress with depth and time, Tests 22, 23, and 25

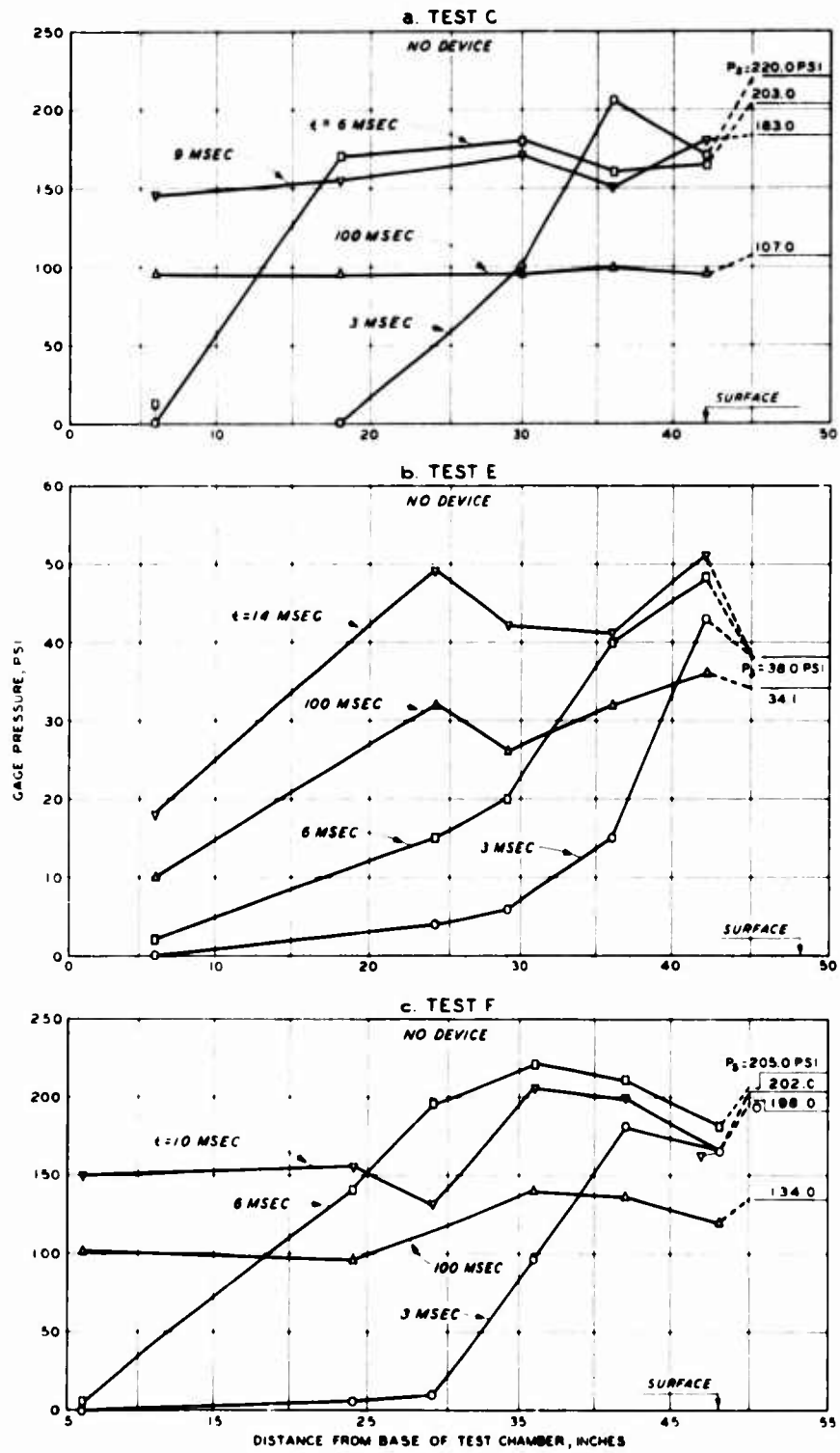


Fig. 67. Variation of soil stress with depth and time, preliminary Tests C, E, and F

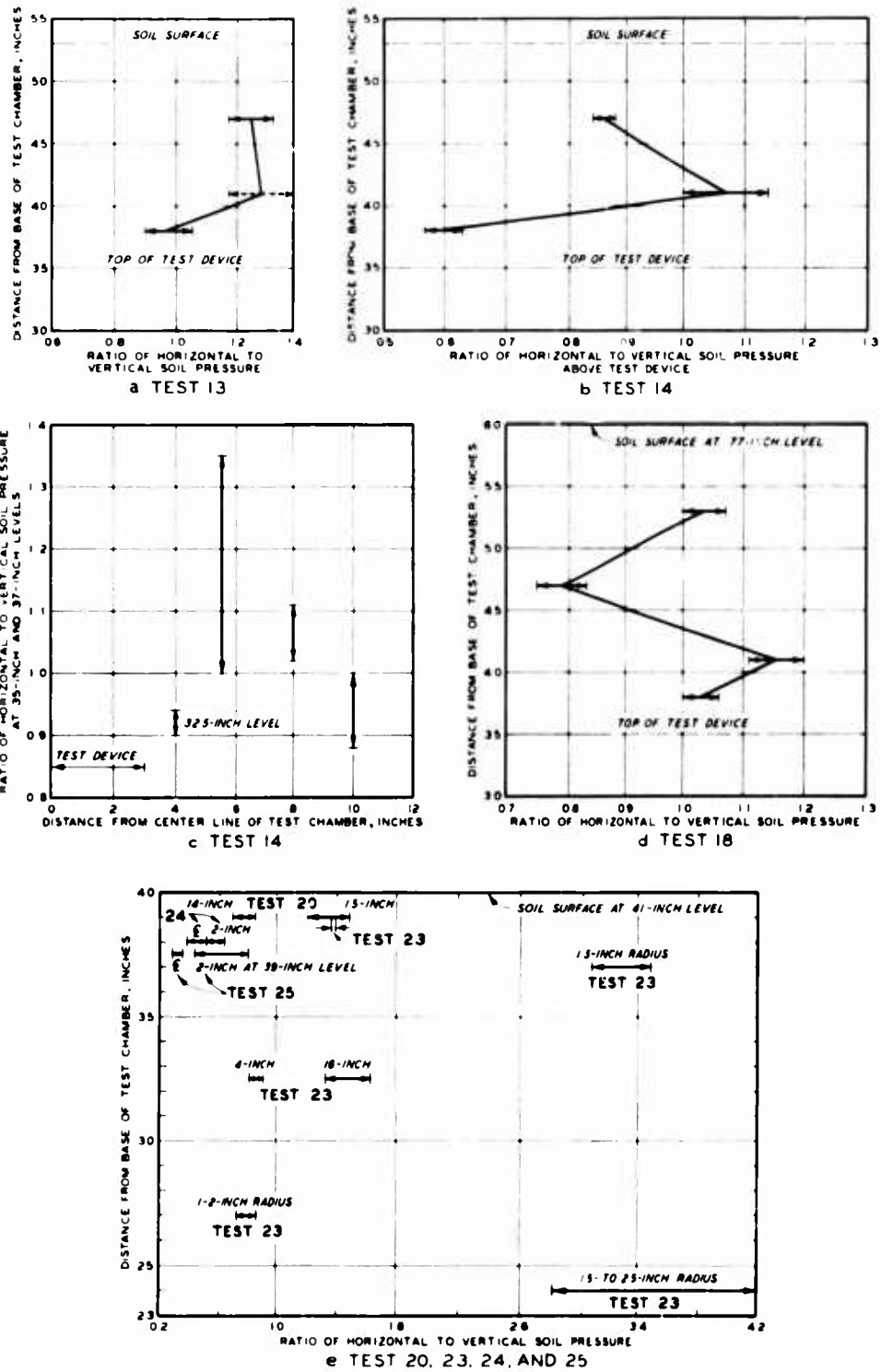


Fig. 68. Variation of horizontal-to-vertical pressure ratio, Tests 13, 14, 18, 20, 23, 24, and 25

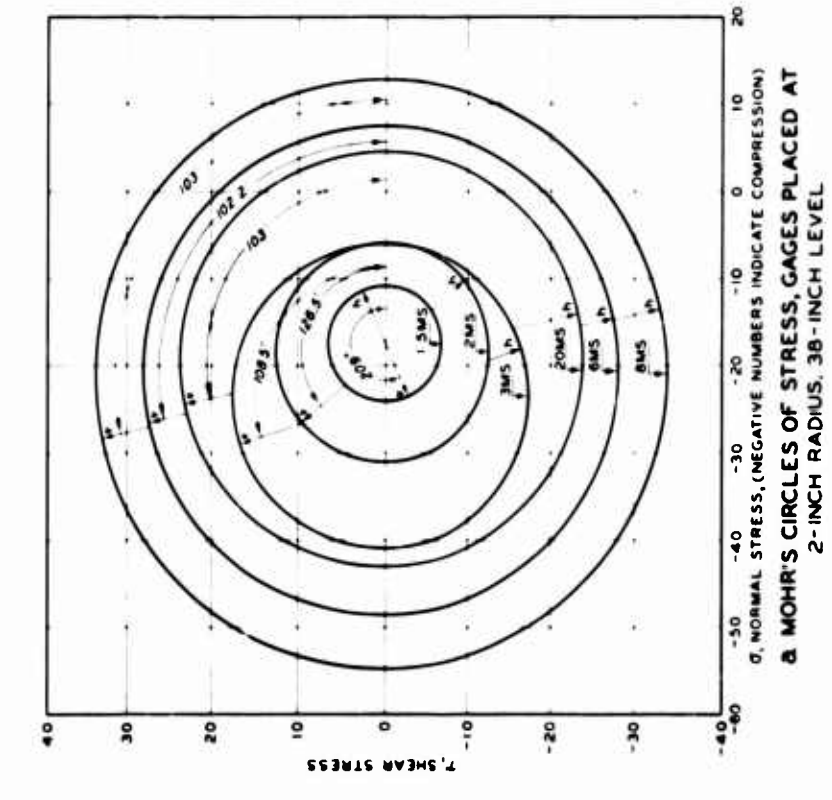
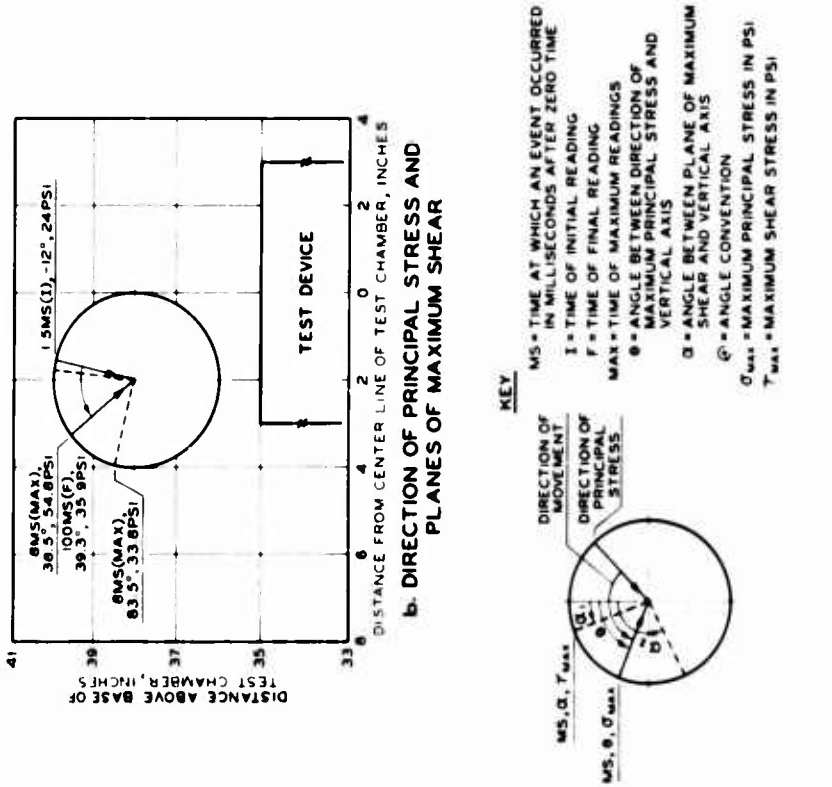
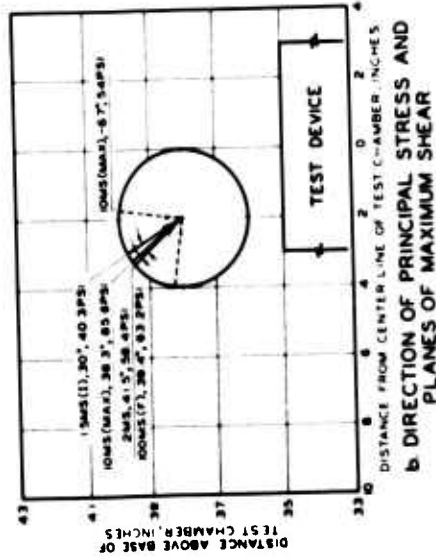
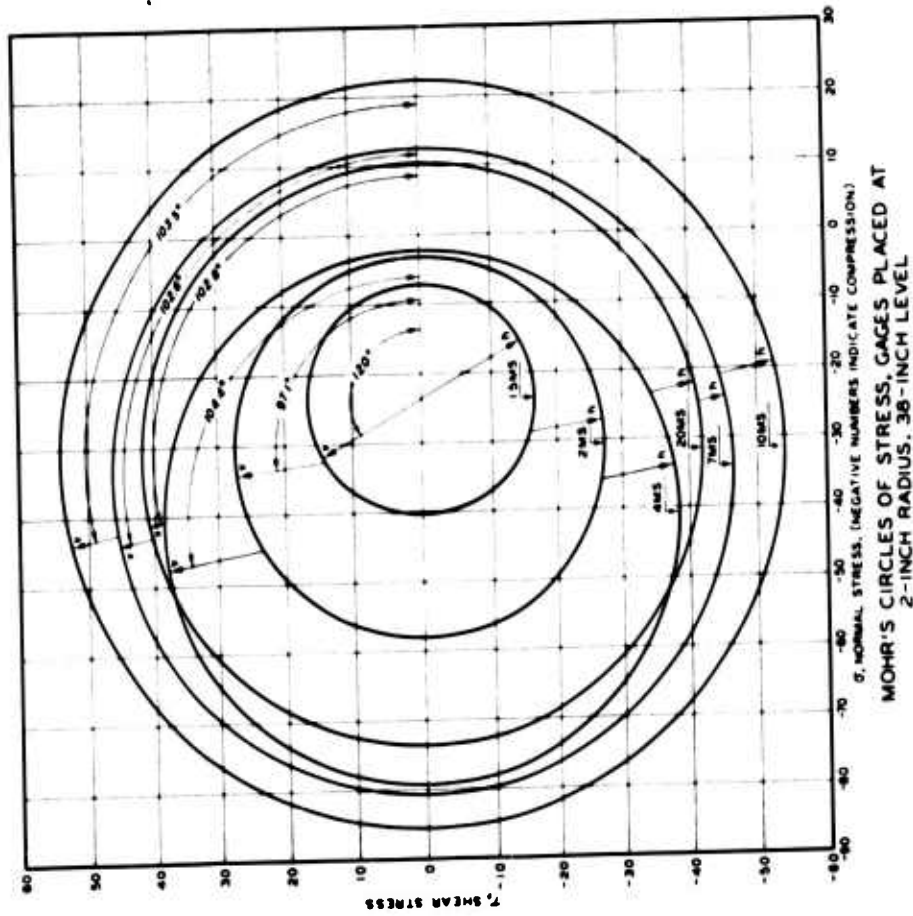


Fig. 69. Determination of direction and magnitude of principal stress, Test 24



KEY

- MS = TIME AT WHICH AN EVENT OCCURRED IN MILLISECONDS AFTER ZERO TIME
- I = TIME OF INITIAL READING
- F = TIME OF FINAL READING
- MAX = TIME OF MAXIMUM READINGS
- θ = ANGLE BETWEEN DIRECTION OF MAXIMUM PRINCIPAL STRESS AND VERTICAL AXIS
- α = ANGLE BETWEEN PLANE OF MAXIMUM SHEAR AND VERTICAL AXIS
- σ = ANGLE CONVENTION
- σ_{MAX} = MAXIMUM PRINCIPAL STRESS IN PSI
- τ_{MAX} = MAXIMUM SHEAR STRESS IN PSI

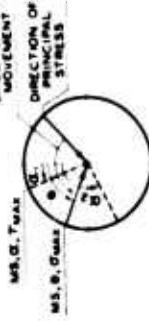


Fig. 70. Determination of direction and magnitude of principal stress, Test 25

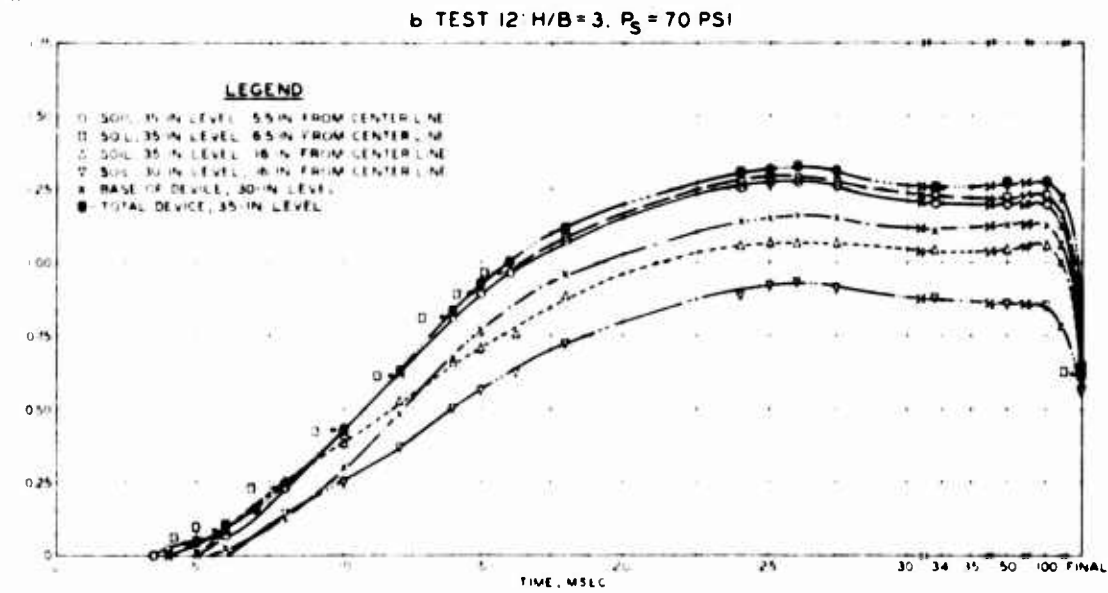
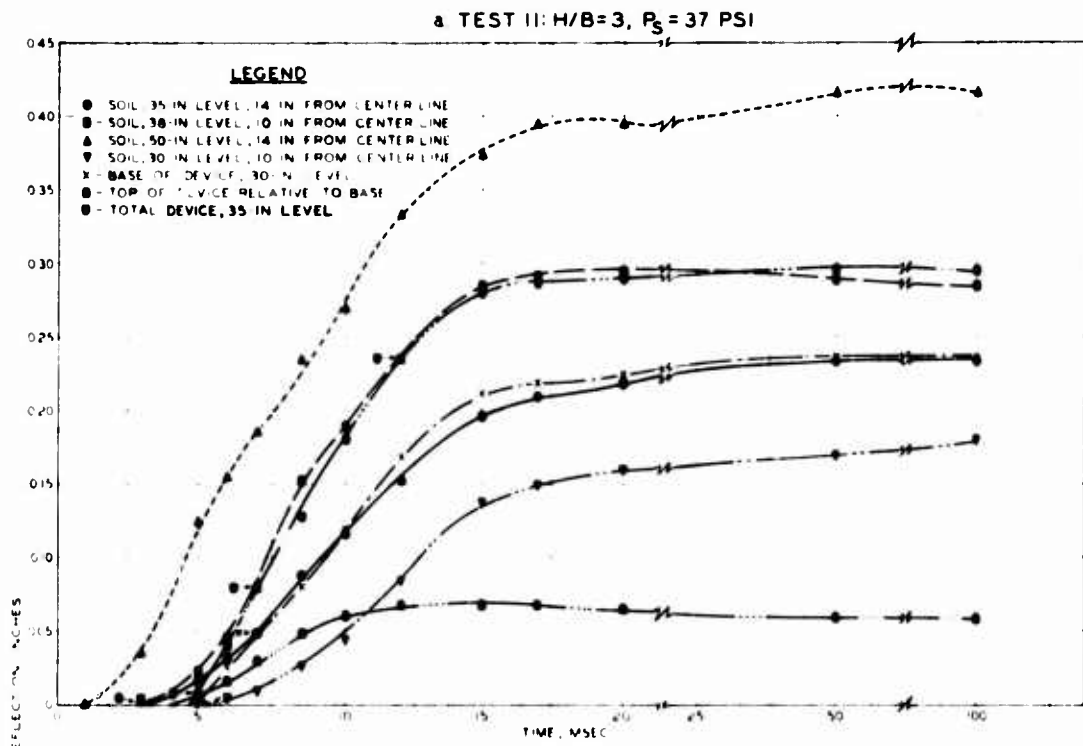


Fig. 71. Soil and structure deflection versus time, Tests 11 and 12

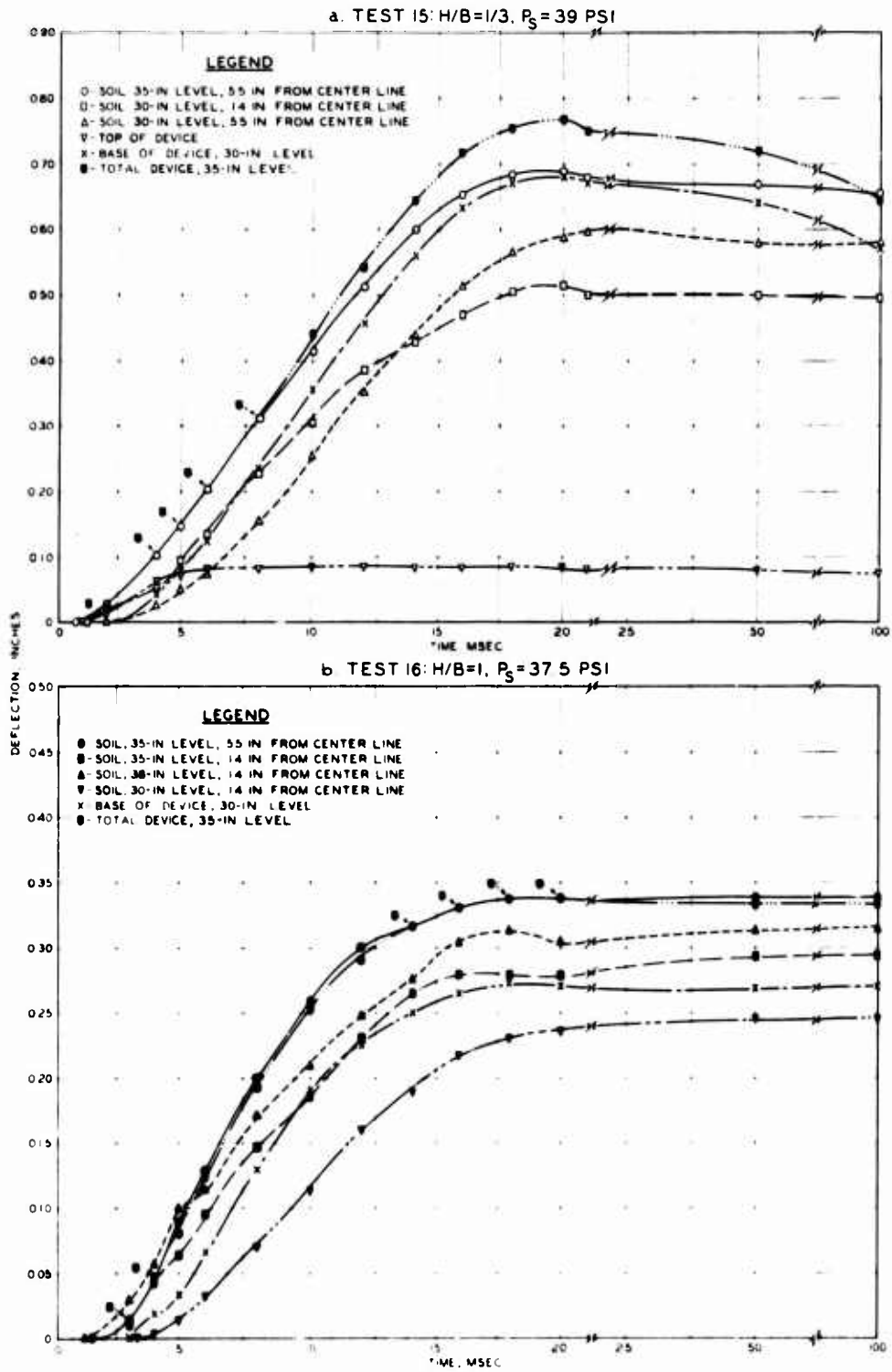


Fig. 72. Soil and structure deflection versus time, Tests 15 and 16

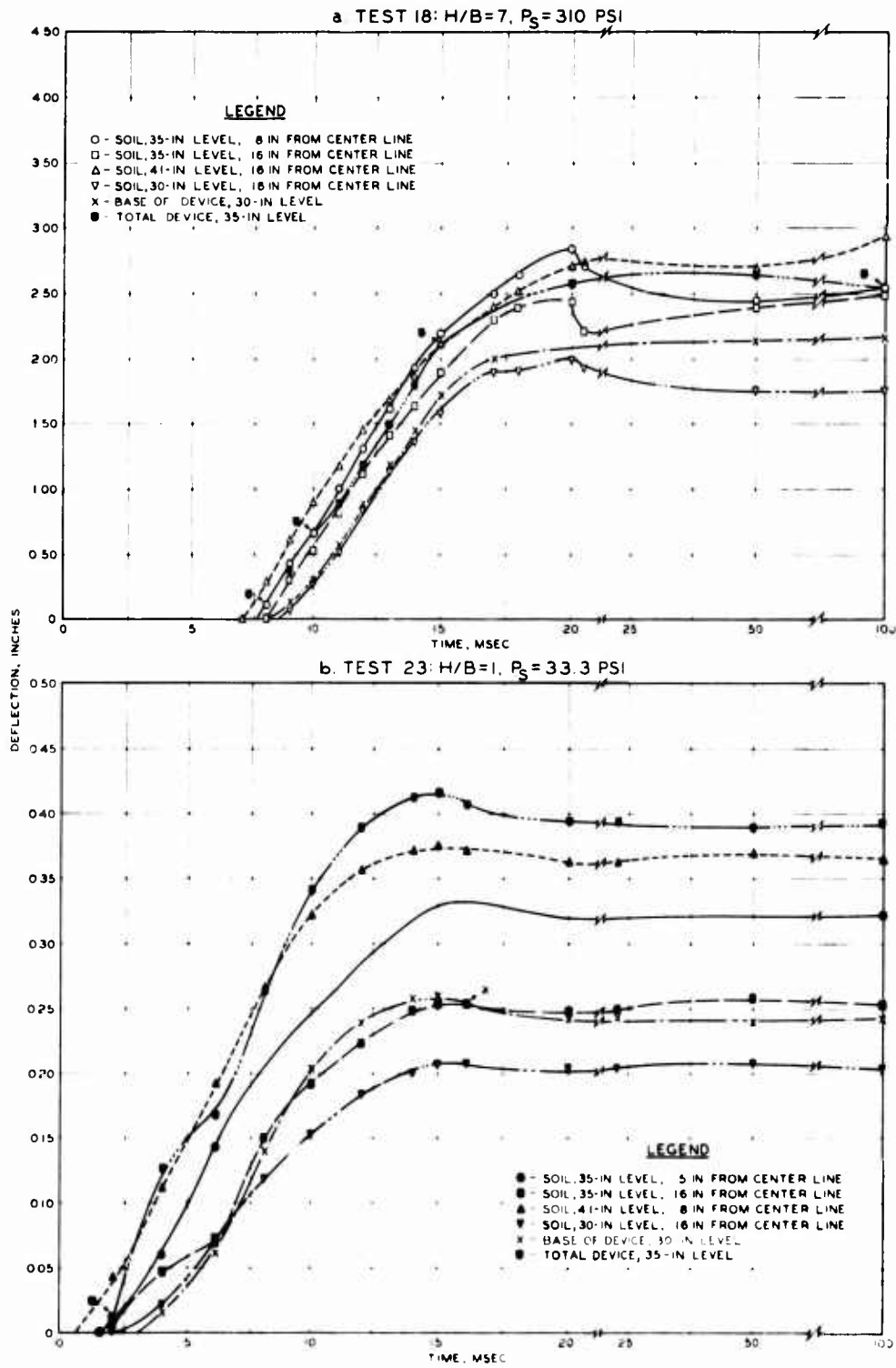


Fig. 73. Soil and structure deflection versus time, Tests 18 and 23

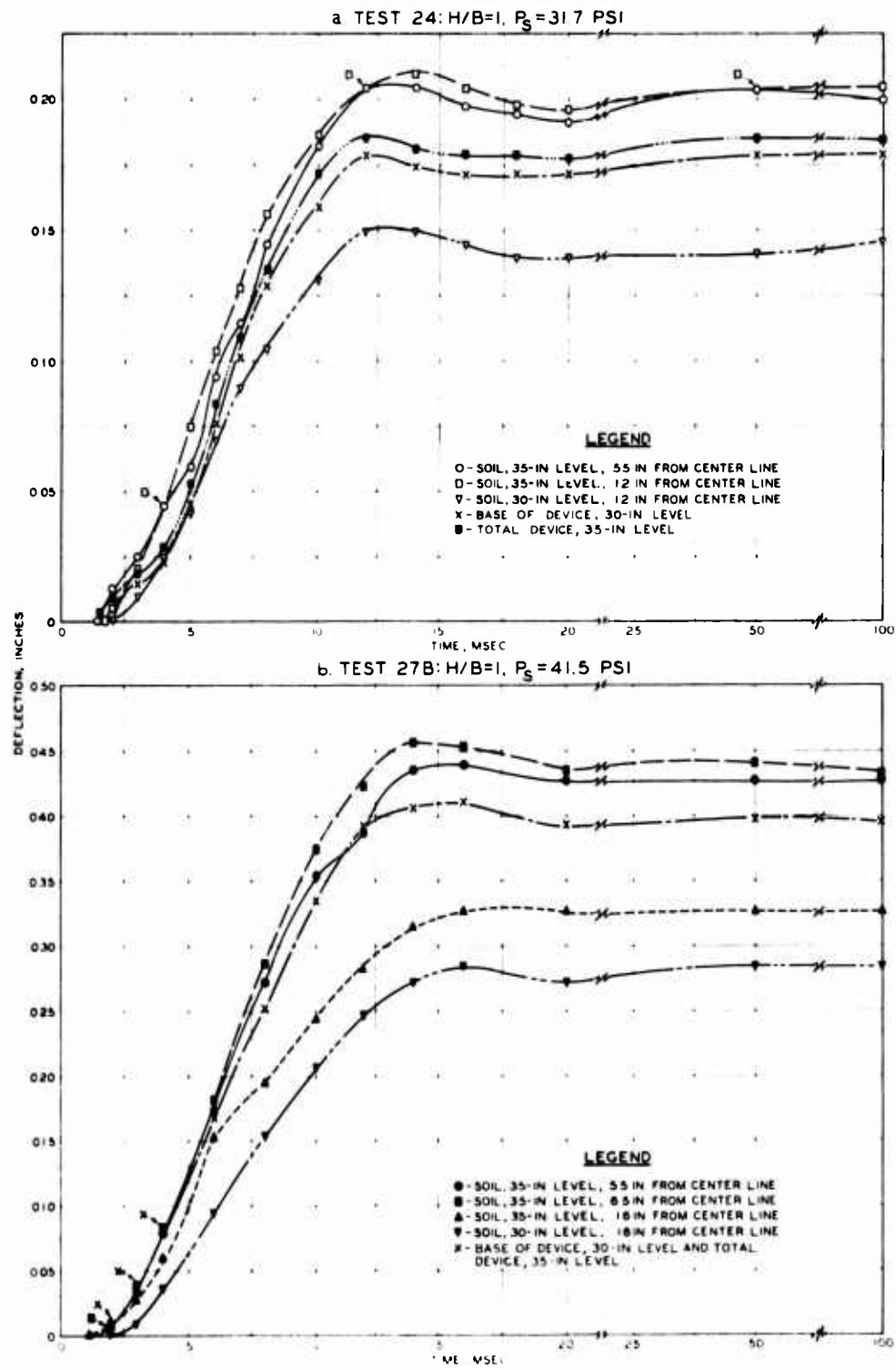


Fig. 74. Soil and structure deflection versus time, Tests 24 and 27B

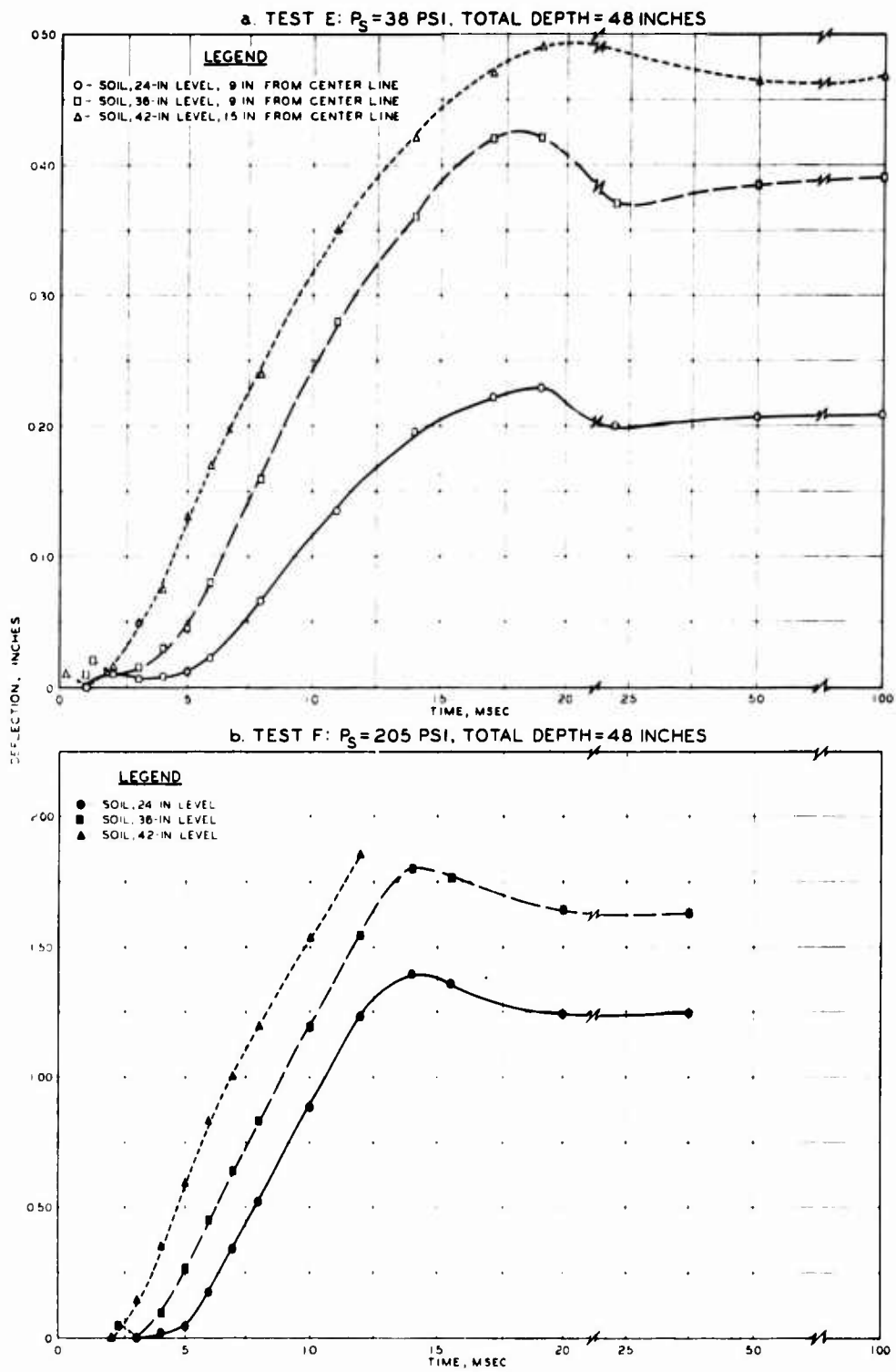


Fig. 75. Soil deflection versus time, preliminary Tests E and F

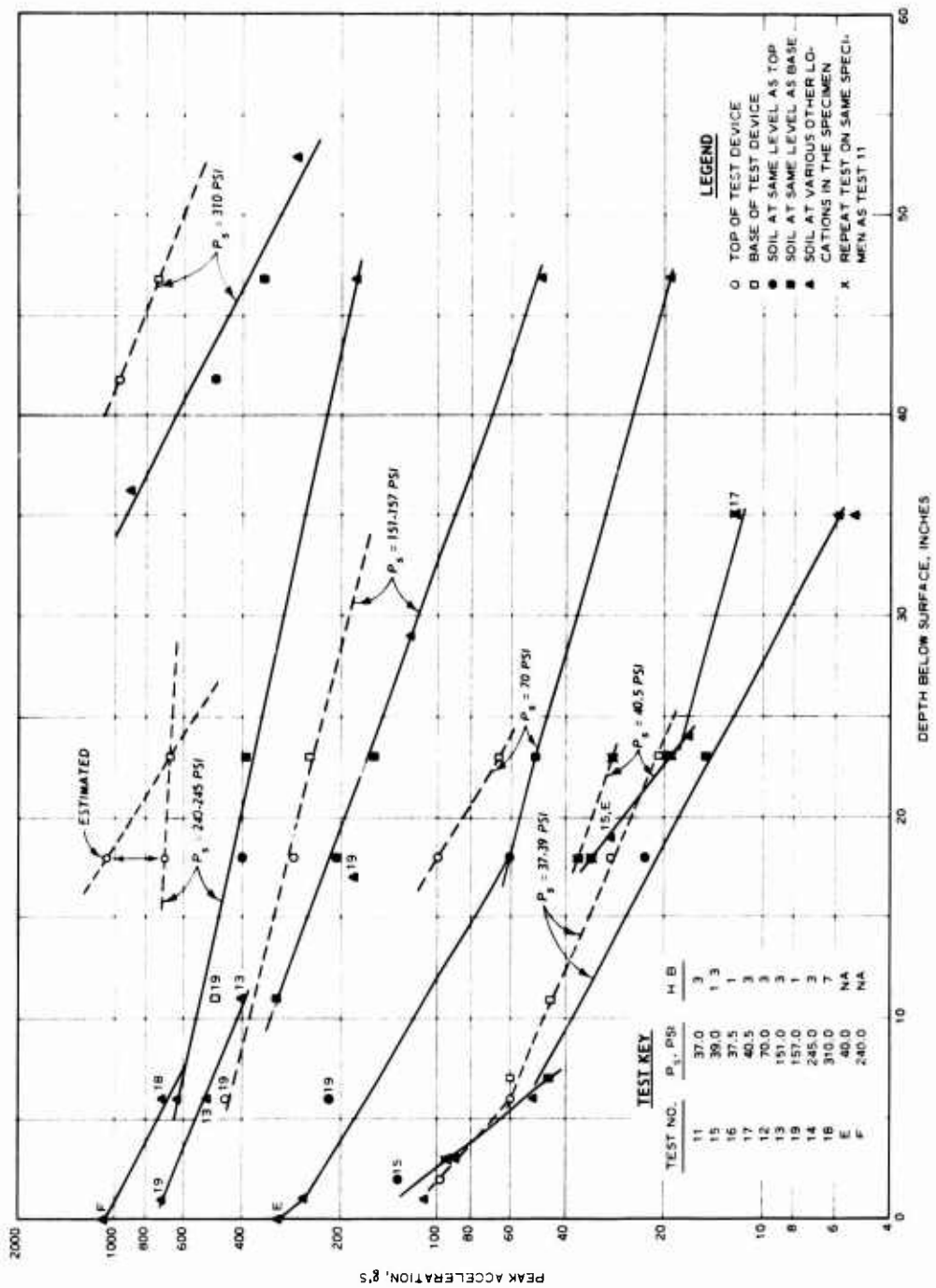
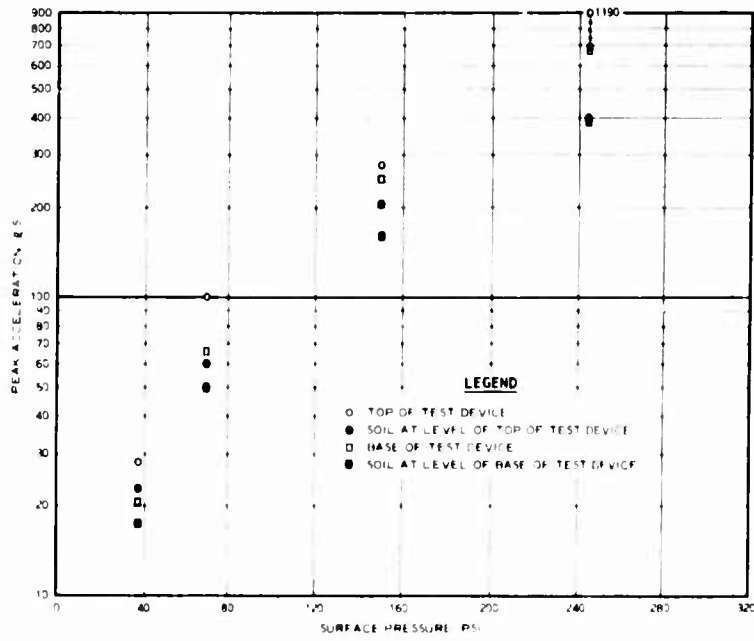
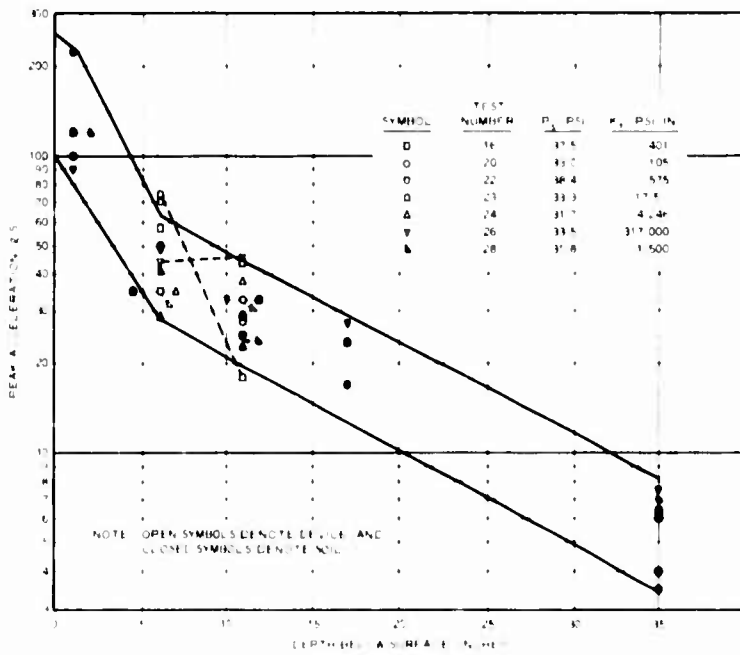


Fig. 76. Variation of soil and structure acceleration with changes in surface pressure and depth of burial at a relatively constant structural stiffness



a. Variation with change in surface pressure at constant depth of burial; Tests 11, 12, 13, and 14; $H/B = 3$



b. Variation with change in structure stiffness; $H/B = 1$, $P_s \approx 32$ to 38 psi

Fig. 77. Variation of soil and structure acceleration with surface pressure and structure stiffness

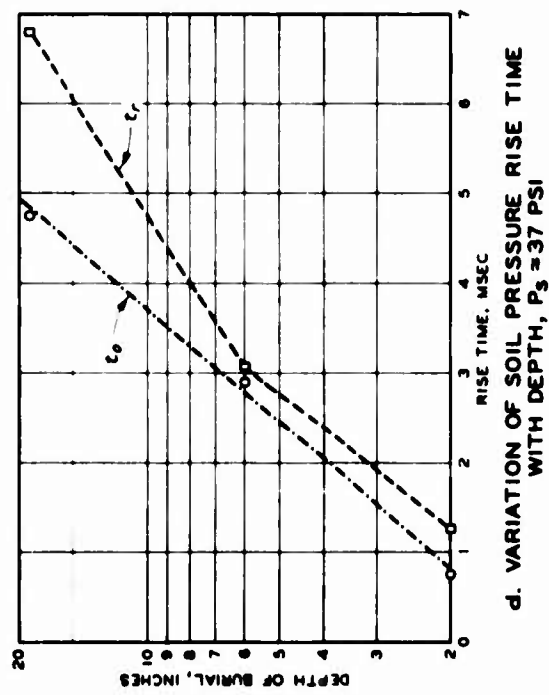
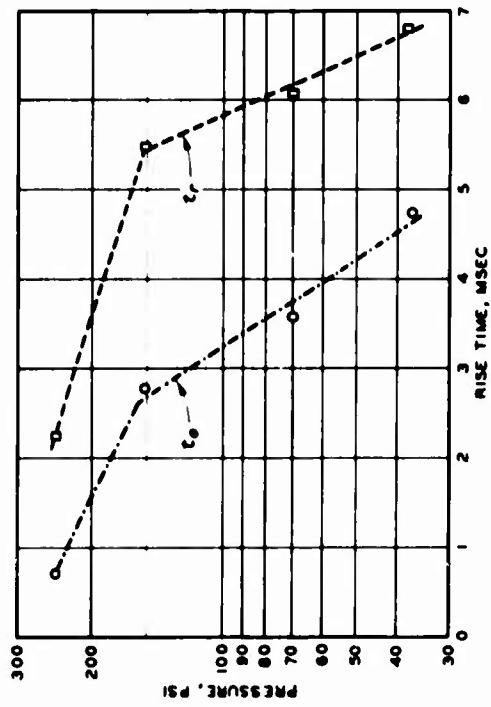
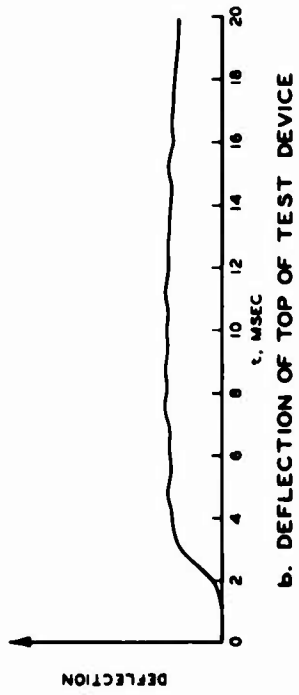


Fig. 78. Rise time data

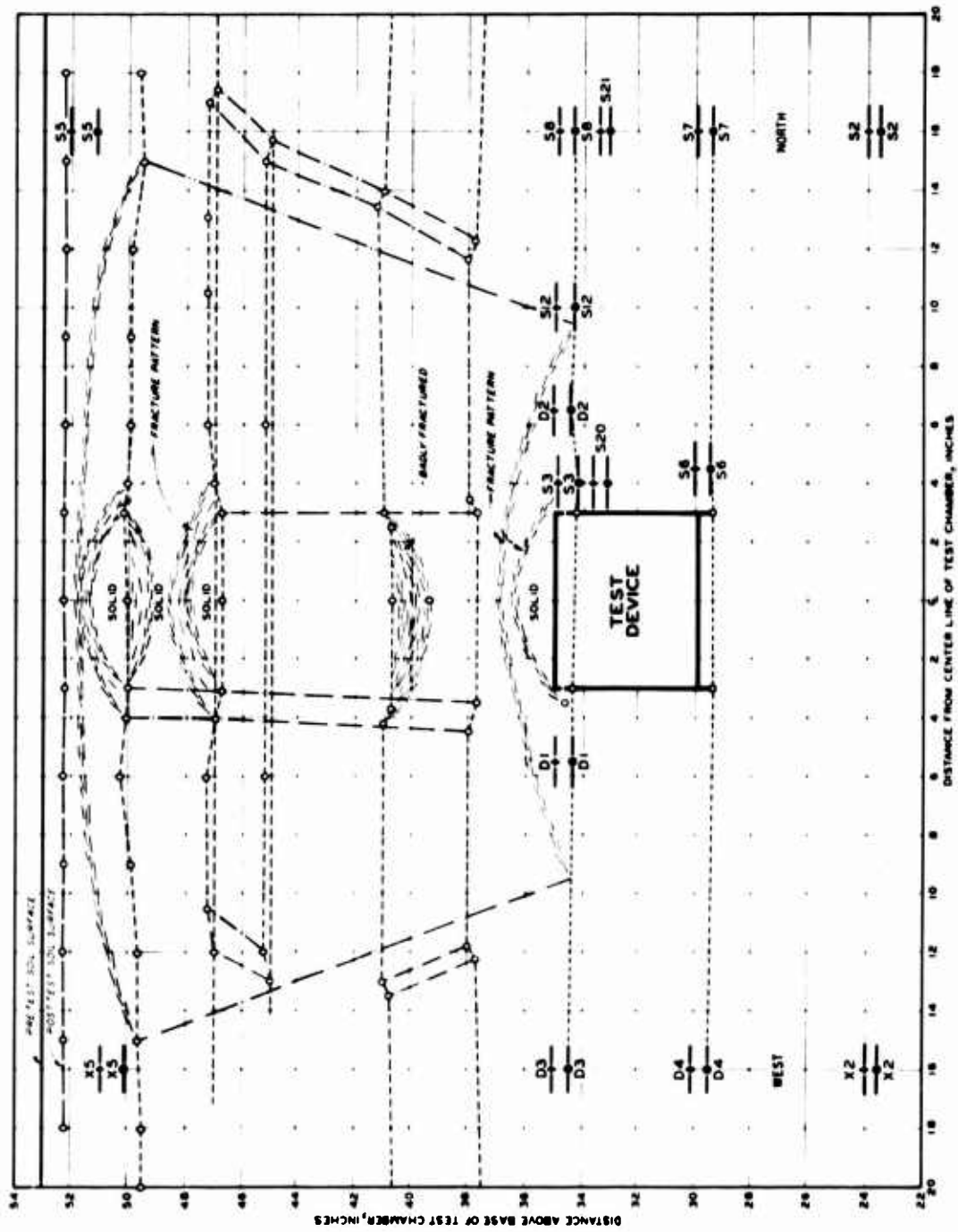
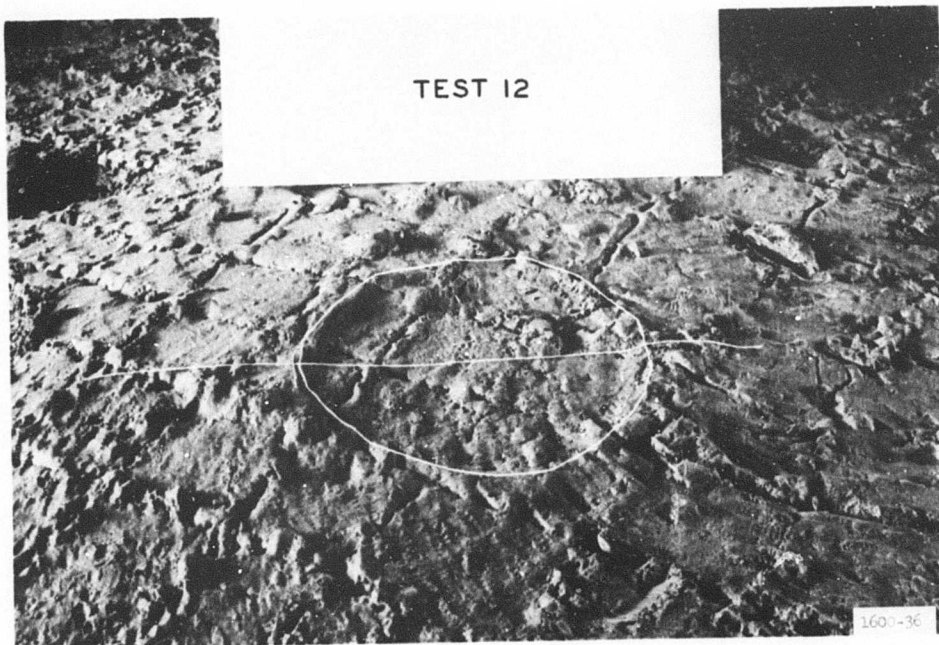
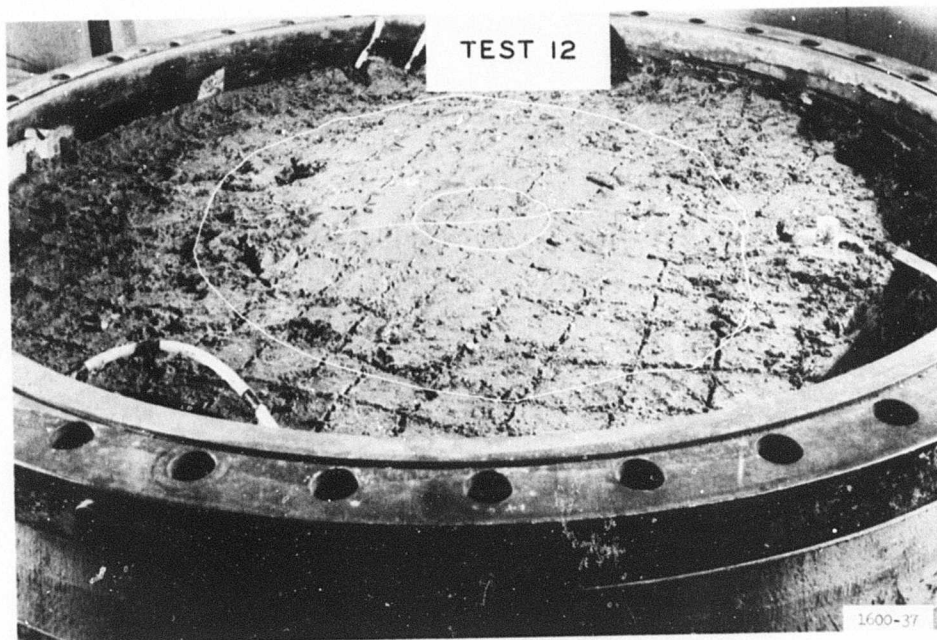


Fig. 79. Cross section of soil deformations, Test 12; $H/B = 3$, $P_s = 70$ psi

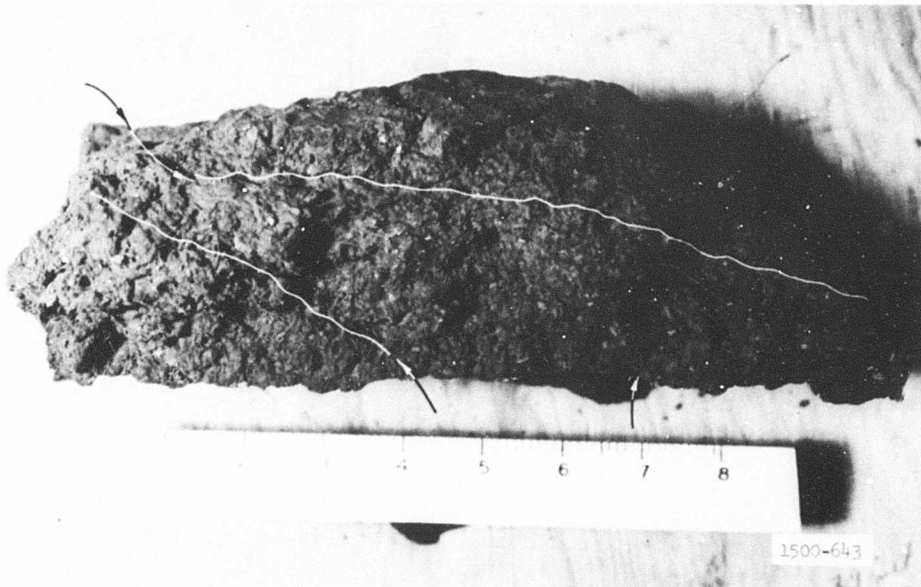


a. Oblique view of soil surface

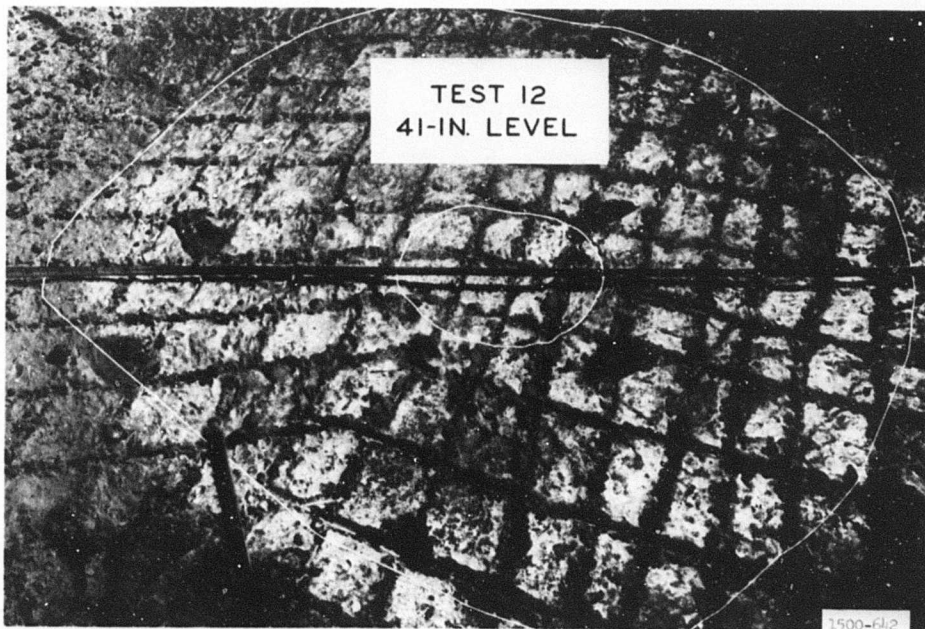


b. Oblique view of depression

Fig. 80. Hump and depression at 50-inch level of Test 12



a. Cross-section view of broken soil layer



b. Oblique view of soil surface

Fig. 81. Views of a soil cross section and the soil surface at 41-inch level, Test 12

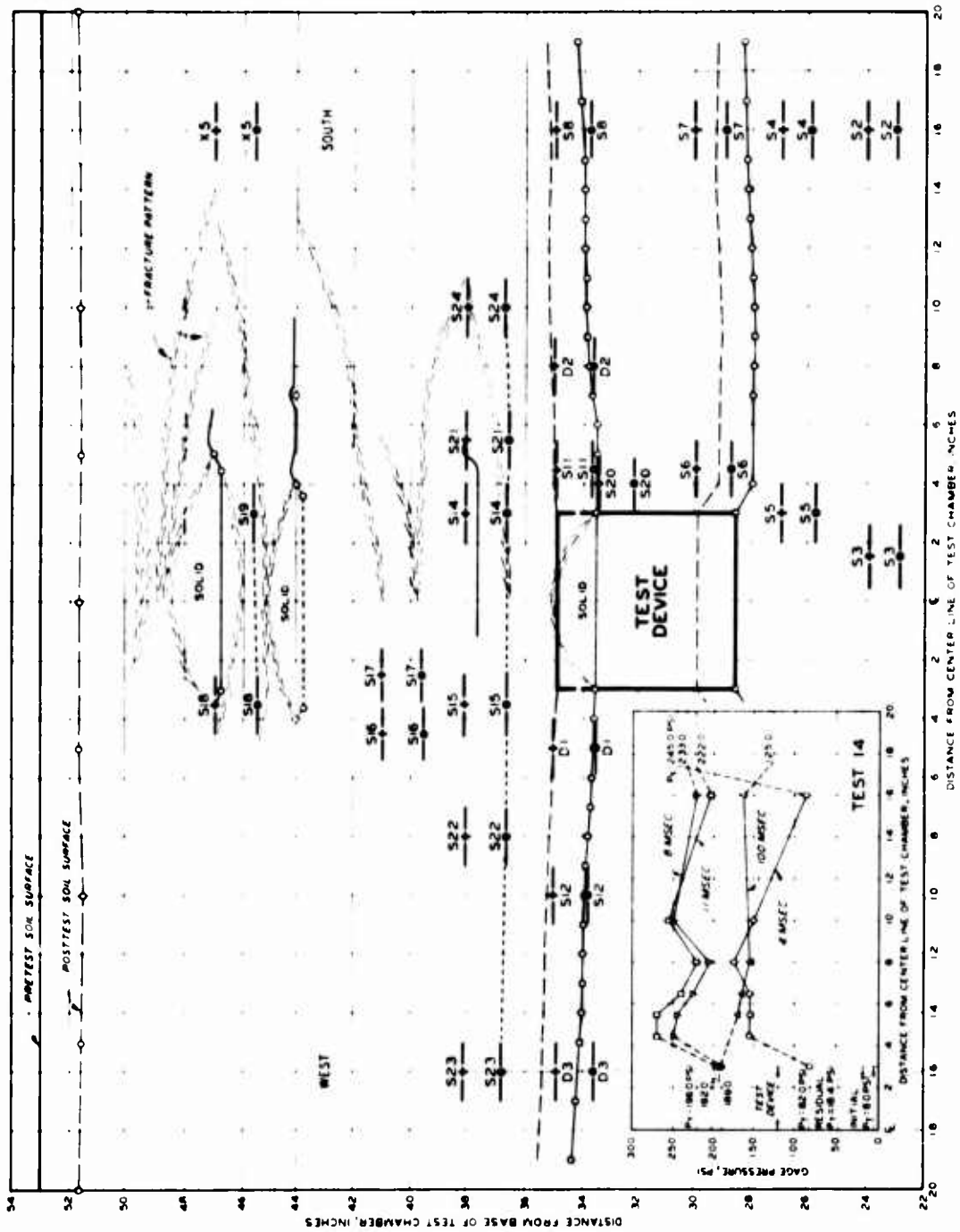


Fig. 82. Cross section of soil deformations, Test 14; $H/B = 3$, $P_S = 245$ psi

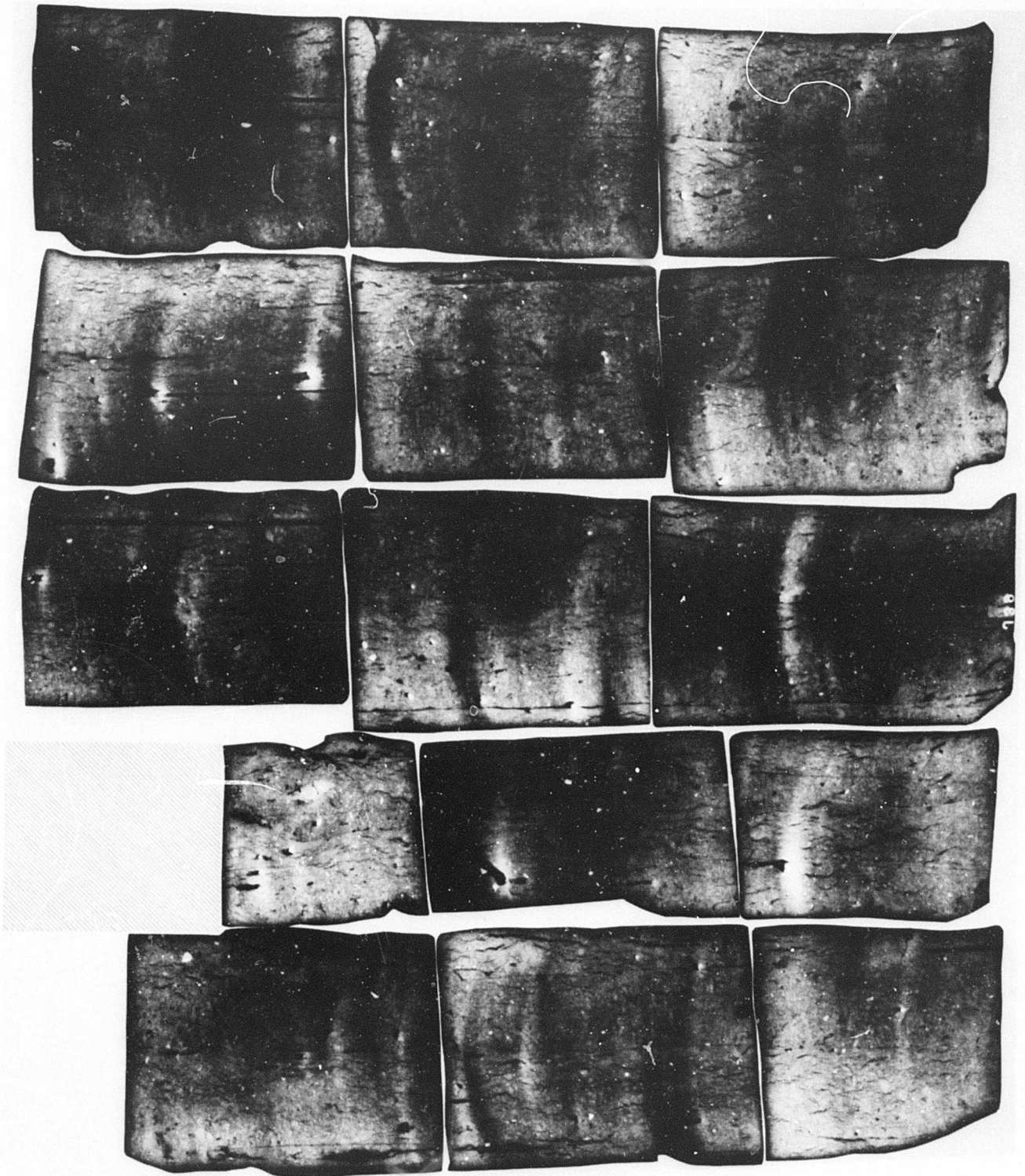
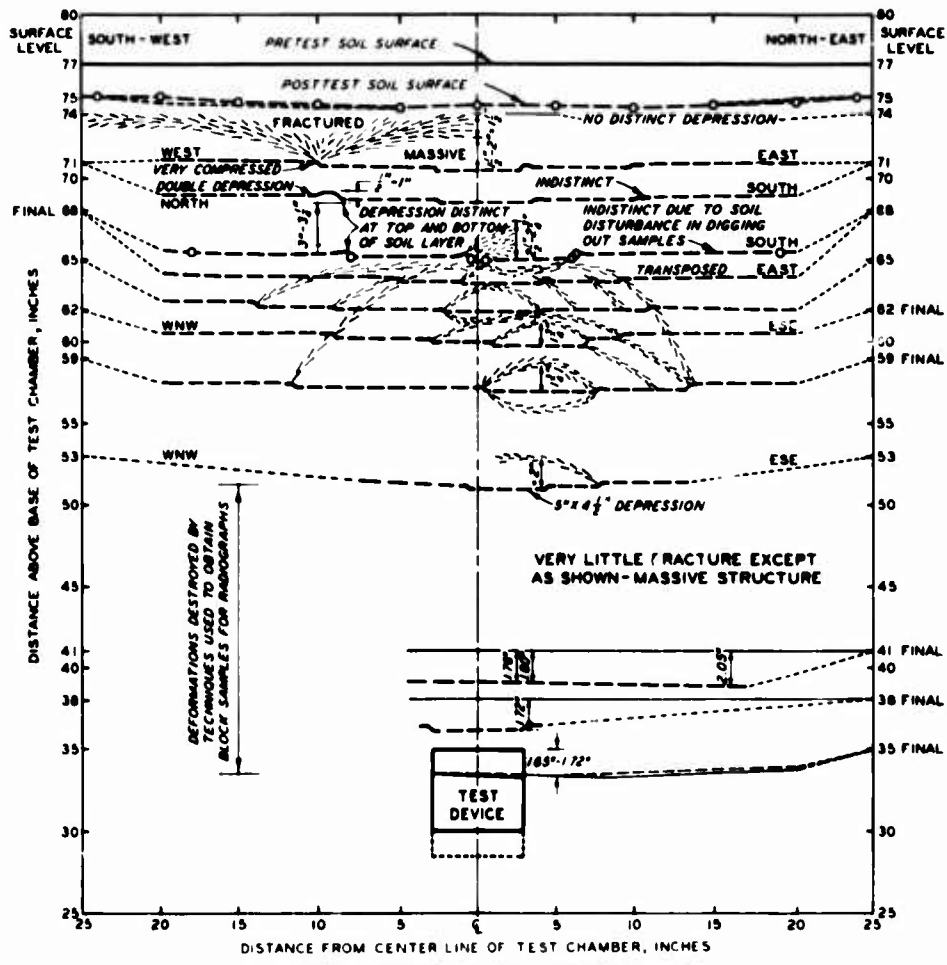
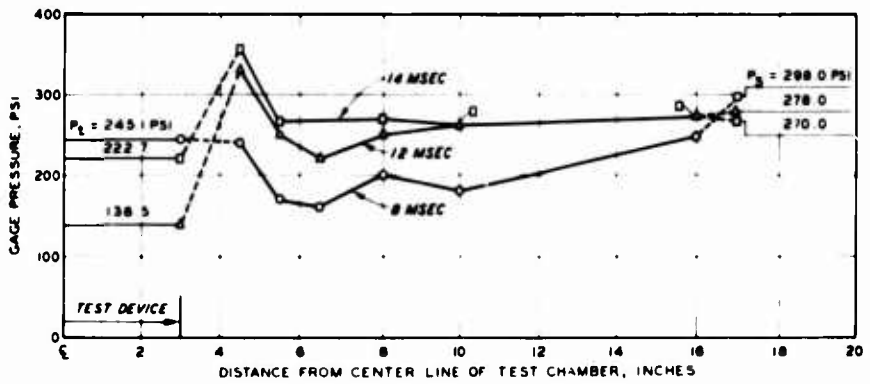


Fig. 83. Radiograph of soil deformation pattern, Test 14;
 $H/B = 3$, $P_S = 245$ psi

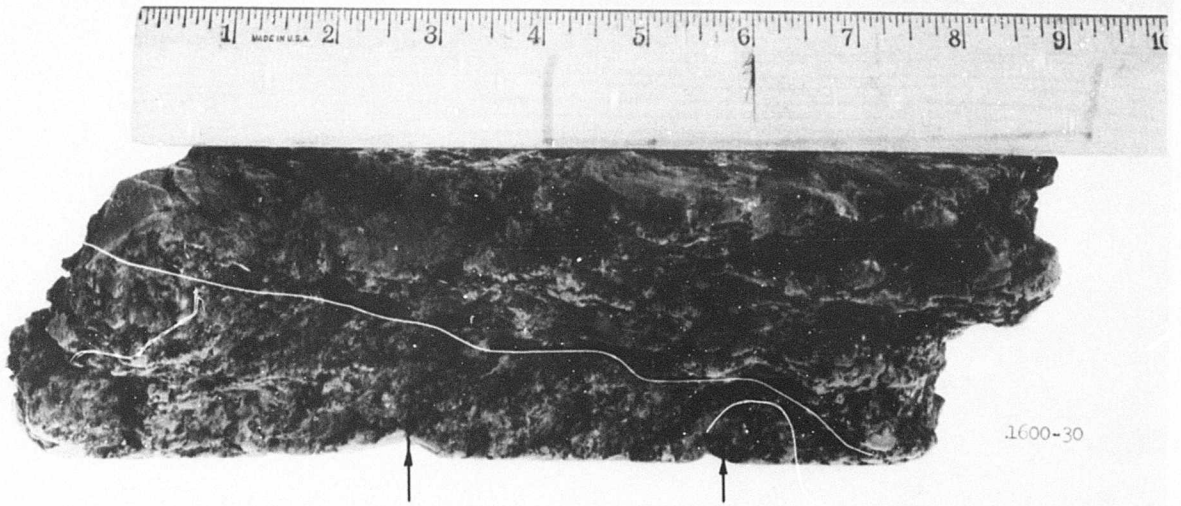


a. CROSS SECTION OF SOIL DEFORMATIONS

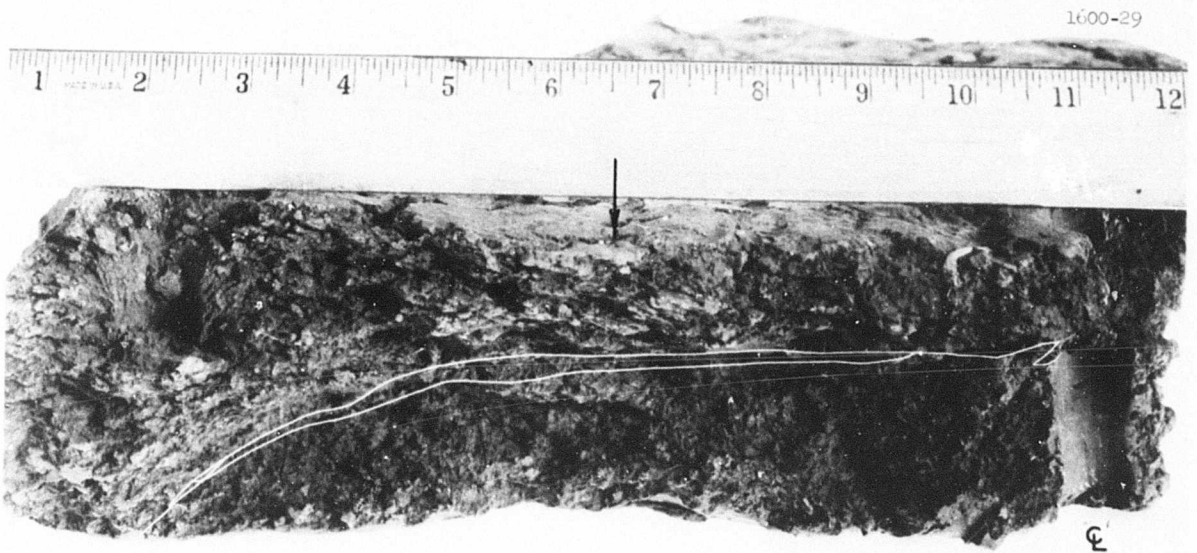


b. VARIATION OF SOIL STRESS WITH TIME AT THE 35-INCH LEVEL

Fig. 84. Cross section of soil deformations, Test 18;
 $H/B = 7$, $P_S = 310 \text{ psi}$

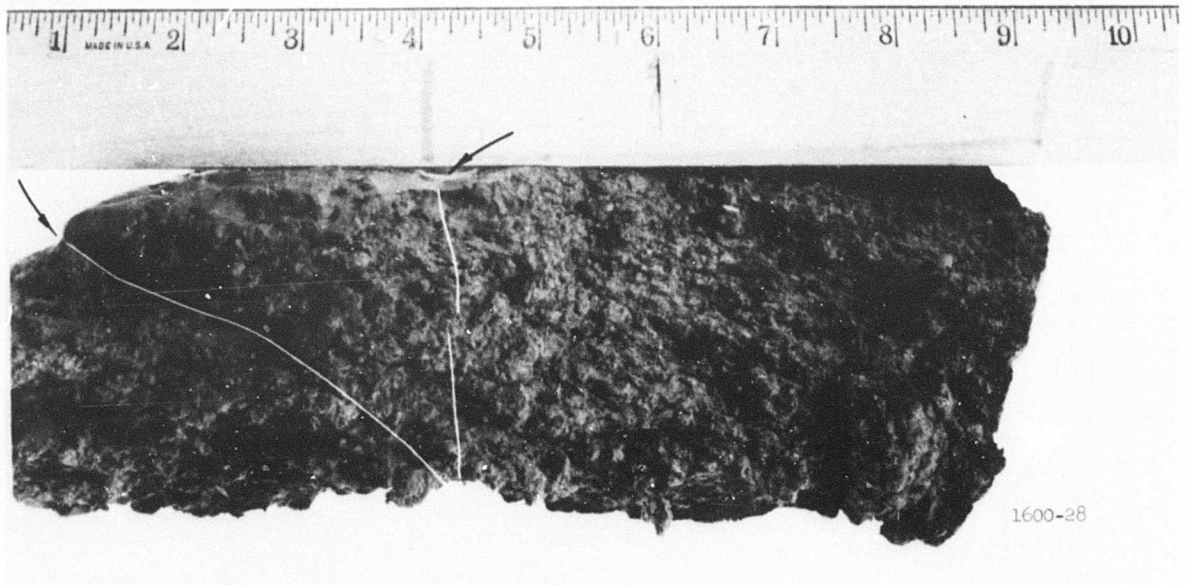


a. Side view of soil between 71- and 74-inch levels

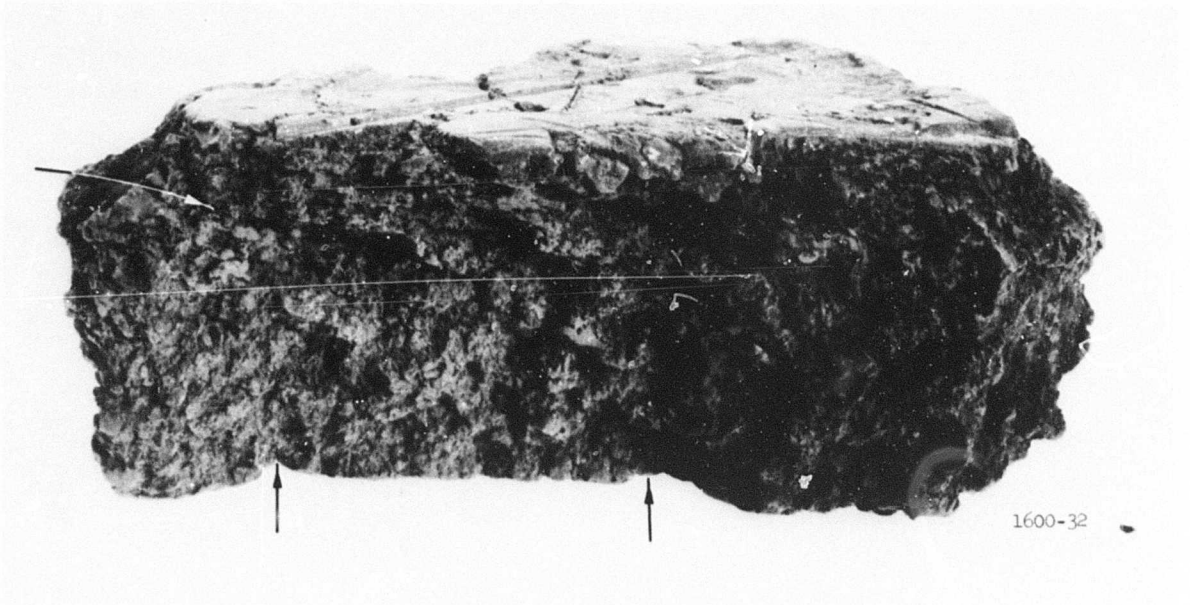


b. Side view of soil between 71- and 74-inch levels

Fig. 85. Soil deformations between 71- and 74-inch levels, Test 18

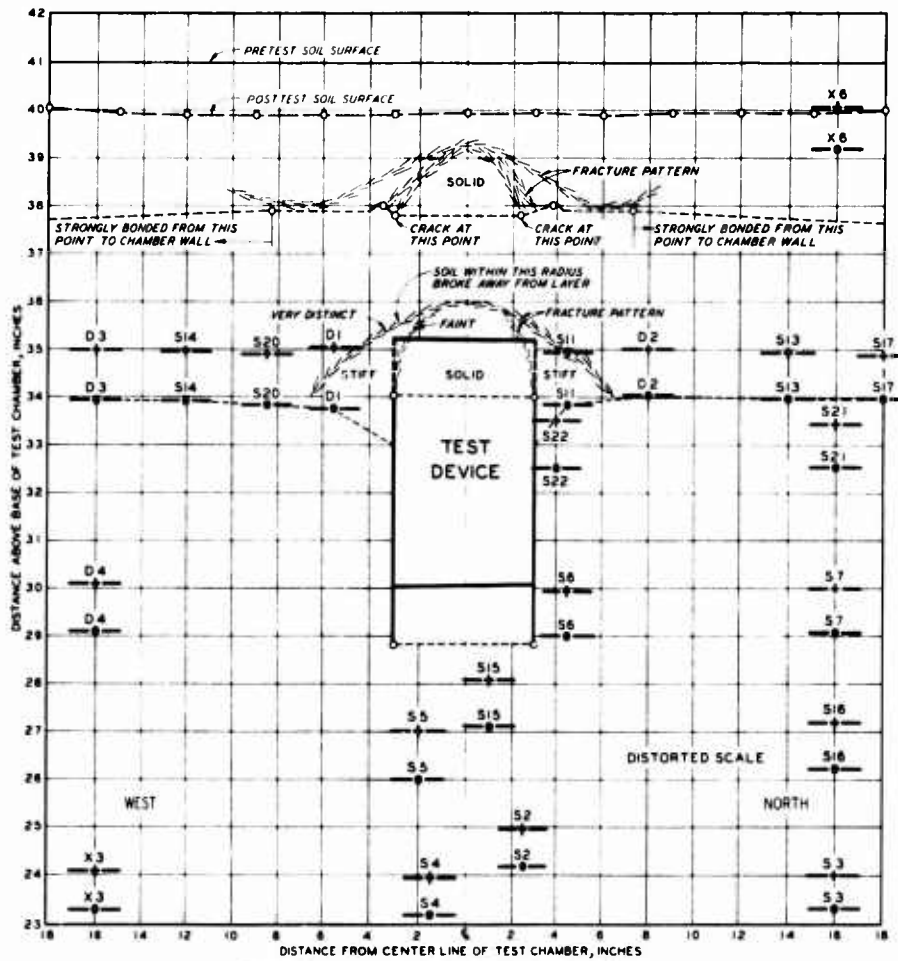


a. Side view of soil between 59- and 62-inch levels

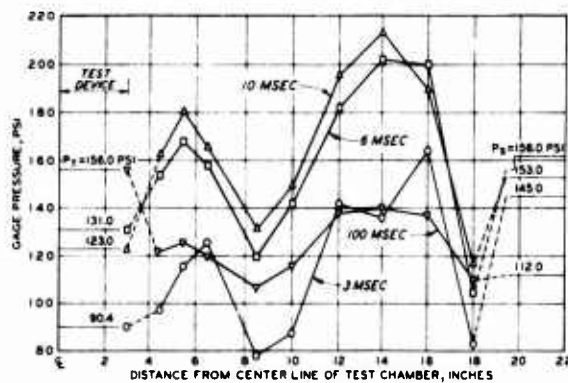


b. Side view of soil between 53- and 56-inch levels

Fig. 86. Soil deformations between 53- and 62-inch levels, Test 18



a. CROSS SECTION OF SOIL DEFORMATIONS



b. VARIATION OF SOIL TEST STRESS WITH TIME AT THE 35-INCH LEVEL

Fig. 87. Cross-section view of soil deformations, Test 19;
 $H/B = 1$, $P_S = 157$ psi

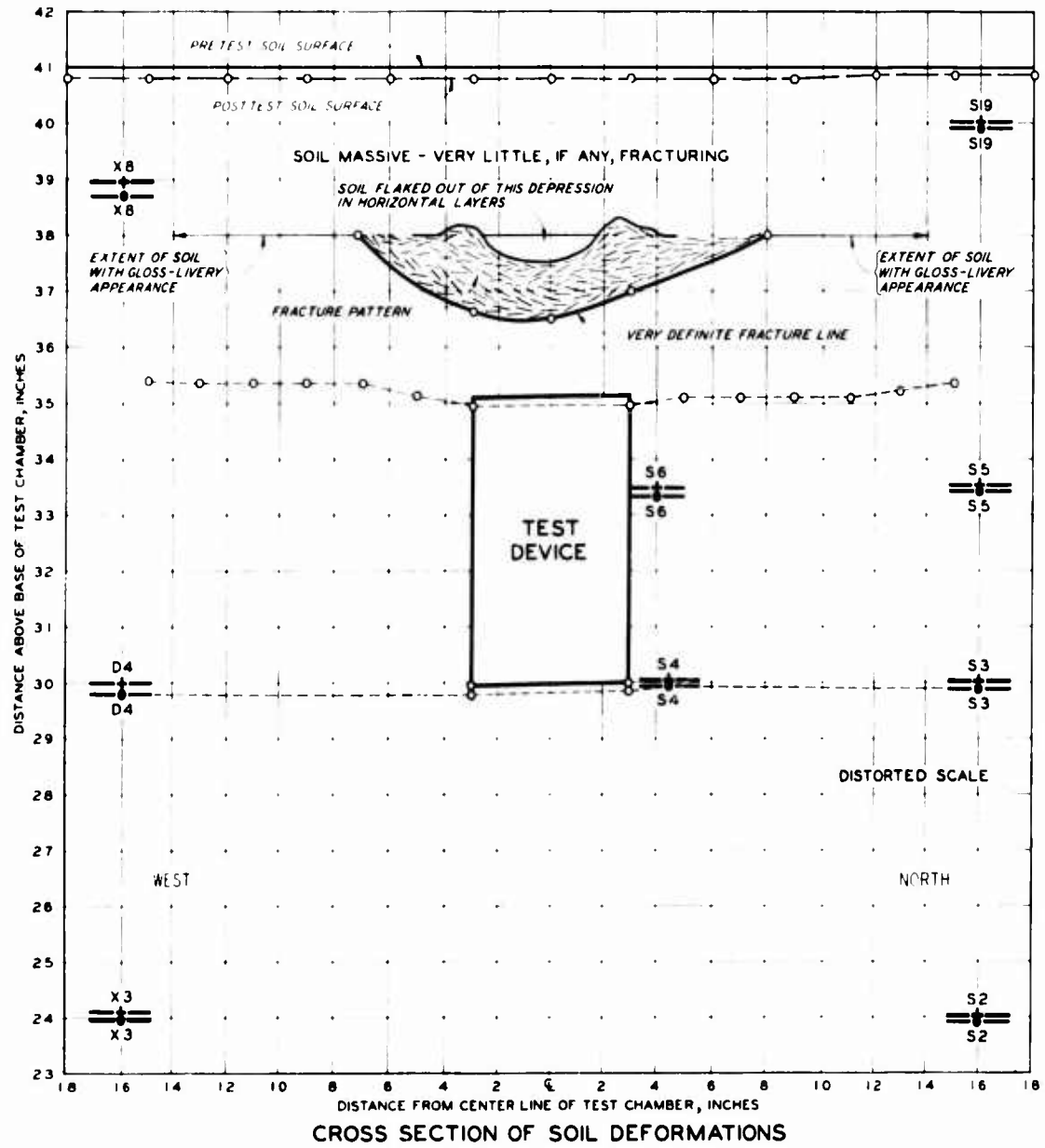


Fig. 88. Cross section of soil deformations, Test 26;
 $H/B = 1$, $P_S = 33.5$ psi

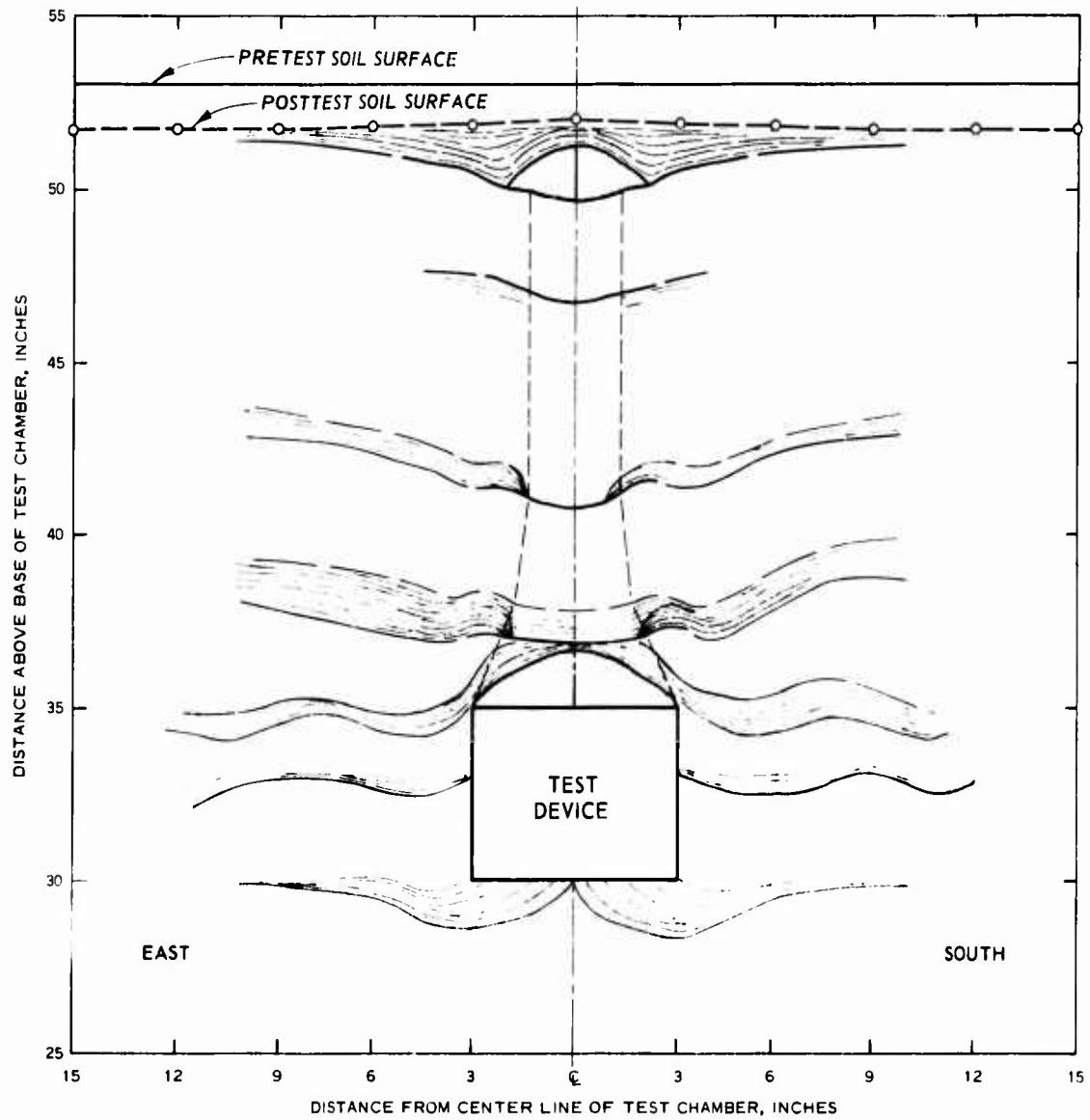


Fig. 89. Composite soil deformation profile under active arching conditions

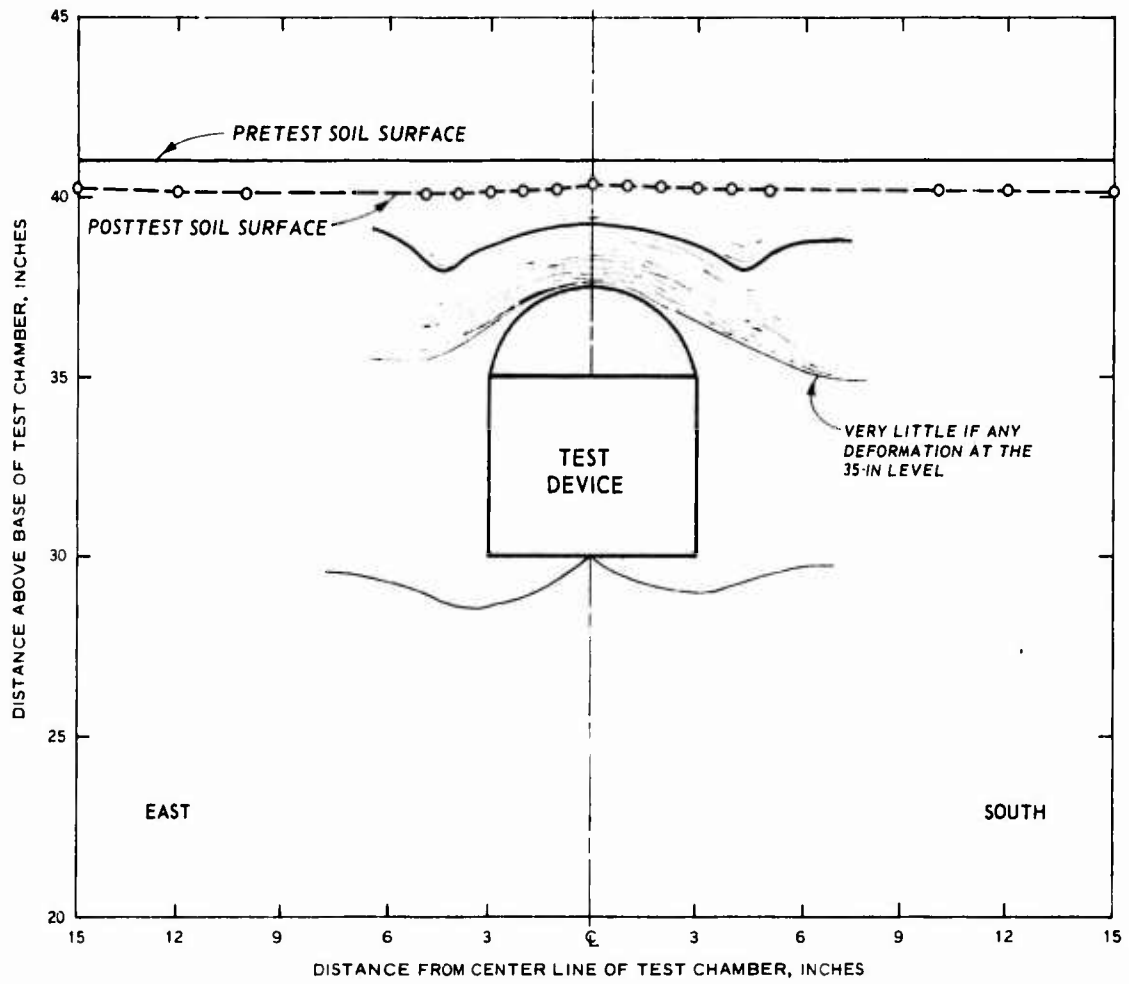


Fig. 90. Hypothetical soil deformations under passive arching conditions

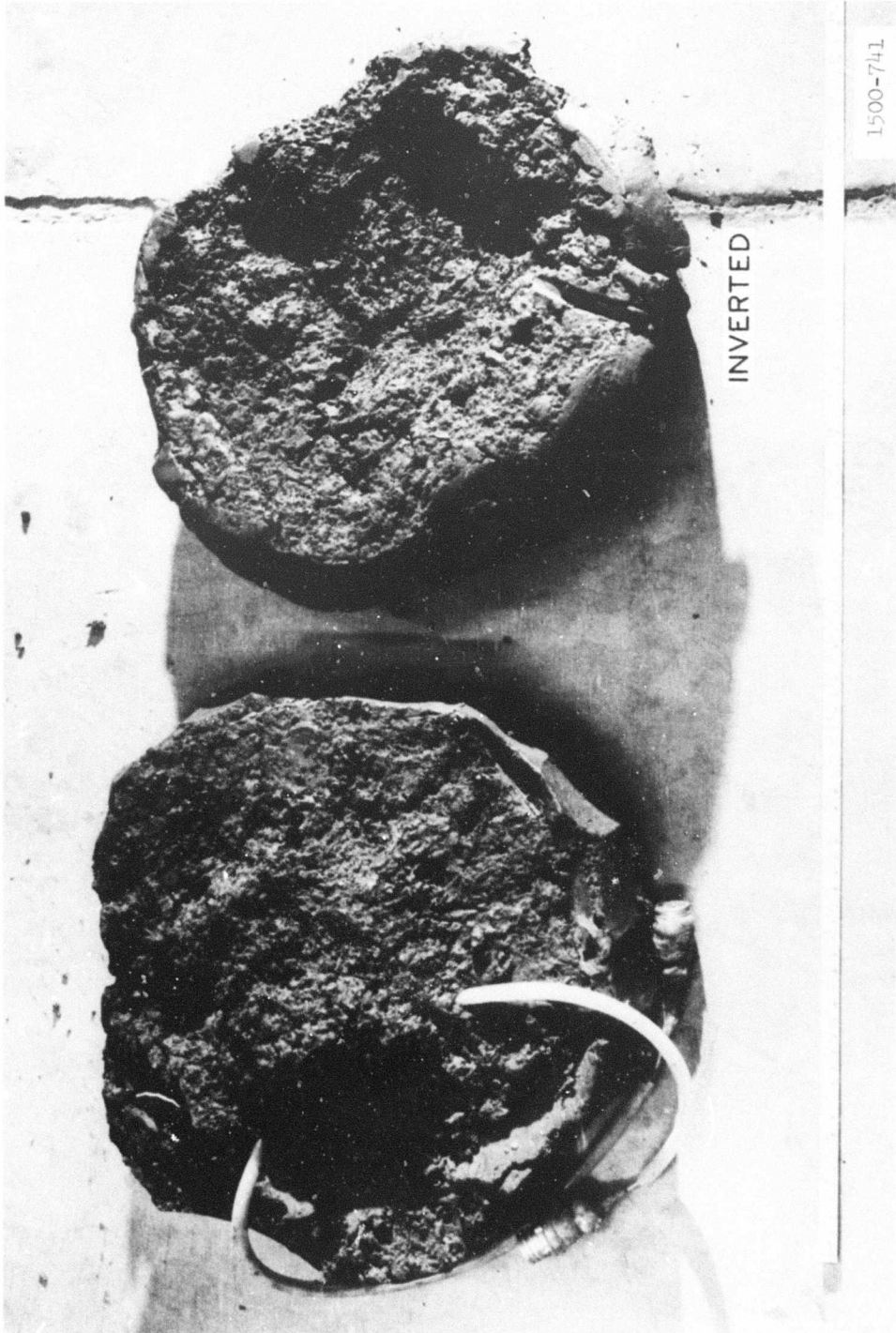


Fig. 91. Soil deformation pattern resulting from a 6-inch plate bearing test;
 $H/B = 3$

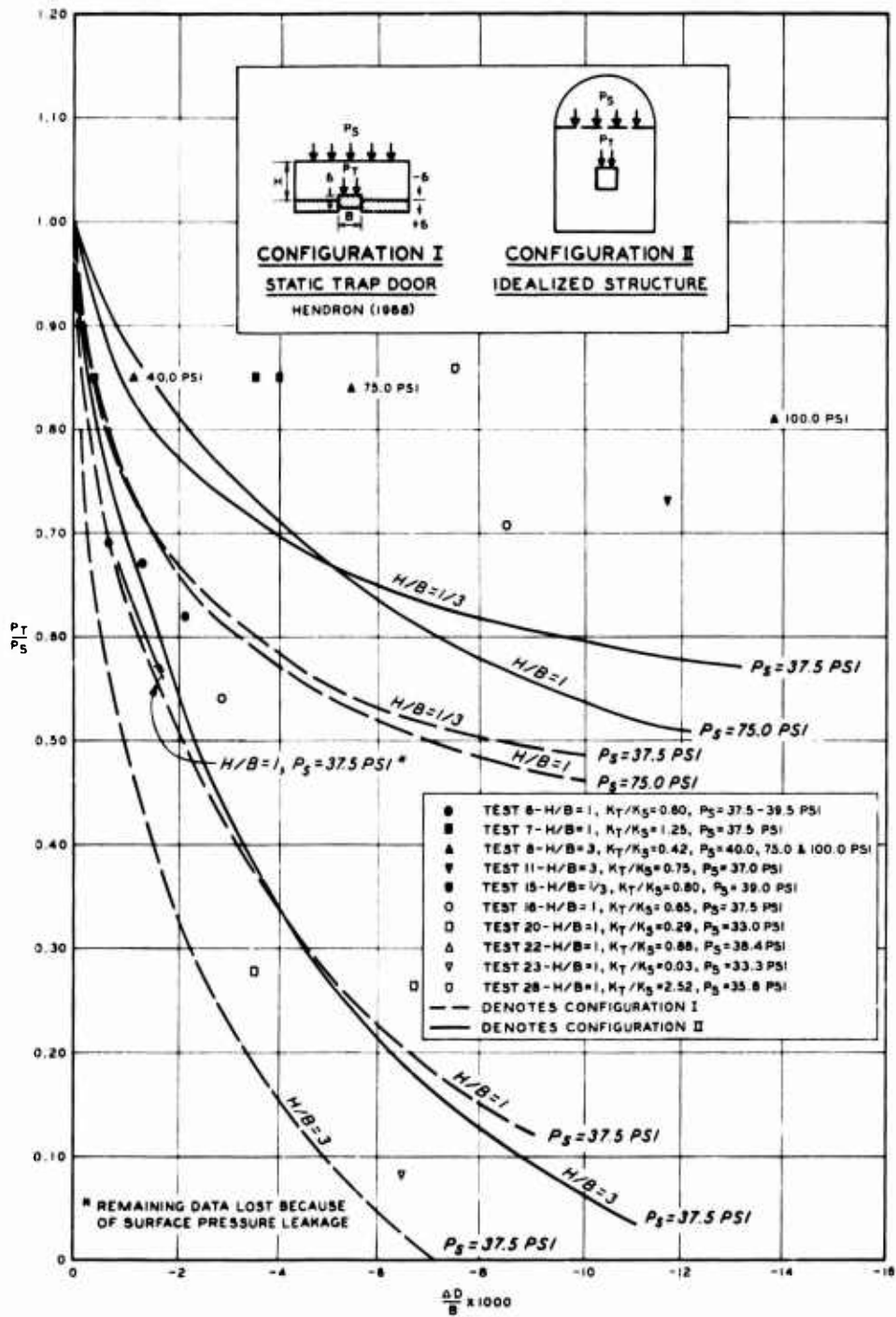


Fig. 92. Active arching curves, static surface pressure

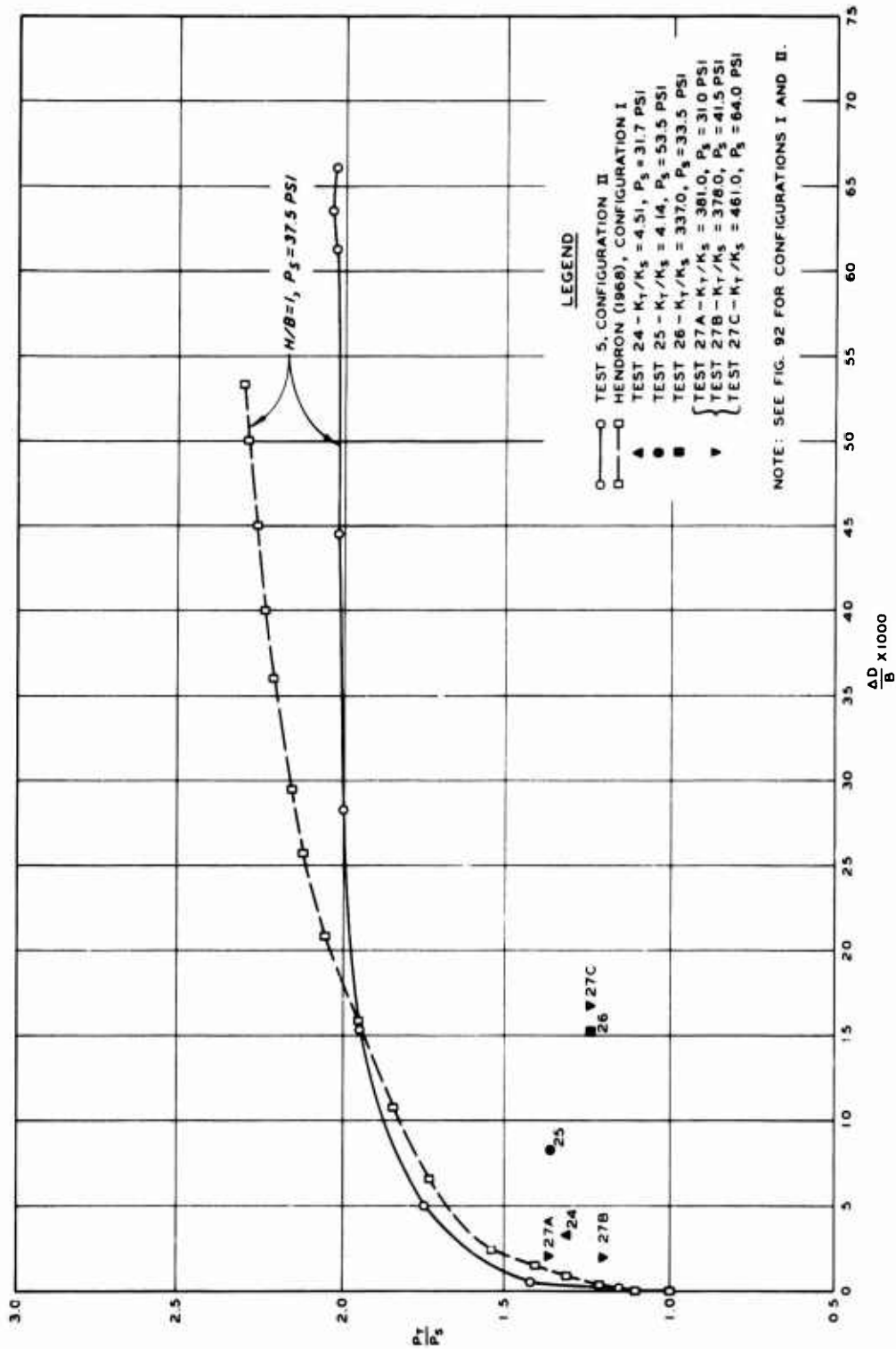


Fig. 93. Passive arching curves, static surface pressure

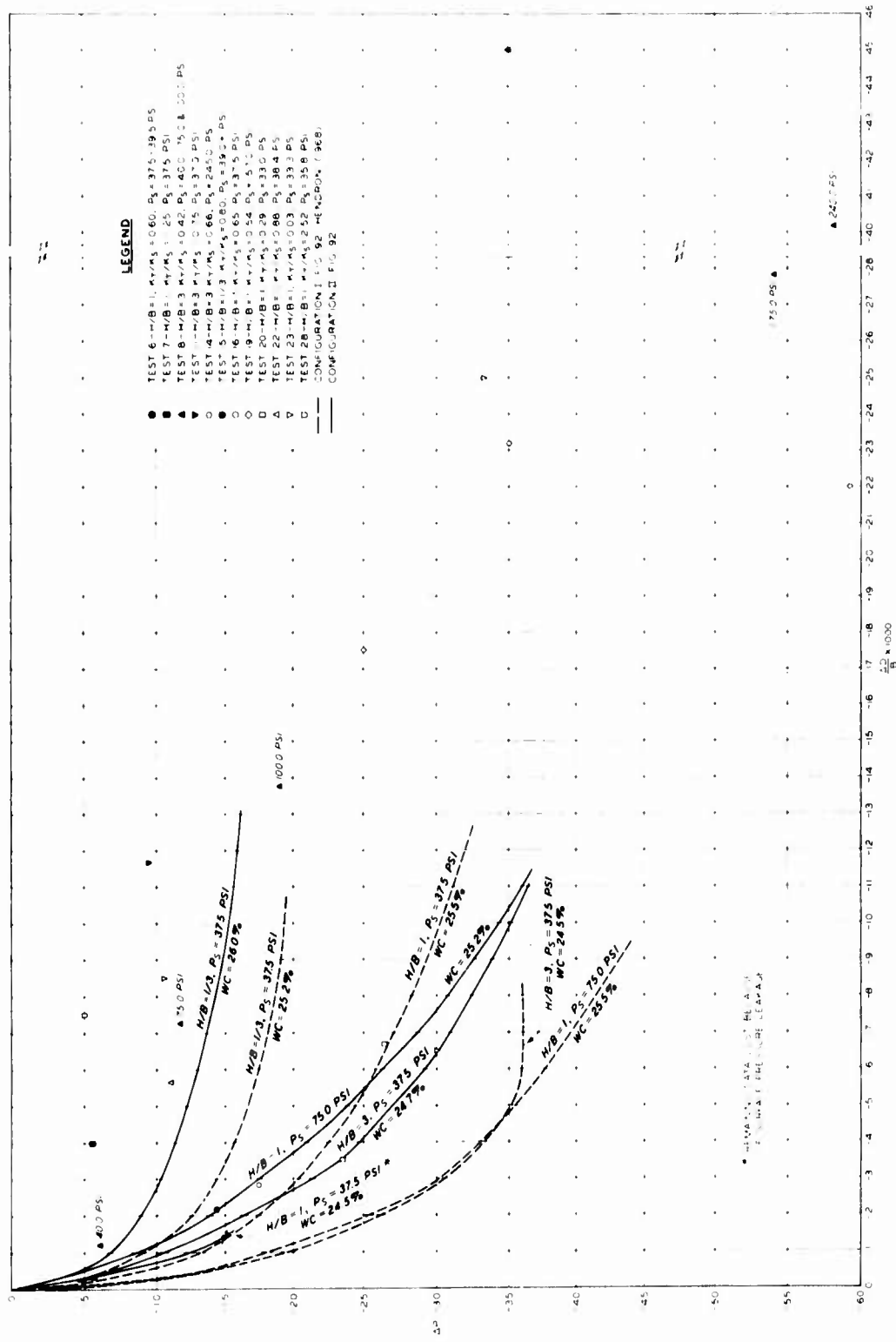
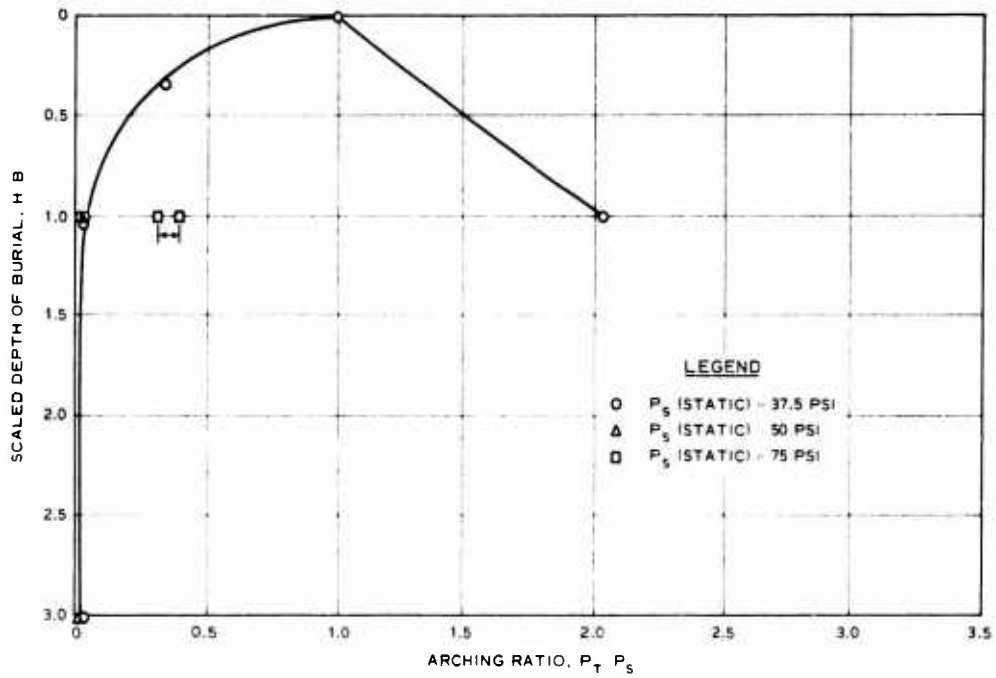
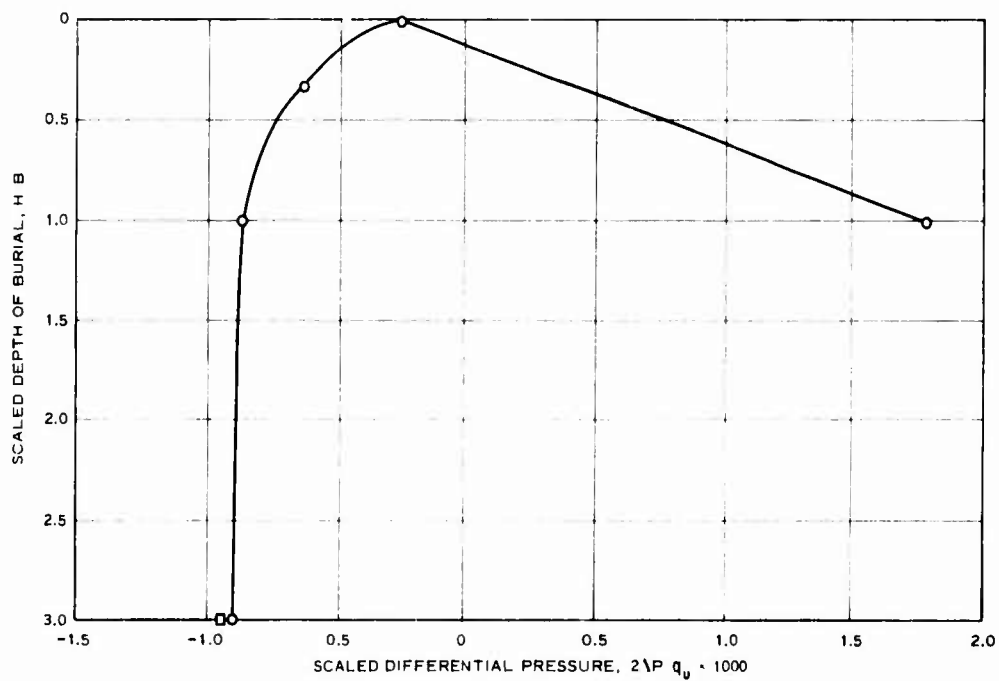


Fig. 94. Active arching, static and dynamic surface pressures, ΔP versus $\frac{\Delta D}{B} \times 1,000$



a. Variation of relative load on the structure



b. Variation of differential pressure at a scaled differen-

tial deflection of $\frac{\Delta D}{B} = \pm 2.5 \times 10^{-3}$

Fig. 95. Variations of relative load and differential pressure with depth of burial



Fig. 36. Composite soil deformation profile under active arching conditions

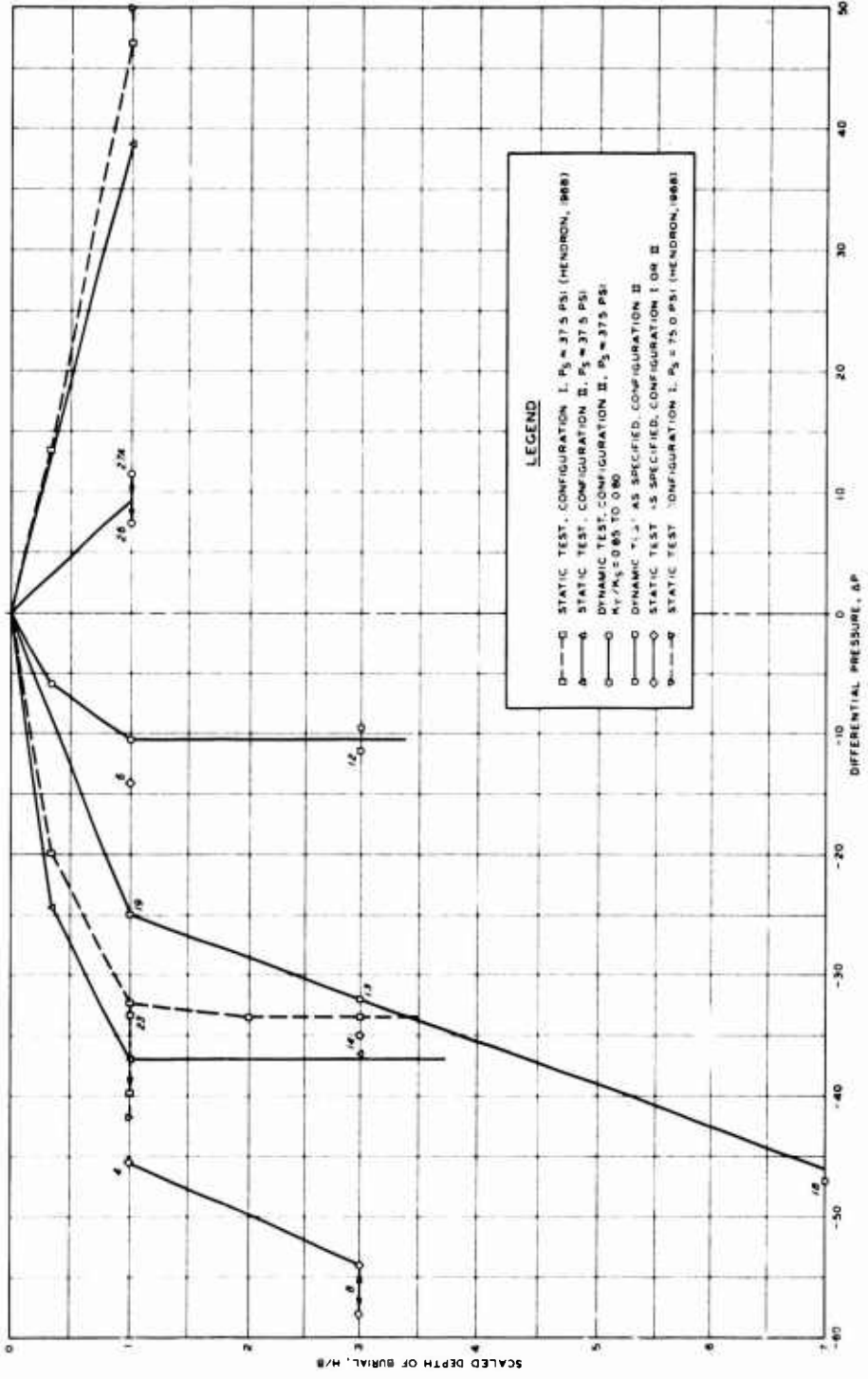
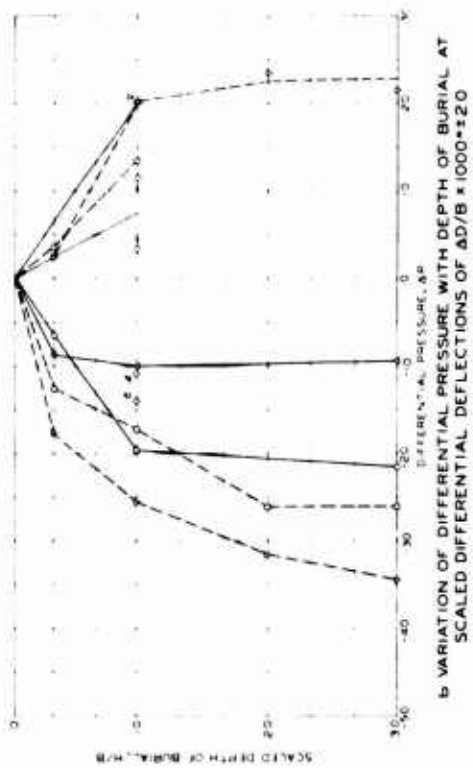


Fig. 97. Differential pressure versus scaled depth of burial, active and passive arching; $WC \approx 26\%$, $B = 6$ inches



LEGEND

- STATIC TEST, CONFIGURATION I, $P_0 = 375$ PSI (HENDON, 1968)
- STATIC TEST, CONFIGURATION II, $P_0 = 375$ PSI
- DYNAMIC TEST, CONFIGURATION I, $P_0 = 375$ PSI, $\Delta P/P_0 = 0.85$ TO 0.80
- DYNAMIC TEST AS SPECIFIED, CONFIGURATION II
- STATIC TEST AS SPECIFIED, CONFIGURATION I OR II
- STATIC TEST, CONFIGURATION I, $P_0 = 75$ PSI (HENDON, 1968)

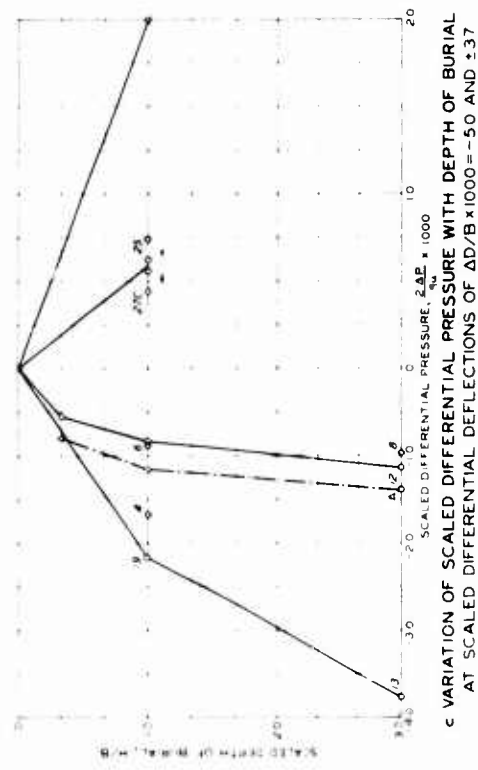
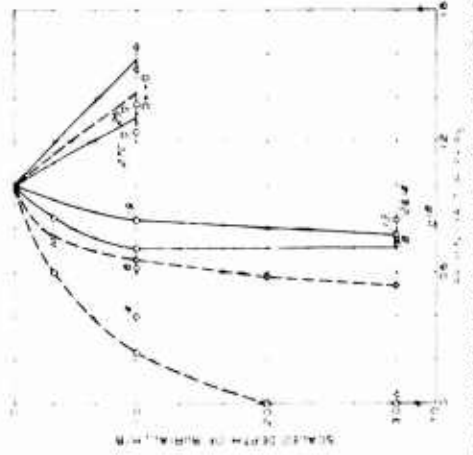
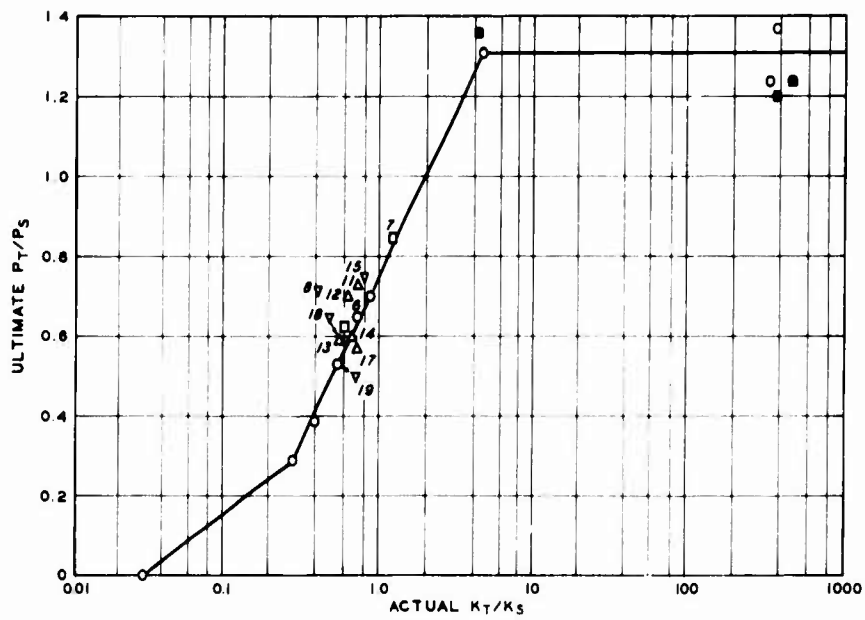
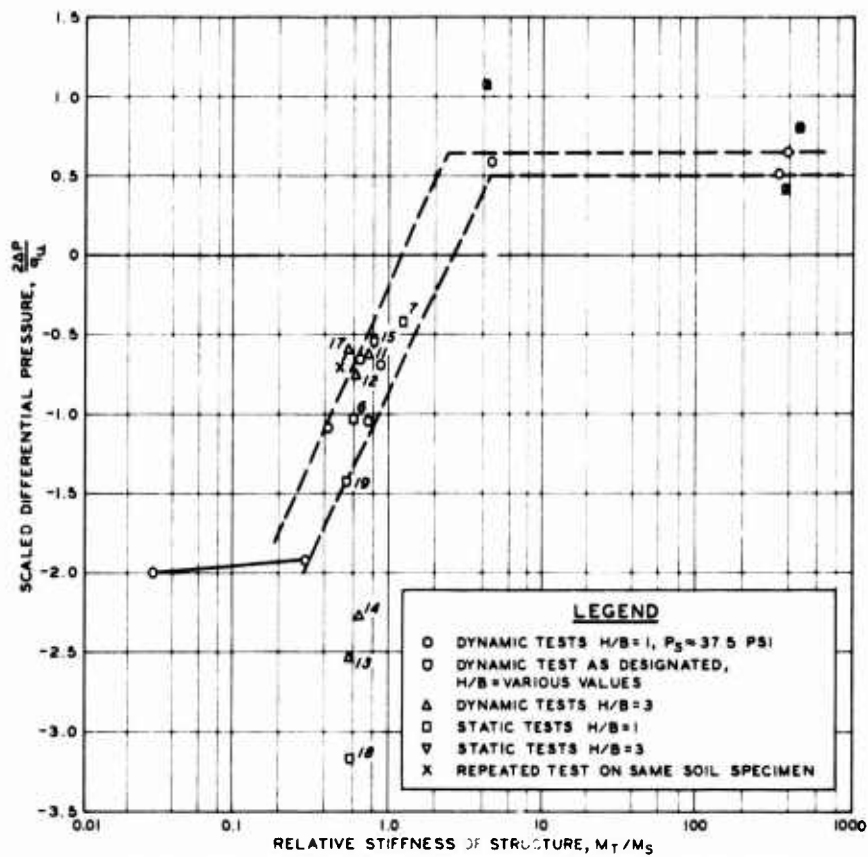


Fig. 98. Variations of relative load on structure and differential pressure with depth of burial



a. RELATION BETWEEN ARCHING FACTOR AND RELATIVE STIFFNESS



b. RELATION BETWEEN DIFFERENTIAL PRESSURE AND RELATIVE STIFFNESS

Fig. 99. Effect of structure stiffness on active and passive arching; WC \approx 24 to 27%, B = 6 inches

APPENDIX A

PROPERTIES OF COMPACTED BUCKSHOT CLAY; WALL FRICTION REDUCTION; SOIL, GAGE, AND TEST DEVICE PLACEMENT

A.1 Occurrence, Nature, and Index Properties of Clay. The soil used throughout this investigation was a highly plastic clay which is an alluvial material deposited in low-lying areas adjacent to the Mississippi River near Vicksburg, Mississippi, U. S. Army Engineer Waterways Experiment Station (1958). This material is generally referred to as "buckshot clay" because it forms small pellets in its dried condition, Jackson and Hadala.

The gradation curve and Atterberg limits for this material are shown in Figure A-1. The limits for all tests to date are generally parallel to the "A" line in the clay of high plasticity portion of the plasticity chart. The clay appears to have the same characteristics as that used by Jackson and Hadala in their study of the dynamic bearing capacity of clay. The material was derived from the same source as that used by both Carroll and Dorris and the properties appear to be very similar.

This material has been used for a considerable number of studies at the Massachusetts Institute of Technology (MIT) and other institutions. Several reports in MIT's study of The Response of Soils to Dynamic Loadings are based on investigations of buckshot or Vicksburg clay, synonymous terms.

Buckshot clay classifies as a CH in the Unified Soil Classification System. The specific gravity of the soil particles is approximately 2.68. The relative consistency of the soil at 26 percent water content is medium with an average unconfined compressive strength of 14 psi.

A.2 Compaction Studies. Initially the test program included a study of the effects of soil saturation on arching. It was known that the constrained modulus of clay was sensitive to this parameter. The compaction study was undertaken to determine the compaction effort and water content required to produce degrees of saturation between 70 and 95 percent.

The soil was placed in the Small Blast Load Generator (SBLG) using the techniques described in Section 3.5 of the main text. The thickness of the soil layers and the amount of compaction effort were varied. The saturation possible to attain within the workable range of water contents was approximately 80-90 percent, Figure A-2. Saturation increased with water content as anticipated. The numbers inserted beside the open data points are the number of passes of the mechanical compactor required.

The results of the tests indicated that it was possible to significantly increase saturation with increased compaction if the initial water content was lower than 20 percent. At water contents of above 25 percent, the effect of compaction on the degree of

saturation was small. At water contents of 30 percent or above, the effects of compaction were negligible (Steen, 1966b). The compaction tests showed that the range of usable water contents fell within an area such that variation of saturation was not practical. The use of the degree of saturation as a test parameter was abandoned.

Based on these tests and previous work by Jackson and Hadala it was decided that a standard compaction technique would be adopted and water content would be used as the principal means of soil strength control. An attempt was made to hold water content constant at 26 percent throughout the main test series. It was only possible to limit water content to 26 ± 2 percent. Saturation varied over a small range between 86 and 92 percent.

In the previously cited work by Jackson and Hadala, a 4-pass compaction technique was developed and related to the standard Proctor compaction curve, Figure A-2. Using this relation, it was possible to prepare large laboratory samples for tests described later in this appendix.

After the test program started, it became evident that the clay was acting as if it were saturated in some tests, especially those involving high pressures and/or long periods of time. From a series of laboratory triaxial tests, the diagram shown in Figure A-3 was constructed. It was assumed that a saturated condition had been reached when the shear stress became constant. This figure was used

as a guide in the planning and analysis of subsequent tests.

A.3 SBLG Wall Friction Reduction Studies. Just prior to and during the initial portions of the test program, a detailed study of wall friction in the SBLG was conducted by Hadala (1967b). Both unlined and lined (grease-polyethylene and grease-neoprene) specimens were tested. A summary of the test results is shown in Figure A-4.

This figure indicates that friction losses for unlined clay specimens was insignificant at static pressures of 250 psi or higher but that the losses could be significant for low pressure static and all dynamic tests. Figure A-4b shows that the friction losses for all lined specimens was less than 10 percent of the applied stress at a depth equal to one diameter.

Hadala also found that the grease-polyethylene liner was susceptible to more damage than the grease-neoprene liner during the construction of the clay specimen in the SBLG.

Based on Hadala's test results and considering the range of static and dynamic incident pressures planned, a double, 1/16-inch neoprene liner covered with a thick layer of G-403 automotive and artillery grease, constructed as explained in Section 3.5 of the main text, was selected for use.

In the preliminary test program and the early static tests, two problems arose which caused a reexamination of the liner problem. Posttest examination of the soil specimen showed that grease was

being squeezed from between the double liner and the friction losses during the static tests were higher than expected.

The horizontal expansion of the clay specimen would negate the one-dimensional compression conditions desired and thus affect the vertical stress wave velocity. Two methods of attacking this problem were tried. First, a neoprene-graphite combination was tested to determine its coefficient of friction. Tests showed that the friction coefficient for the neoprene-graphite combination was 0.13 as compared with a coefficient of 0.02 to 0.08 for the neoprene-thick grease combination. The graphite was abandoned and a second approach was tried. Instead of a thick coat of grease between the neoprene layers, the liners were wiped with a greasy rag. Checkout tests showed this procedure to be satisfactory; no apparent loss of friction-reducing capacity and no excess grease occurred.

The friction losses at depths below one diameter were attacked in another manner. As previously explained, the continuous neoprene liners were taped to the side of the test chamber during the construction of the soil specimen, Figure 11. After the specimen was completed, the tape holding the inside liner was cut. In an attempt to improve the friction-reducing capabilities, it was decided that instead of stopping the inside liner a couple of inches short of the base as was the practice, it would be turned under the soil at the base. Secondly, the inside liner was segmented into 1- to 2-foot

strips. This practice reduced the friction considerably. In all but the low pressure tests, the sidewall friction was practically insignificant. At the depths used for device burial, friction losses were very small even for the low pressure tests.

A.4 Soil Placement Techniques. The soil placement procedures explained in Section 3.5 of the main text were developed by Jackson and Hadala. The soil was generally uniform except between the layers. In spite of the scarifying technique, it was obvious that distinct layers existed and had some effect on the test results.

Although such a condition was undesirable, the time and funds necessary to develop a new soil placement technique were not available. Preliminary study showed that a penetrating device with a tapered head which could work on the sheepsfoot roller principle probably would solve the problem. The device and technique presently are under study at WES. One major problem with this technique is the protection of instrumentation and cables buried in the soil.

A.5 Gage Placement Techniques. The cut-and-cover gage placement technique explained in Section 3.3.2 was patterned after one of the procedures tested by Hadala (1967a) in his gage placement study. The mechanics of placing the gages, such as design of the cutter and the mounding technique, were perfected during this test program, Figure 16.

During the dynamic tests, it was found that cable breaks were

frequent. It was necessary to provide considerable slack in the cables, especially along the chamber wall and near the cable port. In addition, the cables were covered with 1/4-inch plastic tubing, Figure 16.

In the static test program, moisture migration was a problem. It was necessary to carefully wrap and waterproof the cable connectors and the connection between the cable and the gages. The cable had to be changed frequently since any break in the insulation allowed moisture to enter the circuit, especially at high pressures.

The placement program conducted by Hadala (1967a) and Ingram (1965 and 1967) plus the preliminary tests performed in this program showed that soil pressures were normally accurate to less than ± 10 percent. It had been planned to check each soil pressure gage in the soil. The gages were to be installed in soil using the standard procedures and a series of registration tests were to be performed. However, the test device required to accomplish this task was not available soon enough. The soil gages were air calibrated several times during the test program.

A.6 Test Device Placement Techniques. It was necessary to develop a procedure for placing the test device which would minimize the possibility of damage during soil specimen construction and reduce the effects of sidewall friction. A wooden block with a diameter 1/8 inch larger than the device was constructed, Figure A-5a. When the 30-inch

soil level was attained, the block was placed in the position planned for the device. Then, the soil specimen construction was continued in two lifts to the 35-inch level. Extreme caution was required in the use of the mechanical tampers. When the level of the compacted soil reached the planned elevation, the block was removed and the device placed in the hole left by the block, Figures A-5b and 16. The next layer of soil was then placed directly on top of the device. The depth of soil in the next layer was sufficient to protect the top of the device.

To reduce the friction between the soil and the sides of the device and to prevent soil from obstructing movement of the device, it was necessary to cover the device. For this purpose a machined metal shield was used to cover the gap between the top and the main body of the static device. A single 0.015-inch layer of Teflon was wrapped around the entire device, Figure A-5b. For the dynamic device, only the Teflon was required. Preliminary tests to determine the coefficient of friction indicated that friction between the soil and the structure would be insignificant. Examination of the radiographs disclosed that sufficient friction existed to deform the soil in the vicinity of the device, especially at the 32- to 33-inch levels.

A.7 Laboratory Investigation During Test Program. A series of laboratory tests was performed on samples taken from each soil

specimen to control and measure soil strength.

As the soil was being prepared in the pugmill and after delivery to the test site, its water content was checked. As the soil specimen was constructed, the dry density and water content were determined for every other layer. These data were determined from two Little Rock drive density samples removed from these layers. Initially, two Hvorslev unconfined compression tests were performed for every other layer. Because of the large number of tests required, this was later changed so that the Hvorslev tests were used at the 35-inch level and every layer above this level.

The procedures for performing the Hvorslev tests are explained by Hvorslev (1949). The sampler is shown in Figure A-6a and the unconfined compression machine in Figure A-6b. The Hvorslev tests proved to be a very rapid and accurate means of checking soil strength. Initially, it appeared that the Hvorslev data would always plot higher than the strength determined by the normal laboratory unconfined compression test. Later in the test program, when a large amount of data were available, this conclusion was found to be incorrect. Within the scatter of the data, it was not possible to distinguish such a trend, Figure A-7a.

In addition to the samples discussed above, two 4-inch undisturbed cube samples were taken from most soil specimens. These samples were used to perform unconfined compression, triaxial

compression, and consolidation tests in the laboratory. After the correlation between the Hvorslev and laboratory test results was available, the number of undisturbed block samples was reduced, especially when more than one test was performed on the same batch of soil.

After most tests, Hvorslev samples were taken at the surface and at every other layer above and beside the test device. In addition, 4-inch undisturbed block samples were taken during the preliminary test program. Some of the posttest results are plotted in Figure A-7b.

A consolidation of all the density and unconfined compressive strength data is shown in Table 4. It is interesting to note the trends between the pre- and posttest data. In general soil strength increased and water content decreased, though this was not always the case with the water content. The amount of strength change appears to depend on the surface pressure and, for the sample taken directly over the test device, the flexibility of the test device. Stiff devices obviously compressed the soil more and thus raised the strength, while flexible devices had the opposite effect except at the high pressures used in Tests 13 and 14.

The only test in which the "all-samples" soil strength did not increase with testing was Test 25. This is a repeat test on the same soil specimen used in Test 24 so the data are suspect.

The movement of the data upward and to the left, except for the

one test at a water content above 30 percent, can be seen in Figure A-7b. The preponderance of the data increased in shear strength by approximately 3.5 psi and decreased in water content by approximately 0.5 percent.

A range of water contents was used in the preliminary program so that a reasonable one could be selected. A water content that could be expected in the field but which would not mask the test results with effects predominated by water content was desired. Because only one water content was to be used, it was decided to select one wet of optimum if possible. A search of the literature concerning buckshot clay and previous arching studies furnished only a small portion of the information required to design the experiments and their instrumentation.

A.8 Pretest Studies. In order to design the main test program, it was necessary to study: dynamic and static properties of buckshot clay, the soil displacements and accelerations to be expected at various depths, the pressure wave characteristics, and particle velocities.

The constrained modulus was probably the most important soil property determined. It was the basis for establishing the range of relative compressibilities between the test device and soil.

In addition to the parameters used to design the test device, the preliminary test program established the ranges to be expected

for the soil pressure, acceleration, and deflection gages. This was necessary so that proper size gages and gains could be used.

The preliminary test program consisted of two phases which were accomplished simultaneously. Instrumented soil specimens at various water contents were built and tested in the SBIG, Table A-1. Soil samples prepared from the same batch of soil were tested in an impact loading device.

A.8.1 Small Blast Load Generator Tests. A series of five dynamic tests at four water contents were conducted in the SBIG, Table A-1. The variation of soil pressure, displacement, and acceleration with height and water content of specimen were studied. The test layout is shown in Figure A-8. The number and location of the various gages varied somewhat during the tests.

The original Test D was conducted on a soil specimen with 26 percent water content. The planned surface pressure was 40 psi. For some unknown reason, the explosive charge fizzled. The rise time to peak pressure was very long and the desired peak pressure was not attained. Results from this test are not included in this report.

As a result of this failure, a new soil specimen was prepared at a water content of approximately 25.5 percent. It was first exposed to a surface pressure of 41 psi. The results of this test are identified as Test E in Table A-1. After the surface deflection was measured and the gain on the instrumentation changed, the same

specimen was subjected to a surface pressure of 238 psi. This test is identified as Test D.

Copies of the basic oscillograph records from which all time and magnitude measurements were made are contained in Appendix C. The type of instrumentation and its location are shown with each record. The SE soil pressure gage used in these tests was the same type described in the main body of the report. The accelerometers were the same piezoelectric gages explained in Chapter 3. The 2-inch-diameter soil displacement disks were constructed from a density-matched epoxy. These disks were placed at various radii and levels and were used as a basis for measuring permanent soil displacements.

In Tests A, B, and C, a water bag was used at the base of the soil specimen. This water bag was constructed of neoprene, and was 2 to 2-1/2 inches high when evenly compressed. A Norwood and a piezo-gage were located in the water bag. With this test setup, it was possible to study the sidewall friction, base pressure, and reflected pressure waves.

In Tests D and E, soil deflection rods were installed and instrumented for axial strain, Figure 15. The strain was measured as a precaution to ensure that the strain in the rod was small as compared with the movement of the soil disk. The results confirmed the fact that strain in the rods was very small at low pressure and still insignificant at high pressure.

A.8.2 Confined Compression Tests. A series of static and dynamic confined compression tests was made using the gas-actuated impact hammer and instrumentation shown in Figure A-9. The soil was prepared by compacting it into "concrete" molds at the water content and density used in each of the preliminary SBIG tests, Figure A-10. Soils at each of the four water contents (23, 25, 27, and 32 percent) were subjected to static and dynamic pressures of 37.5, 75, 120, and 240 psi.

To prepare the soil for testing, 1-inch-high disks, Figure A-10, were cut from the prepared specimen by use of a piano wire. The edges of each specimen were wrapped in a layer of Teflon before the specimen was placed in the confining chamber. The confining chamber was placed under the impact machine and the head, which was the same diameter as the inside diameter of the confining chamber, was lowered onto the top of the soil disk.

When the trigger mechanism for the hammer was released, a timing device triggered in turn a camera which photographed the display of the stress and strain on the oscilloscope. Typical oscilloscope records are shown in Figure A-11. The stress and strain traces were not coupled to produce X-Y plots for use as stress-strain curves. There is a danger of a phase shift with the viscous buckshot clay.

The test program explained in this section was used since the constrained modulus was so important to the test program and no other

device was readily available. The one-dimensional compression device under design by Schindler was not ready, and the device at the University of Illinois, Kane, Davisson, Oleson, and Sinnamon, was not immediately available. After the test program had been completed, Schindler's device became available and was used to perform one static and one dynamic test on soil specimens prepared at a 26 percent water content. The test results are included in the following sections.

A.9 Static Properties. In order to study the properties of buckshot clay and relate them to the arching actions observed in the soil, a laboratory test program was designed and carried out both prior to and during the main arching test program. Each of the sections below will introduce and explain briefly the various soil tests and their results. Several investigators have shown that the strength and volume change associated with buckshot clay when subjected to a load is a function of the loading rate, Whitman et al. (1962a), Carrol, Kane et al., Perry. The change in shear strength appears to be related to the degree of drainage and some other phenomenon which has not been completely isolated. In spite of the low permeability of buckshot clay, it is important to specify the drainage conditions. In some of the rather long tests in the static program, drainage did occur. This was evidenced by the water seeping from the test chamber at the flanges. This was especially true in Test 8, one of the high pressure static tests. Although the soil was not

saturated in its compacted state at the beginning of the test, it did become saturated during this test, Figures A-2 and A-3. Even in the dynamic tests, the very high pressures may have changed soil volume sufficiently to induce a saturated condition.

In those tests in which the clay became saturated or very nearly saturated and was subjected to strains without drainage, the clay behaved as a cohesive material with ϕ , the friction angle, equal to zero.

From the preceding discussion and the test conditions explained in the main body of the report, it can be seen that no one laboratory test can depict the conditions which existed in each of the arching tests. In order to specify the strength of the material, it was necessary to establish the stress levels which existed, the drainage conditions, and the rise time and/or duration of the load.

The unconfined compression test does not allow control of drainage or confining conditions. For this reason it was initially planned that the unconfined test would be used only to estimate the shear strength. The closer the clay approached a saturated condition and its failure approximated an undrained condition, the more accurate the shear strength computed from the unconfined test became. Due to progressive failure, the average shearing resistance was taken as $q_u/2$, Terzaghi and Peck. When clay is unsaturated, the confining pressure can have measurable effect on its shearing resistance and

the triaxial test is more applicable. It is for these reasons that both unconfined and triaxial tests were used in this program.

Due to the significant nonlinearities in the stress-strain curves for buckshot clay, it was difficult to determine one modulus. The modulus actually was continually changing, depending upon the stress or strain level. Thus it was necessary to use tangent modulus values which were approximately constant over some range of stress or strain or to use a secant modulus which was dependent upon some selected stress or strain.

It would have been desirable to have the same stress and strain conditions in the laboratory test as those to which the soil was subjected in the arching test. Lateral strain appears to be minimized during underground arching; therefore, it was desirable to limit lateral strains. It was for this reason that one-dimensional compression tests were used in the preliminary test program. Time and funds did not allow an appropriate investigation of strain rate effects, and data from other investigations in this field have been used.

A.9.1 Unconfined Compression Tests. As previously explained, two types of unconfined tests were conducted, the normal laboratory test and the Hvorslev test. Figure A-7 compares the maximum strength determined by both type tests. Figure A-12 illustrates the stress-strain results from many of the laboratory tests. Inasmuch as the buckshot clay appeared to be strain rate sensitive, the tests were

separated based on time to failure. In the tests which were conducted in more than 20 minutes, the soil displayed a plastic action. At a strain of approximately 7 percent, the soil became fully plastic and there was very little increase in the soil strength for an increase in strain, especially above 25 percent water content. The drier soil reached this point at approximately 10 percent strain. Obviously, the higher the water content the lower the strength.

The curves for specimens tested to failure at a rate faster than 20 minutes did not indicate as much scatter as those from the slower tests. They generally exhibited a higher strength than the curves from the slower tests with the exception of the soil at a water content of 24 percent. In the faster tests, the soil became fully plastic at lower strains, Figure A-12b.

The failures occurred in the test specimens by both splitting and bulging. In most cases, the failure appeared to be a combination of the two modes of failure. The soils were compacted wet of optimum water content, but were not saturated. Generally the saturation of the test samples varied from 86 to 92 percent, depending on the initial water content.

The unconfined tests were an excellent means of soil strength control. They also indicated relative strengths at various water contents. The test results appear to be applicable to the low pressure static tests which were conducted in a matter of hours rather

than days, where confining pressure and drainage conditions may not have been significant.

A.9.2 Triaxial Tests. These were quick tests with confining pressures approximately equal to those used in the static test program.

Typical examples of the triaxial test results are plotted in Figure A-13. These results indicate cohesion varying from 10 to 16.7 psi and friction angles varying from 1 to 6 degrees depending upon the water content. Thus, the buckshot clay acts almost like a $\phi = 0$ material, especially at the desired water content of 26 percent.

Figure A-13 shows that confining pressures within the range tested had very little effect on the soil strength as compared with a slight change in the water content, except for the soil with a 23 percent water content. The variation was insignificant for the 26 percent water content material.

Time to failure during the triaxial compression tests varied from 50 to 60 minutes or a rate of strain of approximately 0.25 to 0.30 percent per minute.

A comparison of Figures A-12 and A-13 disclosed that at comparable rates of strain and with water contents approximating 26 percent, the average strength of the material as determined by both tests was virtually identical. At 8 percent strain the average

strength as determined by the unconfined tests was 2 psi higher. The ultimate strengths were identical. The unconfined tests conducted in less than 20 minutes disclosed average strengths 8 psi larger than the triaxial results at both 4 and 8 percent strain. At ultimate strength the faster unconfined results were 7.5 psi larger.

For 26 percent water content material it is evident that the effects of confining pressure within the range tested were insignificant as compared with the effects of rate of strain. At comparable strain rates the strengths as determined by unconfined compression tests are as valid as the triaxial test results. Carroll also found that the effects of confining pressure were insignificant as compared to water content and strain rate, Figure A-14.

During the triaxial tests, the samples failed by splitting and/or bulging.

A.2.3 Direct Shear Test. Consolidated-drained direct shear tests were not performed during this test program. Shear strength as determined by the normal shear box is very questionable and has fallen from use except for particular soil types. A large number of these tests were conducted by Jackson and Hadala, and Hadala (1965) during their investigation of the dynamic bearing capacity of buckshot clay. These were stress-controlled tests on 2.4- by 2.4- by 0.4-inch-high specimens. Although it is difficult to compare directly, the shear strength as determined by the direct

shear test using specimens of equal water content was approximately 20 percent higher than comparable triaxial results.

A.9.4 Consolidation Tests. Normal consolidation tests were performed on samples removed from some of the test specimens. Normal $e - \log p$ curves were drawn and, in addition, the stress-strain curves shown in Figure A-15 were constructed. Until such time as better data were available, these curves were used (to obtain an estimate of the one-dimensional modulus of the material).

A.9.5 Stress-Strain Curves. The pretest stress-strain curves plotted in Figure A-16 were generated using confined soil samples prepared as explained in Section A.8.2. The 1-inch-high by 6-inch-diameter specimens were loaded with the MIT constructed loader at the rate of 1,000 pounds per minute or 35.4 psi per minute, Figures A-9 and A-10. Three different specimens were loaded at three different pressures, 37.5, 75, and 240 psi.

The curves in Figure A-16 marked with test numbers were constructed by using data generated at the 30- to 35- or 30- to 38-inch levels of the soil specimens placed in the SBLG. Paired soil deflection and pressure measuring gages were at the same level and radius. The surface pressure was applied at the rate shown in Figure A-16. A more uniform rate was desired but not always attainable. These curves depict the stress-strain relation within the soil and are not necessarily analogous to the one-dimensional compression test.

The posttest curve in Figure A-16c was derived from data developed using Schindler's one-dimensional test device. The soil specimen was 1 inch high by 10 inches in diameter.

The low pressure curves in Figure A-16a indicate a plastic material which tends toward a fully plastic condition. Obviously, the loading rate even at this pressure level has a large effect on the total strain and the shape of the curves.

Figure A-16b contains the medium pressure curves. There is a point of inflection in both curves. This is an indication that some sort of locking action is taking place. In this case, it is probably due to the change in the degree of saturation and not to the type of loading action normally associated with sand.

The high pressure curves are shown in Figure A-16c. In the pre- and posttest curves, the locking action is marked. It is not as obvious in the curve derived from Test 8. The small strains that resulted from the relatively slow rate of load application are difficult to explain. There appeared to be a malfunction in the deflection gage at the 35-inch level which could account for the discrepancies. The curves resulting from the two entirely different compression devices are remarkably similar.

In determining the constrained modulus from the pretest data, a secant modulus was used. In spite of the effects of strain rate, the data proved reliable enough to design the test device. The

modulus calculated from the stress-strain curves in Figure A-14 also were used. They constitute one extreme of the effects of loading rate.

As can be seen from the stress-strain curves, the modulus of this material was continually changing during the course of the tests. This modulus was affected by the pressure, depth of soil, loading rate, and the saturation of the material. In studying the test results in Tables A-1 and A-2 plus those in the main body of the report, this fact should be kept in mind.

A.9.6 Constrained Modulus. Table A-2 contains the range of values derived for the constrained modulus from all sources. In most cases, the values appear to be reasonable. In spite of the disparities in the strain rates, the modulus calculated from the one-dimensional laboratory compression tests related closely to those calculated during the SBLG tests. The one major exception was Test 8 which was discussed in the first paragraph of Section A.9.

The modulus derived from the SBLG tests was calculated by measuring at a designated time the differential strain over a particular gage length, and the average pressure between the top and bottom of the gage length.

A.10 Dynamic Properties. In the study of the dynamic properties of buckshot clay, several properties were of particular interest. Of most importance were the stress-strain and modulus data. These

were required to plan the various stiffnesses for the test device. The constrained modulus was calculated not only by using stress-strain, but also by using propagation velocity of the peak stress wave; thus, a study of velocities was conducted. In dynamic tests, the rise time of the pressure pulse can affect the loading a buried structure experiences; therefore, information on this subject was collected and used in the planning of the test program.

A.10.1 Variation of Propagation Velocities. In the study of propagation velocities two times were of interest: the arrival of the initial disturbance, and the arrival of the peak pressure. The velocities between the soil surface and the level of the test device were of particular interest, i.e. the top 2 to 18 inches of material. The time for the pressure wave to reach the base of the test chamber also was important, since this was used to determine the amount of soil required below the test device and the amount of time available to study structural actions before the reflected waves interfered.

Figure A-17a is a plot of the propagation velocity of the initial disturbance. The data were taken from the records in Appendix C. There is considerable variation in the velocity except for the high water content material in Test C. This uniformity was probably a function of the high degree of saturation. The relation between the velocity and the water content did not appear to be reasonable, i.e. the soil with the lowest water content had the highest velocity and

the soil with the highest water content had the lowest velocity. Further examination disclosed that if Test E, the low pressure test, is omitted, the velocities are in an inverse relation to the water content.

The relation between the pressure and the velocity also appears to be out of order. The low pressure test, E, had a higher propagation velocity than the high pressure test on soil with the same water content. It was not until a point approximately 18 inches below the surface was reached that the position of the velocities appeared to be in proper relation to each other.

In Figure A-17b, the propagation velocity of the initial peak pressure, disregarding reflections, is plotted. These velocities were more uniform from surface to base. In addition, material with a higher water content had a higher velocity than the drier material. The higher pressure tests also developed higher propagation velocities than the low pressure test.

Based on the material shown in Figure A-17, the propagation velocity of the first stress peak was selected as one of the means for calculating the constrained modulus. Although these velocities are not exactly shock velocities, inspection of the pressure signatures in Figures C-73 through C-87 shows that they are close enough for the purposes desired.

Figure A-18 is a plot of the propagation velocities from several

of the program tests. The water content varied from 26.5 to 25.1 percent, Table 4. This figure confirms the rather obvious fact that velocity is dependent upon the surface pressure initiating the stress wave. With the exceptions of Test 12 at 70 psi and Test 17 at 40.5 psi, the curves are in descending order of surface pressure. The reason for the transposition of Test 12 is not clear even though its water content was 26.4 percent and generally high in comparison with the other tests. The position of Test 17 is understandable since this was a repeat shot on the same soil specimen as that used in Test 11. Close examination discloses that the velocities in Test 17 exceeded those in Test 11 at all depths.

Figure A-19 shows the variation of peak stress velocity with surface pressure and soil water content. The pressure curves in Figure A-19a were not normalized for water content even though there was a 1.4 percent range. The water content curves in Figure A-19b were normalized to 200 psi. The 6-inch level was not plotted because of the scatter in the data. These curves indicate that peak pressure waves attained a relatively constant velocity at a water content of approximately 28 percent. This indicates that soil with this water content and above becomes saturated at 200 psi. This does not agree with the results shown in Figure A-3.

Based on Figures A-17b, A-18, and A-19, the calculated modulus should be fairly uniform in relation to depth, but should vary with

pressure and water content. At higher pressures the water content does not appear to have a large effect until a point is reached where the material does not approach saturation at the test pressure of interest.

The velocity of the peak pressure does not appear to vary with depth as some soil model builders believe, at least not within the depths used for these tests. This wave velocity appears to be dependent primarily on the stiffness of the soil, the surface pressure, and, of course, the type material which was a constant for these tests. Thus, the velocity of the peak stress is directly related to the stress-strain characteristics of the soil. These are discussed in Section A.10.3.

The velocities plotted in Figures A-17 and A-18 were not calculated from the stress-strain curves, but were measured directly from the oscillograph records of the soil pressure gages.

A.10.2 Rise Times. Dynamic amplification effects can be very important to buried structures just as they are for surface structures. Figure A-20 is a plot of the variation of rise time of the stress wave with depth, water content, and pressure. The rise time was nondimensionalized by plotting the pressure at the depth of interest over its rise time divided by the surface pressure over the rise time at the surface.

The effects of high water content were dramatic. The effects of

pressure were large at shallow depths. At a depth of 24 inches, the effects of water content below approximately 25.6 percent and of pressure within the range tested appeared to be minimal in the nondimensional form. Figure A-20 appears to confirm the findings reported in the main body of the report. At shallow depths of burial and high pressure levels with water contents around 26 percent, the rise time can affect the load which the test device experiences. Dynamic amplification was possible as the ratio of the rise times to the period of the structure and the test results showed.

A.10.3 Stress-Strain Curves. Stress-strain curves were generated at four water contents and at least four pressure levels using the impact loader previously described. The soil specimens were 6 inches in diameter and 1 inch high. Specimens 2-1/2 inches high were tried but the results were very erratic because of what appeared to be friction losses and the time necessary for the stress wave to traverse the specimen. Figures A-21 and A-22 show the results of these tests. Peak load was reached in 4 to 6 msec. In these curves the material displays a plastic behavior. It was only at high pressures in the wetter material that the shocking action caused by saturation became evident.

In addition to the laboratory stress-strain curves, similar curves were constructed using data developed during the SBIG tests. Data collected with the deflection and pressure gages located within

the soil at the 30- to 35- or 30- to 38-inch levels were used. Figure A-23 contains these curves. The low pressure curves appear reasonable while the high pressure curves are erratic. The total strains and shapes of the curves are considerably different from those in Figure A-22.

Figure A-23b also contains a stress-strain curve generated by using Schindler's one-dimensional compression device. The sample was 1 inch high by 10 inches in diameter. This curve is not similar to all the previously described curves.

It is evident that the rate of strain has a large effect on the characteristics of the stress-strain curve. It almost masks the effect of water content. One-dimensional tests were not as good an approximation of the SBLG conditions as they were in the static tests. This was especially true at high pressures.

Carroll showed similar strain rate effects in his investigation of buckshot clay, Figure A-24.

The stress-strain curves resulting from the laboratory confined compression tests were used to determine the constants in the clay models suggested by Seaman. Using the parameters described in Seaman's report it was not found possible to duplicate his results or to predict the results experienced in the SBLG.

A.10.4 Constrained Modulus. Constrained modulus was required to design the tests and the test devices. This modulus also was

calculated after each test in order to determine the actual relative flexibility of the structure versus the soil.

Prior to the main test program, the one-dimensional laboratory tests discussed above, the preliminary tests in the SBLG, and a method of calculation suggested by Johnson were used to estimate the constrained modulus. The modulus was determined in two ways from the SBLG tests. First the actual stress-strain curves were constructed as previously explained from data generated during Tests D and E. In addition, a modulus was calculated using the velocity of propagation of the peak stress. These were measured velocities and not calculated from the stress-strain curves. The stress waves shown in Appendix C were not considered shock waves, since their rise times, especially at depth, were normally measured in milliseconds and not microseconds. In spite of this "discrepancy," a modulus was calculated using the simple formula, $M_c = C^2 \rho$, where ρ is the wet density of the soil and C is propagation velocity of the peak stress between any two points of interest.

Table A-1 contains the values of constrained modulus derived from all sources. The range of values shown for the SBLG tests was calculated using the velocity from the surface to the 30-inch level and from the surface to the base. The stress-strain data were derived from two different locations, between the 24- and 36-inch levels, and between the 24- and 42-inch levels. When a range of values is shown it signifies that several tests were performed at that

water content and pressure level. The full range of values is given. The secant modulus and not the tangent modulus is used. Based on this, considerable difference was expected in the values of the modulus. The one-dimensional compression tests appear to agree more closely with the velocity data than the strain data which are larger in all cases. The values calculated using Johnson's approach also are shown. They agree with the one-dimensional tests rather well at the intermediate pressures, but appear to be high and low at the upper and lower extreme pressures respectively.

The soil moduli for the main test program are shown in Table 2 of the main text. Note that both velocity and strain data were used. In many cases the agreement was quite good; in others there was considerable difference. The modulus which appeared to be the mean of both ranges normally was used in the stiffness calculations.

Just as in the static tests, the constrained modulus of the soil was changing throughout the tests. These changes were due to the pressure acting on and saturation of the soil. The modulus also was affected by whether the soil was loading or unloading at the particular time in question. Figure 53b contains a curve showing the change in the relative stiffness of the structure versus the soil as Test 16 progressed. The modulus selected and used for most comparisons was calculated at the time of minimum arching. In this manner, the stiffnesses compared should correspond fairly closely to the arching condition examined.

Table A-1

Constrained Modulus of Soil Specimens Derived from All Sources, Preliminary Dynamic Tests

Test No.	Water Content %	PS psi	Height of Specimen in.	Velocity SPLG psi	Constrained Modulus		Calculated psi
					Stress-Strain SPLG psi	1-Dimensional Lab Compression Tests, psi	
A	23.3	236.0 107.0	43.9 1.0	2320		2190-2520	1300 2600 2200 1200
						2340	
B	27.2	212.0 120.0 103.0 118.0	42.1 1.0 1.0 1.0	1100-1230		2945-3210	1000 2200 1900 1550 1050
						2120	
						2180	
						1960	
C	32.1	205.0 97.0 95.0 70.0 43.0	43.1 1.0 1.0 1.0 1.0	3230-5820		1750	4000 2200 1900 1550 1050
						2560	
						2280	
						1920	
D	25.4	238.0 150.0 120.0 81.0	48.7 1.0 1.0 1.0	3520-11130	5710-6340	1230-1500	5100 4350 2700 1900
						2780	
						2420-2720	
						1875-2250	
E	25.6	41.0 41.7 60.4	48.0 1.0 1.0	1100-1581	1830-3360	1500-2100	1120 1150 1500
						2340	
						2560	

Table A-2

Range of Values of Constrained Modulus of Soil Specimens Derived
from All Sources, Preliminary Dynamic Tests

Approx Water Content %	Test Pressure psi	Constrained Modulus		
		1-Dimensional Lab Compression Tests, psi	SBLG Tests psi	Consolidation Tests psi
24.0	37.5	1875-2260	1700-2040	2230
	240.0	3380		6360
25.0	37.5		1570-1870	
	75.0		1650-1700	
26.0	37.5	1920-2175	1500	
	50.0		3830	
	75.0	1850-1920	1875	
	100.0		1545	
	155.0	2980		
	240.0	3660-3840		
27.0	37.5	1500-2160		1910
	75.0	2320		
	175.0		6150	
	240.0	4460	7450-7950	7020
32.0	37.5	1040		1420
	75.0	1940		
	240.0			4660

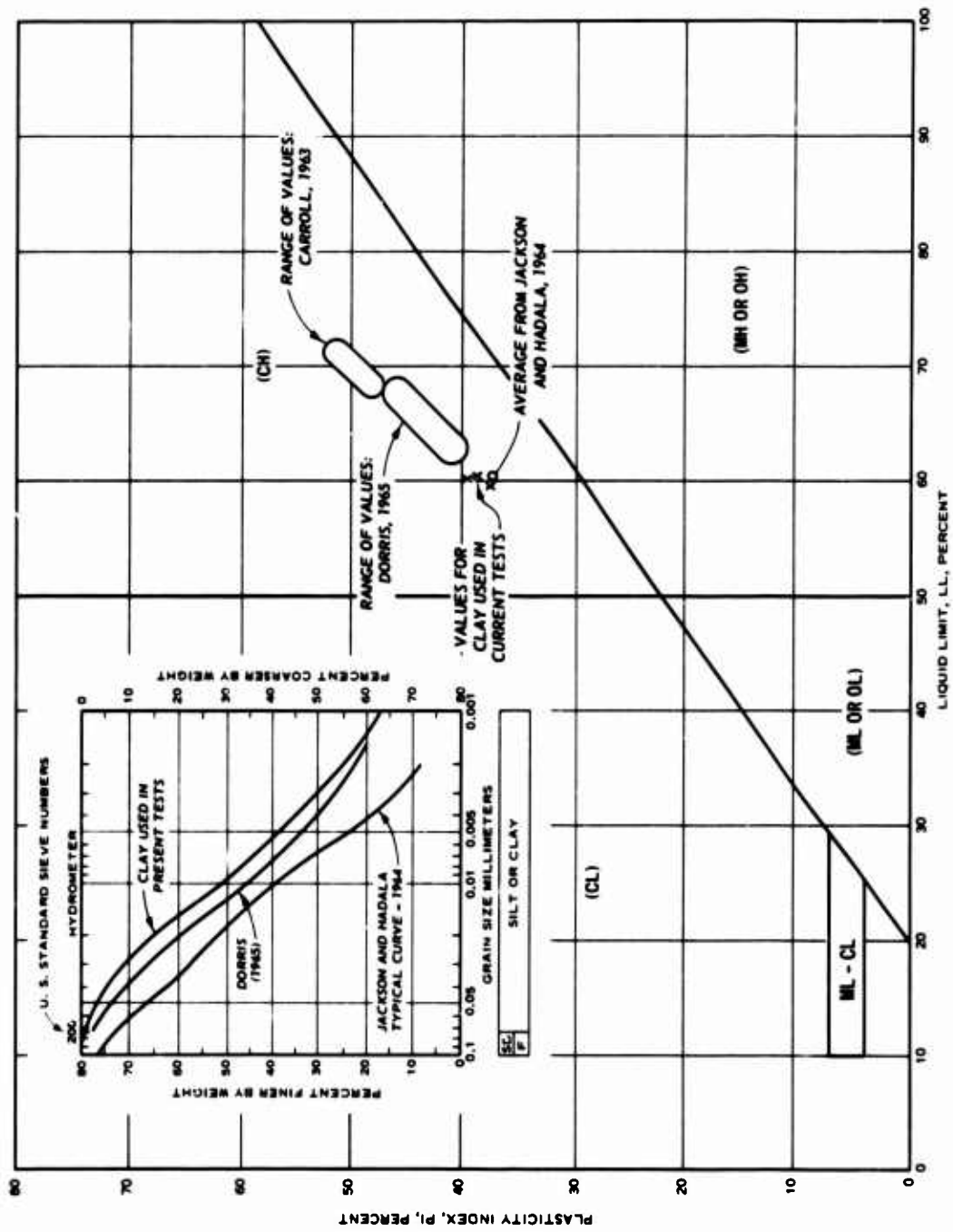


Fig. A-1. Gradation curve and Atterberg limits for buckshot clay

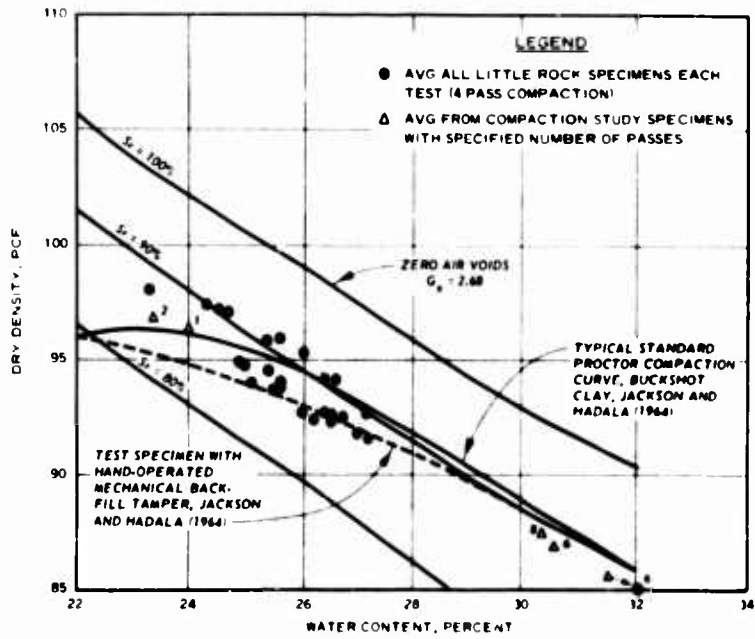


Fig. A-2. Water content-density relations for buckshot clay

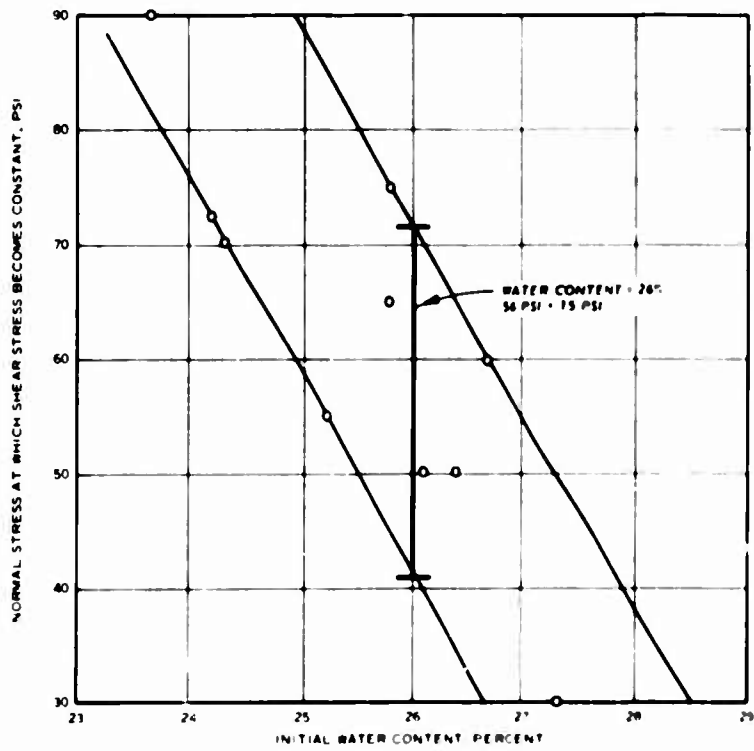
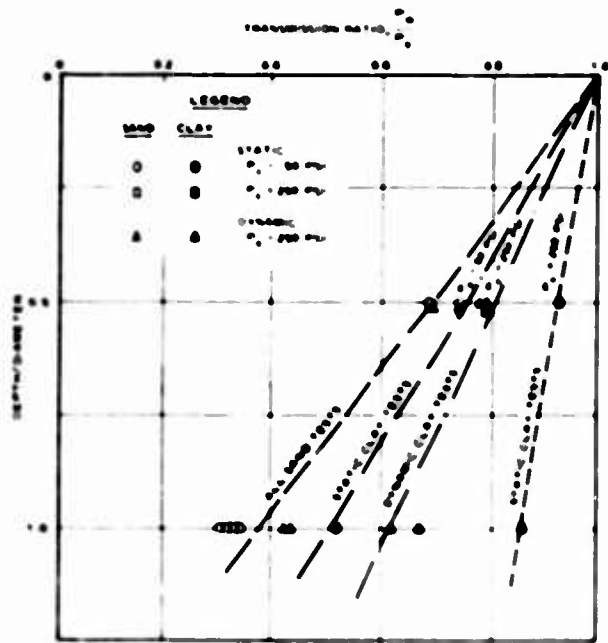
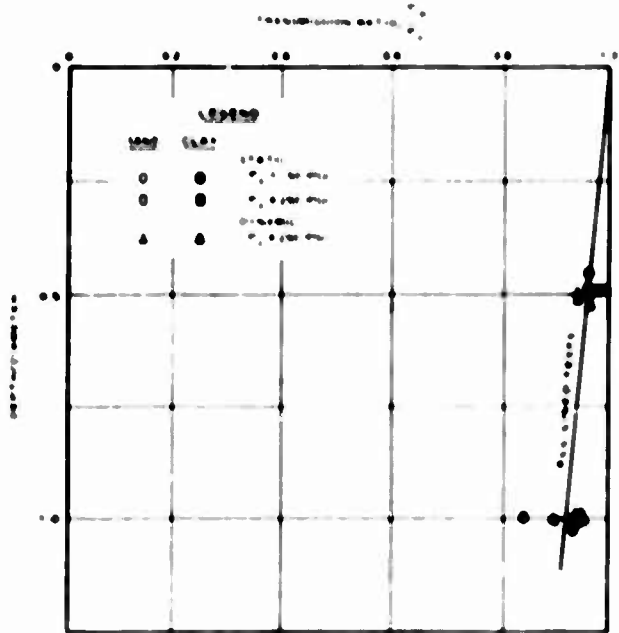


Fig. A-3. Approximate value of stress at which buckshot clay becomes saturated

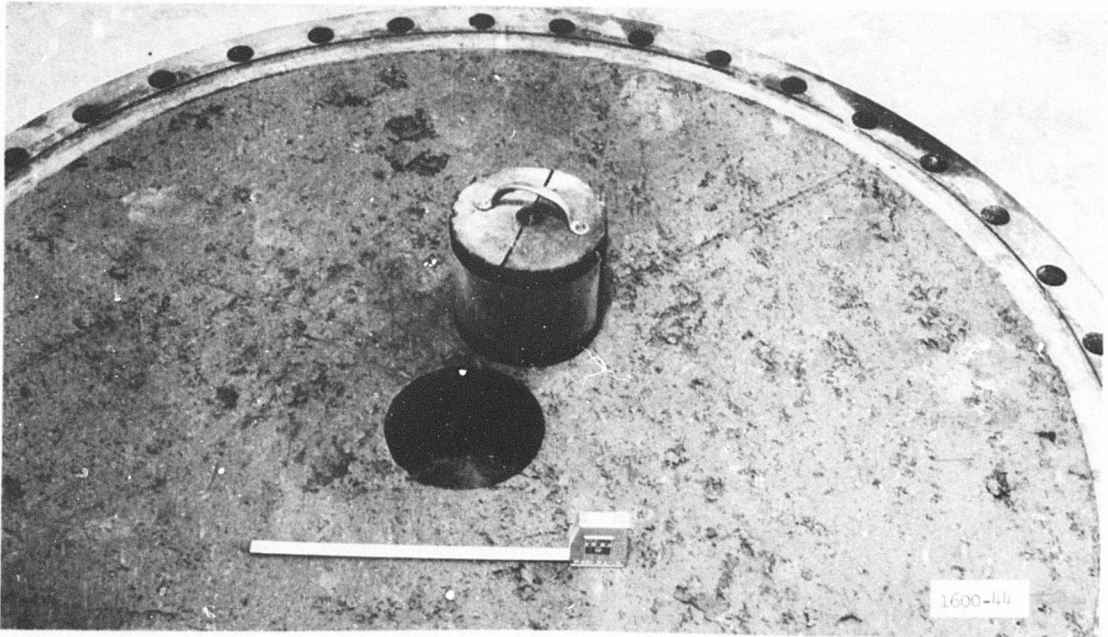


a. Unlined specimens

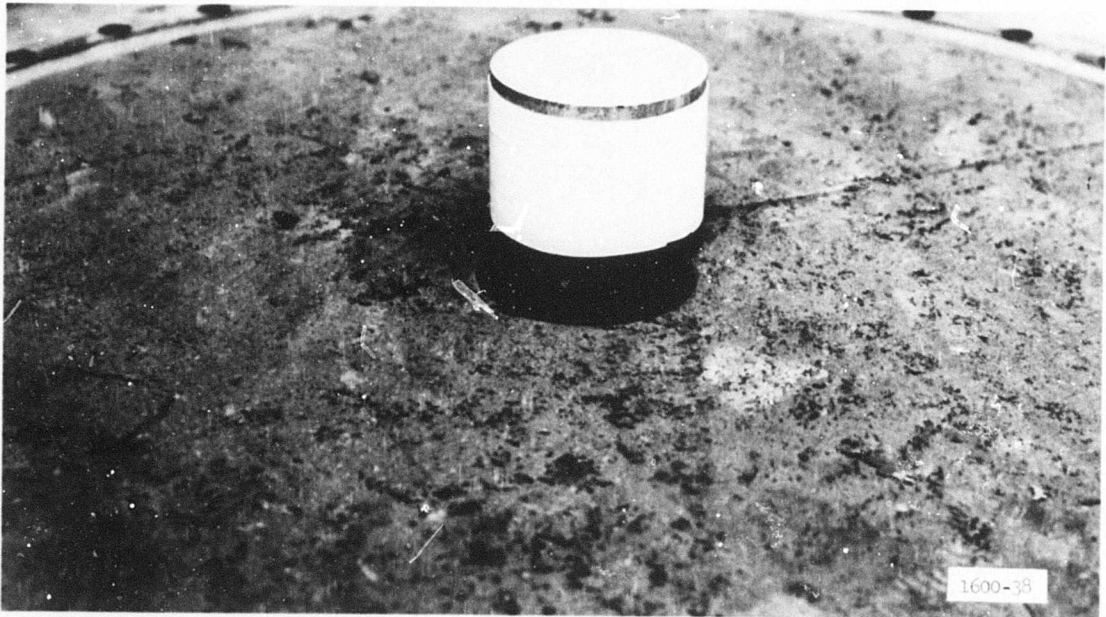


b. Lined specimens.

Fig. A-4. Results of wall-friction studies in the WES-SBLG by Hadala (1967)

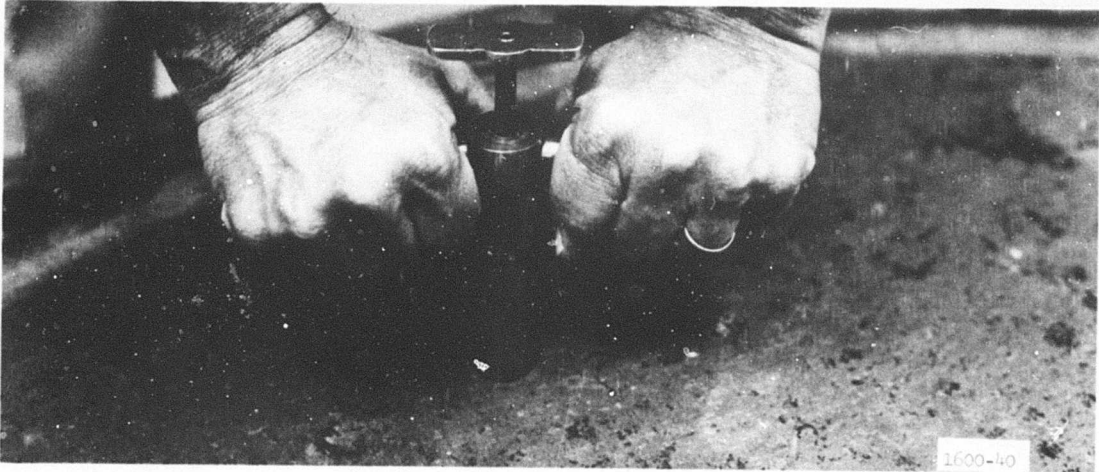


a. Form used for placement of test device

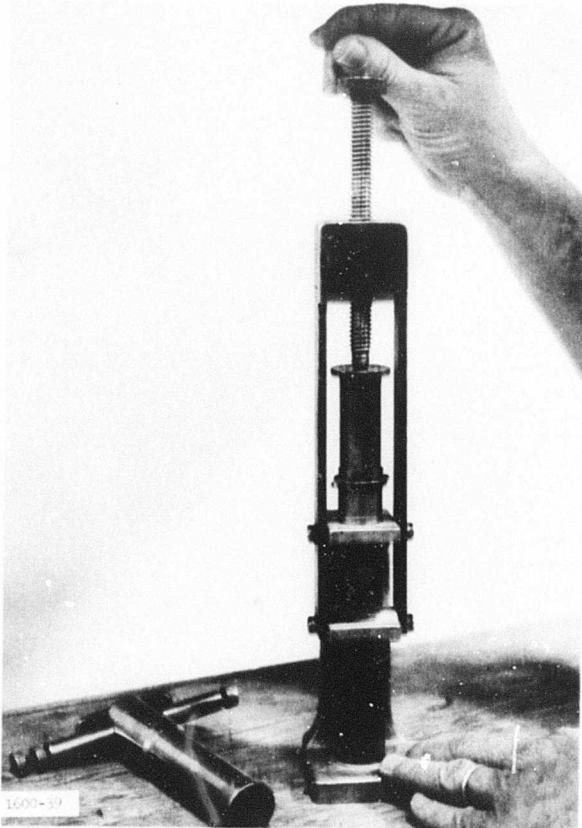


b. Test device with Teflon cover, ready for lowering in prepared hole

Fig. A-5. Placement of test device

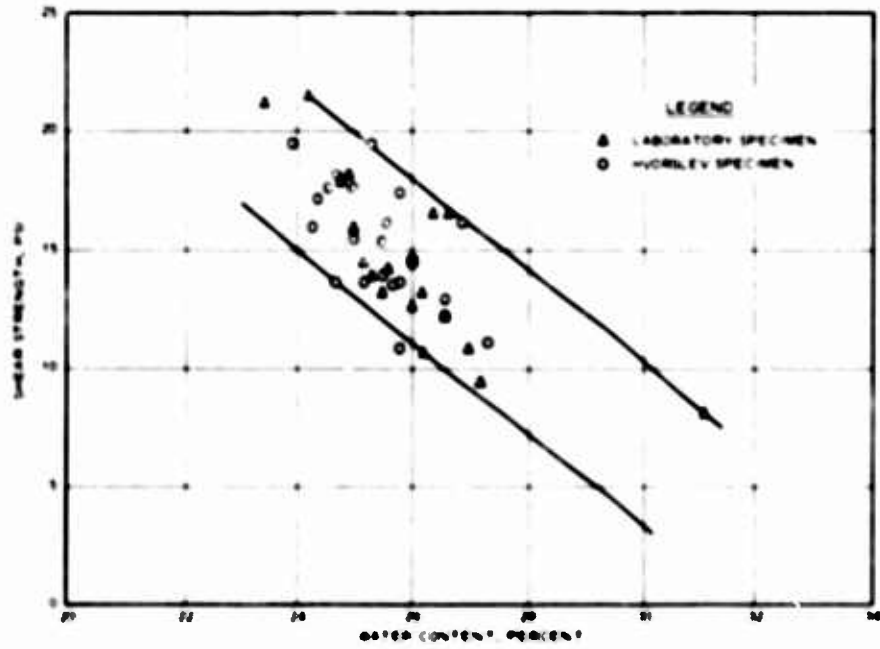


a. Sampler

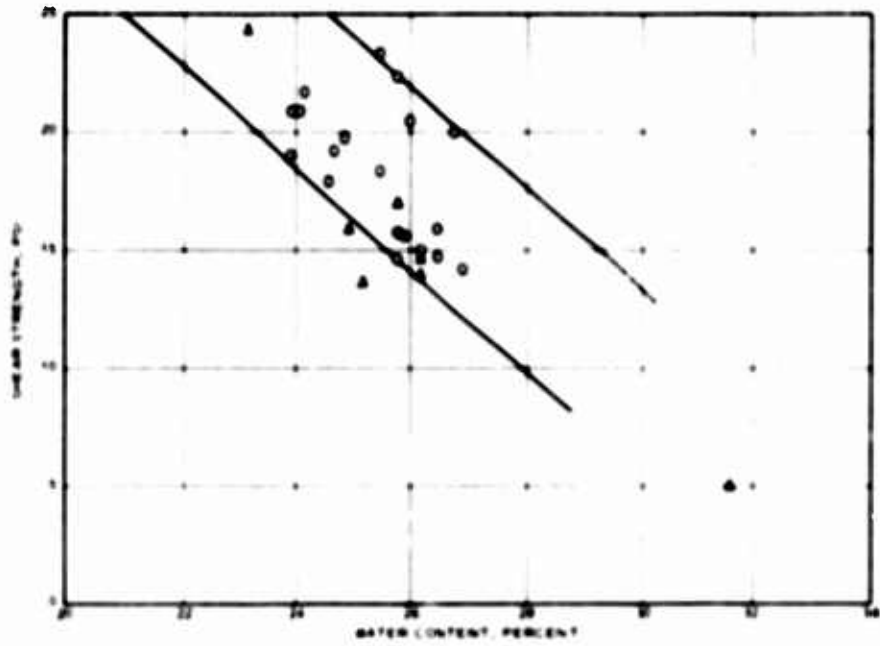


b. Unconfined compression device

Fig. A-6. Use of Hvorslev technique



a. PRETEST UNCONFINED COMPRESSION



b. POSTTEST UNCONFINED COMPRESSION

Fig. A-7. Comparison of unconfined compressive strength as determined by Horsley and laboratory techniques

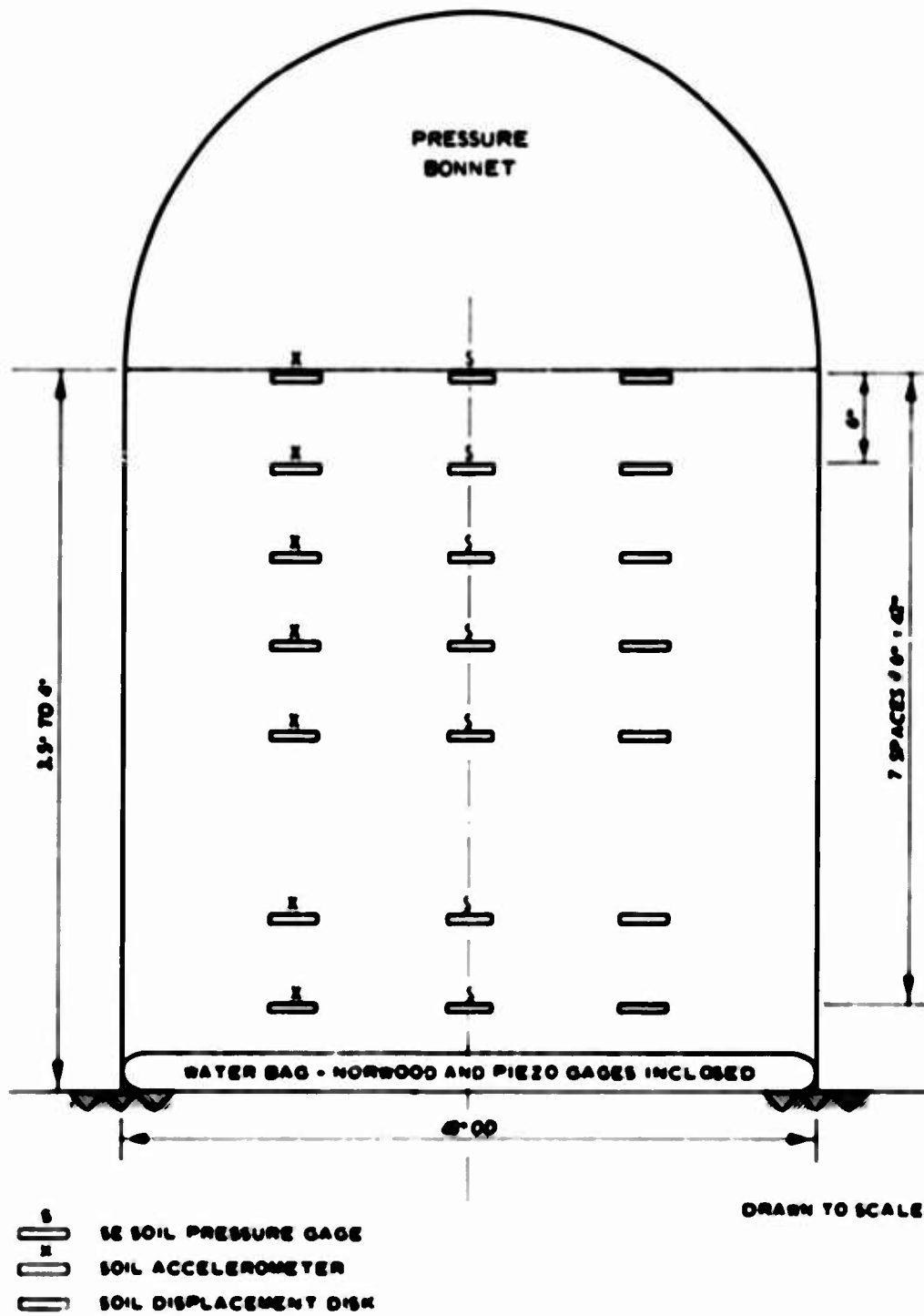
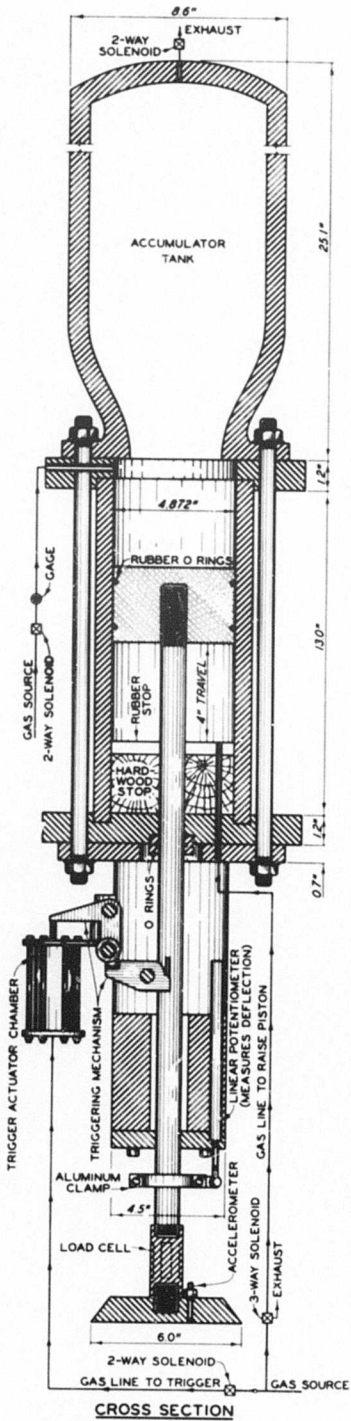
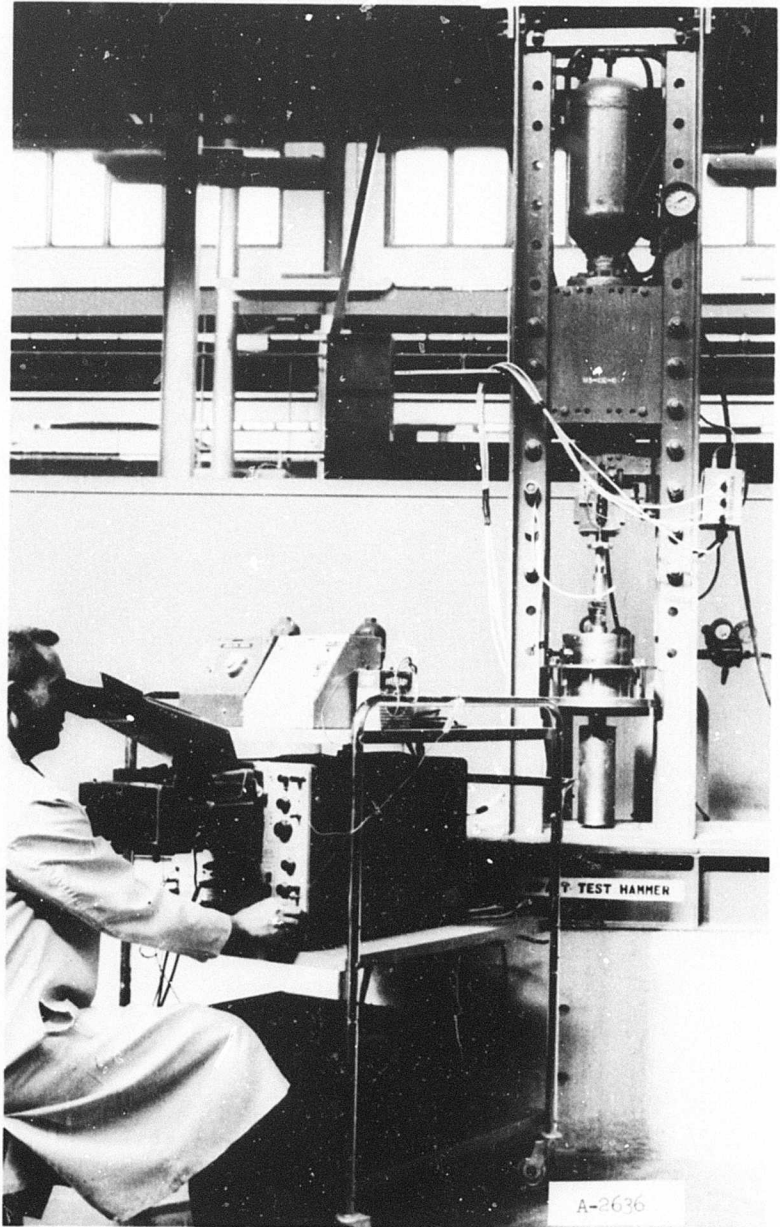


Fig. A-2. Test geometry for preliminary tests in SHLG



CROSS SECTION
IMPACT AIR HAMMER
APPARATUS



b. Impact hammer in test position with instrumentation

a. Cross section of impact hammer

Fig. A-9. Impact hammer used for confined compression tests

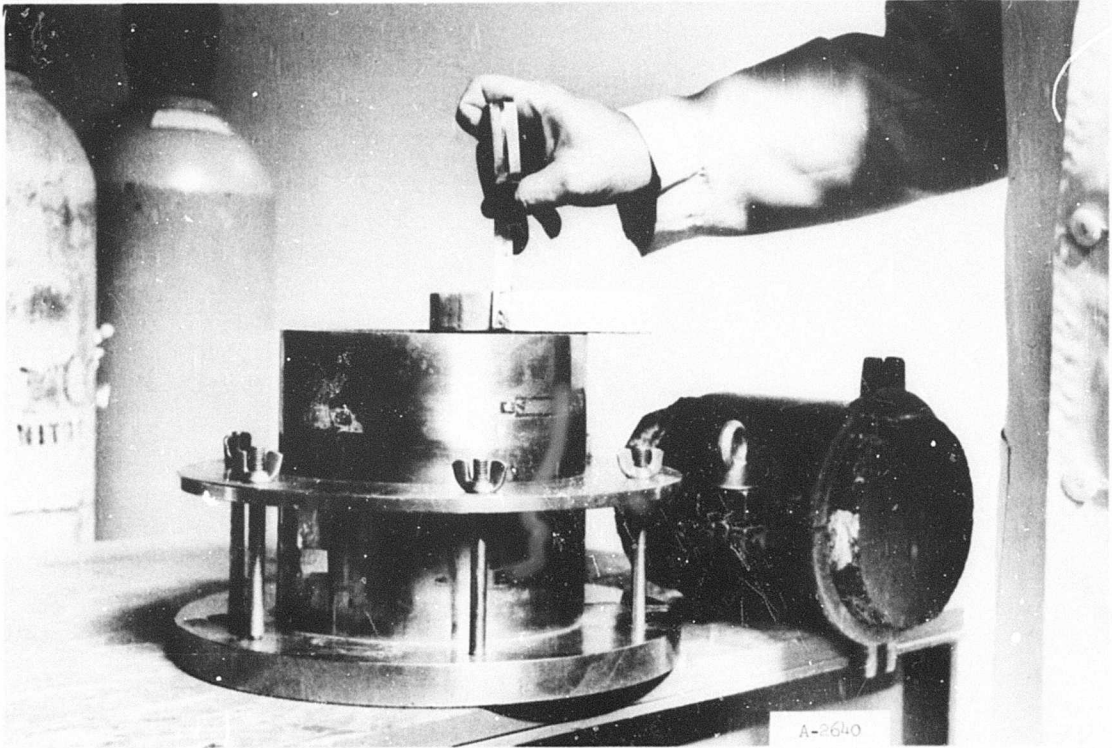


Fig. A-10. Mold, confining chamber, and soil disk used in confined compression tests

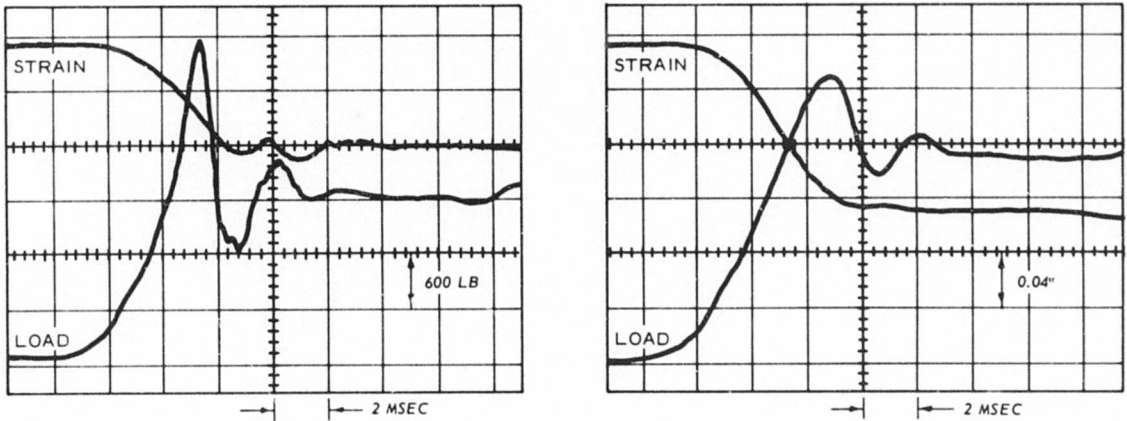
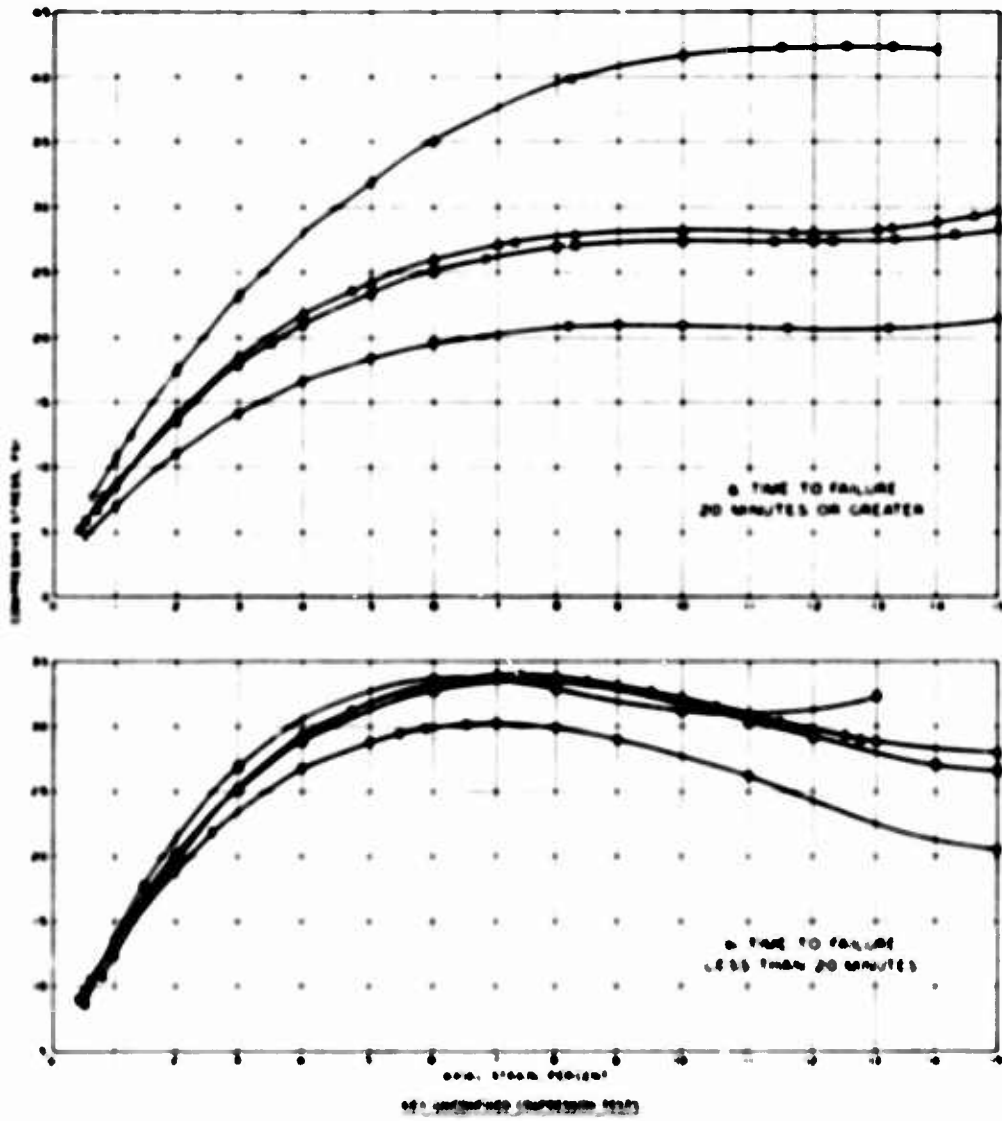


Fig. A-11. Typical oscilloscope records from confined compression tests



Specimen	Specimen Number	Time to Failure (min)	Modulus of Elasticity (psi)	Modulus of Rupture (psi)	Modulus of Resilience (psi)	Modulus of Toughness (psi)
○	20-1-20-1	1	20,000	10,000	10,000	10,000
△	20-1-20-2	1	20,000	10,000	10,000	10,000
□	20-1-20-3	1	20,000	10,000	10,000	10,000
◇	20-1-20-4	1	20,000	10,000	10,000	10,000
●	20-2	1	20,000	10,000	10,000	10,000
⊙	20-3-20-1	1	20,000	10,000	10,000	10,000
⊕	20-3-20-2	1	20,000	10,000	10,000	10,000
⊖	20-3-20-3	1	20,000	10,000	10,000	10,000

Fig. A-12. Stress-strain relations for buckshot clay as determined by unconfined compression test

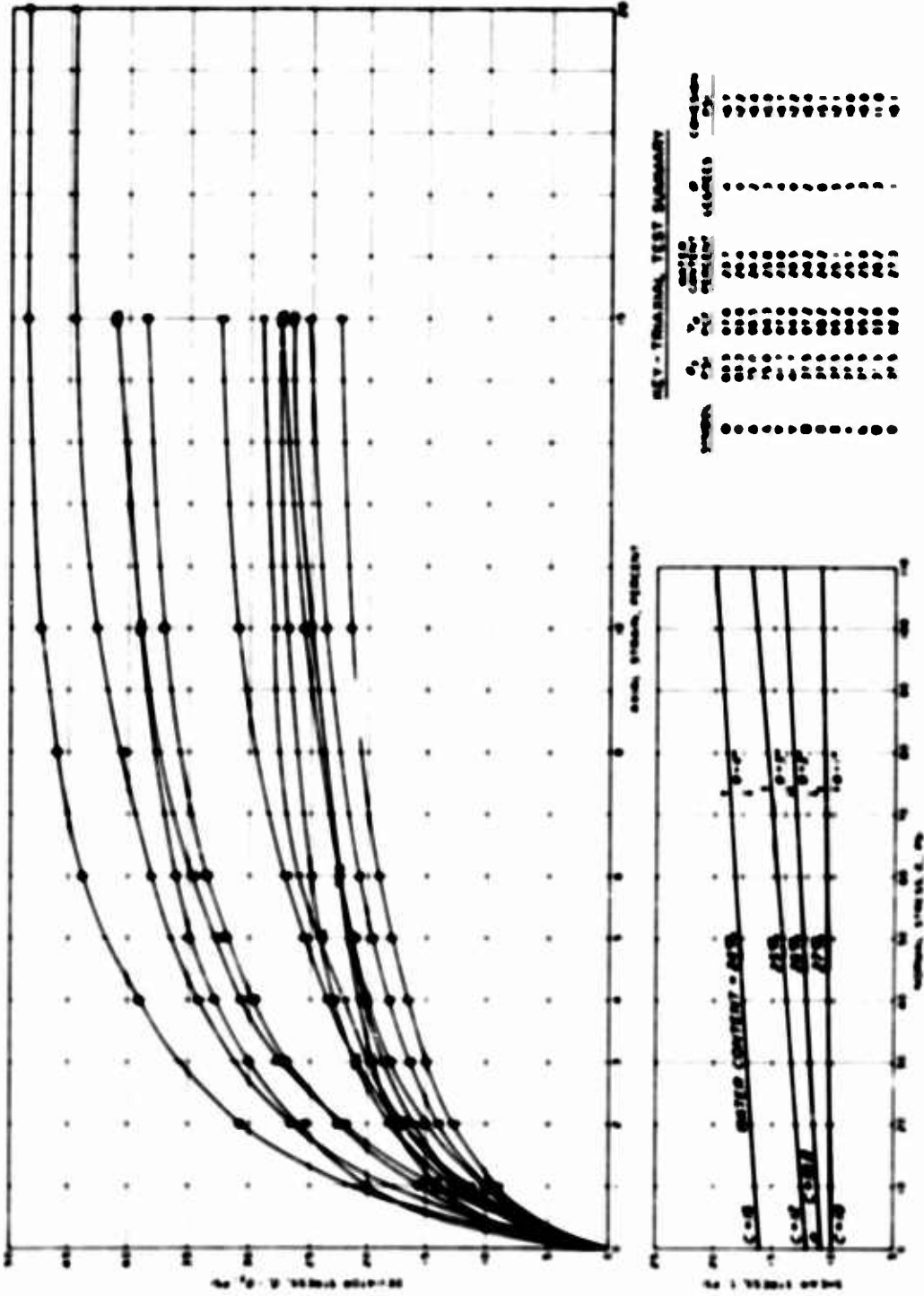
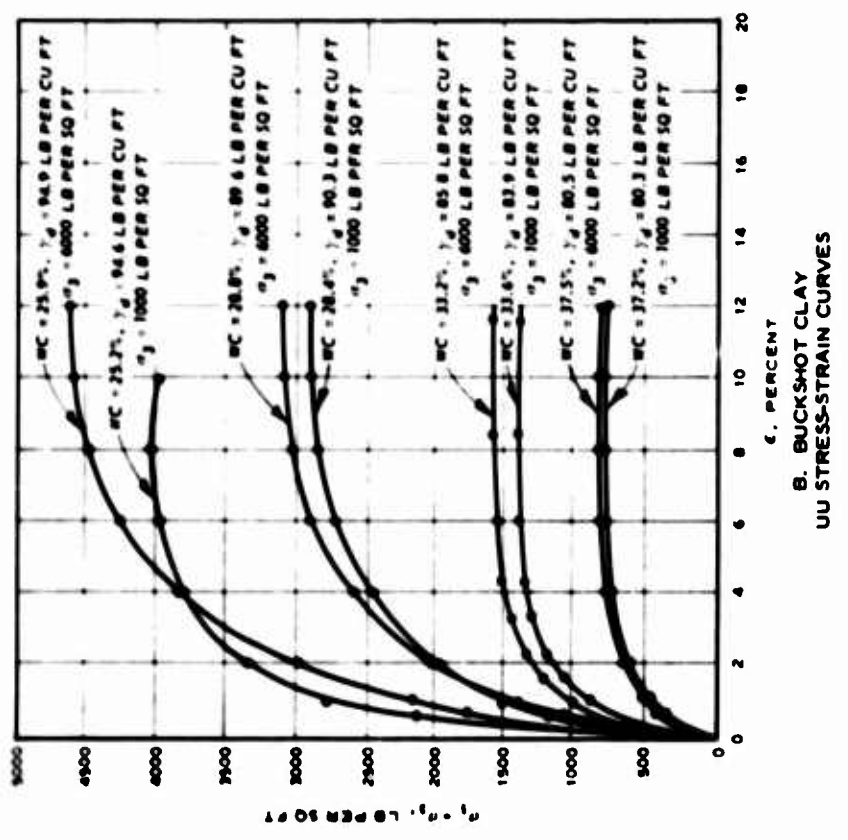
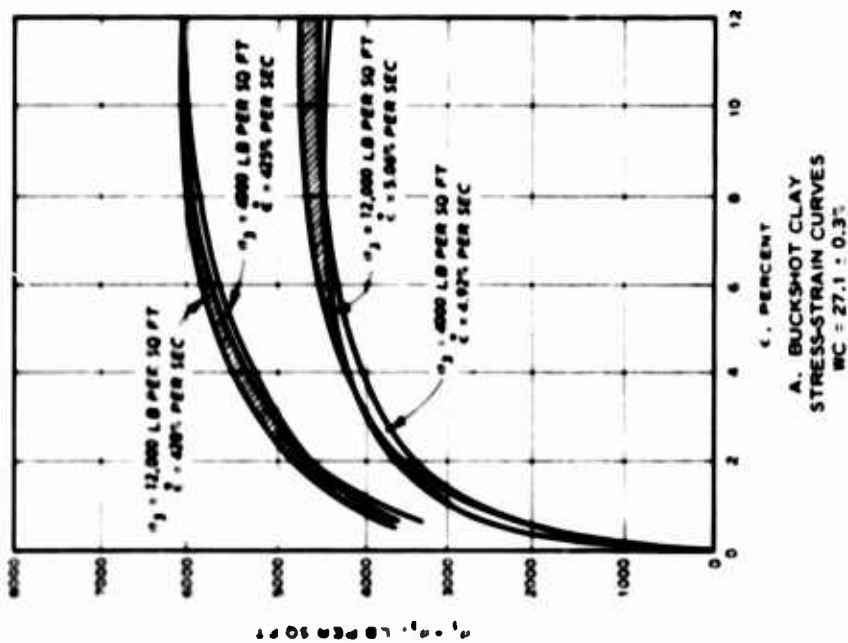


Fig. A-11. Stress-strain relations for buckshot clay as determined by triaxial compression tests



A-14. Effects of confining pressure, water content, and strain rate on the shear strength of buckshot clay (after Carroll)

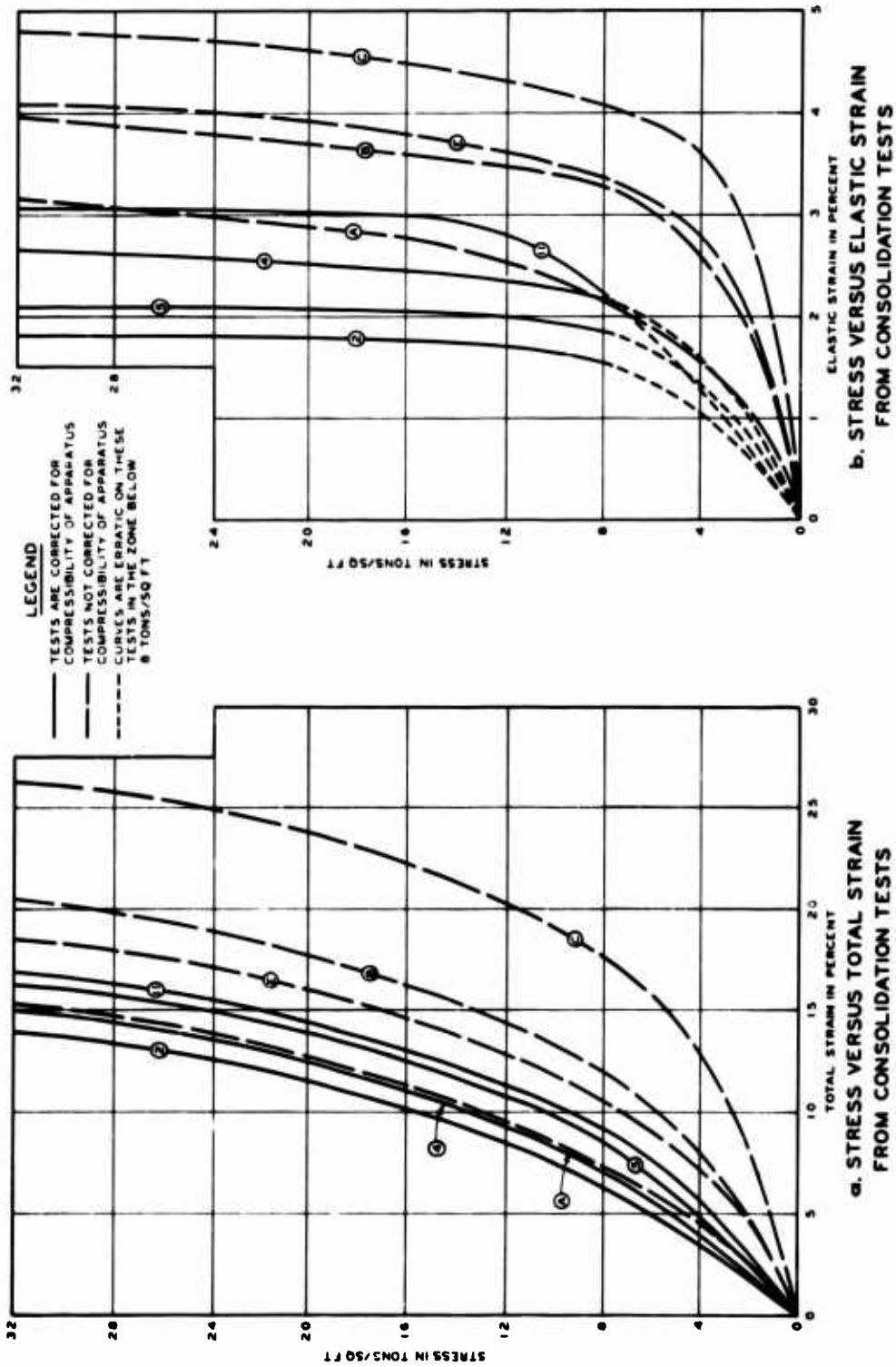


Fig. A-15. Stress-strain curves constructed from consolidation test results

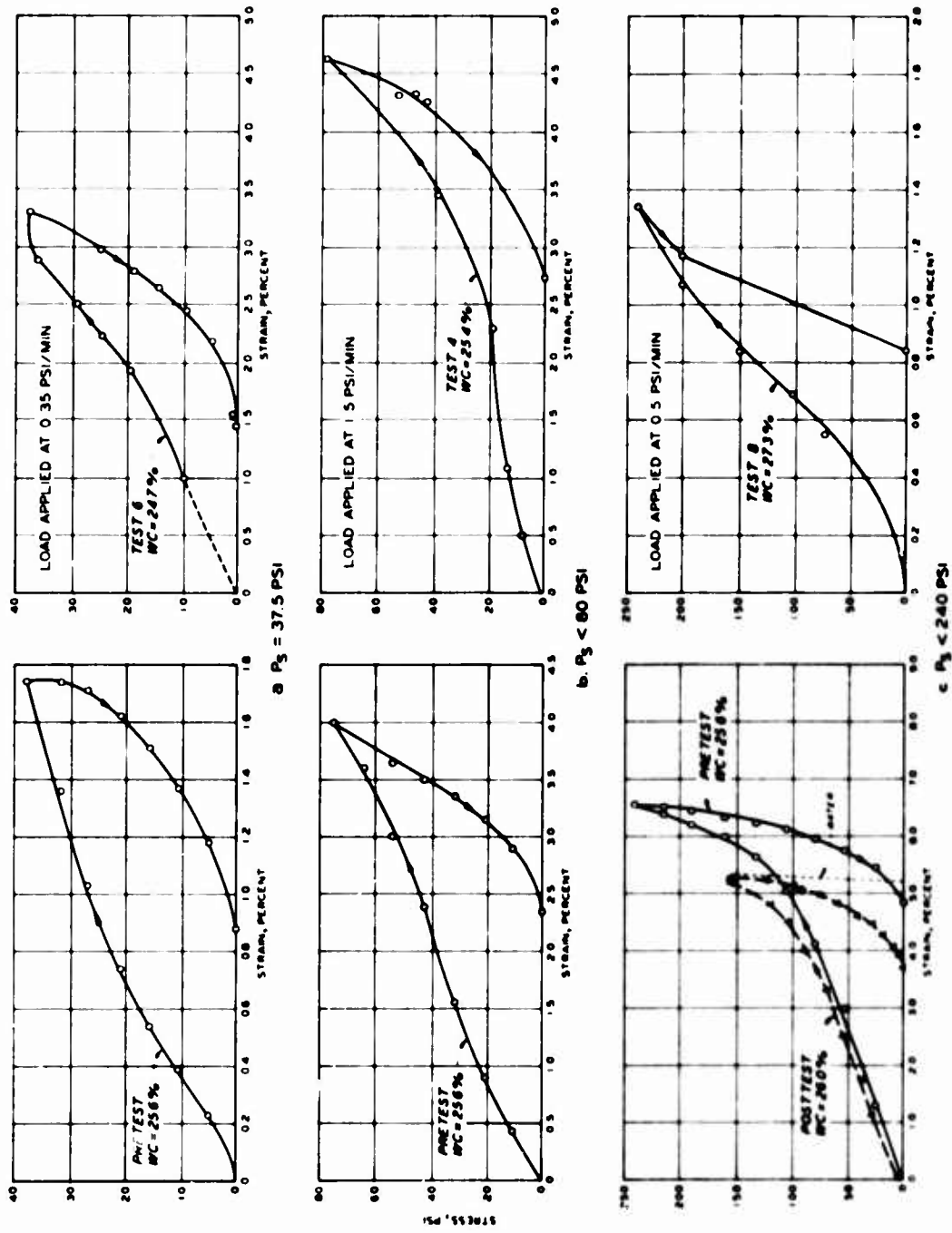


Fig. A-16. Stress-strain curves determined by static one-dimensional tests

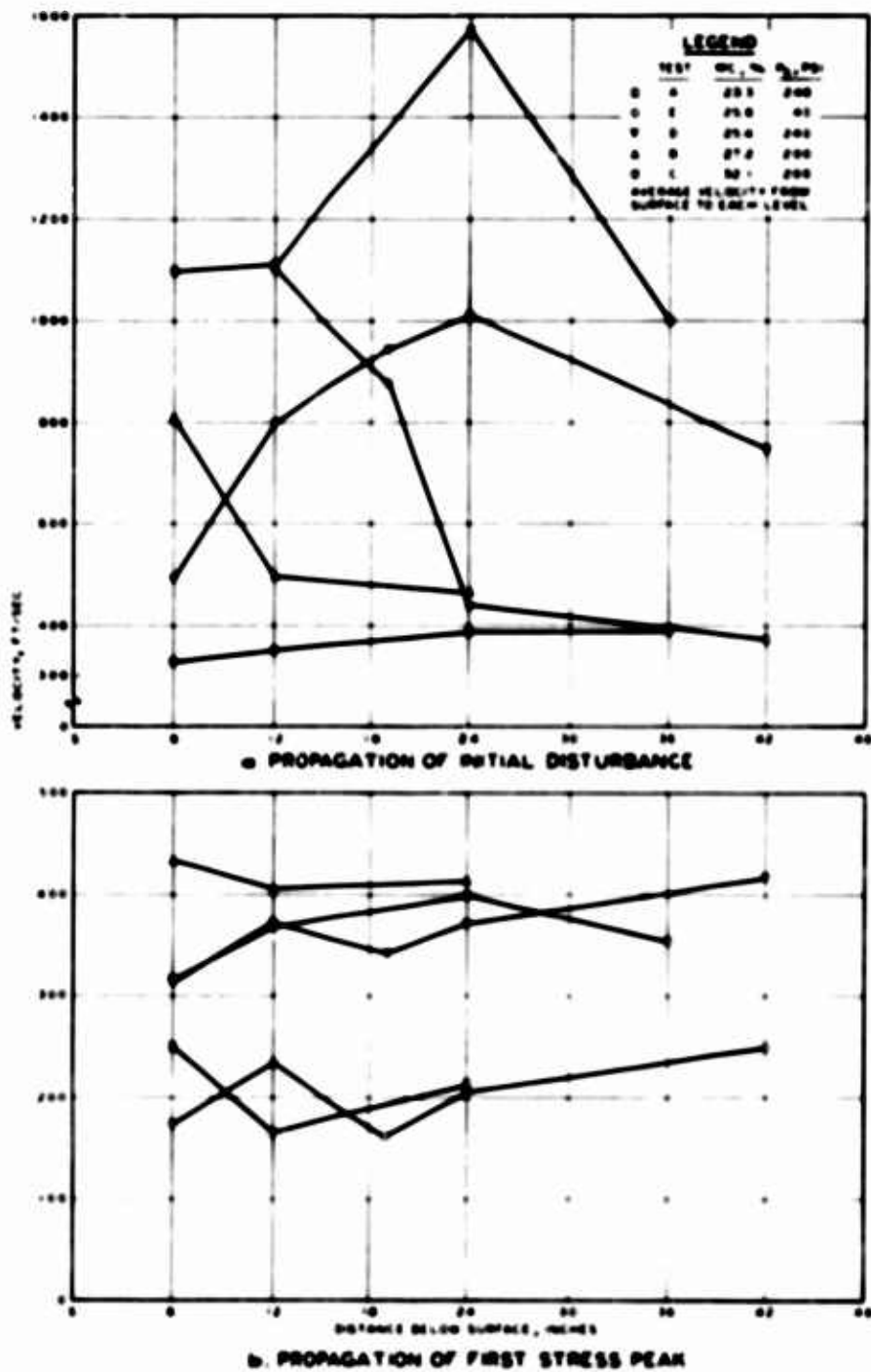


Fig. A-17. Variation of velocities with pressure and soil water content, preliminary SBIG tests

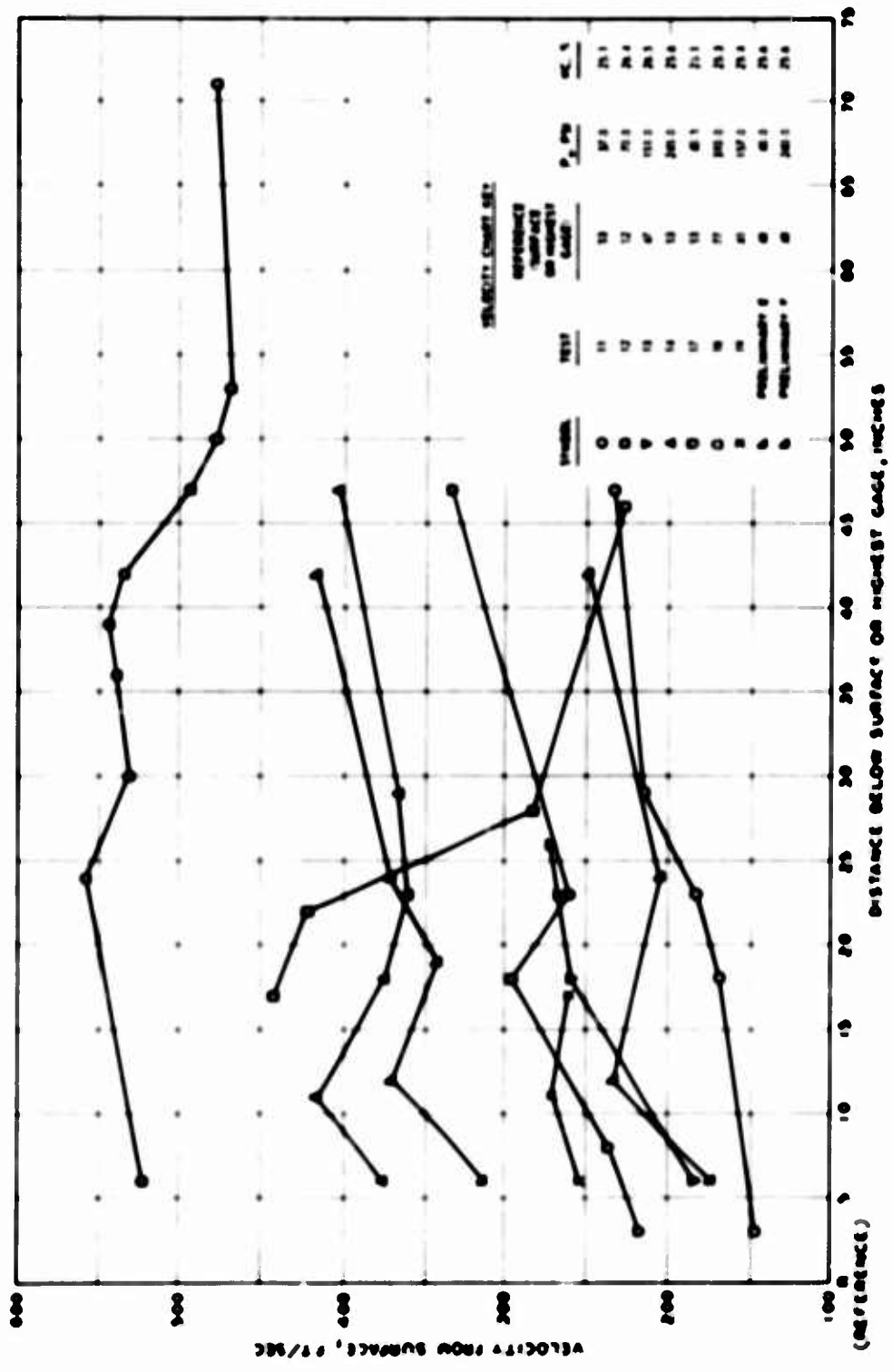
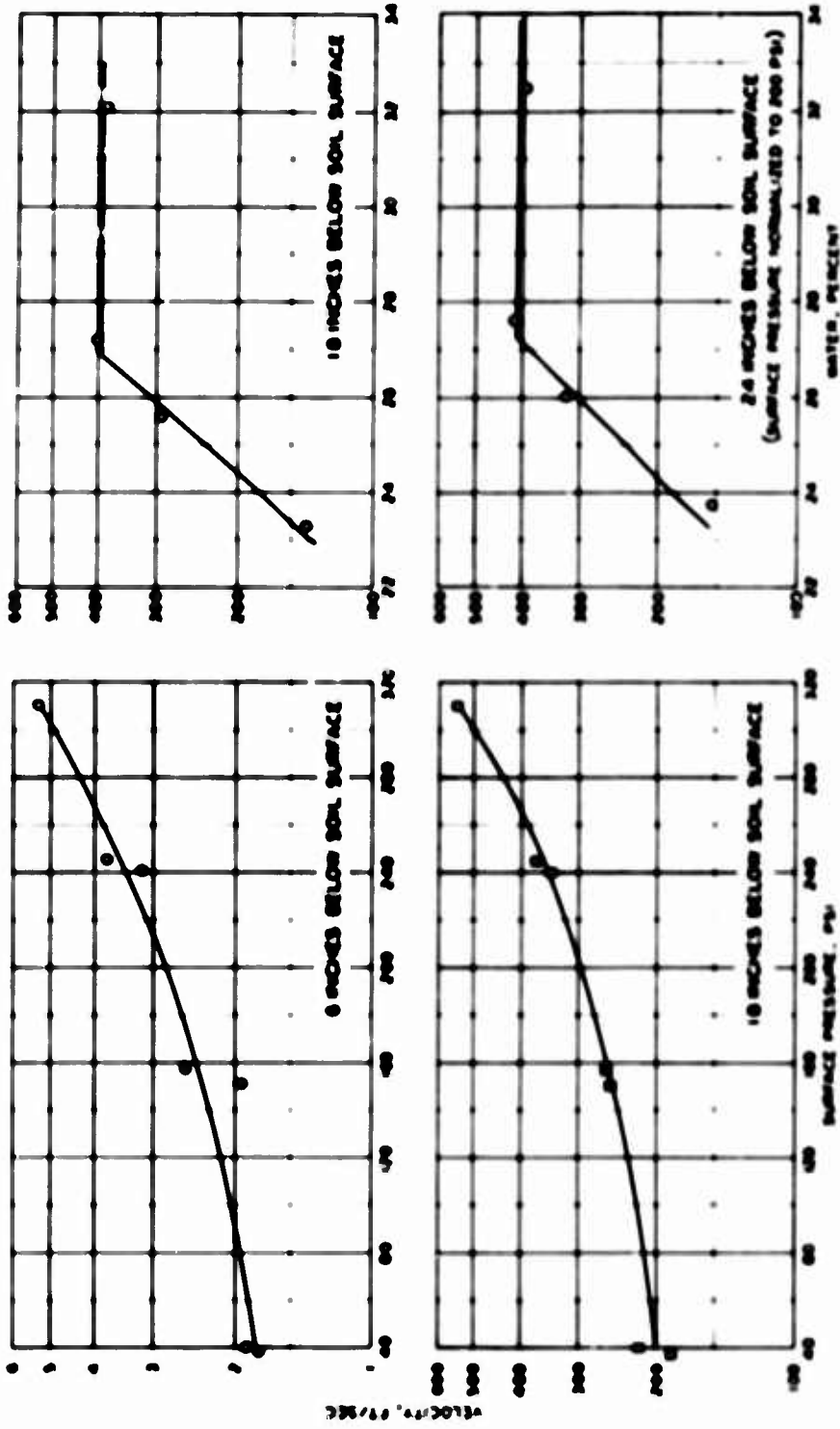


Fig. A-18. Variation of velocity of propagation of first stress peak with surface pressure



b. PEAK STRESS WAVE VELOCITY VERSUS SOIL WATER CONTENT

a. STRESS WAVE VELOCITY VERSUS SURFACE PRESSURE

Fig. A-19. Variation of peak stress velocity with initiating pressure and soil water content

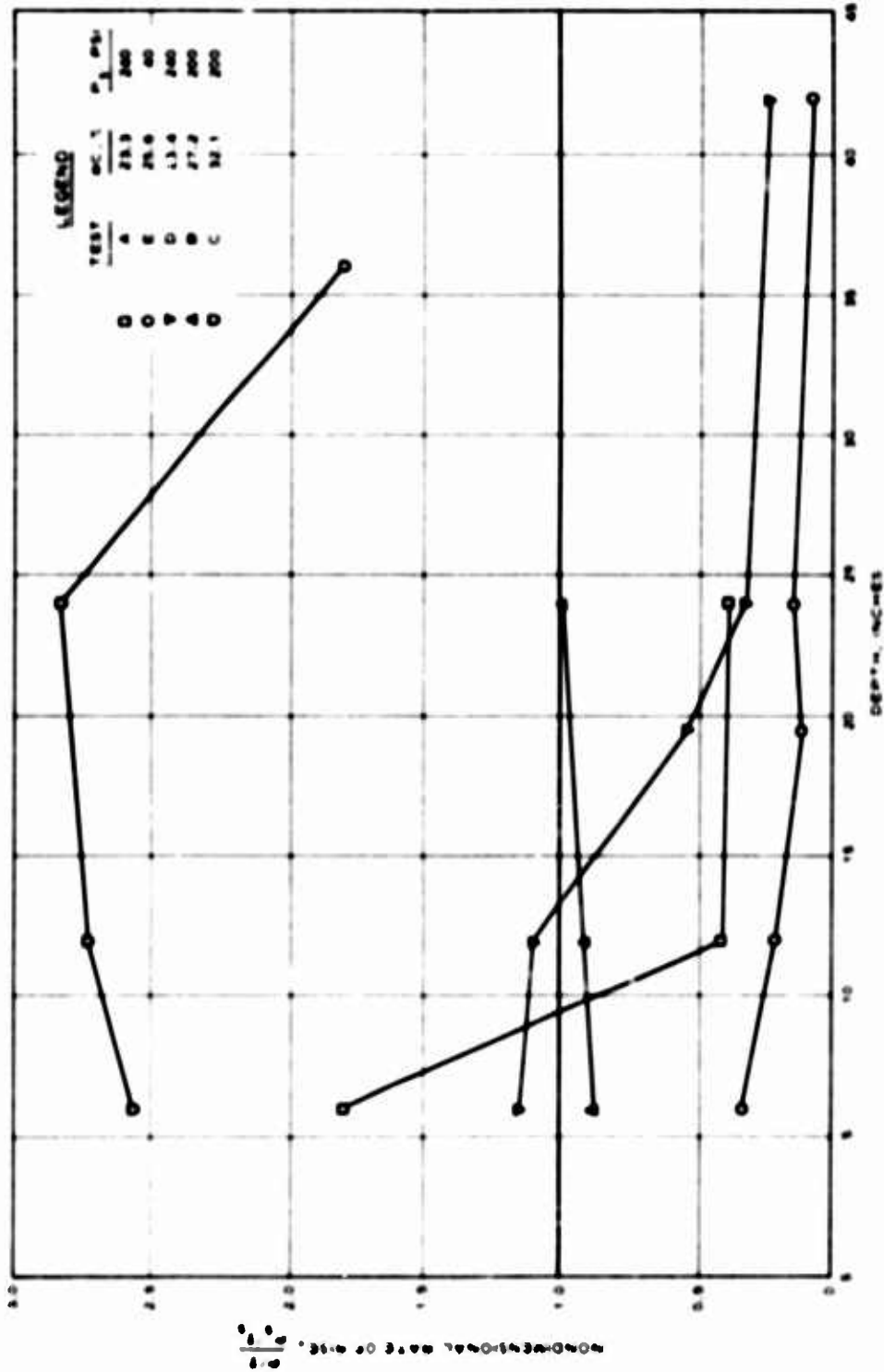


Fig. A-20. Nondimensional rate of rise variation with depth (average of north and south morwood rates of rise set equal to 1.00)

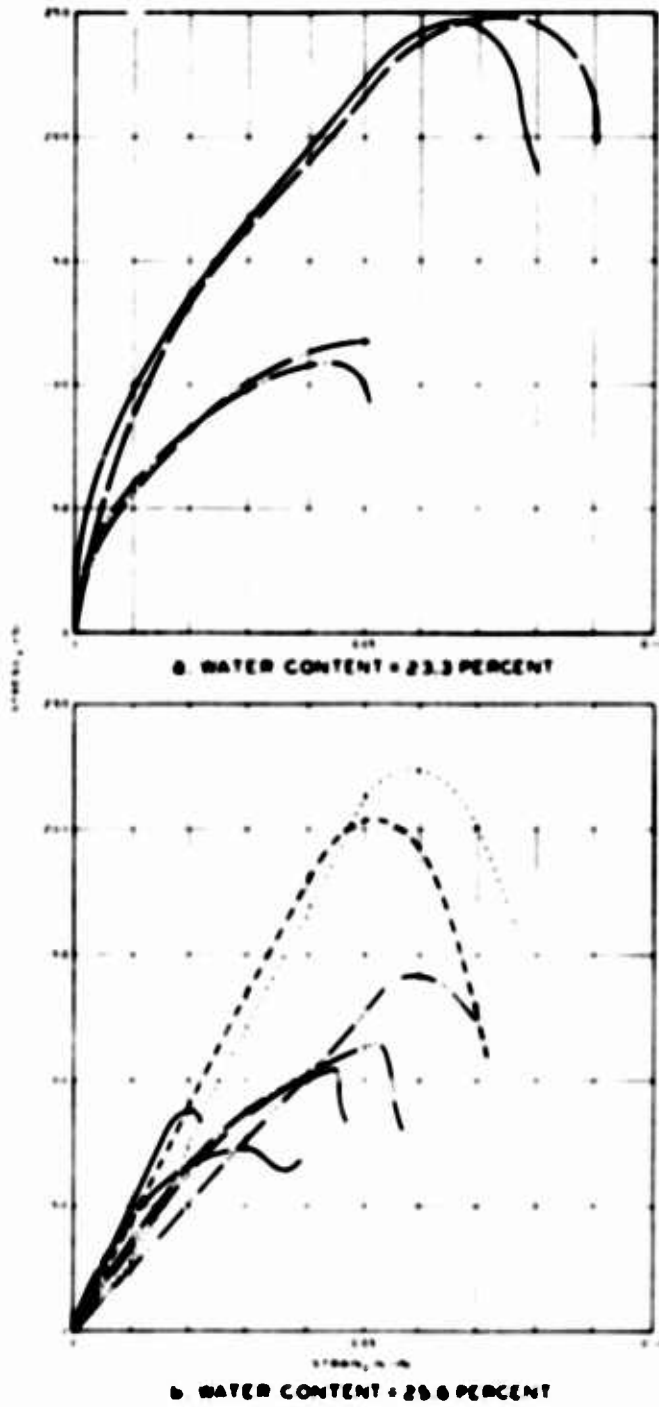


Fig. A-21. Stress-strain curves, buckshot clay, impact loader; water contents, 23.3 and 25.6 percent

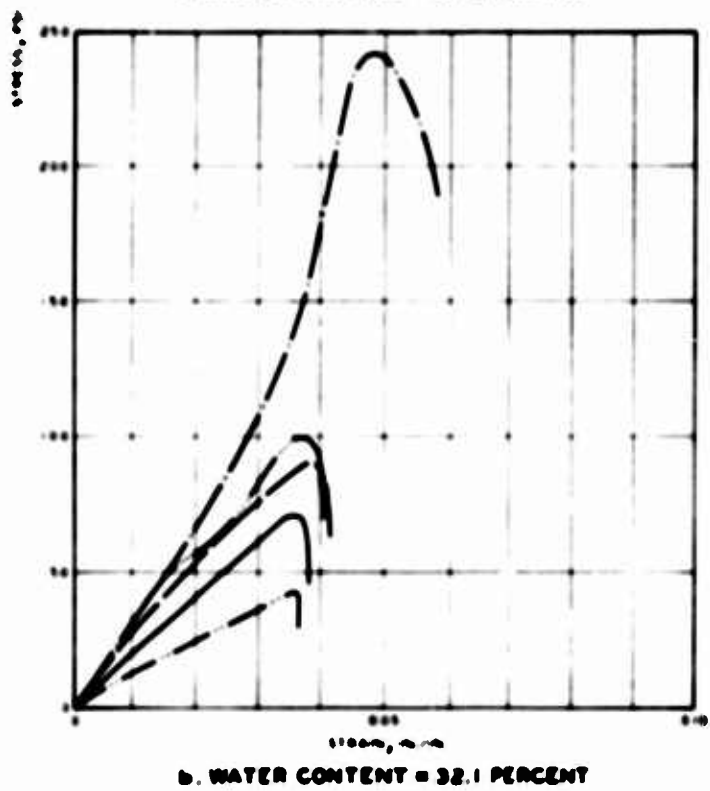
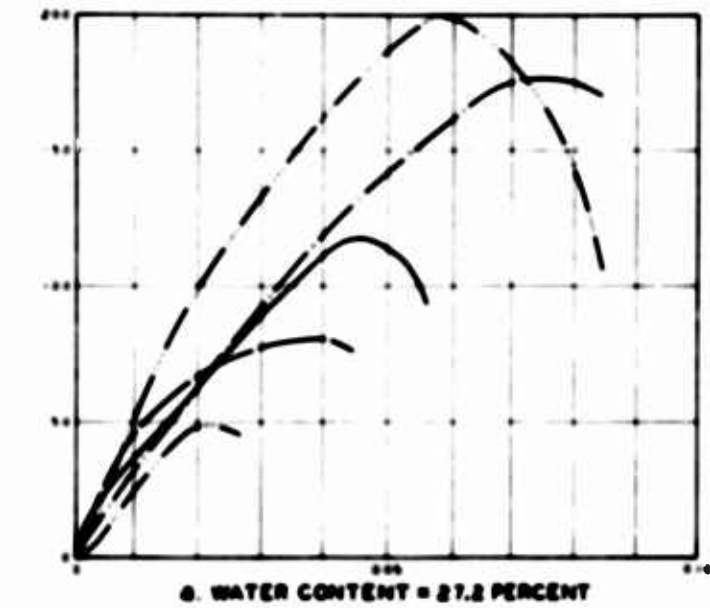


Fig. A-22. Stress-strain curves, buckshot clay, impact loader; water contents, 27.2 and 32.1 percent

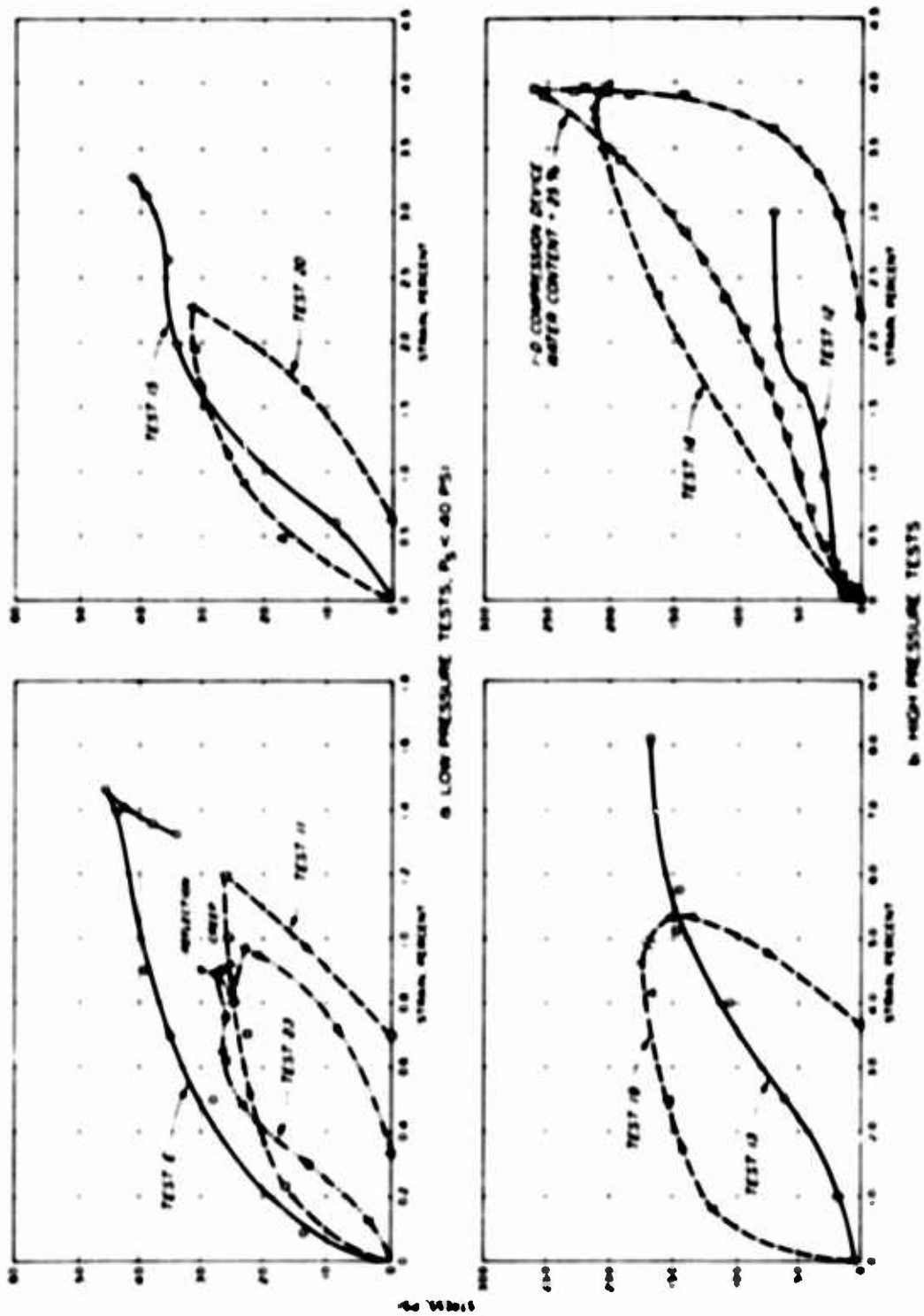


Fig. A-27. Stress-strain curves, buckshot clay, SFLC tests

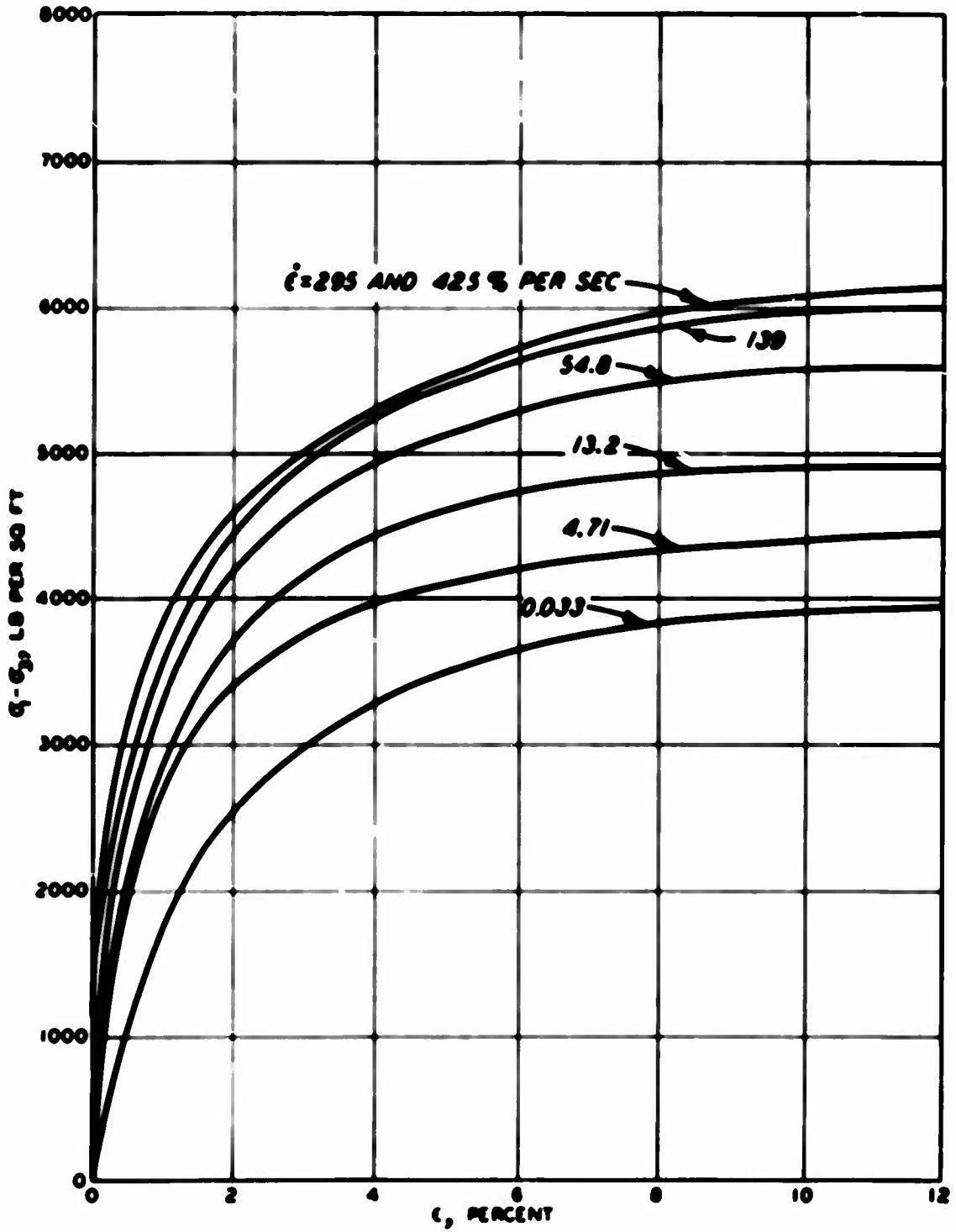


Fig. A-24. Stress-strain curves, buckshot clay (after Carroll)

APPENDIX B

DESIGN OF SPRING-RING TEST DEVICE

The spring-ring test device used in the test program described in the main text is believed to be unique. In order to assist others with a similar design problem and to prevent repetition of similar mistakes, the step-by-step development of this device is outlined in this appendix.

The performance requirements of the flexible test device posed severe problems in the development and design of a structural member which could provide the prescribed elastic and deformation characteristics. The design of the experiments dictated that the size of the test device remain constant for all tests. Additional constraints were: (1) range of spring constants, (2) overall mass of test device, (3) radial stiffness of test device, (4) lateral strength and stiffness of test device, (5) space occupied by the elastic member, and (6) space requirements for displacement and acceleration gages.

Table 3 of the main text shows the range of spring constants desired: 495 lb/in. to 8,950,000 lb/in. These constants were selected based upon the stiffnesses of buckshot clay developed in the preliminary test program described in Appendix A. The main purpose of this program was an investigation of structure stiffness on

soil arching; therefore, a large range of stiffnesses was desired. In addition to the stiffness requirements, sufficient displacement of the top of the device relative to the base was required to develop maximum arching at various depths of burial and surface pressure. These displacement requirements were estimated using the results from Hendron's (1968) trapdoor experiments with the same buckshot clay at similar water contents.

A number of approaches were considered in the initial attempts to design a suitable elastic structural member for the flexible device. In this phase of the design and development a broad range of spring types was surveyed. This survey is summarized in the following paragraphs.

The widely used helical coil spring was the first spring type studied extensively. Structural configurations were evaluated for a single large helix, concentric large helices, and multiple small helix springs within the housing of the test device. Calculations showed that all the configurations tried for this spring type could not provide the required spring constants and displacement range. In addition this spring type had no inherent lateral stiffness and required that other structural members in the test device provide lateral strength. The design calculations using the helical spring were so discouraging that it was dropped from consideration early in the investigation.

Another general spring type considered was the spring column approach attempted by Mason (1965). This approach utilized the differing moduli of elasticity of selected materials such as steel, aluminum, plastic, etc., to fabricate cylinders which gave the desired spring constants. This configuration provides structures with inherently high radial and lateral strength but is very limited in the range of physically realizable spring constants. Calculations using this approach quickly showed that it would be unsuitable for any aspects of the planned experiments except for the extremely rigid devices.

A closely related modification of Mason's approach was considered. Specially formulated plastics and grouts were studied and tested for use as spring cylinders. This approach had some possibilities, but the close control of spring constants and deflections required was not possible.

Other configurations considered were Bellville springs, leaf springs, metal bellows, diaphragms, proving rings, and tapered disk springs as described by Brecht and Wahl. The Bellville springs were eliminated from consideration when their inherently high hysteresis was discovered and also because of the limited displacement range obtainable with their use. Leaf springs could be devised for the lower spring constants only and were laterally weak. Commercially available bellows suffered from the same limitations

as the leaf springs. Diaphragms did not permit the attainment of the necessary displacement range.

Tapered disk springs appeared to have good possibilities. A wide range of spring constants was available within the physical size constraints of the test device. The disk spring was inherently strong radially and was found to have fair lateral strength and stiffness. Several scale drawings were made of the test device utilizing this type of spring design. One of these designs could have been used for some of the desired spring constants. The tapered disk spring approach was finally discarded because of the development of still another spring design concept which had been maturing during the study and evaluation of the spring types described above.

The design approach which eventually lead to the adopted spring system is illustrated in Figure B-1. Initially, flattened proving rings were tried as the spring element (Figure B-1a), but this configuration severely limited the allowable displacement. While the original approach was not suitable, it lead to the idea of using a machined outer cylinder as shown in Figure B-1b. This configuration had a number of structural advantages over any of the other spring designs considered. First, the spring constant could be varied over a very wide range by selecting the machined dimensions of the individual spring elements. Second, the spring element was inherently

rigid radially and fairly stiff laterally. Third, the efficient use of space was superior to any other configurations considered. Fourth, it permitted a greater vertical displacement for a given spring stiffness than any other type of spring studied. In addition, the multiple small slots made it much easier to fabricate a soil barrier around the wall of the test device.

In attempting to extend the slotted cylinder design of Figure B-1b to provide greater vertical displacement, it became apparent that the machining difficulties would be severe for the low spring constant-high displacement spring cylinders. Additional development effort resulted in the configuration shown in Figure B-1c. In this case, the spring cylinder was fabricated from spring rings with spacers bonded between them. This concept made it possible to fabricate, from a relatively small number of spring rings and spacers, a spring cylinder of almost any desired spring constant. Figure B-2 shows some of the spring rings, spacers, and assembled spring cylinders.

Calculations based on nominal 1/16-inch-, 1/8-inch-, and 1/4-inch-thick spring rings, all 6 inches outside diameter and 5 inches inside diameter, showed that these dimensions would satisfy all the spring cylinder stiffness requirements shown in Table 3 of the main text, except for the stiffest device. In order to maintain a constant spring cylinder height, and allow for the space occupied by

the spacers, the final spring-ring thicknesses selected were 0.052 inch, 0.115 inch, and 0.242 inch.

In order to explain the method of fabricating a spring cylinder to a preselected spring constant, a brief review of the action of multiple springs in series and parallel is included. Each spring cylinder is made up of a stack of spring rings in series and the spring constant of the cylinder is the spring constant of the individual rings divided by the number of rings, where the spring rings are all uniform. This can be expressed as,

$$K_T = \frac{K_n}{n} \quad (1)$$

where

K_T = spring constant of cylinder

K_n = spring constant of individual springs

n = number of springs

or more generally:

$$\frac{1}{K_T} = \frac{1}{K_1} + \frac{1}{K_2} + \dots + \frac{1}{K_n} \quad (2)$$

where

K_1 = spring constant of ring 1

K_2 = spring constant of ring 2

K_n = spring constant of ring n

Within the spring cylinder each individual spring ring also acts

as a number of springs in parallel, the number being determined by the number of spacers. The spring constant of springs in parallel is given by the relation:

$$K_p = K_1 + K_2 + K_3 + \dots + K_n \quad (3)$$

where

K_p = ring spring constant

K_1 = segment spring constant

K_n = segment spring constant

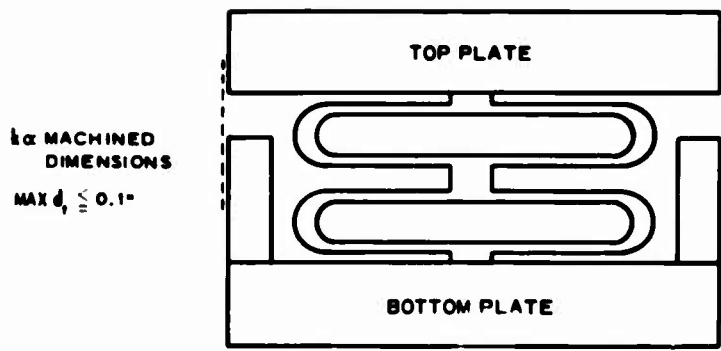
The example of springs in parallel could be applied to the spring rings only in a very general way, for the addition of more spacers was not just a summing of springs. When, for example, the number of spacers was increased from 4 to 5, then each spring element was shortened, with a corresponding increase in stiffness. The resulting spring constant of the ring was therefore significantly greater than the ratio of 5 to 4 which would have been the case for summing springs of a constant K . Experimentally determined curves such as Figure B-3 were used for selecting the number of spacers to obtain a given spring constant. The curves of this figure give the spring constant per ring and this value had to be divided by the number of active rings to obtain the spring constant for the cylinder as explained above.

By the proper choice of spring-ring thickness, number of active

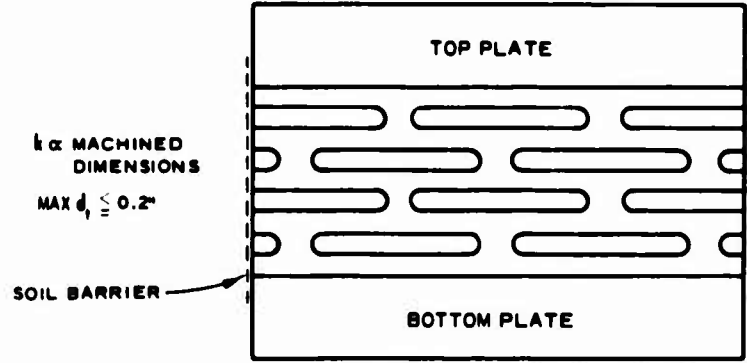
rings, and number of spacers, the desired spring constant was fabricated. In all cases, it was desirable to utilize the largest number of active spring rings possible in order to achieve the largest allowable displacement without overstraining the spring rings. During fabrication, the spring rings and spacers were placed in a fixture which held the parts in place while the epoxy hardened. The fixture consisted of three smooth, round posts screwed into a flat, ground steel plate. The three posts were perpendicular to the base plate and positioned so that a 6-inch-diameter cylinder would fit snugly between them. The spring rings were placed in the assembly fixture one at a time and spacers, coated on both sides with epoxy, were positioned on each spring ring. The angular position of the spacers at each level of assembly was determined with a paper template. The epoxy adhesive used to bond the copper spacers to the steel spring rings was made by mixing three parts by volume of Epon 828 (Shell Oil Co.) with one part by volume of Versamid (Du Pont). The spacers were stamped from sheet copper to the desired sizes, $1/32$ by $1/8$ by $1/2$ inch to go with the $1/16$ -inch rings and $1/16$ by $1/4$ by $1/2$ inch to go with the $1/8$ - and $1/4$ -inch rings (Figure B-2).

Determination of the spring constant of the assembled spring cylinder was made by applying a known force and measuring the resulting deflection. This testing was performed in the apparatus shown

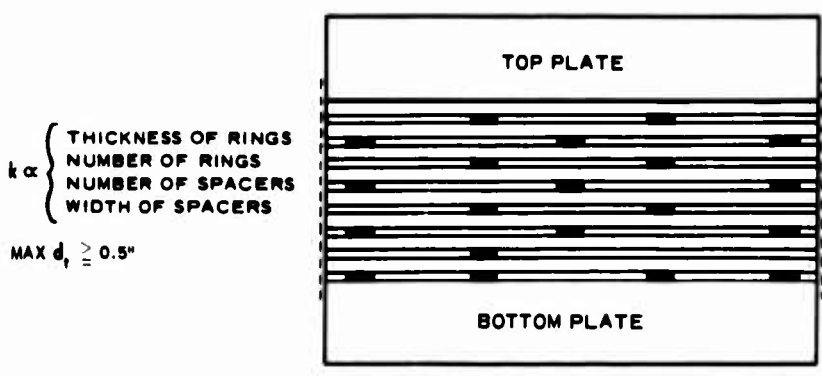
in Figure B-4. In this machine a hydraulic cylinder was used to apply the load and, depending on the test, either a proving ring or a load cell was used to measure the load. Mechanical dial gages and the displacement transducers within the test device were used to monitor the deflection resulting from the load. A typical calibration curve derived from these measurements is shown in Figure 13 in the main text.



a. PROVING RINGS WITHIN TEST DEVICE HOUSING

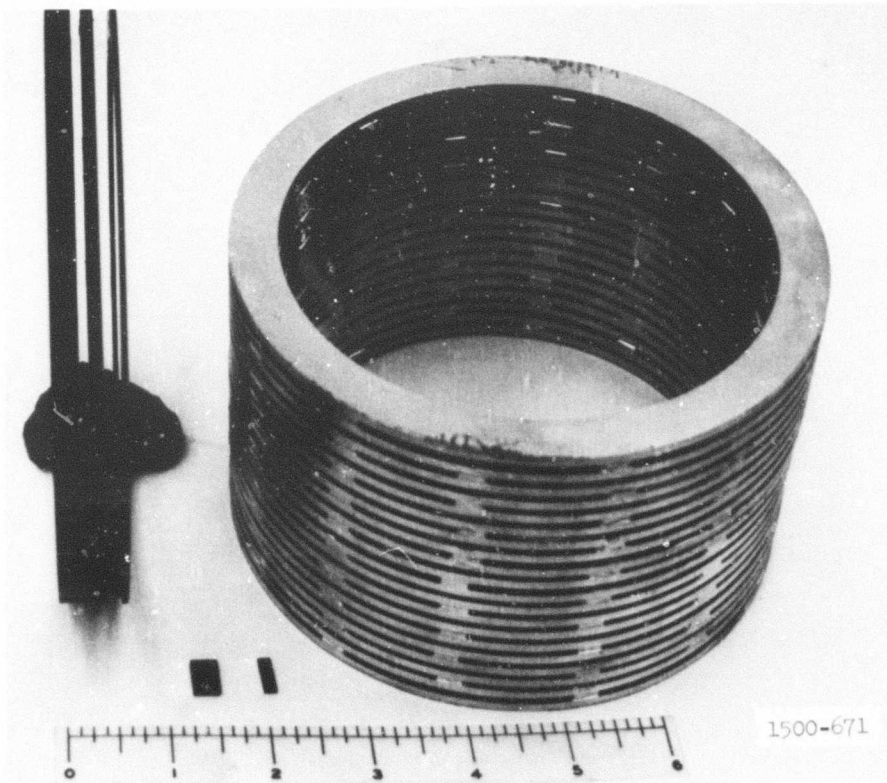


b. ONE-DIMENSIONALLY ELASTIC SURFACE CYLINDER MACHINED AS MULTIPLE PROVING RINGS JOINED TO FORM CYLINDER

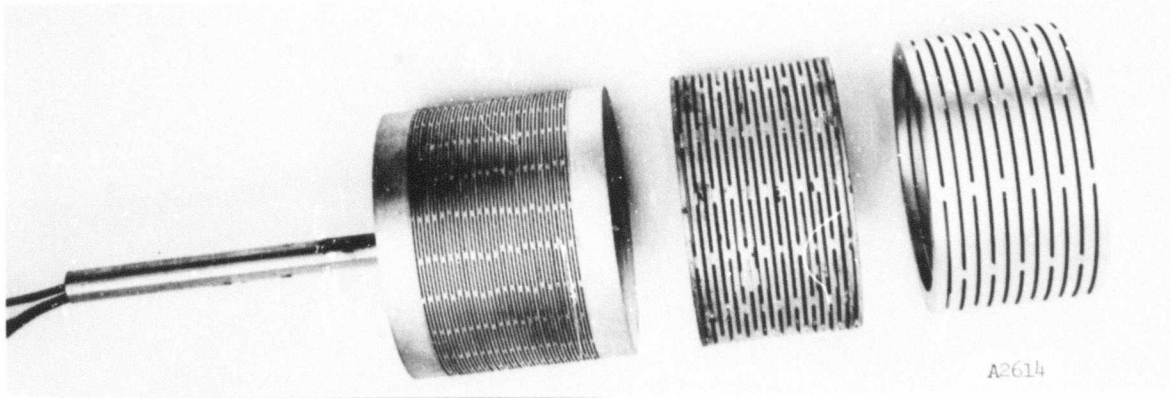


c. ONE-DIMENSIONALLY ELASTIC SURFACE CYLINDER FABRICATED FROM SPRING RINGS AND SPACER SHIMS

Fig. B-1. Stages in the development of the spring-ring concept



a. Springs, spacers, and assembled spring cylinder



b. Spring cylinders fabricated of nominal 1/16-inch, 1/8-inch, and 1/4-inch rings

Fig. B-2. Spring cylinders for spring-ring test device

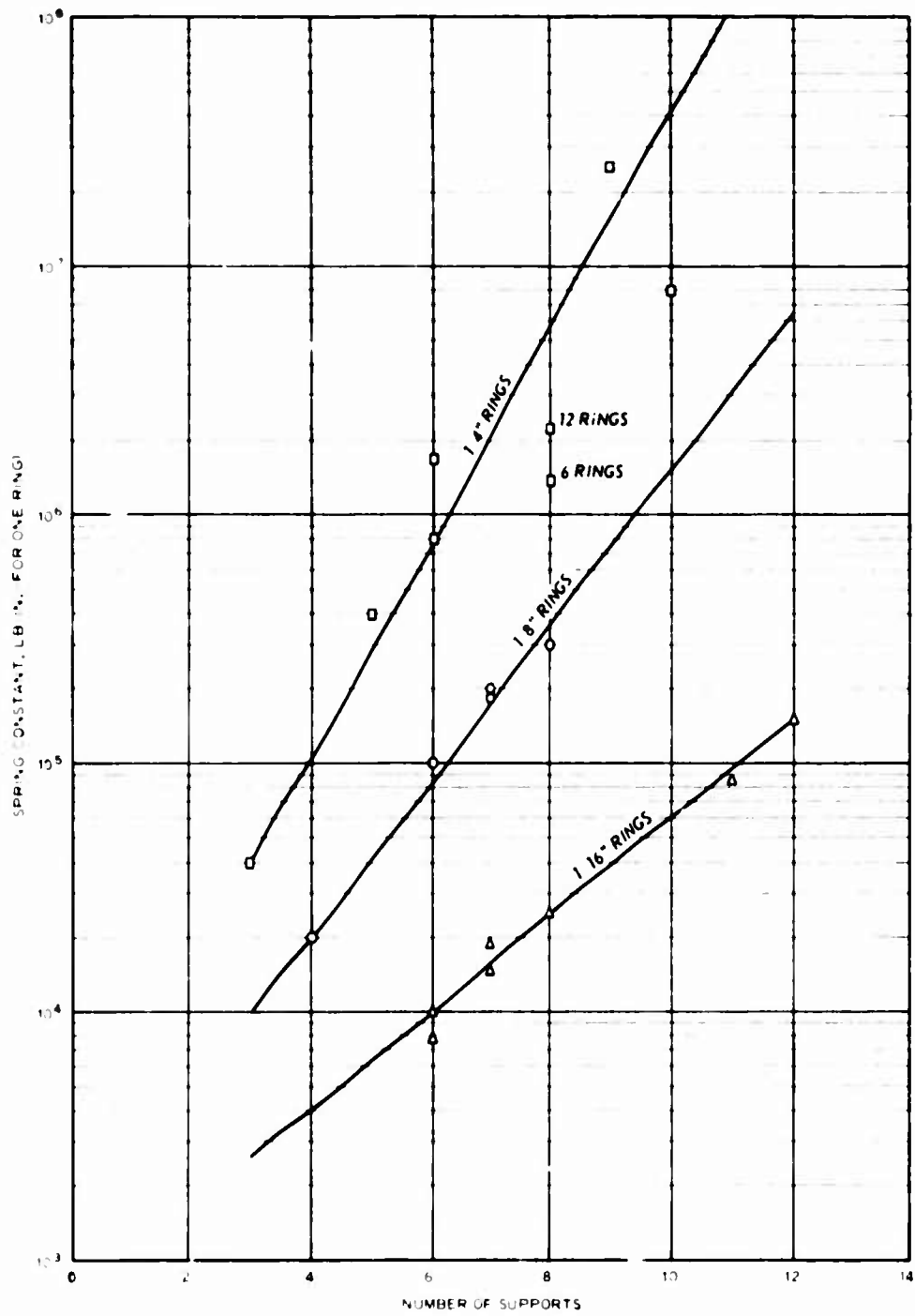


Fig. B-3. Spring constants of individual spring ring

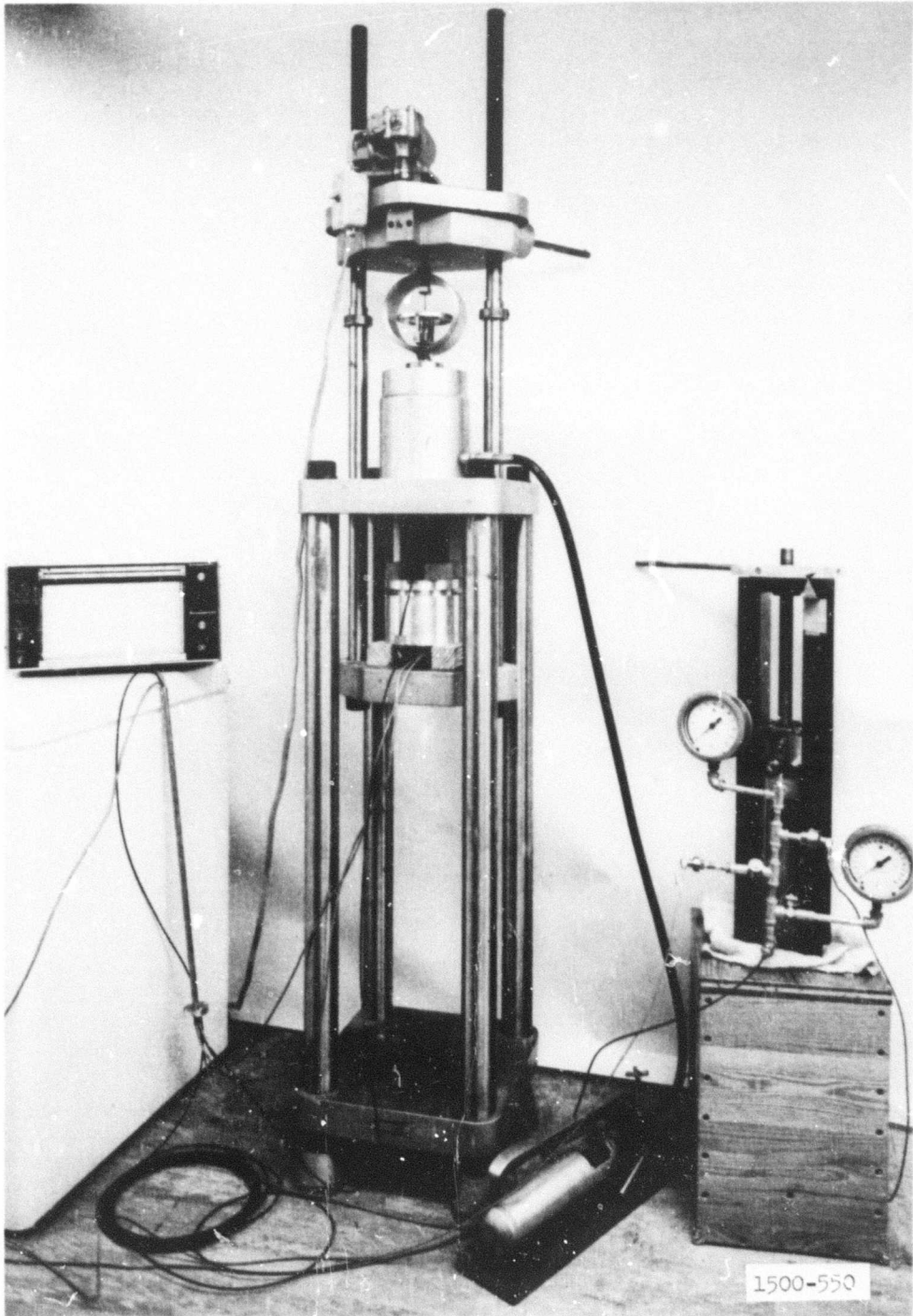


Fig. B-4. Test device calibration apparatus

APPENDIX C

OSCILLOGRAPH RECORDS FROM THE DYNAMIC TESTS

This appendix contains photographic reproductions of many of the oscillograph records from the dynamic test program. These figures are referred to frequently throughout the main text of the report. These records should be of particular value to both investigators and designers in the field of dynamic design.

With the exception of Figure C-1, the records were produced by gages installed in the soil or on the test device. Figure C-1 is a typical record from the tests used to determine the frequency and damping properties of the test devices. Figures C-2 through C-75 were produced during Tests 11 through 28. Figures C-76 through C-87 originated from the preliminary test program.

Normally the first 10 to 20 msec were the most important part of the records. After this time, the records showed considerable disturbance. Therefore only the first 50 msec of the records are shown in continuous form. The 100-msec and final portions, approximately after 1 sec unless specified otherwise, also have been included to show the instrument recovery after the surface pressure had decreased.

The zero timing line during the main test program was produced by using the explosive cap to break a wire placed in the bonnet. In

preliminary Tests A and B, a time of arrival (TOA) gage was placed on the soil surface and compared with the zero time produced by the wire technique. The initiation of the TOA gage lagged the wire break by less than 0.5 msec and corresponded very closely with the initiation of the Norwood pressure gages in the bonnet, Figures C-76, C-77, and C-78. The wire break normally preceded the initiation of the bonnet pressure gages by less than 0.5 msec, Figures C-80, C-83, and C-86. In some of the records, especially those from any type of strain gage, excursions can be seen at zero time. Exploratory tests showed that these disturbances were caused by the E. M. F. generated in the explosion. The pressure gages in the bonnet appeared to initiate at the same time as those placed on the soil surface, Figure C-3.

The format preceding each record identifies the instrumentation channel, the level of the top of the gage measured with reference to the test chamber base, the radial distance from the centerline of the chamber, the radial angle measured clockwise from north, and the final level of the top of the gage. In addition, the calibration for each channel is shown in the last column. As the records have been reduced considerably from their original size, a reference scale is shown on each record. A reference trace also has been placed on each record.

The channel number in the first column identifies the type of

measurement being made; S or SE identifies soil pressure; PN, PS, PE, or FW identifies the bonnet pressure in the north, south, east, or west quadrant; X or ACC signifies an acceleration measurement; D designates deflection; ϵ is a strain measurement; IP designates pressure measurement inside the test device; and F is a measurement of force on the top of the test device produced by a strain gage-bridge arrangement.

When possible, distorted traces have been labeled. Questionable traces also have been labeled.

Timing lines have been placed at the bottom of each record. In addition, important timing lines measured with reference to zero time have been placed on many of the records.

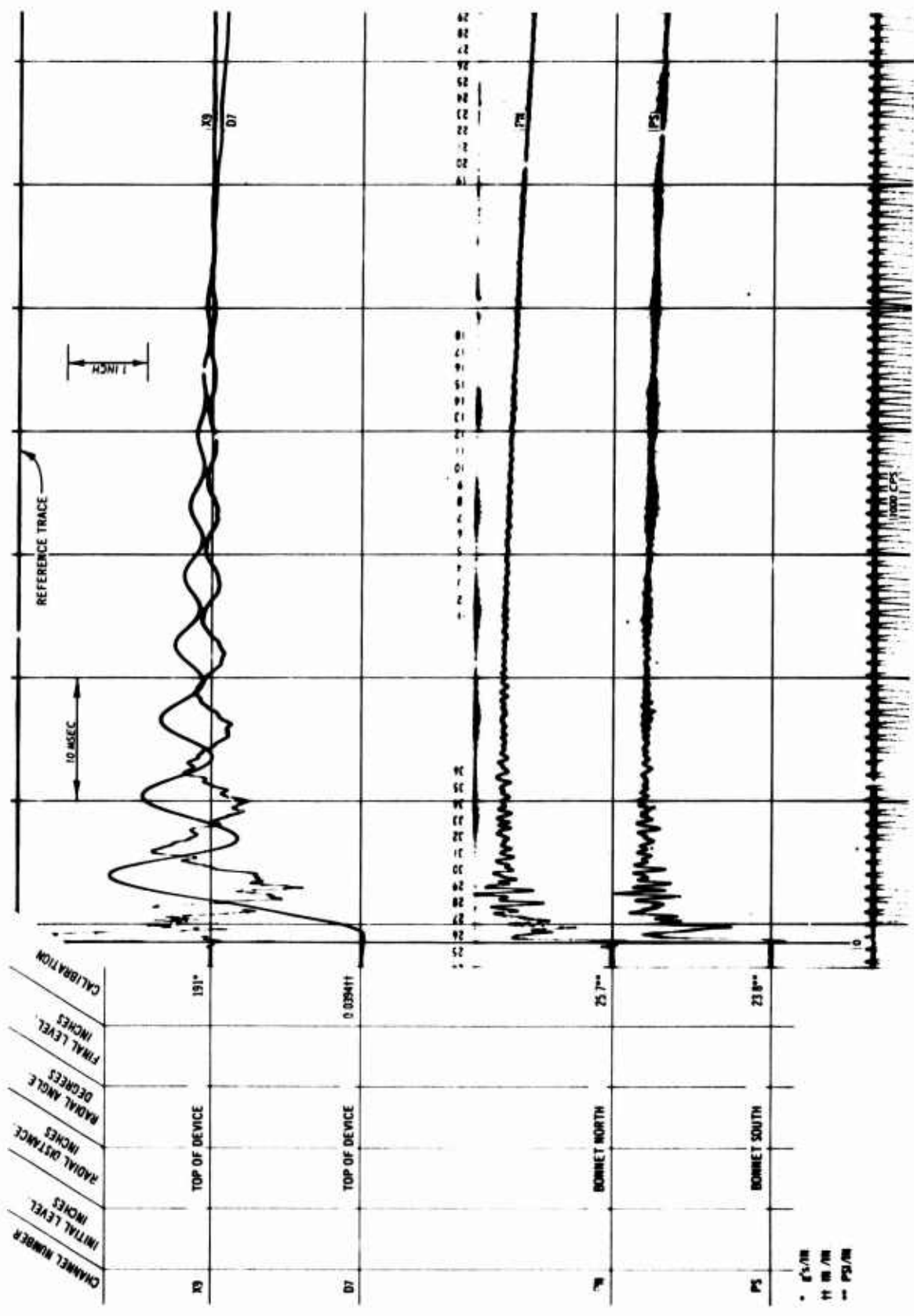


Fig. C-1. Typical dynamic airblast test record for spring-ring test device

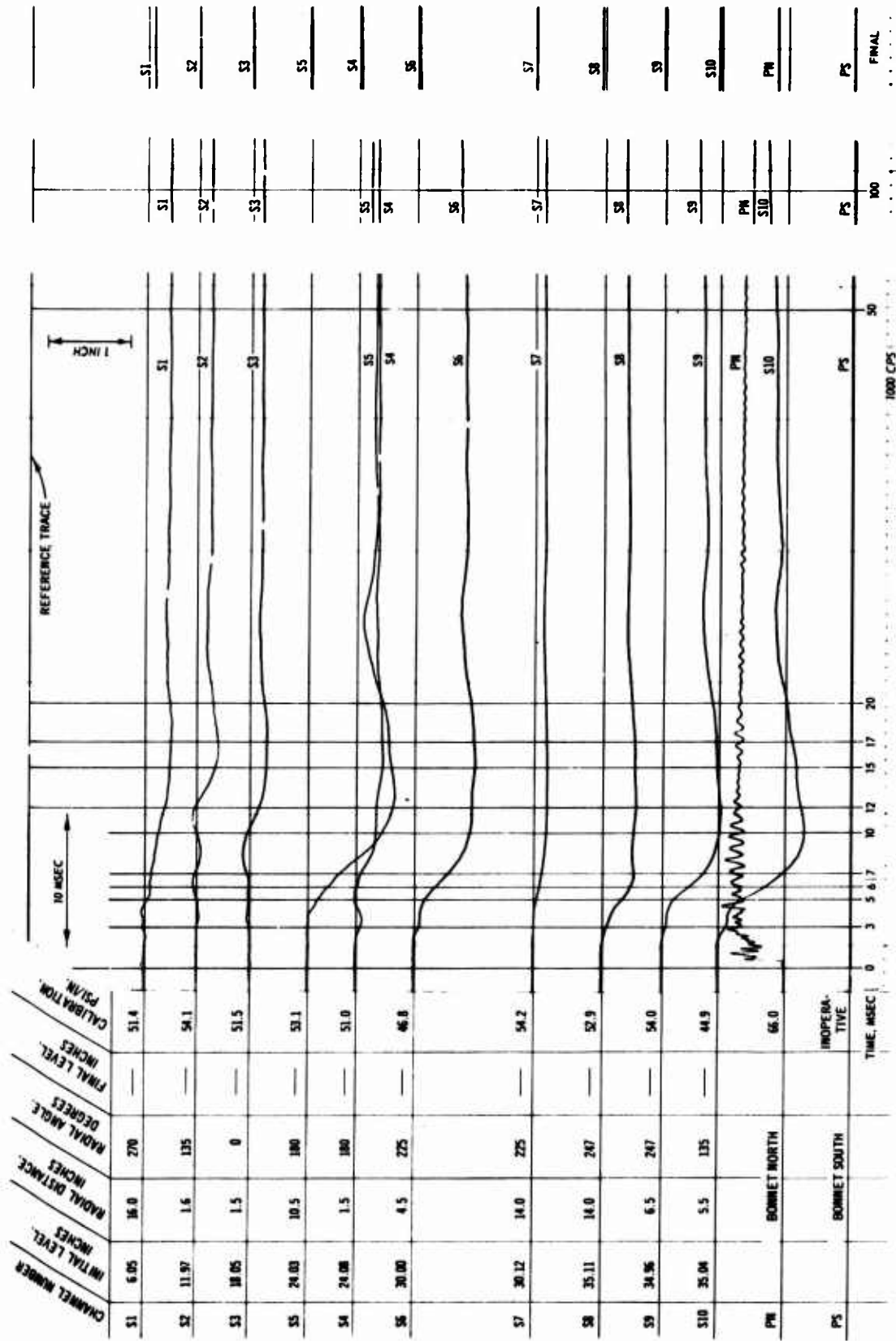


Fig. C-2. Test 11, pressure record (channels S1-S10)

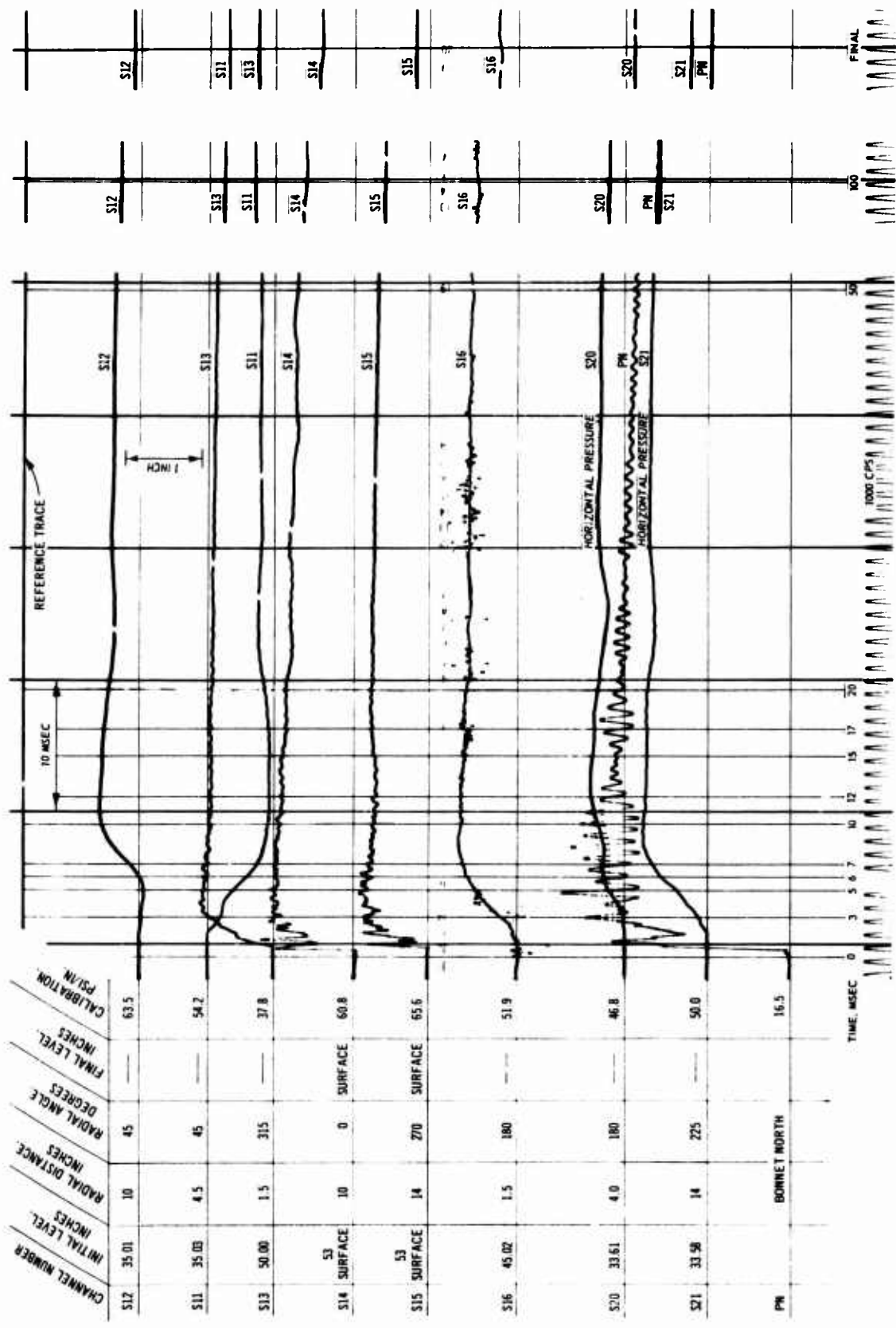


Fig. C-3. Test 11, pressure record (channels S11-S21)

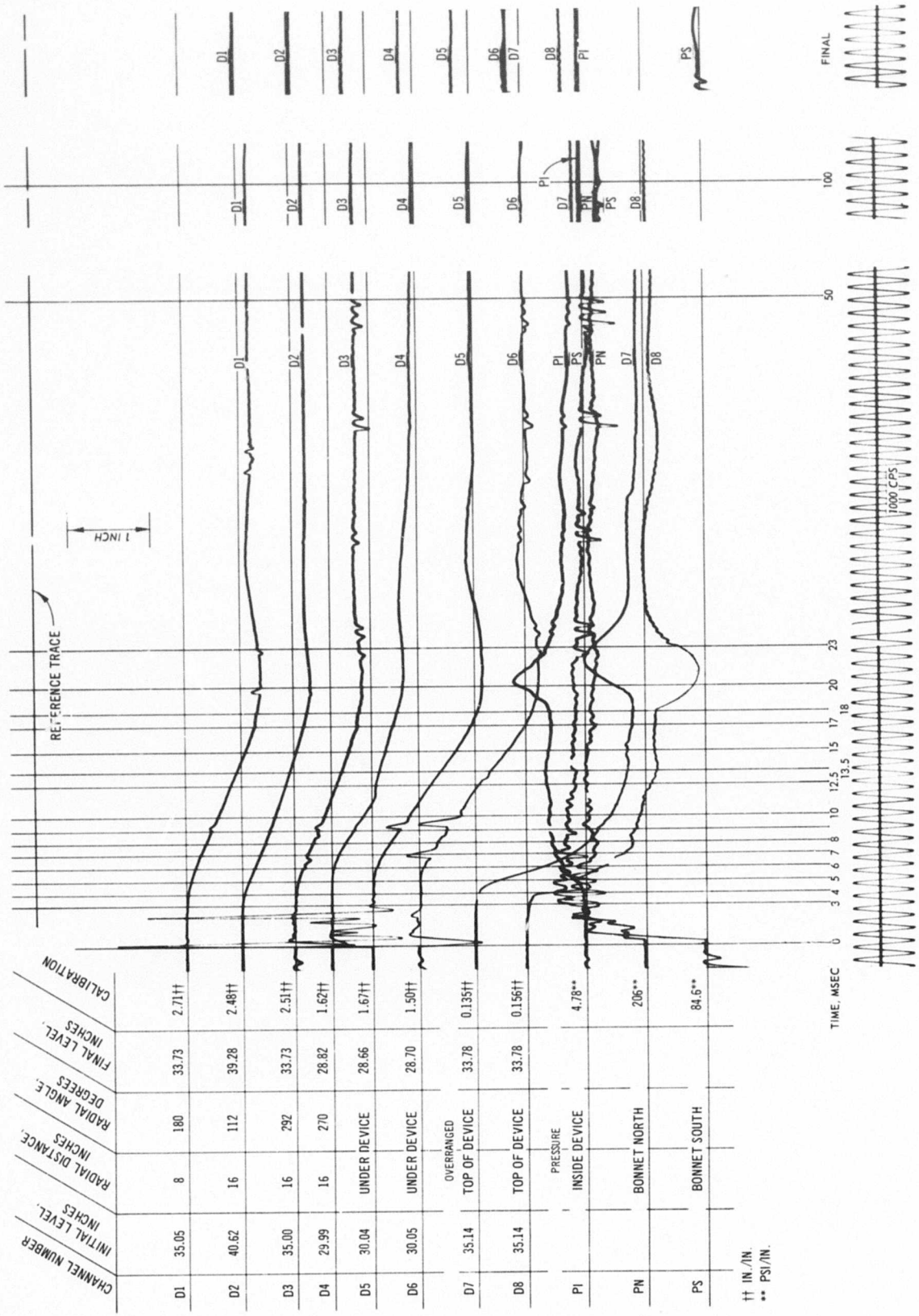


Fig. C-12. Test 13, deflection and pressure record

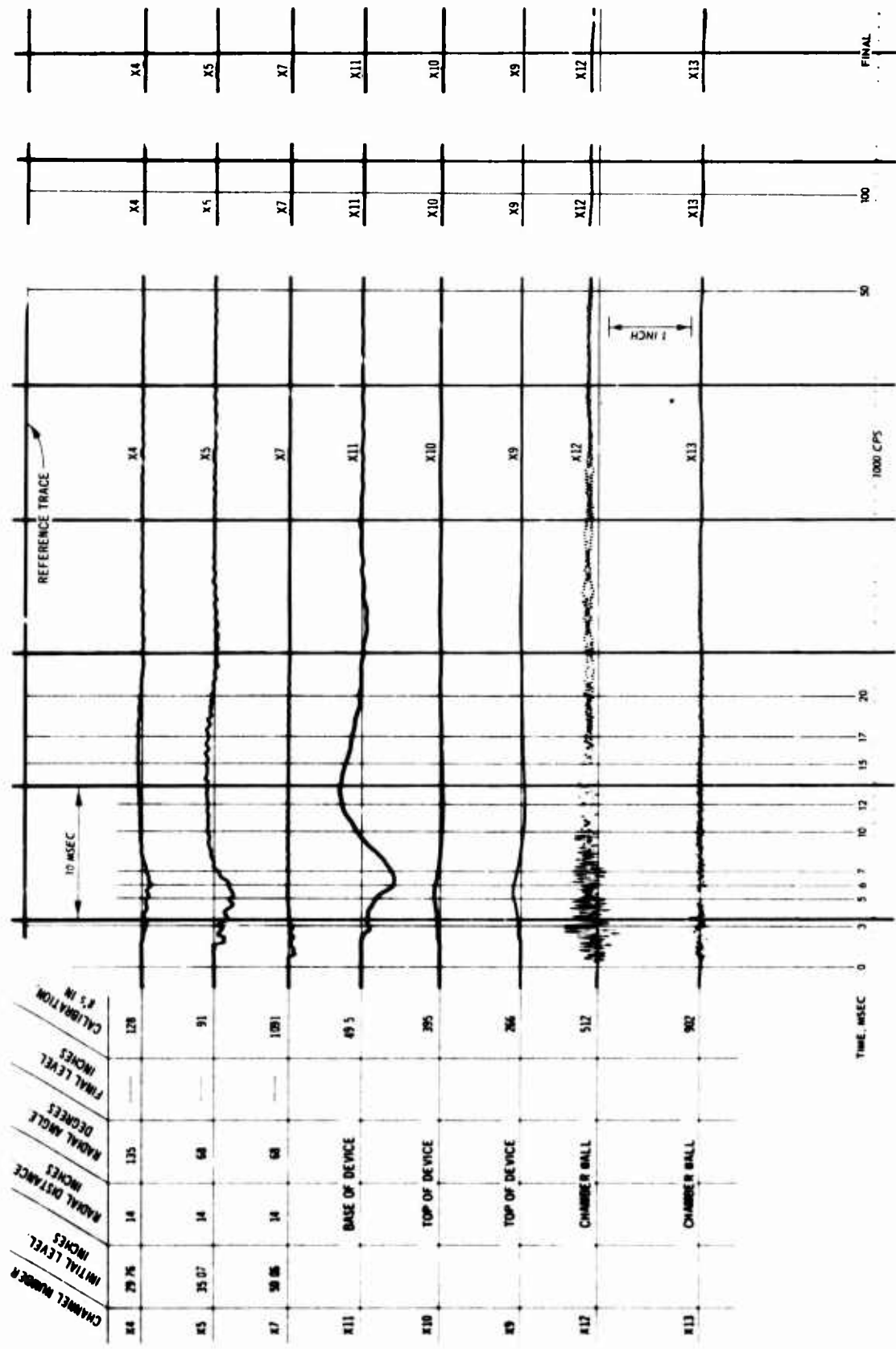


Fig. C-5. Test 11, acceleration record (X4-X13)

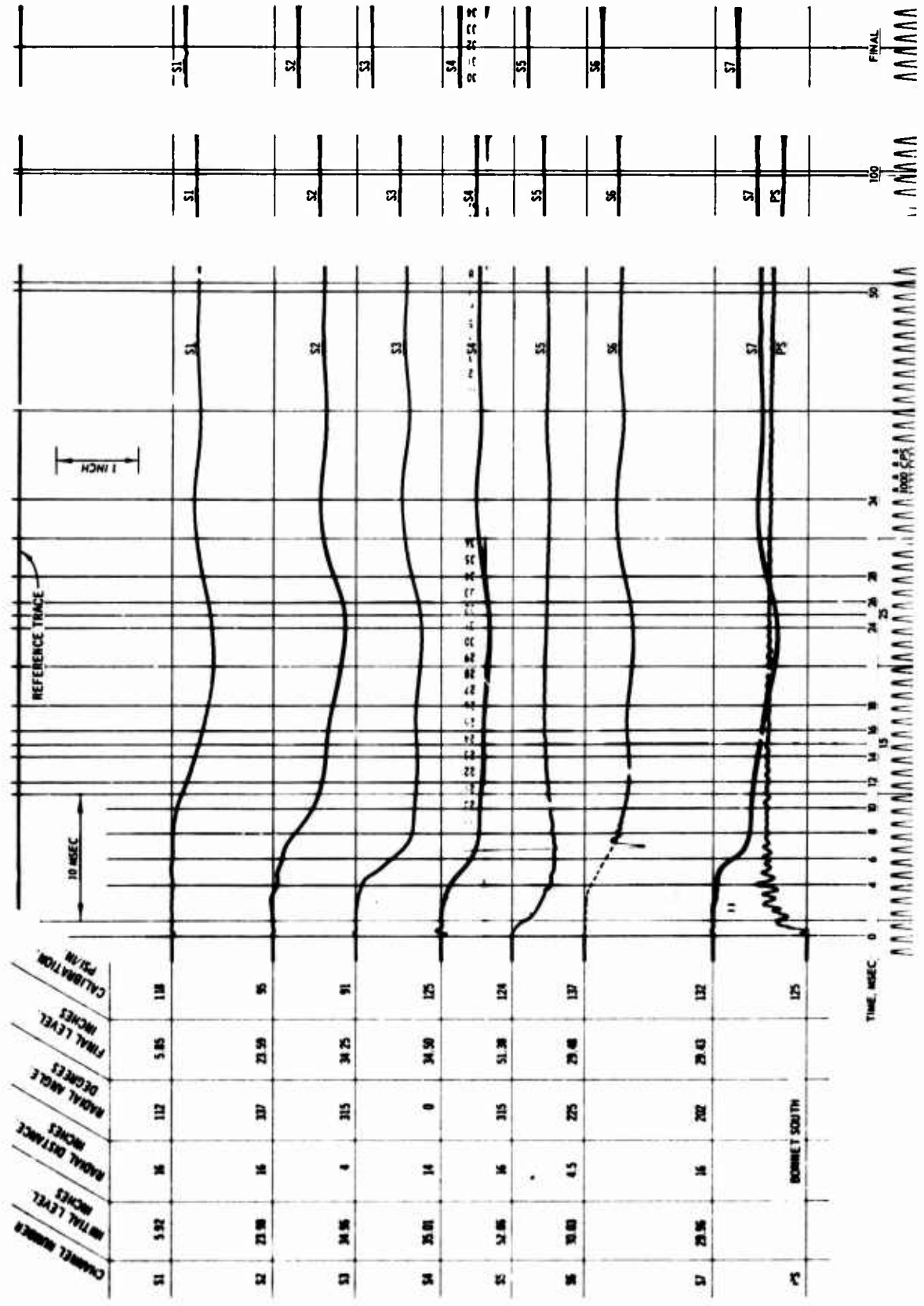


Fig. C-6. Test 12, pressure record (S1-S6)

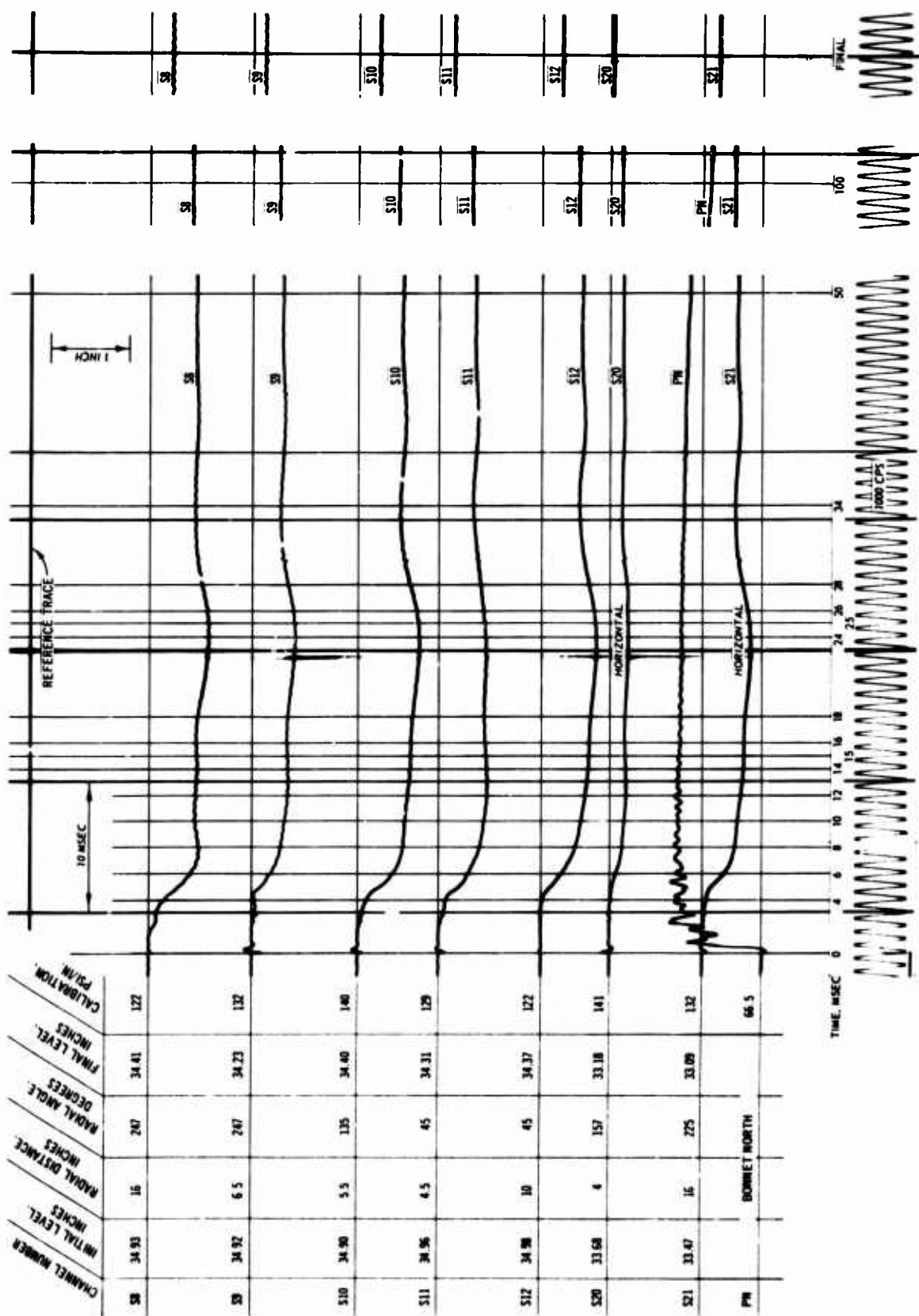


Fig. C-7. Test 12, pressure record (S8-S21)

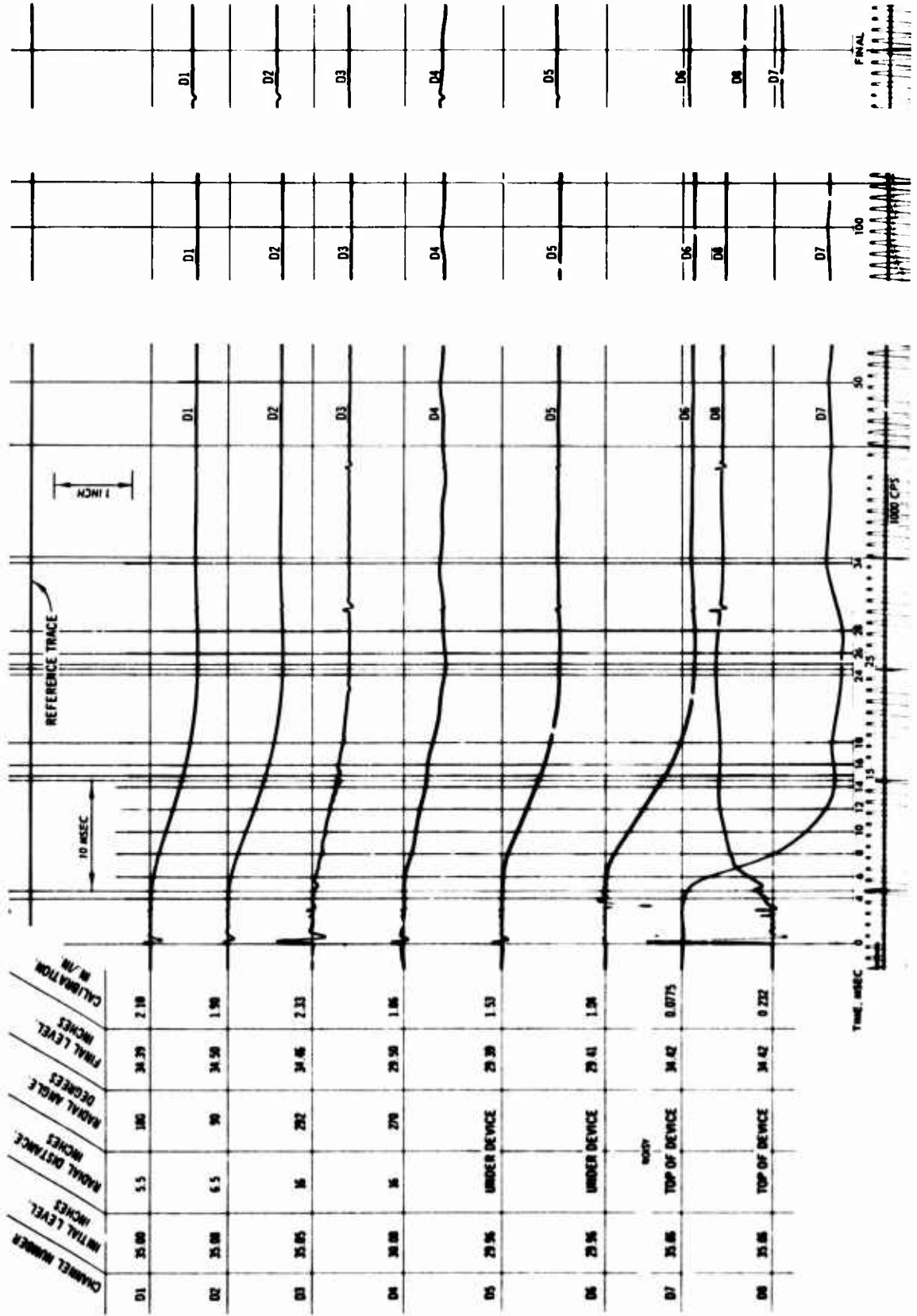


Fig. C-8. Test 12, deflection record

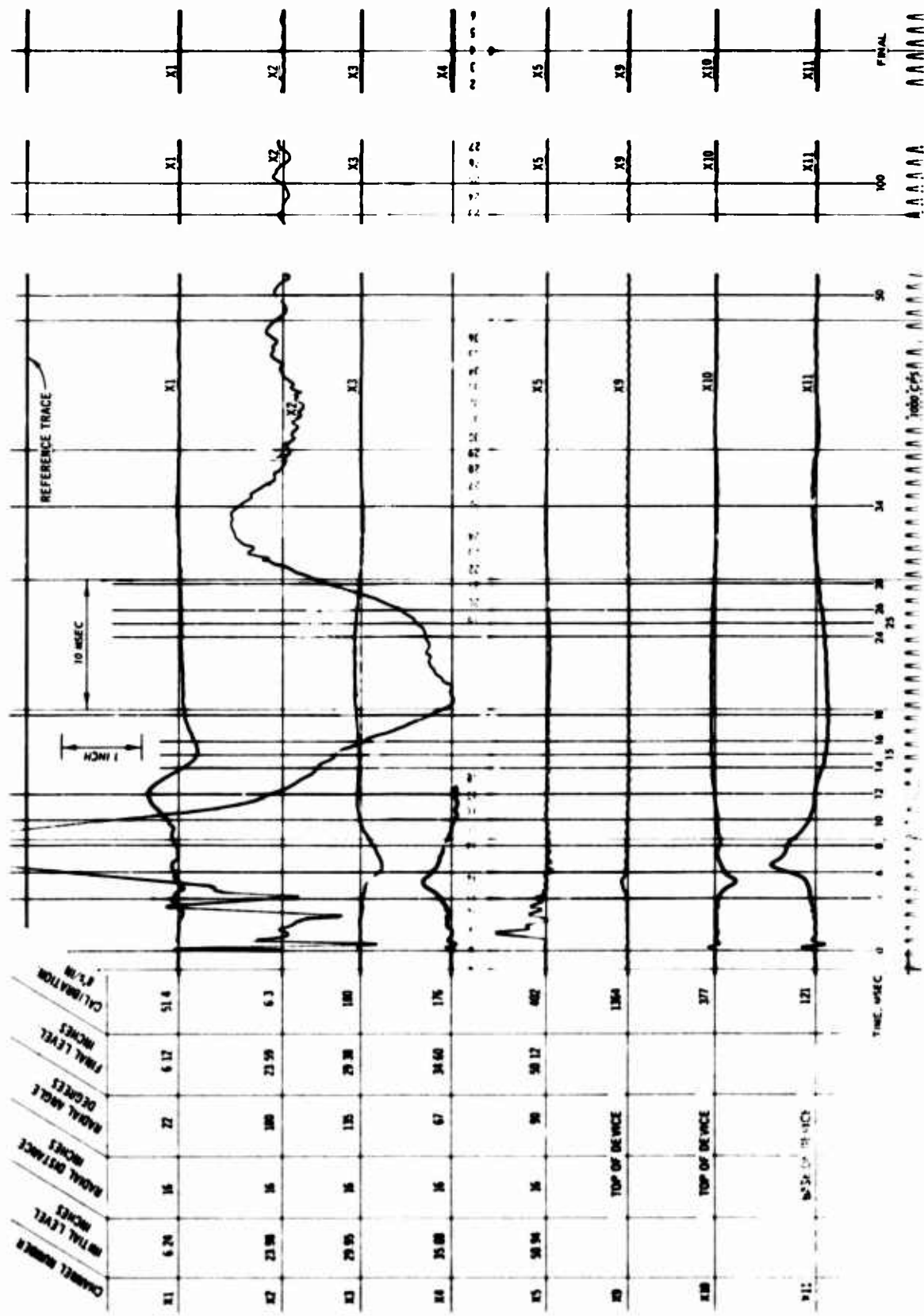


Fig. C-9. Test 12, acceleration record

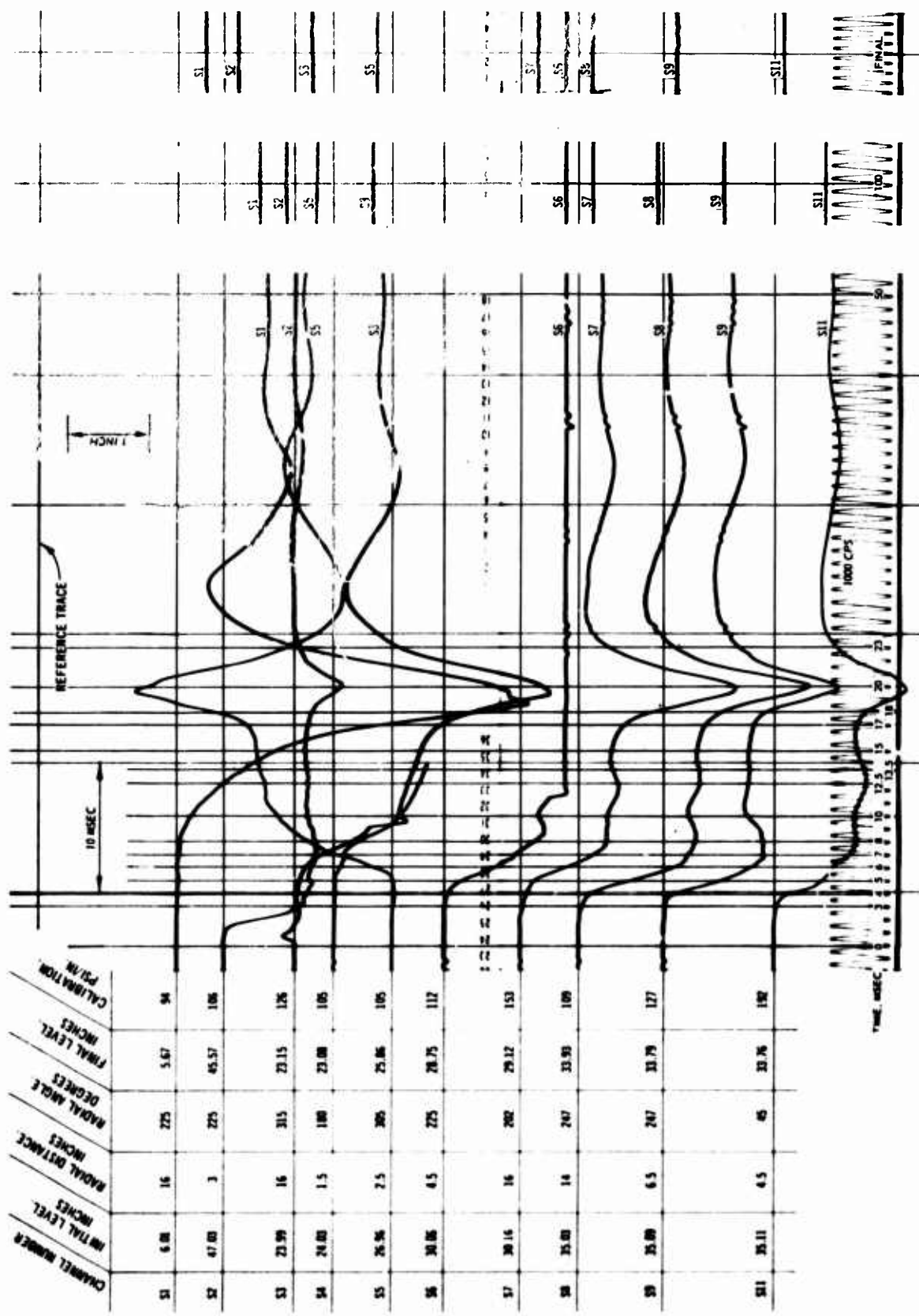


Fig. C-10. Test 13, pressure record (S1-S11)

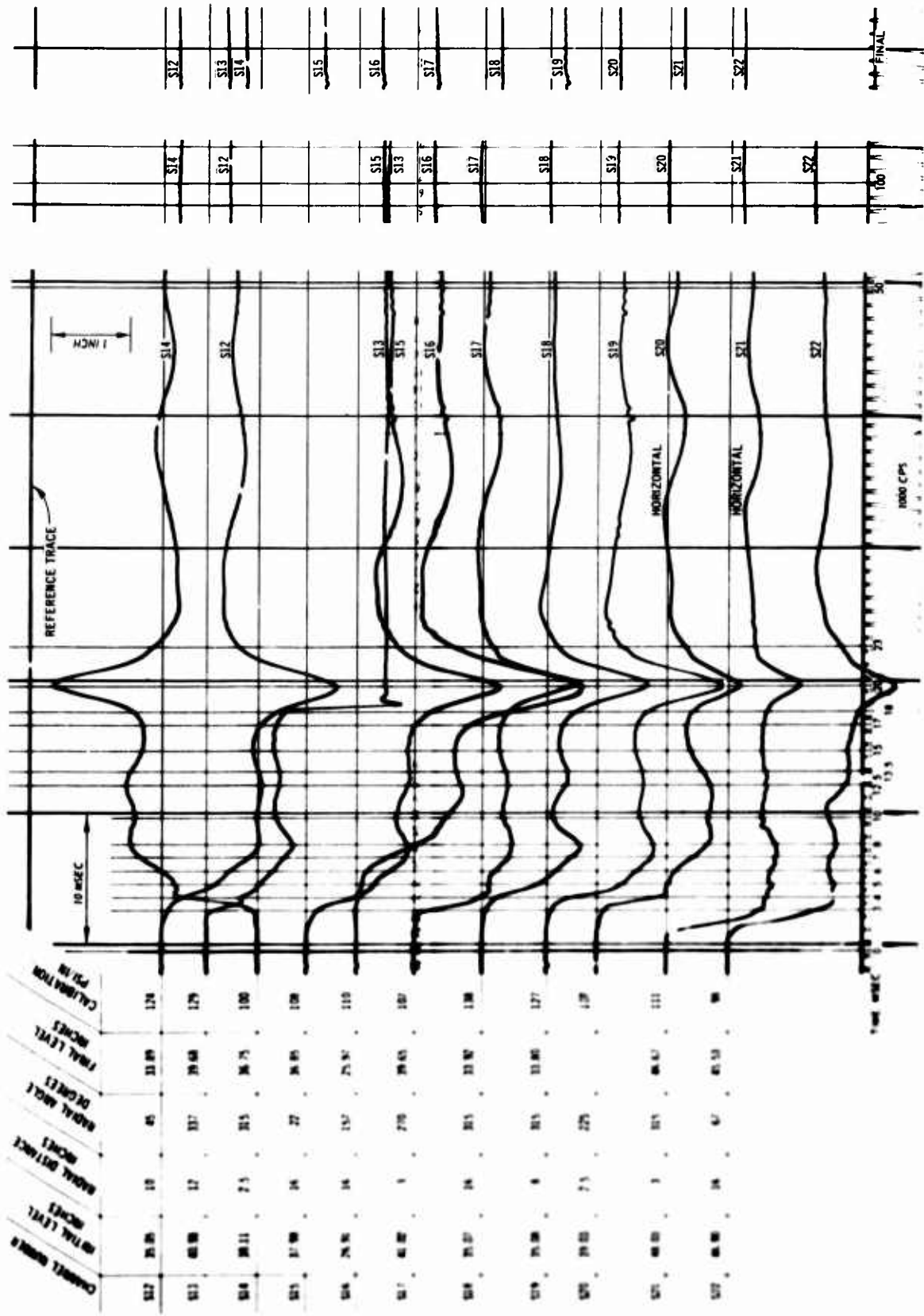


Fig. C-11. Test 13, pressure record (S12-S22)

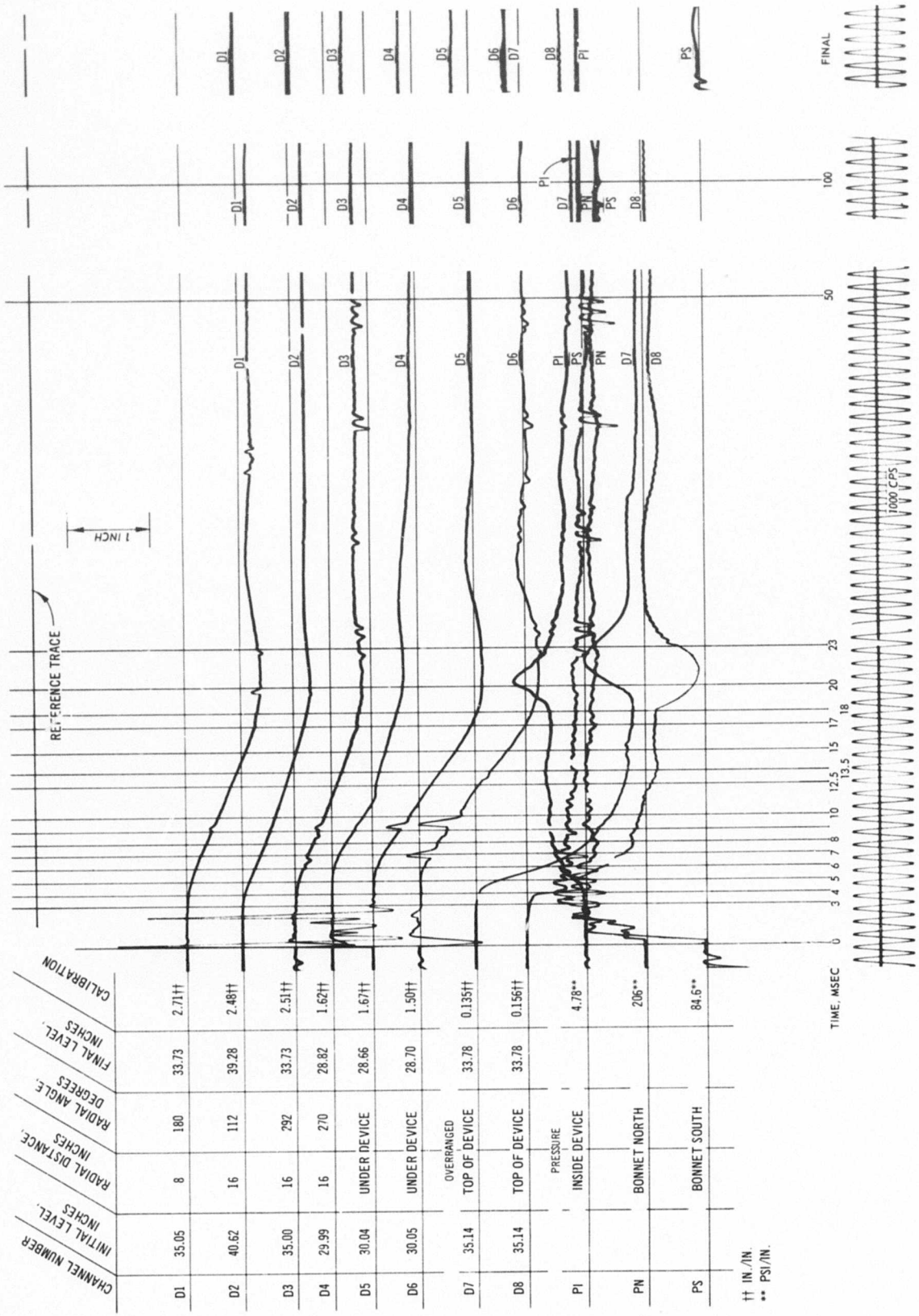
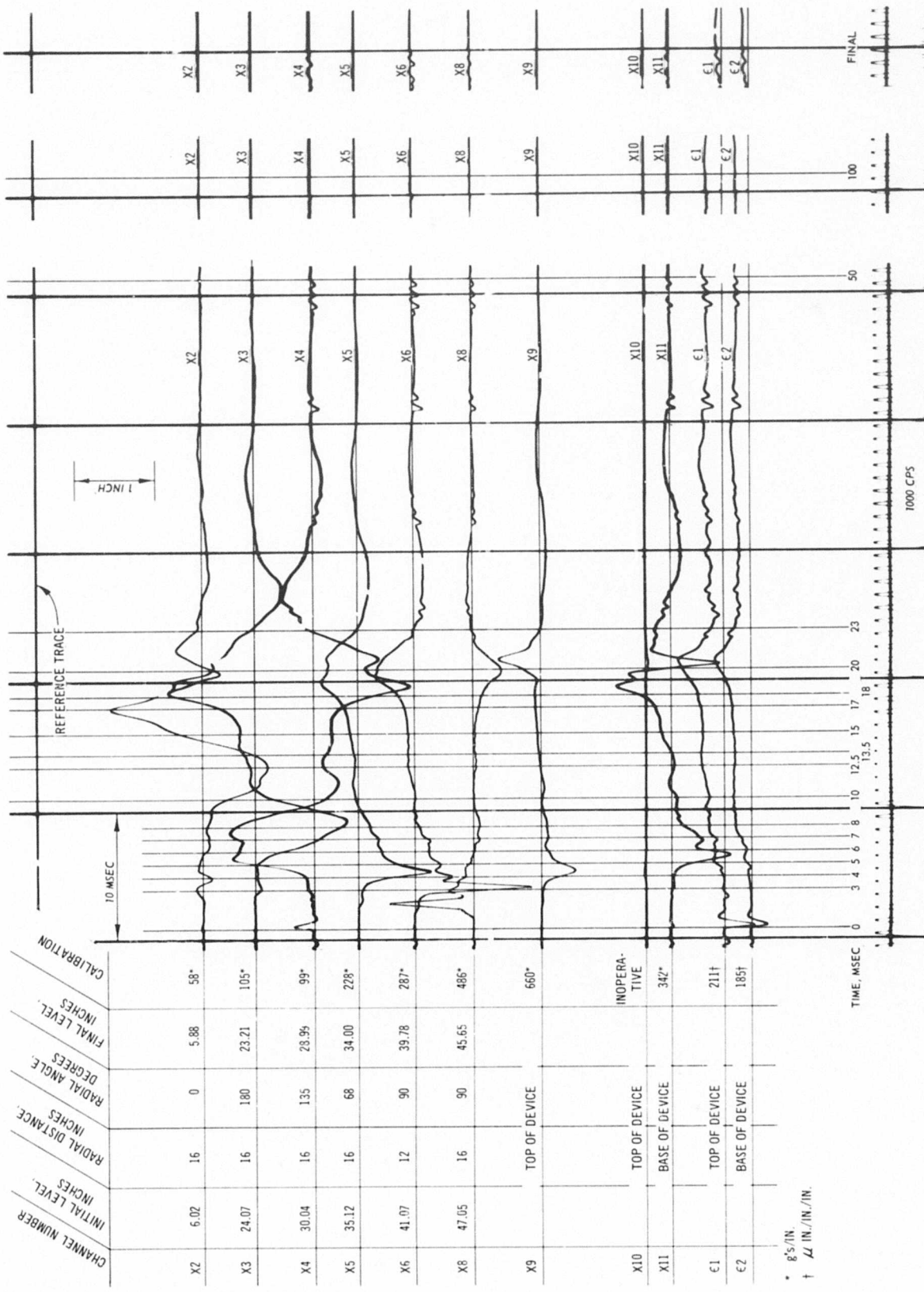


Fig. C-12. Test 13, deflection and pressure record



* g's/IN.
 † IN./IN./IN.

Fig. C-13. Test I3, acceleration and strain record

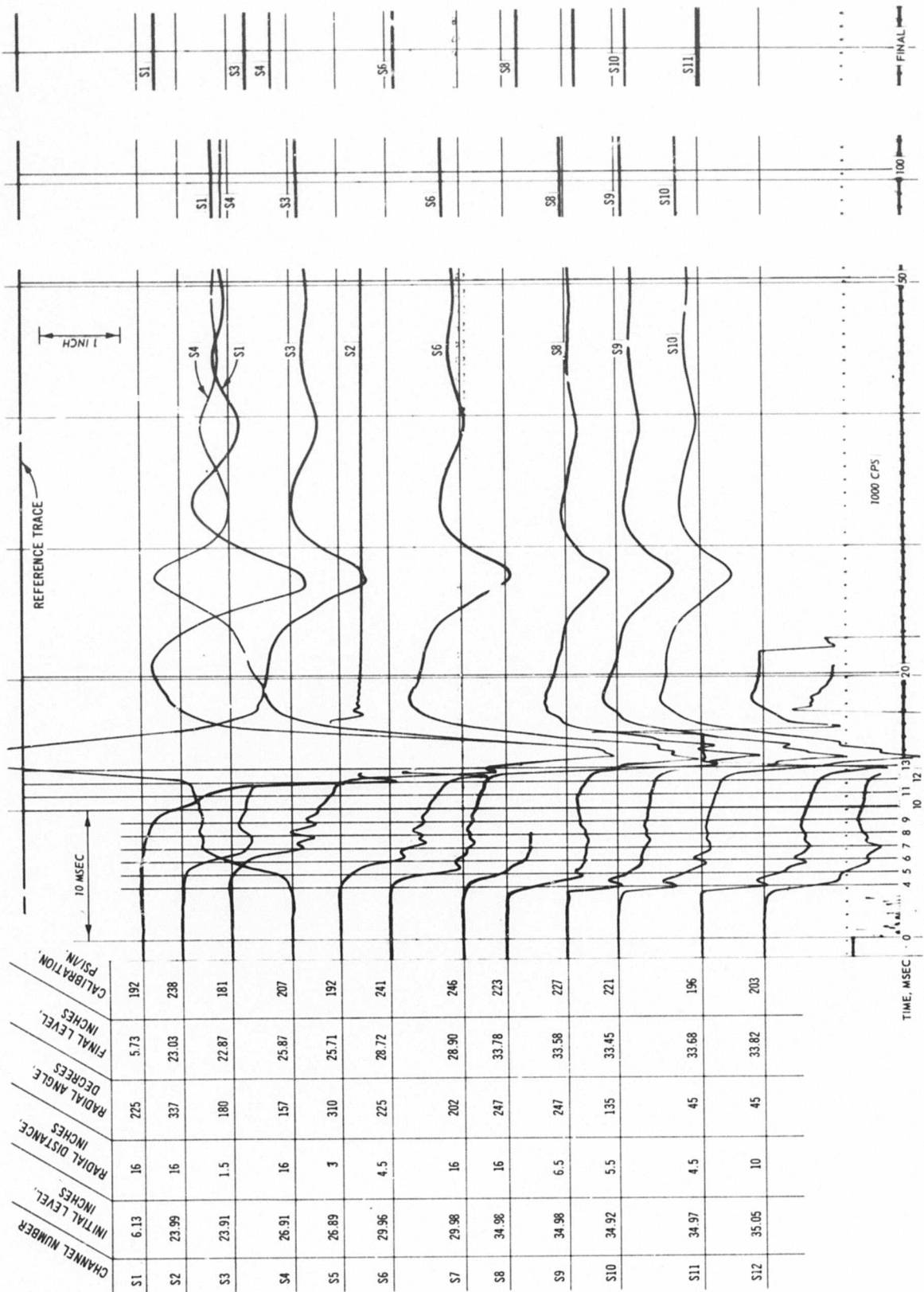


Fig. C-14. Test 14, pressure record (S1-S12)

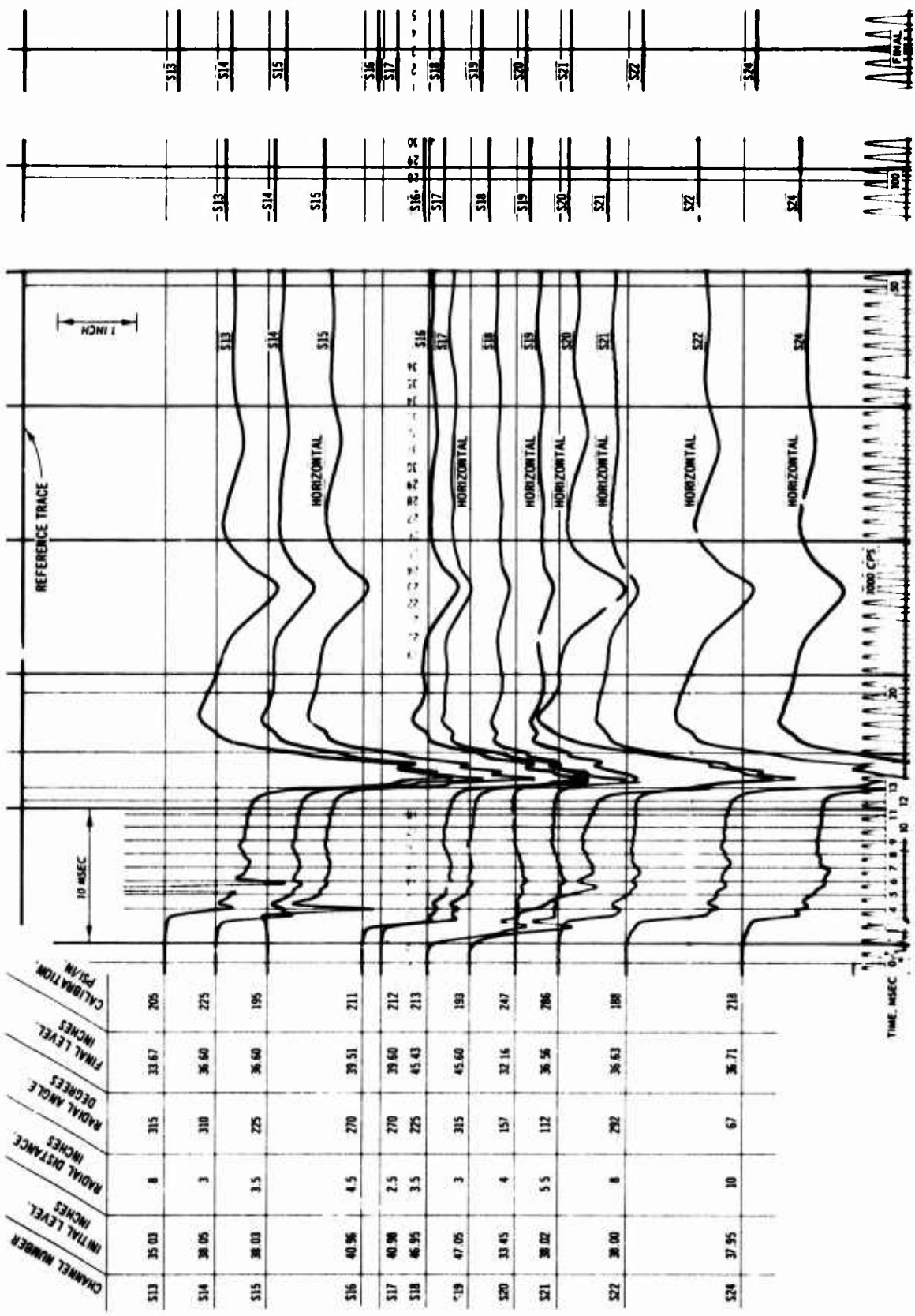


Fig. C-15. Test 14, pressure record (S13-S24)

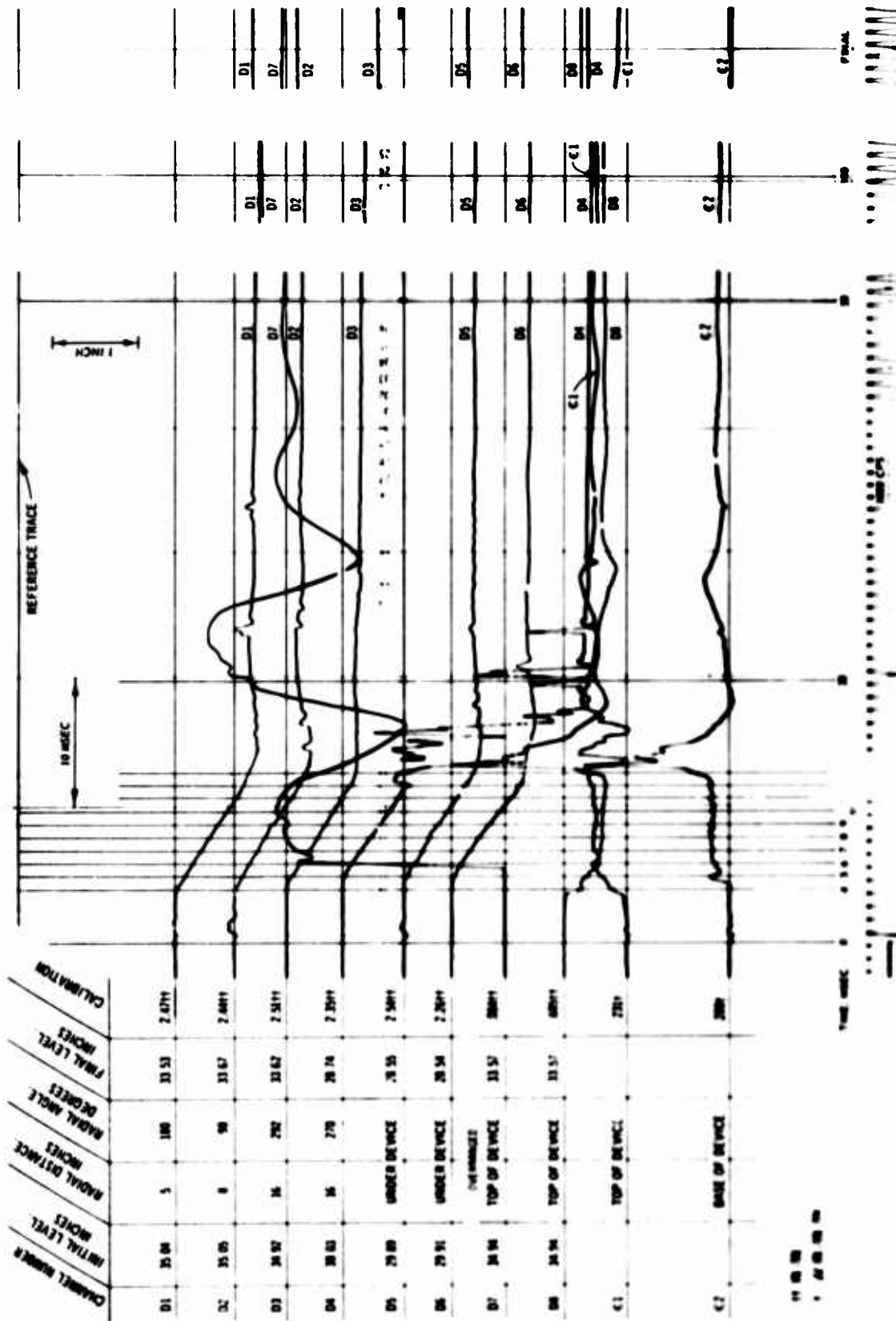
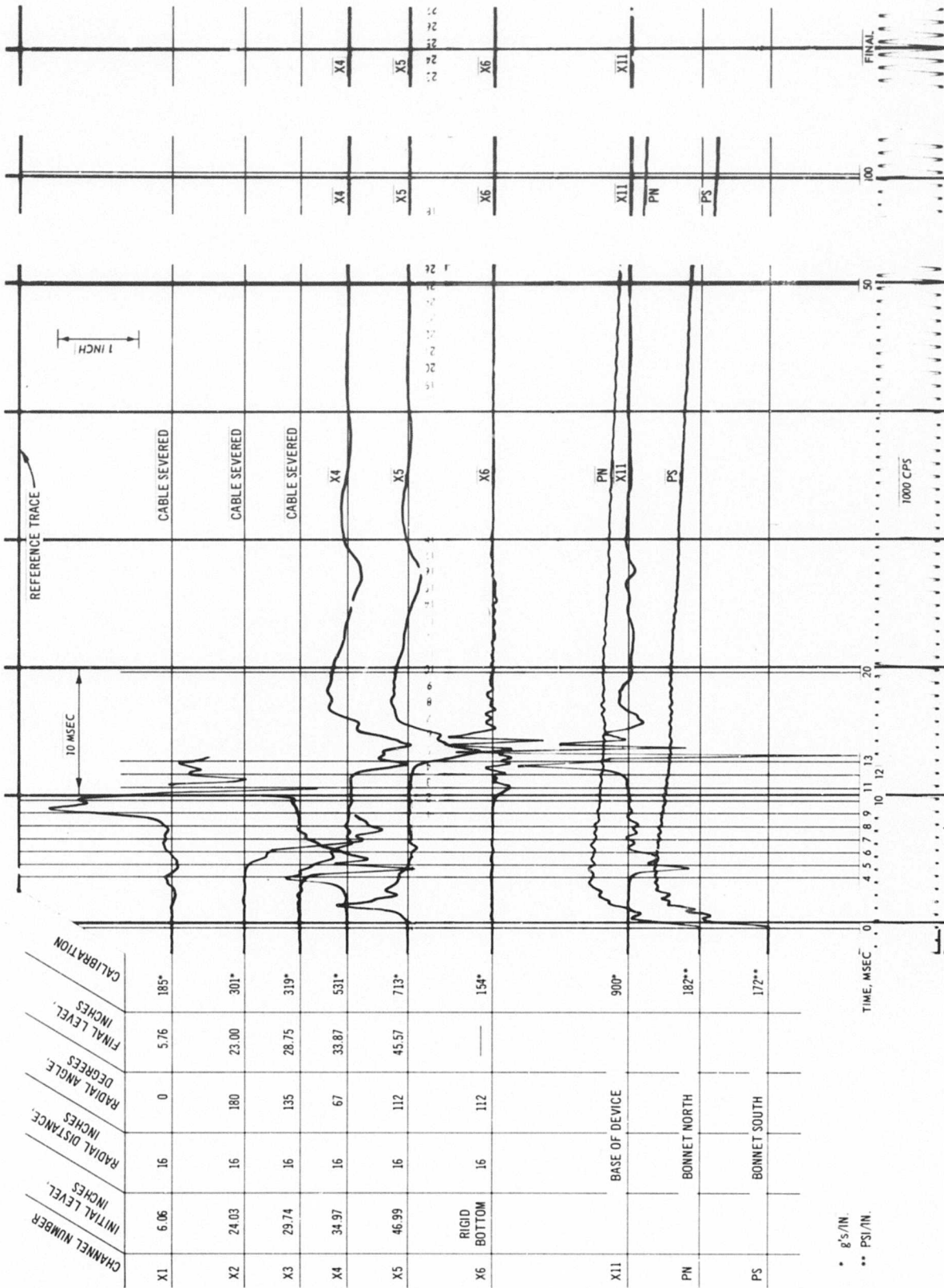


Fig. C-16. Test 14, deflection and strain record



CHANNEL NUMBER	INITIAL LEVEL, INCHES	RADIAL DISTANCE, INCHES	RADIAL ANGLE, DEGREES	FINAL LEVEL, INCHES	CALIBRATION
X1	6.06	16	0	5.76	185*
X2	24.03	16	180	23.00	301*
X3	29.74	16	135	28.75	319*
X4	34.97	16	67	33.87	531*
X5	46.99	16	112	45.57	713*
X6	RIGID BOTTOM	16	112	—	154*
X11		BASE OF DEVICE			900*
PN		BONNET NORTH			182**
PS		BONNET SOUTH			172**

* g's/IN
 ** PSI/IN

Fig. C-17. Test 14, acceleration and pressure record

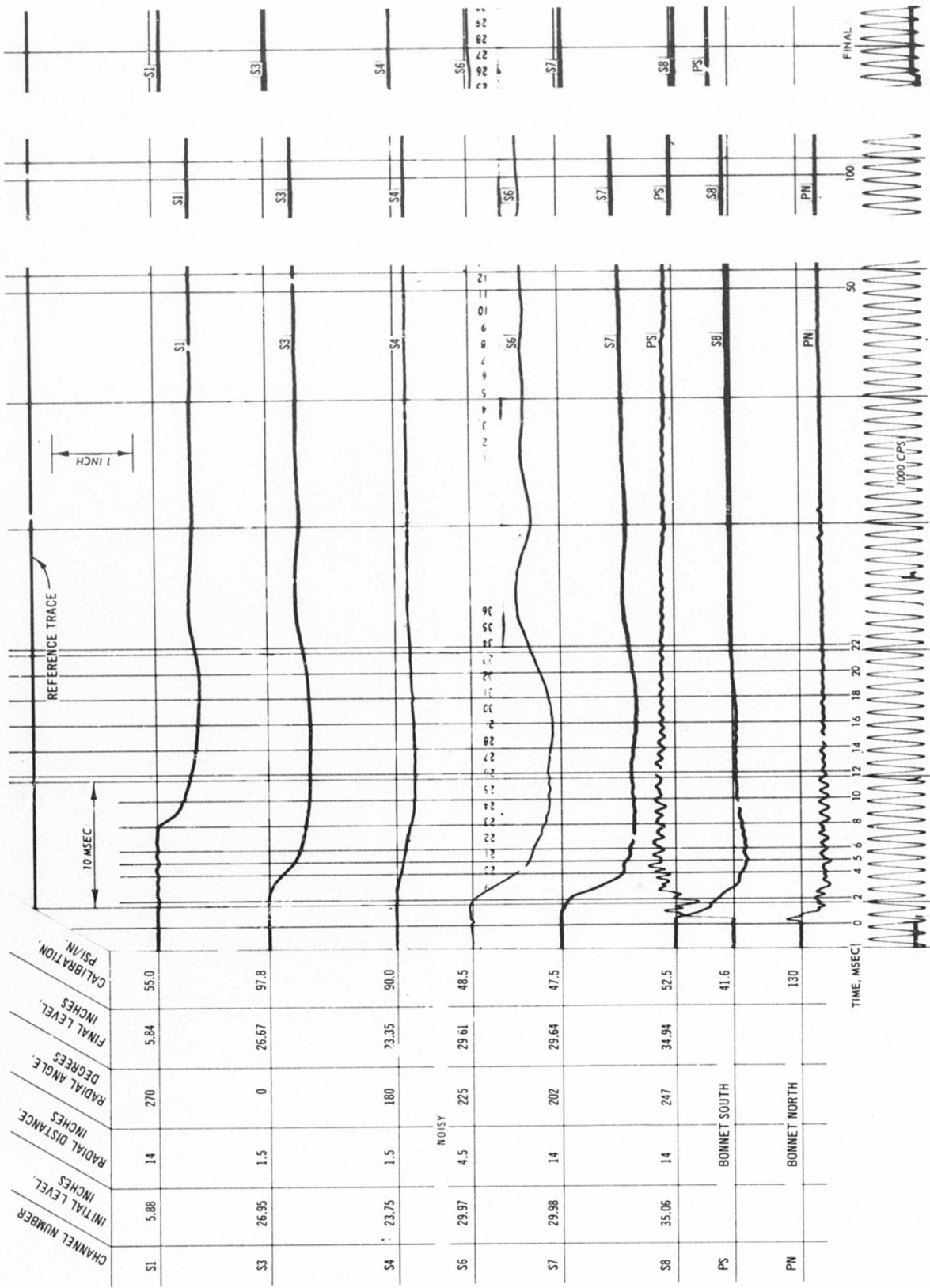


Fig. C-18. Test 15, pressure record (S1-S8)

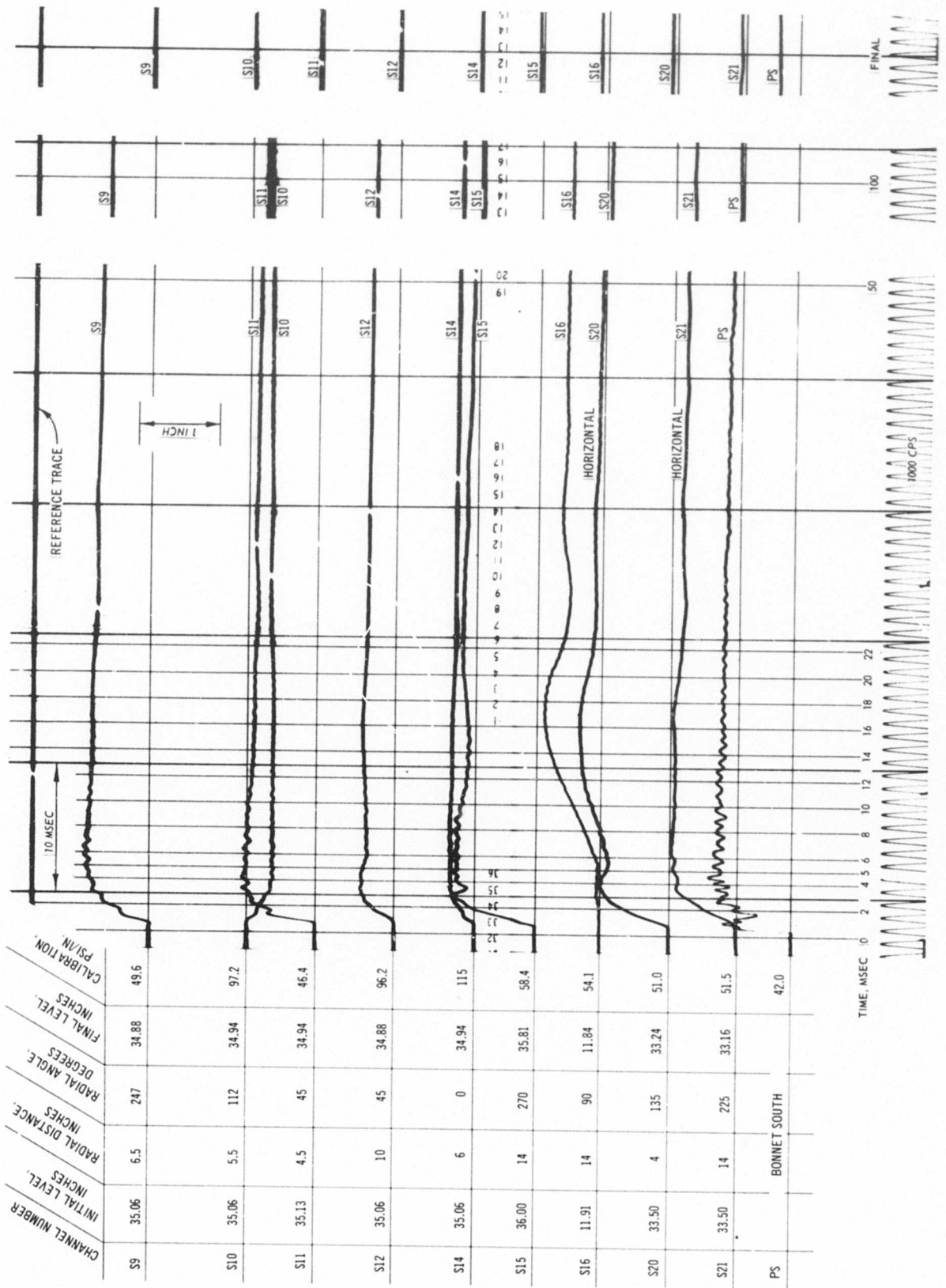


Fig. C-19. Test 15, pressure record (S9-S21)

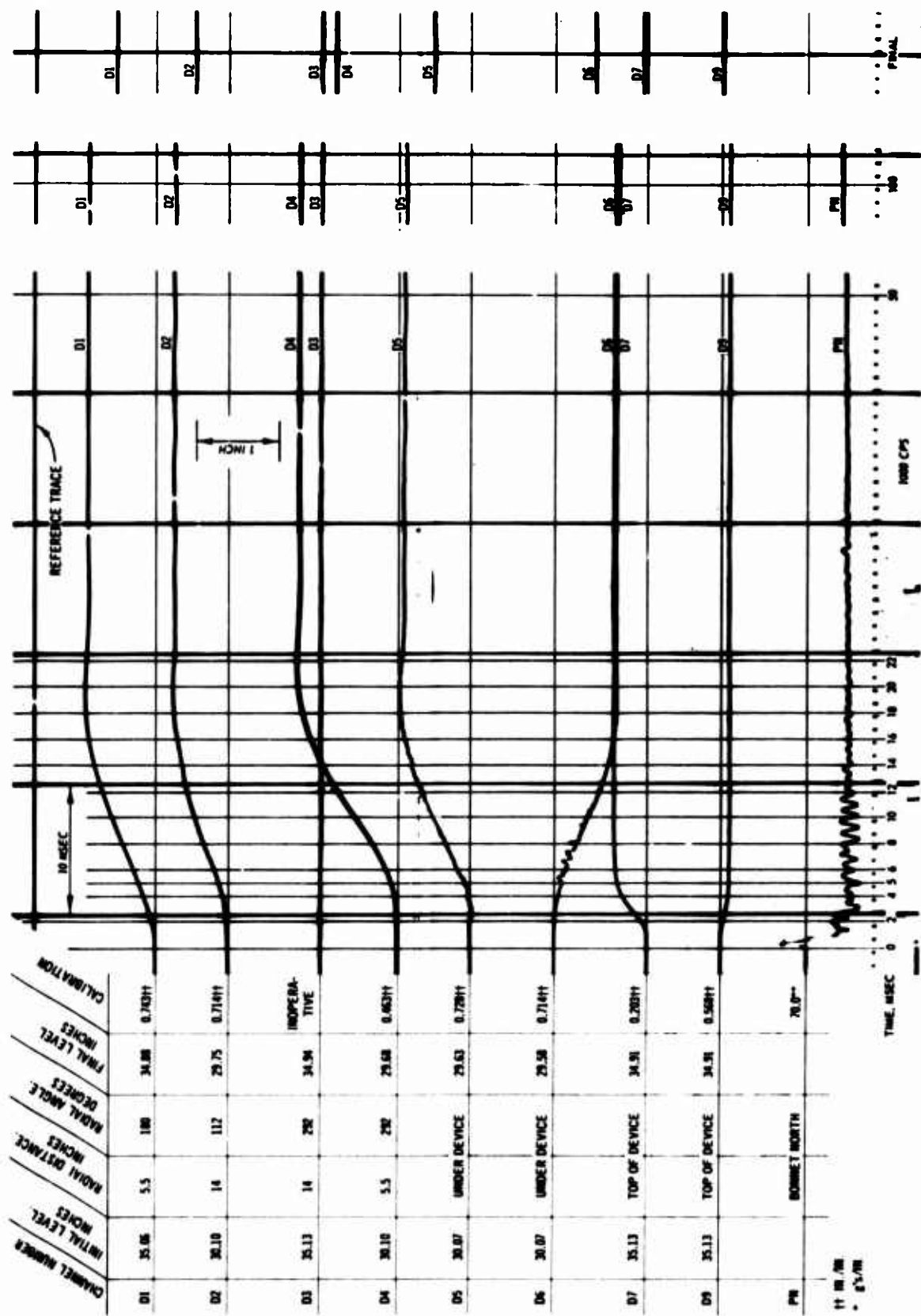


Fig. C-20. Test 15, deflection and pressure record

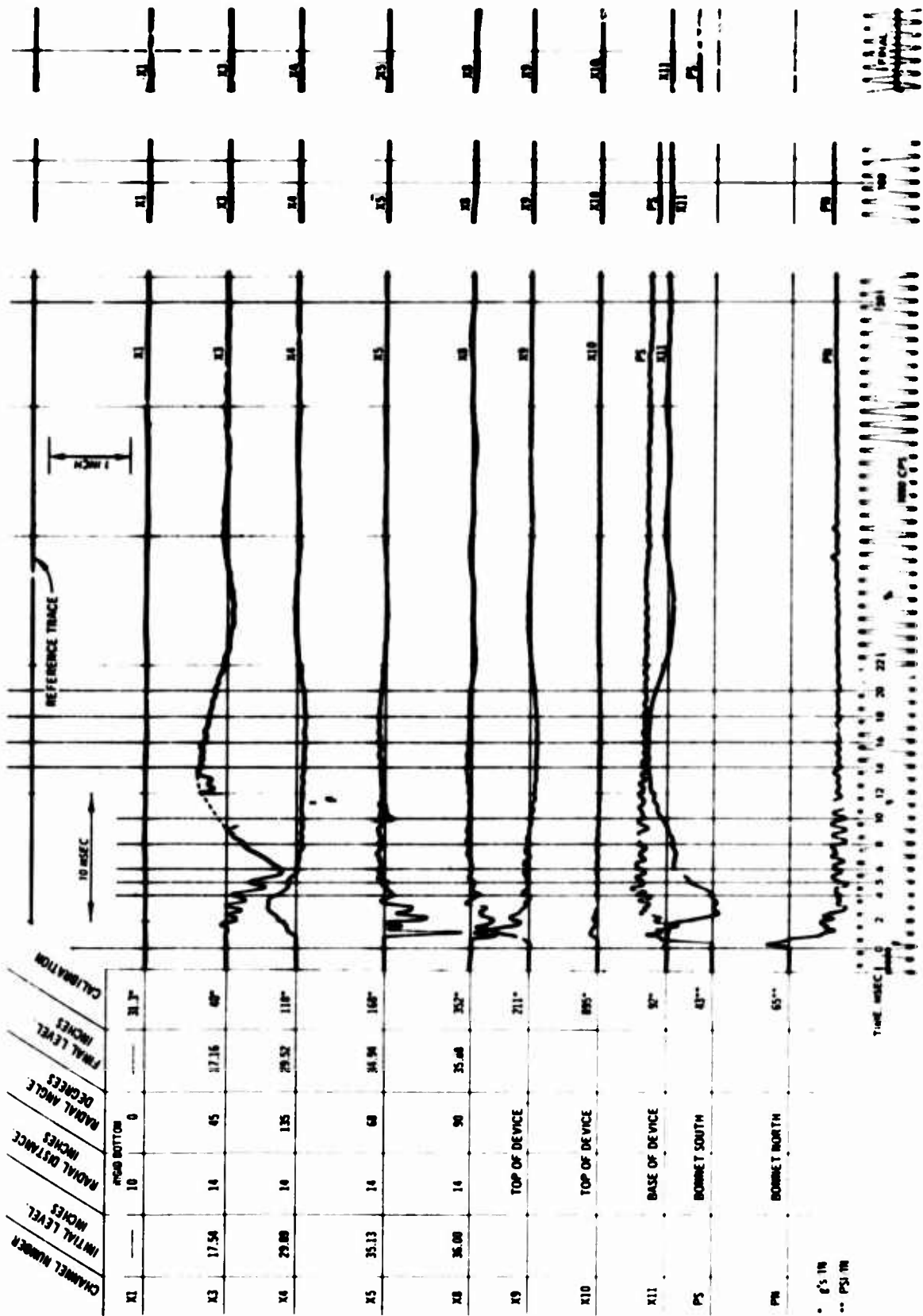


Fig. C-21. Test 15, acceleration and pressure record

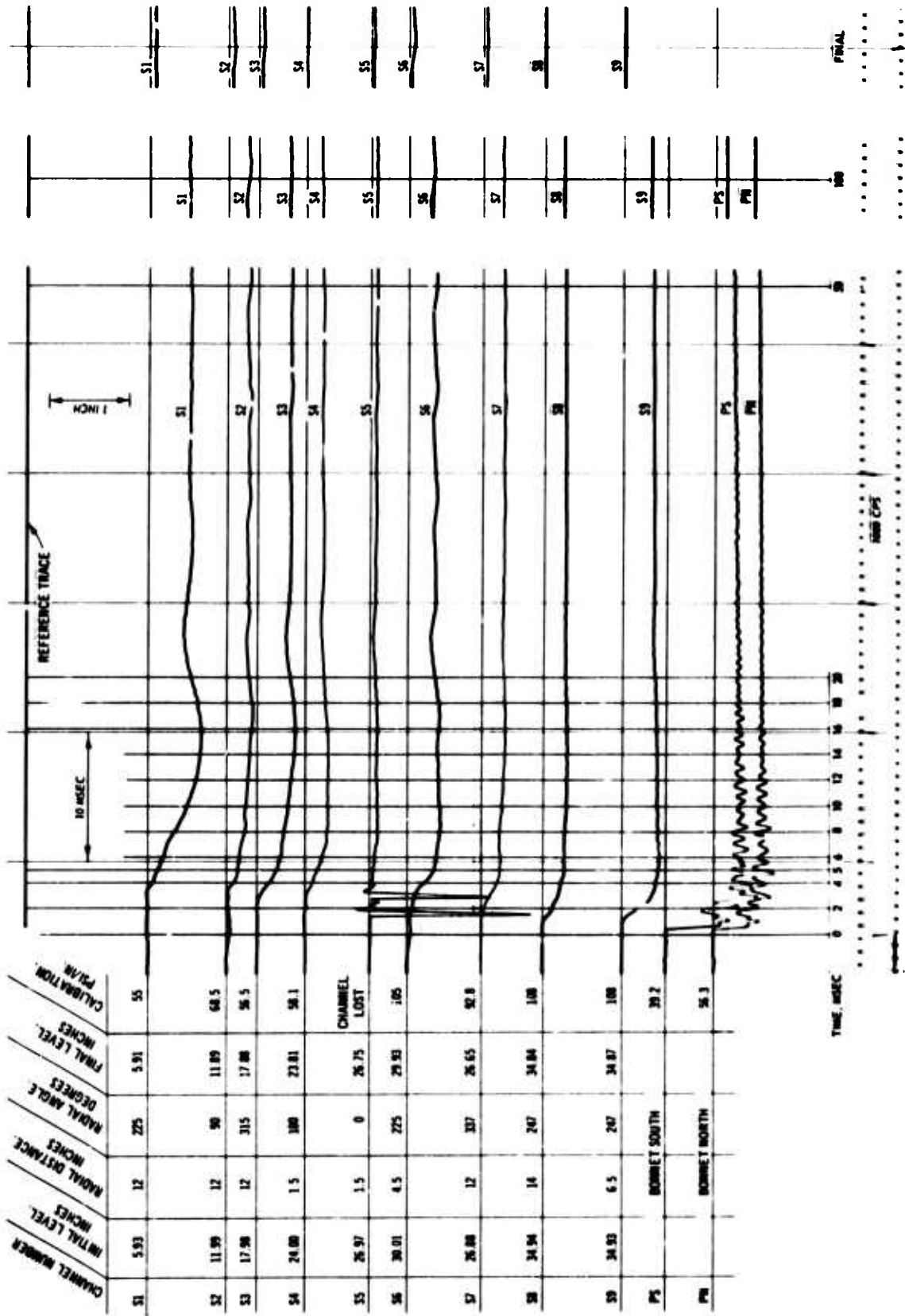


Fig. C-22. Test 16, pressure record (S1-S9)

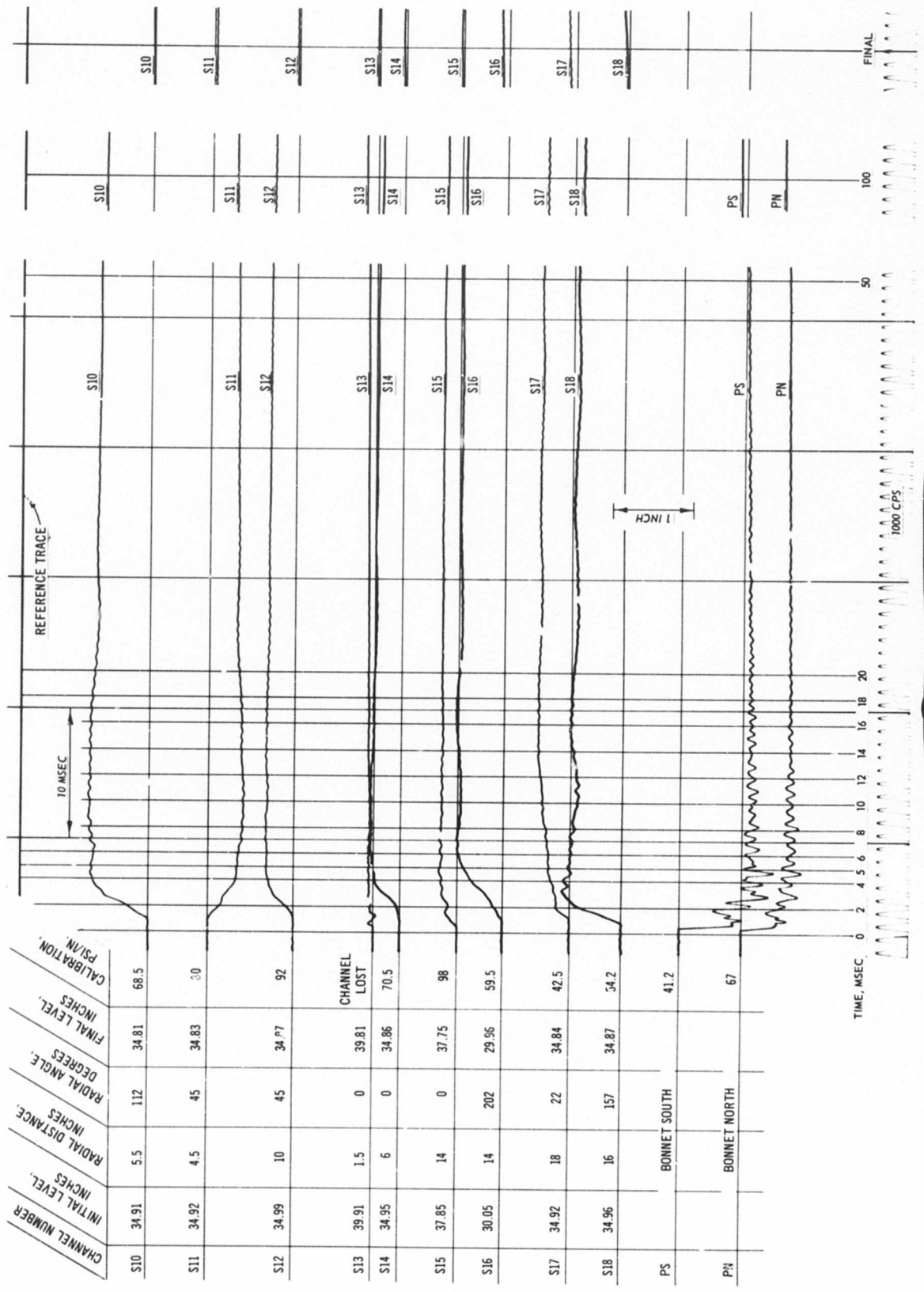


Fig. C-23. Test 16, pressure record (S10-S18)

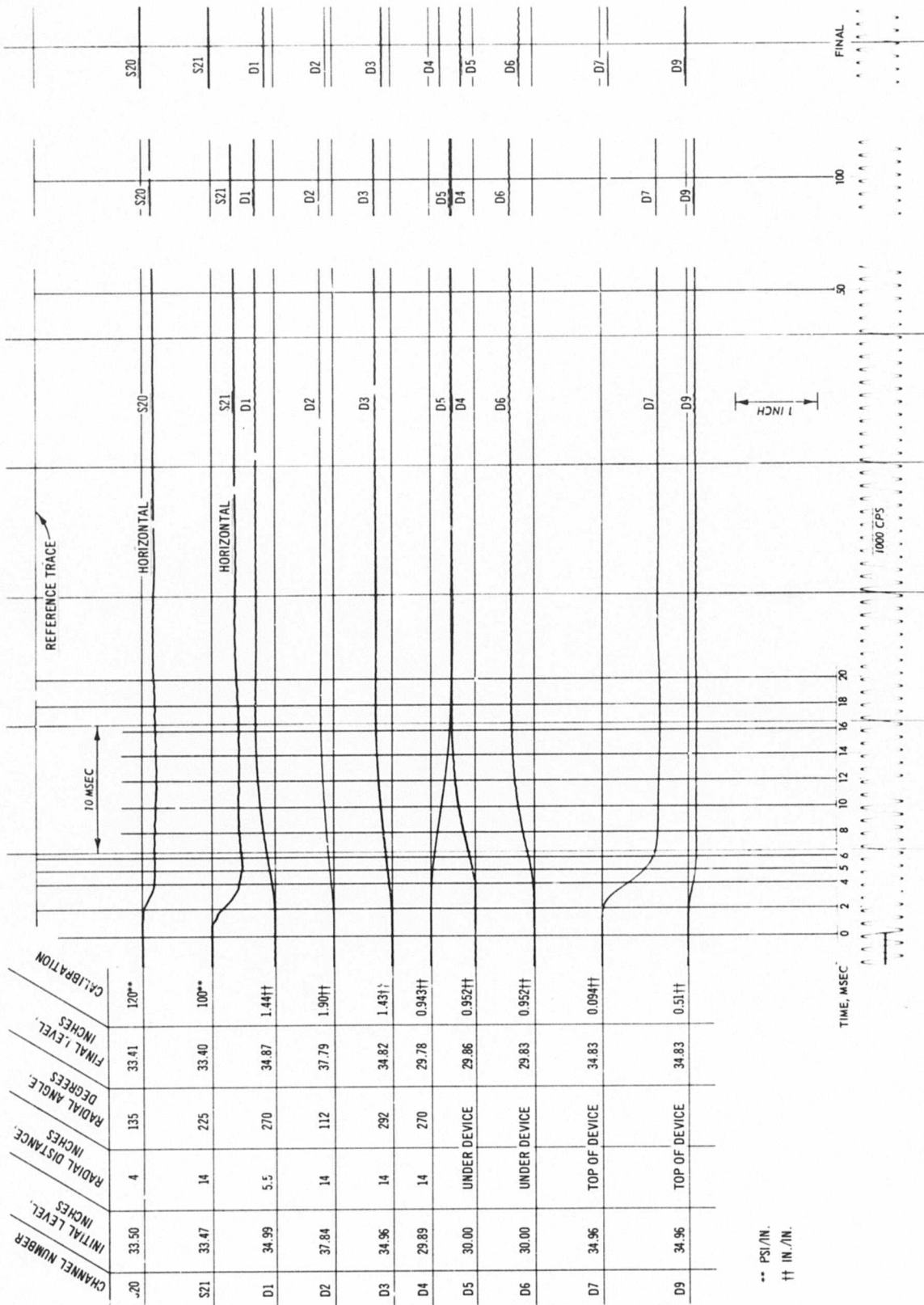


Fig. C-24. Test 16, pressure and deflection record

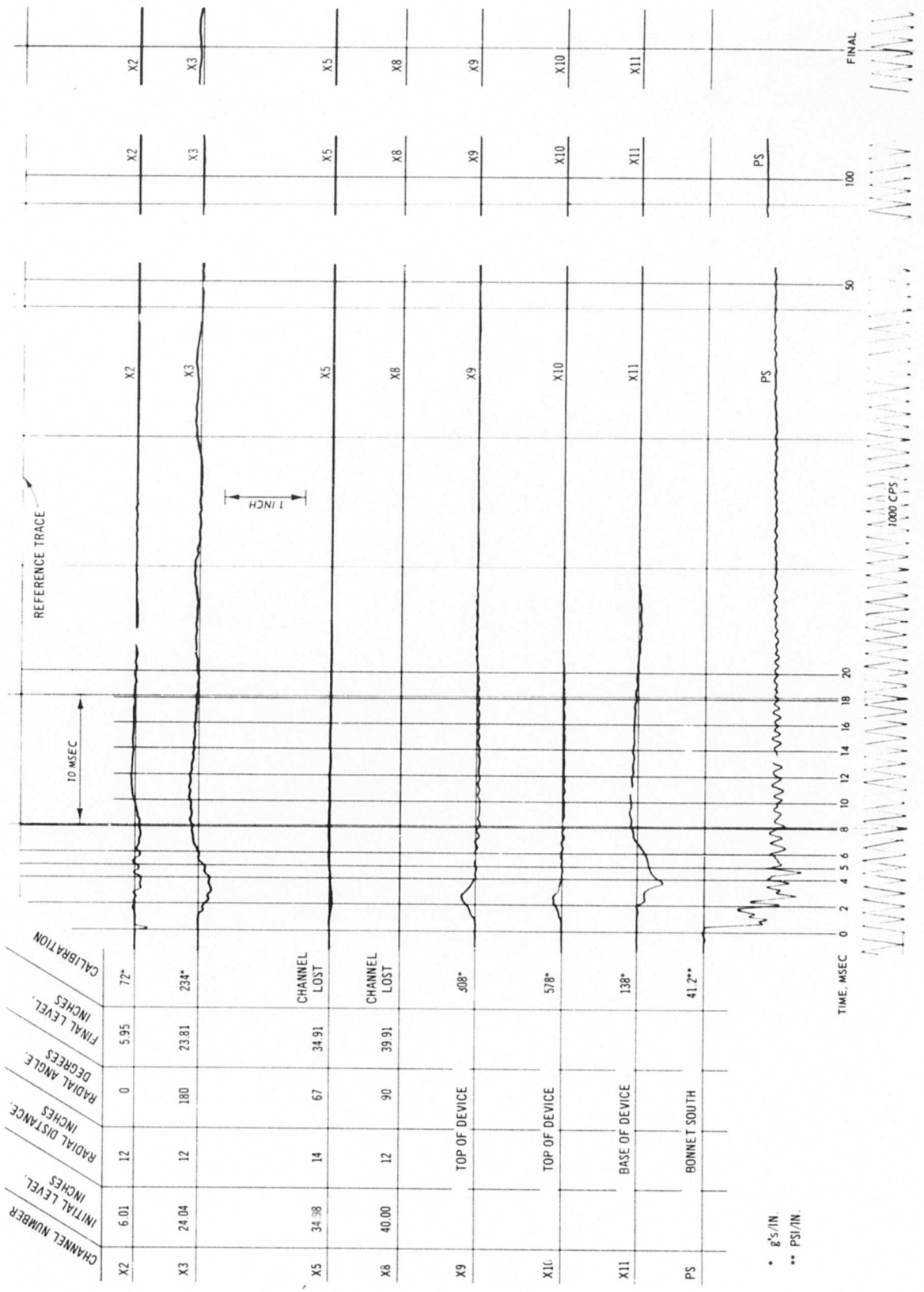


Fig. C-25. Test I6, acceleration and pressure record

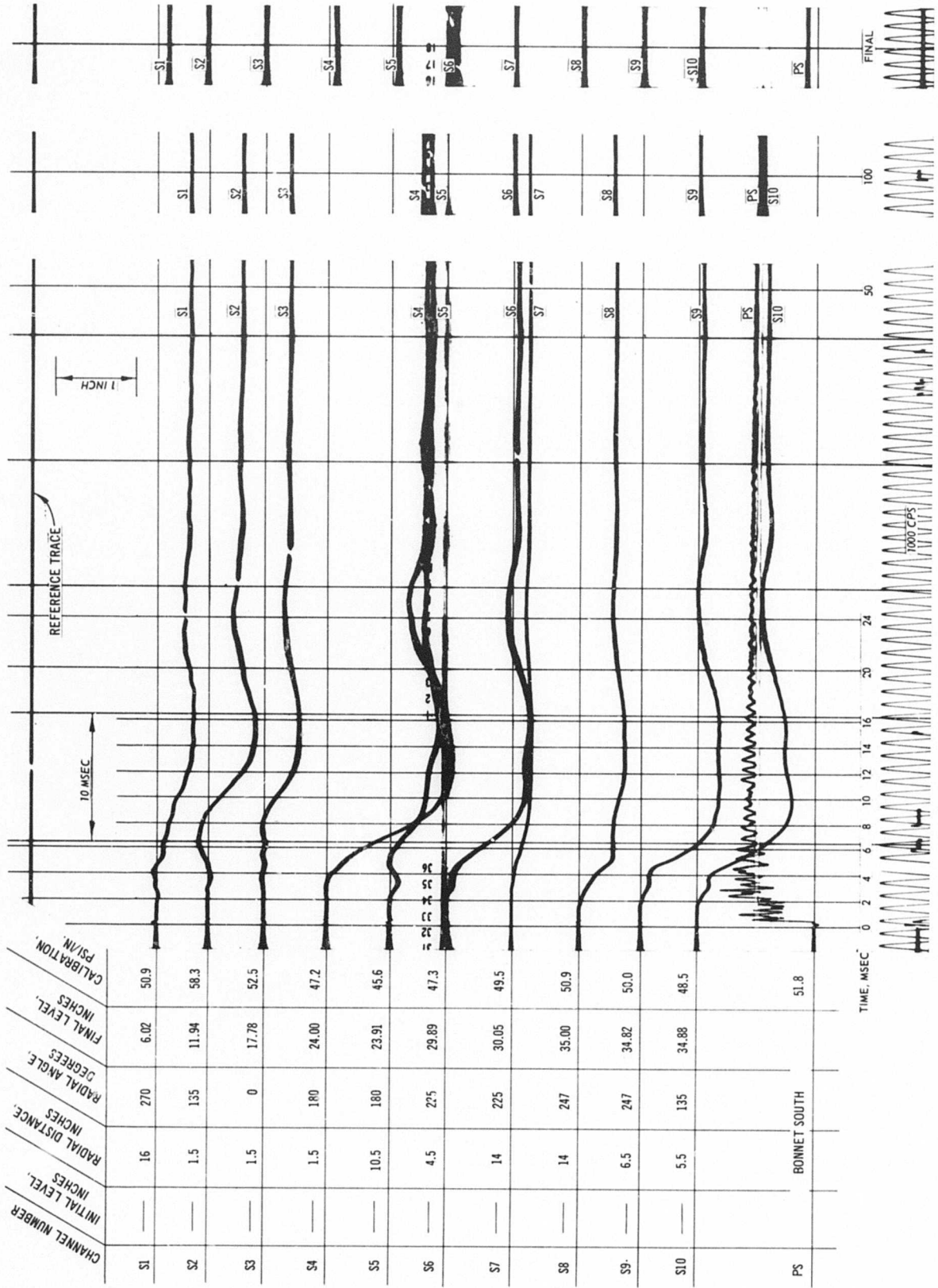


Fig. C-26. Test 17, pressure record (S1-S10)

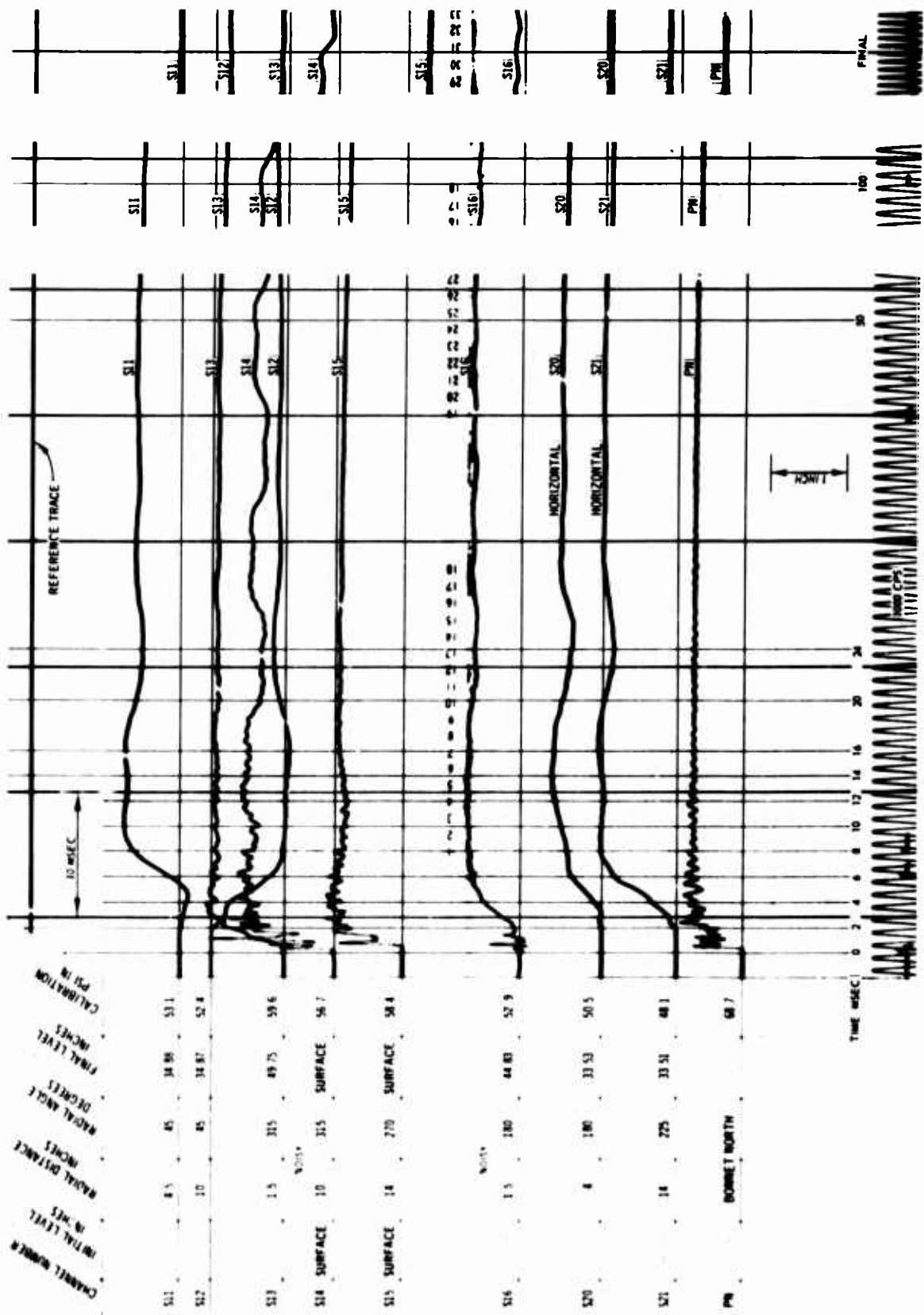


Fig. C-27. Test 17, pressure record (S11-S21)

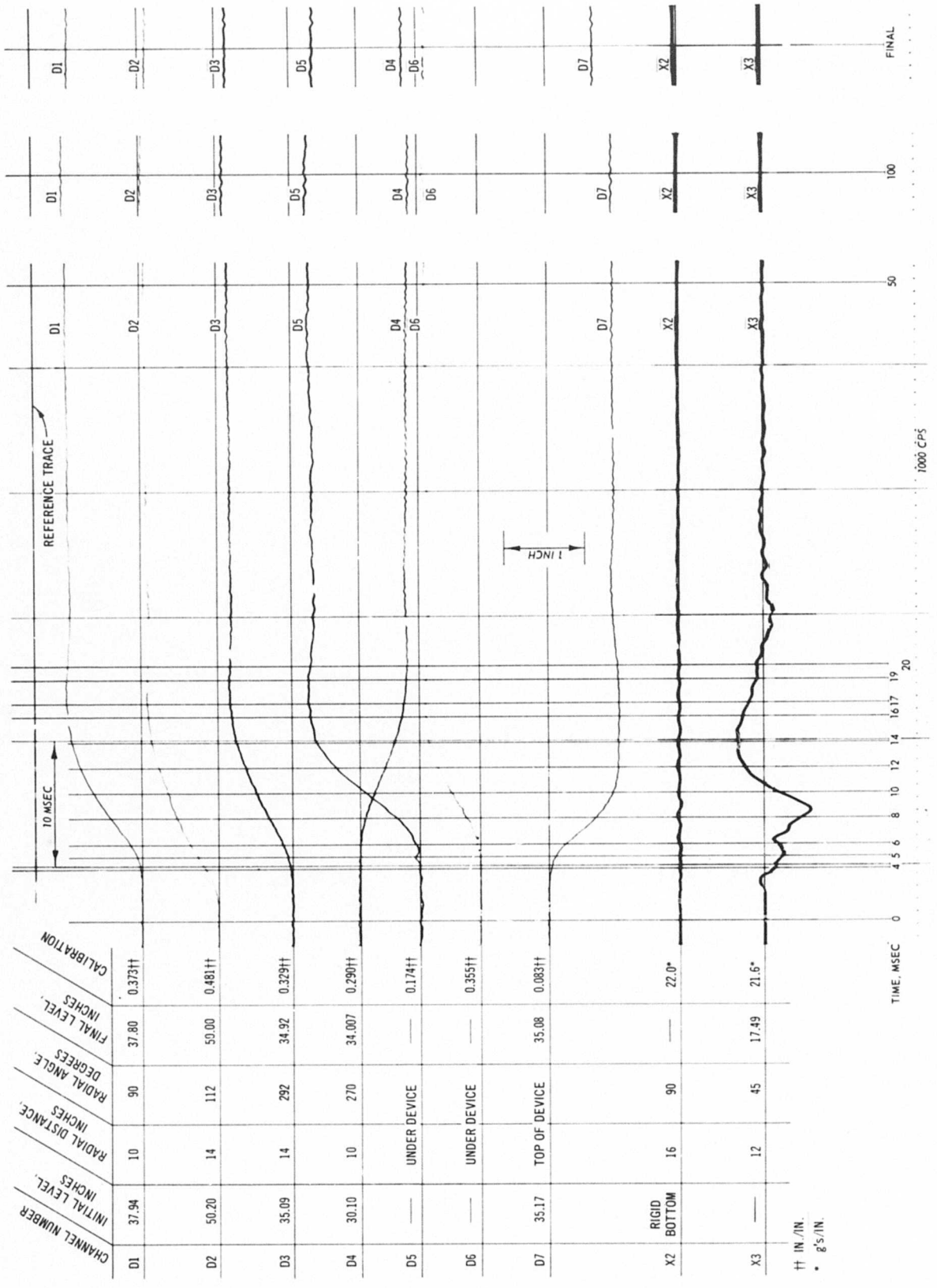


Fig. C-28. Test 17, deflection and acceleration record

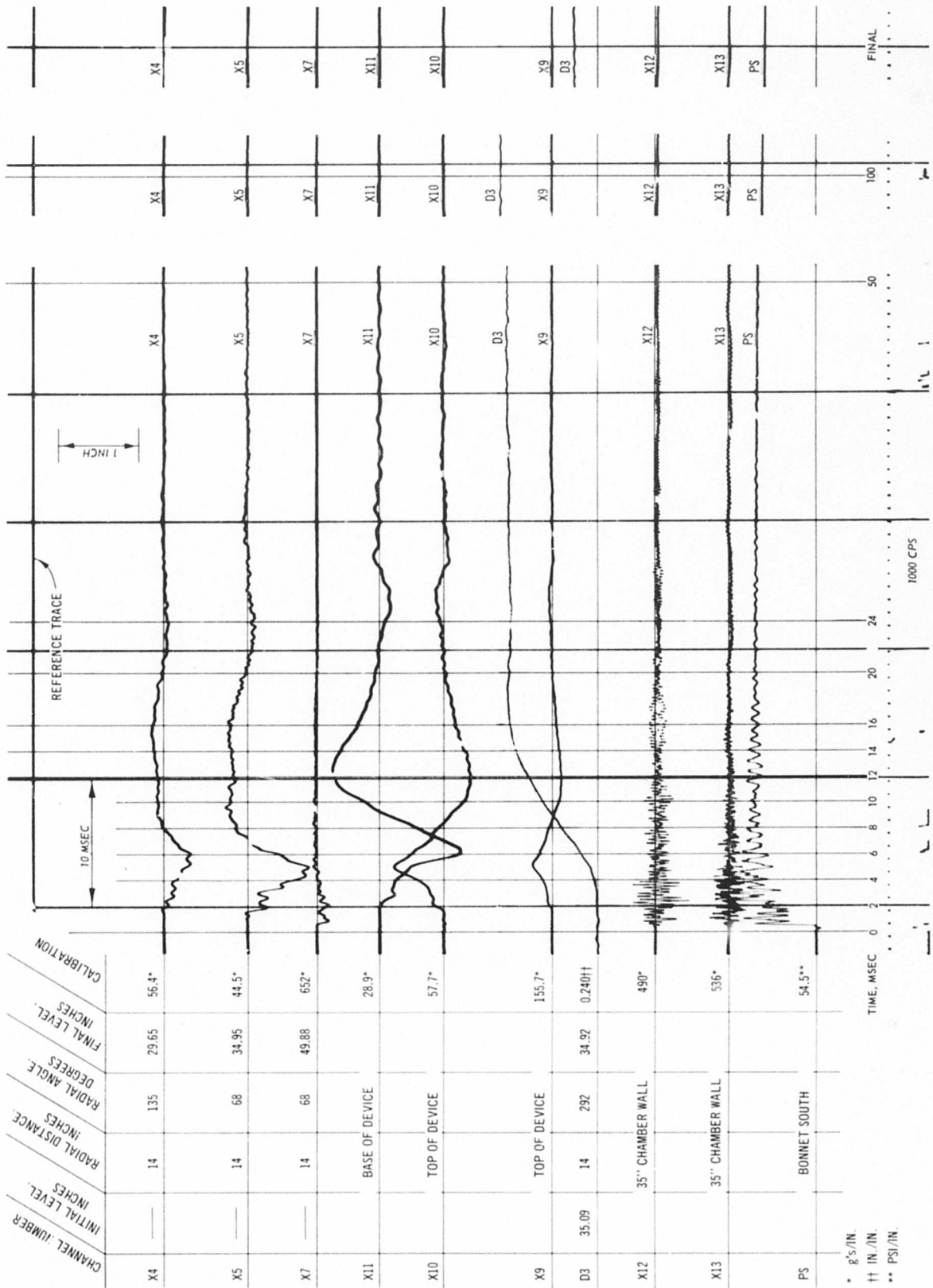


Fig. C-29. Test 17, acceleration, deflection, and pressure record

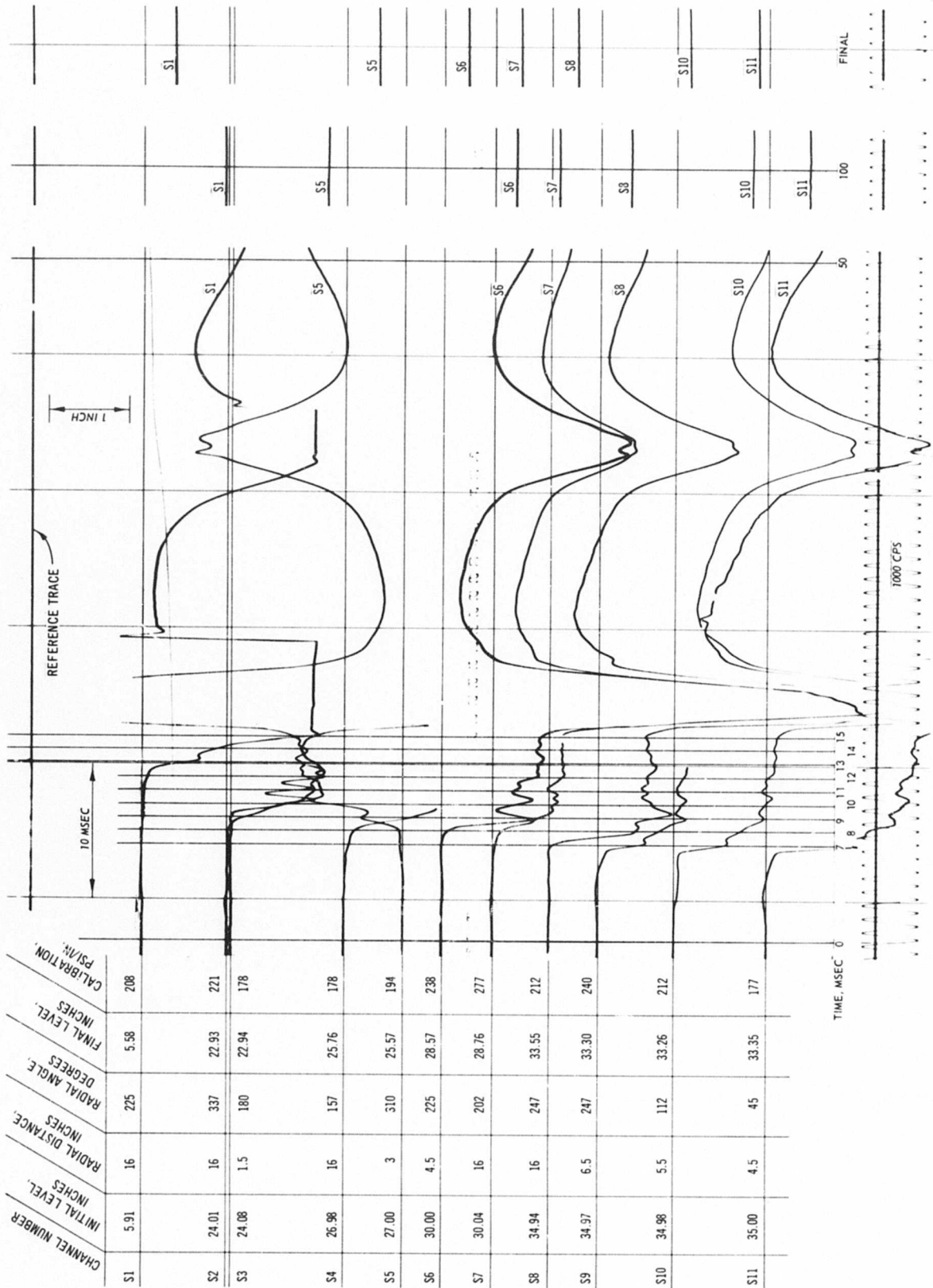


Fig. C-30. Test 18, pressure record (S1-S11)

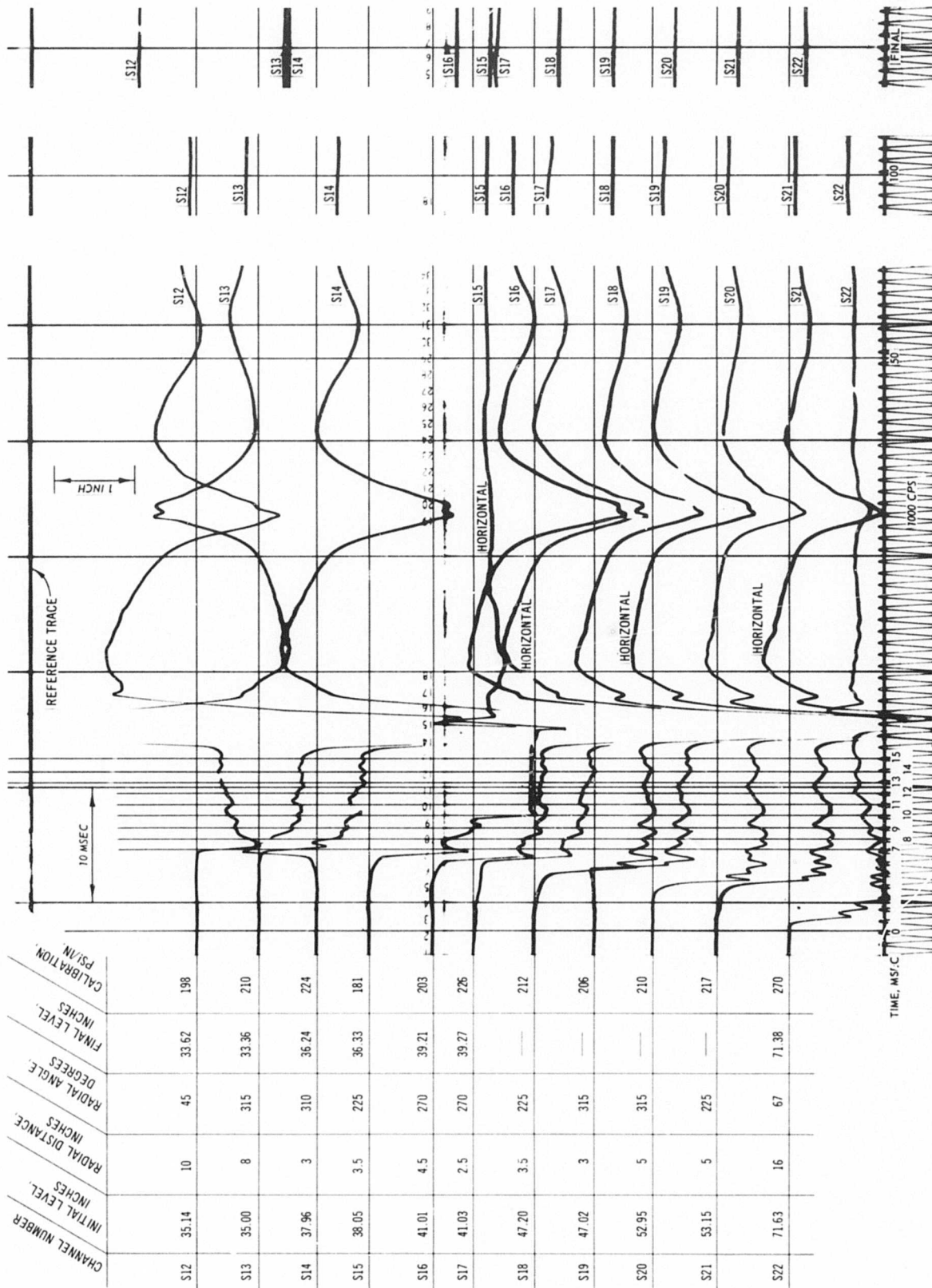


Fig. C-31. Test 18, pressure record (S12-S22)

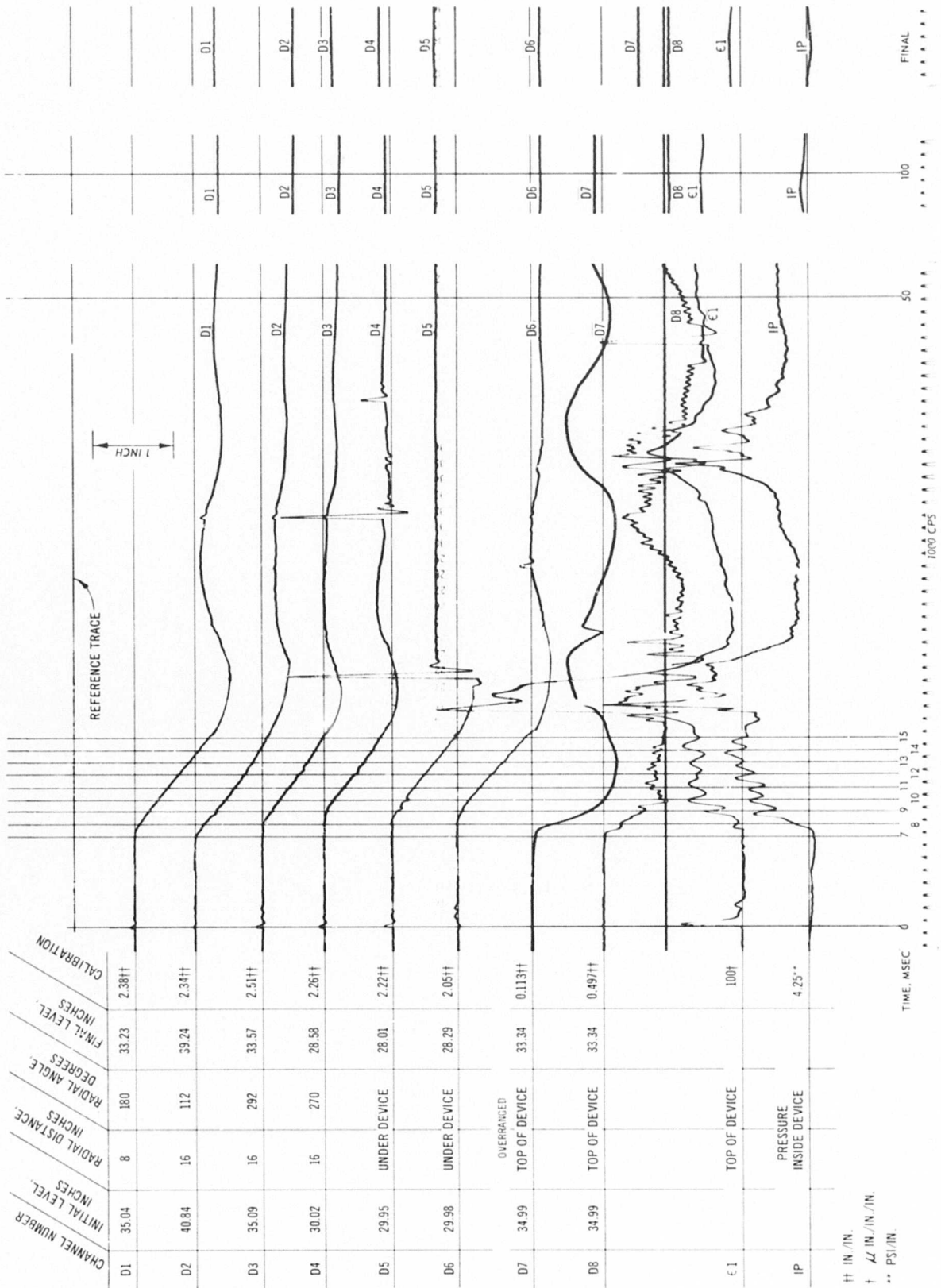


Fig. C-32. Test I8, deflection, strain, and pressure record

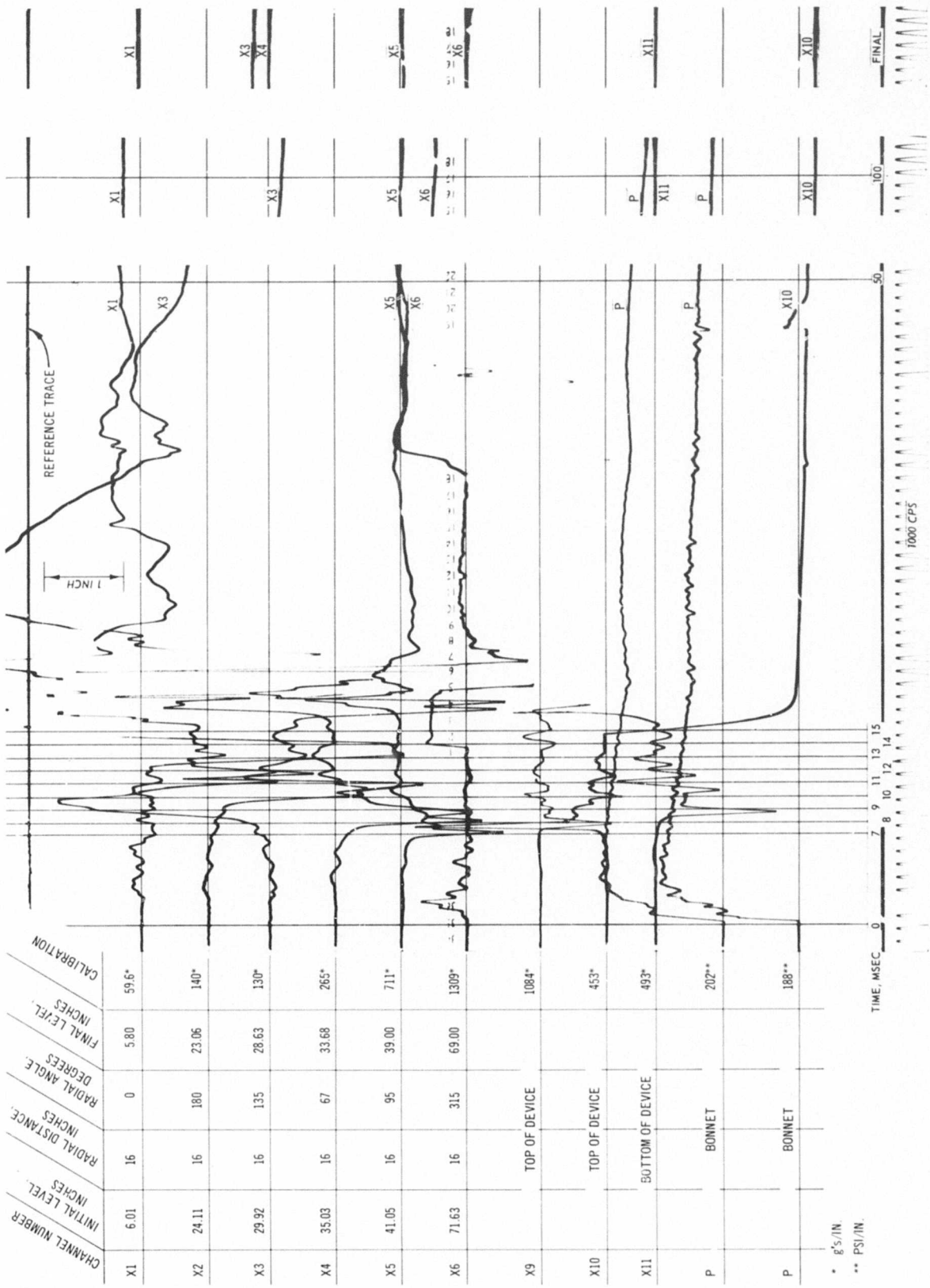


Fig. C-33. Test 18, acceleration and pressure record

* g's/IN.
 ** PSI/IN.

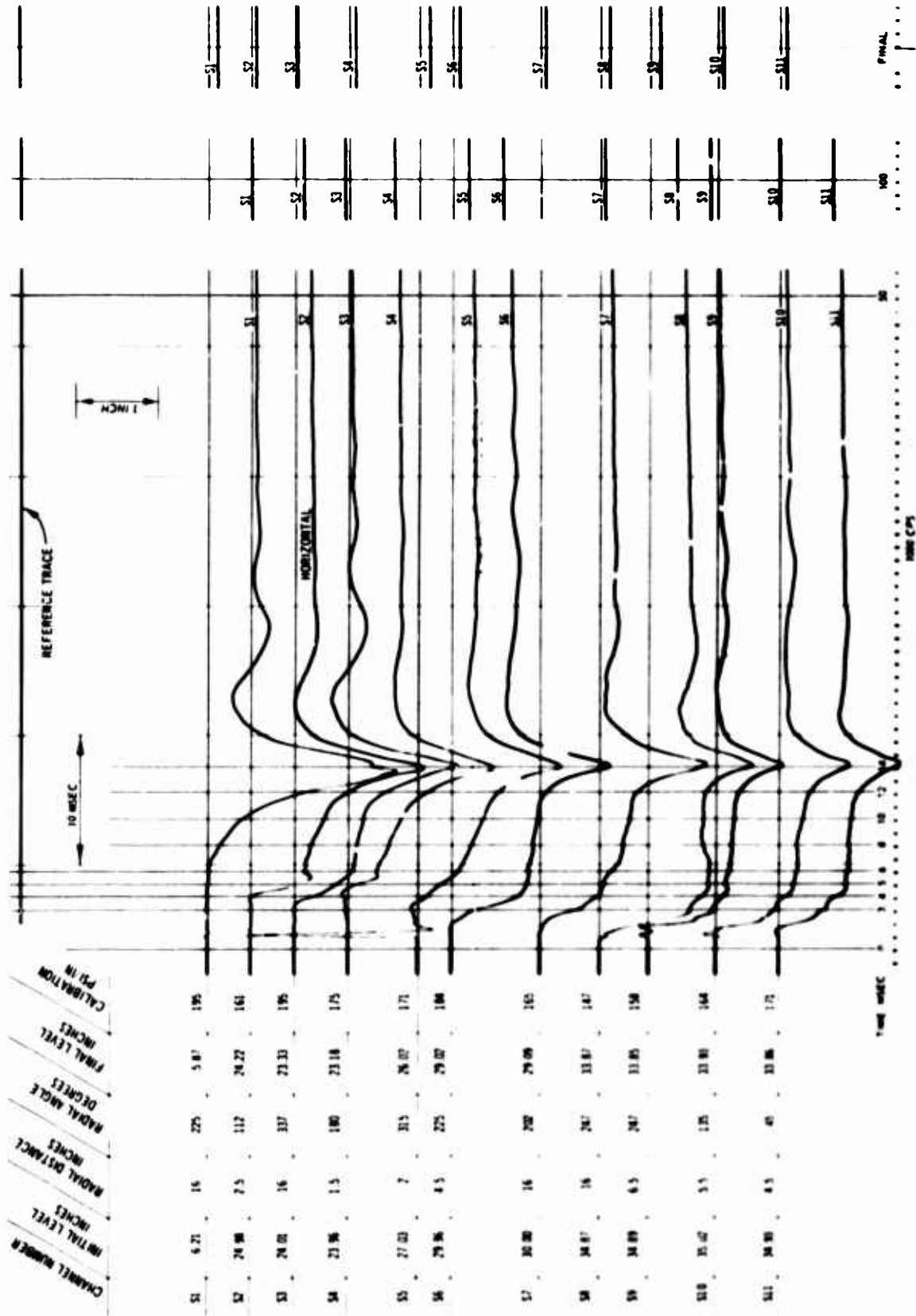


Fig. C-34. Test 19, pressure record (S1-S11)

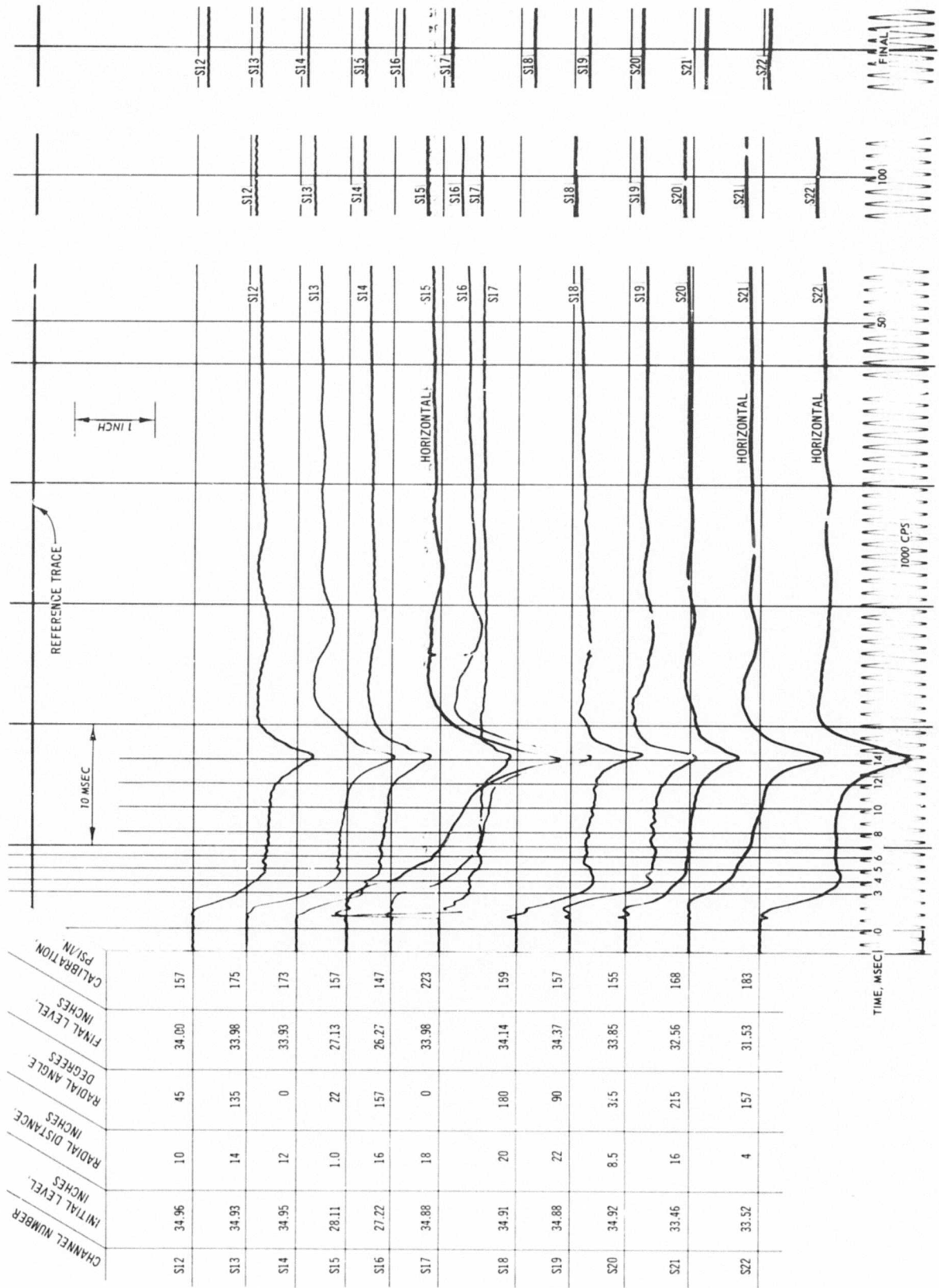


Fig. C-35. Test 19, pressure record (S12-S22)

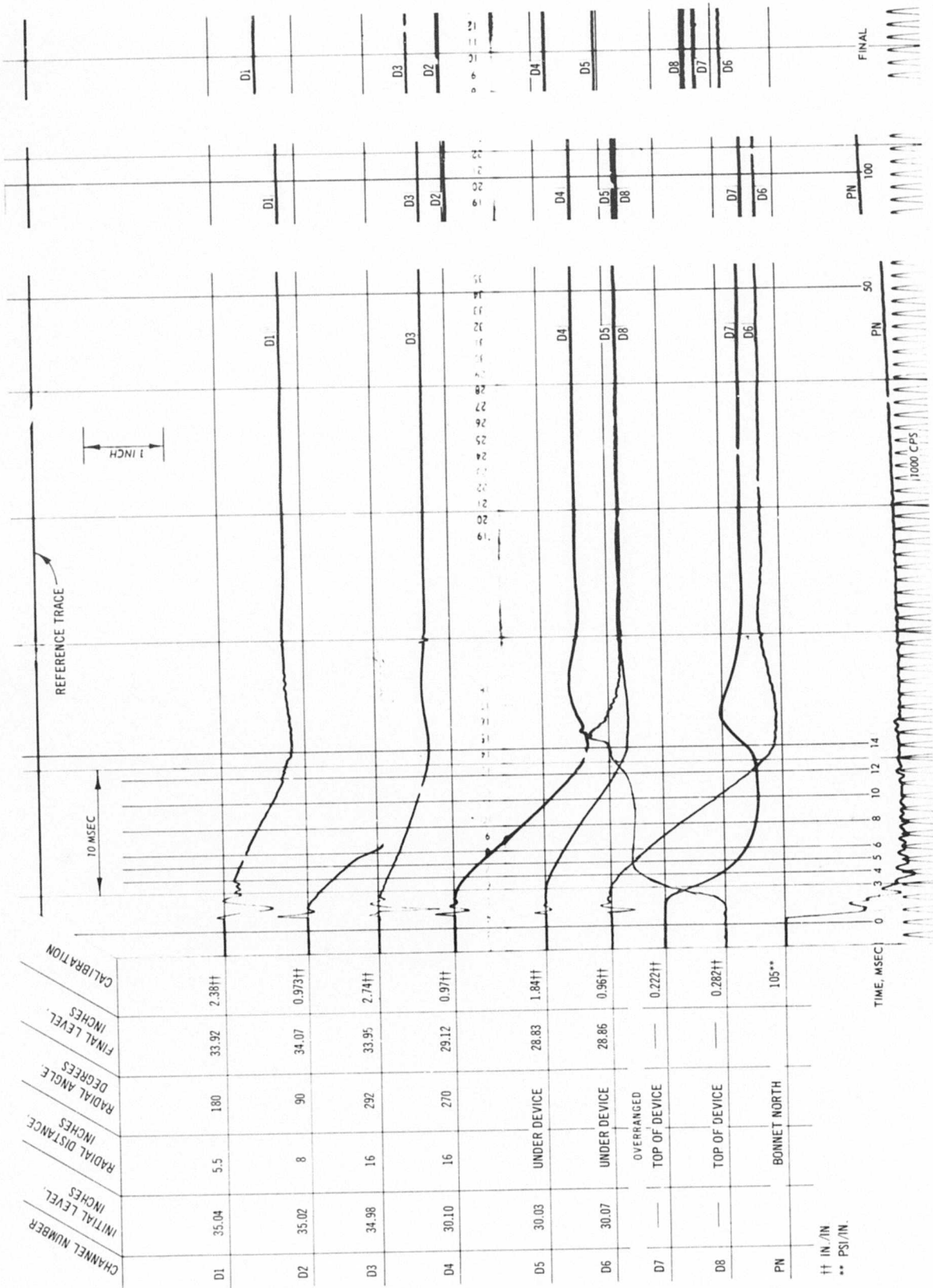


Fig. C-36. Test 19, deflection and pressure record

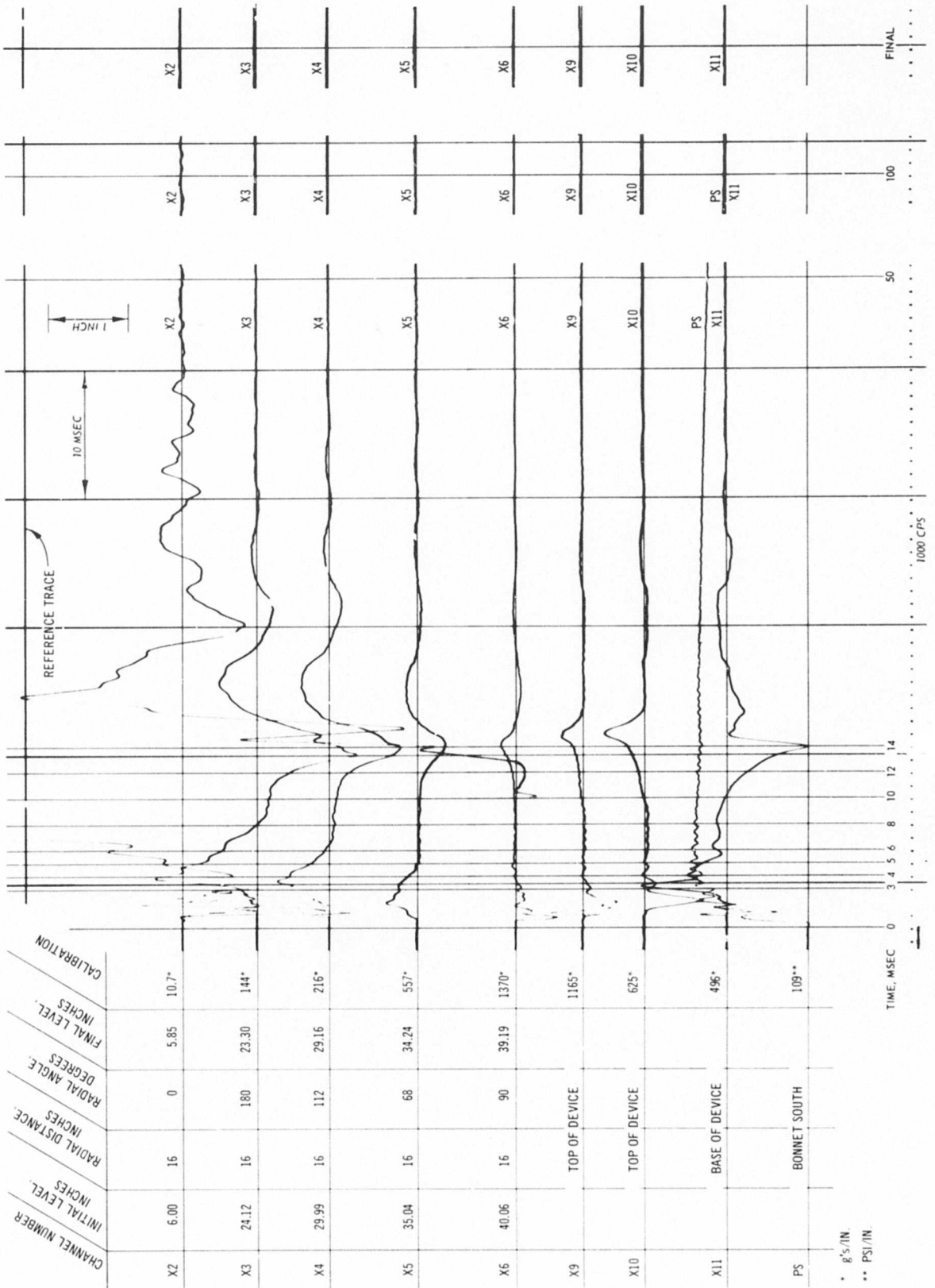


Fig. C-37. Test 19, acceleration and pressure record

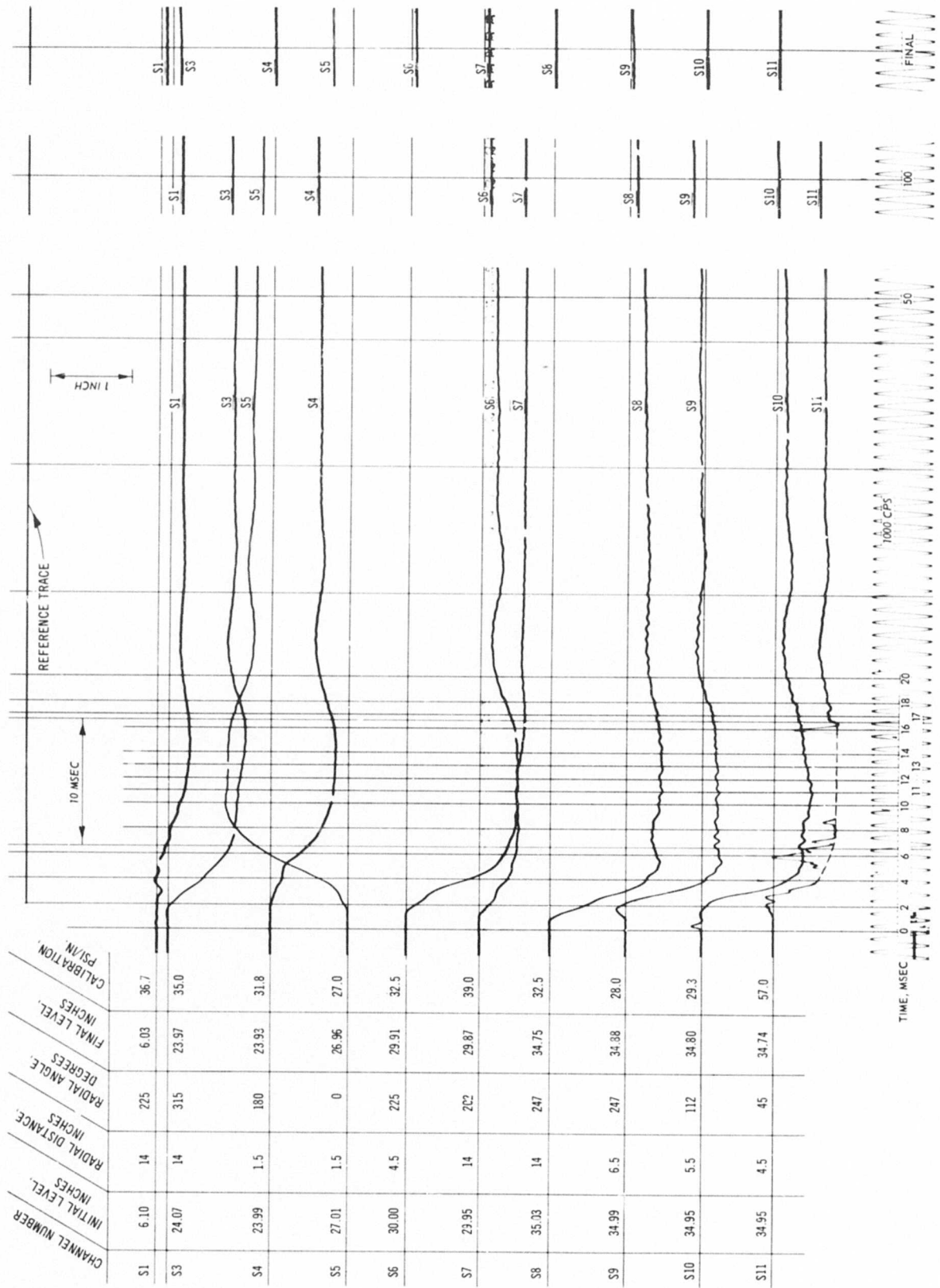


Fig. C-38. Test 20, pressure record (S1-S11)

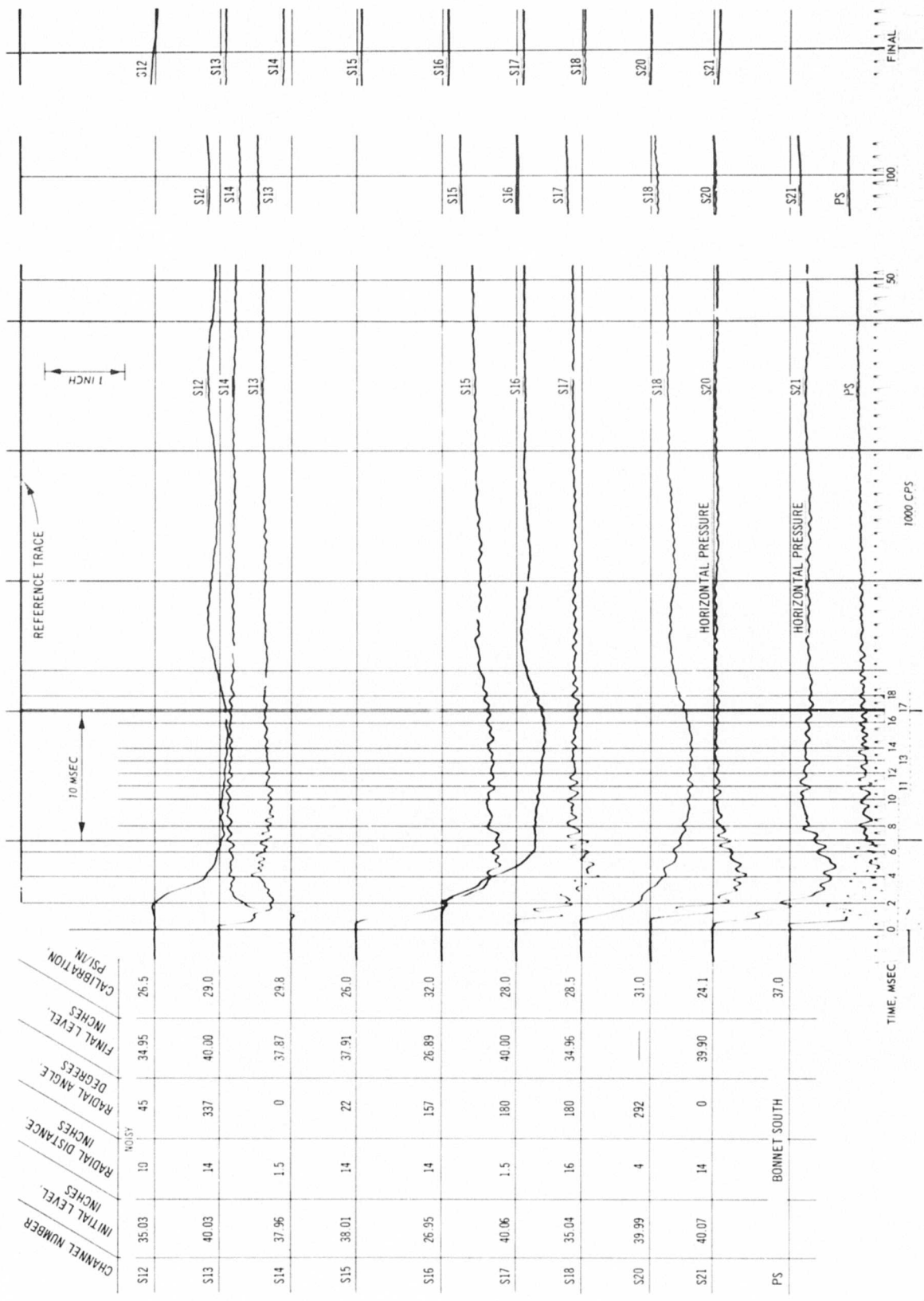


Fig. C-39. Test 20, pressure record (S12-S21)

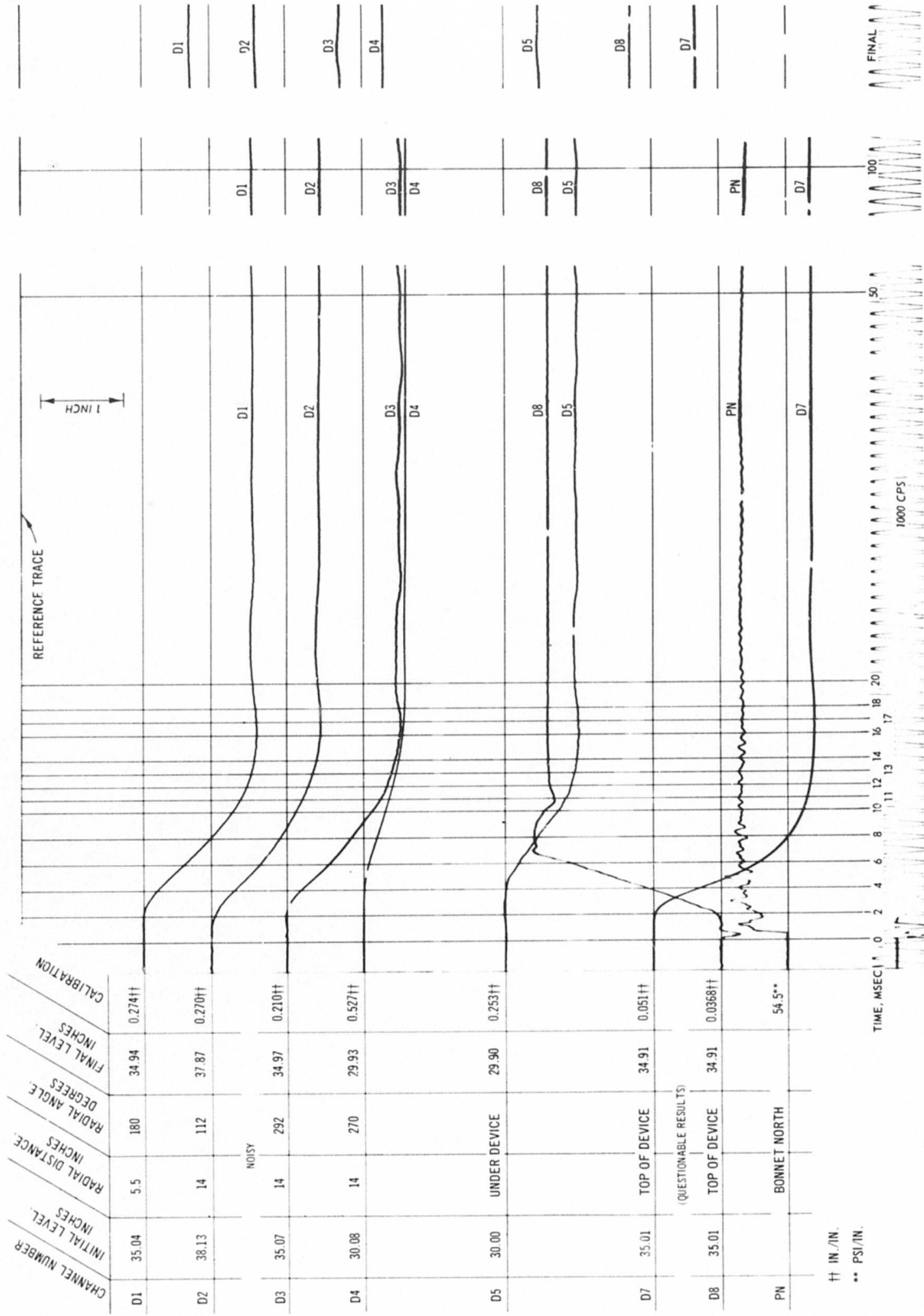


Fig. C-40. Test 20, deflection and pressure record

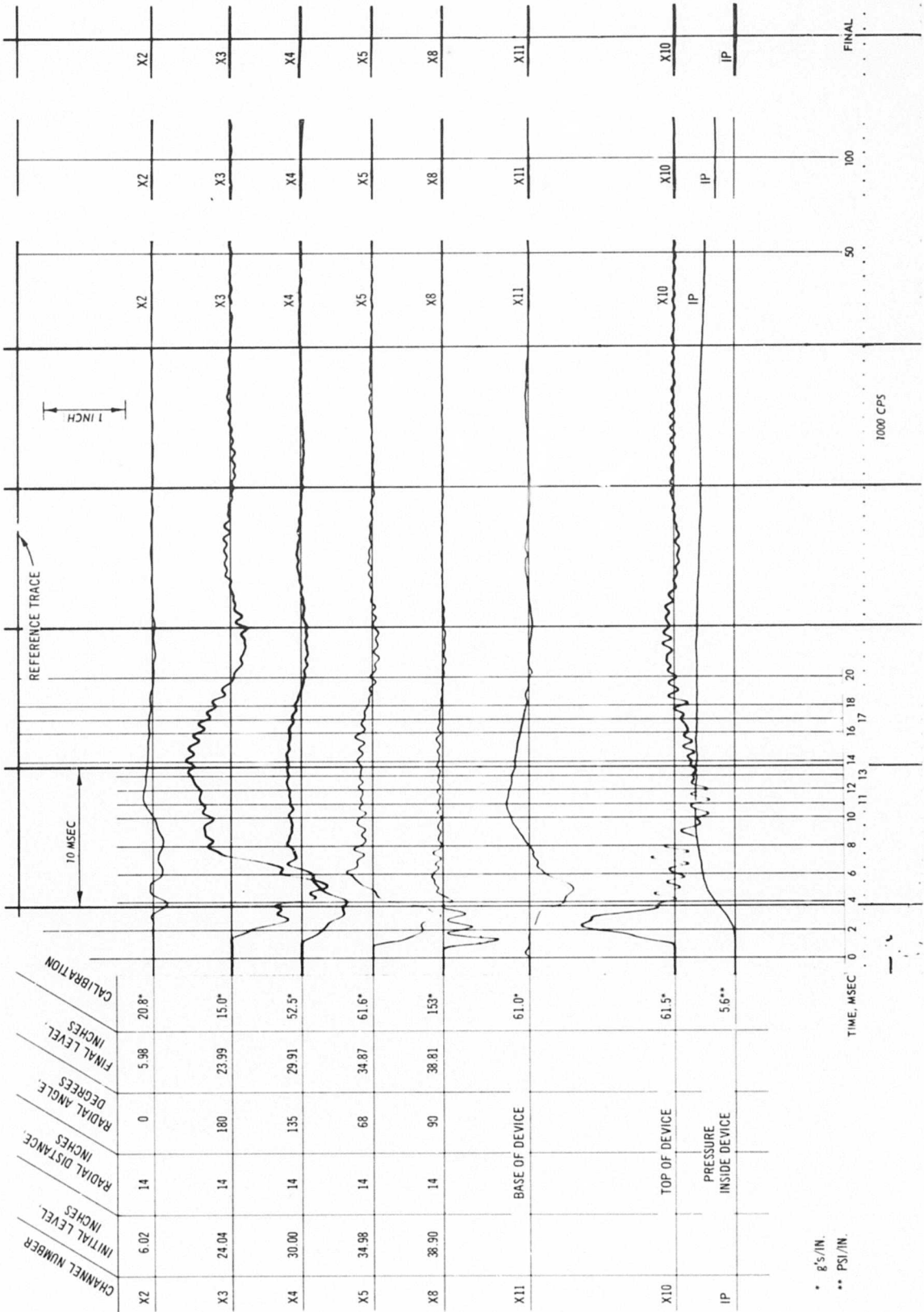


Fig. C-41. Test 20, acceleration and pressure record

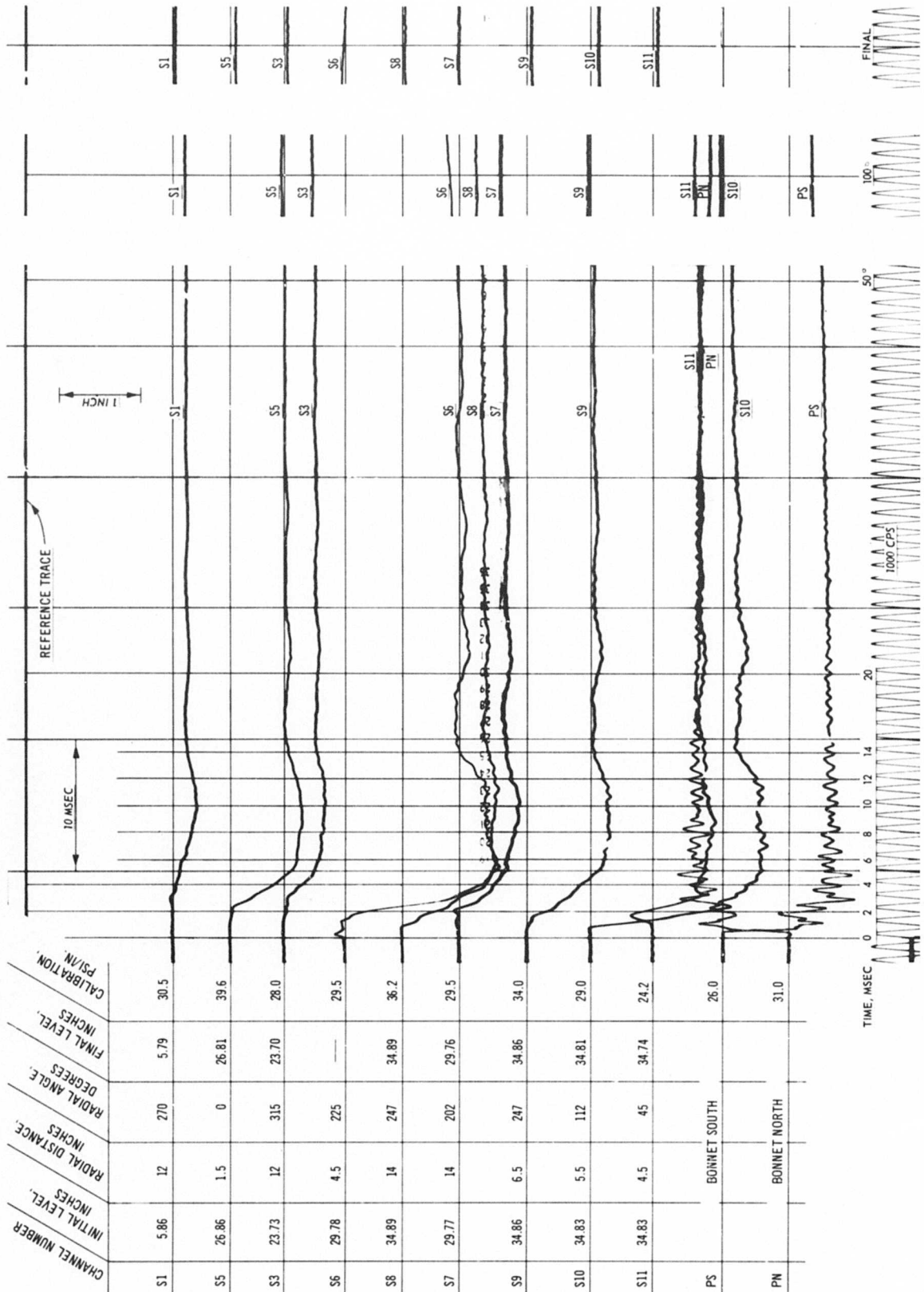


Fig. C-42. Test 21, pressure record

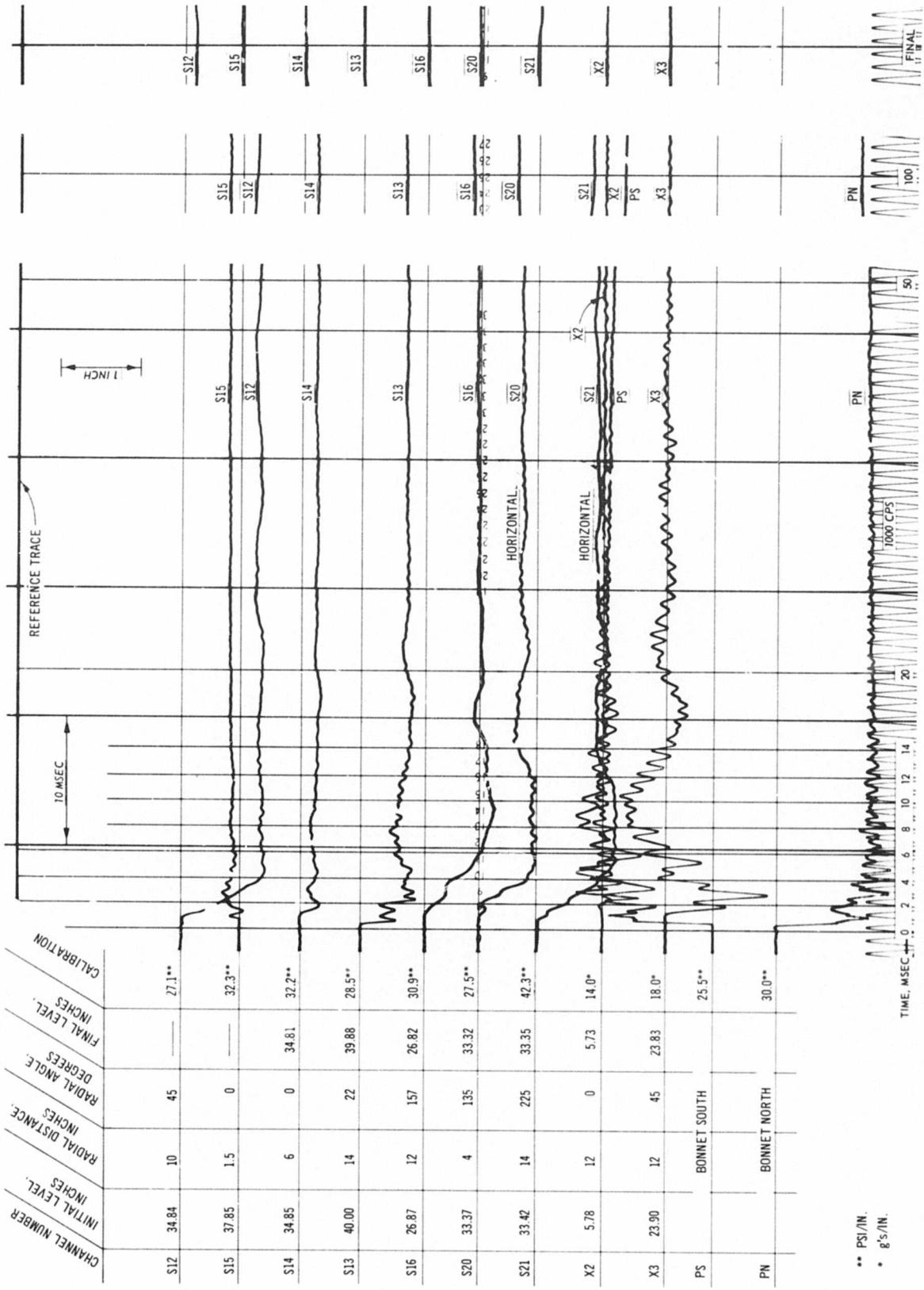


Fig. C-43. Test 21, pressure and acceleration record

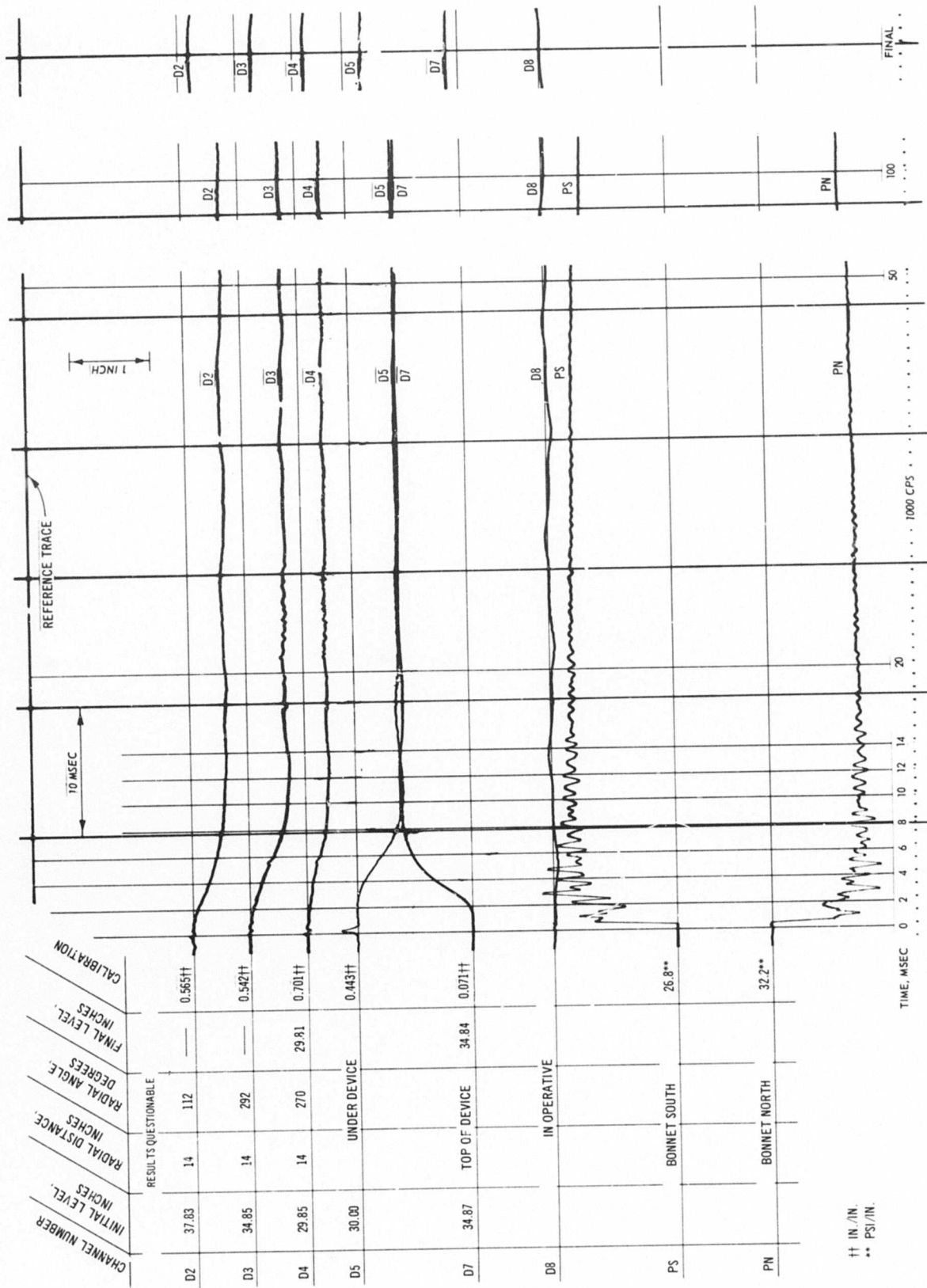
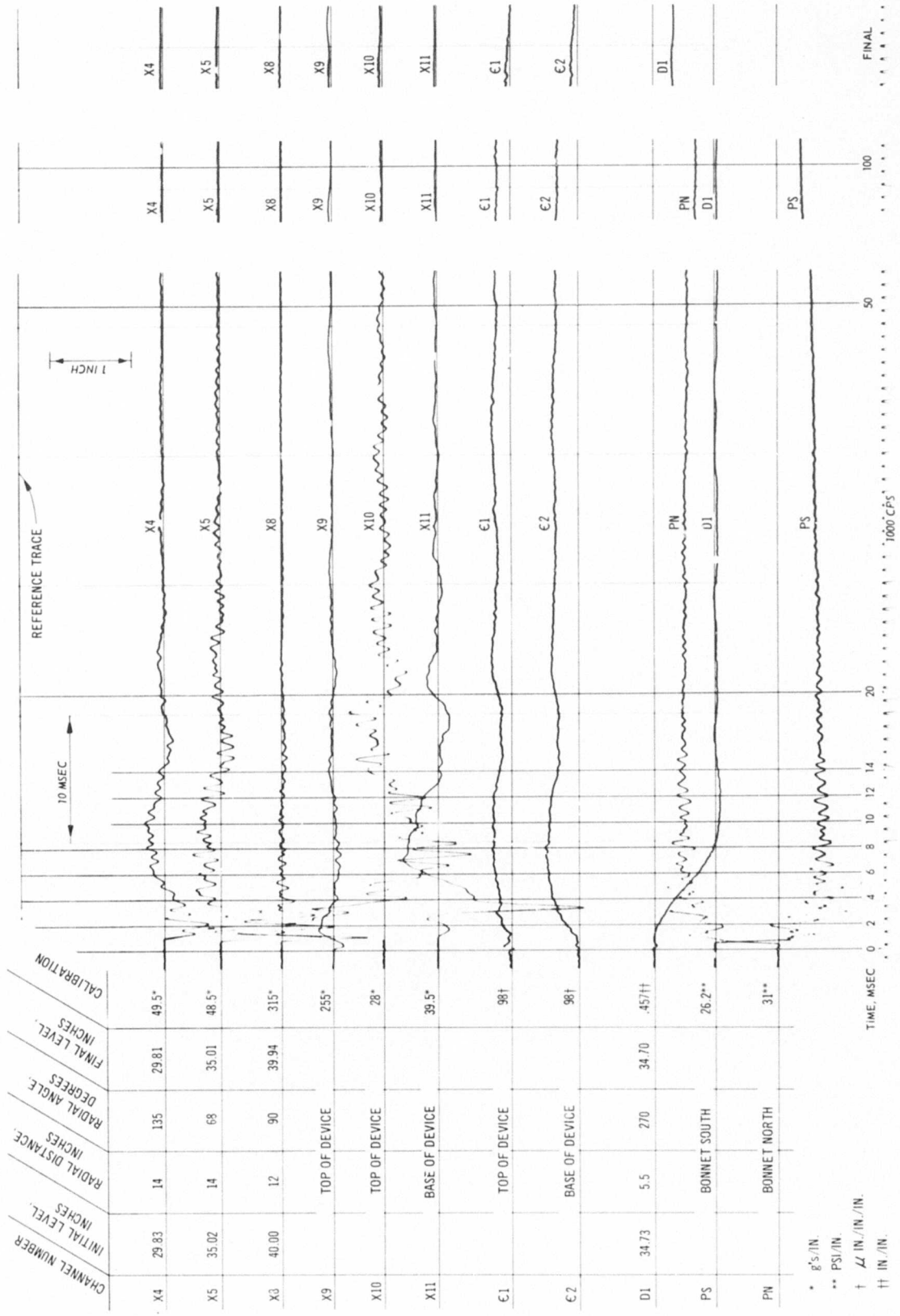


Fig. C-44. Test 21, deflection and pressure record



* g's/IN.
 ** PSI/IN.
 † \angle IN./IN./IN.
 †† IN./IN.

Fig. C-45. Test 21, pressure, acceleration, deflection, and strain record

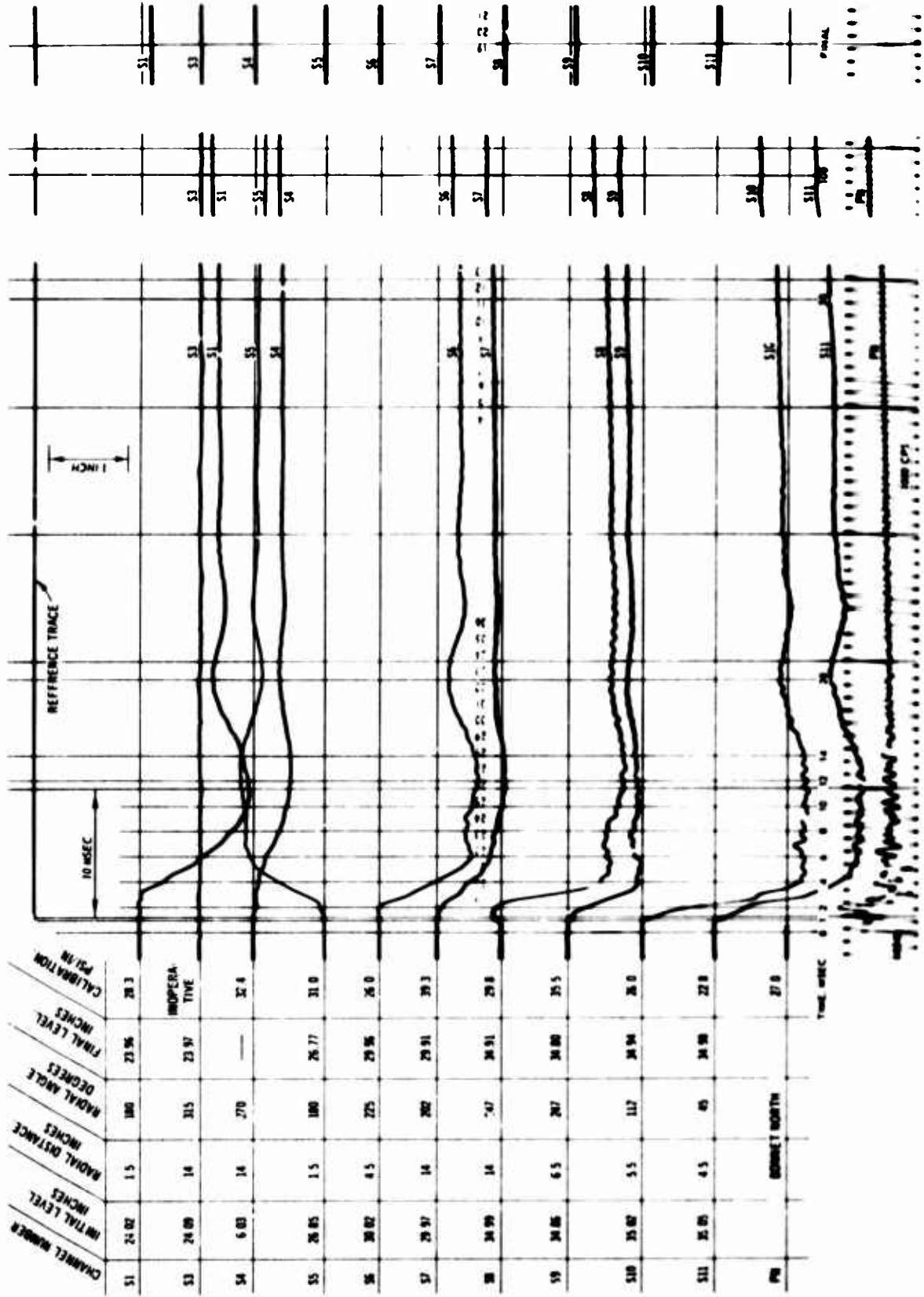


Fig. C-46. Test 22, pressure record (S1-S11)

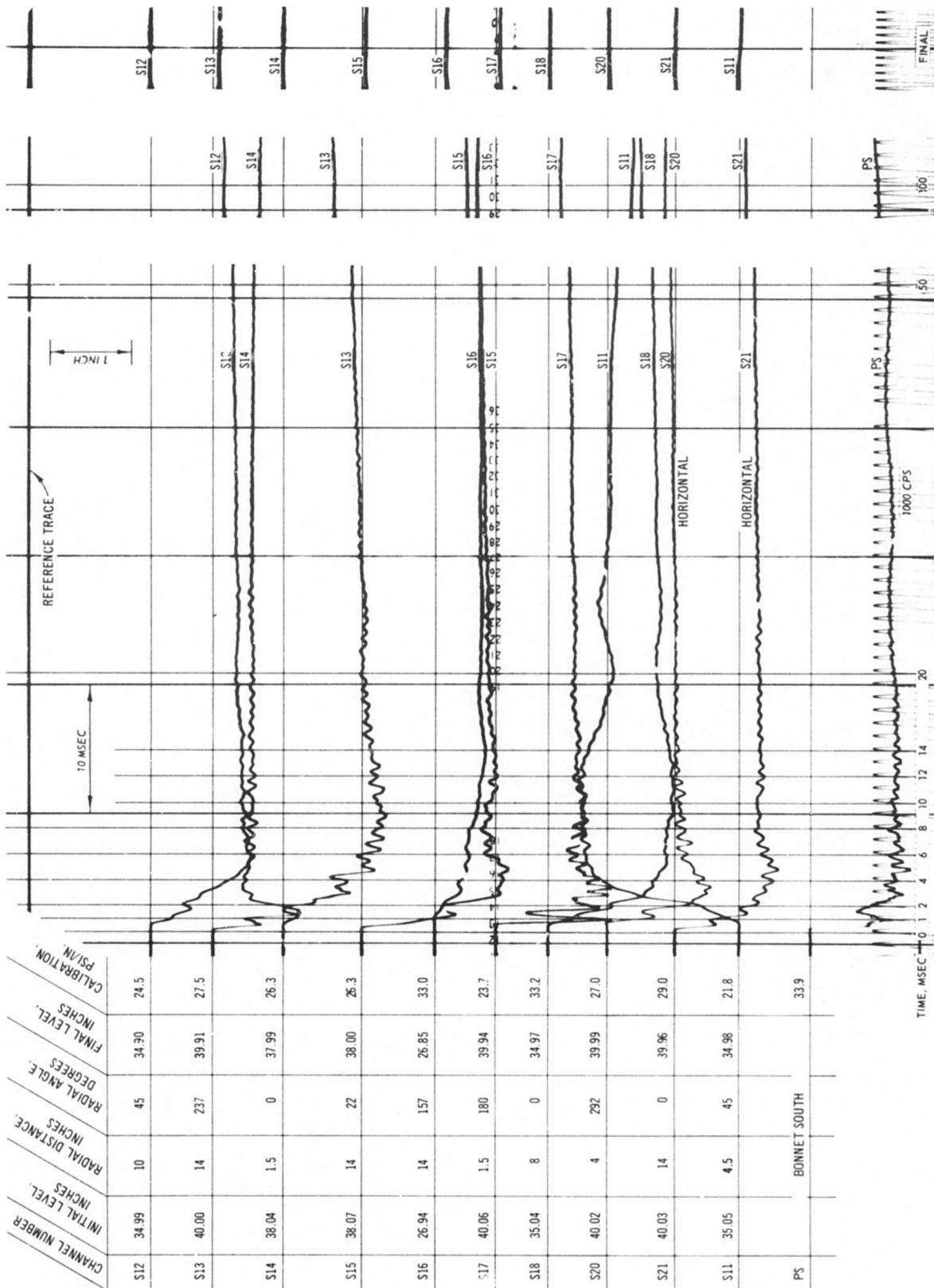


Fig. C-47. Test 22, pressure record (S12-S21, S11)

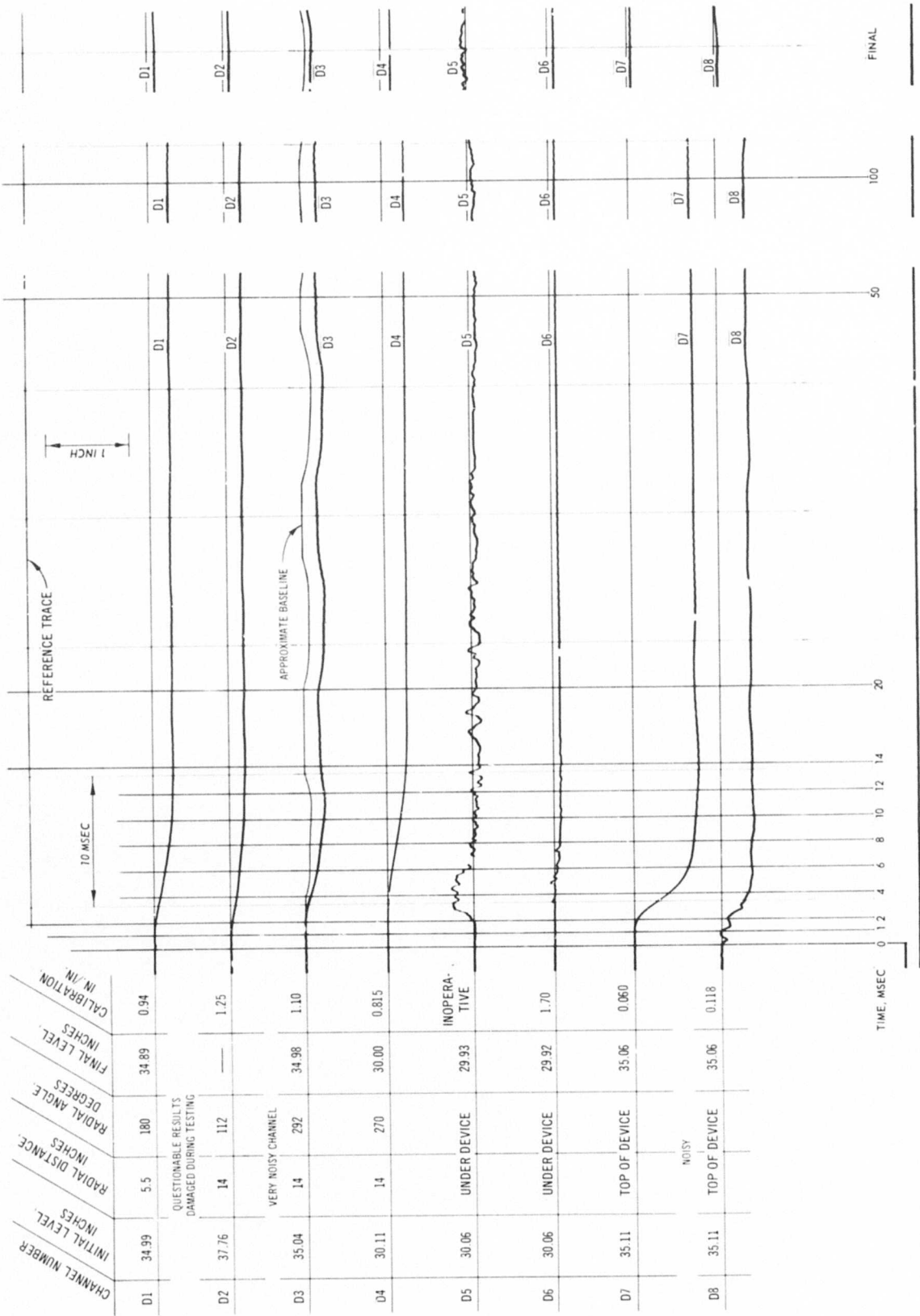


Fig. C-48. Test 22, deflection record

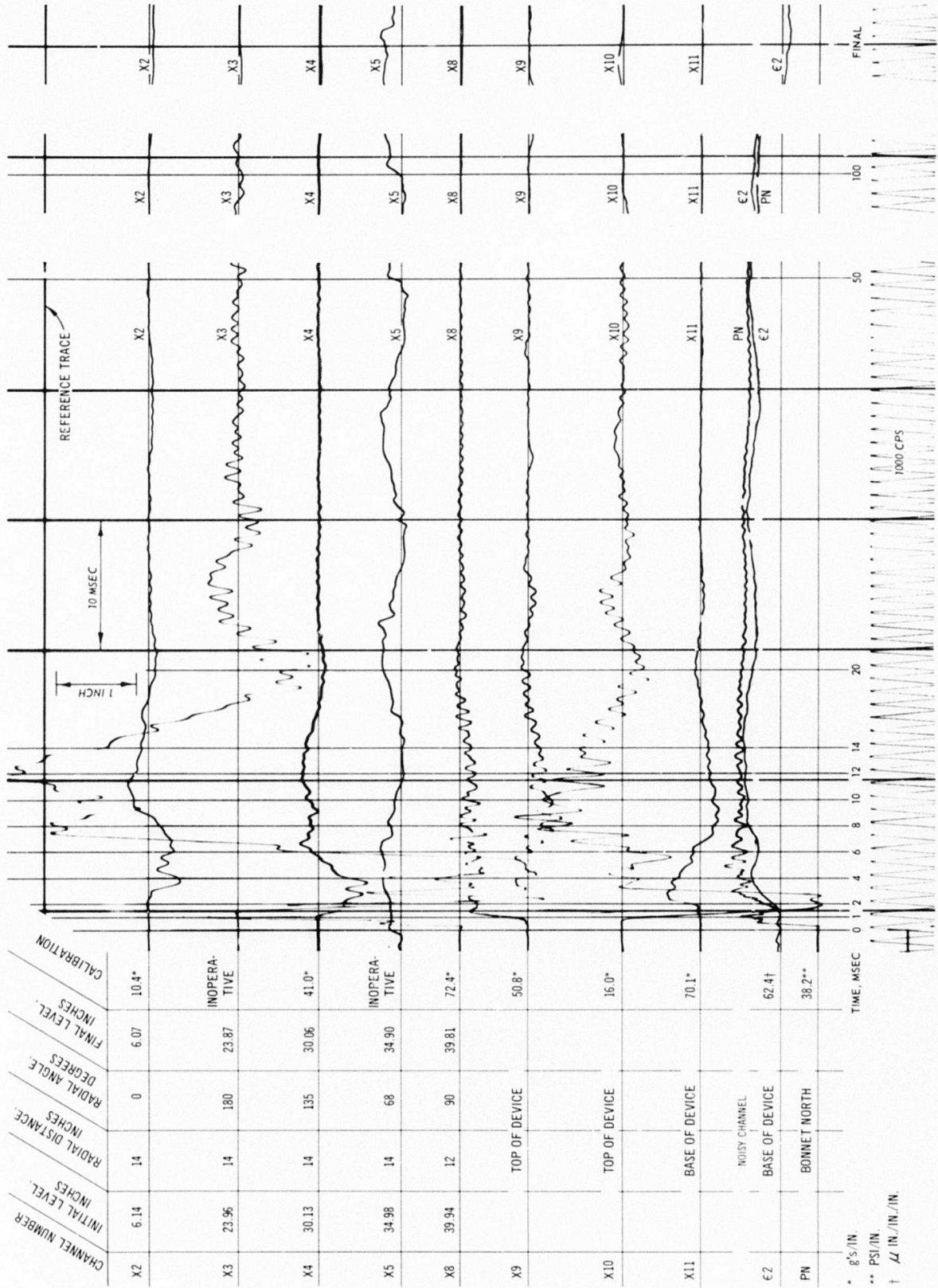
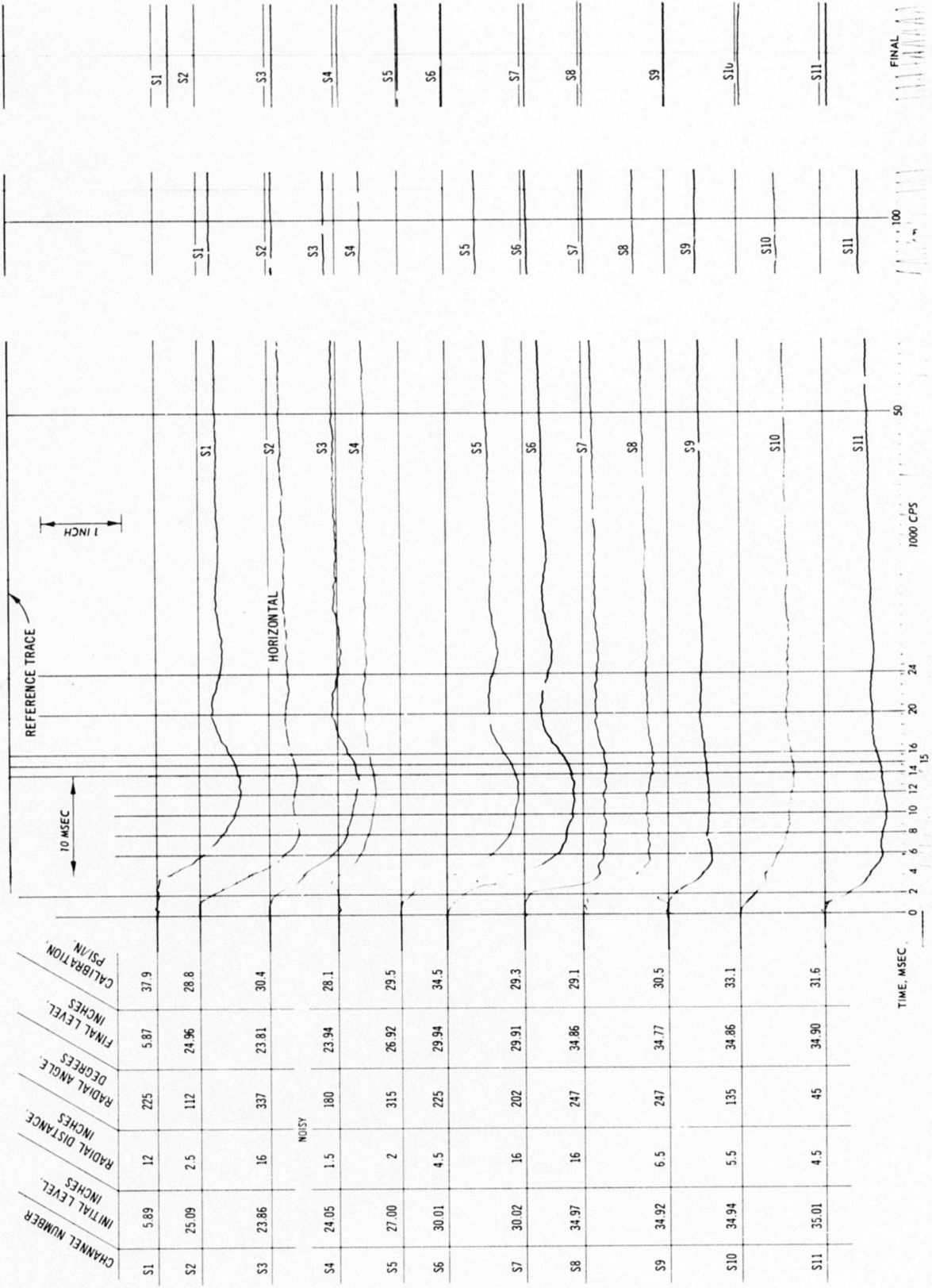
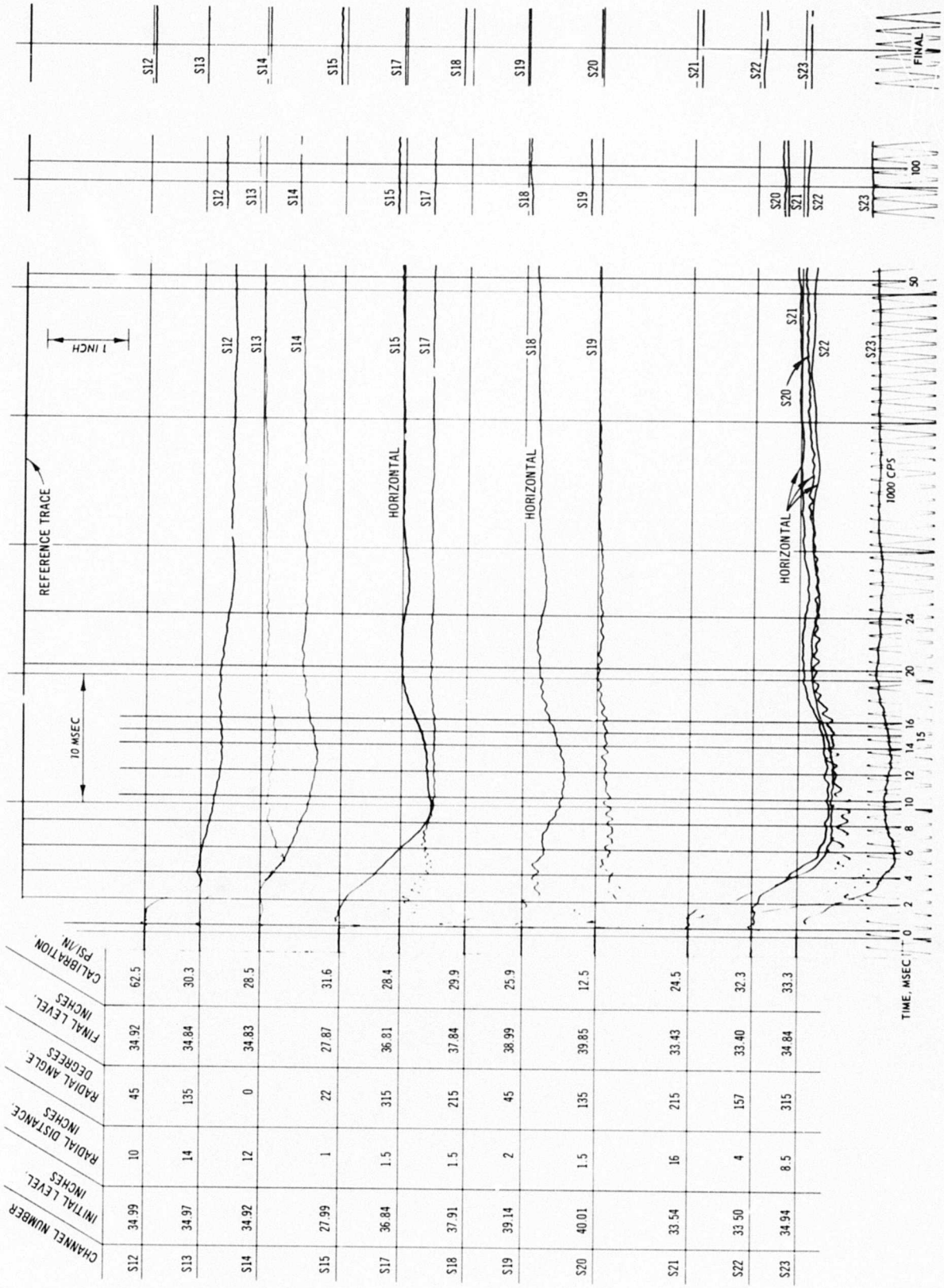


Fig. C-49. Test 22, acceleration, strain, and pressure record



CHANNEL NUMBER	INITIAL LEVEL, INCHES	RADIAL DISTANCE, INCHES	RADIAL ANGLE, DEGREES	FINAL LEVEL, INCHES	CALIBRATION, PSI/IN.
S1	5.89	12	225	5.87	37.9
S2	25.09	2.5	112	24.96	28.8
S3	23.86	16	337	23.81	30.4
NOISY					
S4	24.05	1.5	180	23.94	28.1
S5	27.00	2	315	26.92	29.5
S6	30.01	4.5	225	29.94	34.5
S7	30.02	16	202	29.91	29.3
S8	34.97	16	247	34.86	29.1
S9	34.92	6.5	247	34.77	30.5
S10	34.94	5.5	135	34.86	33.1
S11	35.01	4.5	45	34.90	31.6

Fig. C-50. Test 23, pressure record (S1-S11)



CHANNEL NUMBER	INITIAL LEVEL, INCHES	RADIAL DISTANCE, INCHES	RADIAL ANGLE, DEGREES	FINAL LEVEL, INCHES	CALIBRATION, PSI/IN.
S12	34.99	10	45	34.92	62.5
S13	34.97	14	135	34.84	30.3
S14	34.92	12	0	34.83	28.5
S15	27.99	1	22	27.87	31.6
S17	36.84	1.5	315	36.81	28.4
S18	37.91	1.5	215	37.84	29.9
S19	39.14	2	45	38.99	25.9
S20	40.01	1.5	135	39.85	12.5
S21	33.54	16	215	33.43	24.5
S22	33.50	4	157	33.40	32.3
S23	34.94	8.5	315	34.84	33.3

Fig. C-51. Test 23, pressure record (S12-S23)

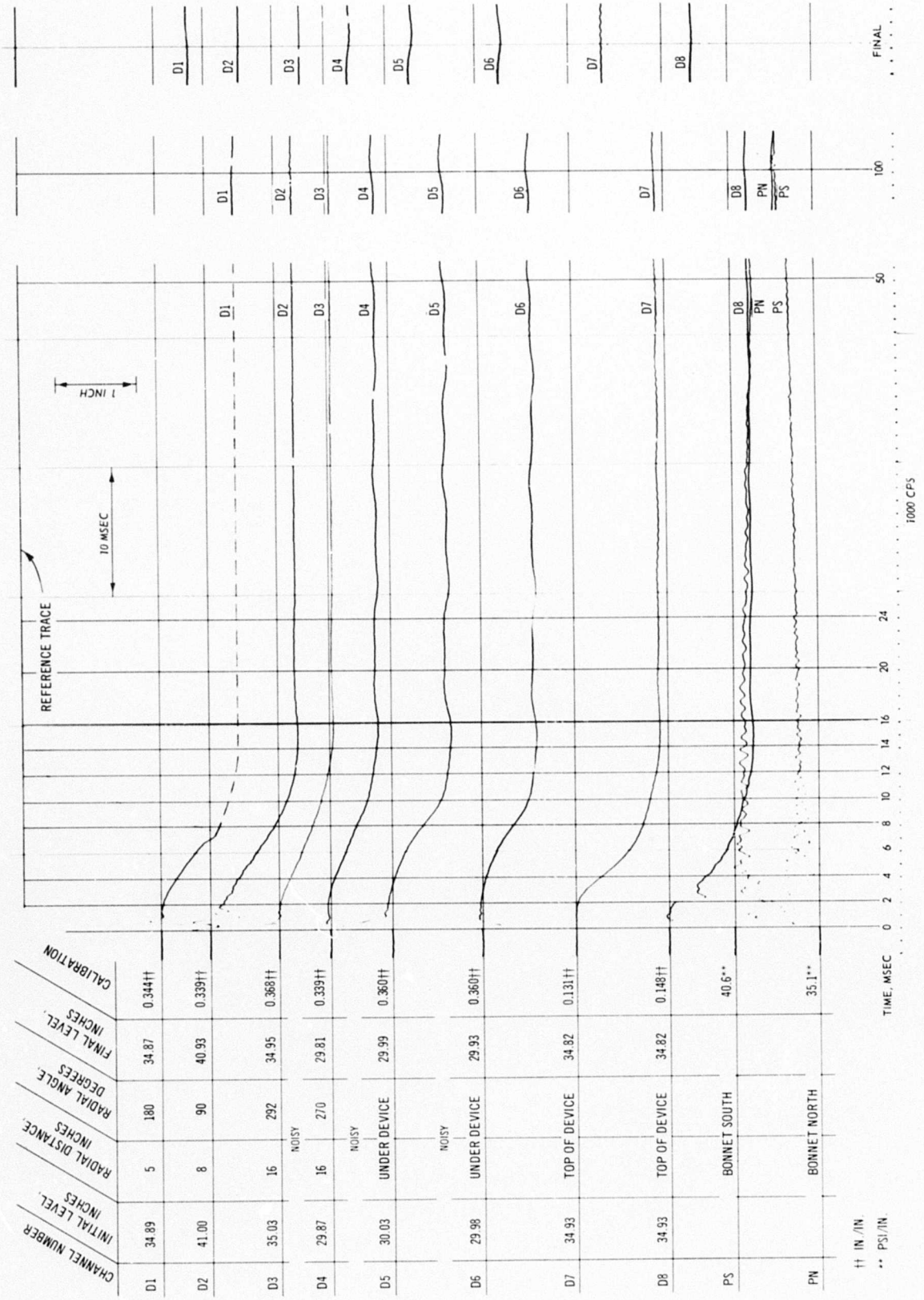


Fig. C-52. Test 23, deflection and pressure record

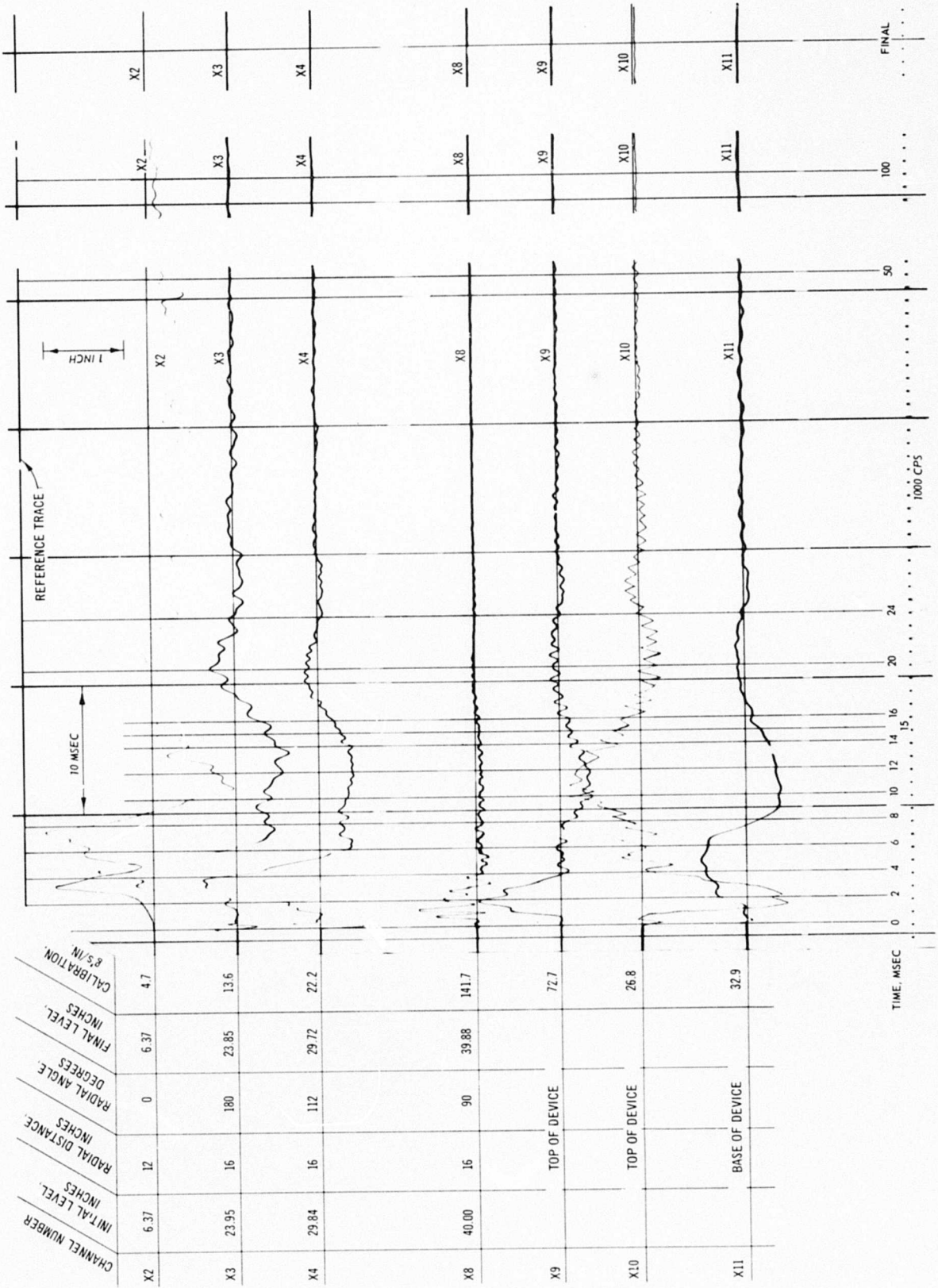


Fig. C-53. Test 23, acceleration record

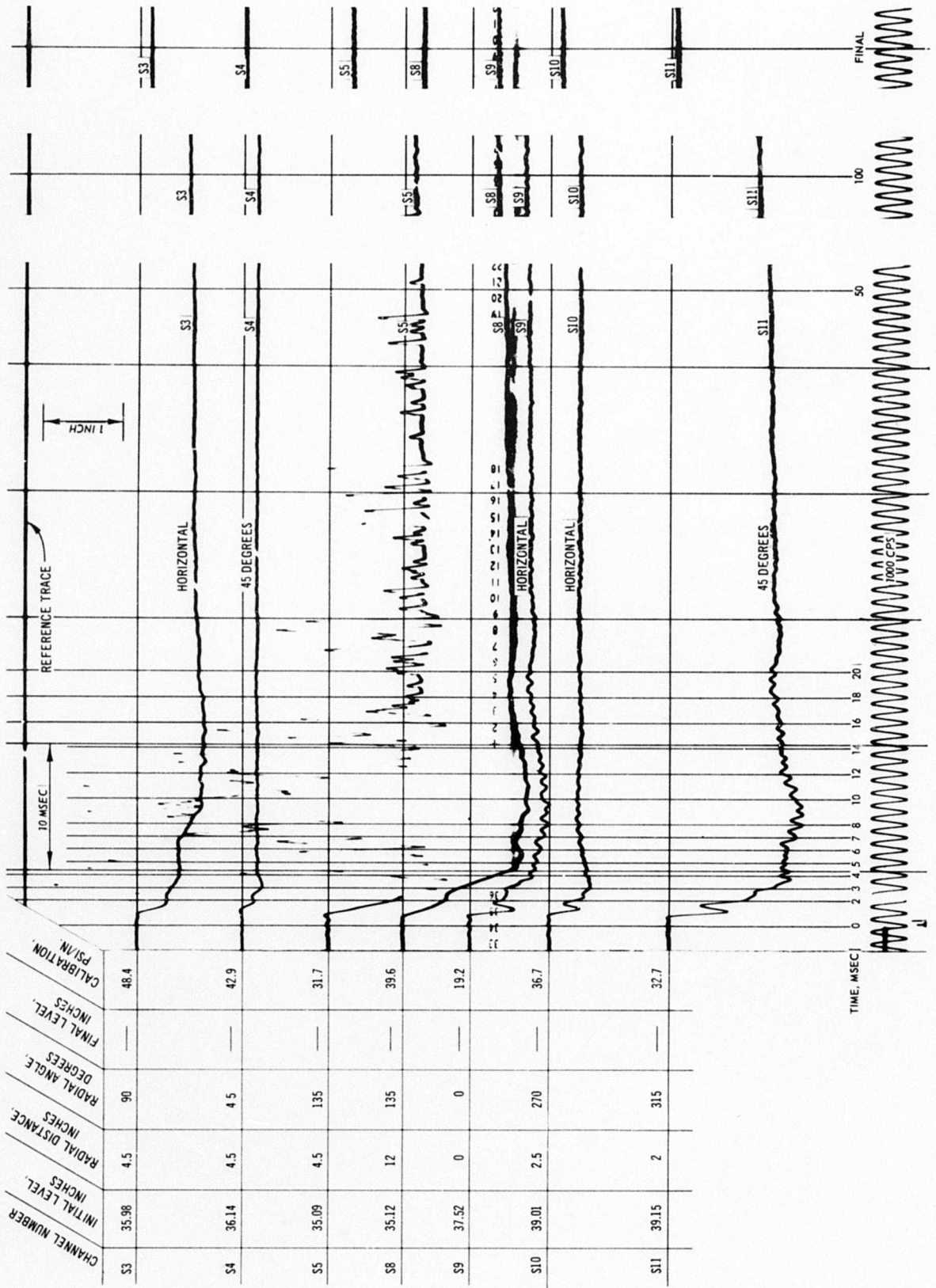


Fig. C-54. Test 24, pressure record

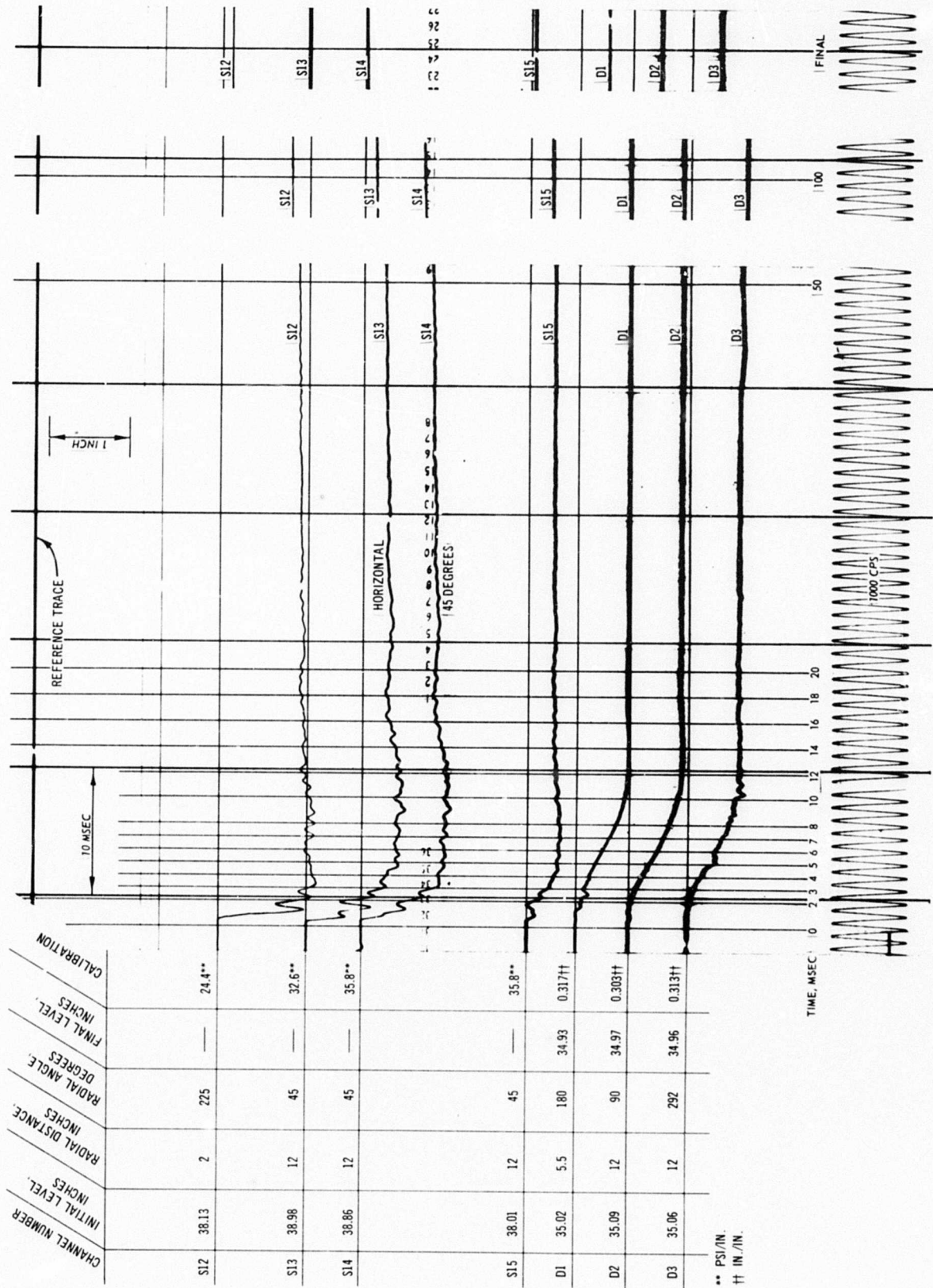


Fig. C-55. Test 24, pressure and deflection record

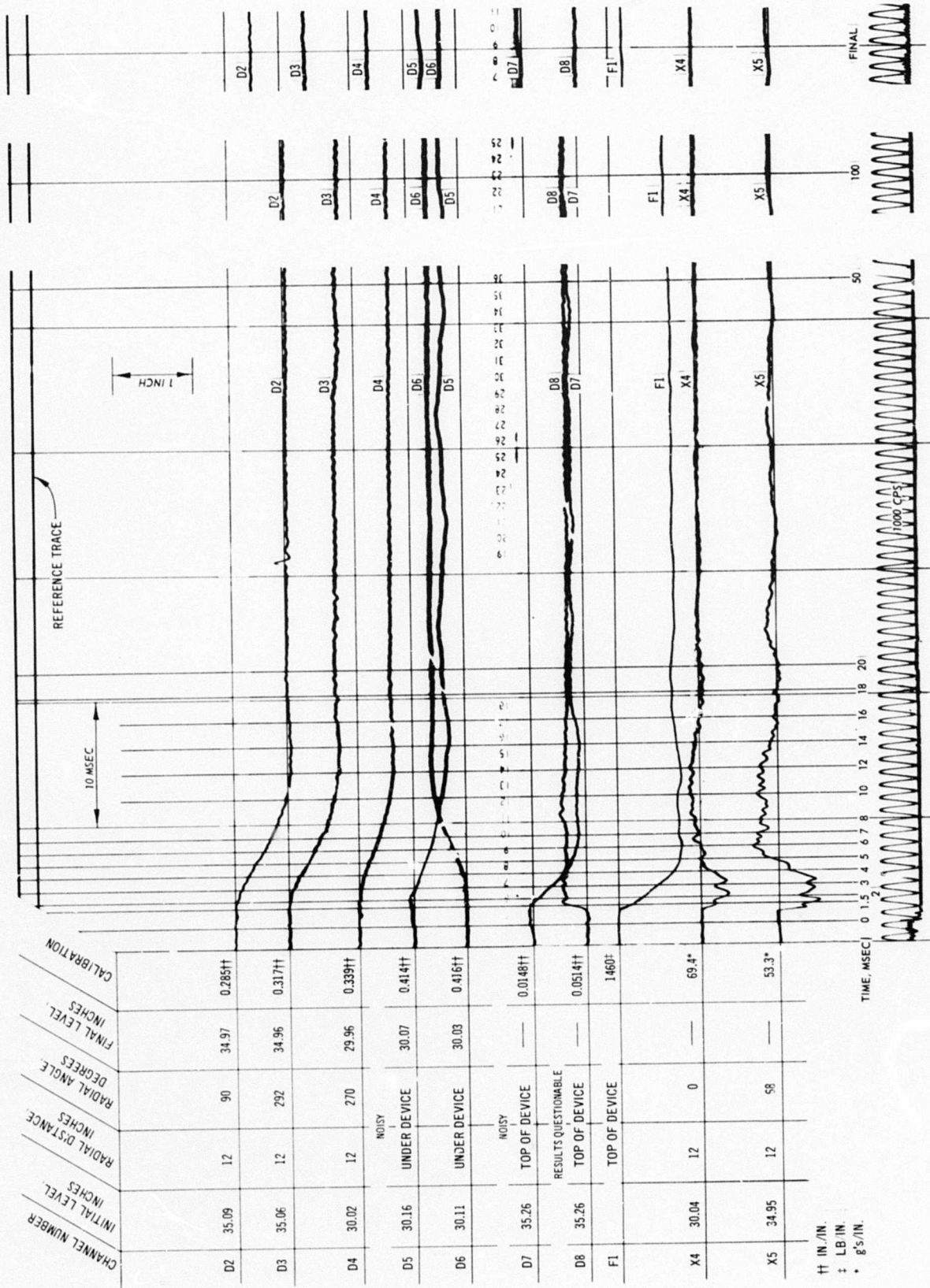


Fig. C-56. Test 24, deflection, force, and acceleration record

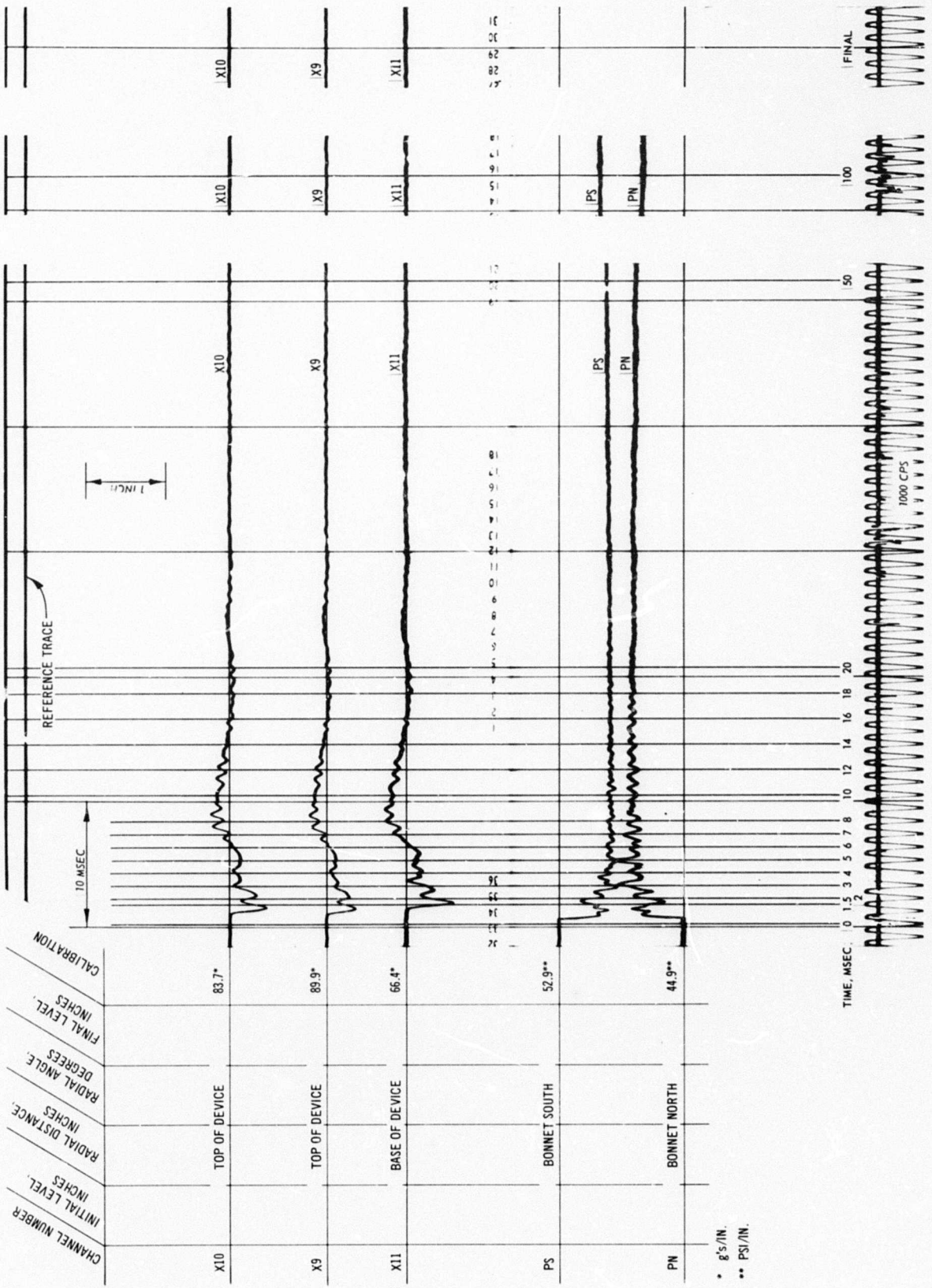


Fig. C-57. Test 24, acceleration and pressure record

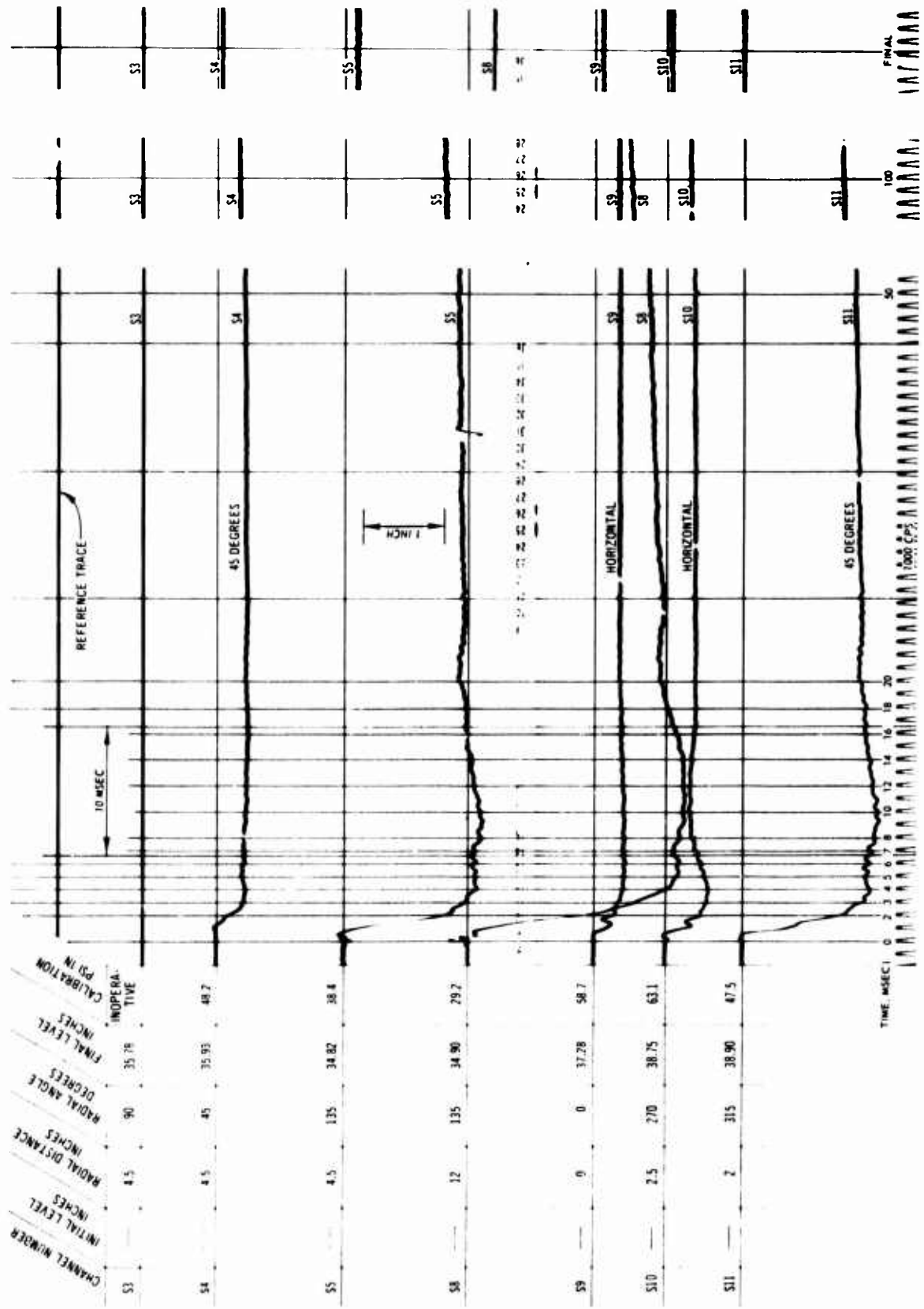


Fig. C-58. Test 25, pressure record

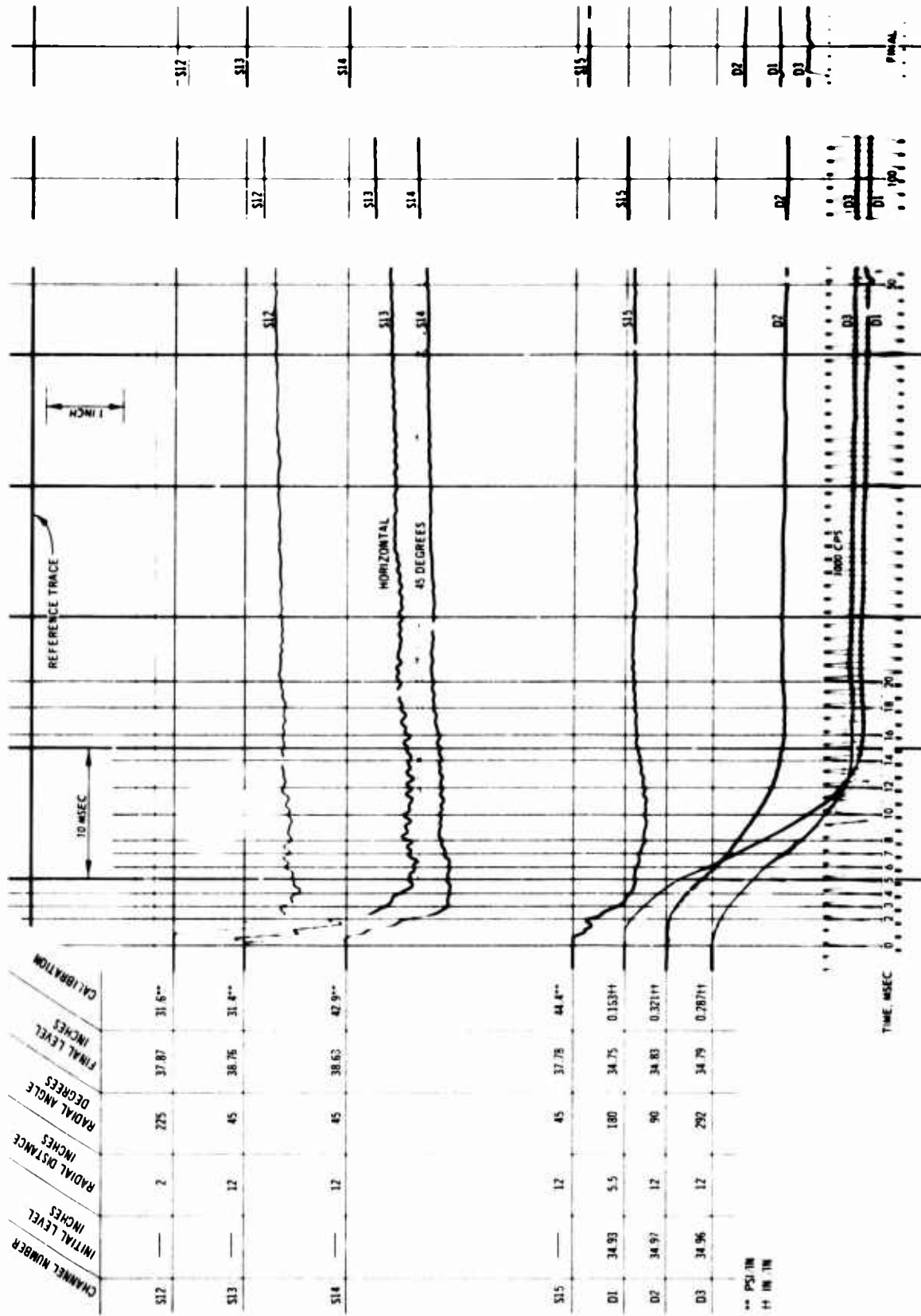


Fig. C-59. Test 25, pressure and deflection record

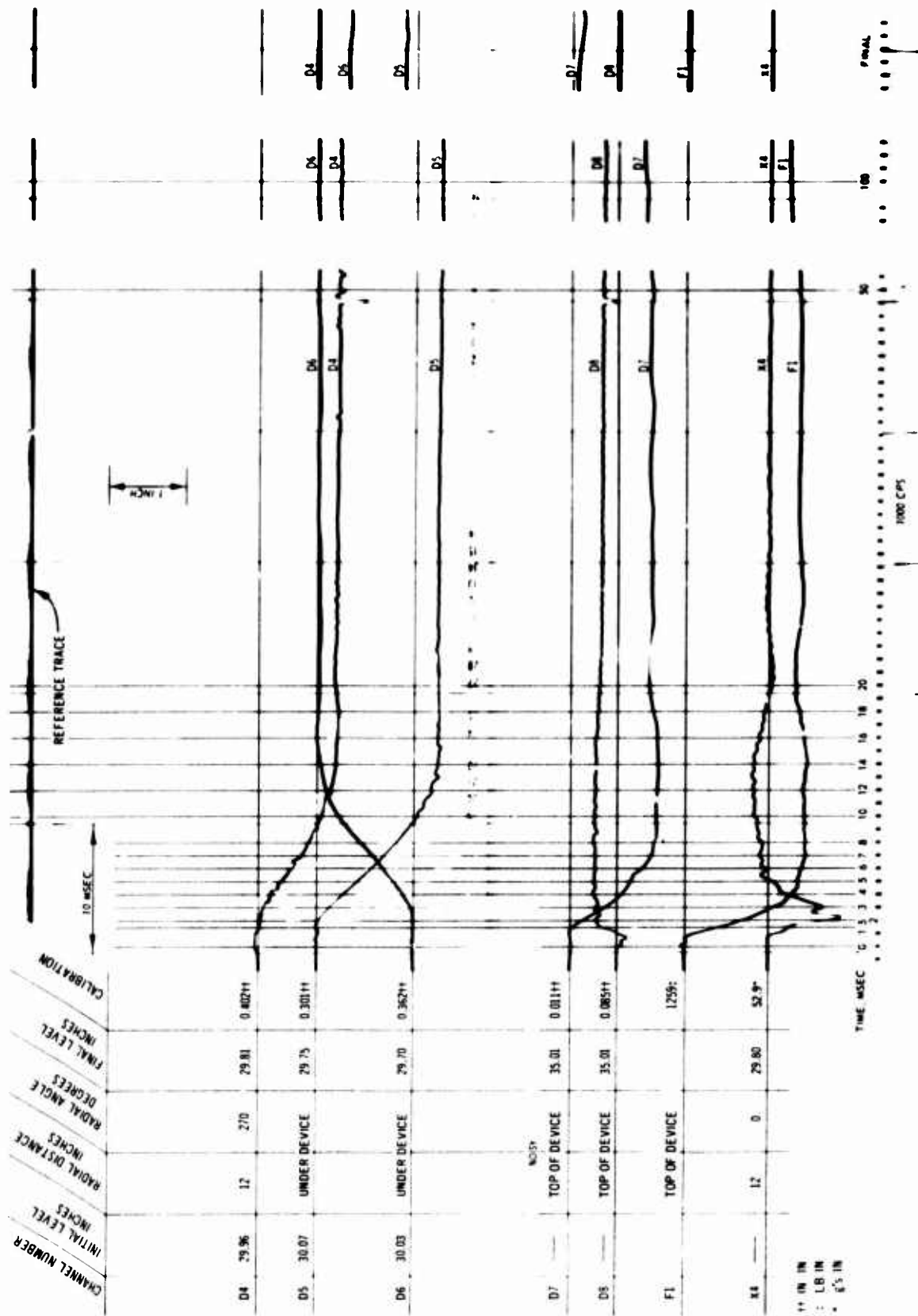


Fig. C-60. Test 25, deflection, force, and acceleration record

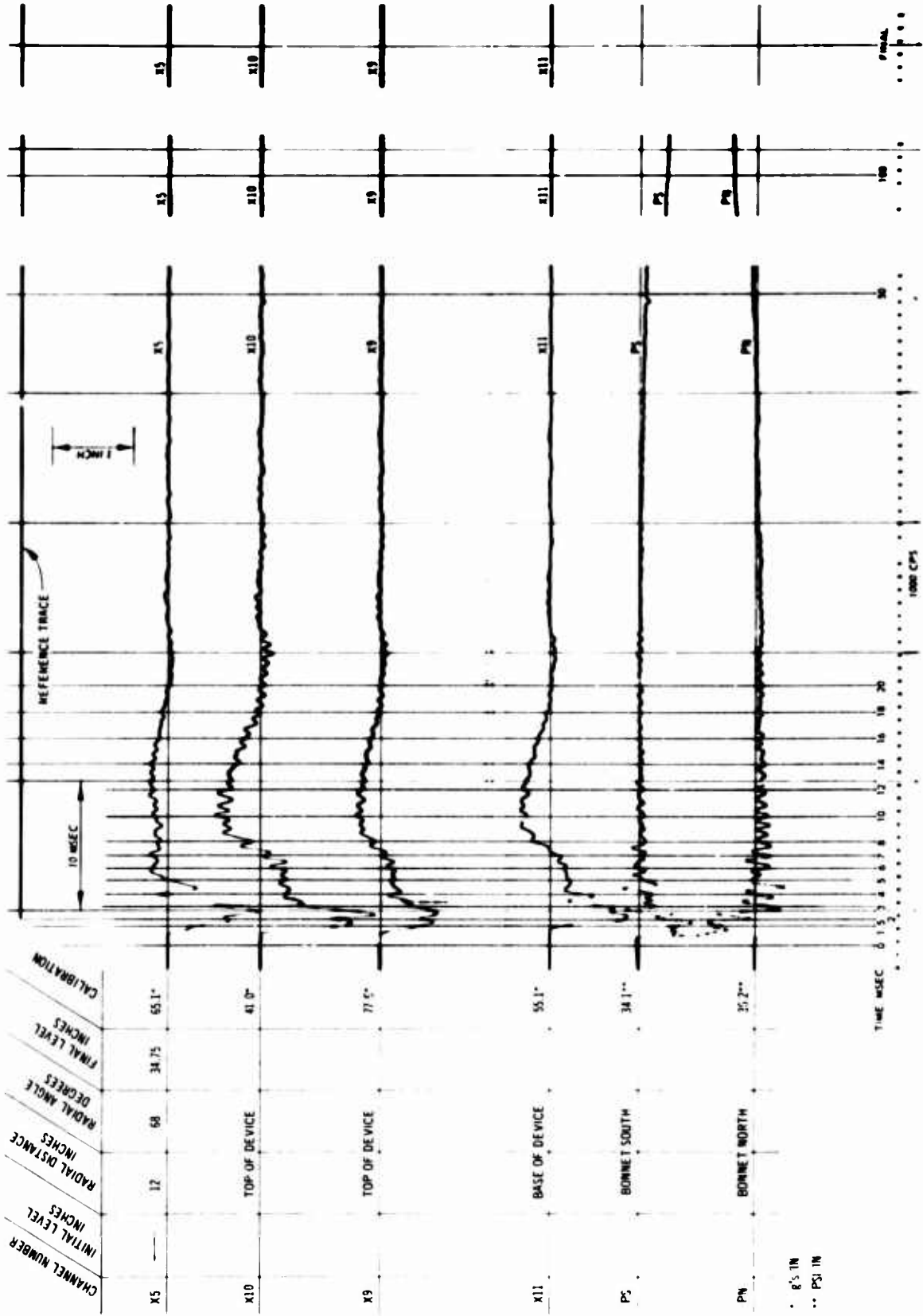


Fig. C-61. Test 25, acceleration and pressure record

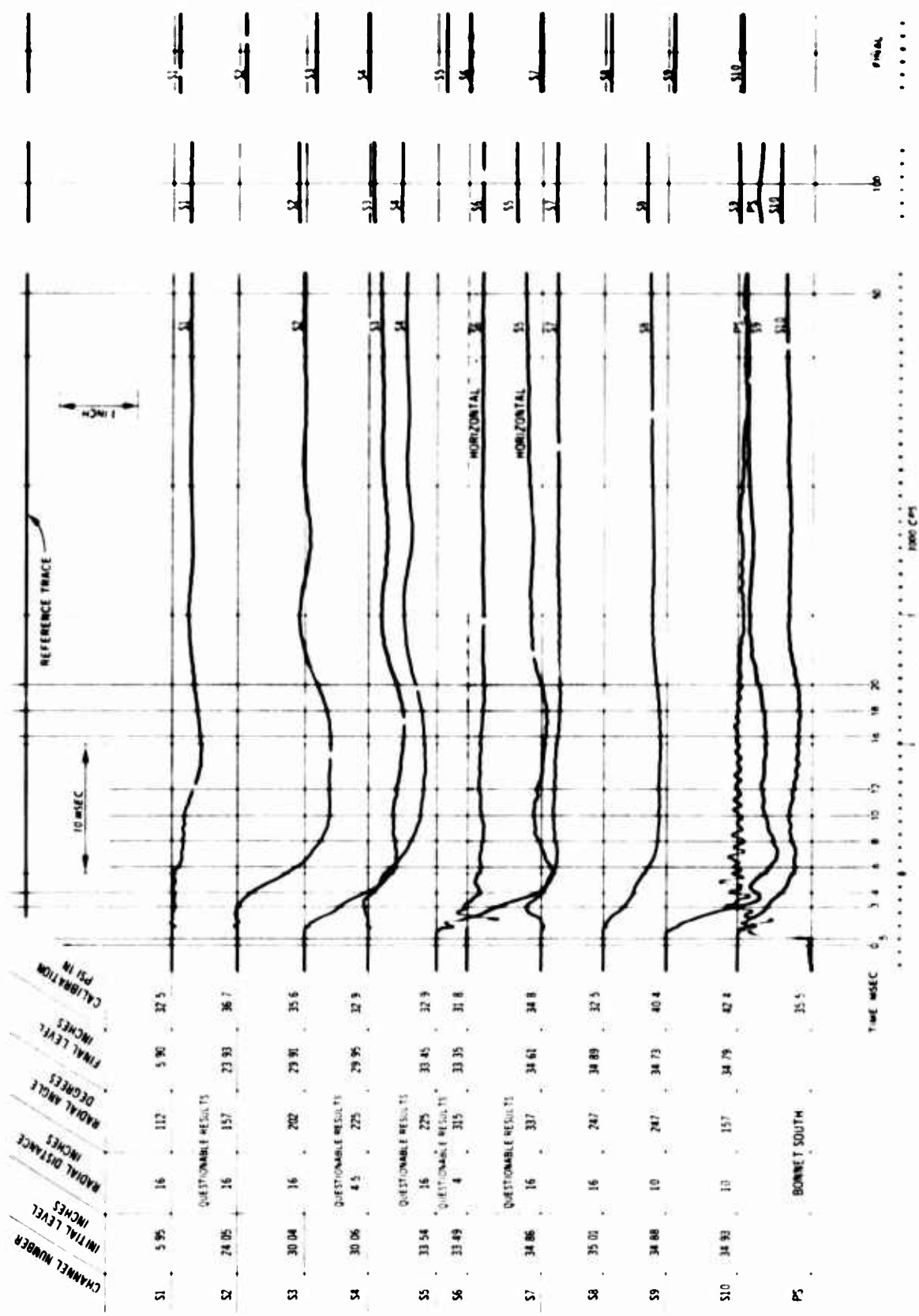


Fig. C-62. Test 26, pressure record (S1-S10)

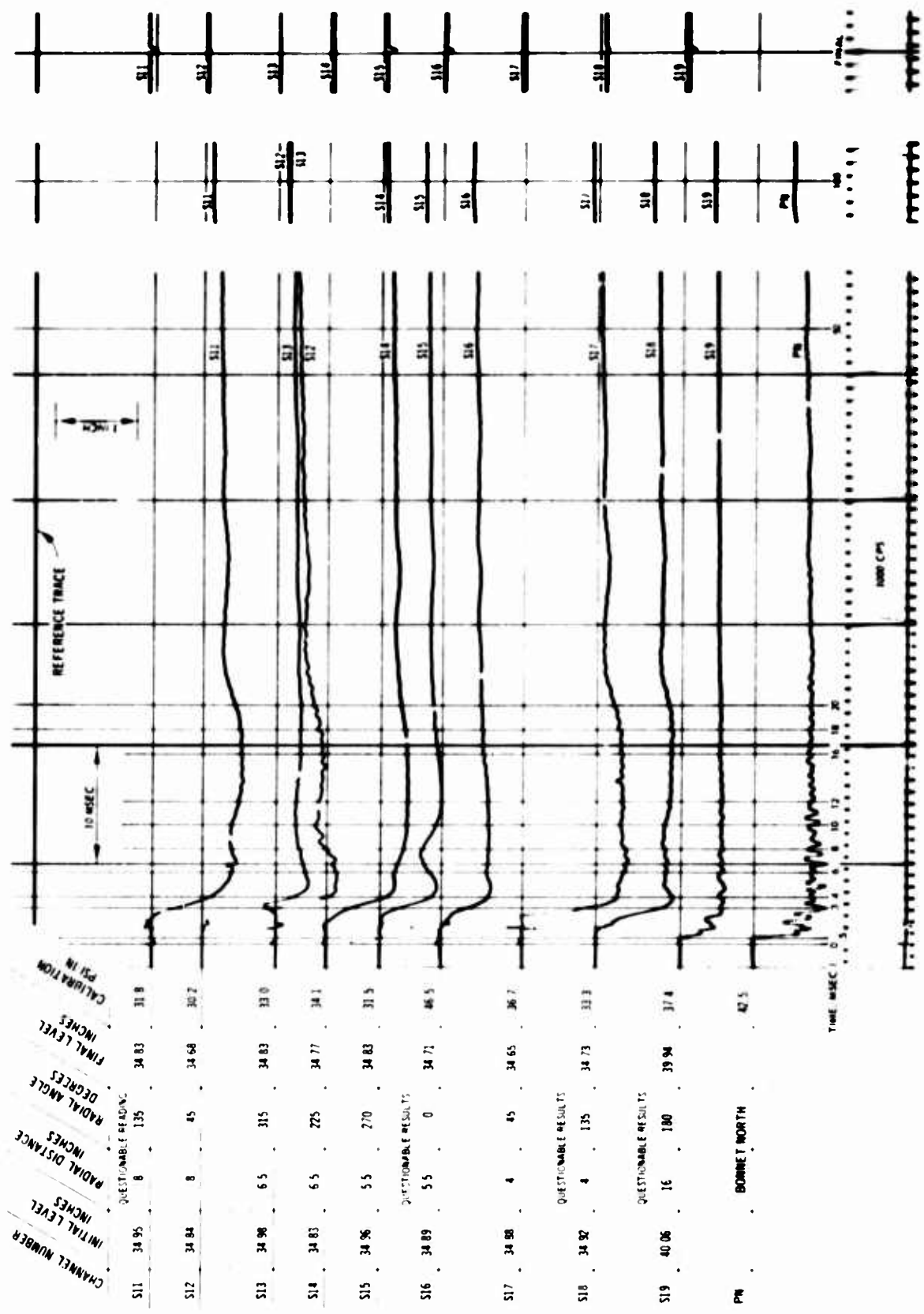


Fig. C-63. Test 26, pressure record (S11-S19)

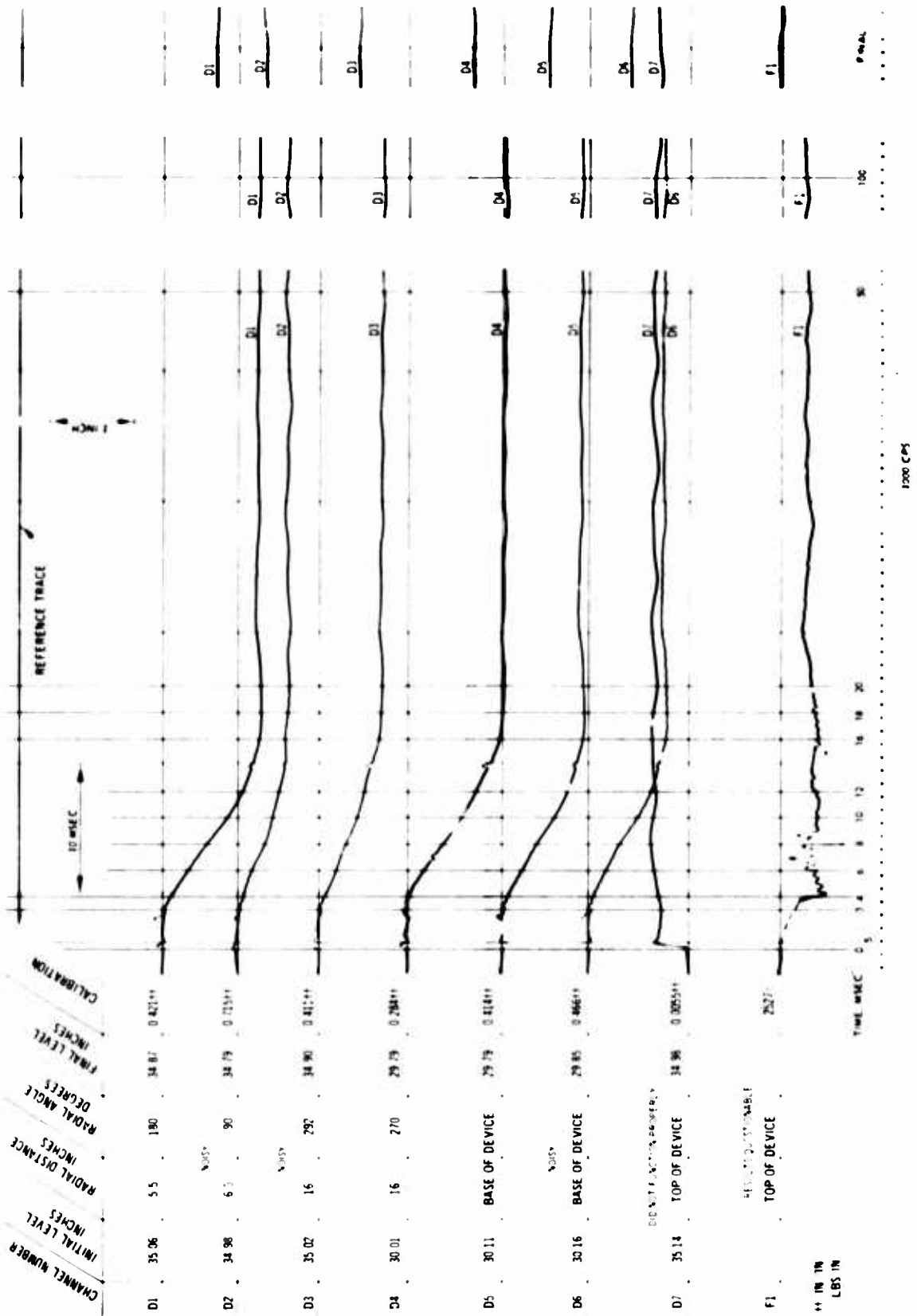


Fig. C-64. Test 26, deflection and force record

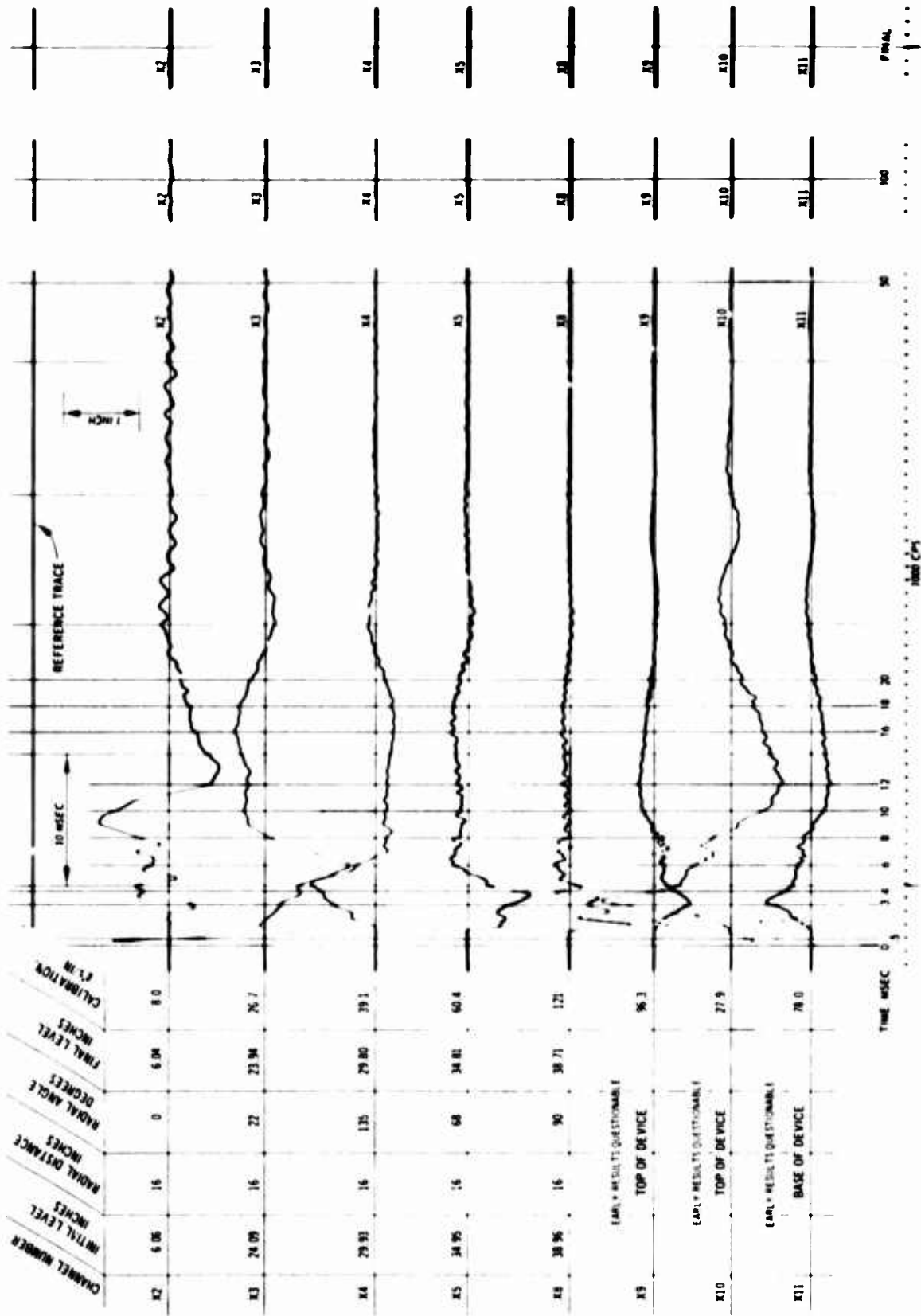


Fig. C-65. Test 26, acceleration record

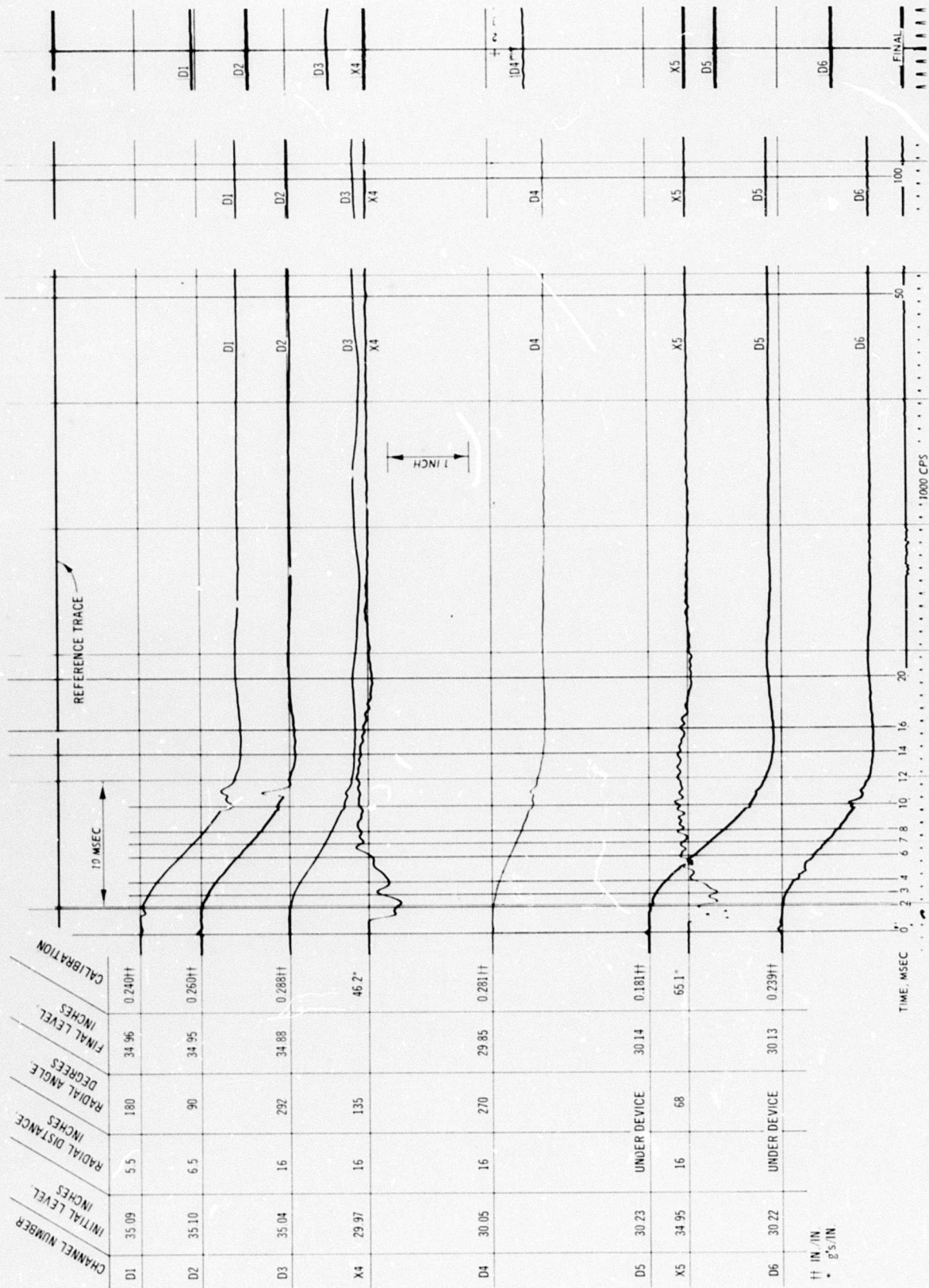


Fig. C-66. Test 27A, deflection and acceleration record

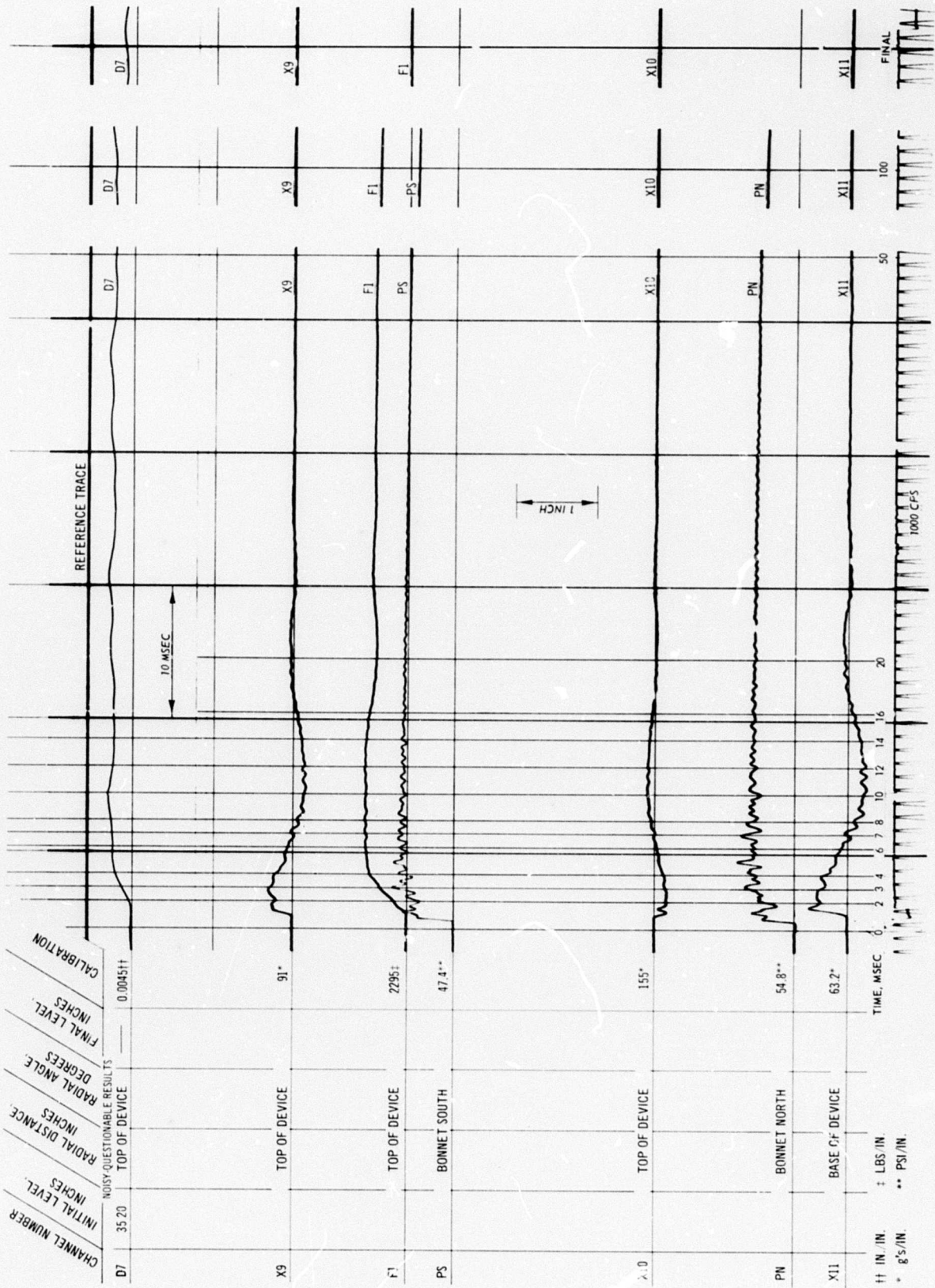


Fig. C-67. Test 27A, deflection, pressure, acceleration, and force record

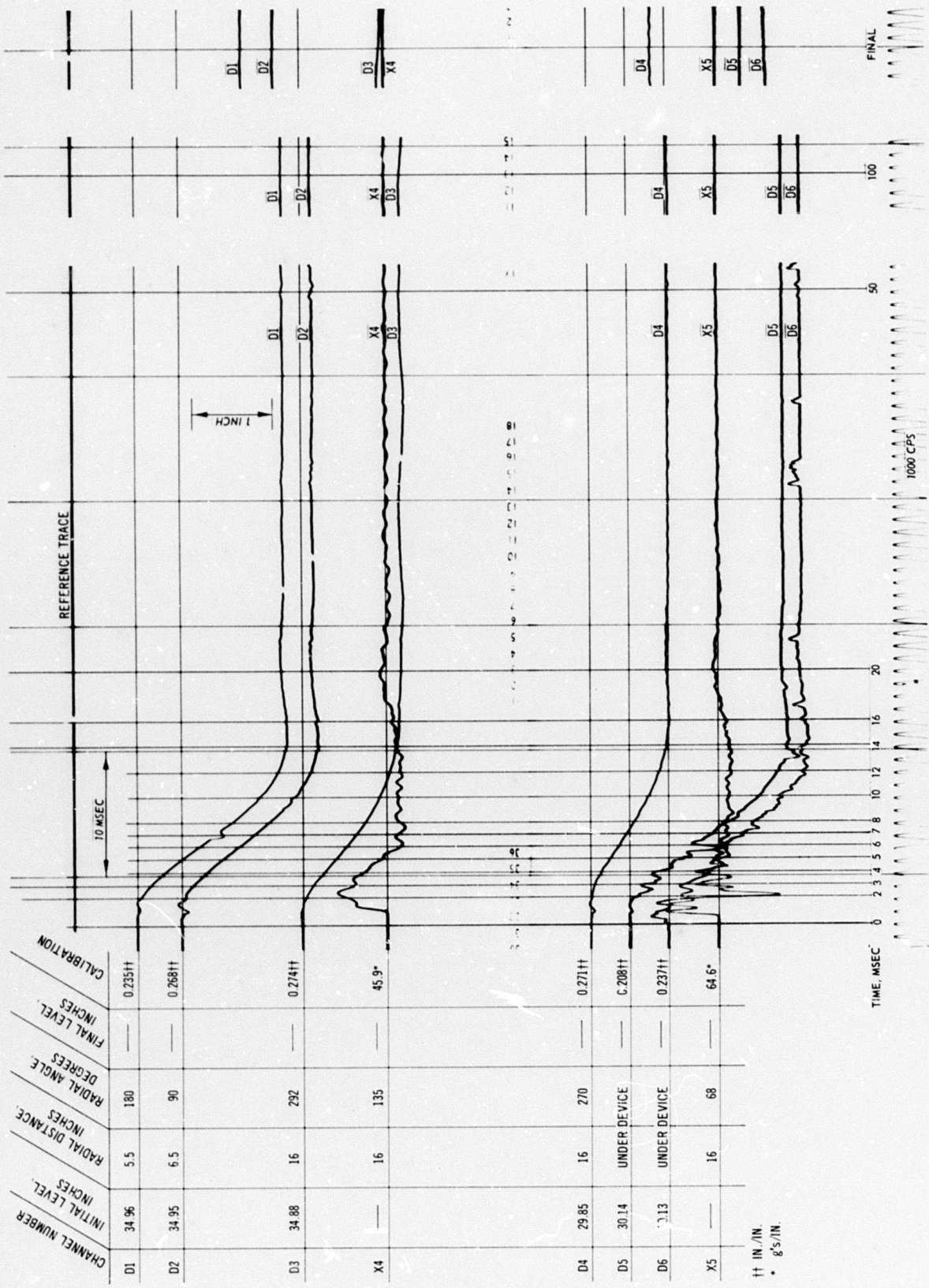


Fig. C-68. Test 27B, deflection and acceleration record

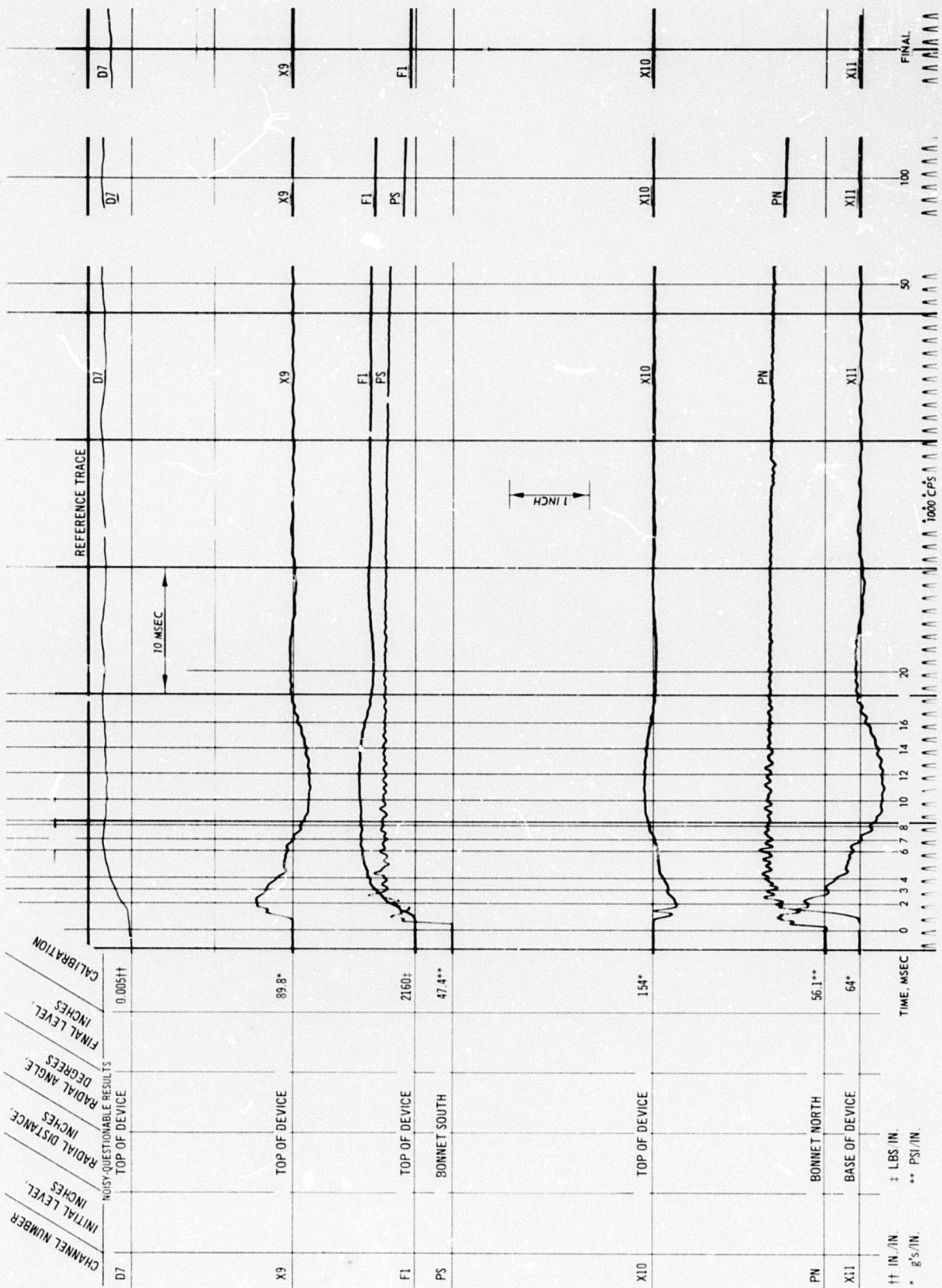


Fig. C-69. Test 27B, deflection, acceleration, pressure, and force record

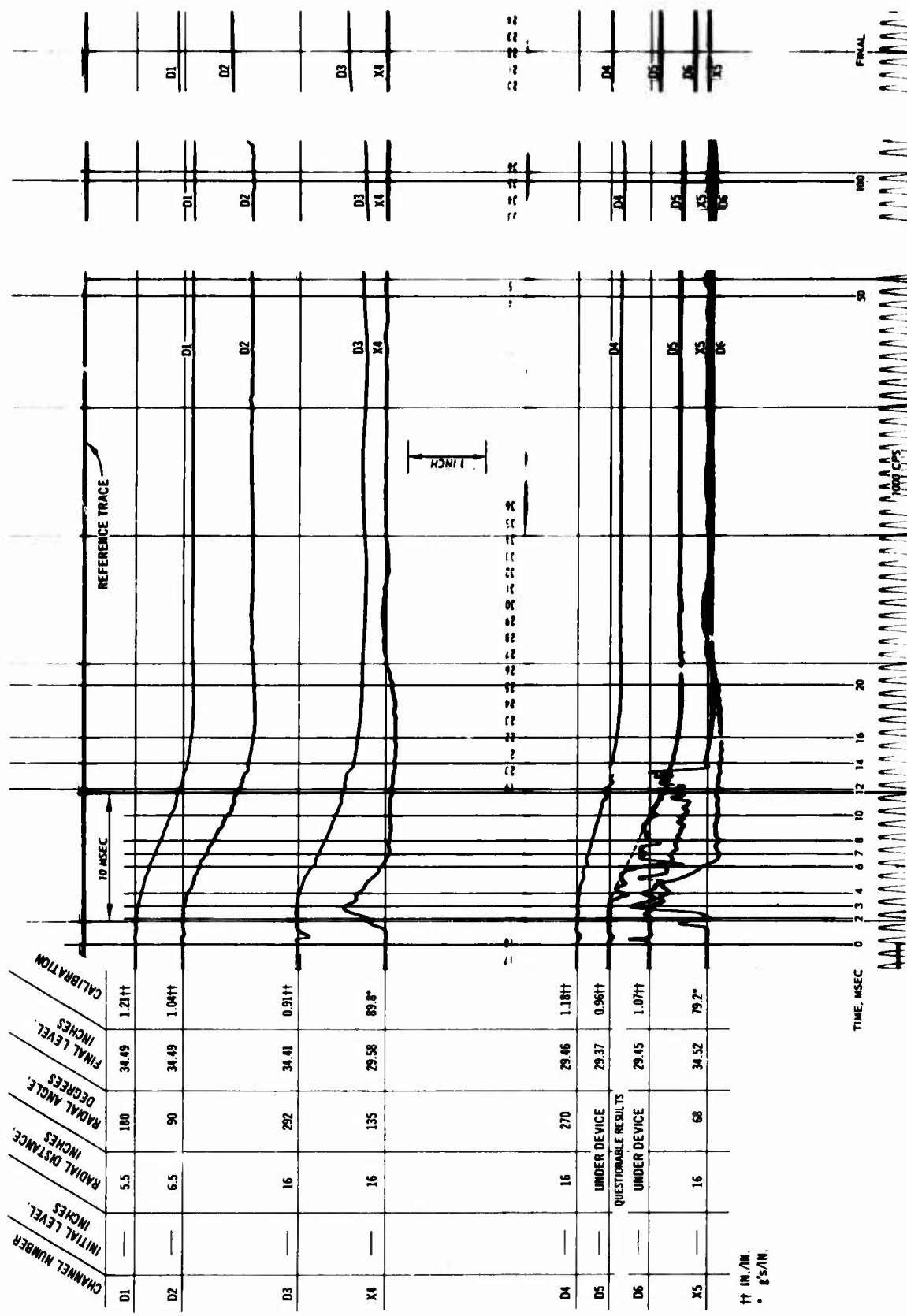


Fig. C-70. Test 27C, deflection and acceleration record

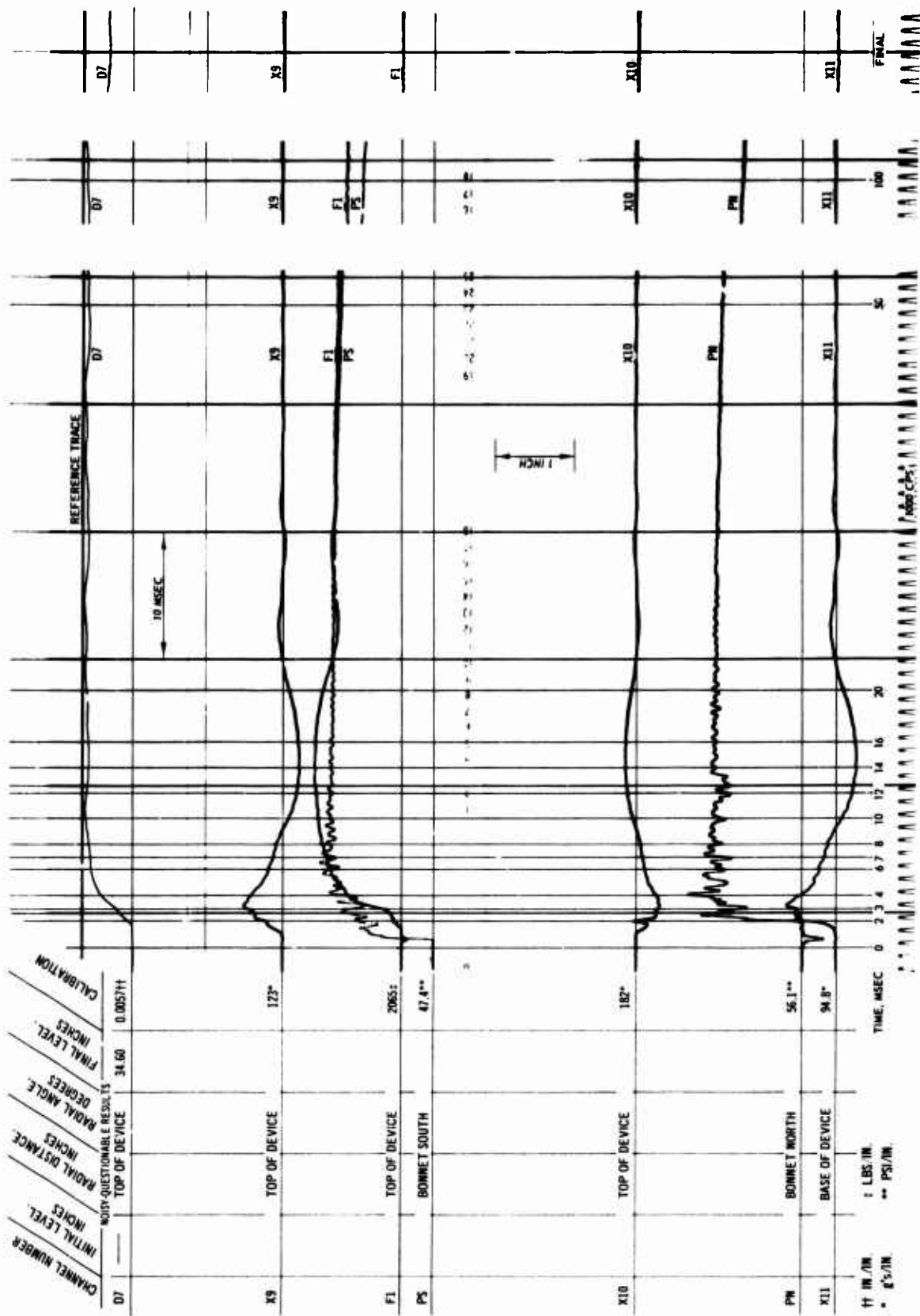


Fig. C-71. Test 27C, deflection, pressure, acceleration, and force record

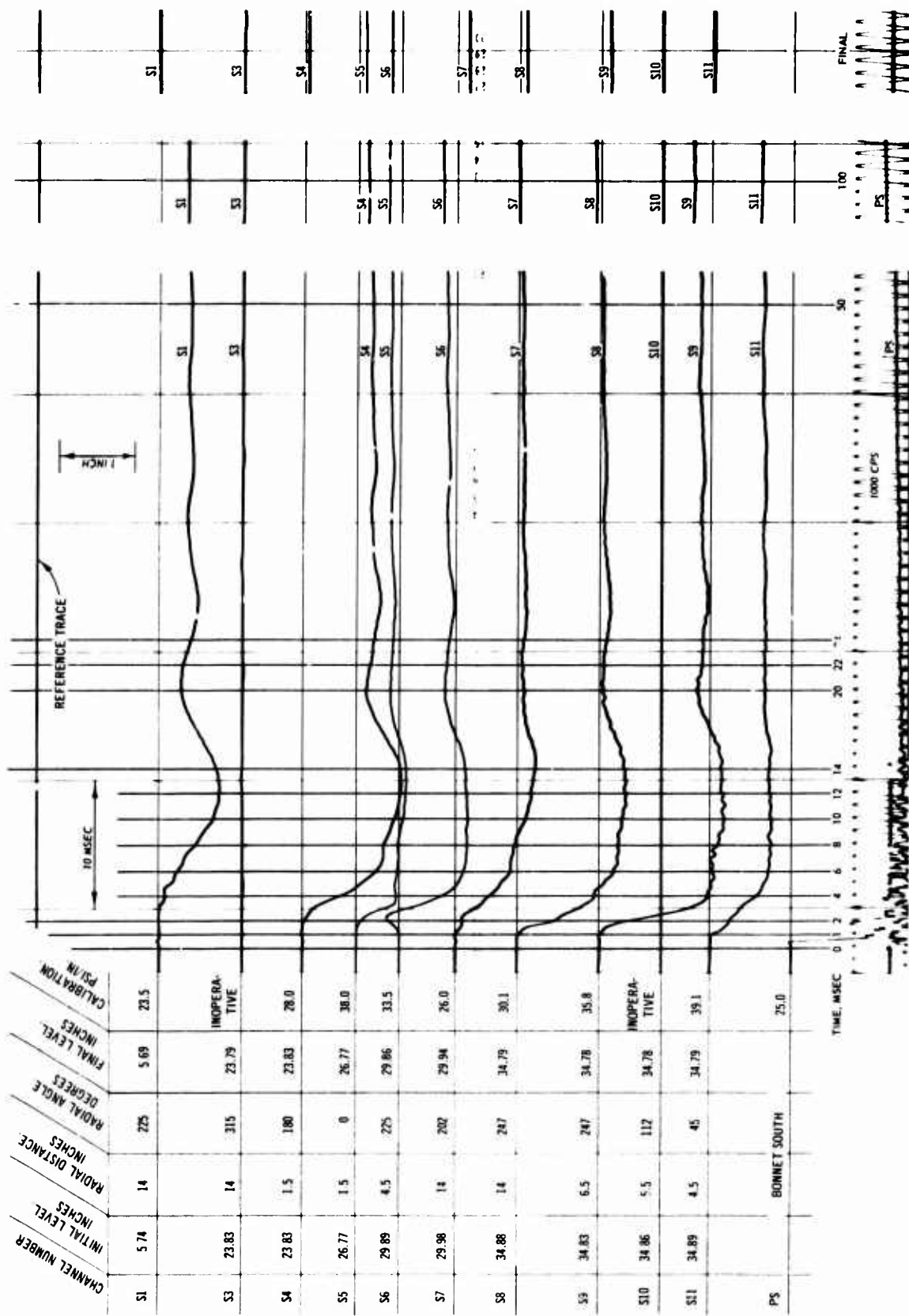


Fig. C-72. Test 28, pressure record (S1-S11)

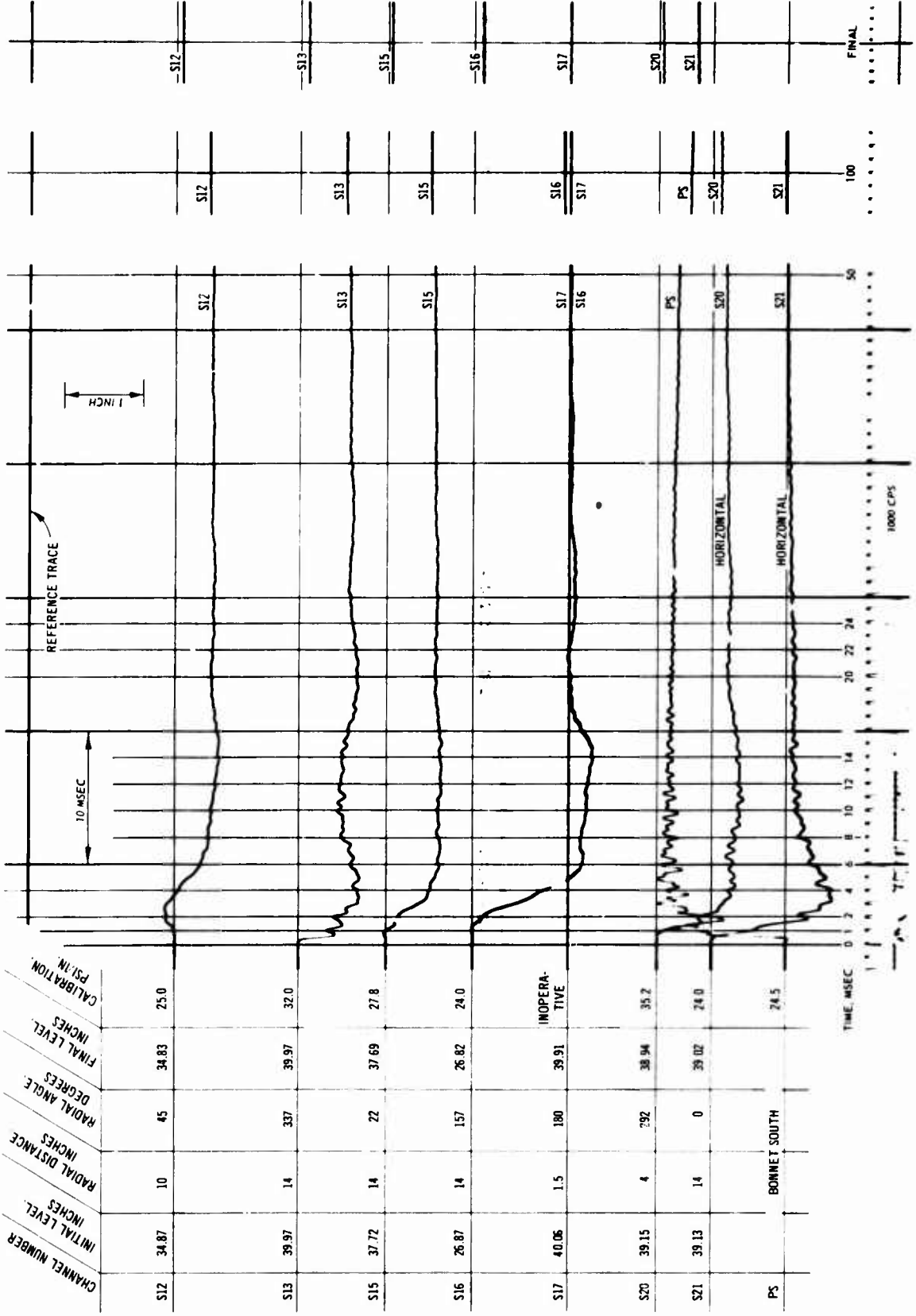


Fig. C-73. Test 28, pressure record (S12-S21)

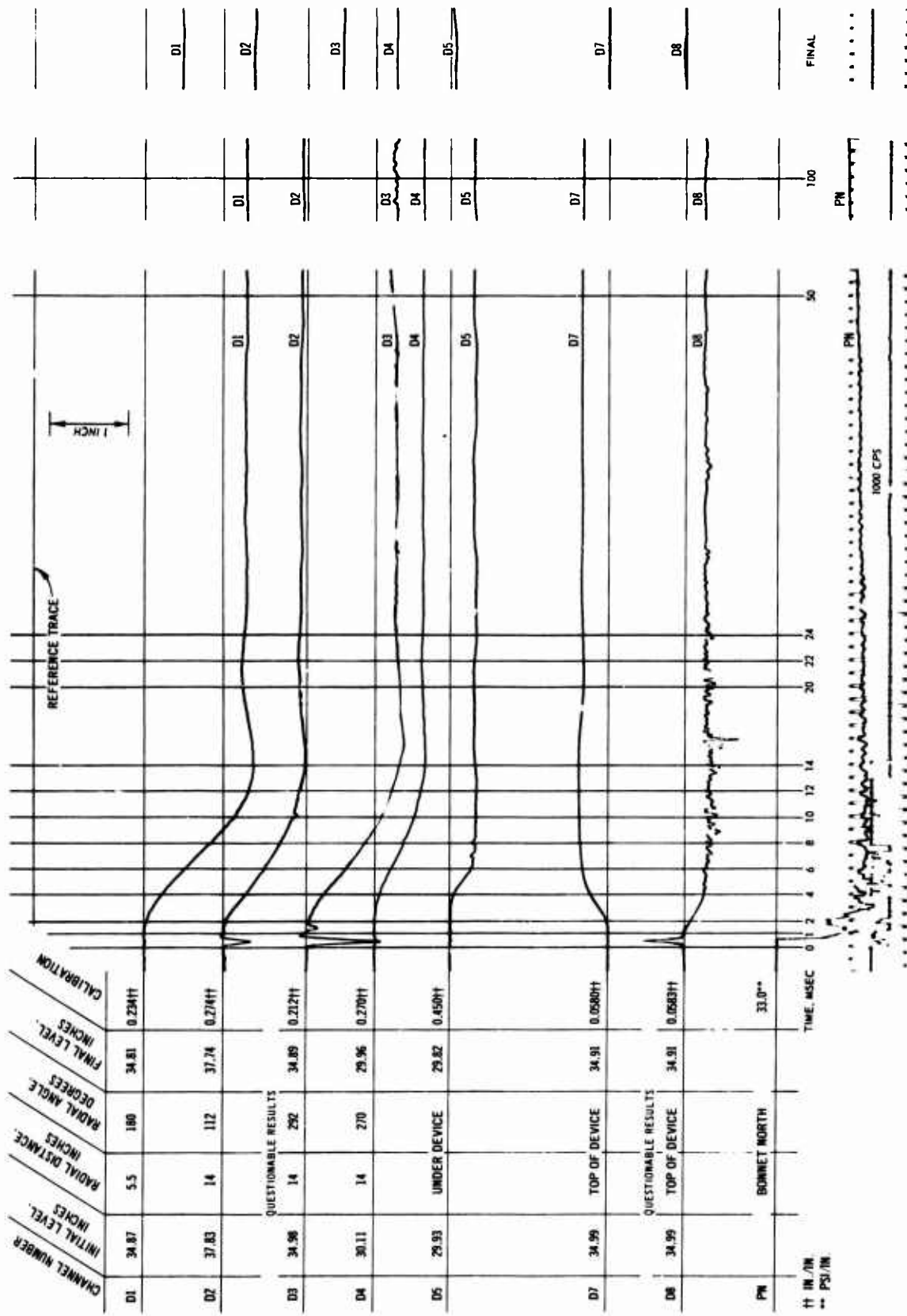


Fig. C-74. Test 28, deflection and pressure record

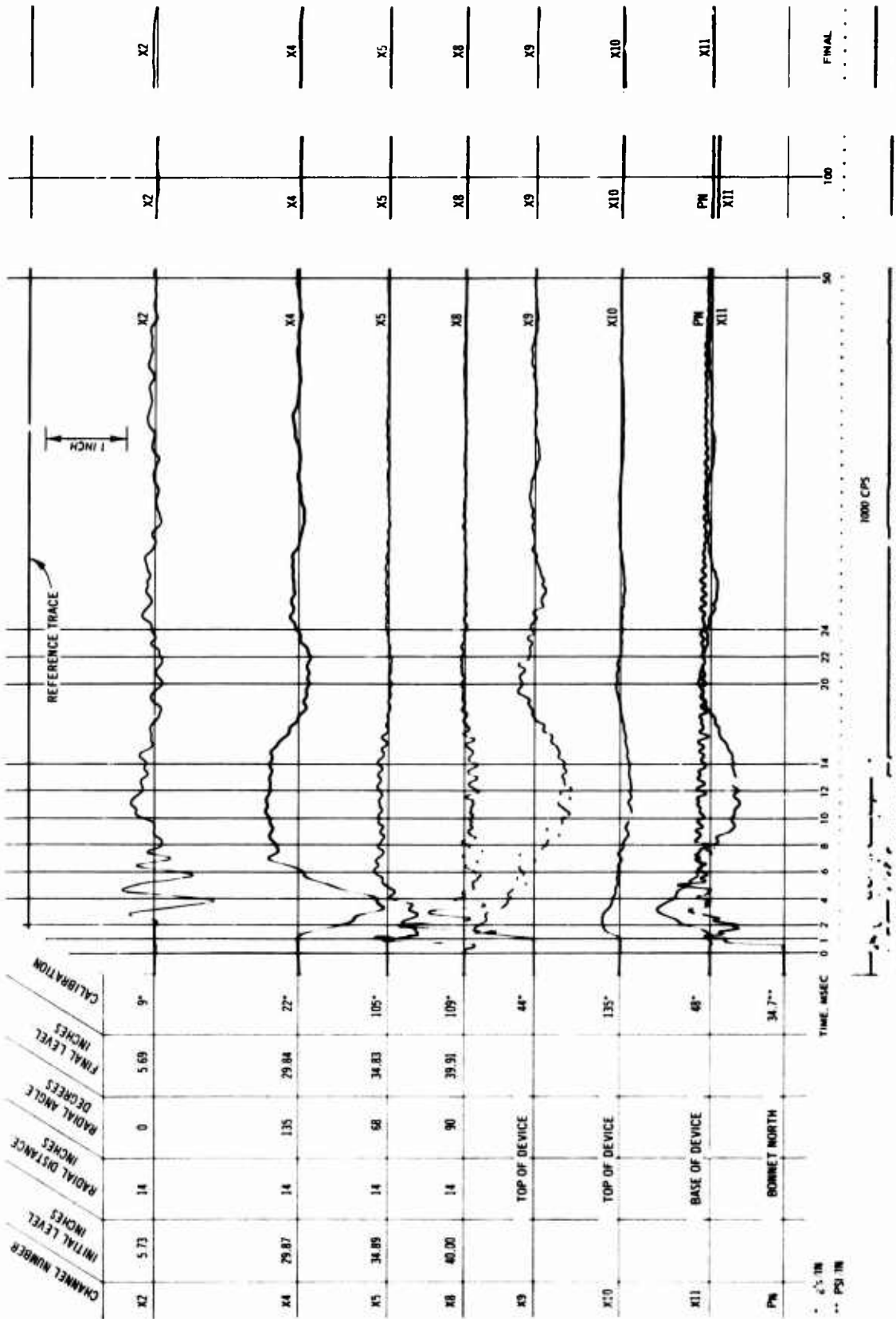
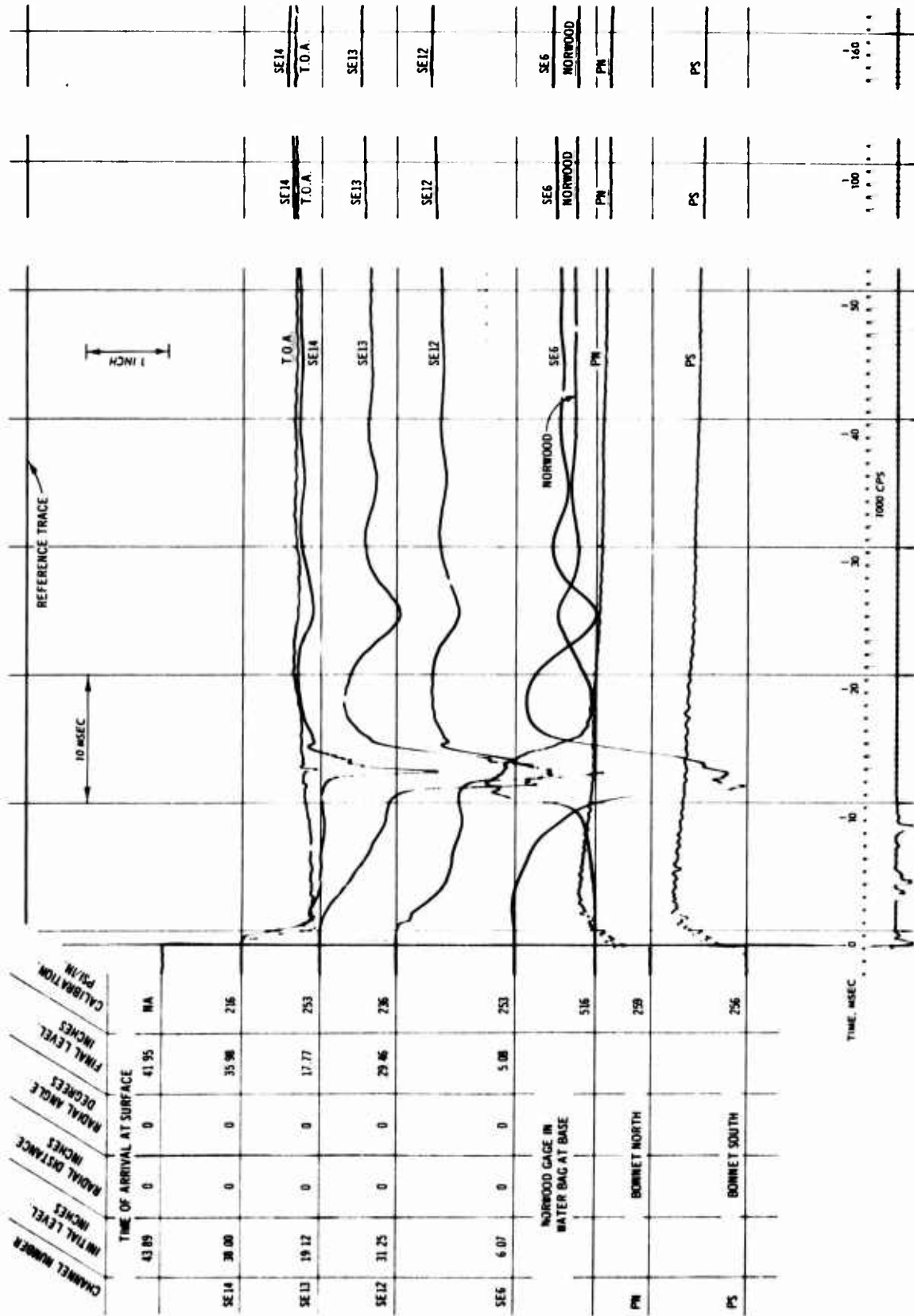
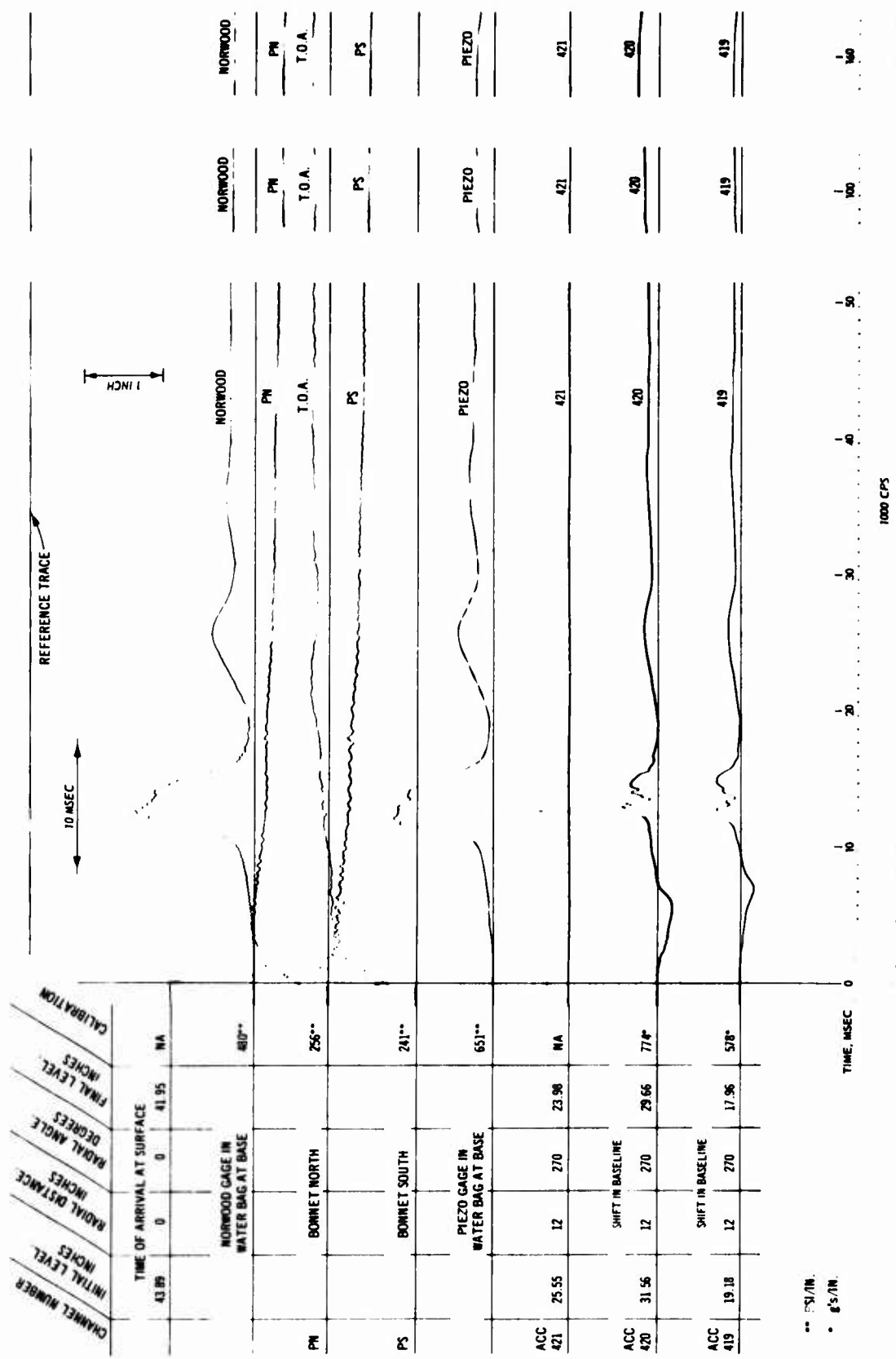


Fig. C-75. Test 28, acceleration and pressure record



CHANNEL NUMBER	INITIAL LEVEL INCHES	RADIAL DISTANCE INCHES	RADIAL ANGLE DEGREES	FINAL LEVEL INCHES	CALIBRATION PSI/IN
	43.89	0	0	41.95	NA
SE14	38.00	0	0	35.98	216
SE13	19.12	0	0	17.77	253
SE12	31.25	0	0	29.46	236
SE6	6.07	0	0	5.08	253
PN					516
PS					259
					256

Fig. C-76. Test A, pressure record



** PSI/IN.
* G'S/IN.

Fig. C-77. Test A, pressure and acceleration record

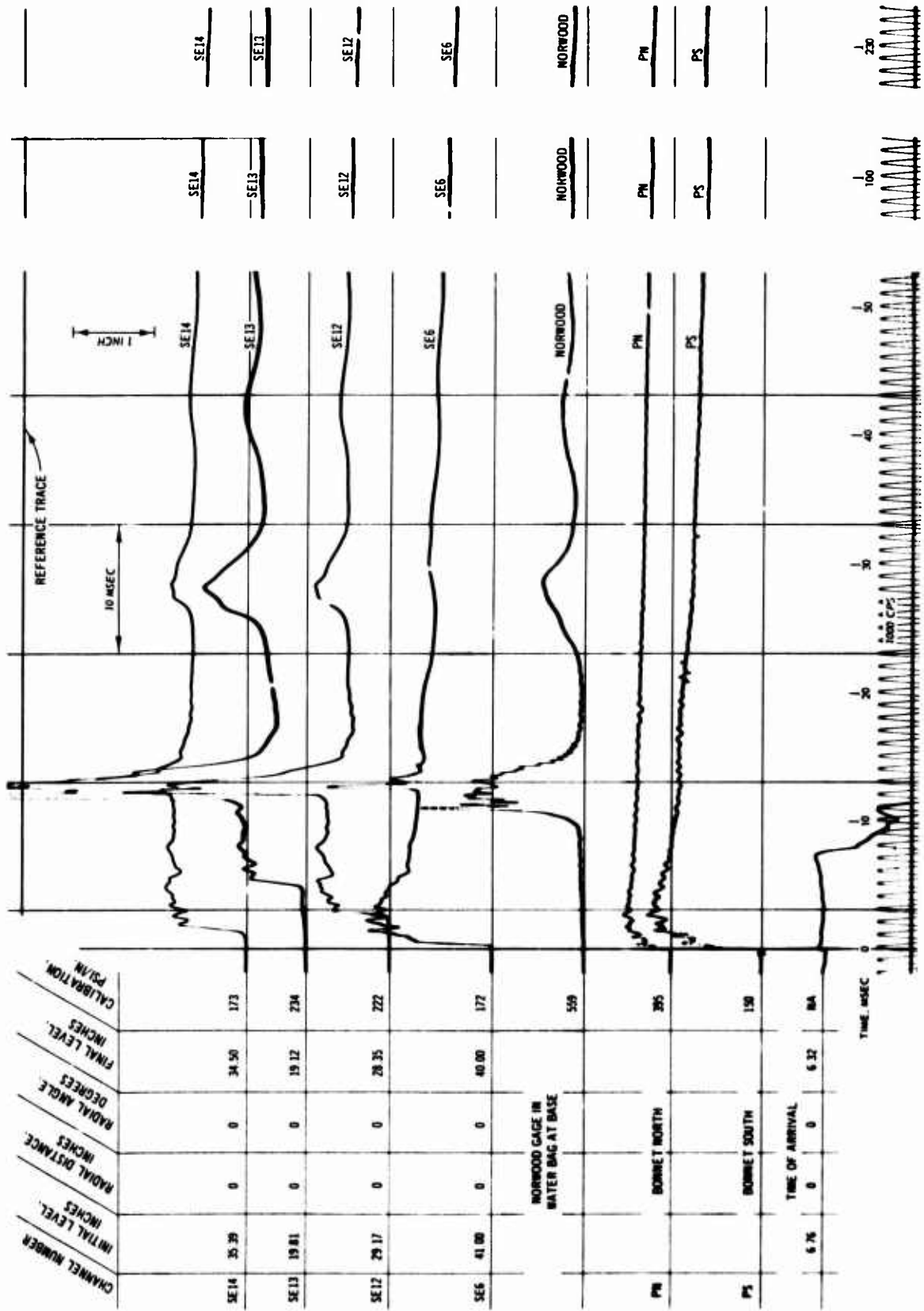


Fig. C-78. Test B, pressure record

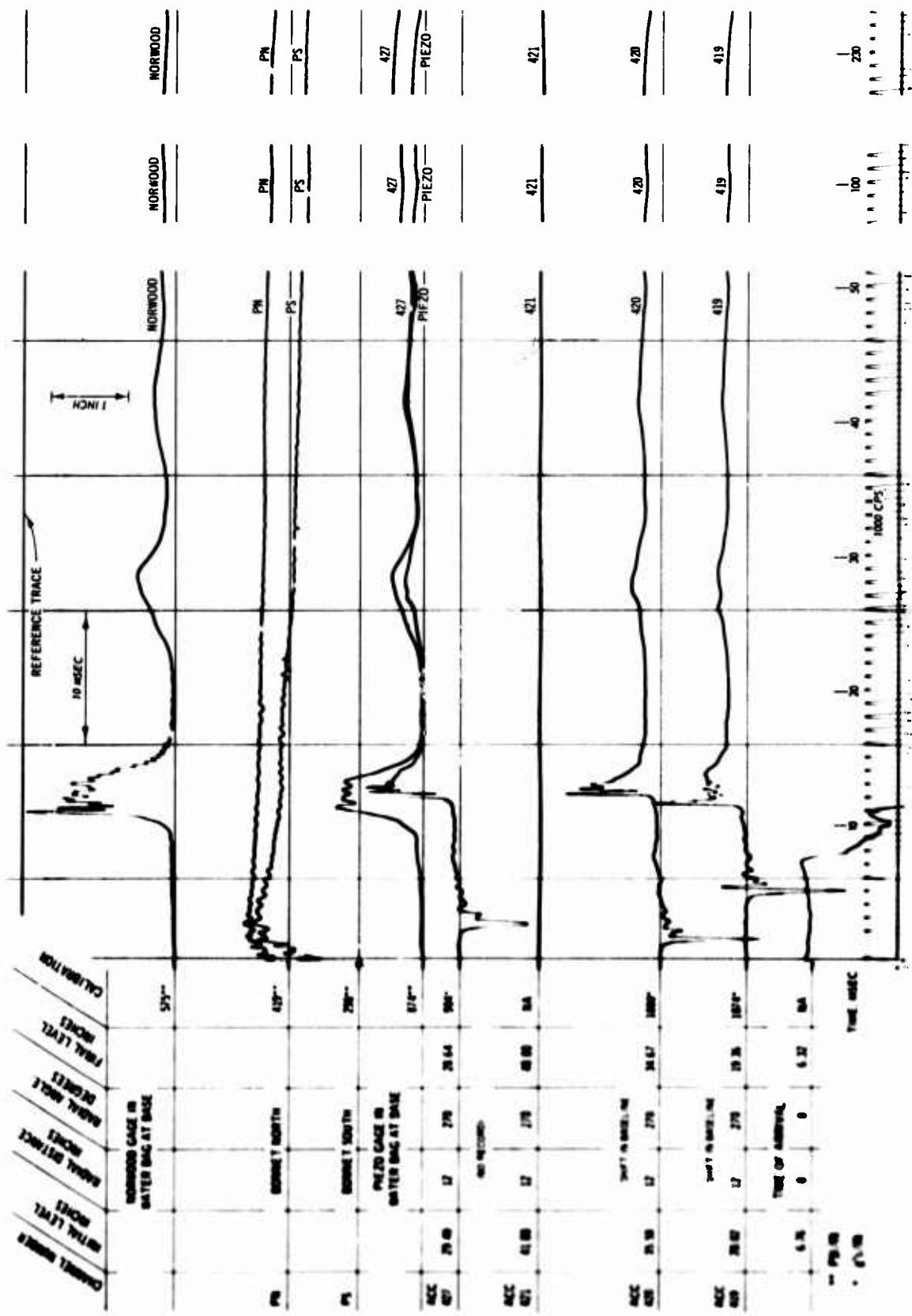


Fig. C-79. Test B, pressure and acceleration record

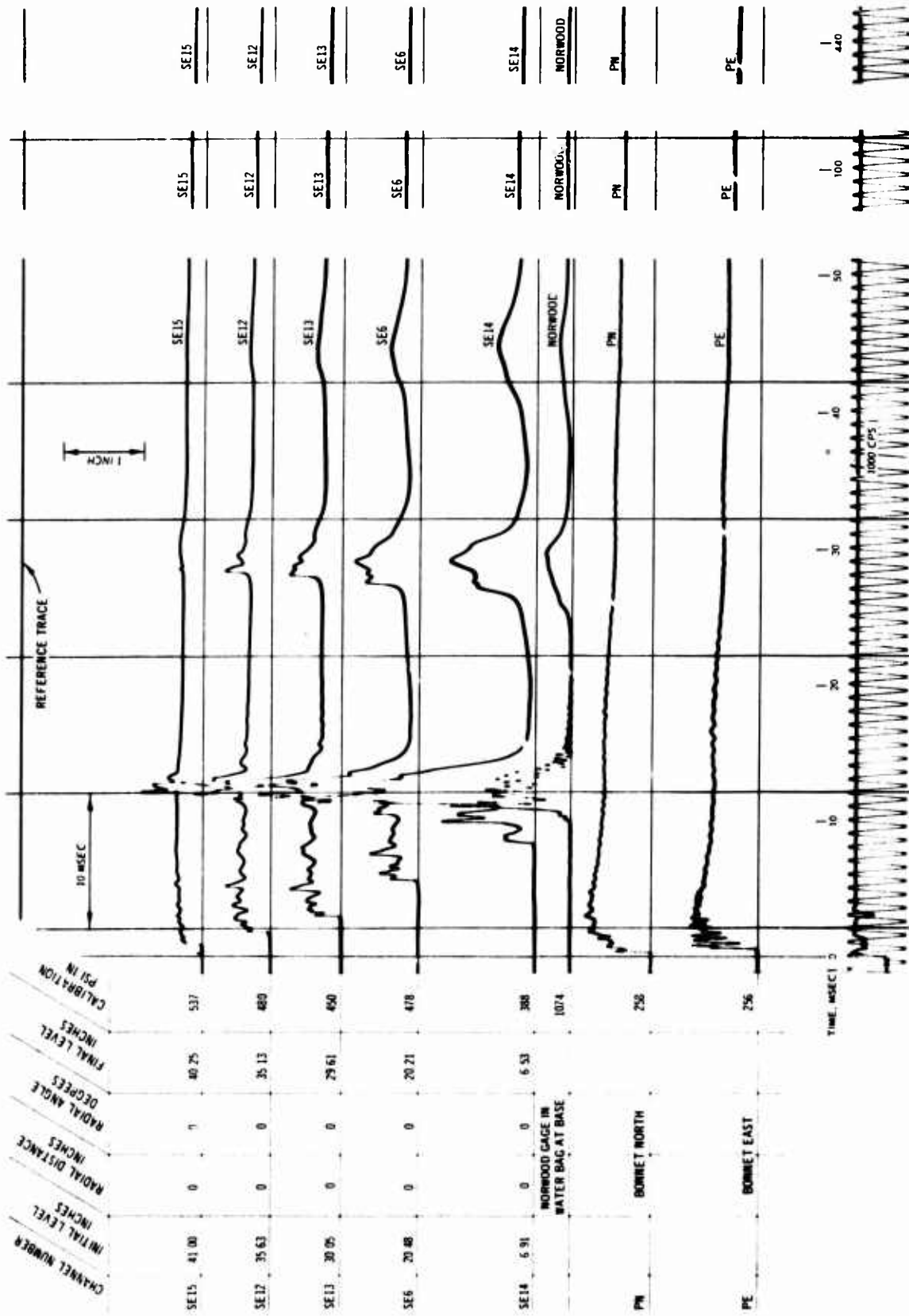


Fig. C-80. Test C, pressure record

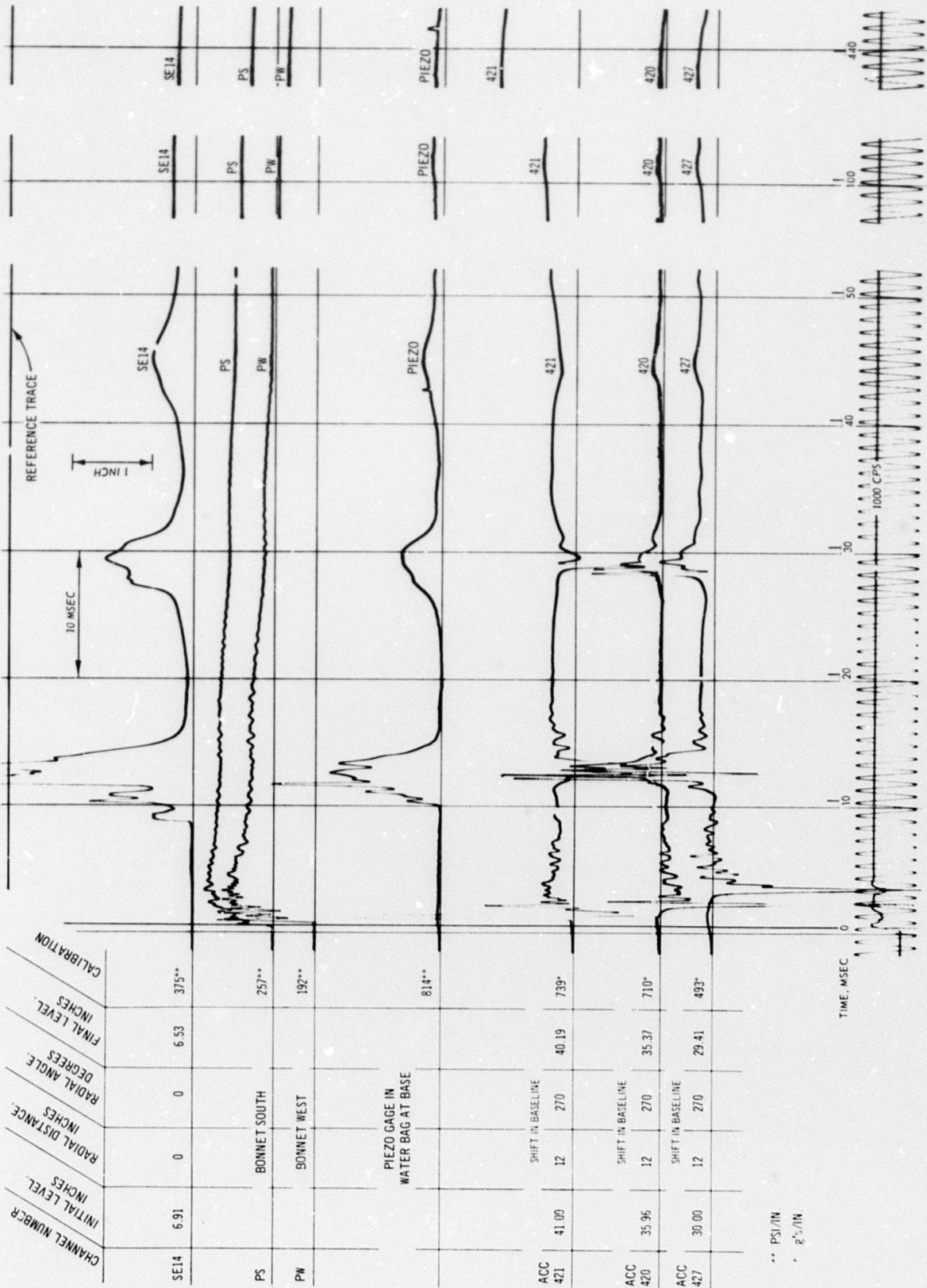


Fig. C-81. Test C, pressure and acceleration record

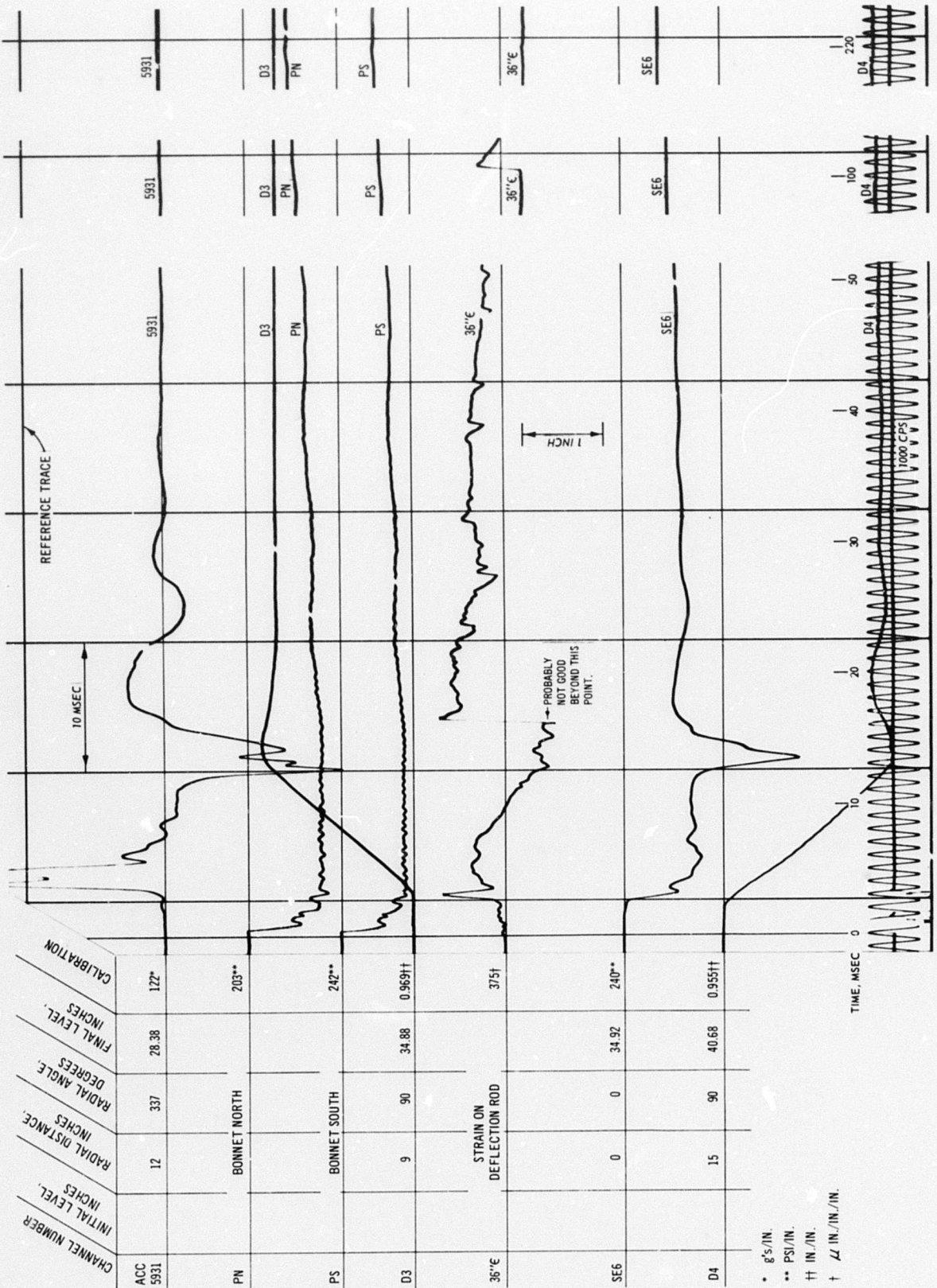


Fig. C-82. Test D, pressure, acceleration, deflection, and strain record

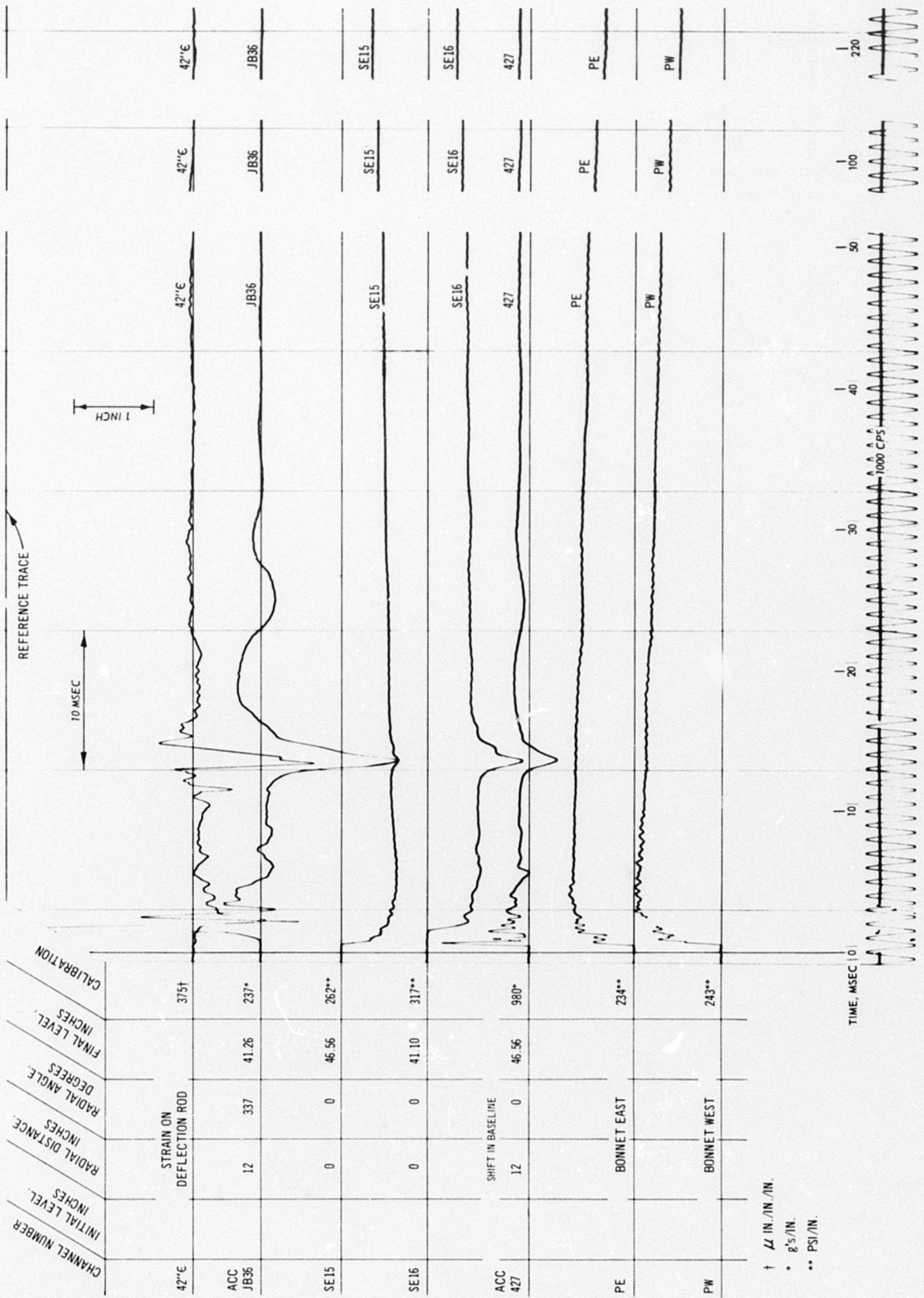
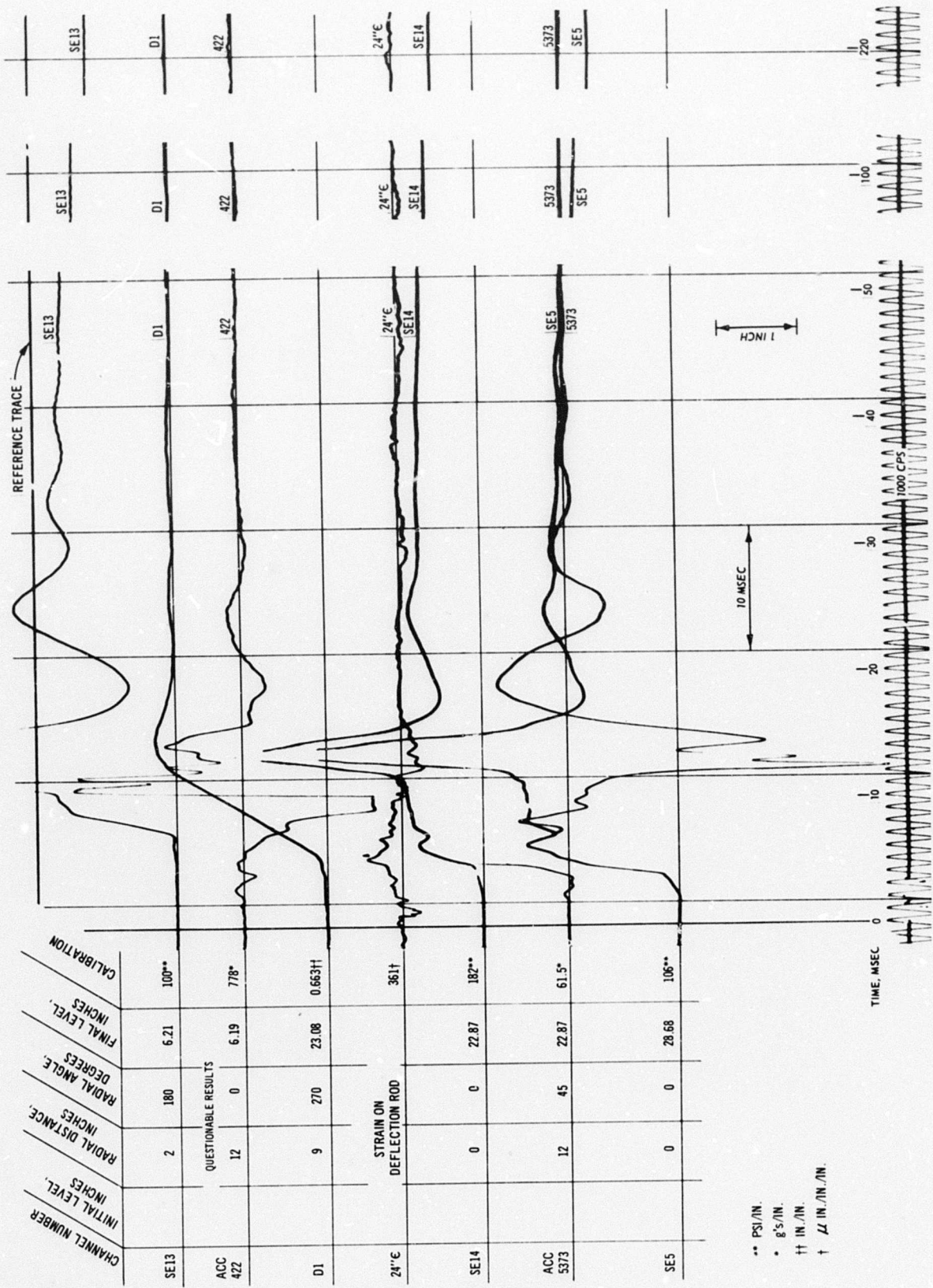


Fig. C-83. Test D, pressure, acceleration, and strain record



** PSI/IN.
 * 8'S/IN.
 †† IN./IN.
 † 1/4 IN./IN.

Fig. C-84. Test D, pressure, acceleration, deflection, and strain record

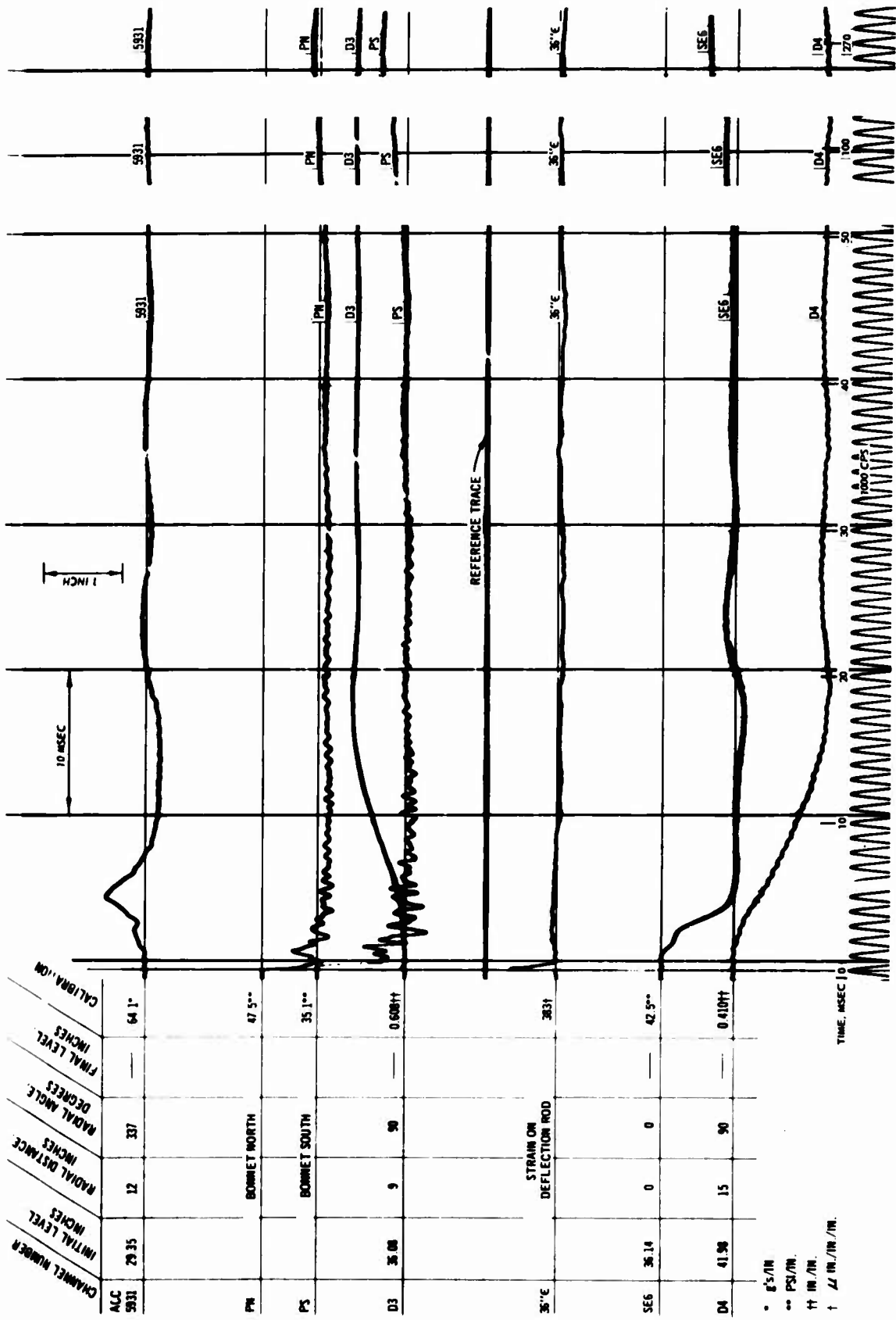


Fig. C-85. Test E, pressure, acceleration, deflection, and strain record

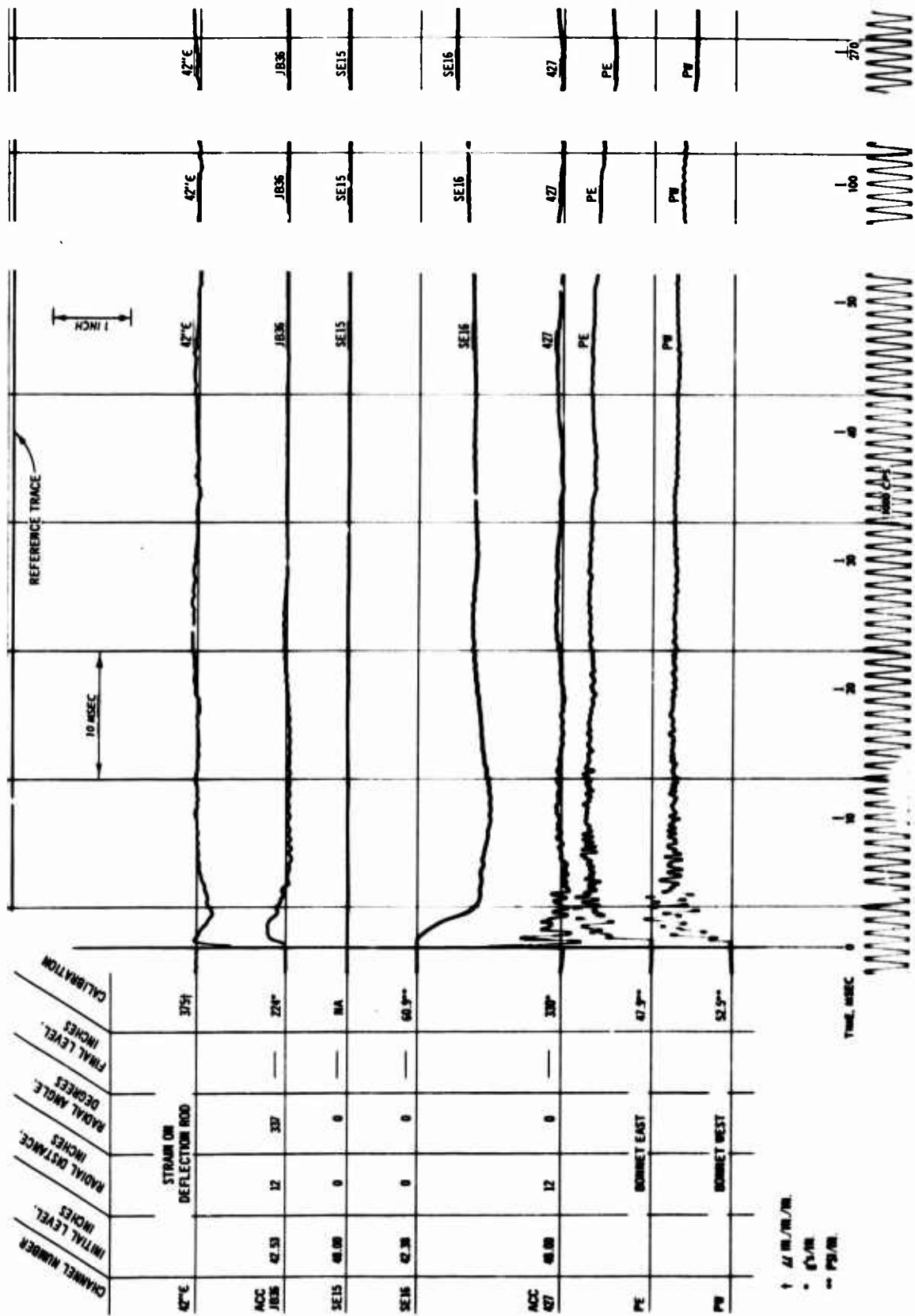


Fig. C-86. Test pressure, acceleration, and strain record

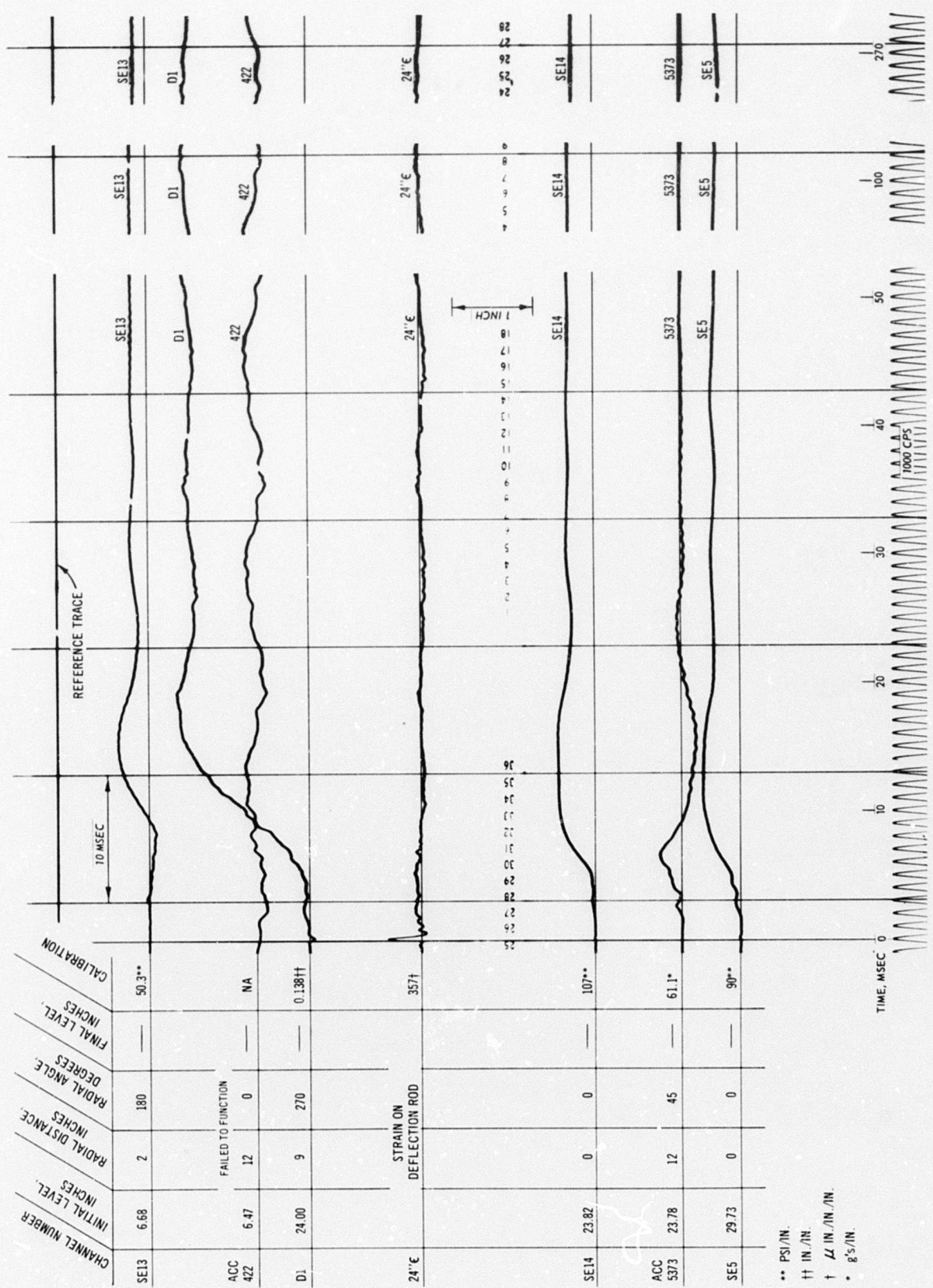


Fig. C-87. Test E, pressure, acceleration, deflection, and strain record

Unclassified

Security Classification

DOCUMENT CONTROL DATA - R & D

(Security classification of title, body of abstract and indexing annotation must be entered when the overall report is classified)

1. ORIGINATING ACTIVITY (Corporate author)		2a. REPORT SECURITY CLASSIFICATION	
U. S. Army Engineer Waterways Experiment Station Vicksburg, Mississippi		Unclassified	
3. REPORT TITLE		2b. GROUP	
AN EXPERIMENTAL INVESTIGATION OF SOIL-STRUCTURE INTERACTION IN A COHESIVE SOIL; VOLUMES I AND II			
4. DESCRIPTIVE NOTES (Type of report and inclusive dates)			
Final report (in two volumes)			
5. AUTHOR(S) (First name, middle initial, last name)			
Guy E. Jester			
6. REPORT DATE	7a. TOTAL NO. OF PAGES	7b. NO. OF REFS	
March 1970	666	133	
8a. CONTRACT OR GRANT NO.	9a. ORIGINATOR'S REPORT NUMBER(S)		
	Technical Report N-70-7; Volumes I and II		
b. PROJECT NO.	9b. OTHER REPORT NO(S) (Any other numbers that may be assigned this report)		
c. NWER Subtask SC210			
d.			
10. DISTRIBUTION STATEMENT			
This document has been approved for public release and sale; its distribution is unlimited.			
11. SUPPLEMENTARY NOTES		12. SPONSORING MILITARY ACTIVITY	
Report was also submitted to University of Illinois, Urbana, Illinois, as thesis for degree of Doctor of Philosophy in Civil Engineering		Defense Atomic Support Agency Washington, D. C.	
13. ABSTRACT			
<p>This study was an experimental investigation of the behavior of an idealized structure buried at various depths in a compacted cohesive soil (buckshot clay, water content = 26%). Eight static and 20 dynamic plane-wave loadings up to 310 psi were conducted. The cylindrical test devices (5 inches high and 6 inches in diameter) were oriented vertically and their stiffness relative to the soil was varied. In addition a device whose top could be extended and contracted hydraulically was buried at various depths and the relation between load and deformation changes was studied at static overpressures of 37.5 and 75 psi. At low static and dynamically applied surface pressures ($P_s = 37.5$ psi) and a depth of burial of one structure diameter ($H/B = 1$), the amount of active arching depended upon the stiffness of the structure relative to that of the soil. Under these conditions, it was possible to relieve practically all the overpressure on the test structure just by decreasing its stiffness. () At $H/B = 1$, the structure behaved as if it were fully buried under dynamic and static pressures less than 40 psi. As the surface pressure was increased, the amount of arching at $H/B \geq 1$ became more dependent upon the shear strength of the soil. When the scaled depth of burial was increased to $H/B = 3$ at surface pressures in the 150- to 250-psi range, the differential pressure, as calculated by subtracting the average pressure acting on the top of the device from the surface pressure at the same time interval, increased but it did not increase as much as the load on the structure. At $P_s = 150$ psi under dynamic conditions the differential pressure was 32 psi or 2.5 times the shear strength of the soil as determined by unconfined compression tests ($q_u/2$) as compared to 25 psi or 1.4 times the shear strength of the soil at $H/B = 1$. When the surface pressure was increased to 240 psi under dynamic conditions at $H/B = 3$, the (Continued)</p>			

DD FORM 1473
1 NOV 65

REPLACES DD FORM 1473, 1 JAN 64, WHICH IS OBSOLETE FOR ARMY USE.

Unclassified

Security Classification

14. KEY WORDS	LINK A		LINK B		LINK C	
	ROLE	WT	ROLE	WT	ROLE	WT
Clays						
Cohesive soils						
Interactions						
Shear properties						
Soil arching						
Soil strength						
Soil-structure interaction						
Structures						
Subsurface structures						

13. ABSTRACT (Continued)

differential pressure was only 35 psi. Under static conditions, the differential pressure was 37 psi at $P_s = 150$ psi and 54 psi at $P_s = 175$ psi. When the static surface pressure was increased to 240 psi, the differential pressure only increased to 58 psi or 5.2 times the shear strength of the soil. Once the strength of the soil at a particular depth had been fully developed, increasing the surface pressure had very little effect on the amount of arching. There was a transition zone between those surface pressures at which the amount of arching was determined by relative structure flexibility and the pressure at which it was more dependent upon soil strength. The pressures which limited the transition zone depended upon depth of burial and the time in which the load was applied. Within the transition zone, the role played by the relative stiffness changed gradually. Based on the very limited amount of data developed in this test program ($P_s < 65$ psi and $H/B = 1$), passive arching does not appear to be sensitive to structure stiffness. Once the relative structure stiffness (K_T/K_S) exceeded a value of approximately 4, there was no increase in the amount of arching with an increase in the structure stiffness. The maximum scaled differential pressure ($2\Delta P/q_u$) never exceeded a value of 1.1. Regardless of the stiffness of the structure or the state of arching considered, static arching curves produced by lowering or raising the top of the structure by internal means could not be used to estimate the amount of arching that a similar spring test device would induce under static or dynamic external loads. In addition it was found that static arching data produced with the spring device could not be used to predict the design loads on a comparable structure at dynamically applied surface pressures in excess of 40 to 70 psi, depending on the depth of burial.